extinguishing metaflammation: mechanisms and therapeutic opportunities for immunological control of metabolic dysfunctions

Zande, H.J.P van der

EXTINGUISHING METAFLAMMATION

Mechanisms and therapeutic opportunities for immunological control of metabolic dysfunctions

Hendrik Johannes Petrus van der Zande

ISBN: 978-94-6458-740-1
Cover design: Miho Suzuki
Layout: Publiss | www.publiss.nl
Printing: Ridderprint | www.ridderprint.nl

The work described in this thesis was performed at the department of Parasitology at the Leiden University Medical Center, Leiden, the Netherlands, and the department of Microbiology at New York University Langone School of Medicine, New York, USA. The work was supported by the graduate program of the Dutch Research Council (NWO, awarded to H.J.P. van der Zande), and a ZonMw TOP Grant (awarded to dr. B.G.A. Guigas and prof.dr. M. Yazdanbakhsh).

Printing of this thesis was financially supported by Bio X Cell, Chipsoft and Valbiotis, which is gratefully acknowledged.

EXTINGUISHING METAFLAMMATION

Mechanisms and therapeutic opportunities for immunological control of metabolic dysfunctions

Proefschrift

ter verkrijging van

de graad van doctor aan de Universiteit Leiden,

op gezag van rector magnificus prof.dr.ir. H. Bijl,

volgens besluit van het college voor promoties

te verdedigen op donderdag 26 januari 2023

klokke 11.15 uur

door

Hendrik Johannes Petrus van der Zande

geboren te Dordrecht

in 1991

Promotor:	prof.dr. M. Yazdanbakhsh
Co-promotor:	dr. B.G.A. Guigas
Leden promotiecommissie:	prof.dr. P.C.N. Rensen prof.dr. C.L. Scott (VIB Universiteit Gent) dr. P. Loke (National Institutes of Health, Bethesda, MA, USA) dr. J. Van den Bossche (Amsterdam UMC, locatie VUmc)

Table of contents

CHAPTER 1

General introduction

Obesity, type 2 diabetes and metaflammation

Chronic imbalance between energy intake and expenditure results in overweight and obesity. These conditions are defined by elevated body mass index (BMI; 25-29.9 kg/m^2 and >30 kg/m^2, respectively) as a gauge for adiposity and predispose for developing co-morbidities like type 2 diabetes, cardiovascular diseases, and some forms of cancer. Although preventable, obesity prevalence has reached epidemic proportions, afflicting over 650 million adults as of 2016 (1), and over 450 million suffered from type 2 diabetes in 2019 (2). Lifestyle interventions - encompassing either dietary, physical, behavioral, or a combination - have been proven efficacious in reducing obesity-associated risks and improving quality of life, yet post-intervention weight maintenance remains a considerable challenge (3). In fact, although mechanistically incompletely understood (4-6), formerly obese individuals are at risk for accelerated post-dieting weight regain (7). Although type 2 diabetes and other obesity-induced metabolic dysfunctions are drug-treatable, most entail symptomatic treatments, and new, innovative therapeutic strategies are still required to both provide alternatives to conventional medicine and act in concert with lifestyle interventions for alleviating disease.

Understanding the pathophysiology of obesity-induced metabolic dysfunctions may assist in developing such new therapeutic strategies. Chronic nutritional overload causes adipocyte hypertrophy and hyperplasia that eventually results in white adipose tissue (WAT) dysfunction, at least partly through hypoxia-induced adipocyte cell death (8, 9). This is believed to trigger inflammation, where recruited immune cells produce proinflammatory cytokines that generate a vicious circle exacerbating inflammation, as well as inhibit adipocyte canonical insulin signaling and promote lipolysis-derived fatty acid efflux. These events promote ectopic lipid deposition in skeletal muscle and the liver, contributing to development of non-alcoholic fatty liver disease (NAFLD). This disruption of skeletal muscle and liver homeostasis promotes local inflammation, hepatic gluconeogenesis and tissue-specific insulin resistance via proinflammatory cytokines and lipotoxicity, together contributing to whole-body insulin resistance and development of type 2 diabetes (10, 11) (**Figure 1**). Hence, type 2 diabetes is driven by so-called chronic, low-grade inflammation particularly in metabolic tissues, also coined metaflammation (12).

Conceivably, most research on metaflammation has focused on WAT, as this is considered the etiological origin of an inflammatory cascade that impairs whole-body insulin sensitivity. It is well-established that cells of both the innate and adaptive immune system accumulate in WAT during obesity and are either associated with or drive insulin resistance (13, 14). A key paradigm herein is the recruitment of monocytes through the monocyte chemoattractant protein 1 (MCP-1)-CCR2 axis and subsequent development into proinflammatory macrophages upon encountering the WAT inflammatory milieu (15-17). .

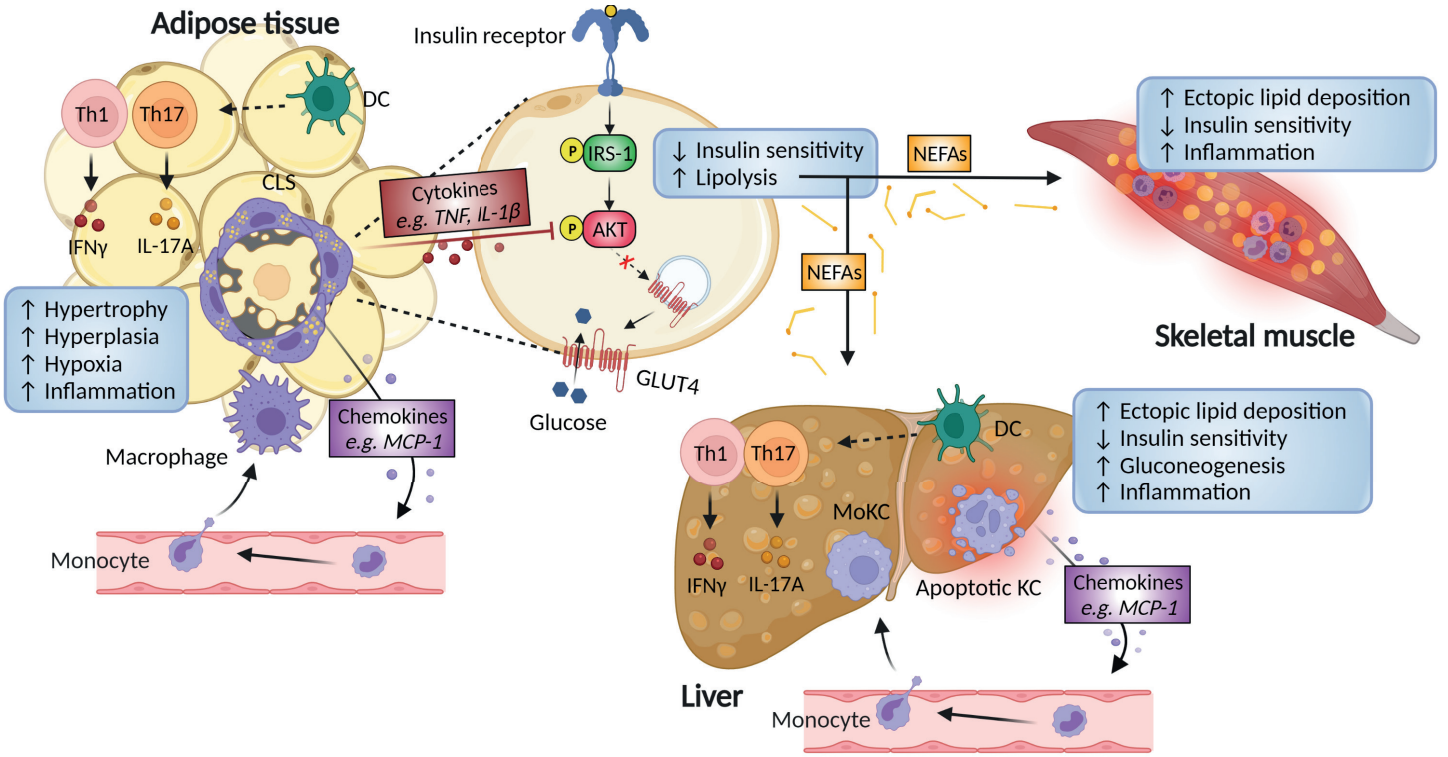

Figure 1. Pathophysiology of obesity-induced metabolic dysfunctions. See text for details. Th: T helper, DC: dendritic cell, IFNγ: interferon gamma, IL: interleukin, CLS: crown-like structure, TNF: tumor necrosis factor, MCP-1: monocyte chemoattractant protein 1, IRS-1: insulin receptor substrate 1, GLUT4: glucose transporter 4, NEFAs: non-esterified fatty acids, KC: Kupffer cell, MoKC: monocyte-derived KC. Created with BioRender.com.

Macrophage-derived proinflammatory cytokines, such as tumor necrosis factor (TNF) and interleukin (IL)-1β, were shown to inhibit tissue-specific insulin signaling (18, 19) (**Figure 1**). Similarly, activation and impaired survival of Kupffer cells (KCs), the liver-resident macrophages, and recruitment of proinflammatory monocyte-derived KCs contribute to NAFLD pathogenesis and progression towards non-alcoholic steatohepatitis (NASH) (20-22) (**Figure 1**). Although well-established, the environmental and cellular changes dictating proinflammatory macrophage activation in the context of obesity are hitherto not fully understood, and identifying new mechanisms may provide novel therapeutic targets or strategies

In addition to macrophages, dendritic cells (DCs) were also shown to contribute to obesity-induced metabolic dysfunctions (23-25). DCs are specialized antigen presenting cells that bridge the innate and adaptive immune system by governing T cell responses dependent on the inflammatory and metabolic context, both aiding in defense against pathogens and maintenance of immune homeostasis. Obesity promotes DC accumulation in metabolic tissues, and mice lacking DCs or with impaired DC migration are protected against metaflammation and insulin resistance (23-25). Furthermore, both WAT and liver are populated by different T cell subsets. Here, interferon (IFN)-γ-producing $CD4^+$ T helper 1 (Th1) cells and IL-17A-producing Th17 cells increase during obesity, and are considered to contribute to insulin resistance (as reviewed in (26) and (27)). The T cell priming capacity of DCs is increasingly recognized to be driven by their cellular metabolic rewiring, facilitating co-stimulatory marker and cytokine expression necessary for skewing T cell differentiation (28). Accordingly, the metabolic microenvironment of DCs has considerable impact on its T cell priming functions (29). However, the mechanistic underpinnings of DC-mediated T cell priming in metabolic tissues in the context of obesity are yet incompletely understood.

Type 2 immunity, metabolic homeostasis and parasitic worms

During homeostasis, the maintenance of insulin sensitivity in metabolic tissues is under the control of the immune system. Specifically in lean WAT, Th2 cells and type 2 innate lymphoid cells (ILC2s) produce the canonical type 2 cytokines IL-4, IL-5 and IL-13, of which IL-5 maintains WAT eosinophil homing (30). These eosinophils are the principal producers of IL-4, and together with Th2 and ILC2-derived IL-4 and IL-13 promote alternative activation of macrophage through IL-4Rα and/or IL-13Rα1/2-mediated activation of the transcription factor STAT6 (30-33). Since tissue macrophages are well-established sentinels of homeostasis (34, 35) and this immunological circuit appears to culminate in alternative activation of macrophages, these cells are considered the effector cells that maintain tissue

insulin sensitivity (**Figure 2**). Although not as extensively studied, similar processes are believed to also contribute to maintenance of insulin sensitivity in the liver (36). One could imagine that restoring this impaired type 2 immunity environment in obese individuals may restore insulin sensitivity and mitigate obesity-induced metabolic dysfunctions.

Parasitic helminth worms are the strongest natural inducers of type 2 immunity (37). Indeed, cross-sectional studies have shown that individuals living in helminth-endemic areas are less likely to develop metabolic dysfunctions (38), and pharmacological elimination of helminths worsened metabolic parameters associated with insulin resistance (39, 40), indicative of an inverse correlation between helminth infection and metabolic dysfunctions. In line with this, experimental infection of obese mice with different helminth species (31, 41-43), as well as treatment with helminth-derived immunomodulatory molecules (41, 42, 44), induced type 2 immunity in metabolic tissues and improved whole-body insulin sensitivity. Together, this suggests that type 2 immunity, induced by helminths or their molecules, may hold promise in treatment of metabolic disorders, although causality and underlying mechanisms remain to be established.

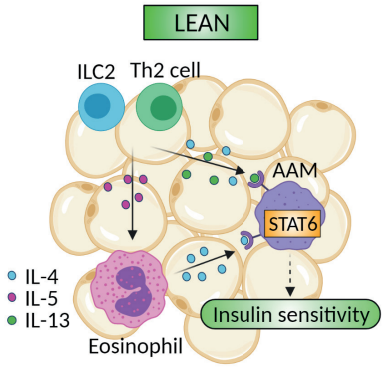

Figure 2. Type 2 immunity in lean WAT. See text for details. AAM: alternatively-activated macrophage. Created with BioRender.com

Thesis outline

Immunometabolism is a rapidly evolving new field at the intersection of immunology and metabolism that consists of two inter-related branches: [1] cellular immunometabolism, *i.e.* how intracellular metabolism dictates immune cell function; and [2] systemic immunometabolism, *i.e.* how immune cells control tissue-specific and whole-body metabolic homeostasis. The work presented in this thesis mainly focuses on how immune cells regulate tissue-specific and whole-body metabolic homeostasis in various experimental contexts. To

this end, we mainly used preclinical mouse models of obesity, insulin resistance and type 2 diabetes to dissect the underlying molecular mechanisms and explore various therapeutic strategies.

In part 1, we investigate the molecular mechanisms involved in the control of metabolic homeostasis by myeloid cells. **Chapter 2** is an example of cross-fertilization of the two arms of immunometabolism, investigating whether manipulation of macrophage metabolism affects immune cell function and, consequently, whole-body metabolism. Here, we investigate the effects of macrophage-specific deletion of ATP citrate lyase (Acly), a metabolic enzyme linking cellular metabolism to immune cell function, on inflammatory disorders such as obesity-induced type 2 diabetes. **Chapter 3** describes the discovery of a new role for the soluble form of the mannose receptor, a cell surface receptor involved in antigen binding and internalization, in the regulation of macrophage proinflammatory activation and metabolic homeostasis. Next, **chapter 4** summarizes and discusses the impact of the mannose receptor and other family members of the C-type lectins on regulating immune cell functions and their effects on metaflammation. Finally, in **chapter 5**, which constitutes another example of a study bridging the two arms of immunometabolism, we investigate how the nutrient sensor liver kinase B1 (LKB1) governs DC function in the context of obesity. Collectively, this section describes novel mechanisms that control metabolic homeostasis, providing potential new leads for therapeutic interventions.

In the second part of this dissertation, we investigate whether immunomodulatory (helminth) molecules improve metabolic dysfunctions of obese mice, and study the underlying mechanisms. **Chapter 6** first provides a literature overview on regulation of metabolic homeostasis by immune cells and the impact of helminths and their immunomodulatory molecules. Among these molecules are the immunomodulatory soluble egg antigens (SEA) of the helminth *Schistosoma mansoni*. In **chapter 7**, we next investigate how *S. mansoni* SEA and ω1, a type 2 immunity-inducing molecule present in *S. mansoni* SEA, may promote insulin sensitivity in a mouse model of diet-induced obesity. Finally, in **chapter 8** we explore the immunometabolic effects of a novel plant extract, named Totum-63 and developed for the treatment of pre-diabetes, on obese mice. Altogether, this part provides new insights into how immunomodulatory (helminth) molecules can regulate whole-body metabolic homeostasis.

To conclude, **chapter 9** highlights the main findings of this thesis and provides suggestions for future research investigating immunological control of obesity-induced metabolic dysfunctions.

References

1. WHO. Obesity and overweight. 2021 [updated 09-06-2021. Available from: https://www.who.int/news-room/fact-sheets/detail/obesity-and-overweight.
2. Williams R, Colagiuri S, Chan J, Gregg E, Ke C, Lim L-L, et al. IDF Atlas 9th Edition 20192019.
3. Webb VL, Wadden TA. Intensive Lifestyle Intervention for Obesity: Principles, Practices, and Results. Gastroenterology. 2017;152(7):1752-64.
4. Thaiss CA, Itav S, Rothschild D, Meijer MT, Levy M, Moresi C, et al. Persistent microbiome alterations modulate the rate of post-dieting weight regain. Nature. 2016;540(7634):544-51.
5. Zou J, Lai B, Zheng M, Chen Q, Jiang S, Song A, et al. CD4+ T cells memorize obesity and promote weight regain. Cell Mol Immunol. 2018;15(6):630-9.
6. van Baak MA, Mariman ECM. Mechanisms of weight regain after weight loss - the role of adipose tissue. Nat Rev Endocrinol. 2019;15(5):274-87.
7. Christou NV, Look D, Maclean LD. Weight gain after short- and long-limb gastric bypass in patients followed for longer than 10 years. Ann Surg. 2006;244(5):734-40.
8. Lee YS, Kim JW, Osborne O, Oh DY, Sasik R, Schenk S, et al. Increased adipocyte O2 consumption triggers HIF-1alpha, causing inflammation and insulin resistance in obesity. Cell. 2014;157(6):1339-52.
9. Seo JB, Riopel M, Cabrales P, Huh JY, Bandyopadhyay GK, Andreyev AY, et al. Knockdown of Ant2 Reduces Adipocyte Hypoxia And Improves Insulin Resistance in Obesity. Nat Metab. 2019;1(1):86-97.
10. Roden M, Shulman GI. The integrative biology of type 2 diabetes. Nature. 2019;576(7785):51-60.
11. Wu H, Ballantyne CM. Skeletal muscle inflammation and insulin resistance in obesity. J Clin Invest. 2017;127(1):43-54.
12. Gregor MF, Hotamisligil GS. Inflammatory mechanisms in obesity. Annual review of immunology. 2011;29:415-45.
13. Lackey DE, Olefsky JM. Regulation of metabolism by the innate immune system. Nature Reviews Endocrinology. 2016;12(1):15-28.
14. Weinstock A, Silva HM, Moore KJ, Schmidt AM, Fisher EA. Leukocyte Heterogeneity in Adipose Tissue, Including in Obesity. Circulation Research. 2020;126(11):1590-612.
15. Lumeng CN, Bodzin JL, Saltiel AR. Obesity induces a phenotypic switch in adipose tissue macrophage polarization. The Journal of Clinical Investigation. 2007;117(1):175-84.
16. Kratz M, Coats Brittney R, Hisert Katherine B, Hagman D, Mutskov V, Peris E, et al. Metabolic Dysfunction Drives a Mechanistically Distinct Proinflammatory Phenotype in Adipose Tissue Macrophages. Cell Metabolism. 2014;20(4):614-25.
17. Hill DA, Lim H-W, Kim YH, Ho WY, Foong YH, Nelson VL, et al. Distinct macrophage populations direct inflammatory versus physiological changes in adipose tissue. Proceedings of the National Academy of Sciences. 2018;115(22):E5096.

18. Hotamisligil GS, Shargill NS, Spiegelman BM. Adipose expression of tumor necrosis factor-alpha: direct role in obesity-linked insulin resistance. Science. 1993;259(5091):87.

19. Stienstra R, Joosten LAB, Koenen T, van Tits B, van Diepen JA, van den Berg SAA, et al. The Inflammasome-Mediated Caspase-1 Activation Controls Adipocyte Differentiation and Insulin Sensitivity. Cell Metabolism. 2010;12(6):593-605.

20. Obstfeld AE, Sugaru E, Thearle M, Francisco A-M, Gayet C, Ginsberg HN, et al. C-C Chemokine Receptor 2 (CCR2) Regulates the Hepatic Recruitment of Myeloid Cells That Promote Obesity-Induced Hepatic Steatosis. Diabetes. 2010;59(4):916.

21. Tran S, Baba I, Poupel L, Dussaud S, Moreau M, Gélineau A, et al. Impaired Kupffer Cell Self-Renewal Alters the Liver Response to Lipid Overload during Non-alcoholic Steatohepatitis. Immunity. 2020;53(3):627-40.e5.

22. Remmerie A, Martens L, Thoné T, Castoldi A, Seurinck R, Pavie B, et al. Osteopontin Expression Identifies a Subset of Recruited Macrophages Distinct from Kupffer Cells in the Fatty Liver. Immunity. 2020;53(3):641-57.e14.

23. Stefanovic-Racic M, Yang X, Turner MS, Mantell BS, Stolz DB, Sumpter TL, et al. Dendritic Cells Promote Macrophage Infiltration and Comprise a Substantial Proportion of Obesity-Associated Increases in CD11c⁺ Cells in Adipose Tissue and Liver. Diabetes. 2012;61(9):2330.

24. Cho KW, Zamarron BF, Muir LA, Singer K, Porsche CE, DelProposto JB, et al. Adipose Tissue Dendritic Cells Are Independent Contributors to Obesity-Induced Inflammation and Insulin Resistance. The Journal of Immunology. 2016:1600820.

25. Deczkowska A, David E, Ramadori P, Pfister D, Safran M, At the B, et al. XCR1+ type 1 conventional dendritic cells drive liver pathology in non-alcoholic steatohepatitis. Nature Medicine. 2021;27(6):1043-54.

26. Wang Q, Wu H. T Cells in Adipose Tissue: Critical Players in Immunometabolism. Frontiers in Immunology. 2018;9(2509).

27. Van Herck MA, Weyler J, Kwanten WJ, Dirinck EL, De Winter BY, Francque SM, et al. The Differential Roles of T Cells in Non-alcoholic Fatty Liver Disease and Obesity. Frontiers in Immunology. 2019;10(82).

28. Patente TA, Pelgrom LR, Everts B. Dendritic cells are what they eat: how their metabolism shapes T helper cell polarization. Current Opinion in Immunology. 2019;58:16-23.

29. Brombacher EC, Everts B. Shaping of Dendritic Cell Function by the Metabolic Micro-Environment. Frontiers in Endocrinology. 2020;11(555).

30. Molofsky AB, Nussbaum JC, Liang H-E, Van Dyken SJ, Cheng LE, Mohapatra A, et al. Innate lymphoid type 2 cells sustain visceral adipose tissue eosinophils and alternatively activated macrophages. Journal of Experimental Medicine. 2013;210(3):535-49.

31. Wu D, Molofsky AB, Liang H-E, Ricardo-Gonzalez RR, Jouihan HA, Bando JK, et al. Eosinophils Sustain Adipose Alternatively Activated Macrophages Associated with Glucose Homeostasis. Science. 2011;332(6026):243.

32. Takeda K, Kamanaka M, Tanaka T, Kishimoto T, Akira S. Impaired IL-13-mediated functions of macrophages in STAT6-deficient mice. The Journal of Immunology. 1996;157(8):3220.

33. Takeda K, Tanaka T, Shi W, Matsumoto M, Minami M, Kashiwamura S-i, et al. Essential role of Stat6 in IL-4 signalling. Nature. 1996;380(6575):627-30.

34. Wynn TA, Chawla A, Pollard JW. Macrophage biology in development, homeostasis and disease. Nature. 2013;496(7446):445-55.

35. Okabe Y, Medzhitov R. Tissue biology perspective on macrophages. Nature Immunology. 2016;17(1):9-17.

36. Ricardo-Gonzalez RR, Red Eagle A, Odegaard JI, Jouihan H, Morel CR, Heredia JE, et al. IL-4/STAT6 immune axis regulates peripheral nutrient metabolism and insulin sensitivity. Proceedings of the National Academy of Sciences. 2010;107(52):22617.

37. Maizels RM, Yazdanbakhsh M. Immune Regulation by helminth parasites: cellular and molecular mechanisms. Nature Reviews Immunology. 2003;3(9):733-44.

38. de Ruiter K, Tahapary DL, Sartono E, Soewondo P, Supali T, Smit JWA, et al. Helminths, hygiene hypothesis and type 2 diabetes. Parasite Immunology. 2017;39(5):e12404.

39. Tahapary DL, de Ruiter K, Martin I, Brienen EAT, van Lieshout L, Djuardi Y, et al. Effect of anthelmintic treatment on leptin, adiponectin and leptin to adiponectin ratio: a randomized-controlled trial. Nutrition & Diabetes. 2017;7(10):e289-e.

40. Rajamanickam A, Munisankar S, Bhootra Y, Dolla C, Thiruvengadam K, Nutman TB, et al. Metabolic Consequences of Concomitant Strongyloides stercoralis Infection in Patients With Type 2 Diabetes Mellitus. Clinical Infectious Diseases. 2019;69(4):697-704.

41. Hussaarts L, García-Tardón N, van Beek L, Heemskerk MM, Haeberlein S, van der Zon GC, et al. Chronic helminth infection and helminth-derived egg antigens promote adipose tissue M2 macrophages and improve insulin sensitivity in obese mice. The FASEB Journal. 2015;29(7):3027-39.

42. Berbudi A, Surendar J, Ajendra J, Gondorf F, Schmidt D, Neumann AL, et al. Filarial Infection or Antigen Administration Improves Glucose Tolerance in Diet-Induced Obese Mice. Journal of Innate Immunity. 2016;8(6):601-16.

43. Khudhair Z, Alhallaf R, Eichenberger RM, Whan J, Kupz A, Field M, et al. Gastrointestinal Helminth Infection Improves Insulin Sensitivity, Decreases Systemic Inflammation, and Alters the Composition of Gut Microbiota in Distinct Mouse Models of Type 2 Diabetes. Frontiers in Endocrinology. 2021;11(1132).

44. Hams E, Bermingham R, Wurlod FA, Hogan AE, O'Shea D, Preston RJ, et al. The helminth T2 RNase ω1 promotes metabolic homeostasis in an IL-33- and group 2 innate lymphoid cell-dependent mechanism. The FASEB Journal. 2016;30(2):824-35.

PART I

I

MOLECULAR MECHANISMS INVOLVED IN THE CONTROL OF METABOLIC HOMEOSTASIS BY MYELOID CELLS

CHAPTER 2

Myeloid ATP citrate lyase regulates macrophage inflammatory responses *in vitro* without altering inflammatory disease outcomes

Sanne G.S. Verberk[#], **Hendrik J.P. van der Zande**[#], Jeroen Baardman, Kyra E. de Goede, Karl J. Harber, Eelco D. Keuning, Joost M. Lambooij, Frank Otto, Anna Zawistowska-Deniziak, Helga E. de Vries, Menno P.J. de Winther, Bruno Guigas, Jan Van den Bossche

[#]These authors contributed equally to this study

Frontiers in Immunology. 12:669920. (2021)
PMID: 33981315
doi: 10.3389/fimmu.2021.669920

Abstract

Macrophages are highly plastic, key regulators of inflammation. Deregulation of macrophage activation can lead to excessive inflammation as seen in inflammatory disorders like atherosclerosis, obesity, multiple sclerosis and sepsis. Targeting intracellular metabolism is considered as an approach to reshape deranged macrophage activation and to dampen the progression of inflammatory disorders. ATP citrate lyase (Acly) is a key metabolic enzyme and an important regulator of macrophage activation. Using a macrophage-specific Acly-deficient mouse model, we investigated the role of Acly in macrophages during acute and chronic inflammatory disorders. First, we performed RNA sequencing to demonstrate that Acly-deficient macrophages showed hyperinflammatory gene signatures in response to acute LPS stimulation *in vitro*. Next, we assessed endotoxin-induced peritonitis in myeloid-specific Acly-deficient mice and show that, apart from increased splenic *Il6* expression, systemic and local inflammation were not affected by Acly deficiency. Also during obesity, both chronic low-grade inflammation and whole-body metabolic homeostasis remained largely unaltered in mice with Acly-deficient myeloid cells. Lastly, we show that macrophage-specific Acly deletion did not affect the severity of experimental autoimmune encephalomyelitis (EAE), an experimental model of multiple sclerosis. These results indicate that, despite increasing inflammatory responses *in vitro*, macrophage Acly deficiency does not worsen acute and chronic inflammatory responses *in vivo.* Collectively, our results indicate that caution is warranted in prospective long-term treatments of inflammatory disorders with macrophage-specific Acly inhibitors. Together with our earlier observation that myeloid Acly deletion stabilizes atherosclerotic lesions, our findings highlight that therapeutic targeting of macrophage Acly can be beneficial in some, but not all, inflammatory disorders.

Introduction

Macrophages are key players in the first line of cellular defense. These highly plastic immune cells can adopt several activation states to respond to the situation at hand. Under homeostatic conditions, functional pro- and anti-inflammatory macrophages are in balance to fight pathogens and to restore tissue damage. Unbalanced macrophage activation may lead to chronic inflammation as seen in atherosclerosis, multiple sclerosis (MS) and obesity or it can lead to hyper-inflammation as occurs during sepsis (1-3).

Metabolic reprogramming of macrophages has been proposed as a promising therapeutic target to combat inflammatory disorders (4, 5). Typical *in vitro* lipopolysaccharide (LPS)-activated inflammatory macrophages switch towards an increased flux through glycolysis and the pentose phosphate pathway to fuel their energy demands for eliciting immune responses, highlighting the central role of metabolism in inflammation (6). Interfering with such metabolic shifts may hamper persistent activation of inflammatory macrophages. Recently, Lauterbach et al. (2019) showed that early after LPS activation, the metabolic enzyme ATP citrate lyase (Acly) becomes activated in macrophages and provides the cell with cytosolic acetyl-CoA from increased glucose uptake and citrate accumulation (7). Increased cytosolic acetyl-CoA allows for histone acetylation to stimulate the expression of inflammatory genes and is involved in fatty acid synthesis and cholesterol biosynthesis (7-9). Hereby, Acly links glycolysis and mitochondrial metabolism to lipid metabolism and histone acetylation, marking Acly as a potential metabolic target for tackling excessive inflammation (9, 10). *In vitro* studies indicated that short-term inhibition of Acly by small molecule inhibitors or knockdown through siRNAs can dampen macrophage inflammation (7, 8, 11). Likewise, systemic inhibition of Acly *in vivo* reduces inflammatory outcomes in endotoxin-induced peritonitis (7). However, through a recently developed myeloid-specific Acly knockout mouse model, we revealed a discrepancy in the translation of *in vitro* findings to *in vivo* settings (12). In contradiction to previous studies, LysM-Cre-mediated Acly-deficient macrophages revealed increased inflammatory signaling in *in vitro* LPS-elicited responses and in atherosclerotic plaques *in vivo* (12). Despite increased inflammatory signaling, myeloid Acly deficiency resulted in increased atherosclerotic plaque stability (12). These data underline the need for a better understanding of targeting of Acly in macrophages specifically in the potential treatment of acute and chronic immune disorders.

Here, to decipher how Acly deficiency in myeloid cells affects acute and chronic inflammatory responses, we first analyzed LPS-activated macrophages by RNA-sequencing (RNA-seq). We demonstrated in an unbiased way that Acly-deficient macrophages display deregulated cholesterol handling and elevated inflammatory gene expression signatures after both 3 and 24 hours of LPS stimulation *in vitro*. Remarkably, we show that *in vivo* disease

outcomes of different inflammatory conditions, *i.e.* endotoxin-induced peritonitis, obesity and experimental auto-immune encephalitis (EAE) remain largely unaffected by myeloid Acly deficiency. Together with our previous findings in atherosclerosis, these data highlight that myeloid-specific targeting of Acly is beneficial only in some inflammatory disorders and is likely compensated in others.

Results

Macrophage Acly deficiency increases inflammatory signaling in vitro

To study the effects of Acly deficiency on inflammatory responses in macrophages, we crossed $Acly^{fl/fl}$ mice with mice expressing Cre under control of the myeloid cell-specific LysM promotor (*Lyz2-Cre*)(12). We have previously shown that naïve, unstimulated Acly-deficient bone marrow-derived macrophages (BMDMs) display deregulated lipid metabolism compared to control BMDMs, whereas inflammatory cytokines were increased only after LPS stimulation (12). Hence, we stimulated control ($Acly^{fl/fl}$) and Acly-deficient ($Acly^{M\text{-}KO}$) bone marrow-derived macrophages (BMDMs) *in vitro* with LPS for 3 and 24 hours to examine inflammatory activation in an unbiased way through RNA-seq (Figure 1A). Efficiency of *Acly* deletion was confirmed at protein level by Western Blot and at gene expression level by RNA-seq since *Acly* was amongst the most downregulated genes in $Acly^{M\text{-}KO}$ macrophages after both 3- and 24-hours LPS stimulation (Figure 1B, Supplementary Figure 1A). Of all significantly regulated genes between control and $Acly^{M\text{-}KO}$ macrophages, only 30 were overlapping after both 3- and 24-hours LPS stimulation, indicating timing-dependent activation patterns (Figure 1C). However, pathway analysis revealed that similar pathways were affected by Acly deletion after 3- and 24-hours LPS activation (Figure 1D). We found Acly-dependent regulation of pathways related to fatty acid and cholesterol biosynthesis and observed that while cholesterol levels were similar, desmosterol levels were still decreased after inflammatory activation with LPS (Supplementary Figure 1B). Next to lipid metabolism, pathway analysis revealed that genes involved in inflammatory signaling were affected upon Acly deletion (Figure 1D). To specifically assess the effect of *Acly* deletion in BMDMs on the expression of inflammatory genes, we first selected the most highly induced genes in LPS-stimulated control macrophages at both time points (Log_2(Fold Change)>5 and adjusted p-value<0.05; Figure 1E-F). 15 out of the 175 genes that were most induced after 3 h LPS treatment were differentially expressed in $Acly^{M\text{-}KO}$ macrophages in comparison to controls (Figure 1E). Likewise, 17 out of the 159 top-induced genes were differentially regulated after 24 h treatment with LPS (Figure 1F). At both time points, the majority of differentially expressed genes was upregulated in $Acly^{M\text{-}KO}$ macrophages,

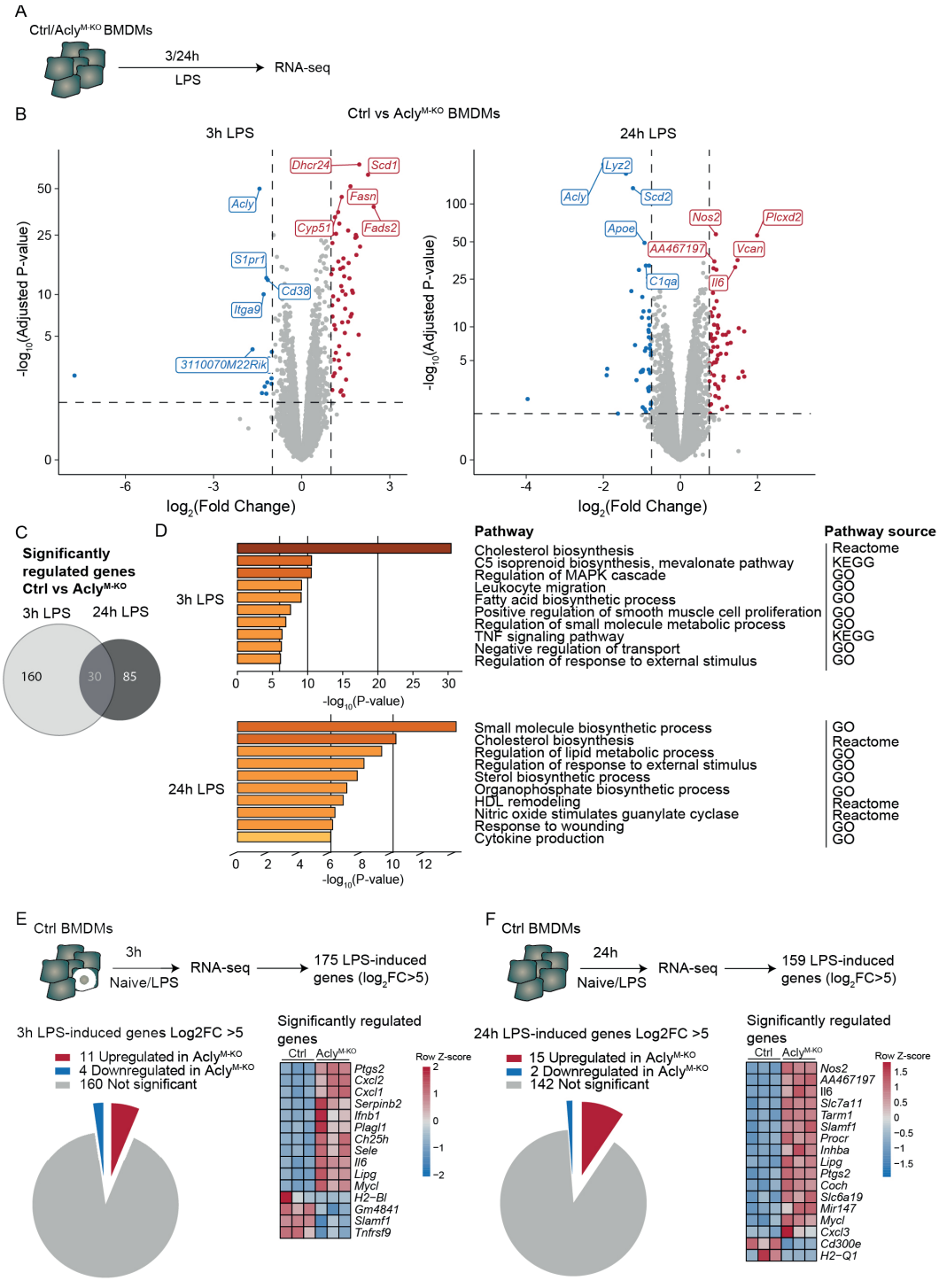
A
Ctrl/Acly^M-KO BMDMs
3/24h
LPS
RNA-seq
B
Ctrl vs Acly^M-KO BMDMs
3h LPS
24h LPS
-log10(Adjusted P-value)
log2(Fold Change)
Dhcr24
Scd1
Fasn
Cyp51
Fads2
Acly
S1pr1
Cd38
Itga9
3110070M22Rik
Lyz2
Scd2
Nos2
Plcxd2
Apoe
AA467197
Vcan
C1qa
Il6
C
Significantly regulated genes Ctrl vs Acly^M-KO
3h LPS
24h LPS
160
30
85
D
3h LPS
-log10(P-value)
Pathway
Pathway source
Cholesterol biosynthesis
C5 isoprenoid biosynthesis, mevalonate pathway
Regulation of MAPK cascade
Leukocyte migration
Fatty acid biosynthetic process
Positive regulation of smooth muscle cell proliferation
Regulation of small molecule metabolic process
TNF signaling pathway
Negative regulation of transport
Regulation of response to external stimulus
Reactome
KEGG
GO
GO
GO
GO
GO
KEGG
GO
GO
24h LPS
-log10(P-value)
Small molecule biosynthetic process
Cholesterol biosynthesis
Regulation of lipid metabolic process
Regulation of response to external stimulus
Sterol biosynthetic process
Organophosphate biosynthetic process
HDL remodeling
Nitric oxide stimulates guanylate cyclase
Response to wounding
Cytokine production
GO
Reactome
GO
GO
GO
GO
Reactome
Reactome
GO
GO
E
Ctrl BMDMs
3h
Naive/LPS
RNA-seq
175 LPS-induced genes (log2FC>5)
3h LPS-induced genes Log2FC >5
11 Upregulated in Acly^M-KO
4 Downregulated in Acly^M-KO
160 Not significant
Significantly regulated genes
Ctrl
Acly^M-KO
Row Z-score
Ptgs2
Cxcl2
Cxcl1
Serpinb2
Ifnb1
Plagl1
Ch25h
Sele
Il6
Lipg
Mycl
H2-Bl
Gm4841
Slamf1
Tnfrsf9
F
Ctrl BMDMs
24h
Naive/LPS
RNA-seq
159 LPS-induced genes (log2FC>5)
24h LPS-induced genes Log2FC >5
15 Upregulated in Acly^M-KO
2 Downregulated in Acly^M-KO
142 Not significant
Significantly regulated genes
Ctrl
Acly^M-KO
Row Z-score
Nos2
AA467197
Il6
Slc7a11
Tarm1
Slamf1
Procr
Inhba
Lipg
Ptgs2
Coch
Slc6a19
Mir147
Mycl
Cxcl3
Cd300e
H2-Q1

▲Figure 1. Legend

Figure 1. Macrophage Acly deficiency upregulates LPS-induced inflammatory gene expression in vitro. (**A**) Control and AclyM-^{KO} BMDMs were stimulated with LPS for 3 or 24 h and analysed by RNA-sequencing. (**B**) Volcano plot of differentially expressed genes between control and Acly-deficient BMDMs after 3 or 24 hour LPS stimulation highlighting the top 5 most significant up- and down-regulated genes. (**C**) Venn diagram showing overlap in deregulated genes by Acly deficiency after 3 and 24 hours LPS activation. (**D**) Deregulated pathways in Acly-deficient macrophages as determined by Reactome, KEGG and GO pathways. (**E-F**) Expression in control versus Acly-deficient BMDMs of genes that are most highly LPS-induced after 3h (*E*) or 24h (*F*) LPS stimulation in control BMDMs. (n=3 per group)

indicating that deletion of Acly in macrophages potentiates inflammatory responses. Among them, the 5 genes that were significantly altered in naive Acly-deficient BMDMs compared to control BMDMs are mainly involved in lipid metabolism and cell cycle regulation, indicating that increased inflammatory responses are likely not due to differences at baseline (Supplementary Figure 1C). *Il6* and *Nos2* were among the most upregulated genes in LPS-stimulated Acly$^{M\text{-}KO}$ macrophages, corresponding with our earlier observations that *Acly*-deficient macrophages secrete more IL-6 and nitric oxide in response to LPS (12). Together, this analysis indicates that inflammatory signaling is increased in LPS-activated Acly$^{M\text{-}KO}$ macrophages *in vitro*.

Acute endotoxin-induced peritonitis is largely unaffected in myeloid-specific Acly-deficient mice

To analyze whether our findings translate to altered acute inflammatory responses *in vivo*, Acly$^{M\text{-}KO}$ and control mice were injected intraperitoneally (i.p.) with LPS (or vehicle control) as a commonly used endotoxin-induced peritonitis model (Figure 2A) (7, 13). In line with the RNA-seq data, we found increased LPS-induced *Il6* expression in spleens of Acly$^{M\text{-}KO}$ mice when compared to control mice, whereas splenic expression of other cytokines remained unaltered (Figure 2B). Both local (peritoneal) and systemic (plasma) cytokine and chemokine levels were induced by LPS to a similar extent in Acly$^{M\text{-}KO}$ and control mice (Figure 2C; Supplementary Figure 2A). However, LPS treatment resulted in slightly decreased relative myeloid cell recruitment and slightly increased relative B cell recruitment to the peritoneum in Acly-deficient mice as assessed by flow cytometry on peritoneal exudate cells (Figure 2D-E; Supplementary Figure 2B). We did not find increased neutrophil-related chemokine gene expression (*Cxcl1*, *Cxcl2*) or tolerogenic cytokine gene expression (*Il10*, *Tgfb*) in peritoneal exudate cells at baseline (Supplementary Figure 2E). However, myeloid cells displayed a decreased percentage of viable cells in the peritoneum upon LPS induction, at least partly explaining the reduced abundance of these cells (Supplementary Figure 2C).

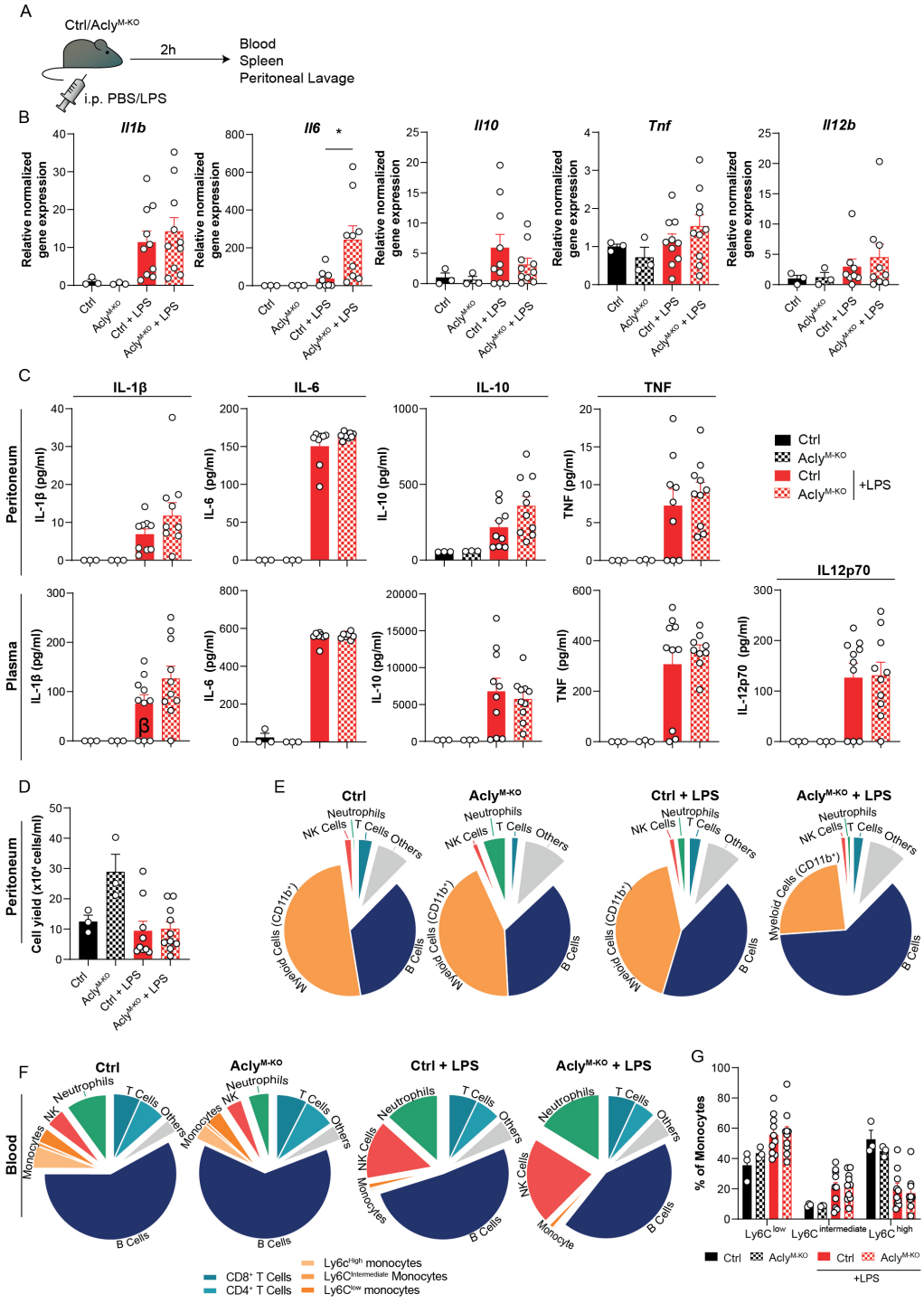
A
Ctrl/Acly M-KO
2h
Blood
Spleen
Peritoneal Lavage
i.p. PBS/LPS
B
Il1b
Il6
Il10
Tnf
Il12b
Relative normalized gene expression
Ctrl
Acly M-KO
Ctrl + LPS
Acly M-KO + LPS
C
IL-1β
IL-6
IL-10
TNF
IL12p70
Peritoneum
Plasma
IL-1β (pg/ml)
IL-6 (pg/ml)
IL-10 (pg/ml)
TNF (pg/ml)
IL-12p70 (pg/ml)
+LPS
D
Peritoneum
Cell yield (x10⁴ cells/ml)
E
Neutrophils
NK Cells
T Cells
Others
Myeloid Cells (CD11b⁺)
B Cells
F
Blood
Monocytes
NK
Neutrophils
T Cells
Others
B Cells
CD8⁺ T Cells
CD4⁺ T Cells
Ly6c^high monocytes
Ly6C^Intermediate Monocytes
Ly6C^low monocytes
G
% of Monocytes
Ly6C low
Ly6C intermediate
Ly6C high
Ctrl
Acly M-KO
+LPS

▲Figure 2. Legend

Figure 2. Myeloid Acly deficiency barely alters systemic and local immune responses in acute endotoxin-induced peritonitis. (**A**) Control and Acly$^{M\text{-}KO}$ mice received an intraperitoneal injection of LPS or vehicle control. After 2 hours, spleens, blood and peritoneal fluid were collected. (**B**) Splenic gene expression of inflammatory cytokines. (**C**) Peritoneal and plasma cytokine levels in vehicle control and LPS-treated control and Acly$^{M\text{-}KO}$ mice. (**D**) Peritoneal exudate cell counts. (**E**) Relative distribution of peritoneal exudate cell levels as assessed by flow cytometry. (**F**) Relative distribution of white blood cells as assessed by flow cytometry. (**G**) Abundance of blood monocyte subsets as defined by Ly6C expression. Values represent mean±SEM (n=3/3/10/10 (Ctrl vehicle/KO vehicle/Ctrl LPS/KO LPS)). *P<0.05 by ordinary one-way ANOVA with Sidak's post hoc test for multiple comparisons.

To investigate whether circulating immune cell levels were altered in the absence of myeloid Acly, we analyzed blood leukocytes. Flow cytometry revealed increased frequencies of NK cells and neutrophils in response to LPS injection, with no differences between control and Acly$^{M\text{-}KO}$ mice (Figure 2F). Interestingly, circulating neutrophils in Acly$^{M\text{-}KO}$ mice displayed also decreased viability in response to LPS, indicating regulation of cell survival by Acly (Supplementary Figure 2D). Circulating monocyte subtypes displayed a similar increase in Ly6C^{low} and Ly6C^{int} abundance at the expense of Ly6C^{high} upon LPS injection in both control and Acly$^{M\text{-}KO}$ mice (Figure 2G). Together, these data indicate that myeloid Acly deficiency alters neither local nor systemic cytokine responses and results in slightly altered cellular responses upon LPS injection locally, potentially through regulation of myeloid cell viability.

Obesity-induced chronic low-grade inflammation and EAE onset and severity are unaffected in myeloid-specific Acly-deficient mice

Obesity and MS are diseases characterized by chronic immune activation, which drives disease progression. During obesity, adipose tissue macrophages (ATMs) are exposed to a lipid-rich environment that drives proinflammatory macrophage activation (14). To assess the effect of obesity on Acly levels in ATMs, we assessed its expression in an RNA-seq data set from ATMs that were sorted from mice fed a control low-fat diet (LFD) or a high-fat diet (HFD) for 16 weeks (Figure 3A). Obesity increased *Acly* expression in ATMs from obese mice (Figure 3B), which led us to investigate the effects of myeloid Acly deficiency on metabolic outcomes in obesity. Hence, we fed control and Acly$^{M\text{-}KO}$ mice a LFD or HFD for 16 weeks and assessed whole-body metabolic parameters and chronic low-grade inflammation in the circulation and metabolic tissues (Figure 3C). Myeloid-specific Acly deficiency did not impact diet-induced body weight changes when compared to controls (Figure 3D). However, Acly$^{M\text{-}KO}$ mice displayed slightly aggravated glucose intolerance after

HFD feeding (Figure 3E), whereas insulin sensitivity was unaffected (Figure 3F). As expected, plasma IL-6 and TNF levels and circulating monocytes were higher in HFD-fed mice, but were not affected by myeloid-specific Acly deficiency (Figure 3G-H; Supplementary Figure 3A). In both visceral white adipose tissue (epididymal; eWAT) and the liver, two of the main metabolic organs, diet-induced changes in myeloid cell composition deteriorate tissue-specific insulin sensitivity. In WAT, depletion of eosinophils, recruitment of monocytes and accumulation of neutrophils and $CD11c^+$ proinflammatory macrophages are associated with metabolic dysfunctions (15). While HFD feeding indeed increased $CD11c^+$ macrophage abundance, myeloid Acly deficiency did not alter these changes (Figure 3I-J; Supplementary Figure 3B-C). Also, neutrophil abundance in WAT was similar after HFD feeding in both genotypes (Supplementary Figure 3D). Likewise, recruitment of neutrophils, monocytes and activation of Kupffer cells are associated with hepatic insulin resistance (16-18). Whereas hepatic neutrophil recruitment was unchanged, Kupffer cells were increasingly activated upon HFD feeding. Acly deficiency did not affect these parameters, but did result in increased hepatic monocyte recruitment upon HFD feeding when compared to HFD fed controls. (Figure 3K-L; Supplementary Figure 3B). Yet, gene expression of typical obesity-induced macrophage and cytokine genes *Adgre* (F4/80)*, Itgax* (CD11c)*, Tnf,* and *Ccl2* remained unaltered by myeloid Acly deficiency in both eWAT and liver (Figure 3M). These data indicate that obesity-induced chronic low-grade inflammation remains unaffected upon myeloid Acly deficiency *in vivo* and causes minor local changes. Lastly, during MS, chronic inflammatory activation affects the central nervous system. We analyzed the effect of myeloid Acly deficiency on disease onset and progression by applying an EAE model (Supplementary Figure 4A). Also in this chronic inflammatory condition, we did not find differences in disease onset and severity between control and $Acly^{M\text{-}KO}$ mice (Supplementary Figure 4B-D). Taken together, our data indicate that deleting Acly in macrophages increased their inflammatory potential *in vitro*, but did not affect acute and chronic inflammatory conditions in peritonitis, obesity and EAE *in vivo*.

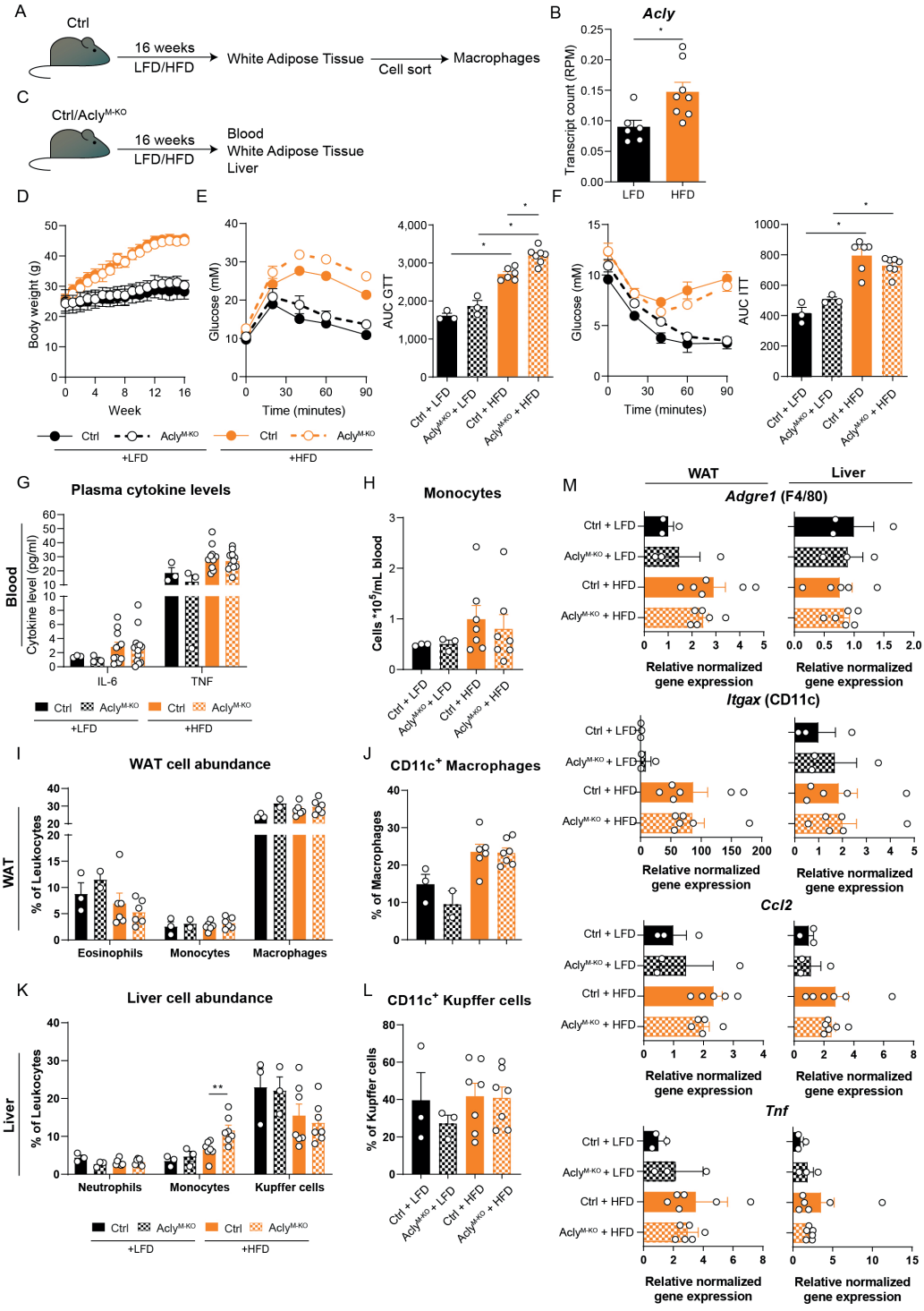
A
Ctrl
16 weeks
LFD/HFD
White Adipose Tissue
Cell sort
Macrophages
C
Ctrl/Acly M-KO
16 weeks
LFD/HFD
Blood
White Adipose Tissue
Liver
B
Acly
Transcript count (RPM)
LFD
HFD
D
Body weight (g)
Week
Ctrl
Acly M-KO
+LFD
+HFD
E
Glucose (mM)
Time (minutes)
AUC GTT
Ctrl + LFD
Acly M-KO + LFD
Ctrl + HFD
Acly M-KO + HFD
F
Glucose (mM)
Time (minutes)
AUC ITT
G
Plasma cytokine levels
Blood
Cytokine level (pg/ml)
IL-6
TNF
H
Monocytes
Cells *10^5/mL blood
I
WAT cell abundance
WAT
% of Leukocytes
Eosinophils
Monocytes
Macrophages
J
CD11c+ Macrophages
% of Macrophages
K
Liver cell abundance
Liver
% of Leukocytes
Neutrophils
Monocytes
Kupffer cells
L
CD11c+ Kupffer cells
% of Kupffer cells
M
WAT
Liver
Adgre1 (F4/80)
Itgax (CD11c)
Ccl2
Tnf
Relative normalized gene expression

◀Figure 3. Legend

Figure 3. Obesity-related chronic low-grade inflammation remains unaffected by myeloid Acly deficiency. (**A**) Control mice received a control low-fat diet (LFD) or a high-fat diet (HFD) for 16 weeks, after which macrophages were sorted from white adipose tissue (WAT). (**B**) *Acly* expression in WAT macrophages after 16 weeks of LFD or HFD. (n=6/8 (LFD/HFD)) (**C**) Control and $Acly^{M\text{-}KO}$ received a LFD or HFD for 16 weeks, after which blood, liver and WAT were collected. (**D**) Body weight during the course of 16 weeks. (**E**) Blood glucose levels during glucose tolerance test (GTT) and derived area under the curve (AUC) in control and $Acly^{M\text{-}KO}$ mice after LFD or HFD. (**F**) Blood glucose levels during insulin tolerance test (ITT) and AUC in control and $Acly^{M\text{-}KO}$ mice after LFD or HFD (n=3/3/6/7 (Ctrl LFD/ KO LFD/Ctrl HFD/KO HFD)). (**G**) Plasma cytokine levels at 12 weeks of diet intervention (n=3/3/10/10 (Ctrl LFD/ KO LFD/Ctrl HFD/KO HFD)). (**H**) Circulating monocyte levels. (**I**) WAT myeloid cell abundance, (**J**) percentage of $CD11c^+$ macrophages in WAT. (**K**) Liver myeloid cell abundance, (**L**) percentage of $CD11c^+$ Kupffer cells. (**M**) Gene expression levels of indicated genes in liver and WAT (n=3/3/6/7 (Ctrl LFD/ KO LFD/Ctrl HFD/KO HFD)). Values represent mean±SEM. *P<0.05, **P<0.01 by ordinary one-way ANOVA with Sidak's post hoc for multiple comparisons.

Discussion

In recent years, Acly arose as a potential metabolic target in combating inflammatory disorders (7, 8, 11, 12). In this study, we demonstrated that Acly-deficient BMDMs have a hyperinflammatory gene signature when activated with LPS *in vitro*. Apart from increased splenic *Il6* expression, other systemic or local inflammatory readouts determined in blood, spleen, and peritoneum were unaltered in myeloid-specific Acly-deficient mice during endotoxin-induced peritonitis *in vivo*. Likewise, neither obesity nor EAE-related inflammation were affected by myeloid Acly deficiency. These results indicate that, although *in vitro* inflammatory responses were increased in LysM-Cre-mediated Acly-deficient cells, myeloid Acly deficiency did not alter acute and chronic inflammatory disease outcomes *in vivo* in mouse models of obesity, peritonitis, and MS. These results highlight that therapeutic targeting of macrophage Acly is likely not beneficial for all inflammatory disorders.

Targeting Acly in inflammation provides the opportunity to target cellular respiration, cholesterol biosynthesis, and histone acetylation (9). In an earlier study, we observed similar cellular respiration and glycolysis rates, alike histone acetylation levels but a disrupted fatty acid and cholesterol biosynthesis in naïve Acly-deficient macrophages (12). Our current observations confirm that even after 3- or 24-hour LPS-activation, cholesterol biosynthesis and related pathways are still among the most deregulated pathways in Acly-deficient macrophages, indicating the persistence of the effect of Acly knockdown in macrophages. Interestingly, RNA-sequencing of BMDMs treated with an Acly inhibitor in combination with LPS for 4 hours does not show a deregulation of cholesterol metabolism, but rather highlights pathways related to immune responses (7). These discrepancies may be explained

by differences in the timing of the Acly inhibition, knockdown and knockout methods. Whereas acute inhibition or siRNA-mediated knockdown might not allow sufficient time for the cell to overcome acute metabolic dysregulation, a genetic knockout approach can induce adaptive changes to rewire metabolic pathways during differentiation and hereby secure sufficient cytosolic acetyl-CoA levels. Indeed, genetic Acly deficiency in multiple mammalian cell types shows an increased abundance of Acetyl-CoA synthetase short chain family member 2 (ACCS2) as well as an increased flux through this enzyme to secure cytosolic acetyl-CoA for *de novo* lipogenesis from endogenous acetate (19-21). In turn, this acetate-derived acetyl-CoA in cancer cells can induce histone acetylation and lipogenesis (22). In line with this, both unstimulated and 3-hour LPS-activated Acly-deficient macrophages display increased expression of *Acss2*, indicating that macrophages can at least partly restore acetyl-CoA levels and adapt metabolism upon long-term Acly deletion (12).

Apart from differences in regulation of metabolism between genetic *Acly* deletion and acute inhibition *in vitro*, both methods of targeting Acly show opposite regulation of inflammatory responses (7, 8, 11). Since metabolism can dictate inflammatory responses in macrophages, the hyperinflammatory response in Acly-deficient macrophages may be an effect of i) increased flux through ACSS2 and/or ii) deregulated cholesterol biosynthesis. Firstly, in line with our results, Acly-deficient adipocytes show increased inflammatory gene signaling in combination with increased *Acss2* expression (21). Also T cells with affected metabolism and an increased flux through ACSS2 have been shown to display an augmented inflammatory response (23). These findings fit with the notion that acetate-derived acetyl-CoA is able to drive increased inflammatory responses (24). The possible link between ACSS2 and inflammation is a potential mechanistic explanation that increased ACSS2 may, at least partly, be a determinant of increased inflammatory signaling during genetic *Acly* deficiency. Secondly, we previously showed in unstimulated Acly-deficient macrophages that a deregulation of cholesterol biosynthesis results in decreased levels of the cholesterol pathway-intermediate desmosterol (12). Decreased desmosterol levels and subsequent blunted inhibition of inflammatory responses by liver X receptor (LXR) may also partly explain the hyperinflammatory genotype of Acly-deficient inflammatory macrophages. Since desmosterol levels are still decreased after 3- and 24-hour LPS stimulation, it highlights that cholesterol-related pathways are still affected on both gene expression and sterol level in LPS-stimulated Acly-deficient macrophages. When such metabolic adaptation occurs during long-term inhibition with small molecule inhibitors of Acly remains unknown and could be examined by using conditional inducible knockouts.

We now demonstrate that genetic *Acly* deletion specifically in macrophages does not alter inflammatory readouts in endotoxin-induced peritonitis except for splenic

Il6 expression, indicating that myeloid Acly deficiency may only mildly alter local LPS-elicited inflammatory responses in the spleen. Splenic *Il6* is expressed by bone marrow-derived myeloid cells upon i.p. LPS injection (25), which indicates that increased splenic *Il6* expression in myeloid Acly-deficient mice is likely due to its higher expression by myeloid cells. However, since only local alterations were evident in myeloid Acly-deficient mice, it implies that there are unidentified factors that explain the lack of a hyperinflammatory response in vivo, which we did observe *in vitro*. While expression of tolerogenic cytokines or chemo-attractant chemokines in peritoneal cells was similar in control and $Acly^{M\text{-}KO}$ at baseline, there could be other unanalyzed factors regulated by myeloid Acly at baseline that attenuate a hyperinflammatory response *in vivo*. Another explanation of differences in responses *in vitro* and *in vivo* could be that tissue-resident macrophages do not all express equal amounts of Acly or the LysM-promotor at baseline or after activation, indicating that myeloid Acly deletion mediated by the LysM-Cre system will not affect all tissues to a similar extent (as can be extracted from GSE63341, GSE122108). Alternatively, decreased viability of myeloid cells upon i.p. injection with LPS might explain a reduced ability to mount inflammatory responses *in vivo*.

In sharp contrast, systemic inhibition of Acly *in vivo* with small molecules resulted in lower circulating cytokine levels in an endotoxin-induced model of peritonitis (7). This implies that beneficial effects from systemic inhibition with a small molecule inhibitor are either not solely mediated by its effect on macrophages, or cells undergoing small molecule-inhibition of Acly are not successive to adaptive metabolic changes as Acly-deficient macrophages are. However, since small molecule inhibition in macrophages *in vitro* shows decreased inflammation, it is likely that beneficial effects in peritonitis are at least partly macrophage-mediated.

Interestingly, Acly inhibition was also shown recently to be utilized for immune evasion by uropathogenic *Escherichia coli* by suppressing cytokine production during cystitis, providing additional evidence that Acly is linked to inflammatory responses (26). Additionally, circulating Acly was recently shown to be increased during sepsis, suggesting an immunological role for Acly in the disease (27). We found a decreased abundance of viable myeloid cells after activation with LPS in $Acly^{M\text{-}KO}$ mice and an increased abundance of neutrophils at baseline, which might indicate that responses to an infection with live pathogen may be altered upon myeloid Acly deficiency. Although sterile, acute LPS-induced peritonitis does not fully reflect bacterial infections, common transcriptional macrophage responses to both gram-positive and –negative bacteria and bacterial compounds have been shown (28). Together with our findings, one could speculate that $Acly^{M\text{-}KO}$ mice respond similar to live pathogen challenge when compared to control mice. However, this should be

examined in more detail in future studies.

Lastly, we show that WAT macrophages display increased expression of *Acly* after HFD feeding. Genetic myeloid *Acly*-deletion, in turn, did not alter inflammatory outcomes, but resulted in a slightly impaired glucose tolerance in obesity. As whole-body insulin sensitivity was not impaired, this hints at a mild inhibition of insulin-independent glucose uptake. Interestingly, obese mice with an adipocyte-specific knockout of *Acly* also showed impaired glucose handling (21). Additionally, Acly expression is positively correlated with glucose transporter 4 (GLUT4) expression in human adipose tissue (21), indicating co-regulation of these proteins in this particular setting. If such co-regulation of glucose transporters exists, one cannot completely exclude the possibility that the observed metabolic defect in Acly$^{M\text{-}KO}$ mice is secondary to decreased glucose uptake in myeloid cells.

Collectively, our results indicate that caution is warranted in prospective long-term or chronic treatments of inflammatory disorders with macrophage-specific Acly inhibitors. The findings of this study aid in further understanding the interaction between macrophage Acly and inflammatory disorders. Further studies into the development of new cell-specific Acly inhibitors can build upon the idea that chronic myeloid Acly therapy does not benefit or worsen inflammatory disorders like sepsis, obesity and EAE.

Methods

Animals, treatment and diet

C57Bl/6J mice with *loxP* sites flanking exon 9 of the *Acly* gene (*Aclyf*^{fl})(20) were crossed with *Lyz2*-Cre transgenic mice to generate mice with a myeloid-specific deletion of *Acly* (Acly$^{M\text{-}KO}$). All mouse experiments were conducted after approval by the Committee for Animal Welfare (University of Amsterdam, VU University Amsterdam and Leiden University Medical Center).

Acute endotoxin-induced peritonitis was achieved by intraperitoneally injecting age-, weight-, and sex-matched 17-week-old control and Acly$^{M\text{-}KO}$ mice with 5 μg/g bodyweight LPS (From Escherichia coli serotype O55:B5; Sigma) in PBS or with PBS only for control. Mice were randomly allocated to either PBS control (n=3) or LPS experimental conditions (n=10). 2 hours after LPS injection, mice were euthanized by CO_2 asphyxiation. Blood was collected by cardiac puncture with ethylene-diamine-tetraacetatic acid (EDTA; Gibco)-pretreated syringes. Peritoneal lavage was performed by injecting 5 mL 2mM EDTA in PBS in the peritoneal cavity followed by careful removal of the maximum volume of lavage fluid possible (3.8-4.6 mL). Subsequently, spleens were harvested and snap frozen in liquid nitrogen for RNA isolation.

EAE was induced in age- and sex-matched 12-week-old control and $Acly^{M\text{-}KO}$ mice by 0.2 mL subcutaneous injection of myelin oligodendrocyte glycopeptide $(MOG)_{35\text{-}55}$ in an emulsion with complete Freund's adjuvant (CFA; Hooke Laboratories) followed by two times intraperitoneal injection of 200 ng pertussis toxin (PTX) dissolved in PBS (Hooke Laboratories) on 2 successive days. Mice were weighed, monitored and scored on EAE symptoms (0 = healthy; 1 = limp tail; 2 = ataxia and/or paresis of hind limbs; 3 = paralysis of hind limbs and/or paresis of forelimbs; 4= tetraplegia; 5 = moribund or dead) (29, 30) daily for the course of 30 days by 2 independent researchers blinded to mouse genotypes. In case clinical signs were less severe than typically observed, clinical scores were graded as 'x-0.5'.

Obesity was induced by feeding mice a high-fat diet (HFD). Group randomization was systematically performed before the start of the experiment, based on age, body weight, fat mass and fasting blood glucose levels. 9- to 17-week-old male control and $Acly^{M\text{-}KO}$ mice were fed a low-fat diet (LFD, 10 kcal% fat, D12450B, Research Diets) (n=4) or a high-fat diet (45 kcal% fat, D12451, Research Diets) (n=8) for 16 weeks, during which body weight was monitored using a conventional weighing scale.

BMDM isolation and BMDM culture

Bone marrow cells were flushed from femurs and tibias of control and $Acly^{M\text{-}KO}$ mice. Bone marrow-derived macrophages (BMDMs) were generated by culturing in complete RPMI-1640 (Gibco) containing 25 mM HEPES, 2 mM L-glutamine, 10% FCS (Gibco), 100 U/ml penicillin, 100 µg/ml streptomycin (Gibco), and 15% L929-conditioned medium (LCM) for 7 days. Control and $Acly^{M\text{-}KO}$ cells were collected and plated for RNA-sequencing at a density of $5*10^5$ cells per well in a 24-well plate and left untreated or stimulated with 100 ng/mL LPS (Sigma) for 3 or 24 hours.

Transcriptomics

Total RNA was isolated from BMDMs using an RNeasy Mini Kit with DNase treatment (QIAGEN) followed by strand-specific library construction using the KAPA mRNA HyperPrep kit (KAPA Biosystems). Samples were sequenced as previously described (12, 31). Briefly, sequencing was performed on an HiSeq 4000 instrument (Illumina). Reads were aligned to mouse genome mm10 using *STAR 2.5.2b*. Indexing and filtering of BAM files was done with *SAMtools* after which raw tag counts and RPKM values were summed using HOMER2's AnalyzeRepeats.pl script. Differentially expressed genes were analyzed using *DESeq2* package in R. Volcano plots and heatmaps were generated using *ggplot2, ggrepel* and *pheatmap* packages. Genes were considered differentially expressed between

control and Acly$^{M\text{-}KO}$ BMDMs when Log2 fold change >0.75 and adjusted p-value <0.05. Pathway analysis was performed by Metascape (32) [http://metascape.org] on regulated genes in 3- or 24-hour LPS-induced Acly$^{M\text{-}KO}$ BMDMs when compared to 3- or 24-hour LPS-induced control BMDMs, respectively.

Immunoblotting

Immunoblotting was performed as described previously (12). Briefly, BMDMs stimulated with LPS for 24 hours and lysed on ice in NP40 cell lysis buffer (ThermoFisher) with fresh protease inhibitor cocktail (Sigma-Aldrich) and fresh PhosSTOP (Sigma-Aldrich). Lysates were analyzed for protein concentration with a BCA assay (ThermoFisher) and inactivated by heating at 95ºC for 10 min. 4-12% Bis-Tris gels (ThermoFisher) were used for protein separation and nitrocellulose membranes (Bio-Rad) for blotting. Membranes were incubated with antibodies against ACLY (1:1000, Abcam, ab40793) and α-Tubulin (1:2000, Sigma-Aldrich, T5168) and signal was visualized using horseradish peroxidase (HRP)-conjugated secondary antibodies in 5% BSA TBS-T and developed using SuperSignal West Pico Chemiluminescent PLUS Substrate (ThermoFisher).

Sterol analysis

Sterol analysis in LPS-activated macrophages was performed as described previously (12). Briefly, LPS-stimulated BMDMs were homogenized and incubated with an internal standard and saponificated during 2-hour incubation at 80°C. Sterols were extracted using hexane and quantified using a GC system (CPSil5 column, Agilent GC 7890B) with FID detection followed by GC-MS and selected ion monitoring of tMS-derivaties on an MSD5977A MS detector in EI+-mode.

Gene expression analysis

Total RNA from snap frozen spleens was isolated using GeneJET RNA Purification Kit from ThermoFisher and following manufacturer's protocol for Total RNA Purification from Mammalian Tissue. Briefly, tissue was disrupted by crushing with mortar and pestle in lysis buffer supplemented with 2% v/v β-mercaptoethanol. Lysates were homogenized by pipetting up and down and transferred to tubes before vortexing. Subsequently, samples were deproteinized by proteinase K. RNA isolation was performed on supernatants after centrifugation using the Purification Columns and wash buffers provided with the isolation kit. cDNA was transcribed using a High-Capacity cDNA Reverse Transcription

Kit (ThermoFisher). Gene expression analysis was performed with SYBR Green Fast mix (Applied Biosystems) on a Viia7 system (Applied Biosystems). Expression levels were normalized to average levels of housekeeping genes ribosomal protein large P0 (*Rplp0*) and Cyclophilin A (*Ppia*).

RNA from snap-frozen adipose tissue and liver samples of LFD and HFD-fed mice was isolated using Tripure RNA Isolation reagent (Roche Diagnostics) and the phenol-chloroform extraction method. Total RNA (1 μg) was reverse transcribed and quantitative real-time PCR was performed with SYBR Green Core Kit on a MyIQ thermal cycler (Bio-Rad). mRNA expression was normalized to *RplP0* mRNA content and expressed as fold change compared to LFD-fed control mice as indicated, using the ΔΔCT method. Primer sequences used are depicted in Supplementary Table 2.

Cytokine and chemokine analysis

Levels of IL-6, TNF, IL-12p70, IL-1β, and IL-10 were quantified in plasma and peritoneal lavage from mice with acute LPS-induced peritonitis using ELISA (Life Technologies), according to manufacturer's protocol. CXCL1 and CXCL2 were analyzed in peritoneal lavage fluid from naïve and LPS-injected mice using ELISA (R&D systems), according to manufacturer's protocol. Circulating IL-6 and TNF levels in obese mice were analyzed on plasma samples from 4h-fasted mice using the Cytometric Bead Array enhanced sensitivity kits (CBA; BD Biosciences) according to the manufacturer's recommendations.

Isolation of stromal vascular fraction from adipose tissue

After 16 weeks on diet, LFD-fed lean and HFD-fed obese mice were sacrificed through an overdose of ketamine/xylazine. eWAT was collected after a 1-minute transcardial perfusion with PBS and digested as described previously (33, 34). In short, collected tissues were minced and incubated for 1 hour at 37°C under agitation (60 rpm) in HEPES-buffered Krebs solution (pH 7.4) containing 0.5 g/L collagenase type I from *Clostridium histolyticum* (Sigma-Aldrich), 2% (w/v) dialyzed bovine serum albumin (BSA, fraction V; Sigma-Aldrich) and 6 mM D-Glucose. The disaggregated adipose tissue was passed through a 200 μm filter (Sefar) that was washed with PBS supplemented with 2.5 mM EDTA and 1% FCS. After allowing the adipocytes to settle, the infranatant, consisting of immune cells, was collected and pelleted at 350 x g for 10 minutes at room temperature. Subsequently, the pellet was treated with erythrocyte lysis buffer (0.15 M NH_4Cl; 1 mM $KHCO_3$; 0.1 mM Na_2EDTA). Cells were next washed with PBS/EDTA/FCS, and counted using a hemocytometer.

Isolation of leukocytes from liver tissue

Livers were collected and digested as described previously (33, 34). In short, livers were minced and incubated for 45 minutes at 37°C in RPMI 1640 + Glutamax (Life Technologies) containing 1 mg/mL collagenase type IV from *C. histolyticum*, 2000 U/mL DNase (both Sigma-Aldrich) and 1 mM $CaCl_2$. The digested liver tissues were passed through a 100 µm cell strainer that was washed with PBS/EDTA/FCS. Following washing with PBS/EDTA/FCS, samples were centrifuged at 50 x g to pellet hepatocytes (3 minutes at 4°C). Next, supernatants were collected and pelleted (530 x g, 10 minutes at 4°C). Following erythrocyte lysis, $CD45^+$ leukocytes were isolated using LS columns and CD45 MicroBeads (35 µL beads per liver, Miltenyi Biotec) according to manufacturer's protocol and counted using a hemocytometer.

Flow cytometry

White blood cells from mice with acute endotoxin-induced peritonitis were collected by centrifugation of 1 mL collected blood and subsequent red blood cell lysis with ACK lysis buffer. Cells from peritoneal lavage were collected by centrifugation. White blood cells and cells collected by peritoneal lavage were labeled by staining for 30 minutes on ice in the dark with the following fluorescently-labelled antibodies diluted in staining buffer: CD8-BV421 (1:100), CD4-BV510 (1:150), Ly6C-BV605 (1:600), CD11c-BV650 (1:100), F4/80-BV711 (1:100), CD45-BV785 (1:500), Ly6G-FITC (1:200), MHC-II-PerCP-Cy5.5 (1:400), CD19-PE (1:100), CD11b-PE-Cy7 (1:400), NK1.1-APC (1:200), CD3-AF700 (1:50) (all from Biolegend). Unspecific antibody binding was blocked by an anti-CD16/32 antibody (1:100, BD Bioscience) and dead cells were excluded from analysis after staining with fixable viability dye-e780 (1:1000, eBioscience). Fluorescence was captured using a BD LSR Fortessa and analyzed using FlowJo 10.0.7 analysis software.

Purified epididymal white adipose tissue (eWAT) stromal vascular cells and liver leukocytes were stained with the fixable live/dead marker Zombie-UV (1:1000; Invitrogen), fixed with 1.9% formaldehyde (Sigma-Aldrich) and stored in staining buffer at 4°C in the dark until subsequent surface staining and flow cytometry within 4 days. Cells were labeled with the following fluorescently-labelled antibodies diluted in staining buffer: Siglec-F-BV605 (1:200; BD Biosciences), CD64-PE (1:100), Ly6C-APC-Cy7 (1:700), CD11c-BV421 (1:100), F4/80-BV711 (1:200), CD45-BV785 (1:400; all Biolegend) and CD11b-PE-Cy7 (1:6000; eBioscience), for analysis of innate immune cells, and CD11c-FITC (1:100), CD11b-FITC (1:100), GR-1-FITC (1:200), CD4-BV650 (1:200; all BD Biosciences), NK1.1-FITC (1:400; eBioscience), B220-PE-Cy7 (1:200), CD3-BV605

(1:400), CD8-BV711 (1:200) and CD45-BV785 (1:400; all Biolegend) for analysis of adaptive immune cells. All antibodies used for flow cytometry are listed in Supplementary Table 3.

Glucose and insulin tolerance tests

An intraperitoneal whole-body glucose tolerance test (ipGTT) was performed after 15 weeks on diet in 6h-fasted mice, as previously reported (33, 34). In short, after an initial blood collection from the tail vein (t = 0), a glucose load (2 g/kg total body weight of D-Glucose; Sigma-Aldrich) was administered i.p., and blood glucose was measured at 20, 40, 60, and 90 min after glucose administration using a hand-held Glucometer (Accu-Chek).

An intraperitoneal whole-body insulin tolerance test (ipITT) was performed after 15 weeks on diet in 4h-fasted mice, as described previously (33, 34). Briefly, a bolus of insulin (0.75U/kg total body mass; NOVORAPID) was administered i.p. after an initial blood collection from the tail vein (t = 0), and blood glucose was measured at 20, 40, 60, and 90 min after insulin administration using a Glucometer.

Statistical analysis

Data are presented as mean ± standard error of the mean (SEM). Statistical significance was tested using either a two-tailed Student's *t* test for comparing 2 samples or an ordinary one-way ANOVA followed by Sidak's correction for multiple comparisons in GraphPad Prism software (8.2.1). P-values < 0.05 were considered statistically significant indicated by *p<0.05, **p<0.01, ***p<0.001.

Data availability

RNA-sequencing data of BMDM experiments is deposited in the GEO-database under accession number: GSE169189. Remaining raw data supporting the conclusions of this article will be made available by the authors upon reasonable request.

Acknowledgements

We would like to express gratitude to Kathryn E. Wellen for providing the Acly$^{fl/fl}$ mice, and to Mike de Kok, Koen H.M. Prange and Guillermo R. Griffith for their help with acquiring and analyzing transcriptomics data. Lastly, we would like to thank Priscilla Heijnen, Susanne van der Pol, Merel Rijnsburger, and Lynn van Olst for their extensive help with the animal experiments performed. J.V.d.B. received a VENI grant from ZonMW (91615052) and a

Netherlands Heart Foundation junior postdoctoral grant (2013T003) and senior fellowship (2017T048). M.P.J.d.W. is an established investigator of the Netherlands Heart Foundation, is supported by grants from the Netherlands Heart Foundation and Spark-Holding BV (2015B002 and 2019B016), and Fondation Leducq (16CVD-01), and holds an AMC fellowship. BG received a ZonMW TOP grant from NWO (91214131) and HZ received a grant supported by the NWO Graduate School Program (022.006.010).

Conflicts of interest

All authors declare no competing interests.

References

1. Osuchowski MF, Welch K, Siddiqui J, Remick DG. Circulating cytokine/inhibitor profiles reshape the understanding of the SIRS/CARS continuum in sepsis and predict mortality. J Immunol. 2006;177(3):1967-74.
2. Moore KJ, Sheedy FJ, Fisher EA. Macrophages in atherosclerosis: a dynamic balance. Nat Rev Immunol. 2013;13(10):709-21.
3. Chawla A, Nguyen KD, Goh YP. Macrophage-mediated inflammation in metabolic disease. Nat Rev Immunol. 2011;11(11):738-49.
4. O'Neill LA, Pearce EJ. Immunometabolism governs dendritic cell and macrophage function. J Exp Med. 2016;213(1):15-23.
5. Van den Bossche J, O'Neill LA, Menon D. Macrophage Immunometabolism: Where Are We (Going)? Trends Immunol. 2017;38(6):395-406.
6. Jha AK, Huang SC, Sergushichev A, Lampropoulou V, Ivanova Y, Loginicheva E, et al. Network integration of parallel metabolic and transcriptional data reveals metabolic modules that regulate macrophage polarization. Immunity. 2015;42(3):419-30.
7. Lauterbach MA, Hanke JE, Serefidou M, Mangan MSJ, Kolbe CC, Hess T, et al. Toll-like Receptor Signaling Rewires Macrophage Metabolism and Promotes Histone Acetylation via ATP-Citrate Lyase. Immunity. 2019;51(6):997-1011 e7.
8. Langston PK, Nambu A, Jung J, Shibata M, Aksoylar HI, Lei J, et al. Glycerol phosphate shuttle enzyme GPD2 regulates macrophage inflammatory responses. Nat Immunol. 2019;20(9):1186-95.
9. Wellen KE, Hatzivassiliou G, Sachdeva UM, Bui TV, Cross JR, Thompson CB. ATP-citrate lyase links cellular metabolism to histone acetylation. Science. 2009;324(5930):1076-80.
10. Verberk SG, de Goede KE, Van den Bossche J. Metabolic-epigenetic crosstalk in macrophage activation: an updated view. Epigenomics. 2019;11(7):719-21.
11. Infantino V, Iacobazzi V, Palmieri F, Menga A. ATP-citrate lyase is essential for macrophage inflammatory response. Biochem Biophys Res Commun. 2013;440(1):105-11.
12. Baardman J, Verberk SGS, van der Velden S, Gijbels MJJ, van Roomen CPPA, Sluimer JC, et al. Macrophage ATP citrate lyase deficiency stabilizes atherosclerotic plaques. Nature Communications. 2020;11(1).
13. Lewis AJ, Seymour CW, Rosengart MR. Current Murine Models of Sepsis. Surg Infect (Larchmt). 2016;17(4):385-93.
14. Kratz M, Coats Brittney R, Hisert Katherine B, Hagman D, Mutskov V, Peris E, et al. Metabolic Dysfunction Drives a Mechanistically Distinct Proinflammatory Phenotype in Adipose Tissue Macrophages. Cell Metabolism. 2014;20(4):614-25.
15. Lackey DE, Olefsky JM. Regulation of metabolism by the innate immune system. Nat Rev Endocrinol. 2016;12(1):15-28.
16. Obstfeld AE, Sugaru E, Thearle M, Francisco AM, Gayet C, Ginsberg HN, et al. C-C chemokine receptor 2 (CCR2) regulates the hepatic recruitment of myeloid cells that promote obesity-induced hepatic steatosis. Diabetes. 2010;59(4):916-25.

17. Talukdar S, Oh DY, Bandyopadhyay G, Li D, Xu J, McNelis J, et al. Neutrophils mediate insulin resistance in mice fed a high-fat diet through secreted elastase. Nat Med. 2012;18(9):1407-12.

18. Tran S, Baba I, Poupel L, Dussaud S, Moreau M, Gelineau A, et al. Impaired Kupffer Cell Self-Renewal Alters the Liver Response to Lipid Overload during Non-alcoholic Steatohepatitis. Immunity. 2020;53(3):627-40 e5.

19. Liu X, Cooper DE, Cluntun AA, Warmoes MO, Zhao S, Reid MA, et al. Acetate Production from Glucose and Coupling to Mitochondrial Metabolism in Mammals. Cell. 2018;175(2):502-13 e13.

20. Zhao S, Torres A, Henry RA, Trefely S, Wallace M, Lee JV, et al. ATP-Citrate Lyase Controls a Glucose-to-Acetate Metabolic Switch. Cell Rep. 2016;17(4):1037-52.

21. Fernandez S, Viola JM, Torres A, Wallace M, Trefely S, Zhao S, et al. Adipocyte ACLY Facilitates Dietary Carbohydrate Handling to Maintain Metabolic Homeostasis in Females. Cell Rep. 2019;27(9):2772-84 e6.

22. Gao X, Lin SH, Ren F, Li JT, Chen JJ, Yao CB, et al. Acetate functions as an epigenetic metabolite to promote lipid synthesis under hypoxia. Nat Commun. 2016;7:11960.

23. Leone RD, Zhao L, Englert JM, Sun I-M, Oh M-H, Sun I-H, et al. Glutamine blockade induces divergent metabolic programs to overcome tumor immune evasion. Science. 2019;366(6468):1013-21.

24. Kendrick SF, O'Boyle G, Mann J, Zeybel M, Palmer J, Jones DE, et al. Acetate, the key modulator of inflammatory responses in acute alcoholic hepatitis. Hepatology. 2010;51(6):1988-97.

25. Zhang Z, La Placa D, Nguyen T, Kujawski M, Le K, Li L, et al. CEACAM1 regulates the IL-6 mediated fever response to LPS through the RP105 receptor in murine monocytes. BMC Immunol. 2019;20(1):7.

26. Zhang Z, Wang M, Zhang Y, Zhang Y, Bartkuhn M, Markmann M, et al. Uropathogenic Escherichia coli virulence factor α hemolysin reduces histone acetylation to inhibit expression of pro-inflammatory cytokine genes. The Journal of Infectious Diseases. 2021.

27. Wang C, Zhu X, Cui Y, Miao H, Xu Y, Xiong X, et al. Serum proteome-wide identified ATP citrate lyase as a novel informative diagnostic and prognostic biomarker in pediatric sepsis: A pilot study. Immun Inflamm Dis. 2020.

28. Benoit M, Desnues B, Mege JL. Macrophage polarization in bacterial infections. J Immunol. 2008;181(6):3733-9.

29. Brini E, Ruffini F, Bergami A, Brambilla E, Dati G, Greco B, et al. Administration of a monomeric CCL2 variant to EAE mice inhibits inflammatory cell recruitment and protects from demyelination and axonal loss. J Neuroimmunol. 2009;209(1-2):33-9.

30. Ummenthum K, Peferoen LA, Finardi A, Baker D, Pryce G, Mantovani A, et al. Pentraxin-3 is upregulated in the central nervous system during MS and EAE, but does not modulate experimental neurological disease. Eur J Immunol. 2016;46(3):701-11.

31. Baardman J, Verberk SGS, Prange KHM, van Weeghel M, van der Velden S, Ryan DG, et al. A Defective Pentose Phosphate Pathway Reduces Inflammatory Macrophage Responses during Hypercholesterolemia. Cell Rep. 2018;25(8):2044-52 e5.

32. Zhou Y, Zhou B, Pache L, Chang M, Khodabakhshi AH, Tanaseichuk O, et al. Metascape provides a biologist-oriented resource for the analysis of systems-level datasets. Nat Commun. 2019;10(1):1523.

33. Hussaarts L, Garcia-Tardon N, van Beek L, Heemskerk MM, Haeberlein S, van der Zon GC, et al. Chronic helminth infection and helminth-derived egg antigens promote adipose tissue M2 macrophages and improve insulin sensitivity in obese mice. FASEB J. 2015;29(7):3027-39.

34. van der Zande HJP, Gonzalez MA, de Ruiter K, Wilbers RHP, Garcia-Tardon N, van Huizen M, et al. The helminth glycoprotein omega-1 improves metabolic homeostasis in obese mice through type 2 immunity-independent inhibition of food intake. FASEB J. 2021;35(2):e21331.

Supplementary information

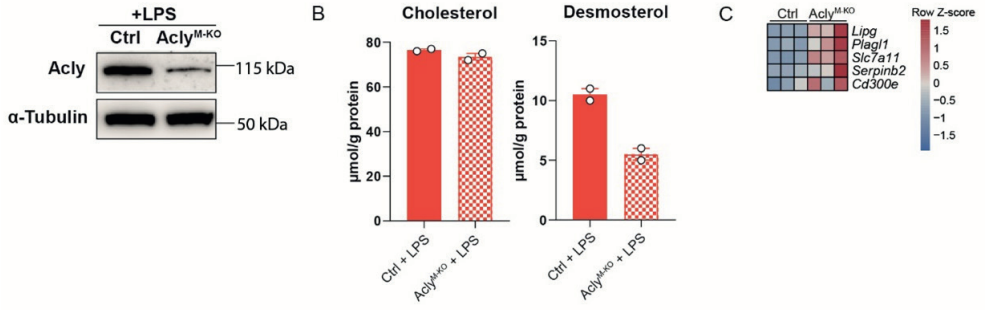

Supplementary Figure 1. (**A**) Protein levels of Acly in 24-hour LPS-activated BMDMs, assessed by immunoblotting analysis (**B**) Cholesterol and desmosterol levels in 24-hour LPS-activated BMDMs. (**C**) Significantly regulated LPS-induced genes in unstimulated BMDMs.

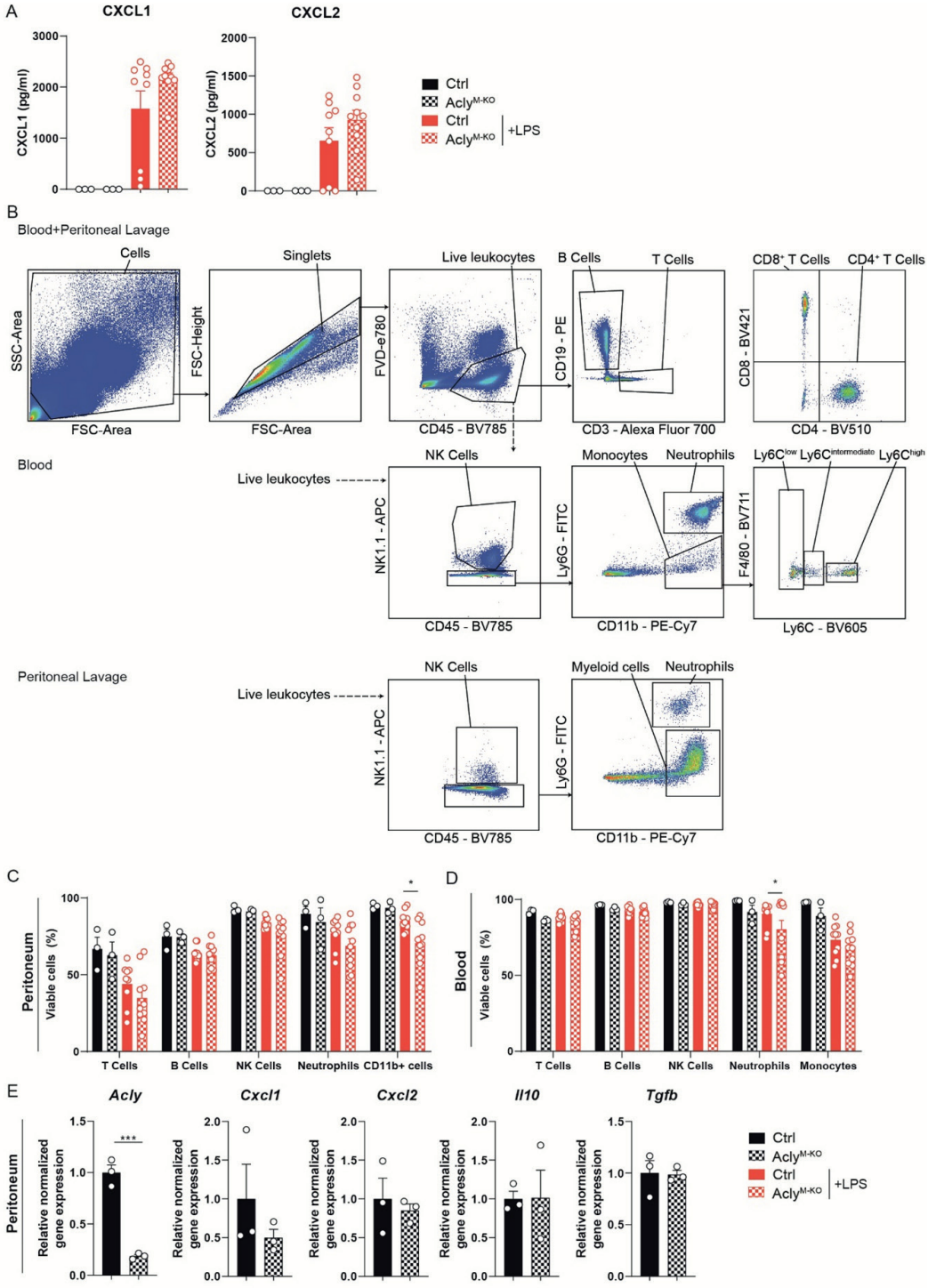
A
CXCL1
CXCL2
CXCL1 (pg/ml)
CXCL2 (pg/ml)
Ctrl
Acly M-KO
Ctrl
Acly M-KO
+LPS
B
Blood+Peritoneal Lavage
Cells
Singlets
Live leukocytes
B Cells
T Cells
CD8+ T Cells
CD4+ T Cells
SSC-Area
FSC-Area
FSC-Height
FSC-Area
FVD-e780
CD45 - BV785
CD19 - PE
CD3 - Alexa Fluor 700
CD8 - BV421
CD4 - BV510
Blood
Live leukocytes
NK Cells
Monocytes
Neutrophils
Ly6Clow Ly6Cintermediate Ly6Chigh
NK1.1 - APC
CD45 - BV785
Ly6G - FITC
CD11b - PE-Cy7
F4/80 - BV711
Ly6C - BV605
Peritoneal Lavage
Live leukocytes
NK Cells
Myeloid cells
Neutrophils
NK1.1 - APC
CD45 - BV785
Ly6G - FITC
CD11b - PE-Cy7
C
Peritoneum
Viable cells (%)
T Cells
B Cells
NK Cells
Neutrophils
CD11b+ cells
D
Blood
Viable cells (%)
T Cells
B Cells
NK Cells
Neutrophils
Monocytes
E
Peritoneum
Acly
Cxcl1
Cxcl2
Il10
Tgfb
Relative normalized gene expression
***
Ctrl
Acly M-KO
Ctrl
Acly M-KO
+LPS

▲Supplementary Figure 2. Legend

Supplementary Figure 2. (**A**) Levels of CXCL1 and CXCL2 in peritoneal lavage. (**B**) Flow cytometry gating strategy for analysis of blood and peritoneal B cells, T cells, $CD4^+$/$CD8^+$ T cells, NK cells, Monocytes/Myeloid cells, and Neutrophils. (**C**-**D**) Viability of cell subsets as defined by flow cytometry in peritoneum (*C*) and blood (*D*). (**E**) Gene expression on peritoneal exudate cells atbaseline. Values represent mean±SEM (n=3/3/10/10 (Ctrl vehicle/KO vehicle/Ctrl LPS/KO LPS)). *P<0.05 by ordinary Two-way ANOVA with Sidak's post hoc test for multiple comparisons.

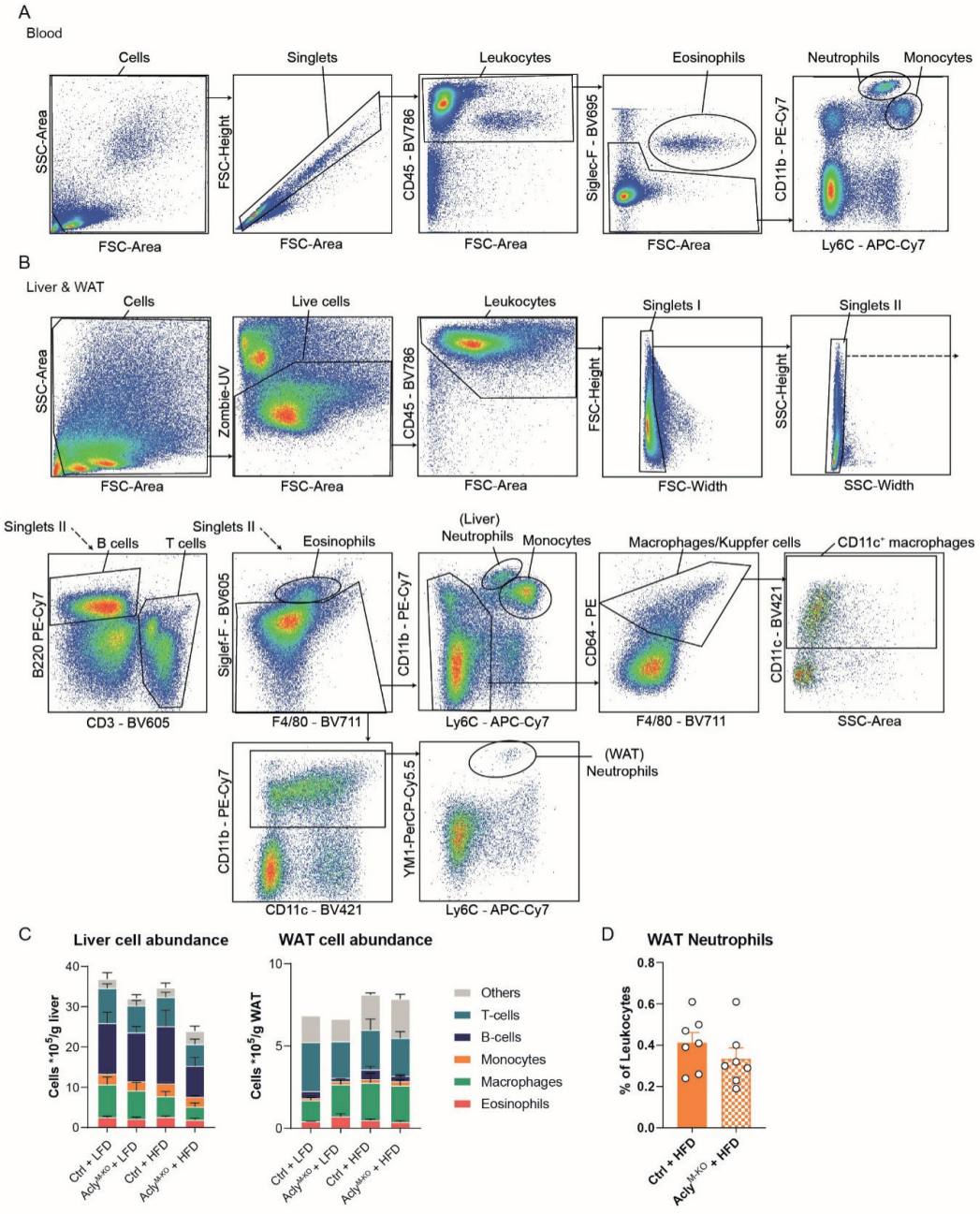

Supplementary Figure 3. (**A-B**) Flow cytometry gating for eosinophils, neutrophils and monocytes in blood (**A**) and for eosinophils, neutophils, monocytes, macrophages (Kuppfer cells in liver), CD11c⁺ macrophages, B cells and T cells in liver and WAT. (**C**) Flow cytometric detmination of immune cell composition in liver and WAT per gram of tissue. (**D**) Neutrophil abundance in WAT upon HFD feeding. Values represent mean ± SEM (n=3/3/6/7 (Ctrl LFD, KO LFD, Ctrl HFD, KO HFD))

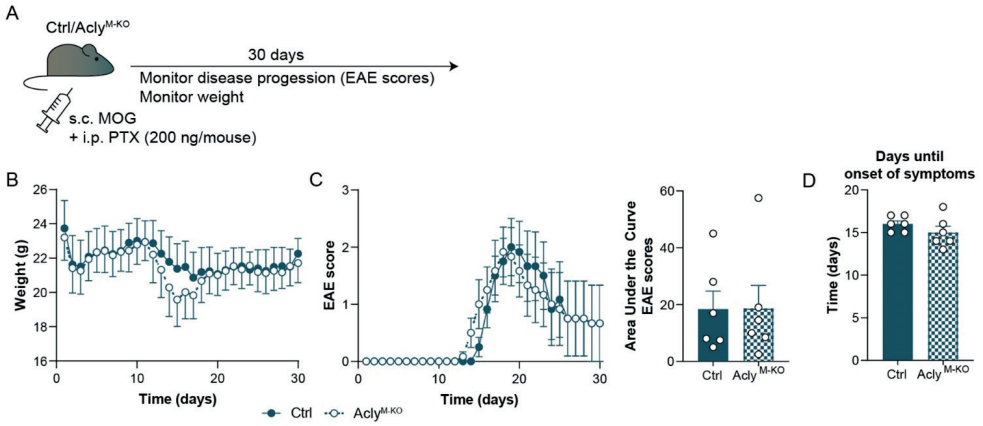

Supplementary Figure 4. Experimental autoimmune encephalitis (**A**) Control and Acly$^{M\text{-}KO}$ mice were injected subcutaneously with a myelin oligodendrocyte (MOG)-solution and intraperitoneally wth pertussis toxin (PTX). (**B**) Weight progression during the course of 30 days in control and Acly$^{M\text{-}KO}$ mice. (**C**) EAE scoring during the course of 30 days and derived area under the curve (AUC) in control and Acly$^{M\text{-}KO}$ mice. (**D**) Days until onset of symptoms in control and Acly$^{M\text{-}KO}$ mice. Values represent mean ± SEM (n=6/6 (ctrl/Acly$^{M\text{-}KO}$)

Supplementary Table 1. Cell abundance in blood an peritoneal lavage (PL), accompanying Figure 2E,F

	Ctrl		Acly$^{M\text{-}KO}$		Ctrl + LPS		ACLY$^{M\text{-}KO}$ + LPS	
PL	**Average**	**SD**	**Average**	**SD**	**Average**	**SD**	**Average**	**SD**
NK Cells	1.8	0.5	1.3	0.2	1.3	0.5	1.2	0.3
Neutrophils	0.4	0.2	5.6 *	4.0	2.0	1.3	0.8#	2.6
CD11b+ cells	50.4	8.0	44.0	17.2	42.1	13.5	24.1 *	9.7
B Cells	35.0	7.8	36.1	14.4	42.4	10.3	61.5	11.4
T Cells	5.2	0.8	3.1	0.6	4.3	0.9	3.4	0.4
- CD8+ T Cells	12.3	1.4	9.3	3.1	10.6	3.5	8.8	1.6
- CD4+ T Cells	67.4	8.3	55.7	18.4	69.0	6.0	75.2	7.6
(n=)	3		3		9		10	
	Ctrl		**Acly$^{M\text{-}KO}$**		**Ctrl + LPS**		**ACLY$^{M\text{-}KO}$ + LPS**	
Blood	**Average**	**SD**	**Average**	**SD**	**Average**	**SD**	**Average**	**SD**
NK Cells	4.7	1.2	4.0	0.2	14.4	5.6	21.2	7.3
Neutrophils	10.0	5.3	5.1	3.1	13.3	4.6	16.1#	12.4
Monocytes	10.4	0.5	9.1	3.1	2.1	1.1	1.9	0.8
B Cells	57.7	6.4	62.3	3.8	51.2	7.8	42.8	8.5
T Cells	13.8	4.7	15.7	3.1	13.8	5.0	12.7	4.8
- CD8+ T Cells	48.4	2.4	47.7	1.1	51.4	2.0	54.9	4.0
- CD4+ T Cells	49.2	2.1	49.4	0.9	45.5	2.4	41.8	5.3
(n=)	3		3		10		10	

1 outlier detected with ROUT's outlier test (Graphpad Prism 8.2.1)
* P<0.05, significanT difference between Ctrl and Acly$^{M\text{-}KO}$ from same stimulation

Supplementary Table 2. List of primer sequences

Marker	Forward primer	Reverse primer
Endotoxin-induced peritonitis model		
Rplp0	GGACCCGAGAAGACCTCCTT	GCACATCACTCAGAATTTCAATGG
Ppia	TTCCTCCTTTCACAGAATTATTCCA	CCGCCAGTGCCATTATGG
Il1b	AAAGAATCTATACCTGTCCTGTGTAATGAAA	GGTATTGCTTGGGATCCACACT
Il6	GCTACCAAACTGGATATAATCAGGAAA	CTTGTTATCTTTTAAGTTGTTCTTCATGTACTC
Il10	TTTGAATTCCCTGGGTGAGAA	CTCCACTGCCTTGCTCTTATTTTC
Tnf	CATCTTCTCAAAATTCGAGTGACAA	TGGGAGTAGACAAGGTACAACCC
Il12b	GGTGCAAAGAAACATGGACTTG	CACATGTCACTGCCCGAGAGT
Acly	CCCCAAGATTCAGTCCCAAGT	GCCTTGGTATGTCGGCTGAA
Cxcl1	ACCCAAACCGAAGTCATAGCC	AGACAGGTGCCATCAGAGC
Cxcl2	CATCCAGAGCTTGAGTGTGAC	CTTTGGTTCTTCCGTTGAGGG
Tgfb	GTCACTGGAGTTGTACGGCA	AGCCCTGTATTCCGTCTCCT
Obesity model		
Rplp0	TCTGGAGGGTGTCCGCAACG	GCCAGGACGCGCTTGTACCC
Adgre	CTTTGGCTATGGGCTTCCAGTC	GCAAGGAGGACAGAGTTTATCGTG
Itgax	GCCACCAACCCTTCCTGGCTG	TTGGACACTCCTGCTGTGCAGTTG
Ccl2	TCAGCCAGATGCAGTTAACGCCC	GCTTCTTTGGGACACCTGCTGCT
Tnf	GTCCCCAAAGGGATGAGAAG	CACTTGGTGGTTTGCTACGA

Supplementary Table 3. List of antibodies used

Marker	Fluorochrome	Clone	Supplier	Catalog Number
Endotoxin-induced peritonitis model				
FVD	e780		eBioscience	65-0865-14
CD45	BV785	30-F11	Biolegend	103149
CD19	PE	6D5	Biolegend	115507
CD3	Alexa Fluor 700	17A2	Biolegend	100215
CD8a	BV421	53-6.7	Biolegend	100753
CD4	BV510	RM4-5	Biolegend	100553
NK1.1	APC	PK136	Biolegend	108709
Ly6G	FITC	1A8	Biolegend	127605
CD11b	BV650	M1/70	Biolegend	101239
F4/80	BV711	BM8	Biolegend	123147
Ly6C	BV605	HK1.4	Biolegend	128035
Obesity model				
Zombie	UV		Invitrogen	423107
CD45	BV785	30-F11	Biolegend	103149
Siglec-F	BV605	E50-2440	BD Biosciences	740388
CD11b	PE-Cy7	M1/70	eBioscience	25-0112
CD11b	FITC	M1/70	eBioscience	11-0112
Ly6C	APC-Cy7	HK1.4	Biolegend	128026
CD64	PE	X54-5/7.1	Biolegend	139304
F4/80	BV711	BM8	Biolegend	123147
CD11c	BV421	N418	Biolegend	117330
CD11c	FITC	HL3	BD Biosciences	553801
B220	PE-Cy7	RA3-6B2	Biolegend	103221
CD3	BV605	17A2	Biolegend	100237
GR-1	FITC	RB6-8C5	BD Biosciences	553126
NK1.1	FITC	PK136	eBioscience	11-5941

CHAPTER 3

Soluble mannose receptor induces proinflammatory macrophage activation and metaflammation

Maria Embgenbroich[#], **Hendrik J.P. van der Zande**[#], Leonie Hussaarts[#], Jonas Schulte-Schrepping, Leonard R. Pelgrom, Noemí García-Tardón, Laura Schlautmann, Isabel Stoetzel, Kristian Händler, Joost M. Lambooij, Anna Zawistowska-Deniziak, Lisa Hoving, Karin de Ruiter, Marjolein Wijngaarden, Hanno Pijl, Ko Willems van Dijk, Bart Everts, Vanessa van Harmelen, Maria Yazdanbakhsh, Joachim L. Schultze, Bruno Guigas*, Sven Burgdorf*

[#]These authors contributed equally to this study
*These authors contributed equally to this study

PNAS. 118(31):e2103304118. (2021)
PMID: 34326259
doi: 10.1073/pnas.2103304118

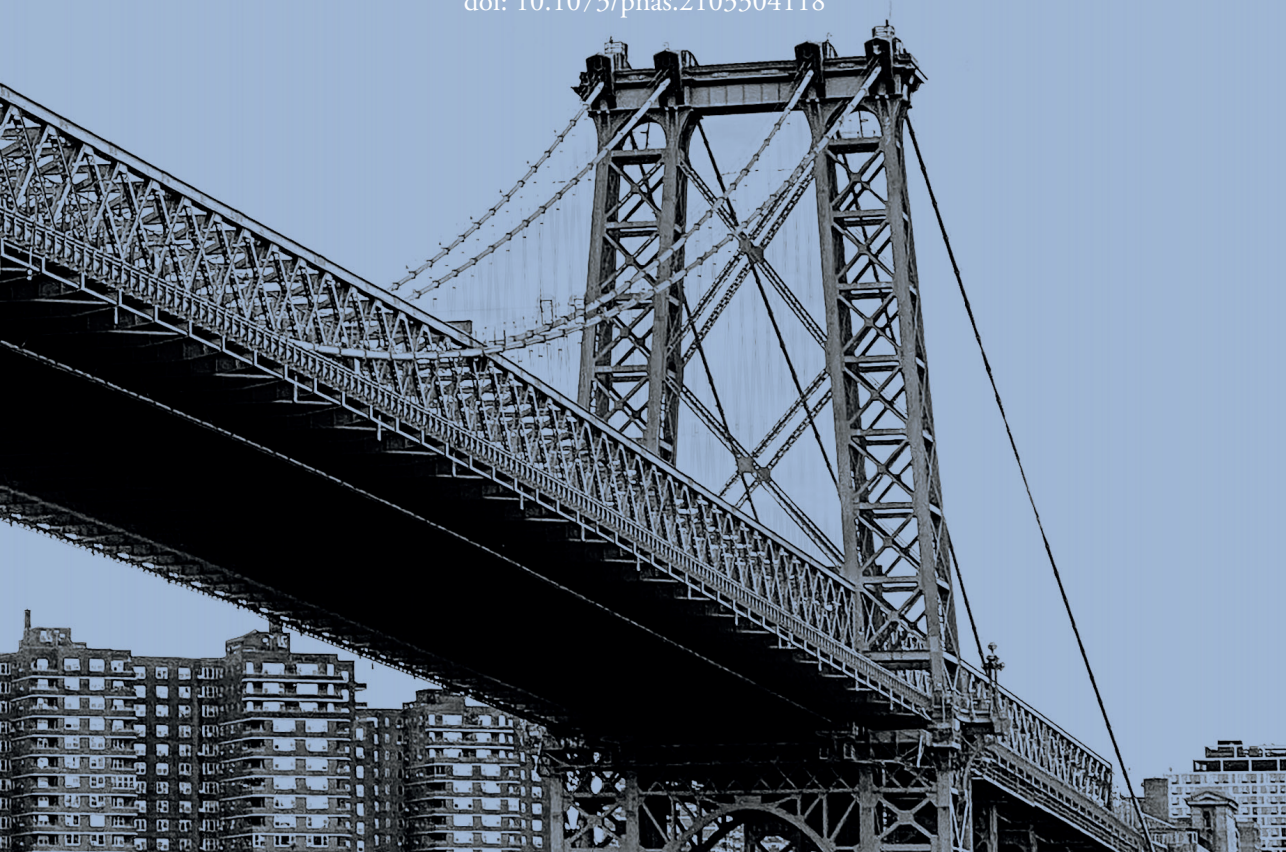

Abstract

Proinflammatory activation of macrophages in metabolic tissues is critically important in the induction of obesity-induced metaflammation. Here, we demonstrate that the soluble mannose receptor (sMR) plays a direct, functional role in both macrophage activation and metaflammation. We show that sMR binds CD45 on macrophages and inhibits its phosphatase activity, leading to a Src/Akt/NF-κB-mediated cellular reprogramming toward an inflammatory phenotype both *in vitro* and *in vivo*. Remarkably, increased serum sMR levels were observed in obese mice and humans and directly correlated with body weight. Importantly, enhanced sMR levels increase serum proinflammatory cytokines, activate tissue macrophages and promote insulin resistance. Altogether, our results reveal sMR as regulator of proinflammatory macrophage activation, which could constitute a therapeutic target for metaflammation and other hyperinflammatory diseases.

Introduction

Metaflammation defines a chronic inflammatory state in response to prolonged excessive nutrient intake and is characterized by low-grade inflammation of metabolic tissues (1). Macrophage reprogramming toward an inflammatory phenotype plays a critical role in obesity-induced metaflammation (2, 3). In lean individuals, macrophages in metabolic tissues maintain tissue homeostasis and insulin sensitivity, potentially through secreting anti-inflammatory cytokines, for example, TGF-b and IL-10 (1). In metaflammation, however, macrophages in adipose tissue and liver are activated through proinflammatory factors in their microenvironment, such as high levels of saturated free fatty acids (FA) and IFN-γ. Consequently, these macrophages produce high amounts of tumor necrosis factor (TNF), which directly inhibits canonical insulin signaling (4), leading to ectopic fat deposition in the liver and in skeletal muscles (5). Additionally, activation of Kupffer cells (KCs), the liver-resident macrophages, promotes recruitment and activation of inflammatory monocytes, which contribute to hepatic insulin resistance and steatosis (6-8).

The MR (also termed CD206) is a type I transmembrane protein belonging to the C-type lectin family, which is mainly expressed by subpopulations of macrophages, dendritic cells and endothelial cells (9, 10). The MR consists of a cysteine-rich region, a fibronectin type II domain, eight C-type lectin-like domains (CTLDs), a transmembrane region and a short cytosolic tail. Due to its high affinity for glycosylated antigens, the MR plays an important role in antigen uptake and presentation (11, 12). In addition to its functions as a transmembrane protein, the extracellular part of the MR can be shed by metalloproteases and released into the extracellular space (13, 14). Hence, soluble MR (sMR) can be detected in murine and human serum, and its level was found to be increased in patients with a variety of inflammatory diseases (15-20), correlating with severity of disease and even mortality. However, a physiological role of the sMR has not been studied yet, and it remains unclear whether the sMR can actively trigger inflammation.

Here, we report that sMR enhances macrophage proinflammatory activation, both *in vitro* and *in vivo*, and promotes metaflammation. We demonstrate that the sMR directly interacts with CD45 on the surface of macrophages and inhibits its phosphatase activity, leading to Src/Akt/NF-κB-mediated cellular reprogramming toward an inflammatory phenotype. Additionally, we found enhanced sMR serum levels in obese mice and humans and show that sMR-induced activation of macrophages triggers metaflammation *in vivo*.

Results

Soluble MR enhances proinflammatory cytokine secretion by macrophages

To investigate whether the MR is involved in the proinflammatory activation of macrophages, we first stimulated bone marrow-derived macrophages from wild-type or MR-deficient mice

with LPS. We found increased secretion of the proinflammatory cytokines TNF, IL-6, IL-1β and IL-12 in MR-expressing wild-type macrophages (Figure 1A). Because the MR itself lacks intracellular signaling motifs and hence no MR-mediated signaling has been described so far, we hypothesized that the sMR, resulting from the shedding of the MR extracellular region (Supplementary Figure 1A), might play a role in macrophage activation through direct interaction with macrophage surface proteins. To investigate this hypothesis, we generated a fusion protein consisting of the Fc region of human IgG1 and the extracellular region of the MR (encompassing the cysteine-rich region, the fibronectin region, and CTLD1-2) (FcMR) (21). We showed that treatment of MR-deficient macrophages with FcMR also enhanced proinflammatory cytokine secretion after LPS stimulation compared to isotype control-treated cells (Figure 1B). We observed similar results when treating MR-deficient macrophages with commercially available recombinant MR protein, consisting of the complete extracellular region of the protein (Figure 1C), suggesting that binding of sMR to the macrophage surface might indeed be responsible for the observed effects. To definitively prove that the sMR causes the observed increase in cytokine production, we purified sMR from the supernatant of MR-expressing macrophages (Supplementary Figure 1B) and showed that its administration to MR-deficient macrophages increased the secretion of TNF after LPS stimulation (Supplementary Figure 1C). Similar results were obtained from FcMR-treated primary macrophages isolated from murine liver, spleen or peritoneal cavity (Figure 1D), and in human monocyte-derived macrophages (moMϕ) after addition of recombinant human MR (Figure 1E) or after small interfering RNA (siRNA)-mediated down-regulation of the MR (Figure 1F). Interestingly, sMR also promoted a shift in cellular energy metabolism toward increased glycolysis in both murine and human macrophages (Supplementary Figure 1D-E), a bioenergetic hallmark of proinflammatory activation in macrophages (22, 23). Taken together, these data demonstrate that the sMR enhances proinflammatory activation of both murine and human macrophages.

sMR induces a proinflammatory phenotype in macrophages

To further dissect the effect of the sMR on macrophages, we treated MR-deficient macrophages with FcMR for 4, 12 or 24 h and performed RNA sequencing (RNA-seq) analysis (Figure 2A). Principle component analysis (PCA) revealed clear transcriptomic distinction of the samples in all analyzed conditions (Figure 2B). A heatmap of the 1,366 differentially expressed (DE) genes between FcMR treatment and control presented the substantial changes in gene expression due to the FcMR treatment over time with overlapping and unique gene sets (Figure 2C, Supplementary Figure 2A). Gene ontology enrichment analysis based on these shared and specific DE gene sets up-regulated upon FcMR treatment clearly confirmed inflammatory activation of macrophages (Supplementary Figure 2B).

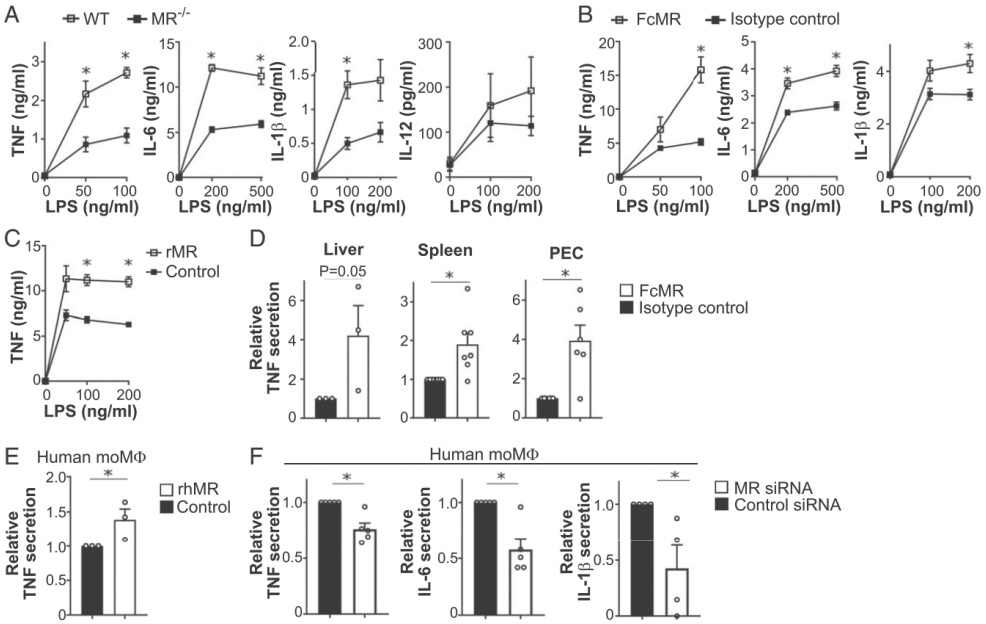

Figure 1: sMR induces proinflammatory cytokine secretion by macrophages. (A) Secretion of TNF, IL-6, IL-1β, and IL-12 by LPS-treated WT or MR-deficient ($MR^{-/-}$) macrophages. **(B)** TNF, IL-6, and IL-1β secretion by LPS-treated MR-deficient macrophages after incubation with FcMR. **(C)** Secretion of TNF by LPS-stimulated MR-deficient macrophages after addition of 0.3 μg/mL recombinant murine MR (rMR). **(D)** Primary murine macrophages were isolated from liver, spleen, or peritoneal cavity (PEC) of WT mice by magnetic separation of $F4/80^{+}$ cells. Secretion of TNF after LPS treatment and stimulation with FcMR were determined by ELISA. **(E)** Secretion of TNF by LPS-treated human monocyte-derived macrophages (moMΦ) after stimulation with 0.3 μg/mL recombinant human MR (rhMR). **(F)** Secretion of TNF, IL-6, and IL-1β by LPS-stimulated human moMΦ after siRNA-mediated down-regulation of the MR. All graphs are depicted as mean ± SEM; for all experiments, $n \geq 3$. *$P < 0.05$

The most significantly up-regulated genes in response to FcMR treatment further emphasized the strong and dynamic proinflammatory activation of macrophages, with well-known immunological key mediators such as TNF, IL-6, IL-1b, and IL-12 (Figure 2D, Supplementary Figure 2C). To classify the response elicited by sMR within the broad spectrum of macrophage activation phenotypes, we performed an enrichment analysis using macrophage activation signatures derived from our previous study comprising macrophages treated with 28 different immunological stimuli (24) and the gene sets of FcMR-mediated up-regulated genes per time point. This analysis revealed a striking similarity of FcMR-induced expression patterns to macrophage signatures associated with a chronic inflammatory phenotype, as induced by TNF, PGE2, and P3C (TPP) in our previous stimulation study (Figure 2E, Supplementary Figure 2D), further substantiating that the sMR reprograms macrophages toward a proinflammatory phenotype.

sMR activates macrophages by binding and inhibiting CD45

Next, we investigated the molecular mechanisms regulating sMR-induced macrophage reprogramming and searched for binding partners of the MR on the macrophage surface. To this end, we isolated cell lysates from macrophages that previously underwent surface biotinylation and performed immunoprecipitation using FcMR. Western blot analysis using streptavidin allowed us to monitor cell surface proteins interacting with sMR, including a clear band at the molecular weight of the phosphatase CD45 (between 180 and 220 kDa, depending on the splice variant; Supplementary Figure 3A), a known binding partner of the MR (25). Indeed, coimmunoprecipitation experiments revealed a physical interaction between the MR and CD45 on macrophages (Figure 3A-B).

CD45 can be expressed as different isoforms, depending on alternative splicing of its three exons A, B, and C. To identify the CD45 isoform interacting with sMR, we assessed their respective expression using isoform-specific antibodies. Analysis by Western blot and flow cytometry clearly showed the absence of exons A, B, and C in bone marrow-derived macrophages (Supplementary Figure 3B), pointing out that these cells only express the CD45RO isoform. This is in accordance with our RNA-seq data, which showed a specific read coverage of all exons of *Cd45* except for exons A, B, and C (Supplementary Figure 3C). Additionally, we showed that primary macrophages from spleen, white adipose tissue (WAT), liver, and the peritoneal cavity also expressed the CD45RO isoform (Supplementary Figure 3D), which is in agreement with previous literature (26). Accordingly, we confirmed the direct interaction of FcMR with CD45RO from primary splenic macrophages by far Western blot (Supplementary Figure 3E).

Since little is known about CD45 phosphatase activity in macrophages, we next investigated whether CD45 is active in these cells. Therefore, we immunoprecipitated CD45 from macrophage lysates and added 4-nitrophenyl phosphate (pNPP), from which dephosphorylation by CD45 can be quantified using colorimetry. We monitored a clear phosphatase activity, which was blocked by a CD45-specific inhibitor (Supplementary Figure 3F), demonstrating the presence of active CD45 in macrophages. Next, we tested the effect of sMR on CD45 phosphatase activity. To this end, we immunoprecipitated CD45 from lysates of FcMR-treated macrophages and showed that dephosphorylation of pNPP was reduced when compared to isotype control-treated cells (Figure 3C), indicating that the MR inhibited CD45 phosphatase activity. In a second approach, we assessed the dephosphorylation of a synthetic peptide containing pY505 of Lck, a specific substrate of CD45. We showed that preincubation of macrophages with FcMR increased pY505 phosphorylation (Figure 3D), confirming the inhibitory effect of the MR on CD45 phosphatase activity.

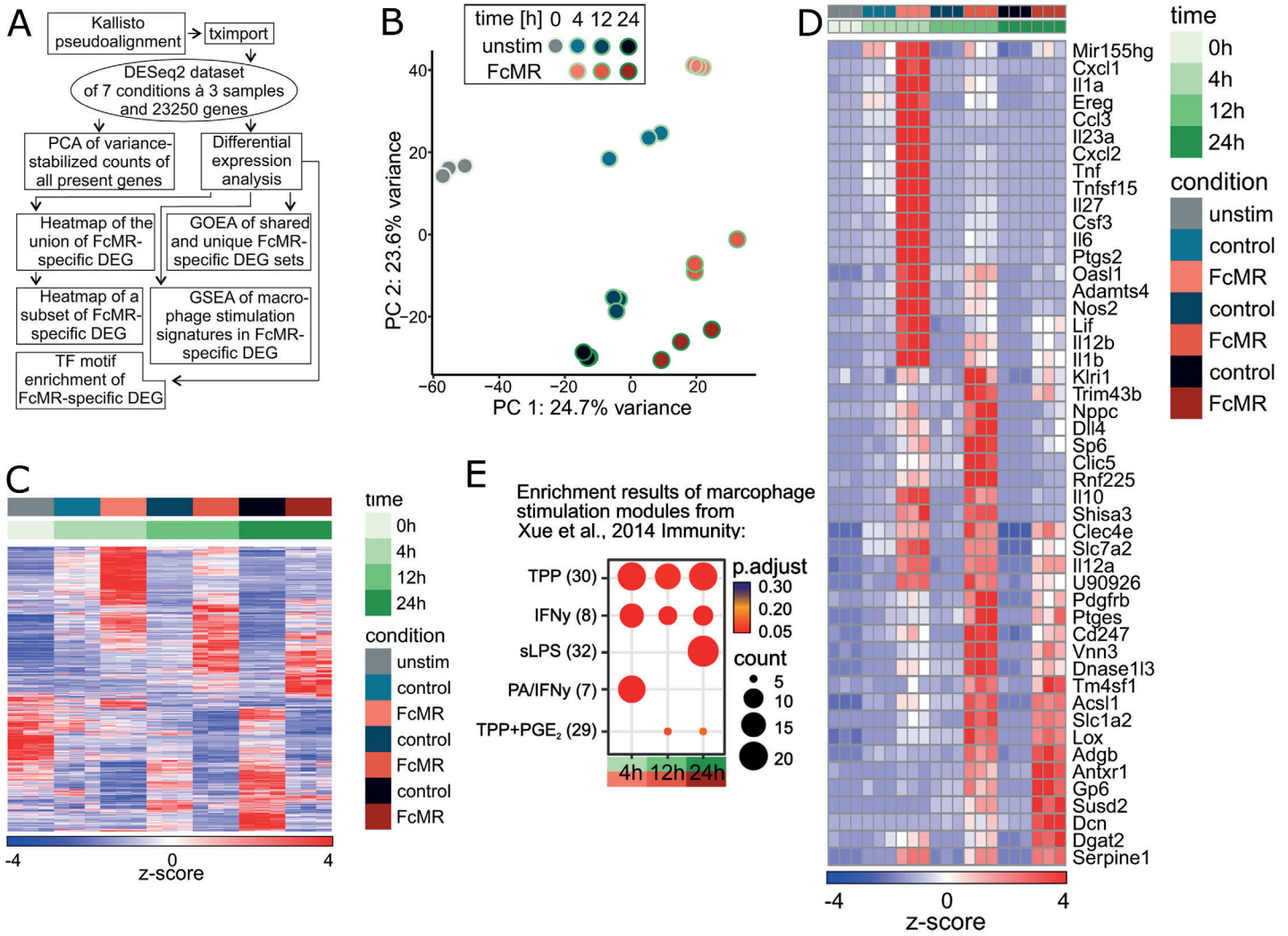
A
Kallisto pseudoalignment
tximport
DESeq2 dataset of 7 conditions à 3 samples and 23250 genes
PCA of variance-stabilized counts of all present genes
Differential expression analysis
Heatmap of the union of FcMR-specific DEG
GOEA of shared and unique FcMR-specific DEG sets
Heatmap of a subset of FcMR-specific DEG
GSEA of macrophage stimulation signatures in FcMR-specific DEG
TF motif enrichment of FcMR-specific DEG
B
time [h] 0 4 12 24
unstim
FcMR
PC 2: 23.6% variance
PC 1: 24.7% variance
C
time
0h
4h
12h
24h
condition
unstim
control
FcMR
control
FcMR
control
FcMR
-4
0
4
z-score
D
time
0h
4h
12h
24h
condition
unstim
control
FcMR
control
FcMR
control
FcMR
Mir155hg
Cxcl1
Il1a
Ereg
Ccl3
Il23a
Cxcl2
Tnf
Tnfsf15
Il27
Csf3
Il6
Ptgs2
Oasl1
Adamts4
Nos2
Lif
Il12b
Il1b
Klri1
Trim43b
Nppc
Dll4
Sp6
Clic5
Rnf225
Il10
Shisa3
Clec4e
Slc7a2
Il12a
U90926
Pdgfrb
Ptges
Cd247
Vnn3
Dnase1l3
Tm4sf1
Acsl1
Slc1a2
Lox
Adgb
Antxr1
Gp6
Susd2
Dcn
Dgat2
Serpine1
-4
0
4
z-score
E
Enrichment results of marcophage stimulation modules from Xue et al., 2014 Immunity:
TPP (30)
IFNγ (8)
sLPS (32)
PA/IFNγ (7)
TPP+PGE2 (29)
4h
12h
24h
p.adjust
0.30
0.20
0.05
count
5
10
15
20

▲Figure 2. Legend

Figure 2: RNAseq analysis identifies a proinflammatory phenotype in MR-treated macrophages. (**A**) Schematic overview of the bioinformatics RNA-seq analysis strategy. (**B**) Principal component analysis based on variance-stabilized counts of all 23,250 present genes. (**C**) Heatmap of hierarchically clustered, normalized, and z-scaled expression values of the union of 1,366 DE genes between FcMR-treated and control samples. (**D**) Normalized and z-scaled expression values of the union of the top 25 DE genes of each time point significantly up-regulated in at least two consecutive time points ranked according to their FcMR vs control samples visualized in a heatmap. (**E**) Dot plot of gene set enrichment analysis results of 49 predefined stimulus-specific macrophage expression signatures comprising 28 different stimuli on the FcMR-specific DE genes for each time point. TPP: TNF, PGE2, and Pam3Cys; PA: palmitic acid.

To investigate whether sMR-mediated inhibition of CD45 phosphatase activity plays a role in macrophage activation, we down-regulated CD45 expression using siRNA (Supplementary Figure 3G). Similar to inhibition of CD45 by sMR, CD45 down-regulation resulted in increased expression of TNF, IL-6, IL-1β and IL-12 after stimulation with LPS (Figure 3E). Importantly, addition of FcMR after down-regulating CD45 had no further effect on cytokine secretion (Figure 3F), demonstrating that the activating effect of the MR on macrophages was indeed due to its inhibition of CD45.

sMR-mediated inhibition of CD45 activates a Src/Akt/NF-κB signaling cascade in macrophages

We next investigated how sMR-mediated inhibition of CD45 results in macrophage reprogramming toward a proinflammatory phenotype. First, we screened for overrepresented transcription factor (TF) binding motifs in the nonprotein coding regions of FcMR-specific up-regulated DE genes. Network visualization of enriched TF binding motifs and their potential target DE genes clearly exposed NF-κB as the dominating transcriptional regulator of differential gene expression across all three time points (Figure 4A). In fact, from 351 known NF-κB target genes, 118 genes (34%) were significantly DE after FcMR treatment on at least one time point (Supplementary Figure 4A-B, Supplementary Dataset 1). Moreover, from all 351 NF-κB target genes, only 269 genes displayed a clear expression (BaseMean expression value ≥ 10) in macrophages, of which 117 genes (43%) were increased by FcMR. This proportion even increased up to 49% for all target genes with BaseMean expression value ≥ 1,000 (61 out of 124 target genes), suggesting a clear activation of NF-κB by the sMR. Indeed, macrophage treatment with FcMR significantly downregulated IkBa (Figure 4B), an inhibitor of NF-κB, which disables its nuclear translocation retaining NF-κB in the cytosol. Accordingly, enhanced nuclear translocation of both NF-κB subunits p65 and p50

(Figure 4C) and increased recruitment of p65 toward the TNF promotor (Supplementary Figure 4D) were observed after treatment with FcMR.

Subsequently, we aimed at identifying the signaling cascade leading from FcMR-mediated inhibition of CD45 to activation of NF-κB. Since CD45 can lead to the activation of Src kinases (27), Src in turn can activate Akt (28), and both Src and Akt have been associated with NF-κB activation (29-32), we investigated whether FcMR-mediated inhibition of CD45 resulted in NF-κB activation through signaling via Src and Akt. Indeed, FcMR treatment increased phosphorylation and hence activation of Src (Figure 4D). Furthermore, blocking Src using three different chemical inhibitors (PP2, KX2-391 and A419259) markedly decreased TNF secretion (Figure 4E). Of note, the effect of FcMR on TNF secretion was abolished in the presence of these Src inhibitors (Figure 4F), demonstrating that FcMR-induced macrophage activation depends on Src signaling. Similarly, FcMR treatment clearly increased phosphorylation of Akt (Figure 4G) and addition of an Akt-specific inhibitor decreased LPS-induced secretion of TNF, IL-6 and IL-1β (Figure 4H). Also here, the stimulatory effect of FcMR on cytokine secretion was abolished by Akt inhibition (Figure 4I), showing an important role for Akt signaling in FcMR-enhanced TNF secretion. Accordingly, inhibition of Akt prevented FcMR-induced translocation of NF-κB into the nucleus (Supplementary Figure 4D).

Taken together, these data demonstrate that sMR-mediated inhibition of CD45 results in activation of a Src/Akt signaling pathway leading to nuclear translocation of NF-κB and macrophage reprogramming toward an inflammatory phenotype.

Serum sMR is up-regulated in obesity and promotes high-fat diet-induced metabolic dysfunctions and hepatic steatosis

Next, we monitored whether the inflammatory effect of the MR on macrophages regulates inflammatory processes *in vivo* using a murine model of obesity-induced metaflammation. We first investigated whether high fat diet (HFD) feeding resulted in changes in serum sMR levels (Supplementary Figure 5A) and we demonstrated significantly increased sMR concentrations in the serum of HFD-fed obese mice, as compared to lean control diet (CD)-fed mice (Figure 5A). Additionally, serum sMR levels positively correlated with body weight and fat mass of the mice (Figures 5B-C). In humans, serum sMR levels were also increased in obese individuals when compared to lean subjects (Figure 5D) and correlated positively with body mass index and fat mass (Figures 5E-F), indicating a direct correlation between serum sMR levels and obesity in both humans and mice.

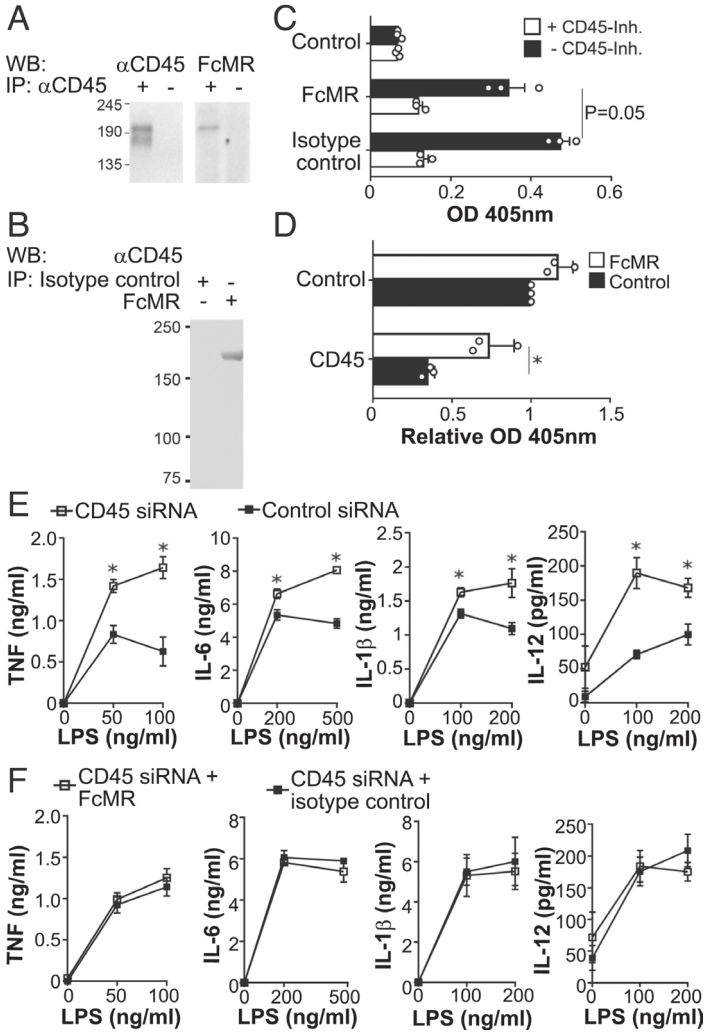

Figure 3: MR inhibits phosphatase activity of CD45 on macrophages. (**A**) Macrophage cell lysates were immune precipitated using a CD45-specific and body and stained for FcMR binding by far Western blot. (**B**) Macrophage lysates were immune precipitated with FcMR or isotype control and stained for CD45 by Western blot. (**C**) CD45 was precipitated from lysates of FcMR- or isotype control-treated macrophages and incubated with 4-NPP in the presence or absence of the CD45 inhibitor SF1670. Graph depicts CD45-mediated dephosphorylation of 4-NPP measured by colorimetry. Samples precipitated without CD45 antibody were used as controls. (**D**) CD45 was precipitated from lysates of FcMR- or isotype control-treated macrophages and incubated with the CD45 substrate TATEGQ-pY-QPQ. Graph depicts the phosphorylation status of TATEGQ-pY-QPQ. Samples precipitated without CD45 antibody were used as controls. (**E**) Secretion of TNF, IL-6, IL-1β, and IL-12 by LPS-stimulated macrophages after siRNA-mediated down-regulation of CD45. (**F**) Influence of FcMR on secretion of TNF, IL-6, IL-1β, and IL-12 by LPS-stimulated macrophages after siRNA-mediated down-regulation of CD45. All graphs are depicted as mean ± SEM; for all experiments, n ≥ 3. *$P < 0.05$.

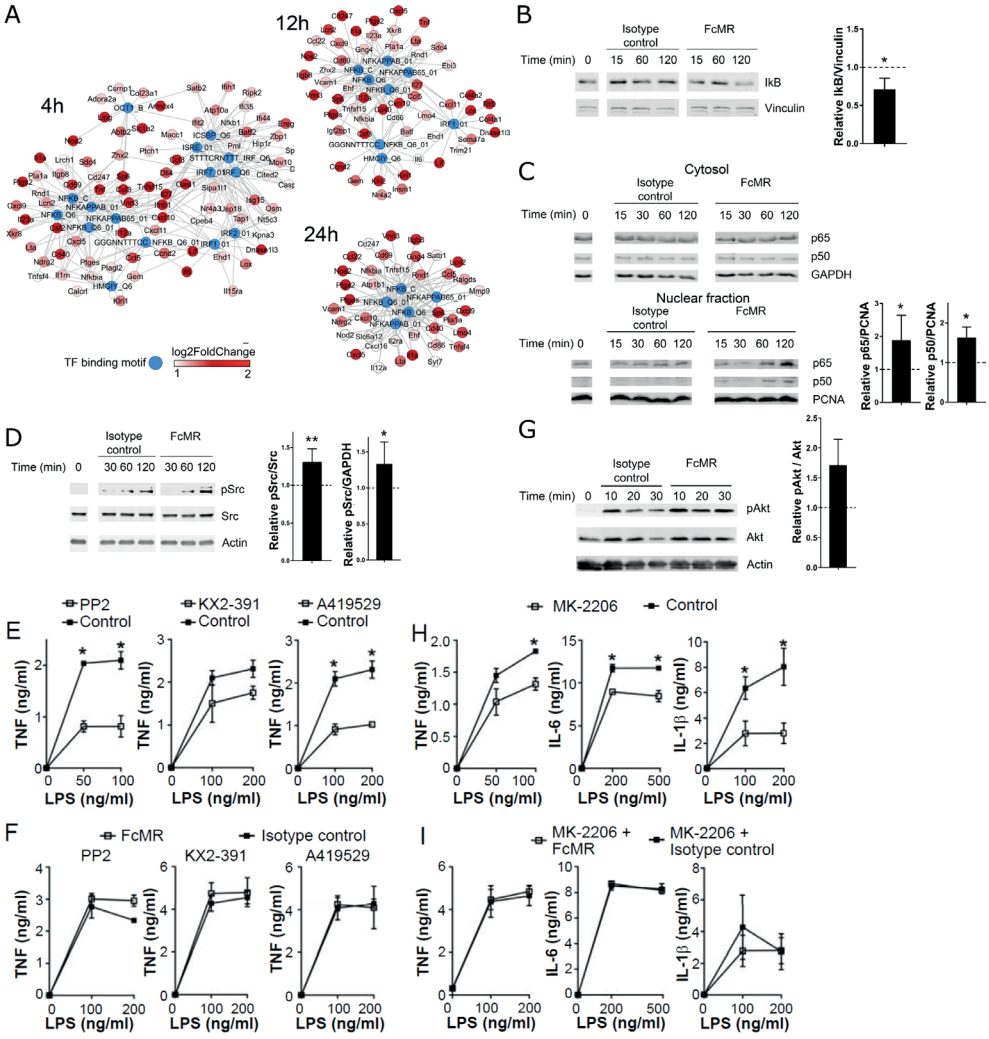

Figure 4: MR reprograms macrophages to a proinflammatory phenotype via Src/Akt/NF-κB signaling. (**A**) Network visualization of significantly enriched (q-value < 0.1) TF binding motifs (blue) of the MSigDB motif gene set and their potential targets (colored in red according to their FC) among the up-regulated DE genes after 4, 12, or 24 h of FcMR treatment. (**B**) MR-deficient macrophages were treated with FcMR or isotype control. Total IκB was determined by Western blot. (**C**) MR-deficient macrophages were treated with FcMR or isotype control. p65 and p50 were monitored in the cytosolic and nuclear fraction by Western blot. (**D**) MR-deficient macrophages were treated with FcMR or isotype control. Src and phosphorylated Src (pSrc) were determined by Western blot. (**E**) MR-deficient macrophages were treated with 3 mM PP2, 1 mM KX2-391, or 1 mM A419529 and stimulated with LPS. TNF secretion was monitored by ELISA. (**F**) FcMR or isotype control-treated MR-deficient macrophages were incubated with PP2, KX2-391, or A419259 and stimulated with LPS. Secretion of TNF was determined by ELISA. (**G**) MR-deficient macrophages

▲Figure 4. Legend

were treated with FcMR or isotype control for 30 min. Akt and phosphorylated Akt (pAkt) were determined by Western blot. (**H**) MR-deficient macrophages were treated with 5 mM MK-2206 and stimulated with LPS. TNF, IL-6, and IL-1β secretion was monitored by ELISA. (**I**) FcMR or isotype control-treated MR-deficient macrophages were incubated with MK-2206 and stimulated with LPS. Secretion of TNF, IL-6, and IL-1β was determined by ELISA. All graphs are depicted as mean ± SEM; for all experiments, n ≥ 3. $*P < 0.05$.

Subsequently, we analyzed changes in MR-expressing cells as putative source for increased sMR serum levels in HFD-fed mice. In spleen and WAT of both CD- and HFD-fed mice, nearly all MR-expressing cells were $CD45^+$, whereas in liver, $CD45^-$ cells also expressed the MR. These latter cells were identified as $CD31^+CD146^+$ liver sinusoidal endothelial cells (LSECs), which were indeed previously reported to express the MR (9). Importantly, whereas no differences in MR expression could be detected in $CD45^-$ cells, a clear increase in MR^+ cells was observed in $CD45^+$ hematopoietic cells in spleen, liver and WAT of HFD-fed obese mice compared to CD-fed mice (Figure 5G). Of note, $CD45^+MR^+$ cells in all three organs were mainly identified as $CD64^+F4/80^+$ macrophages (Supplementary Figure 5B-C). Taken together, this demonstrates that obesity increased MR-expressing macrophages in spleen, liver and WAT.

To test whether increased sMR levels regulate macrophage-mediated inflammatory diseases *in vivo*, we then analyzed the development of obesity-induced metaflammation in MR-deficient mice (Figure 6A). Whereas no differences in body weights were found between wild-type and MR-deficient mice on CD, MR-deficient mice gained slightly less weight on HFD (Figure 6B). This effect was not due to a decrease in caloric intake, as HFD-fed $MR^{-/-}$ mice rather displayed a mild increase in food consumption when compared to WT mice (Supplementary Figure 6A). Furthermore, the HFD-induced reductions in locomotor activity, energy expenditure, and carbohydrate oxidation observed in WT obese mice were found to be partly reverted in $MR^{-/-}$ mice (Supplementary Figure 6B-E). Analysis of body composition showed that the lower body weight in HFD-fed MR-deficient mice resulted exclusively from a reduction in fat mass, without affecting lean mass (Figure 6C). Accordingly, the weights of epididymal, mesenteric and subcutaneous (inguinal) WAT, as well as brown adipose tissue (BAT), were lower in HFD-fed MR-deficient mice (Supplementary Figure 7A-B). This decrease in WAT mass in HFD-fed $MR^{-/-}$ mice appears to be due to reduced adipocyte hyperplasia rather than hypertrophy (Supplementary Figure 8A-E). Of note, no significant differences between genotypes were observed in gene expression of proteins involved in adipocyte differentiation and FA metabolism in epididymal white adipose tissue (eWAT; Supplementary Figure 8F) nor in beiging or thermogenic markers in

inguinal white adipose tissue (iWAT) and BAT, respectively (Supplementary Figure 8G-H). Liver weight was also markedly lower in HFD-fed MR-deficient mice as compared to wild-type controls (Figure 6D), suggesting a reduction in hepatic steatosis. Indeed, MR-deficient mice were completely protected against HFD-induced hepatic steatosis (Figure 6F-G). Accordingly, hepatic triglycerides, total cholesterol and phospholipids contents (Figure 6H, Supplementary Figure 7F), and hepatic gene expression of lipid droplet-associated proteins (Supplementary Figure 7H) were markedly lower in HFD-fed $MR^{-/-}$ mice. Furthermore, the expression of various genes encoding proteins involved in FA transport and storage were significantly decreased in HFD-fed $MR^{-/-}$ mice, whereas no changes in expression of genes implicated in FA oxidation were observed (Supplementary Figure 7I). Circulating alanine aminotransaminase (ALAT) levels were also markedly decreased in HFD-fed MR-deficient mice (Supplementary Figure 7G).

We next assessed metabolic consequences of MR deficiency. Although no differences in metabolic parameters were observed between genotypes in CD-fed mice, HFD-fed MR-deficient mice displayed lower fasting plasma insulin levels than wild-type mice, whereas fasting glucose levels were unchanged (Supplementary Figure 7C-D). The calculated Homeostasis Model Assessment of Insulin Resistance index was significantly reduced in HFD-fed MR-deficient mice (Figure 6E), suggesting that insulin resistance is less severe in these mice. In line with this, whole-body insulin sensitivity (Figure 6I) and glucose tolerance (Figure 6J) were higher, despite similar insulin levels (Supplementary Figure 7E), in HFD-fed MR-deficient mice compared to wild-type mice. Importantly, the alleviated hepatic steatosis and whole-body metabolic homeostasis were still observed when HFD-fed MR-deficient mice were weight-paired to their wild-type counterparts (Supplementary Figure 11A-D), indicating that MR deficiency protects against HFD-induced metabolic dysfunctions independently of body weight changes. Altogether, these data indicate that the MR might contribute to obesity-induced metabolic dysfunctions.

MR promotes inflammatory macrophage accumulation in eWAT and liver during obesity

Since our *in vitro* data demonstrate that the MR reprograms macrophages toward an inflammatory phenotype, we next investigated whether the observed metabolic changes in MR-deficient mice might be caused by reduced proinflammatory macrophage activation in metabolic tissues.

As previously reported, HFD significantly increased obesity-associated proinflammatory $CD11c^{+}$ adipose tissue macrophages (ATMs) in eWAT of wild-type mice (33), whereas total

ATMs and monocytes were not affected (Figures 6K-M, Supplementary Figure 9). Remarkably, while no significant differences in total ATMs and monocyte numbers were observed between genotypes, inflammatory CD11c$^+$ ATM numbers were found to be significantly higher in HFD-fed MR-expressing wild-type mice as compared to MR-deficient mice (Figure 6K-M), and strongly correlated with whole-body insulin resistance (Figure 6N).

In the liver, HFD significantly increased proinflammatory CD11c$^+$ KCs and monocytes in wild-type mice, while total KCs were not affected (Figure 6O-Q). Similar to what was observed in eWAT, inflammatory CD11c$^+$ KCs, but also monocytes, were more abundant in liver of MR-expressing wild-type mice as compared to MR-deficient mice, of which the CD11c$^+$ KCs again correlated strongly with insulin resistance (Figure 6R), while total KCs were not affected (Figure 6O-Q). This was associated with higher expression of genes involved in proinflammatory macrophage activation in liver and WAT of MR-expressing wild-type mice (Supplementary Figure 10B,D). Importantly, these differences in proinflammatory macrophage abundances in metabolic tissues were still present when wild-type and MR-deficient mice were weight-paired (Supplementary Figure 11E-F), indicating that also the regulation of obesity-induced proinflammatory macrophages by the MR is independent of changes in body weight. By contrast, MR deficiency neither affected other myeloid and lymphocyte subsets nor T cell-associated cytokines gene expression in eWAT or liver from HFD-fed mice (Supplementary Figure 10).

Taken together, these data provide first indications that the MR might contribute to obesity-induced metaflammation.

sMR treatment induces proinflammatory cytokines, metabolic dysfunctions, and increased proinflammatory macrophages

To univocally determine the role of the MR in metaflammation, we investigated whether *in vivo* administration of sMR in lean mice is able to induce macrophage activation and metabolic dysfunctions, by intraperitoneally injecting FcMR or isotype control every three days for four weeks (Figure 7A). We first monitored circulating cytokine levels in response to a single intraperitoneal injection of FcMR in CD-fed mice. In accordance with our *in vitro* experiments, even a single injection of FcMR acutely increased serum levels of TNF and IL-6 and the chemokine MCP-1/CCL2 compared to isotype control-treated mice (Figure 7B).

After four weeks of treatment, we monitored a mild increase in body weight in FcMR-treated mice compared to control mice (Figs. 7C-D). In addition, insulin sensitivity, as measured by an acute drop in blood glucose levels following insulin intraperitoneal (i.p.) injection, was reduced in FcMR-treated mice compared to control mice (Figs. 7E-F), confirming the detrimental effect of the sMR on whole-body metabolic homeostasis. Importantly, the effect

of FcMR on HFD-induced insulin resistance was even more pronounced when mice were fed an HFD concomitantly with FcMR treatment for four weeks, underlining the inflammatory effect of the sMR in mice fed an HFD (Supplementary Figure 12).

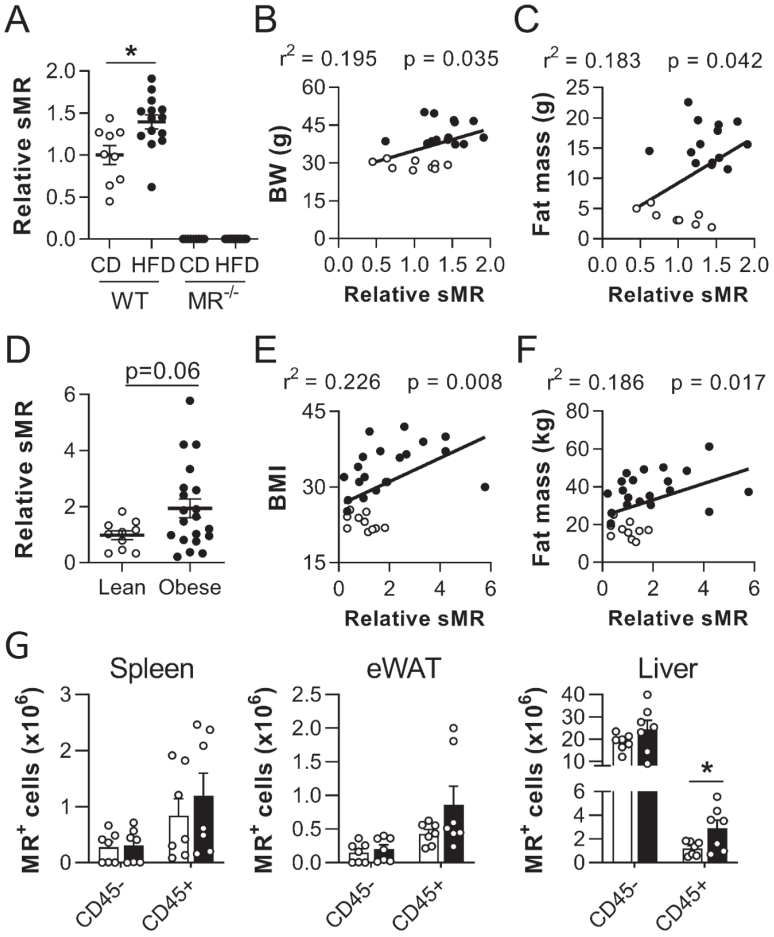

Figure 5: sMR is up-regulated in obesity. (**A**) sMR levels in the serum of wild-type or MR-deficient mice after HFD or CD feeding. (**B-C**) Correlation of sMR serum levels and body weight (*B*) or fat mass (*C*) of all mice depicted in *A*. (**D**) sMR levels in the serum of lean and obese humans. (**E-F**) Correlation between sMR serum levels and body mass index (*E*) or fat mass (*F*). (**G**) Wild-type mice were fed an HFD or CD for 18 weeks. MR-expressing cells were quantified in different organs. Results are expressed as means ± SEM; n=7 mice per group for G. **P* < 0.05.

FcMR treatment increased macrophage numbers in eWAT of lean mice (Figure 7G). Moreover, gene expression of *Il1b, Tnf, Il6* and *Ccl2* was increased in eWAT of FcMR-treated

lean mice (Figure 7H). Accordingly, macrophages isolated from these mice showed increased secretion of most of these cytokines upon stimulation with LPS (Figure 7I), demonstrating that, in lean mice, increased serum sMR levels induce the secretion of proinflammatory cytokines, induce whole-body insulin resistance and promote macrophage activation in metabolic tissues *in vivo*.

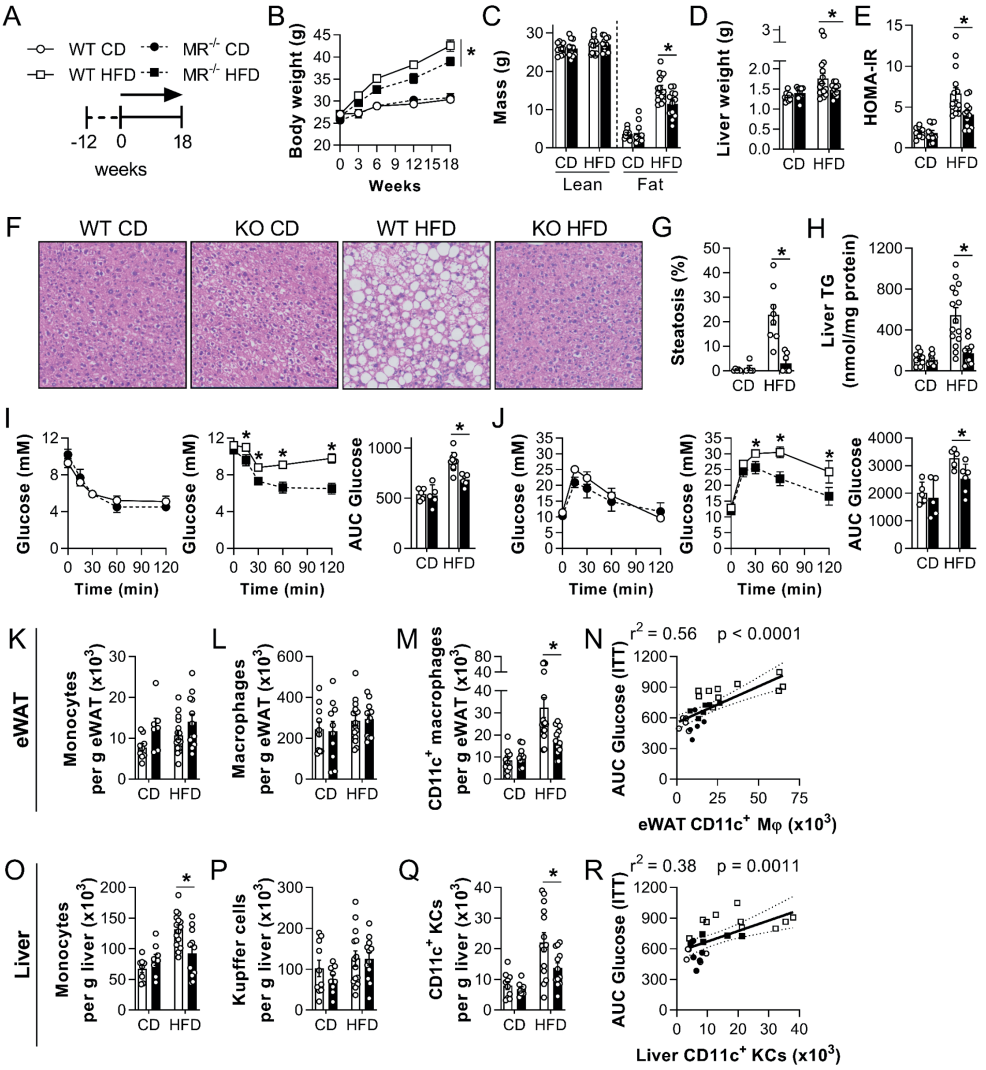

Figure 6: MR regulates WAT and liver macrophage activation, hepatic steatosis, and metabolic homeostasis after HFD feeding. (**A**) Wild-type (WT) and MR-deficient ($MR^{-/-}$) mice were fed an HFD or CD for 18 weeks. (**B**) Body weight of mice on diet for 18 weeks. (**C**) Lean and fat mass after

◀Figure 6. Legend (Continued)

18 weeks on diet determined by MRI. (**D**) Liver weight after 18 weeks on diet. (**E**) Homeostasis Model Assessment of Insulin Resistance index (HOMA-IR) based on blood glucose and fasting insulin. (**F-G**) Hematoxylin and eosin staining (*F*) and quantification (*G*) of hepatic steatosis. (**H**) Levels of liver triglycerides. (**I**) Intraperitoneal insulin tolerance test. Blood glucose levels were measured at the indicated time points, and the area under the curve (AUC) of the glucose excursion curve was calculated as a surrogate measure for whole-body insulin resistance. (**J**) Intraperitoneal glucose tolerance test. The AUC of the glucose excursion curve was calculated as a surrogate measure for whole-body glucose intolerance. (**K-M**) Numbers of total monocytes (*K*), macrophages (*L*), and CD11c$^+$ macrophages (*M*) per gram eWAT determined by flow cytometry. (**N**) Correlation between eWAT CD11c$^+$ macrophages and whole-body insulin resistance, assessed by the AUC of the glucose excursion curve. (**O-Q**) Numbers of total monocytes (*O*), KCs (*P*), and CD11c$^+$ KCs (*Q*) per gram liver determined by flow cytometry. (**R**) Correlation between CD11c$^+$ KCs and whole-body insulin resistance. Results are expressed as means ± SEM; n=5-15 mice per group. **P* <0.05.

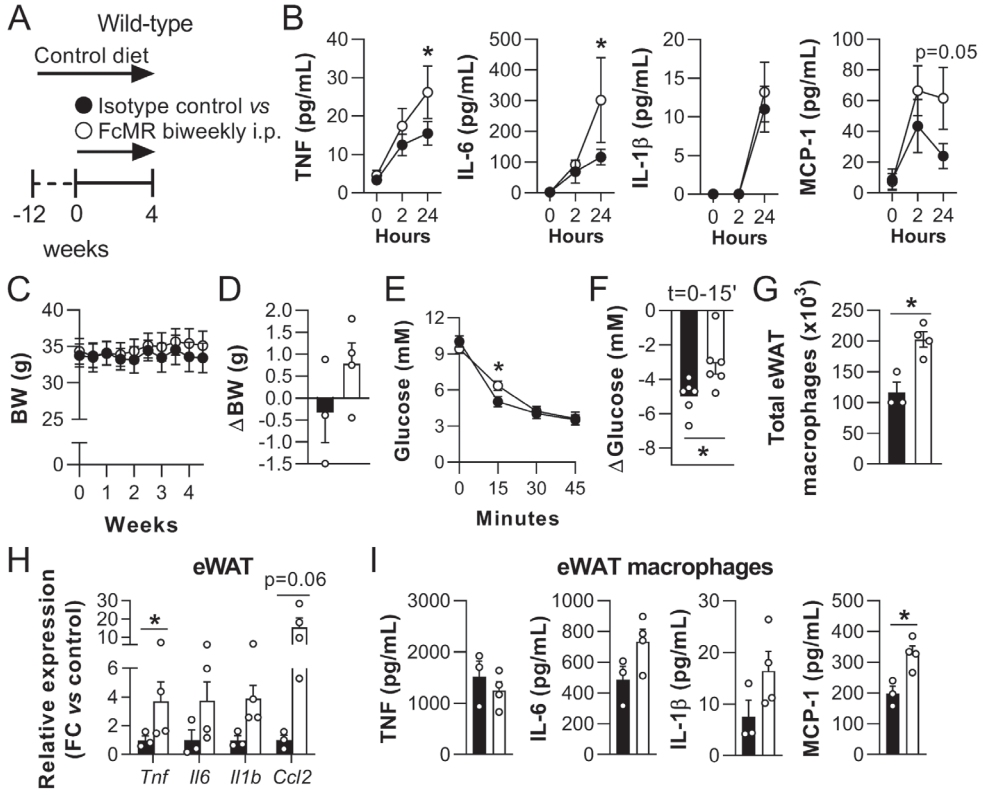

Figure 7: Increased MR levels regulate whole-body metabolism and promote inflammation. (**A**) CD-fed WT mice were injected i.p. with 4.82 μmoles/mouse FcMR or isotype control for 4 weeks. (**B**) Serum cytokine concentrations were determined by cytometric bead array (CBA) at the

▲Figure 7. Legend (Continued)

indicated timepoints post-first injection. (**C-D**) Graphs depicting body weight over time (*C*) and overall change in body weight (*D*). (**E-F**) Intraperitoneal insulin tolerance test after FcMR treatment of CD-fed mice. Changes in circulating glucose levels at 15 min post insulin i.p. (*F*). (**G**) The number of F4/80$^+$ magnetic cell separation (MACS)-sorted eWAT macrophages was determined after 4 weeks of treatment. (**H**) Expression of inflammatory genes in eWAT was monitored by qPCR. (**I**) Cytokine secretion by F4/80$^+$ macrophages from eWAT was determined by CBA after stimulation with 100 ng/ml LPS. BW: body weight. Results are expressed as means ± SEM; n=3-5 mice per group. *P <0.05.

Discussion

The MR as a member of the C-type lectin family has mainly been described as an endocytic receptor recognizing glycosylated antigens and mediating antigen processing and presentation (34, 35). However, the extracellular region of the MR can be shed by metalloproteases and released as a soluble protein in the extracellular space. Consequently, the sMR is detectable in murine and human serum (13, 14), and recent studies reported an increase of serum sMR levels in a variety of inflammatory diseases and serum sMR levels directly correlated with severity of disease and mortality (15-20). Here, we demonstrated that, in addition to a mere phenotypic correlation, the sMR plays a direct, functional role in macrophage activation, driving reprogramming toward a proinflammatory phenotype. By interacting with and inactivating CD45, the sMR reprograms macrophages via activation of Src/Akt signaling and nuclear translocation of NF-κB. *In vivo*, sMR levels were increased in obese mice and humans as compared to lean controls, and we found that MR deficiency reduced adipose tissue and liver proinflammatory macrophages and protected against obesity-induced metabolic dysfunctions. Consistently, treatment of lean mice with sMR acutely increased serum proinflammatory cytokines and induced both tissue macrophage activation and systemic insulin resistance.

Although wild-type (WT) and MR$^{-/-}$ mice on CD were phenotypically similar in term of body composition and whole-body metabolic homeostasis, MR$^{-/-}$ mice on HFD appeared to be slightly resistant to HFD-induced body weight gain and displayed markedly improved insulin sensitivity and glucose tolerance when compared to WT mice. However, it is important to underline that body weight pairing of obese mice from the two genotypes clearly indicated that the lower body weight observed in HFD-fed MR$^{-/-}$ mice only marginally contributed to their lower hepatic steatosis, improved whole-body metabolic homeostasis and phenotypic changes in AT and liver macrophages. In addition, we found that sMR injections promoted inflammation but only induced mild insulin resistance in lean WT mice. Although significant, this effect was modest and may be explained by several factors, including the timing of administration and dosage, but also by the fact

that lean mice are highly insulin sensitive. Of note, injecting sMR at the start of HFD feeding accelerated the development of insulin resistance, which supports a role for sMR in promoting metaflammation.

In this study, we found increased MR^+ cells in spleen, liver, and eWAT upon HFD feeding, which were almost exclusively macrophages. Since cell surface MR can be shed and released as a soluble form, obesity-induced changes in tissue homeostasis may increase MR expression and sMR release by macrophages, creating increased local and systemic sMR levels to promote macrophage-mediated inflammation and metabolic dysfunctions. An important factor in this process could be the ligand-inducible TF PPAR-γ, which is activated, among others, by free FAs. Indeed, single-cell RNA sequencing analysis of adipose tissue immune cells revealed that PPAR signaling is among the up-regulated pathways in obesity-induced lipid-associated macrophages in both mice and humans (36). Since *Mrc1* (encoding the MR) is also a direct target gene of PPAR-γ (37), obesity-induced activation of PPAR-γ in macrophages may lead to enhanced transcription of the MR, eventually resulting in increased sMR levels. One of the limitations of our study was the use of constitutive whole-body $MR^{-/-}$ mice instead of a myeloid cell-specific knockout model, which is currently not available. As such, the main cellular source of circulating proinflammatory sMR remains to be confirmed, although it is conceivable that a significant part of the increased circulating sMR during obesity may also be derived from non-myeloid MR-expressing cells, such as LSECs.

Our data demonstrate that macrophage activation by the MR was due to MR-mediated inhibition of CD45, which in turn leads to activation of Src and Akt, and nuclear translocation of NF-κB. CD45 has been postulated to inhibit Src kinases (27) and Akt (28), a known regulator of NF-κB (30, 31, 38). Here, we show that CD45-mediated dephosphorylation of Src induces Akt-mediated nuclear translocation of NF-κB, and that the sMR uses this signaling pathway to induce macrophage reprogramming toward an inflammatory phenotype. MR-mediated macrophage activation depended on Akt signaling, as its inhibition abrogated MR-mediated nuclear translocation of NF-κB and ensuing TNF and IL-6 secretion by macrophages. Additionally, Akt has been postulated as a regulator that can fine tune NF-κB-mediated responses through regulating efficient binding of p65 to specific target promoters (32). Of note, these authors demonstrated that NF-κB-mediated expression of TNF was particularly sensitive to Akt signaling, which is in accordance with the Akt-dependency of TNF expression after MR-induced activation of macrophages described here.

The immunometabolic phenotype of obese MR-deficient mice resembles that of mice deficient for MGL/CLEC10A, another member of the C-type lectin family. Indeed,

these mice displayed reduced hepatic steatosis, insulin resistance and glucose intolerance upon HFD when compared to wild-type mice, a feature that was associated with lower AT proinflammatory macrophages (39). In another context, MGL/CLEC10A was also shown to bind and inactivate CD45 (40), offering the possibility that MGL/CLEC10A can directly induce macrophage reprogramming by inhibition of CD45, similar to the MR. Future studies will have to reveal whether MGL/CLEC10A indeed plays a direct role in macrophage activation, whether its expression is also increased in HFD-induced obesity, and whether this may be mediated by a soluble form of MGL/CLEC10A.

In summary, we demonstrate that a soluble form of the MR reprograms macrophages toward an inflammatory phenotype by interacting with CD45 on the surface of these macrophages. MR-mediated inhibition of CD45 activated Src and Akt kinases, leading to nuclear translocation of NF-κB and induction of a transcriptional program that ultimately results in enhanced inflammatory cytokine production. Furthermore, sMR levels in serum of obese mice and humans are increased, strongly correlating with body weight and adiposity, a feature that needs however to be confirmed in female mice and larger population studies. Accordingly, MR deficiency resulted in fewer adipose tissue and liver proinflammatory macrophages and protection against hepatic steatosis and metaflammation, whereas increased MR levels induced elevated serum proinflammatory cytokines, macrophage activation and metabolic dysfunctions. Altogether, our results identify sMR as a regulator of proinflammatory macrophage activation and could contribute to the development of new therapeutic strategies for metaflammation and other hyperinflammatory diseases. Targeting MR-mediated activation of macrophages using antibodies, nanobodies, aptamers or small molecules that could prevent MR interacting with macrophage CD45RO might open new possibilities for therapeutics aimed at dampening (meta)inflammation.

Material and Methods

Antibodies and Reagents

A detailed list of antibodies and reagents is included in the Supplementary information.

Generation of bone marrow-derived macrophages

Bone marrow was flushed from the femurs and tibias of mice and cultured for 7 days in medium containing 2.5 % supernatant of a Granulocyte Macrophage Colony-Stimulating Factor (GM-CSF)-producing cell line (total concentration 150 ng/mL).

Generation and purification of FcMR

FcMR proteins (encompassing the CR region, the FN II domain and CTLD1-2 fused to the Fc region of hIgG1) and isotype controls (Fc region of hIgG1) were generated as described previously (21). For all *in vitro* experiments, FcMR and isotype controls were used in a concentration of 10 μg/mL.

Monitoring secretion of TNF, IL-6, IL-1β and IL-12

Macrophages were incubated with 10 μg/mL FcMR or isotype control, 300 ng/mL recombinant MR (2535-MM-050, R&D Systems), 30 ng/mL purified sMR, 3 μM PP2, 1 μM KX2-391, 1 μM A419259 or 5 μM MK-2206. After 2 h, LPS was added in the given concentrations. Unless indicated differently, supernatants were collected at 3 h (TNF) or 18 h (IL-6, IL-12p70) post-LPS stimulation. For secretion of IL-1β, cells were incubated with LPS for 3 h and with 10 mM nigericin for another 1 h. Secreted cytokine levels were measured by enzyme-linked immunosorbent assay (ELISA). Levels of TNF, IL-6, IL-1β, and MCP-1 in the circulation at 2 h post-FcMR, or isotype control injection, or in culture supernatant of LPS-treated eWAT macrophages were measured using the cytometric bead array kits (BD Biosciences), per manufacturer's recommendations.

Mice and diet

All animal experiments were performed in accordance with the Guide for the Care and Use of Laboratory Animals of the Institute for Laboratory Animal Research and have received approval from the university Ethical Review Boards (DEC No. 12199; Leiden University Medical Center, Leiden, The Netherlands). To reduce variation due to sex hormone cycles on whole-body metabolism, male mice were used for all *in vivo* experiments. $MR^{-/-}$ mice were generated on C57BL/6J background, regularly backcrossed to C57BL/6J, and compared to age-matched C57BL/6J wild-type mice from the same mouse facility. To minimize eventual effects of genotype-dependent microbiota differences on metabolic and immunological outcomes, the beddings of WT and $MR^{-/-}$ mice were frequently mixed before randomization. All mice were housed in a temperature-controlled room with a 12-hour light-dark cycle. Throughout the experiment, food and tap water were available ad libitum. The 8- to 10-weeks-old male mice were randomized according to total body weight, lean and fat mass, and fasting plasma glucose, insulin, TC and TG levels, after which they were fed an HFD (45% energy derived from fat, D12451, Research Diets) or a CD (10% energy derived from fat, D12450B, Research Diets) for 18 weeks. An *a priori* power calculation was done. Analysis was performed blinded to the conditions. For *in vivo* FcMR treatment,

C57BL/6J wild-type littermate mice were randomized as above. Subsequently, mice were biweekly intraperitoneally injected with 50 μg FcMR or 6.75 μg isotype control, to yield the same administered dose of hIgG1, for four weeks while either on CD or concomitant with the start of HFD feeding.

Quantification and statistical analysis

All data are presented as mean ± SEM. Statistical analysis was performed using GraphPad Prism 8.0 (GraphPad Software) with unpaired t-test, one-way or two-way ANOVA, followed by Fisher's post hoc test. Differences between groups were considered statistically significant at $P < 0.05$. Outliers were identified according to the two-SD method. Single data points represent mean values of distinct independent experiments (*in vitro*) or individual mice (*in vivo*).

Data and Software availability

The complete RNAseq analysis including code and count data can be found under jsschrepping/Embgenbroich_2020 at https://github.com/schultzelab. Additionally, the unprocessed RNA-seq data is available online in the Gene Expression Omnibus database (https://www.ncbi.nlm.nih.gov) under accession number GSE145369.

Acknowledgements

This work is funded by the Deutsche Forschungsgemeinschaft (DFG, German Research Foundation) SFB1454 (project number 432325352) and under Germany´s Excellence Strategy EXC2151 (project number 390873048) (to S.B.), a European Federation for the Study of Diabetes (EFSD)/Lilly Research Grant Fellowship from the European Federation for the Study of Diabetes (to B.G.), Dutch Research Council (NWO) Graduate School Program 022.006.010 (to H.J.P.v.d.Z.), and the Dutch Organization for Scientific Research (ZonMW TOP Grant 91214131 to B.G. and M.Y.). We thank Frank Otto and Arifa Ozir-Fazalalikhan for their invaluable technical help. The authors declare no competing interests.

References

1. Brestoff JR, Artis D. Immune regulation of metabolic homeostasis in health and disease. Cell. 2015;161(1):146-60.
2. Hotamisligil GS. Inflammation, metaflammation and immunometabolic disorders. Nature. 2017;542(7640):177-85.
3. Lackey DE, Olefsky JM. Regulation of metabolism by the innate immune system. Nat Rev Endocrinol. 2016;12(1):15-28.
4. Hotamisligil GS, Murray DL, Choy LN, Spiegelman BM. Tumor necrosis factor alpha inhibits signaling from the insulin receptor. Proc Natl Acad Sci U S A. 1994;91(11):4854-8.
5. Shulman GI. Ectopic fat in insulin resistance, dyslipidemia, and cardiometabolic disease. N Engl J Med. 2014;371(23):2237-8.
6. Neuschwander-Tetri BA. Hepatic lipotoxicity and the pathogenesis of nonalcoholic steatohepatitis: the central role of nontriglyceride fatty acid metabolites. Hepatology. 2010;52(2):774-88.
7. Lanthier N, Molendi-Coste O, Horsmans Y, van Rooijen N, Cani PD, Leclercq IA. Kupffer cell activation is a causal factor for hepatic insulin resistance. Am J Physiol Gastrointest Liver Physiol. 2010;298(1):G107-16.
8. Morinaga H, Mayoral R, Heinrichsdorff J, Osborn O, Franck N, Hah N, et al. Characterization of distinct subpopulations of hepatic macrophages in HFD/obese mice. Diabetes. 2015;64(4):1120-30.
9. Martinez-Pomares L. The mannose receptor. J Leukoc Biol. 2012;92(6):1177-86.
10. Takahashi K, Donovan MJ, Rogers RA, Ezekowitz RA. Distribution of murine mannose receptor expression from early embryogenesis through to adulthood. Cell Tissue Res. 1998;292(2):311-23.
11. Burgdorf S, Kautz A, Bohnert V, Knolle PA, Kurts C. Distinct pathways of antigen uptake and intracellular routing in CD4 and CD8 T cell activation. Science. 2007;316(5824):612-6.
12. Burgdorf S, Lukacs-Kornek V, Kurts C. The mannose receptor mediates uptake of soluble but not of cell-associated antigen for cross-presentation. J Immunol. 2006;176(11):6770-6.
13. Jordens R, Thompson A, Amons R, Koning F. Human dendritic cells shed a functional, soluble form of the mannose receptor. Int Immunol. 1999;11(11):1775-80.
14. Martinez-Pomares L, Mahoney JA, Kaposzta R, Linehan SA, Stahl PD, Gordon S. A functional soluble form of the murine mannose receptor is produced by macrophages in vitro and is present in mouse serum. J Biol Chem. 1998;273(36):23376-80.
15. Saha B, Tornai D, Kodys K, Adejumo A, Lowe P, McClain C, et al. Biomarkers of Macrophage Activation and Immune Danger Signals Predict Clinical Outcomes in Alcoholic Hepatitis. Hepatology. 2019;70(4):1134-49.
16. Suzuki Y, Shirai M, Asada K, Yasui H, Karayama M, Hozumi H, et al. Macrophage mannose receptor, CD206, predict prognosis in patients with pulmonary tuberculosis. Sci Rep. 2018;8(1):13129.

17. Rodgaard-Hansen S, Rafique A, Weis N, Wejse C, Nielsen H, Pedersen SS, et al. Increased concentrations of the soluble mannose receptor in serum from patients with pneumococcal bacteraemia, and prediction of survival. Infect Dis (Lond). 2015;47(4):203-8.

18. Ding D, Song Y, Yao Y, Zhang S. Preoperative serum macrophage activated biomarkers soluble mannose receptor (sMR) and soluble haemoglobin scavenger receptor (sCD163), as novel markers for the diagnosis and prognosis of gastric cancer. Oncol Lett. 2017;14(3):2982-90.

19. Loonen AJM, Leijtens S, Serin O, Hilbink M, Wever PC, van den Brule AJC, et al. Soluble mannose receptor levels in blood correlate to disease severity in patients with community-acquired pneumonia. Immunol Lett. 2019;206:28-32.

20. Andersen ES, Rodgaard-Hansen S, Moessner B, Christensen PB, Moller HJ, Weis N. Macrophage-related serum biomarkers soluble CD163 (sCD163) and soluble mannose receptor (sMR) to differentiate mild liver fibrosis from cirrhosis in patients with chronic hepatitis C: a pilot study. Eur J Clin Microbiol Infect Dis. 2014;33(1):117-22.

21. Schuette V, Embgenbroich M, Ulas T, Welz M, Schulte-Schrepping J, Draffehn AM, et al. Mannose receptor induces T-cell tolerance via inhibition of CD45 and up-regulation of CTLA-4. Proc Natl Acad Sci U S A. 2016;113(38):10649-54.

22. Van den Bossche J, O'Neill LA, Menon D. Macrophage Immunometabolism: Where Are We (Going)? Trends Immunol. 2017;38(6):395-406.

23. Viola A, Munari F, Sanchez-Rodriguez R, Scolaro T, Castegna A. The Metabolic Signature of Macrophage Responses. Front Immunol. 2019;10:1462.

24. Xue J, Schmidt SV, Sander J, Draffehn A, Krebs W, Quester I, et al. Transcriptome-based network analysis reveals a spectrum model of human macrophage activation. Immunity. 2014;40(2):274-88.

25. Martinez-Pomares L, Crocker PR, Da Silva R, Holmes N, Colominas C, Rudd P, et al. Cell-specific glycoforms of sialoadhesin and CD45 are counter-receptors for the cysteine-rich domain of the mannose receptor. J Biol Chem. 1999;274(49):35211-8.

26. Pilling D, Fan T, Huang D, Kaul B, Gomer RH. Identification of markers that distinguish monocyte-derived fibrocytes from monocytes, macrophages, and fibroblasts. PLoS One. 2009;4(10):e7475.

27. Shrivastava P, Katagiri T, Ogimoto M, Mizuno K, Yakura H. Dynamic regulation of Src-family kinases by CD45 in B cells. Blood. 2004;103(4):1425-32.

28. Chen J. The Src/PI3K/Akt signal pathway may play a key role in decreased drug efficacy in obesity-associated cancer. J Cell Biochem. 2010;110(2):279-80.

29. Bai D, Ueno L, Vogt PK. Akt-mediated regulation of NFkappaB and the essentialness of NFkappaB for the oncogenicity of PI3K and Akt. Int J Cancer. 2009;125(12):2863-70.

30. Xie X, Lan T, Chang X, Huang K, Huang J, Wang S, et al. Connexin43 mediates NF-kappaB signalling activation induced by high glucose in GMCs: involvement of c-Src. Cell Commun Signal. 2013;11(1):38.

31. Abu-Amer Y, Ross FP, McHugh KP, Livolsi A, Peyron JF, Teitelbaum SL. Tumor necrosis factor-alpha activation of nuclear transcription factor-kappaB in marrow macrophages is mediated by c-Src tyrosine phosphorylation of Ikappa Balpha. J Biol Chem. 1998;273(45):29417-23.

32. Cheng J, Phong B, Wilson DC, Hirsch R, Kane LP. Akt fine-tunes NF-kappaB-dependent gene expression during T cell activation. J Biol Chem. 2011;286(41):36076-85.

33. Lumeng CN, Bodzin JL, Saltiel AR. Obesity induces a phenotypic switch in adipose tissue macrophage polarization. J Clin Invest. 2007;117(1):175-84.

34. Rauen J, Kreer C, Paillard A, van Duikeren S, Benckhuijsen WE, Camps MG, et al. Enhanced cross-presentation and improved CD8+ T cell responses after mannosylation of synthetic long peptides in mice. PLoS One. 2014;9(8):e103755.

35. Kreer C, Kuepper JM, Zehner M, Quast T, Kolanus W, Schumak B, et al. N-glycosylation converts non-glycoproteins into mannose receptor ligands and reveals antigen-specific T cell responses in vivo. Oncotarget. 2017;8(4):6857-72.

36. Jaitin DA, Adlung L, Thaiss CA, Weiner A, Li B, Descamps H, et al. Lipid-Associated Macrophages Control Metabolic Homeostasis in a Trem2-Dependent Manner. Cell. 2019;178(3):686-98 e14.

37. Klotz L, Hucke S, Thimm D, Classen S, Gaarz A, Schultze J, et al. Increased antigen cross-presentation but impaired cross-priming after activation of peroxisome proliferator-activated receptor gamma is mediated by up-regulation of B7H1. J Immunol. 2009;183(1):129-36.

38. Lluis JM, Buricchi F, Chiarugi P, Morales A, Fernandez-Checa JC. Dual role of mitochondrial reactive oxygen species in hypoxia signaling: activation of nuclear factor-{kappa}B via c-SRC and oxidant-dependent cell death. Cancer Res. 2007;67(15):7368-77.

39. Westcott DJ, Delproposto JB, Geletka LM, Wang T, Singer K, Saltiel AR, et al. MGL1 promotes adipose tissue inflammation and insulin resistance by regulating 7/4hi monocytes in obesity. J Exp Med. 2009;206(13):3143-56.

40. van Vliet SJ, Gringhuis SI, Geijtenbeek TB, van Kooyk Y. Regulation of effector T cells by antigen-presenting cells via interaction of the C-type lectin MGL with CD45. Nat Immunol. 2006;7(11):1200-8.

Supplementary Materials and Methods

Antibodies and Reagents

α-mouse actin (20-33), α-phosphotyrosine (4G10) and α-mouse GAPDH (10B13) were obtained from Merck, α-mouse vinculin (4650), α-mouse IκBa (44D4), α-mouse PCNA (PC10), α-mouse Akt (9272), α-mouse pAkt (Ser473)(9271), α-mouse Src (L4A1), α-mouse pSrc (Tyr416)(2101) and α-mouse p65 (D14E12) from Cell Signaling Technology, α-mouse calnexin (ab22595) from Abcam and α-mouse p50 (E10) from Santa Cruz. All antibodies used in flow cytometry are listed in Supplementary Table 1. Recombinant MR was obtained from R&D Systems, KX2-391 from Biotrend, A-419259 from Biomol, MK-2206 from Enzo Life Sciences, Biotin from Roth, SF1670 from Merck and rhM-CSF from BioLegend. All other chemicals were obtained from Sigma.

Purification of sMR from the supernatant of MR-expressing cells

Supernatant of bone marrow-derived macrophages was collected and loaded on an affinity chromatography column containing Sepharose beads that were covalently linked to an anti-MR antibody (MR5D3, BIO-RAD). After extensive washing, sMR was eluted in 0.1 M Glycin (pH 2.5), neutralized with 1 M Tris (pH 9.0) and dialyzed against PBS containing 10% PEG for 24 h.

Sample preparation for Western Blot analysis

For whole cell lysates, samples were lysed in 10 mM triethanolamine, 150 mM NaCl, 1 mM $MgCl_2$, 1 mM $CaCl_2$ and 1% Triton X-100. For the extraction of nuclear extracts, cells were lysed first in 50 mM HEPES-KOH, 1 mM EDTA (pH 8.0), 140 mM NaCl, 0.25% Triton X-100, 0.5% Igepal and 10% glycerol and the cytosolic fraction was harvested. Afterwards, pellets were resuspended in 10 mM Tris-HCl (pH 8.0), 1 mM EDTA, 100 mM NaCl, 0.5 mM EGTA, 0.1% Sodium desoxycholic acid and 0.5% sodium N-lauryl sarcosine, sonicated and centrifuged, yielding the nuclear fraction.

Surface biotinylation and co-immunoprecipitation experiments

Bone marrow-derived macrophages were incubated with 0.5 mg/ml biotin for 30 min and washed extensively. Afterwards, cells were lysed and 10 μg/ml FcMR was added for 1 h on ice. Subsequently, FcMR was immunoprecipitated using protein A/G-based affinity chromatography and samples were loaded on an SDS-PAGE for analysis by Western Blot using streptavidin or a CD45-specific antibody. Alternatively, a CD45-specific antibody was

added to macrophage lysates and precipitated by protein A/G-based affinity chromatography for subsequent far Western Blot analysis using FcMR.

CD45 phosphatase assay

CD45 was immunoprecipitated from macrophage lysates and incubated with 2 mM pNPP for 18 h at 37°C in the presence or absence of 1 μM of the CD45-specific inhibitor SF1670. Dephosphorylation of pNPP was quantified by colorimetry at 405 nm. Alternatively, immunoprecipitated CD45 was incubated with 0.25 μg of the biotinylated peptide TATEGQpYQPQ for 18 h at 37 °C in the presence or absence of SF1670. Phosphorylated TATEGQpYQPQ was monitored after affinity chromatography using streptavidin-agarose, staining with the phosphospecific primary antibody 4G10 (Milipore), a HRP-conjugated secondary antibody and addition of the HRP substrate TMB One (Kementec).

siRNA-mediated down-regulation of CD45

siRNA against CD45 (Mm-Ptprc_6 Flexitube siRNA, Qiagen) or control siRNA (AAAAACAUGCAGAAAUGCUGU; containing a specific sequence of the luciferase gene) were obtained from Qiagen. After five days of culture in GM-CSF-containing medium, cells were electroporated with 4 μg siRNA using a Gene Pulser Xcell Electroporation Systems (Bio-Rad) with two sequential pulses of 1000 V for 0.5 ms each. Cells were incubated for 2 days before subsequent experiments were performed.

Blood monocyte-derived macrophages and siRNA-mediated down-regulation of MR expression

Human $CD14^+$ monocytes were isolated from blood of anonymous healthy volunteers, as described previously (1), and cultured in RPMI 1640 (Invitrogen) supplemented with 10% heat-inactivated FSC, 100 U/ml penicillin, 100 μg/ml streptomycin and 50 ng/mL of recombinant human M-CSF (BioLegend) in plates with Nunclon™ Delta Surface coating (Nunc). On day 4 of differentiation, cells were electroporated with either 455 nM anti-*Mrc1* siRNA or 455 nM scrambled siRNA (Dharmacon) using the Neon® transfection system (Invitrogen) using one pulse of 1600V for 20 ms. Cells were incubated for 2 days and next incubated for 24 h with 100 ng/ml LPS and 50 ng/ml IFN-γ. Supernatant was harvested after 24 h for analyses of TNF, IL-6, and IL-1β by ELISA using a commercially available kit (BioLegend).

RNA isolation and RNAseq analysis

RNA of $5x10^6$ bone marrow-derived macrophages treated with FcMR or isotype control for 4, 12, and 24 h was isolated with Trizol and miRNeasy micro kit (Qiagen) according to the manufacturer's protocol. RNA quality was assessed by visualization of 28S and 18S band integrity on a Tapestation 2200 (Agilent). 100 ng of RNA was converted into cDNA libraries using the TruSeq RNA library preparation kit v2. Size distribution of cDNA libraries was measured using the Agilent high sensitivity DNA assay on a Tapestation 2200 (Agilent). cDNA libraries were quantified using KAPA Library Quantification Kits (Kapa Biosystems). After cluster generation on a cBot, 75 bp single read sequencing was performed on a HiSeq1500.

Bioinformatic analysis

After base calling and de-multiplexing using CASAVA version 1.8.2 and subsequent quality control using fastQC, the 75 bp single-end reads were pseudoaligned to the mm10-based mouse Gencode reference transcriptome vM16 using kallisto version 0.44.0. Transcript abundance estimations were imported to R and summarized on gene level using tximport (2). Downstream analyses were performed using DESeq2 (3). After filtering of lowly expressed genes (rowSums > 10) and variance stabilizing transformation, principal component analysis was performed on all present genes using the prcomp package. Differential expression analysis was performed comparing FcMR-treated samples versus controls for each time point without pre-defined $\log_2$ fold change threshold and using independent hypothesis weighting (IHW) as the multiple testing procedure. Genes with an adjusted p-value < 0.05 and a fold change (FC) > 2 were determined as significantly differentially expressed. Normalized and z-scaled expression values of the union of differentially expressed (DE) genes over all three time points were visualized in a heatmap. Gene ontology enrichment analyses were performed on those genes shared between all three DE gene sets (shared), as well as the respective gene sets for each time point (4 h, 12 h, and 24 h) and those genes unique for each time point (4h.u, 12 h.u, and 24 h.u) using the R package ClusterProfiler and visualized in a dot plot. Based on the differential expression analysis, genes with significant upregulation in at least two consecutive time points were selected and ranked according to their FC at each timepoint. Normalized and z-scaled expression values of the union of the top 25 genes for each comparison were visualized in a heatmap. Furthermore, enrichment analysis on the FcMR-specific DE genes for each time point was performed based on 49 previously defined, stimulus-specific macrophage expression signatures encompassing 28 different immunological stimuli, using ClusterProfiler's 'enricher' function. Significantly enriched

signatures were visualized in a dot plot and normalized and z-scaled expression values of the genes to the enriched signatures were plotted in a heatmap. To identify transcriptional regulators responsible for the FcMR-induced changes in gene expression, transcription factor motif enrichment analyses was performed using ClusterProfiler's 'enricher' function based on the MSigDB motif gene sets on the FcMR-specific DE genes for each time point. Motifs with q-value < 0.1 were selected and results were visualized in networks showing the enriched TF motifs and their potential targets among the DE genes of the respective comparison using Cytoscape v3.4.0. For determination of the *Cd45* transcript variant expressed in the cells of this data set, reads were aligned to the reference genome mm10 using Hisat2 v2.1.0 (4) and visualized using the R package Gviz (5). For additional analysis of the NF-κB pathway, we downloaded a comprehensive list of NF-κB target genes from *https://www.bu.edu/nf-kb/gene-resources/target-genes/* and matched the human genes with their murine orthologs. The curated NF-κB target gene list can be found as Dataset S1. Intersecting the resulting list of 417 murine NF-κB target genes with the set of genes detected in our bulk RNA-seq experiment revealed the presence of 351 genes in our data set, of which 118 genes were significantly DE on at least one time point comparing the FcMR-treated cells with controls. Normalized and z-scaled expression values of the 351 present NF-κB target genes were visualized in a heatmap. In addition, fold changes and mean expression values of the significantly DE genes comparing the FcMR-treated cells with controls at the respective time points were visualized in MA plots with colored dots indicating NF-κB targets among the sets of DE genes.

ChIP-qPCR

Bone marrow-derived macrophages were stimulated with 10 μg/ml FcMR or isotype control for 1 h prior to stimulation with 200 ng/ml LPS for another 90 min. Cell fixation, chromatin isolation and ChIP was performed as described previously (6). Briefly, cells were fixed in 1% methanol-free formaldehyde for 5 min at RT, followed by blocking in 125 mM glycine. Nuclei were isolated by NEXSON and chromatin preparation was done using a Covaris S220 focused ultrasonicator (Peak Power: 75 W; Duty factor: 2%; Cycles/burst: 200; 8 min and Peak Power: 140 W; Duty factor: 5%; Cycles/burst: 200; 20 min, respectively). Chromatin preparation was incubated overnight at 4 °C with anti-p65 (clone D14E12, Cell Signaling) or isotype control (rabbit IgG, 31235, Thermo Scientific), followed by incubation for 2 h with Dynabeads (10003D, Thermo Scientific). Samples were eluted by 50 mM glycine pH 2.8 and decrosslinked with Proteinase K and RNase A for 30 min at 37°C and overnight at 65°C. DNA was purified by NucleoSpin Gel and PCR Clean-up Kit (740609.250, Macherey-

Nagel). qPCR was performed with Absolute qPCR Mix (AB1162B, Thermo Scientific) on a CFX96 Real-Time System (BioRad) using 5'-GAGGCTCCGTGGAAAACTCACTTG-3' and 5'-GCAGAGCAGCTTGAGAGTTGGGAA-3' (TNF promoter region 1) and 5'-CAGTTCTCAGGGTCCTATACAACACA-3' and 5'-GGTAGTGGCCCTACACCTCT GTC-3' (TNF promoter region 2) as primers.

Human samples

Serum samples from twenty-six healthy, weight-stable, nonsmoking Caucasian volunteer subjects, 12 lean (2 males, 10 females, BMI 23.3 +/- 0.5 kg/m^2) and 14 obese (2 males, 12 females, BMI 35.2 +/- 1.2 kg/m^2), this latter before and after weight loss, were collected in the framework of a clinical trial (7) and used to measure circulating sMR in a subset of still available samples. This study (Clinical Trial Registration No. NTR2401) was approved by the Medical Ethics Committee of the Leiden University Medical Centre and performed in accordance with the principles of the revised Declaration of Helsinki. All volunteers gave written informed consent before participation.

Plasma analysis

Blood samples were collected from the tail tip of 4 h-fasted mice using chilled paraoxon-coated capillaries. sMR serum levels were determined after immune precipitation using a MR-specific antibody, followed by fluorimetry. Blood glucose levels were determined using a Glucometer (Accu-Check, Roche Diagnostics). Plasma total cholesterol (TC; Instruchemie), triglycerides (TG; Instruchemie) and insulin (Chrystal Chem) were determined using commercially available kits according to the manufacturer's instructions. The homeostatic model assessment of insulin resistance (HOMA-IR) adapted to mice was calculated as ([glucose (mg/dl)*0.055] × [insulin (ng/ml) × 172.1])/3857 and used as a surrogate measure of whole-body insulin resistance (8). Plasma alanine aminotransferase (ALAT) was measured using a Reflotron® kit (Roche diagnostics).

Body composition and indirect calorimetry

Body composition was measured by MRI using an EchoMRI (Echo Medical Systems). Groups of 6-8 mice with free access to food and water were subjected to individual indirect calorimetric measurements at 16 weeks after the start of diet feeding for a period of 5 consecutive days using a Comprehensive Laboratory Animal Monitoring System (Columbus Instruments). Before the start of the measurements, the animals were acclimated to the cages and the single housing for a period of 48 h. Feeding behavior was assessed by real-time

food intake. Spontaneous locomotor activity was determined by the measurement of beam breaks. Oxygen consumption and carbon dioxide production were measured at 15 min intervals. Energy expenditure and carbohydrate and fatty acid oxidation were calculated and normalized for body surface area ($kg^{0.75}$), as previously described (9). The adipocyte number per fat pad and mean adipocyte volume were determined as previously described (10).

Insulin and glucose tolerance tests

Whole-body insulin sensitivity was assessed after the indicated time on CD or HFD in 4 h fasted mice by an i.p. insulin tolerance test (ipITT). After an initial blood collection (t=0), an i.p. bolus of insulin (1 U/kg lean body mass; NOVORAPID, Novo Nordisk) was administered to the mice. Blood glucose was measured by tail bleeding at indicated time points after insulin administration using a Glucometer. Whole-body glucose tolerance was assessed after the indicated time on CD or HFD in 6 h fasted mice by an intraperitoneal glucose tolerance test (ipGTT). After an initial blood collection (t=0), an i.p. injection of glucose (2g D-Glucose/kg total body weight, Sigma-Aldrich) was administered in conscious mice. Blood glucose was measured by tail bleeding at indicated time points after glucose administration using a Glucometer (Accu-Check, Roche Diagnostics). At 15 minutes, blood was also collected for analysis of plasma insulin levels as described above.

Histological analyses

A piece of eWAT or liver (~30 mg) was fixed in 4% paraformaldehyde (PFA; Sigma-Aldrich), paraffin-embedded, sectioned at 4 μm and stained with Hematoxylin and Eosin (H&E). Six fields at 20x magnification (total area 1.68 mm^2) were used for the analysis of crown-like structures and hepatic steatosis.

Hepatic lipid composition

Liver lipids were extracted as previously described (11). Briefly, liver samples (~50 mg) were homogenized in ice-cold methanol. After centrifugation, lipids were extracted with CH_3OH:$CHCl_3$ (1:3 v/v), followed by phase separation with centrifugation (13,000 x g; 15 min at RT). The organic phase was dried and dissolved in 2% Triton X-100 in water. Triglycerides (TG), total cholesterol (TC) and phospholipids (PL) concentrations were measured using commercial kits (Roche Molecular Biochemicals). Liver lipids were expressed as nanomoles per mg protein, which was determined using the Bradford protein assay kit (Sigma-Aldrich).

RNA purification and qRT-PCR

RNA was extracted from snap-frozen tissue samples using Tripure RNA Isolation reagent (Roche Diagnostics). Total RNA (1 μg) was reverse transcribed and quantitative real-time PCR was next performed with the SYBR Green Core Kit on a MyIQ thermal cycler (Bio-Rad). mRNA expression was normalized to *Rplp0* mRNA content and expressed as fold change compared to wild-type CD-fed mice using the ΔΔCT method. Primers are listed in Supplementary Table 2.

Isolation of stromal vascular fraction from adipose tissue

Epididymal adipose tissues were collected in PBS, then minced and digested for 1 h at 37°C in HEPES-buffered Krebs solution (pH 7.4) containing 0.5 mg/mL collagenase type I from *Clostridium histolyticum* (Sigma-Aldrich), 2% (w/v) bovine serum albumin (BSA, fraction V, Sigma-Aldrich) and 6 mM glucose, as previously described (12). Disaggregated adipose tissues were passed through 100 μm cell strainers or 200 μm filters and washed with PBS supplemented with 2.5 mM EDTA and 5% FCS. Filtrate was either directly centrifuged (350 x *g*, 10 min at RT) or rested for 10 minutes, after which infranatant was collected and centrifuged. After centrifugation, the supernatant was discarded and the pellet containing the stromal vascular fraction (SVF) was treated with erythrocyte lysis buffer (BD Biosciences). After washing, cells were either directly counted, or macrophages were isolated using LS columns and F4/80 microbeads according to the manufacturer's protocol. Cells were next stained with the live/dead marker Aqua or Zombie-UV (Invitrogen), fixed with 1.9% paraformaldehyde (Sigma-Aldrich) and stored in FACS buffer (PBS, 2 mM EDTA, 0.5% BSA [w/v]) at 4°C in the dark until subsequent analysis performed within 4 days.

Isolation of leukocytes from liver tissue

Livers were collected in ice-cold RPMI 1640 + Glutamax (Life Technologies), minced and digested for 45 min at 37°C in RPMI 1640 + Glutamax supplemented with 1 mg/mL collagenase type IV from *Clostridium histolyticum*, 2000 U/mL DNase (both Sigma-Aldrich) and 1 mM $CaCl_2$, as previously described (12). In short, the digested tissues were next passed through 100 μm cell strainers and washed with PBS/EDTA/FCS. Following centrifugation (530 x g, 10 min at 4 °C), the cell pellet was resuspended in PBS/EDTA/FCS and centrifuged at 50 x g to pellet hepatocytes (3 minutes at 4 °C). The supernatant was next collected and pelleted (530 x g, 10 min at 4 °C), followed by treatment with erythrocyte lysis buffer. After washing, either macrophages or total leukocytes were isolated using LS columns and F4/80 or CD45 MicroBeads (35 μl beads per liver; Miltenyi Biotec),

respectively, according to the manufacturer's protocol. Isolated $CD45^+$ cells were counted and processed for flow cytometry as for SVF, and $F4/80^+$ cells were stimulated with FcMR and LPS as described above.

Isolation of peritoneal macrophages

Peritoneal wash was collected in PBS supplemented with 2 mM EDTA and centrifuged (530 x g, 10 min at 4°C). Cell pellet was treated with erythrocyte lysis buffer, counted and processed for flow cytometry as for SVF, or macrophages were isolated using MS columns and F4/80 microbeads according to the manufacturer's protocol.

Isolation of splenic macrophages

Spleens were collected in ice-cold RPMI 1640 + Glutamax, minced and digested for 20 min at 37°C in RPMI 1640 + Glutamax supplemented with 1 mg/mL collagenase D (Sigma) and 2000 U/mL DNase. The digested tissues were next passed through 100 µm cell strainers and washed with PBS/EDTA/FCS. Following centrifugation (530 x g, 10 min at 4°C), the cell pellet was treated with erythrocyte lysis buffer. Cells were either counted and processed for flow cytometry as for SVF, or macrophages were isolated using MS columns and F4/80 microbeads according to the manufacturer's protocol.

Flow cytometry

For analysis of myeloid subsets, part of the cells was first permeabilized with 0.5% saponin (Sigma-Aldrich) or eBioscience permeabilization buffer (Invitrogen) and stained with an antibody against YM1 conjugated to biotin prior to staining with an antibody cocktail including streptavidin-PerCP. Cells were either next or directly stained with antibodies directed against CD11b, CD11c, CD45, CD45.2, CD45RA, CD45RB, CD45RC, CD64, F4/80, Ly6C, and Siglec-F in either 0.5% saponin, permeabilization, or FACS buffer. For assessing MR-expressing cells in obesity, samples were additionally incubated with antibodies specific for CD31, CD146, and MR. For analysis of lymphocyte subsets, cells were stained with antibodies directed against B220, CD3e, CD11b, CD11c, GR-1, NK1.1 (all for lineage cocktail), CD4, CD8a, CD19, IL-13, and Thy1.2. For detection of intracellular cytokines, isolated immune cells were first *ex vivo* cultured for 4 hours in culture medium in the presence of 100 ng/mL phorbol myristate acetate (PMA), 1 µg/ml ionomycin and 10 µg/ml Brefeldin A (all from Sigma-Aldrich) prior to viability staining and fixation. Cells were measured on a FACSCanto flow cytometer or LSR-II (both BD Biosciences), and gates were set according to Fluorescence Minus One (FMO) controls. Gating strategies can be

found in Supplementary Figure 9. The source and information on antibodies used for flow cytometry are listed in Supplementary Table 1.

Extracellular flux analysis

Extracellular Flux Analysis was performed as described before (13). Briefly, BMDMs or human moM's were incubated with FcMR or isotype control (18h) or rhMR (5h) respectively and settled in RPMI-1640 (Sigma; pH = 7.4) supplemented with 5% FCS on a 96-well assay plate (Agilent) and rested at 37°C in 0% CO_2 for 1 hour. Extracellular acidification rate (ECAR) was recorded with the XF96e Extracellular Flux analyzer (Agilent) in response to glucose (10 mM; Sigma) and oligomycin (1.5 μM; Cayman Chemical) injection.

Supplementary references

1. Hussaarts L, Smits HH, Schramm G, van der Ham AJ, van der Zon GC, Haas H, et al. Rapamycin and omega-1: mTOR-dependent and -independent Th2 skewing by human dendritic cells. Immunol Cell Biol. 2013;91(7):486-9.
2. Soneson C, Love MI, Robinson MD. Differential analyses for RNA-seq: transcript-level estimates improve gene-level inferences. F1000Res. 2015;4:1521.
3. Love MI, Huber W, Anders S. Moderated estimation of fold change and dispersion for RNA-seq data with DESeq2. Genome Biol. 2014;15(12):550.
4. Kim D, Paggi JM, Park C, Bennett C, Salzberg SL. Graph-based genome alignment and genotyping with HISAT2 and HISAT-genotype. Nat Biotechnol. 2019;37(8):907-15.
5. Hahne F, Ivanek R. Visualizing Genomic Data Using Gviz and Bioconductor. Methods Mol Biol. 2016;1418:335-51.
6. Arrigoni L, Richter AS, Betancourt E, Bruder K, Diehl S, Manke T, et al. Standardizing chromatin research: a simple and universal method for ChIP-seq. Nucleic Acids Res. 2016;44(7):e67.
7. Wijngaarden MA, van der Zon GC, van Dijk KW, Pijl H, Guigas B. Effects of prolonged fasting on AMPK signaling, gene expression, and mitochondrial respiratory chain content in skeletal muscle from lean and obese individuals. Am J Physiol Endocrinol Metab. 2013;304(9):E1012-21.
8. Lee S, Muniyappa R, Yan X, Chen H, Yue LQ, Hong EG, et al. Comparison between surrogate indexes of insulin sensitivity and resistance and hyperinsulinemic euglycemic clamp estimates in mice. Am J Physiol Endocrinol Metab. 2008;294(2):E261-70.
9. Hussaarts L, Garcia-Tardon N, van Beek L, Heemskerk MM, Haeberlein S, van der Zon GC, et al. Chronic helminth infection and helminth-derived egg antigens promote adipose tissue M2 macrophages and improve insulin sensitivity in obese mice. FASEB J. 2015;29(7):3027-39.
10. van Beek L, Vroegrijk IO, Katiraei S, Heemskerk MM, van Dam AD, Kooijman S, et al. FcRgamma-chain deficiency reduces the development of diet-induced obesity. Obesity (Silver Spring). 2015;23(12):2435-44.
11. Geerling JJ, Boon MR, van der Zon GC, van den Berg SA, van den Hoek AM, Lombes M, et al. Metformin lowers plasma triglycerides by promoting VLDL-triglyceride clearance by brown adipose tissue in mice. Diabetes. 2014;63(3):880-91.
12. van der Zande HJP, Gonzalez MA, de Ruiter K, Wilbers RHP, Garcia-Tardon N, van Huizen M, et al. The helminth glycoprotein omega-1 improves metabolic homeostasis in obese mice through type 2 immunity-independent inhibition of food intake. FASEB J. 2021;35(2):e21331.
13. Pelgrom LR, van der Ham AJ, Everts B. Analysis of TLR-Induced Metabolic Changes in Dendritic Cells Using the Seahorse XF(e)96 Extracellular Flux Analyzer. Methods Mol Biol. 2016;1390:273-85.

Supplementary information

Supplementary Table 1. FACS antibodies.

Target	Clone	Conjugate	Source	Identifier
B220	RA3-6B2	FITC	eBioscience	11-0452
B220	RA3-6B2	eF450	eBioscience	48-0452
CD3e	17A2	APC	eBioscience	17-0032
CD3e	17A2	FITC	eBioscience	11-0032
CD4	GK1.5	PE-Cy7	eBioscience	25-0041
CD4	GK1.5	PerCP-eF710	eBioscience	46-0041
CD8a	53-6.7	APC-Cy7	Biolegend	100714
CD11b	M1/70	FITC	eBioscience	11-0112
CD11b	M1/70	PE-Cy7	eBioscience	25-0112
CD11c	HL3	FITC	BD Biosciences	553801
CD11c	HL3	V450	BD Biosciences	560521
CD19	eBio1D3	eF450	eBioscience	48-0193
CD31	MEC 13.3	FITC	BD Biosciences	561813
CD45	30-F11	BV785	Biolegend	103149
CD45.2	104	FITC	Biolegend	109806
CD45RA	RA3-6B2	Pacific Blue	Biolegend	103230
CD45RB	16A	FITC	BD Biosciences	553099
CD45RC	DNL-1.9	PE	BD Biosciences	557357
CD64	X54-5/7.1	PE	Biolegend	139304
CD146	ME-9F1	PE-Cy7	Biolegend	134713
CD206/MR	MR5D3	APC	Bio-Rad	MCA2235
F4/80	BM8	APC	eBioscience	17-4801
F4/80	BM8	BV711	Biolegend	123147
GR-1	RB6-8C5	FITC	BD Biosciences	553126
IL-13	eBio13A	eF450	eBioscience	48-7133
Ly6C	HK1.4	APC-Cy7	Biolegend	128025
NK1.1	PK136	FITC	eBioscience	11-5941
Siglec-F	E50-2440	BV605	BD Biosciences	740388
Siglec-F	E50-2440	PE	BD Biosciences	552126
Thy1.2	30-H12	APC-eF780	eBioscience	47-0902
YM1	Polyclonal	Biotin	R&D Systems	BAF2446
Other reagents			**Source**	**Identifier**
LIVE/DEAD™ Fixable Aqua Dead Cell Stain Kit			Invitrogen	L34957
Zombie UV™ Fixable Viability Kit			Biolegend	423107
Streptavidin - PerCP			BD Biosciences	554064

Supplementary Table 2. qPCR primers.

Gene	Accession number	Forward primer	Reverse primer
Acaca	NM_133360.2	CAGCTGGTGCAGAGGTACCG	TCTACTCCGCAGGTACTGCCG
Acadm	NM_007382	TACCCGTTCCCTCTCATCAA	CACCCATACGCCAACTCTTC
Acox1	NM_015729	GGGACCCACAAGCCTCTGCCA	GTGCCGTCAGGCTTCACCTGG
Adipoq	NM_009605	GGAATGACAGGAGCTGAAGG	CGAATGGGTACATTGGGAAC
Ccl2	NM_011333.3	TCAGCCAGATGCAGTTAACGCCC	GCTTCTTTGGGACACCTGCTGCT
Cd36	NM_001159558	GCAAAGAACAGCAGCAAAATC	CAGTGAAGGCTCAAAGATGG
Cebpa	NM_007678.3	TGCCGGGAGAACTCTAACTC	CTCTGGAGGTGACTGCTCAT
Cidea	NM_007702	CTCGGCTGTCTCAATGTCAA	CCGCATAGACCAGGAACTGT
Cidec	NM_178373	CCATCAGAACAGCGCAAGAAG	AGAGGGTTGCCTTCACGTTC
Cox8b	NM_007751.3	GACCCCGAGAATCATGCCAA	CCTGCTCCACGGCGGAA
Cpt1a	NM_013495	AGGAGACAAGAACCCCAACA	AAGGAATGCAGGTCCACATC
Dlk1	NM_010052.5	GTACCCCTAACCCATGCGAG	TGCACAGACACTCGAAGCTC
Fabp1	NM_017399.4	GCCACCATGAACTTCTCCGGCA	GGTCCTCGGGCAGACCTATTGC
Fasn	NM_007988	CACAGGCATCAATGTCAACC	TTTGGGAAGTCCTCAGCAAC
Infg	NM_008337	CGGCACAGTCATTGAAAGCC	TGTCACCATCCTTTTGCCAGT
Il1b	NM_008361	GACCCCAAAAGATGAAGGGCT	ATGTGCTGCTGCGAGATTTG
Il4	NM_021283	CCTCACAGCAACGAAGAACA	ATCGAAAAGCCCGAAAGAGT
Il6	NM_031168.1	TGTGCAATGGCAATTCTGAT	CTCTGAAGGACTCTGGCTTTG
Il10	NM_010548	GACAACATACTGCTAACCGACTC	ATCACTCTTCACCTGCTCCACT
Il12a	NM_001159424	GGTGAAGACGGCCAGAGAAA	GTAGCCAGGCAACTCTCGTT
Il17a	NM_010552	TCATCCCTCAAAGCTCAGCG	TTCATTGCGGTGGAGAGTCC
Itgax	NM_021334.2	GCCACCAACCCTTCCTGGCTG	TTGGACACTCCTGCTGTGCAGTTG
Lep	NM_008493	CCCTGTGTCGGTTCCTGTGGC	GCGGATACCGACTGCGTGTGT
Mrc1	NM_008625.2	TTCAGCTATTGGACGCGAGG	GAATCTGACACCCAGCGGAA
Pparg	NM_011146	TACATAAAGTCCTTCCCGCTGAC	GTGATTTGTCCGTTGTCTTTCCT
Ppargc1a	NM_008904.2	CCCAGAGTCACCAAATGACCCCA	CCTCTTGGTTGGCGGTGGCA
Rplp0	NM_007475	TCTGGAGGGTGTCCGCAACG	GCCAGGACGCGCTTGTACCC
Ly6a/Sca1	NM_001271416.1	TGCCCATCAATTACCTGCCC	TTGAGAATCCACAATAACTGCTGC
Scd1	NM_009127.4	GCTCTACACCTGCCTCTTCGGGAT	TCCAGAGGCGATGAGCCCCG
Tbx1	NM_011532.2	CAAGGCAGGCAGACGAATGT	TACCGGTAGCGCTTGTCATC
Tgfb1	NM_011577	GCTGAACCAAGGAGACGGAA	ATGTCATGGATGGTGCCCAG
Tnf	NM_013693	GTCCCCAAAGGGATGAGAAG	CACTTGGTGGTTTGCTACGA
Tnfrsf9	NM_011612.2	GGAGCTAACGAAGCAGGGTT	CGTCTAGAGAGCAGTTCGTCC
Ucp1	NM_009463	TCAGGATTGGCCTCTACGAC	TGCATTCTGACCTTCACGAC

Dataset S1. NF-κB-targeted genes regulated by sMR.
https://www.pnas.org/doi/suppl/10.1073/pnas.2103304118/suppl_file/pnas.2103304118.sd01.xlsx

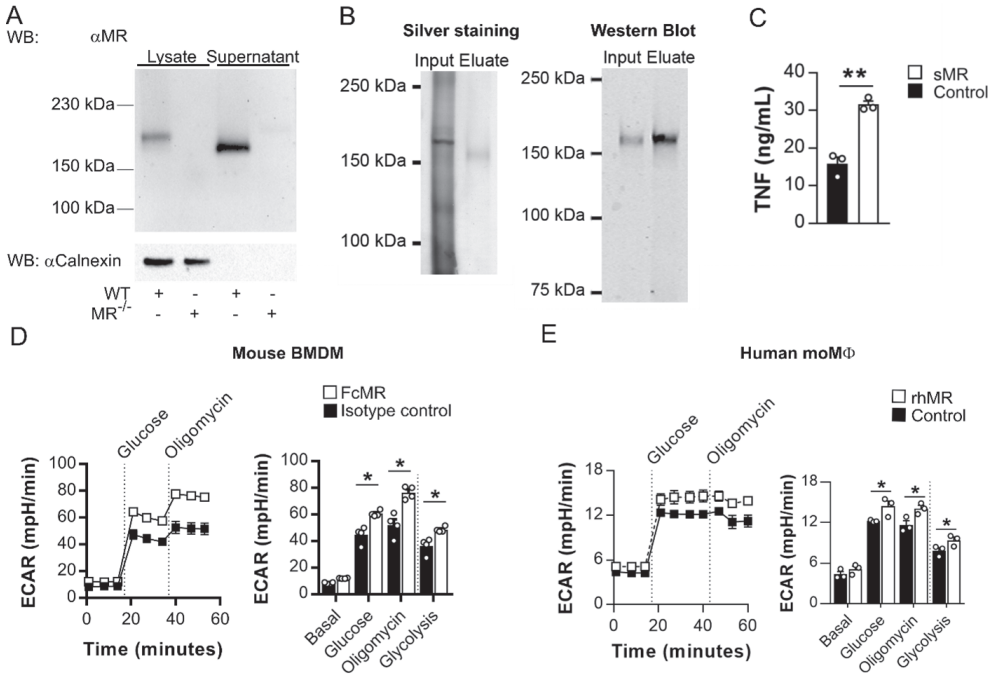

Supplementary Figure 1. Purification of sMR from the supernatant of MR-expressing cells and its effect on cytokine secretion. (**A**) The presence of the MR in the cell lysates or supernatant from wild-type or MR-deficient macrophages was determined by Western blot. (**B**) sMR was purified by affinity chromatography using a Protein A/G column covalently linked to an MR-specific antibody. Images depict silver staining (left) and Western blot using a MR-specific antibody (right). (**C**) MR-deficient macrophages were treated with purified sMR (30 ng/mL) and stimulated with LPS. Secretion of TNF was determined after 18 h by ELISA. (**D-E**) Real-time glycolysis in FcMR or isotype control-treated mouse macrophages (*D*) or recombinant human MR-treated human monocyte-derived macrophages (*E*) as measured through extracellular acidification rate (ECAR). Cells were pre-incubated in glucose-free medium (basal), followed by sequential addition of glucose and oligomycin. Glycolysis is calculated as the increase in ECAR in response to glucose ([ECAR Glucose] – [ECAR Basal]). All graphs are depicted as mean ± SEM; for all experiments, n ≥ 3. **P* <0.05.

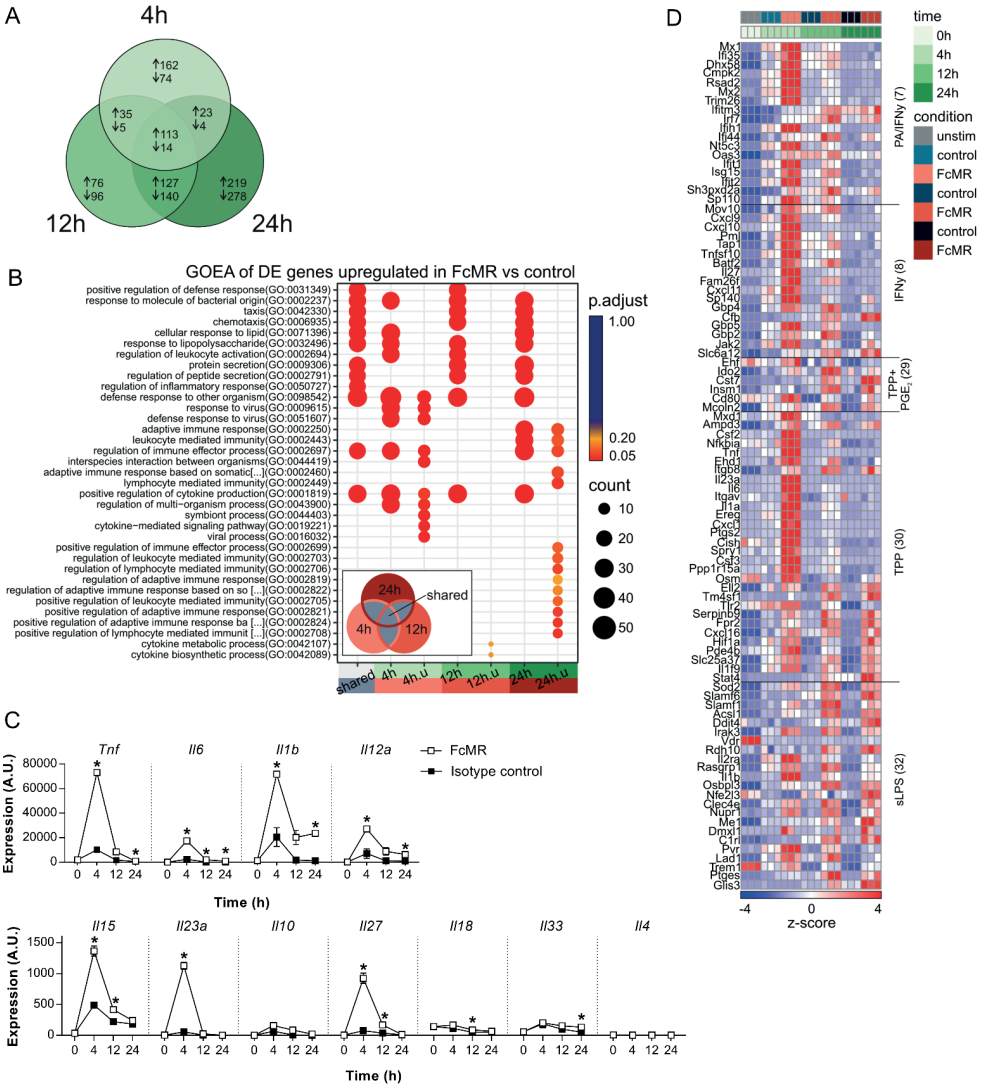

Supplementary Figure 2. RNAseq analysis of bone marrow-derived macrophages incubated with FcMR or isotype control for 4, 12, or 24h. (**A**) Venn diagram of 1,366 DE genes in FcMR-treated versus control samples. (**B**) Dot plot of gene ontology enrichment analysis (GOEA) results of the DE genes shared between all three DE gene sets (shared), the respective DE gene sets for each time point (4 h, 12 h, and 24 h) and those DE genes unique for each time point (4 h.u, 12 h.u, and 24 h.u). (**C**) Expression of indicated cytokines after treatment with FcMR or isotype control as measured by RNAseq. (**D**) Heatmap of hierarchically clustered, normalized and z-scaled expression values of the genes corresponding to the enriched stimulus-specific macrophage expression signatures shown in Figure 2E. *P <0.05.

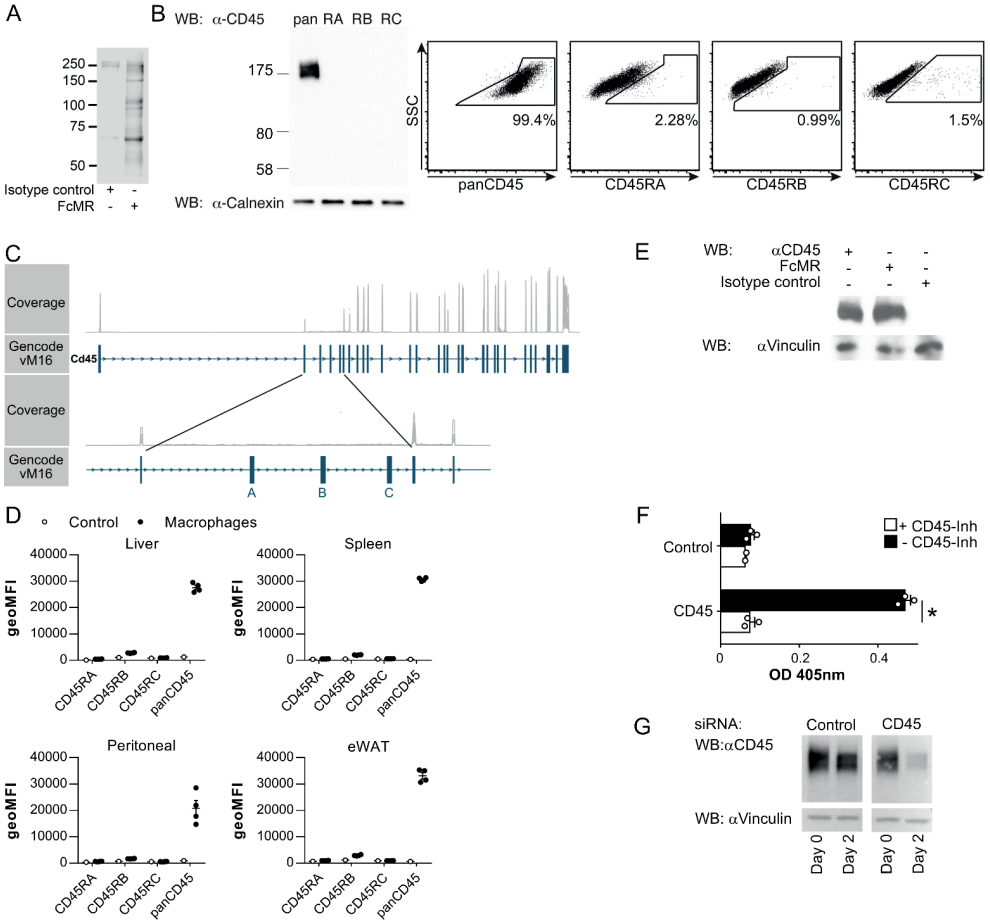

Supplementary Figure 3. Inhibition of CD45 by the MR. (**A**) Lysates from surface biotinylated macrophages were immune precipitated with FcMR or isotype control and analyzed by Western blot using neutravidin. (**B**) CD45 isoforms on bone marrow-derived macrophages (BMDMs) analyzed by Western blot and flow cytometry. (**C**) Visualization of the RNAseq read coverage of the murine *Cd45* locus. (**D**) Analysis of CD45 isoforms on macrophages from spleen, liver, white adipose tissue (WAT) and the peritoneal cavity (PEC) by flow cytometry. Open circles indicate fluorescence minus one (FMO) controls. (**E**) F4/80^{+} splenic macrophages were isolated by magnetic separation. Cell lysates were analyzed by far Western blot after staining with FcMR or isotype control or by Western blot with antibodies against CD45 and vinculin. (**F**) CD45 was immune precipitated from cell lysates from BMDMs and incubated with 4-NPP in the presence or absence of the CD45 inhibitor SF1670. Graph depicts dephosphorylation of 4-NPP. Samples without CD45 antibody were used as controls. (**G**) siRNA-mediated down-regulation of CD45. All graphs are depicted as mean ± SEM; for all experiments, n ≥ 3. *P <0.05.

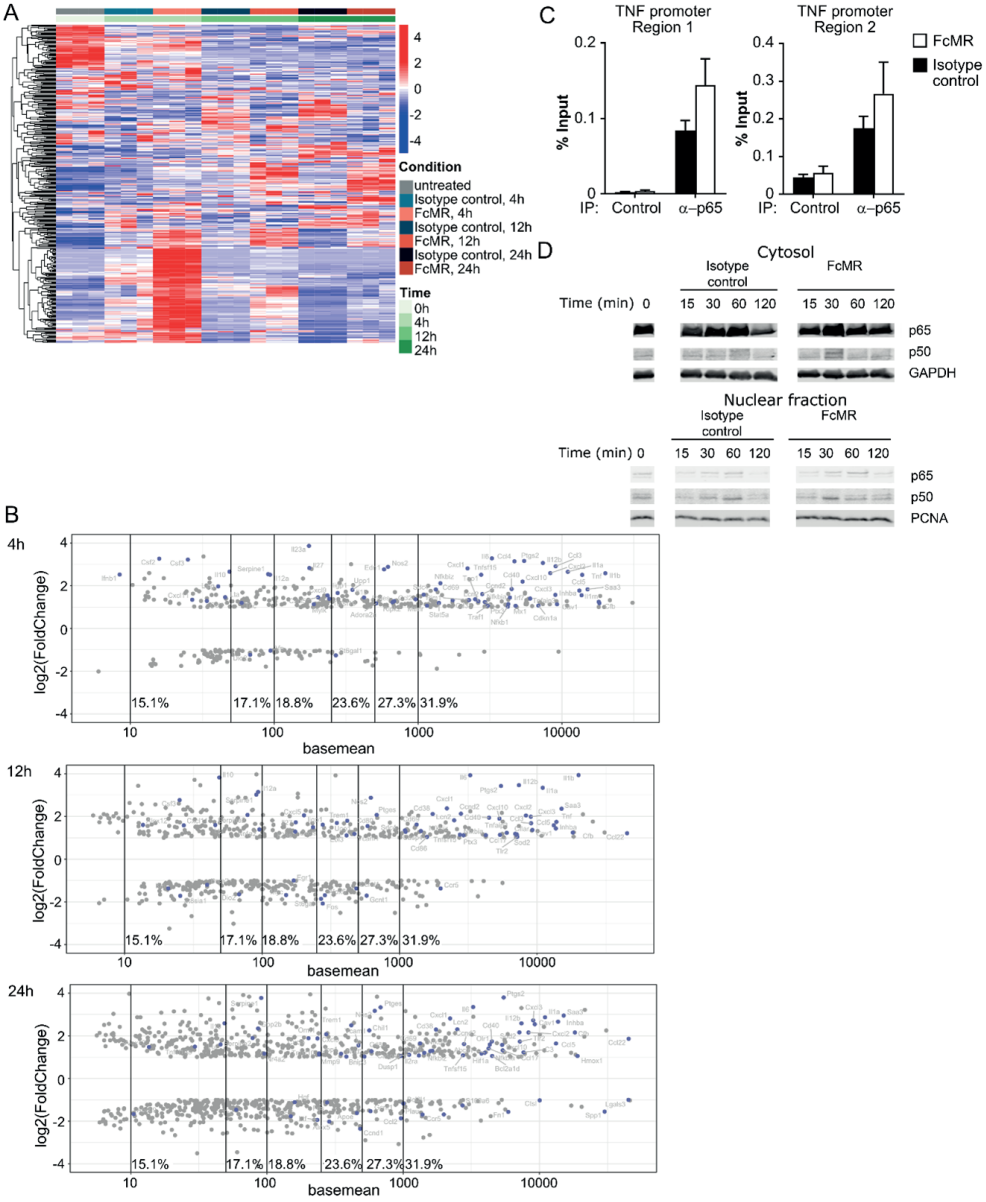

Supplementary Figure 4. Regulation of NF-κB target genes by FcMR. (**A**) Normalized and z-scaled expression values of 351 NF-κB target genes present in our data set across time and treatments. 118 genes were significantly differentially expressed at least one time point comparing the FcMR-treated cells with controls. (**B**) MA plots showing fold changes and mean expression values (BaseMean) of significantly differentially expressed genes comparing the FcMR-treated cells with controls at the respective time point. Blue dots indicate NF-κB target genes. Numbers indicate the percentage of NF-κB target genes amongst all

◀Supplementary Figure 4. Legend (Continued)

DE genes that display a BaseMean value of at least 10, 50, 100, 250, 500, or 1,000. (**C**) BMDMs were incubated with FcMR or isotype control for 60 min. Recruitment of p65 towards the TNF promoter was monitored by ChIP. (**D**) MR-deficient macrophages were incubated with FcMR or isotype control in the presence of the Akt inhibitor MK-2206 (5 mM). p65 and p50 were determined in the cytosolic and nuclear fraction by Western Blot.

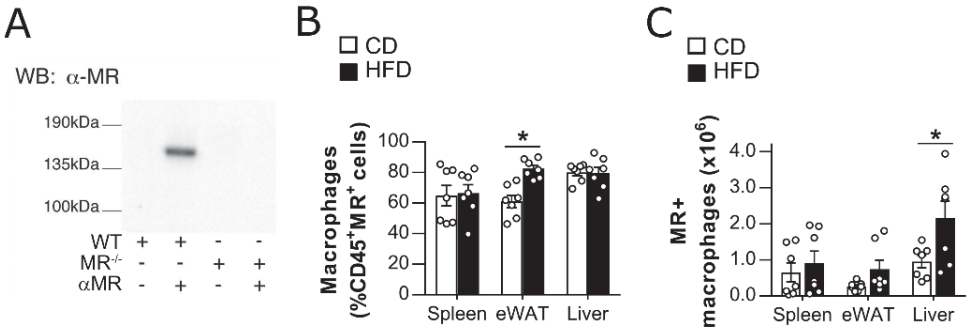

Supplementary Figure 5. MR serum levels and numbers of MR expressing macrophages in metabolic tissues during obesity. (**A**) sMR serum levels from wild-type or MR-deficient mice and depicted by Western blot. (**B**) Percentage of F4/80$^+$CD64$^+$ macrophages within CD45$^+$MR$^+$ cells in indicated tissues of HFD or CD-fed mice. (**C**) Absolute numbers of MR$^+$F4/80$^+$CD64$^+$ macrophages in the indicated tissues. All graphs are depicted as mean ± SEM; n = 6-7 per group. $^*P$ <0.05.

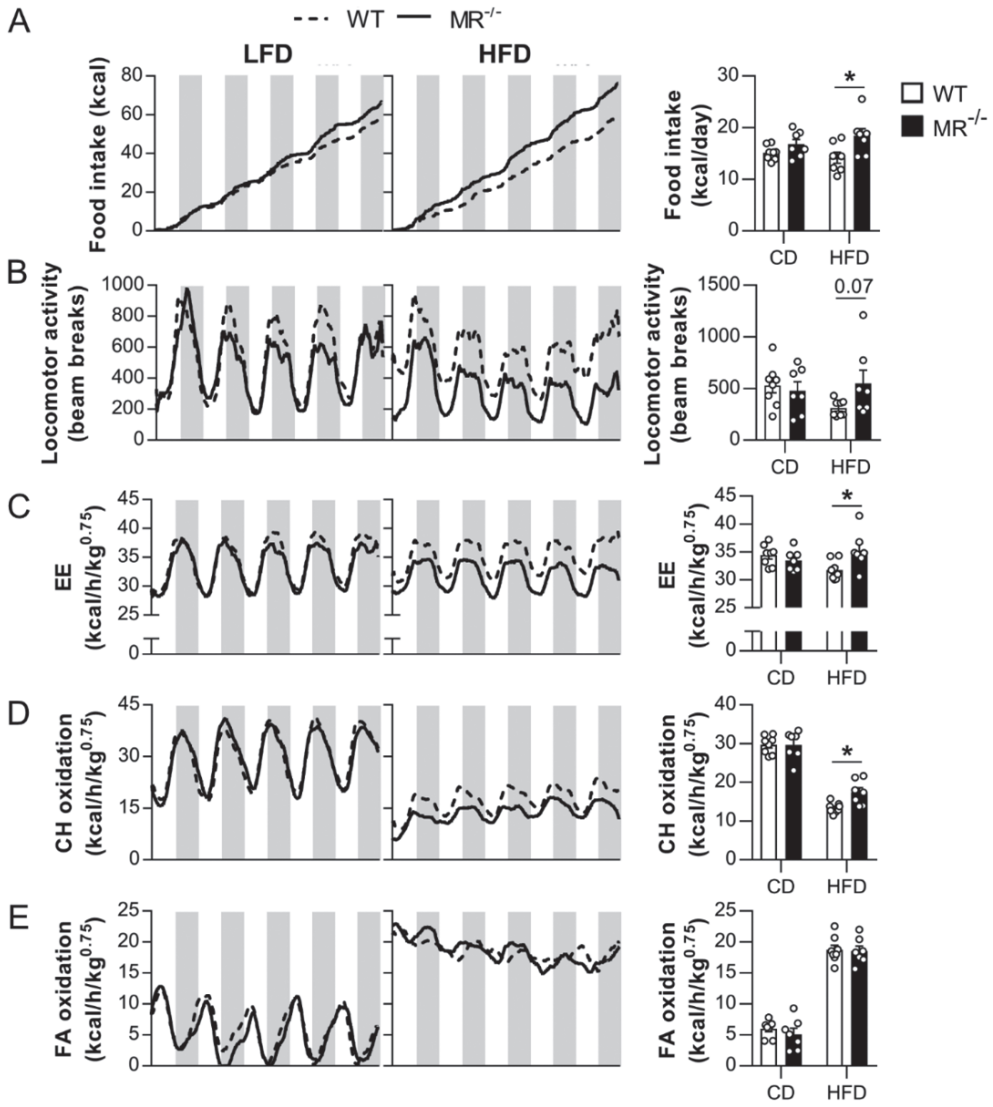

Supplementary Figure 6. MR deficiency counteracts HFD-induced decrease in locomotor activity, whole-body energy expenditure, and carbohydrate oxidation. (**A-E**) Wild-type (WT) and MR-deficient (MR$^{-/-}$) mice were fed either CD or HFD. At week 16, mice were subjected to individual indirect calorimetric measurements using fully automated metabolic cages with free access to food and water. After 48 h acclimatization, cumulative food intake (*A*), spontaneous locomotor activity (*B*), energy expenditure (EE; *C*), carbohydrate (CH; *D*) and fatty acid (FA; *E*) oxidation were measured for 5 consecutive days (white part = light phase; grey part = dark phase). The daily averages for each of the abovementioned parameters were calculated. Results are expressed as means ± SEM; n = 6-8 mice per group. *P <0.05.

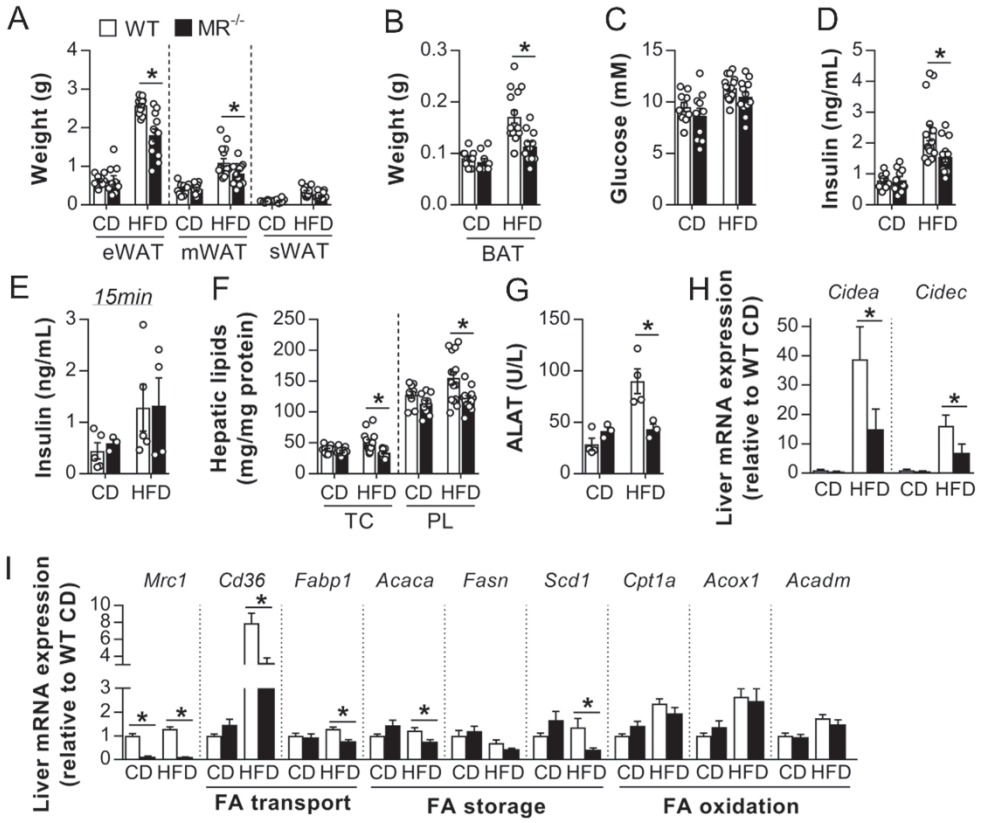

Supplementary Figure 7. MR regulates whole-body metabolic homeostasis. Wild-type and MR$^{-/-}$ mice were fed a CD or HFD for 18 weeks. (**A**) Weight of different white fat pads. (**B**) Weight of intrascapular brown adipose tissue. (**C-D**) Fasting blood glucose and plasma insulin levels. (**E**) Plasma insulin levels at 15 minutes post glucose injection during GTT. (**F**) Liver triglycerides (TG) and phospholipids (PL). (**G**) The plasma concentrations of alanine aminotransferase (ALAT) in pooled samples of 2-3 mice from two separate experiments (3-4 pooled samples per group). (**H**) Hepatic expression of the indicated genes. (**I**) Hepatic expression of the indicated genes. All the RT-qPCR results are expressed as relative to the housekeeping gene *Rplp0* (RPLP0/36B4) as fold change vs WT-CD mice. Results are expressed as means ± SEM; n = 9-16 mice per group, except for E (n = 3-5 per group), G (n = 3-4 mice per group) and H (n = 5 mice per group). **P* <0.05.

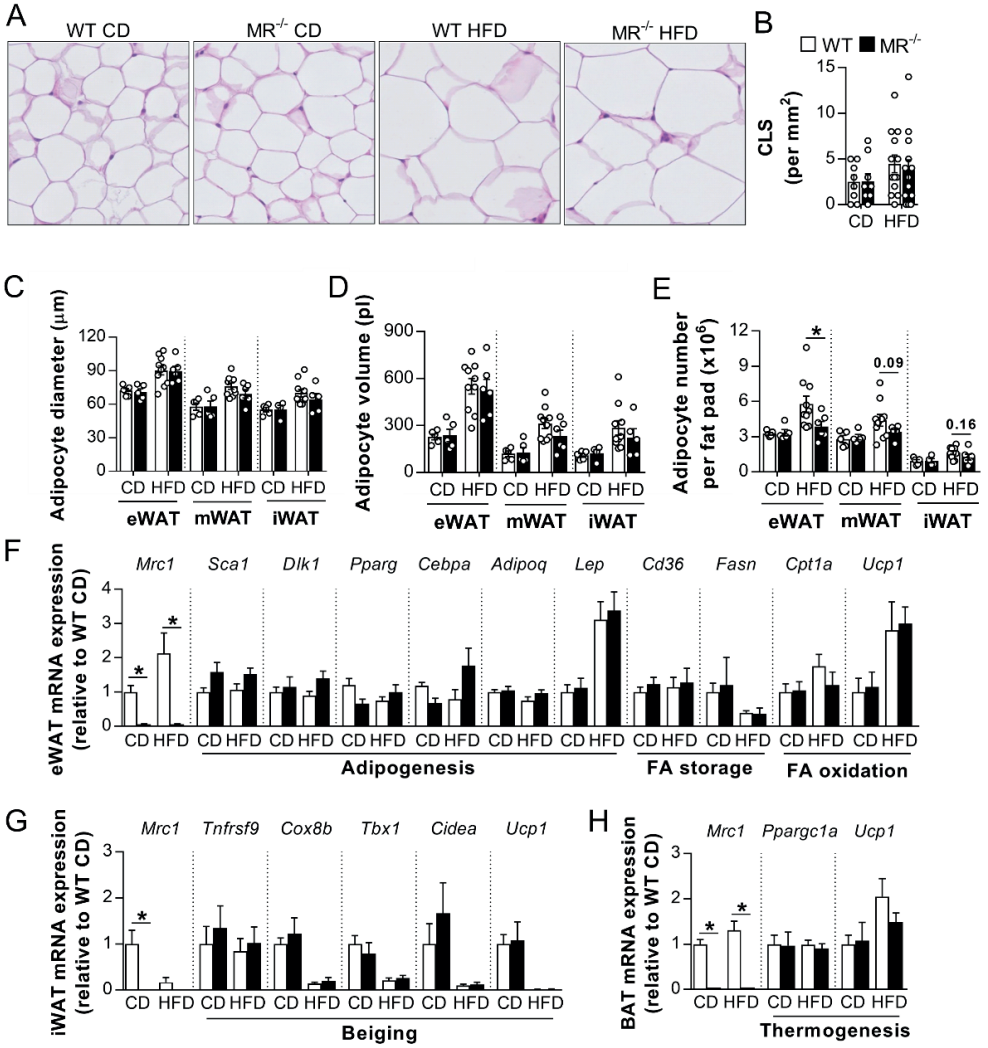

Supplementary Figure 8. MR deficiency did not affect adipocyte hypertrophy, brown adipose tissue thermogenesis, and white adipose tissue beiging. (**A-B**) Wild-type and MR-deficient mice were fed either CD or HFD for 18 weeks. At sacrifice, epididymal white adipose tissues (eWAT) were collected (*A*) and crown-like structures (*B*) were determined. (**C-E**) Adipocyte diameter (*C*), volume (*D*) and number (*E*) per fat pad were determined in eWAT, mesenteric (mWAT) and inguinal adipose tissues (iWAT). (**F**) The mRNA expression of *Mrc1* (MR) and indicated key genes involved in adipocyte physiology were measured by RT-qPCR in eWAT. (**G-H**) The mRNA expression of *Mrc1* and thermogenic (*G*) or beiging (*H*) markers were measured by RT-qPCR in iWAT and BAT, respectively. All the RT-qPCR results are expressed as relative to the housekeeping gene *Rplp0* (RPLP0/36B4) as fold change vs WT-CD mice. Results are expressed as means ± SEM. n = 10-15 mice per group. **P* <0.05.

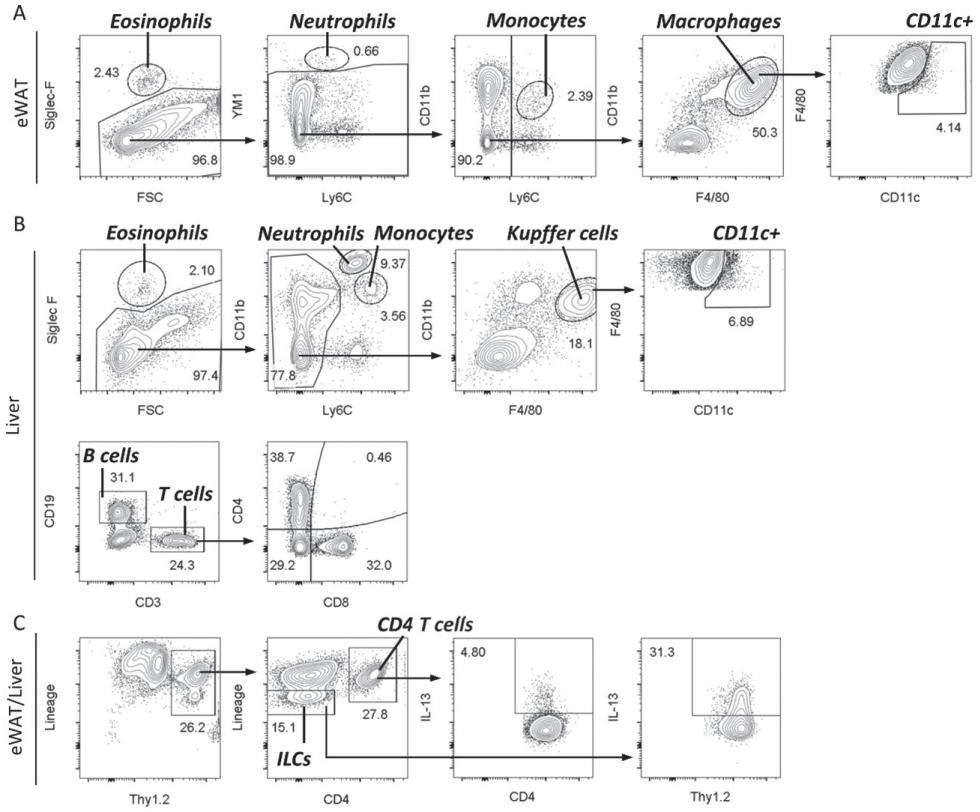

Supplementary Figure 9. Gating strategies. (**A-B**) Gating strategies for indicated cell populations in eWAT (*A*) and liver (*B*). Cells were pre-gated on live, singlet, CD45+ cells. (**C**) Gating strategy for identification of Th2 cells (IL-13$^+$ CD4 T cells) and ILC2s (IL-13$^+$ ILCs) after *ex vivo* restimulation with PMA, ionomycin and Brefeldin A. Example is shown for eWAT sample, but gating strategy is similar for liver samples.

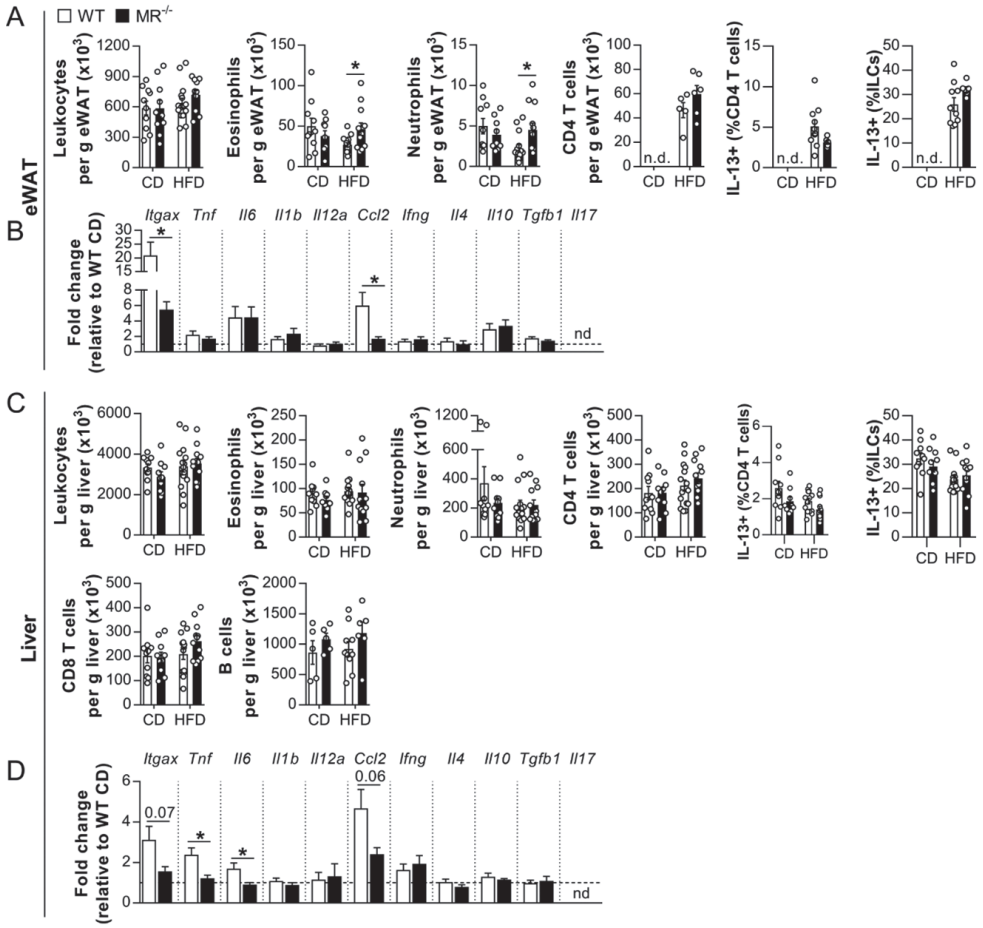

Supplementary Figure 10. Effect of MR deficiency on metabolic tissue immune cells. Wild-type and MR-deficient mice were fed either CD or HFD for 18 weeks. (**A**) Numbers of leukocytes, eosinophils, neutrophils and CD4 T cells per gram tissue, and percentages of IL-13$^+$ CD4 T cells and ILCs in eWAT. (**B**) mRNA expression levels of selected cytokines and activation markers in eWAT after 18 weeks on HFD monitored by RT-qPCR. (**C**) Numbers of leukocytes, eosinophils, neutrophils, CD4 T cells, CD8 T cells and B cells per gram tissue, and percentages of IL-13$^+$ CD4 T cells and ILCs in liver. (**D**) mRNA expression levels of selected cytokines and activation markers in liver after 18 weeks on HFD. All the RT-qPCR results are expressed as relative to the housekeeping gene *Rplp0* (RPLP0/36B4) as fold change vs WT-CD mice. Gating strategies are shown in Supplementary Figure 9. Results are depicted as means ± SEM; n = 10-15 mice per group for all, except eWAT CD4 T cells (n = 5-6 mice per group). **P* <0.05.

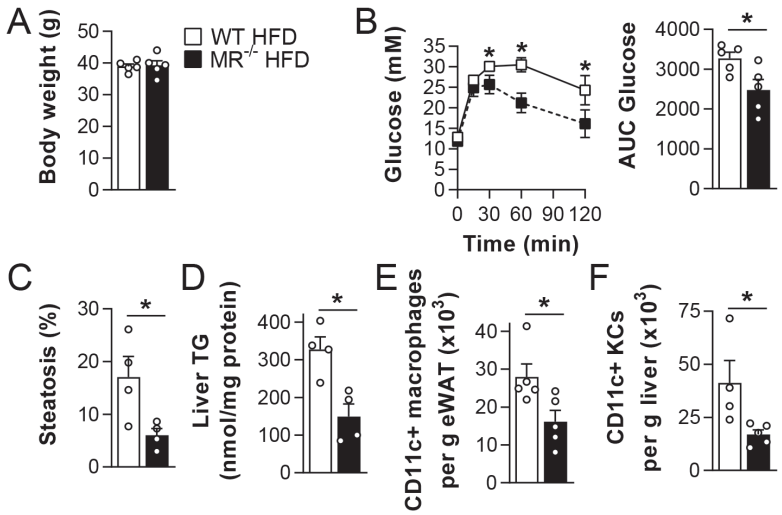

Supplementary Figure 11. MR regulates whole-body metabolic homeostasis and proinflammatory activation of metabolic tissue macrophages independently of changes in body weight in obese mice. (**A**) Wild-type and MR-deficient mice were matched on body weight after 18 weeks on HFD. (**B**) At week 17, an intraperitoneal glucose tolerance test was performed. (**C**) After sacrifice, hepatic steatosis was quantified from H&E-stained slides. (**D**) Liver TG content was measured. (**E-F**) The numbers of CD11c$^+$ macrophages were determined in eWAT (*E*) and liver (*F*). Results are expressed as means ± SEM; (n = 4-5 mice per group). *P <0.05.

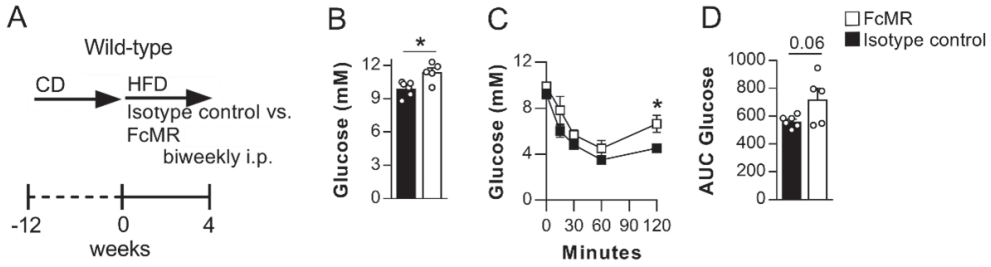

Supplementary Figure 12. sMR treatment regulates whole-body metabolism in HFD-fed mice. (**A**) Wild-type mice were fed a HFD and concomitantly injected i.p. with 4.82 mmoles/mouse FcMR or isotype control every 3 days. (**B-D**) After 4 weeks, fasting blood glucose levels were measured (*B*) and an intraperitoneal insulin tolerance test (*C, D*) was performed. Results are expressed as means ± SEM; n = 6 mice per group. **P* <0.05.

CHAPTER 4

The mannose receptor: from endocytic receptor and biomarker to regulator of (meta)inflammation

Hendrik J.P. van der Zande[#], Dominik Nitsche[#], Laura Schlautmann[#], Bruno Guigas[*], Sven Burgdorf[*]

[#]These authors contributed equally to this study
[*]These authors contributed equally to this study

Frontiers in Immunology. 12:765034. (2021)
PMID: 34721436
doi: 10.3389/fimmu.2021.765034

Abstract

The mannose receptor is a member of the C-type lectin (CLEC) family, which can bind and internalize a variety of endogenous and pathogen-associated ligands. Because of these properties, its role in endocytosis as well as antigen processing and presentation has been studied intensively. Recently, it became clear that the mannose receptor can directly influence the activation of various immune cells. Cell-bound mannose receptor expressed by antigen-presenting cells was indeed shown to drive activated T cells towards a tolerogenic phenotype. On the other hand, serum concentrations of a soluble form of the mannose receptor have been reported to be increased in patients suffering from a variety of inflammatory diseases and to correlate with severity of disease. Interestingly, we recently demonstrated that the soluble mannose receptor directly promotes macrophage proinflammatory activation and trigger metaflammation. In this review, we highlight the role of the mannose receptor and other CLECs in regulating the activation of immune cells and in shaping inflammatory responses.

Introduction

The mannose receptor (MR), also termed CD206, is a member of the C-type lectin (CLEC) family. Members of this family contain C-type lectin domains (CTLDs), which play an important function in ligand recognition. Typically, type I transmembrane CLECs contain multiple CTLDs at their extracellular region, whereas type II membrane CLECs only contain a single CLEC (Figure 1). In addition, type II transmembrane CLECs can bear signaling motifs at their cytosolic tail (Figure 1).

The MR is mainly expressed by subpopulations of macrophages, immature dendritic cells (DCs) and endothelial cells (1, 2). Its expression level varies upon the situation and can be differentially regulated by cytokines (e.g. IL-10, IL-4, IL-13 and IFNγ), prostaglandins, LPS and the transcription factor PPARγ (3-7). Hence, MR expression is closely related to the activation status of the MR-expressing cell.

The MR encompasses a nearly 175 kDa type I transmembrane protein, consisting of an N-terminal cysteine-rich (CR) domain, a fibronectin (FN) type II domain, eight C-type lectin domains (CTLDs), a transmembrane region and a short cytosolic region. Similar to most other CLECs, a main feature of the MR is the recognition and internalization of specific ligands.

Since every MR region has its own binding specificity, ligands can vary substantially in their molecular structure. The cysteine-rich domain mediates binding to sulphated sugars (8) including glycosylated hormones, chondroitin sulphate and sulphated $Lewis^X$ and $Lewis^A$ (9), but also specific proteins attached to sulphated glycostructures, such as CD169 and CD45 (10). With its fibronectin type II domain, the MR recognizes collagen (especially type I-IV) (2, 11), and mediates collagen internalization by macrophages and liver sinusoidal endothelial cells (2). Its CTLDs are responsible for the recognition of glycoconjugates. More precisely, CTLD4 binds to glycostructures with terminal mannose, fucose or N-Acetylglucosamine (GlcNAc) in a calcium-dependent fashion (12, 13). Since these sugar moieties are often exposed on microorganisms, the MR contributes to the clearance of a variety of infections, including *Candida albicans* (14), Leishmania (15, 16), *Mycobacterium tuberculosis* (17) and *Klebsiella pneumoniae* (18). Hence, the MR can bind to and internalize a variety of both endogenous ligands and pathogens (Figure 2).

Since the intracellular region of the MR lacks any known signaling domains, no MR-intrinsic signaling has been reported yet. Still, the presence of the MR has been linked to a direct induction of several target genes (19-21), probably because the MR might assist other receptors in their signaling cascade (Figure 2). For example, it has been demonstrated that the MR interacts with TLR2 after binding to *Pneumocystis carinii* and stimulates a TLR2-mediated signaling cascade (22). The molecular mechanisms enabling MR-mediated stimulation of signaling events, however, remain to be elucidated.

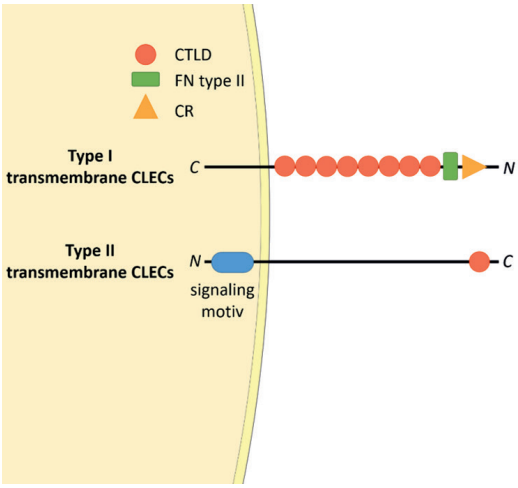

including

	expressed on	# of CTLDs
DEC205	myeloid DCs	10
MR	myeloid DCs, MΦs, endothelial cells	8

	expressed on	signaling motiv
CLEC2	platelets, DCs, Kupffer cells, neutrophils	ITAM
DC-SIGN	myeloid DCs, MΦs	ITIM-/ITAM-independent
Dectin-1	myeloid DCs, MΦs, monocytes, B cells, neutrophils, T cells	ITAM
Lox-1	endothelial cells, MΦs, DCs, B cells, platelets	-
MGL	myeloid DCs, MΦs	-
Mincle	myeloid DCs, MΦs, monocytes, B cells, neutrophils	via FcRγ

Figure 1. The CLEC family. Type I transmembrane CLECs typically contain multiple CTLDs at their extracellular region, whereas type II CLECs contain only one CLEC. All CLECs display individual expression patterns. Parts of the figure were created using templates from Servier Medical Art, which are licensed under a Creative Commons Attribution 3.0 Unported License; https://smart.servier.com. CTLD: C-type lectin domain, FN type II: fibronectin type II domain, CR: cysteine-rich domain, CLEC: C-type lectin, ITAM: immunoreceptor tyrosine-based activation motif, ITIM: immunoreceptor tyrosine-based inhibitory motif; DC: dendritic cell; Mϕ: macrophage; FcRγ: Fc receptor gamma chain; C: C-terminus; N: N-terminus.

Apart from its membrane-bound form, the MR can also be proteolytically cleaved by metalloproteases and released into the extracellular space as a soluble form (sMR) (Figure 2) (23, 24). Consequently, sMR can be detected in the supernatant of MR-expressing cells and in the serum of mice and humans as a soluble protein. Additionally, a recent study also indicated the presence of sMR in extracellular vesicles (25).

As the sMR encompasses all extracellular regions of full-length MR, preserving its main ligand binding properties (23, 24), this suggests that proteolytic cleavage must occur directly after the transmembrane region, in close proximity to the cell membrane. MR shedding occurs constitutively and levels of sMR correlate with the amount of total MR expressed in the cells (23). In addition to constitutive shedding in MR-expressing cells, MR shedding is specifically stimulated by fungal particles (*P. carinii, Candida albicans, Aspergillus fumigatus* and zymosan) and requires Dectin-1-mediated signaling (9, 26). However, whether this is due to activation of specific proteases involved in MR shedding or to other reasons has not been elucidated so far.

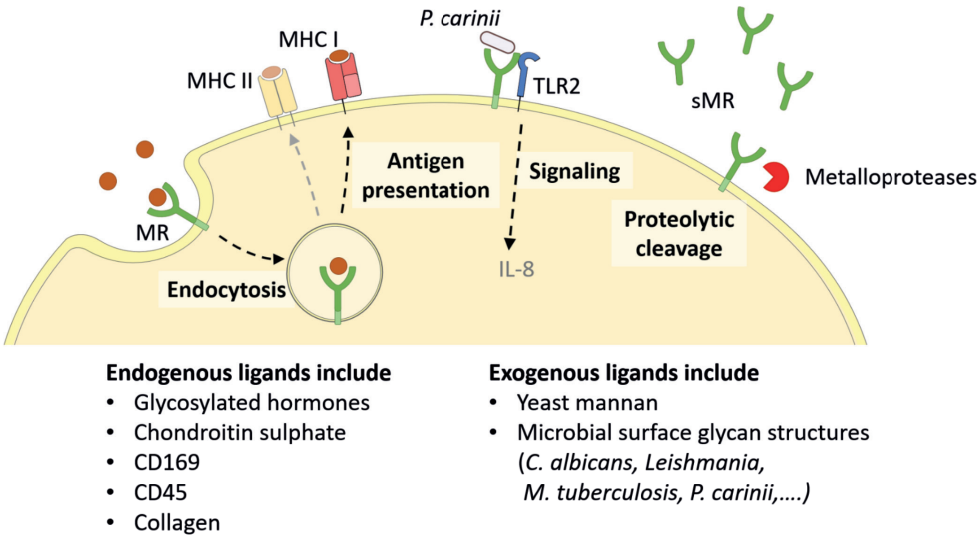

Figure 2. Cellular functions of the MR. The membrane-bound MR can recognize extracellular ligands, leading to their internalization. Endocytosed antigens are targeted into early endosomes, from which they are processed mainly for cross-presentation onto MHC I molecules and subsequent CD8+ T cell activation. Furthermore, the MR can assist other molecules in their signaling cascade, like enhanced TLR2 signaling after recognition of P. carinii. Finally, the MR can be shed by metalloproteases and released as a soluble form (sMR) in the extracellular space. MHC, major histocompatibility complex; MR, mannose receptor. Parts of the figure were created using templates from Servier Medical Art, which are licensed under a Creative Commons Attribution 3.0 Unported License; https://smart.servier.com.

The MR mediates antigen uptake and processing for cross-presentation

Due to its ligand binding capacities and its role in the clearance of multiple pathogens, the endocytic properties of the MR have been extensively studied. Under normal conditions, the MR localizes to the plasma membrane and in early endosomes, from where it is constantly recycled, even in the absence of ligands. Upon ligand binding, the MR is internalized in a clathrin-dependent fashion, a process mediated by the FENTLY motif in the cytoplasmic tail of the receptor. The di-aromatic YF motif is responsible for its intracellular trafficking into early endosomes (27).

Specific intracellular routing of MR-internalized antigens into early endosomes(28-33) was shown to have pronounced consequences for its role in antigen presentation. In fact, MR-internalized antigens are targeted towards a distinct non-degradative early endosome population, where they are rescued from lysosomal degradation and concomitant

presentation on MHC II molecules (28). Mechanistically, the MR has been postulated to actively prevent the fusion of such early endosomes with lysosomes (34, 35). From this early endosomal compartment, MR-internalized antigens are predominantly processed for antigen presentation on MHC I molecules, a process called cross-presentation (Figure 2) (28, 36). Additionally, ligand binding to the MR induces its ubiquitination, which in turn contributes to the recruitment of the cross-presentation machinery. Interestingly, MR cross-linking using antigens conjugated to MR-specific antibodies can also induce lysosomal targeting and concomitant MHC II-restricted presentation of the internalized antigens (37-39). Additionally, antibody-mediated cross-linking of the MR has been demonstrated to activate an anti-inflammatory immunosuppressive program in antigen-presenting cells (APCs) (19), pointing out the possibility that ligand binding and receptor cross-linking might regulate the functional outcome of MR-mediated antigen recognition. The role of the MR in antigen uptake, processing and presentation, however, is extensively described elsewhere (40-42) and is not a central topic of this review.

In addition to its role in endocytosis, the MR has also been postulated to be involved in macrophage migration, as MR-deficient bone marrow-derived macrophages display increased migration independent of a CSF-1 gradient (43). Although the underlying molecular mechanisms remain to be identified, it is thinkable that these effects were mediated by MR-mediated interaction with collagen.

Membrane-bound MR on antigen presenting cells induce T cell tolerance

Apart from its function in antigen recognition, internalization and processing for cross-presentation in APCs, the membrane-bound MR has been shown to directly regulate the function of other immune cells. Due to its association with antigen uptake and presentation, the MR became an attractive receptor in antigen targeting strategies. Such antigen targeting towards the MR has been linked to the induction of antigen-specific tolerance (44). In fact, in a mouse model of experimental autoimmune encephalomyelitis, injection of mannosylated myelin peptides surprisingly inhibited the onset of disease (45). Additionally, MR engagement on monocyte-derived DCs contributed to the induction of a regulatory phenotype (19, 46) and MR expression is mainly restricted to immunoregulatory cells, including tolerogenic DC subtypes, liver sinusoidal endothelial cells and alternatively activated macrophages (47, 48), for which the MR constitutes one of the main marker proteins.

Recent advances demonstrate that the membrane-bound MR is not a mere marker for tolerogenic cells, but also plays an active role in the induction of T cell tolerance (Figure 3) (11). Indeed, $CD8^+$ T cells activated by MR-expressing DCs displayed a clearly reduced cytotoxicity. This impaired T cell activation was mediated by a direct interaction of the membrane-bound MR on APCs with CD45 on T cells. CD45 is an immune cell-specific phosphatase which can be expressed as different isoforms depending on the immune cell subset. CD45 isoforms differ in the presence of the alternatively spliced exons A, B and C (49) and are frequently used to identify or distinguish bone marrow-derived immune cell subsets. Functionally, CD45 has been shown to play an important role in signaling mediated by the T and B cell receptors (50), whereas little is known about the role of CD45 in other immune cells. Importantly, the interaction of membrane-bound MR with CD45 on $CD8^+$ T cells during T cell activation caused inhibition of its phosphatase activity, which resulted in T cell reprogramming and a significant upregulation of tolerance-associated genes. One of these genes encodes CTLA-4, which was mainly responsible for the impaired T cell cytotoxicity (11).

Surprisingly, MR-mediated inhibition of CD45 did not alter T cell receptor (TCR) signaling, as TCR-induced Lck activity, phosphorylation of ZAP70, LAT and ERK, intracellular calcium release and NFAT activation were not clearly influenced by the presence of the MR on the APC. However, transcription factor binding prediction analysis at the CTLA-4 promoter identified B-cell lymphoma 6 (Bcl-6), a transcription repressor normally involved in the differentiation of T follicular helper cells (51), as novel regulator of CTLA-4 expression. Using computational analyses, Electrophoretic Mobility Shift Assay (EMSA) and chromatin immunoprecipitation (ChIP) experiments, two Bcl-6 binding sites were identified within the CTLA-4 promoter. Indeed, Bcl-6 recruitment towards the CTLA-4 promoter prevented CTLA-4 transcription. Moreover, Bcl-6 expression was induced by CD45 phosphatase activity during T cell activation. Hence, MR-mediated inhibition of CD45 prevented the induction of Bcl-6 in activated T cells, eventually leading to the expression of CTLA-4 and the induction of T cell tolerance (Figure 3) (11), which was also confirmed *in vivo*. Injection of wild-type or MR-deficient DCs, that were previously transduced with OVA-expressing adenoviruses, resulted in an upregulation of CLTA-4 and impaired cytotoxic activity of antigen-specific T cells after priming by MR-expressing DCs (11). Accordingly, MR-deficient mice displayed a higher capacity of clearing an adenoviral infection when compared to wild-type mice (11), substantiating a regulatory function of the membrane-bound MR *in vivo*.

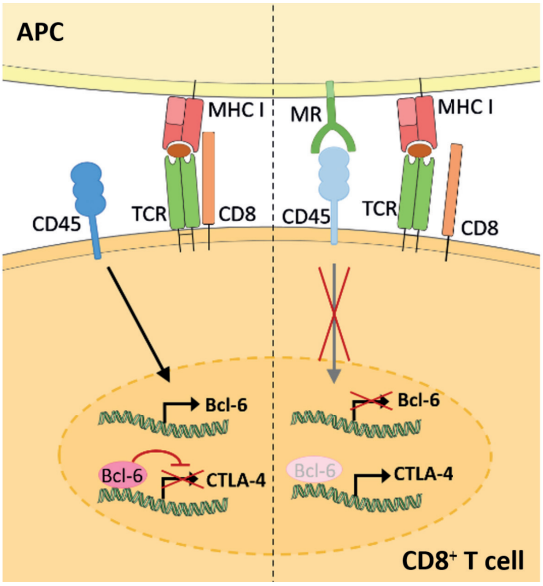

Figure 3. Membrane-bound MR on antigen presenting cells induces CD8⁺ T cell tolerance. Upon CD8⁺ T cell activation in the absence of the MR (left), expression of the transcriptional inhibitor Bcl-6 is induced. Bcl-6 binds to the CTLA-4 promoter and prevents its expression. During T cell activation in the presence of the MR (right), the MR on APCs interacts with CD45 on cytotoxic T cells. Such interaction prevents the upregulation of Bcl-6 and induces CTLA-4 expression and CD8⁺ T cell tolerance. APC, antigen presenting cell; MR, mannose receptor; TCR, T cell receptor. Parts of the figure were created using templates from Servier Medical Art, which are licensed under a Creative Commons Attribution 3.0 Unported License; https://smart.servier.com.

sMR correlates with inflammatory diseases and induces macrophage activation

As mentioned above, the MR can be shed by proteolytic cleavage and released into the extracellular space. In contrast to the regulatory effect of the membrane-bound MR on T cell activation, the soluble form of MR has rather been associated with inflammation, as increased sMR serum levels have been observed in patients suffering from diverse inflammatory diseases.

First evidence for an association between sMR serum levels and disease progression came from a study in which increased sMR serum levels were observed in hospitalized patients when compared to a healthy control population (52). These differences were already pronounced in endocrinological and hematological patients, but became obvious in critically ill patients with sepsis and severe liver disease. Accordingly, the highest sMR concentrations were measured in the serum of patients from the intensive care unit. Similar observations were made in patients with liver cirrhosis, alcoholic liver disease and acute-on-chronic liver

failure, a condition characterized by acute decompensation and organ failure following an extreme inflammatory response. Here, sMR concentrations were demonstrated to correlate with disease severity, portal hypertension, gut permeability, bacterial translocation and even mortality, displaying increased levels in non-survivors (53-58). Additionally, a modest but significant gender-independent correlation of sMR serum levels with age was observed (52).

Increased sMR levels were also observed in patients with a wide variety of inflammatory diseases, such as pulmonary tuberculosis (59), pulmonary fibrosis (60), multiple myeloma (61, 62), rheumatoid arthritis (63), chronic joint inflammation (64), pneumonia (65, 66), interstitial lung disease (67, 68) and gastric cancer (69). Strikingly, in these studies, sMR levels positively correlated with disease severity and mortality. As such, the sMR has been proposed as a new biomarker for inflammation (56, 57, 69-71). In fact, for several inflammatory diseases, including sepsis and pulmonary fibrosis, the sMR has even been suggested to be a better biomarker than those previously reported, such as sCD163, C-reactive protein or procalcitonin (60, 72). However, in all these studies, a functional role of the sMR in the onset of these inflammatory diseases has not been investigated so far.

The hypothesis of a putative functional role of sMR in inflammatory diseases is further supported by observations that MR-deficient mice are protected against inflammation-mediated renal injury in a mouse model of crescentic glomerulonephritis (CGN) (73). Macrophage infiltration in the kidney plays a dominant role in the pathophysiology of CGN (74, 75) and their phenotype is shaped by the kidney resident mesangial cells (MCs) (76). Interestingly, the protective effect of MR deficiency on CGN was associated with reduced macrophage infiltration in the kidney and impaired MC-mediated macrophage activation, as demonstrated by a reduction in both TNF secretion and phagocytosis-induced reactive oxygen species production. Although the potential contribution of sMR deficiency to CGN protection was not considered, these results provided the first evidence that MR may regulate proinflammatory activation of macrophages.

Importantly, a recent study demonstrated that the sMR can actually drive proinflammatory macrophage activation (77). sMR induced an inflammatory phenotype of both murine and human macrophages, as reflected by increased secretion of proinflammatory cytokines (TNF, IL-6, IL-12 and IL-1β) and a shift in cellular metabolism towards increased glycolysis (77), a hallmark of proinflammatory macrophage activation (78). In addition, RNAseq analyses also supported macrophage reprogramming towards an inflammatory phenotype (77), as the transcriptomic signature of sMR-treated macrophages displayed close similarities with the one of macrophages treated with TNF, prostaglandin E2 and the TLR2 ligand Pam3CSK4, a combination of stimuli used in a previous study to mimic a macrophage

phenotype associated with chronic inflammation (79). Together, this demonstrates that sMR triggers an inflammatory response in macrophages.

At a mechanistic level, and similar to the effect of membrane-bound MR on T cells, sMR binds CD45 on macrophages, leading to an inhibition of CD45 phosphatase activity (77). Using specific inhibitors and siRNA-mediated downregulation of CD45, it was confirmed that sMR-induced proinflammatory macrophage activation was dependent on inhibition of CD45 (Figure 4). A screening for overrepresented transcription factor motifs in the promoter regions of all differentially expressed genes and identified NF-κB as the major transcription factor involved in sMR-induced macrophage activation. Accordingly, sMR treatment resulted in downregulation of IκBa, an inhibitor of NF-κB, and enhanced nuclear translocation of both NF-κB subunits p65 and p50 as well as recruitment of p65 to the TNF promotor. One of the known substrates of CD45 that has been associated with activation of NF-κB is Src, a kinase that is inactivated under homeostatic conditions by CD45-mediated dephosphorylation (80). Activated Src was shown to phosphorylate Akt (81), and both phosphorylated Src and Akt were reported to promote NF-κB activation (82-85). Using a combination of pharmacological and genetic tools, it was demonstrated that sMR-mediated inhibition of CD45 indeed resulted in a Src/Akt/NF-κB-mediated cellular reprogramming toward an inflammatory phenotype (Figure 4) (77).

sMR is a novel driver of metaflammation

Proinflammatory macrophage accumulation in metabolic tissues is one of the hallmarks of obesity-induced metaflammation, a chronic state of low-grade inflammation that is triggering metabolic dysfunctions. Indeed, recruitment of $CCR2^+$ monocytes to visceral white adipose tissue (WAT) and the liver promotes tissue inflammation, insulin resistance and impaired glucose homeostasis (86-89). This detrimental effect is believed to be mainly driven by monocyte differentiation into CD11c-expressing proinflammatory macrophages and enhanced production of TNF and IL-1β, leading to inhibition of canonical insulin signaling (90-92). Consequently, tissue-specific insulin resistance promotes ectopic lipid deposition and the development of hepatic steatosis, together contributing to whole-body insulin resistance. In support of this, genetic or pharmacological inhibition of CCR2-dependent monocyte recruitment to WAT and liver was shown to mitigate tissue inflammation and metabolic dysfunctions in obese mice (87, 88, 93).

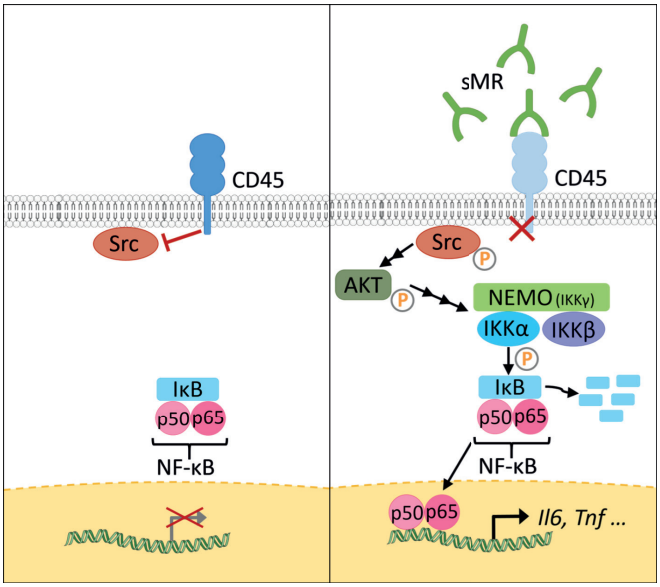

Figure 4. The sMR induces proinflammatory activation of macrophages. Under homeostatic conditions (left), CD45 in macrophages dephosphorylates Src. At increased sMR concentrations (right), binding of sMR to CD45 inhibits its phosphatase activity, leading to phosphorylation and activation of Src, which in turn activates an Akt/NF-κB pathway, causing macrophage reprogramming towards an inflammatory phenotype. sMR, soluble mannose receptor. Parts of the figure were created using templates from Servier Medical Art, which are licensed under a Creative Commons Attribution 3.0 Unported License; https://smart.servier.com.

In accordance with other inflammatory diseases discussed above, we recently reported that serum sMR levels were increased in high-fat diet (HFD)-fed obese mice and obese humans, and positively correlated with adiposity (77). Given that the sMR induces a proinflammatory phenotype in macrophages as described above and proinflammatory macrophages drive insulin resistance in metabolic tissues, these observations suggested the possibility that sMR-mediated proinflammatory macrophage activation in obesity may contribute to metabolic dysfunctions. Indeed, HFD-fed MR-deficient mice exhibited reduced numbers of CD11c-expressing obesity-associated macrophages in both WAT and liver, and were protected against hepatic steatosis, insulin resistance and glucose intolerance, independent of body weight changes (77) (Figure 5A). Of note, acute diphtheria toxin (DT)-mediated depletion of MR-expressing cells in obese CD206-DTR mice was also previously reported to improve whole-body glucose tolerance and insulin sensitivity when compared to wild-type mice (94), further substantiating a role for the MR in regulating metabolic homeostasis. In this study, the authors attributed

the improved metabolic phenotype of these MR-deficient mice to increased proliferation and differentiation of adipocyte precursors in WAT secondary to downregulation of transforming growth factor (TGF)-β signaling pathway. However, since inflammatory macrophages and proinflammatory gene markers, especially *Tnf*, were also significantly reduced in WAT from obese MR-depleted mice, at least part of these observations could also be due to impaired MR-induced activation of macrophages.

More importantly, intraperitoneal administration of recombinant sMR to healthy lean mice acutely increased circulating proinflammatory cytokines (77), supporting that sMR can also trigger proinflammatory macrophage activation *in vivo*. As such, chronic treatment with sMR increased adipose tissue macrophage numbers, WAT expression of proinflammatory cytokines (Figure 5B) and reduced whole-body insulin sensitivity in lean mice, a detrimental metabolic effect that was even more pronounced when mice were concomitantly fed a HFD (77). These findings unequivocally identified the sMR as novel driver of macrophage activation and metaflammation.

Other CLECs in the regulation of metaflammation

The proinflammatory effect of the MR on macrophages and its role in the development of obesity-induced metaflammation raises the question whether such properties are unique to the MR or rather a general feature of CLECs.

In general, CLECs can play a role in different kinds of immune responses. However, there are some striking similarities in the regulation of immune cell function between the MR and macrophage galactose-type lectin (MGL), another CLEC member that is also highly expressed on alternatively-activated macrophages. Similar to the MR, MGL lacks internal signaling motifs, but has been reported to enhance TLR2-mediated signaling (95). Additionally, membrane-bound MGL on APCs interacts with CD45 on T cells, inhibiting its phosphatase activity (96). Of note, in this study, the underlying molecular mechanisms seem to involve reduced T cell receptor signaling, and therefore differ slightly from MR-induced T cell tolerance. Nevertheless, MGL-induced inhibition of CD45 prevented effective activation of cytotoxic T cells (96). Strikingly, the immunometabolic phenotype of obese MGL-deficient mice resembles the phenotype of obese MR-deficient mice (97). Upon HFD feeding, both genotypes display reduced body weight gain, exclusively due to lower fat mass accumulation, protection against hepatic steatosis, and improved glucose tolerance and insulin sensitivity when compared to wild-type mice. Interestingly, these metabolic features were associated with reduced numbers of inflammatory macrophages in adipose tissue and a tissue-specific decreased in gene expression of *Ccl2* (MCP-1) and *Tnf* (77, 97). Although a potential interaction between MGL and CD45 on macrophages has not been investigated yet, it is tempting to speculate that

MGL may inhibit CD45 phosphatase activity in macrophages, resulting in proinflammatory macrophage activation. The absence of such an interaction could potentially contribute to the protective immunometabolic phenotype of obese MGL-deficient mice. However, it is worth underlining that a soluble form of MGL has not been reported so far, suggesting that MGL-mediated effects, unlike those induced by the sMR, might require direct cell-cell interaction.

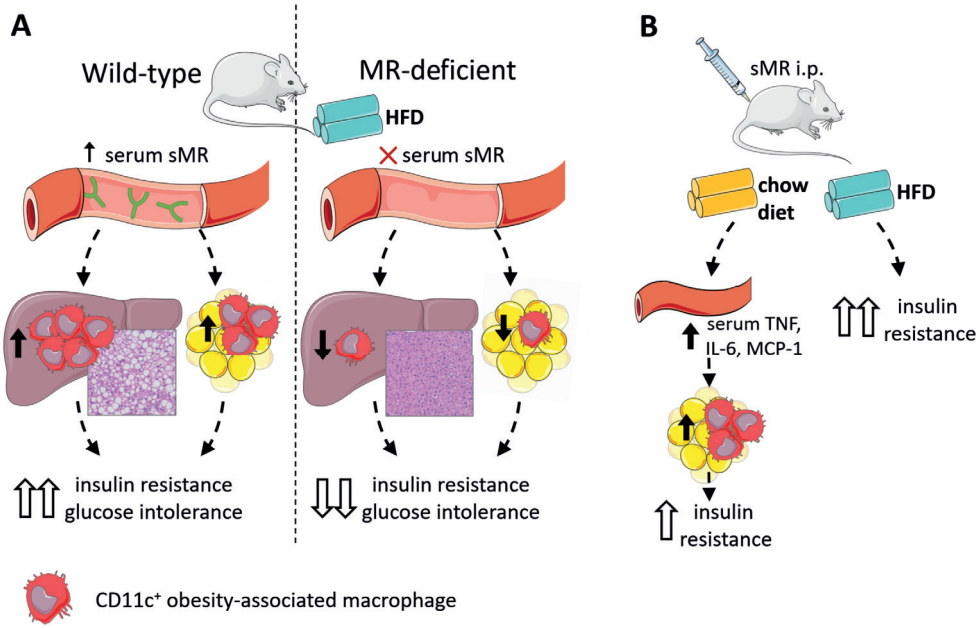

Figure 5. The sMR in metaflammation. (A) Wild-type mice on HFD (left) have high serum sMR, which is associated with increased hepatic steatosis, CD11c+ KCs and CD11c+ ATMs. Together, this is associated with increased insulin resistance and glucose intolerance. MR-deficient mice on HFD (right) have no serum sMR, which is associated with protection against hepatic steatosis, lower CD11c+ KCs and ATMs. Together, this is associated with lower insulin resistance and glucose intolerance. **(B)** sMR i.p. injections in mice on chow diet increased serum proinflammatory cytokines, associated with increased proinflammatory macrophages in adipose tissue, both associated with mild insulin resistance. sMR i.p. injection in mice on HFD increased insulin resistance. ATMs; adipose tissue macrophages; i.p., intraperitoneal; HFD, high-fat diet; KCs, Kupffer cells; sMR, soluble mannose receptor. Parts of the figure were created using templates from Servier Medical Art, which are licensed under a Creative Commons Attribution 3.0 Unported License; https://smart.servier.com.

Another CLEC that has been involved in metaflammation is Dectin-1. As for MR-deficient mice, Dectin-1-deficient mice are protected from HFD-induced obesity (98). Dectin-1 expression was upregulated in WAT from obese mice and humans, and associated with proinflammatory adipose tissue macrophages (ATMs). Accordingly, treatment with a Dectin-1 antagonist

improved insulin sensitivity in obese mice and reduced adipose tissue $CD11c^+$ obesity-associated macrophages, while treatment with a Dectin-1 agonist did the opposite. However, since Dectin-1 ligation induces cellular signaling that directly leads to activation of NF-κB (99), it is likely that Dectin-1 promotes metaflammation through a different molecular mechanism than the MR. Nevertheless, increased metalloprotease-mediated MR shedding in response to *Candida albicans* and β-glucan particles was dependent on Dectin-1 and its intracellular signaling pathway (9), which offers the possibility that the immunometabolic phenotype of obese Dectin-1-deficient mice may in part be explained by reduced sMR production.

Macrophage-inducible C-type lectin (Mincle) has also been associated with a variety of inflammatory diseases, such as rheumatoid arthritis, allergic contact dermatitis, hepatitis and diet-induced obesity (100-103). Macrophage expression of Mincle was shown to be induced by saturated fatty acids and macrophage-adipocyte interactions (103). Accordingly, WAT Mincle expression was localized to crown-like structures of macrophages surrounding dying adipocytes during obesity (104). Although Mincle-deficient mice display similar weight gain compared to wild-type mice upon HFD feeding, obesity-induced crown-like structures, hepatic steatosis and whole-body insulin resistance and glucose intolerance are significantly mitigated when compared to wild-type mice (104, 105). As Mincle ligation induces FcRγ-mediated signaling, eventually resulting in activation of NF-κB in macrophages (99), Mincle-mediated macrophage activation is probably occurring via distinct molecular pathways, independent of CD45 and the MR.

Of note, there is a variety of other CLECs that were associated with metaflammation or chronic inflammatory diseases for which the mechanistic underpinnings are poorly defined. For example, expression of the lectin-like oxidatively-modified low-density lipoprotein (Ox-LDL) receptor (LOX-1) – also named CLEC8A – is increased in visceral WAT of HFD-fed obese mice (106). Obese LOX-1-deficient mice display reduced HFD-induced CCL2/MCP-1, macrophage inflammatory protein-1α (MIP-1α) and IL-6 expression in WAT, suggesting a role for LOX-1 in regulating adipose tissue inflammation. Interestingly, LOX-1 is expressed on endothelial cells (107) and human macrophages (108), and similar to the MR, it can be proteolytically cleaved to release a soluble form (109, 110). Although no functional role has been described for soluble LOX-1 to date, it is known that cleavage of LOX-1 is triggered by the proinflammatory factors oxLDL, C-reactive protein, TNF, IL-8 and IL-18 and regulated by membrane cholesterol (111-114). Its cleavage is mediated via serine proteases that have been shown to be upregulated during obesity, potentially increasing bioavailability of soluble LOX-1 in these conditions (115). Interestingly, soluble LOX-1 serum levels have been shown to be correlated with the occurrence and severity of a variety of inflammatory cardiovascular diseases, including stroke, atherosclerosis and acute

coronary syndrome (116-122). Whether soluble LOX-1 is merely a biomarker for these diseases, or might be functionally involved in disease progression, remains to be identified.

The Dendritic Cell-Specific Intercellular adhesion molecule-3-Grabbing Non-integrin (DC-SIGN) - also termed CD209 or CLEC4L - is increased on monocyte-derived dendritic cells (Mo-DCs) from post-menopausal type 2 diabetic obese women, which is thought to modulate their adhesion capacity to vascular cell walls and migration to peripheral tissues (123). Besides this association with obesity, there is limited data on the putative role of DC-SIGN in the context of metaflammation. Similar to the MR, DC-SIGN can be detected as soluble form (sDC-SIGN) in serum (124) but its functions remain also largely unknown and would definitely require dedicated studies.

In contrast to the abovementioned detrimental roles of several CLECs in the context of obesity-induced metabolic dysfunctions, *in vivo* overexpression or administration of a soluble form of CLEC2 improved hepatic steatosis, hepatic fatty acid oxidation and whole-body glucose tolerance (125, 126). CLEC2 is expressed on platelets, dendritic cells, neutrophils and Kupffer cells, and its soluble form induced alternative activation of hepatic Kupffer cells, a feature that was postulated to drive the metabolic benefits, although this remains to be firmly established.

In conclusion, the proinflammatory effects of sMR and its role in obesity-induced metaflammation are not a general feature of CLECs. However, while the number of studies is limited, different CLECs have been linked to metaflammation, with the majority playing detrimental roles in the control of insulin sensitivity. Although some homogeneity in molecular mechanisms might exist (*e.g.* immunometabolic phenotypes of MGL-deficient and MR-deficient mice), other CLECs likely aggravate metabolic dysfunctions independent of interaction with CD45 on macrophages. As the conclusions from these studies were mostly drawn using whole-body knockout mice, future studies using conditional knockout models are warranted to identify the cellular source and underlying molecular mechanisms responsible for CLEC-mediated control of metabolic homeostasis.

Discussion and further perspectives

Since the MR lacks signaling motifs, it was generally assumed that it functions as a mere endocytic receptor, internalizing extracellular material for clearance and antigen presentation. Recent advances have made clear that the MR can actively shape immune responses by directly regulating immune cell activity (11, 73, 77). Until now, the membrane-bound MR has been shown to induce T cell tolerance, whereas the sMR stimulates an inflammatory response in macrophages, both via inhibition of CD45. However, it remains unclear whether these observed differences are merely due to a distinct cell type-dependent role of CD45 or

rather to different effects of the soluble versus membrane-bound MR. As membrane-bound MR could cross-link CD45 or alter its composition and clustering in the cell-membrane, a different response in terms of immune cell activation compared to its soluble form could be possible. First indications suggested that sMR might also promote T cell tolerance (11), pointing out that the recipient cell might determine the MR-induced effects rather than the form of MR interacting with the cells. Future studies will have to validate this hypothesis and show whether interaction of macrophages with membrane-bound MR also results in the induction of an inflammatory response. Similarly, the exact role of other soluble CLEC receptors, such as LOX-1, needs to be investigated carefully.

Moreover, it remains unclear whether the MR also influences the functionality of other immune cells, like $CD4^+$ T cells, DCs and B cells. Since all these cells express CD45, a similar regulation by interaction with MR could be possible. Therefore, the identification of the CD45 isoforms interacting with the MR needs to be monitored carefully, since these isoforms differ substantially depending on the cell type and inflammatory status.

Another important open question regarding increased sMR serum concentrations during inflammation is the identification of its source. As mentioned above, the MR is mainly expressed by macrophages, DCs and endothelial cells (1, 2). During metaflammation, we observed increased MR expression in liver and adipose tissue but not spleen, in particular in macrophages and liver sinusoidal endothelial cells (77). As such, it can be expected that these cells are responsible for increased sMR production, resulting in enhanced local and systemic sMR concentrations and in macrophage-mediated metaflammation. Since the expression of the MR is directly regulated by PPARγ (7), and free fatty acid-activated PPARγ signaling is upregulated in lipid-associated macrophages during obesity (127), this transcription factor could be one of the key players in the regulation of MR expression and shedding. It is thus tempting to speculate that increased MR expression and hence sMR serum levels might be a result of metaflammation-associated activation of PPARγ in macrophages. In addition, MR is constitutively cleaved by yet unidentified metalloproteases (23, 24). Since obesity was shown to alter the metalloprotease expression profiles of adipose tissue and liver (128-130), it needs to be investigated whether obesity-induced metalloprotease expression in metabolic tissues may increase MR shedding.

Additionally, the correlation of sMR serum concentrations with the inflammatory status of various human populations should be monitored carefully and in an unbiased fashion, using a large and representative cohort not selected for specific inflammatory conditions. Naturally, future studies should address whether sMR-mediated activation of macrophages plays a functional role in the onset and progression of such conditions. In order to experimentally address this putative function of the sMR in different diseases, the

availability of reliable methods to quantify sMR serum levels is a prerequisite. For this purpose, ELISA-based methods to quantify human and mouse sMR are commercially available. Such ELISA kits have been reported manyfold to reliably determine sMR levels in human serum (52). However, studies reporting sMR levels in murine sera are rare, which might be explained by a lack of reliability of the available products. Indeed, we recently developed a method based on immunoprecipitation and fluorimetry to monitor murine sMR serum levels in the context of metaflammation (77), as we obtained false positive detection of sMR serum levels from MR-deficient mice using a commercially available ELISA kit. However, since this technique is elaborate and time-consuming, the establishment of a reliable ELISA is of interest to monitor sMR in mouse serum in future investigations.

In conclusion, should the sMR be confirmed to contribute to the induction of inflammation in a broad spectrum of diseases, it would definitely constitute a potential target for therapeutic intervention. As such, approaches aimed at reducing, eliminating or inactivating sMR might reduce macrophage activation and could contribute to mitigation of disease. In addition, the molecular mechanisms leading to increased sMR serum concentrations are also of great interest, as these could provide additional leads for therapeutic interventions.

Acknowledgements

This work is funded by the Deutsche Forschungsgemeinschaft (DFG, German Research Foundation) - SFB1454 (project number 432325352 to SB) under Germany´s Excellence Strategy EXC2151 (project number 390873048 to SB), the NWO Graduate School Program (022.006.010 to HJPvdZ), an EFSD/Lilly Research Grant Fellowship from the European Federation for the Study of Diabetes (to BG) and the Dutch Organization for Scientific Research (ZonMW TOP Grant 91214131 to BG).

Conflict of Interest

The authors declare that this work was conducted in the absence of any commercial or financial relationships that could be construed as a potential conflict of interest.

References

1. East L, Isacke CM. The mannose receptor family. Biochim Biophys Acta. 2002;1572(2-3):364-86.
2. Taylor PR, Gordon S, Martinez-Pomares L. The mannose receptor: linking homeostasis and immunity through sugar recognition. Trends Immunol. 2005;26(2):104-10.
3. Longoni D, Piemonti L, Bernasconi S, Mantovani A, Allavena P. Interleukin-10 increases mannose receptor expression and endocytic activity in monocyte-derived dendritic cells. Int J Clin Lab Res. 1998;28(3):162-9.
4. Schreiber S, Blum JS, Chappel JC, Stenson WF, Stahl PD, Teitelbaum SL, et al. Prostaglandin E specifically upregulates the expression of the mannose-receptor on mouse bone marrow-derived macrophages. Cell Regul. 1990;1(5):403-13.
5. Shepherd VL, Abdolrasulnia R, Garrett M, Cowan HB. Down-regulation of mannose receptor activity in macrophages after treatment with lipopolysaccharide and phorbol esters. J Immunol. 1990;145(5):1530-6.
6. Harris N, Super M, Rits M, Chang G, Ezekowitz RA. Characterization of the murine macrophage mannose receptor: demonstration that the downregulation of receptor expression mediated by interferon-gamma occurs at the level of transcription. Blood. 1992;80(9):2363-73.
7. Klotz L, Hucke S, Thimm D, Classen S, Gaarz A, Schultze J, et al. Increased antigen cross-presentation but impaired cross-priming after activation of peroxisome proliferator-activated receptor gamma is mediated by up-regulation of B7H1. J Immunol. 2009;183(1):129-36.
8. Fiete DJ, Beranek MC, Baenziger JU. A cysteine-rich domain of the "mannose" receptor mediates GalNAc-4-SO4 binding. Proc Natl Acad Sci U S A. 1998;95(5):2089-93.
9. Gazi U, Rosas M, Singh S, Heinsbroek S, Haq I, Johnson S, et al. Fungal recognition enhances mannose receptor shedding through dectin-1 engagement. J Biol Chem. 2011;286(10):7822-9.
10. Martinez-Pomares L, Crocker PR, Da Silva R, Holmes N, Colominas C, Rudd P, et al. Cell-specific glycoforms of sialoadhesin and CD45 are counter-receptors for the cysteine-rich domain of the mannose receptor. J Biol Chem. 1999;274(49):35211-8.
11. Schuette V, Embgenbroich M, Ulas T, Welz M, Schulte-Schrepping J, Draffehn AM, et al. Mannose receptor induces T-cell tolerance via inhibition of CD45 and up-regulation of CTLA-4. Proc Natl Acad Sci U S A. 2016;113(38):10649-54.
12. Taylor ME, Bezouska K, Drickamer K. Contribution to ligand binding by multiple carbohydrate-recognition domains in the macrophage mannose receptor. J Biol Chem. 1992;267(3):1719-26.
13. Taylor ME, Drickamer K. Structural requirements for high affinity binding of complex ligands by the macrophage mannose receptor. J Biol Chem. 1993;268(1):399-404.
14. Marodi L, Korchak HM, Johnston RB, Jr. Mechanisms of host defense against Candida species. I. Phagocytosis by monocytes and monocyte-derived macrophages. J Immunol. 1991;146(8):2783-9.
15. Chakraborty P, Ghosh D, Basu MK. Modulation of macrophage mannose receptor affects the uptake of virulent and avirulent Leishmania donovani promastigotes. J Parasitol. 2001;87(5):1023-7.

16. Chakraborty R, Chakraborty P, Basu MK. Macrophage mannosyl fucosyl receptor: its role in invasion of virulent and avirulent L. donovani promastigotes. Biosci Rep. 1998;18(3):129-42.

17. Tailleux L, Schwartz O, Herrmann JL, Pivert E, Jackson M, Amara A, et al. DC-SIGN is the major Mycobacterium tuberculosis receptor on human dendritic cells. J Exp Med. 2003;197(1):121-7.

18. Zamze S, Martinez-Pomares L, Jones H, Taylor PR, Stillion RJ, Gordon S, et al. Recognition of bacterial capsular polysaccharides and lipopolysaccharides by the macrophage mannose receptor. J Biol Chem. 2002;277(44):41613-23.

19. Chieppa M, Bianchi G, Doni A, Del Prete A, Sironi M, Laskarin G, et al. Cross-linking of the mannose receptor on monocyte-derived dendritic cells activates an anti-inflammatory immunosuppressive program. J Immunol. 2003;171(9):4552-60.

20. Fernandez N, Alonso S, Valera I, Vigo AG, Renedo M, Barbolla L, et al. Mannose-containing molecular patterns are strong inducers of cyclooxygenase-2 expression and prostaglandin E2 production in human macrophages. J Immunol. 2005;174(12):8154-62.

21. Zhang J, Tachado SD, Patel N, Zhu J, Imrich A, Manfruelli P, et al. Negative regulatory role of mannose receptors on human alveolar macrophage proinflammatory cytokine release in vitro. J Leukoc Biol. 2005;78(3):665-74.

22. Tachado SD, Zhang J, Zhu J, Patel N, Cushion M, Koziel H. Pneumocystis-mediated IL-8 release by macrophages requires coexpression of mannose receptors and TLR2. J Leukoc Biol. 2007;81(1):205-11.

23. Martinez-Pomares L, Mahoney JA, Kaposzta R, Linehan SA, Stahl PD, Gordon S. A functional soluble form of the murine mannose receptor is produced by macrophages in vitro and is present in mouse serum. J Biol Chem. 1998;273(36):23376-80.

24. Jordens R, Thompson A, Amons R, Koning F. Human dendritic cells shed a functional, soluble form of the mannose receptor. Int Immunol. 1999;11(11):1775-80.

25. Nielsen MC, Andersen MN, Gronbaek H, Damgaard Sandahl T, Moller HJ. Extracellular vesicle-associated soluble CD163 and CD206 in patients with acute and chronic inflammatory liver disease. Scand J Gastroenterol. 2020;55(5):588-96.

26. Fraser IP, Takahashi K, Koziel H, Fardin B, Harmsen A, Ezekowitz RA. Pneumocystis carinii enhances soluble mannose receptor production by macrophages. Microbes Infect. 2000;2(11):1305-10.

27. Schweizer A, Stahl PD, Rohrer J. A di-aromatic motif in the cytosolic tail of the mannose receptor mediates endosomal sorting. J Biol Chem. 2000;275(38):29694-700.

28. Burgdorf S, Kautz A, Bohnert V, Knolle PA, Kurts C. Distinct pathways of antigen uptake and intracellular routing in CD4 and CD8 T cell activation. Science. 2007;316(5824):612-6.

29. Kreer C, Kuepper JM, Zehner M, Quast T, Kolanus W, Schumak B, et al. N-glycosylation converts non-glycoproteins into mannose receptor ligands and reveals antigen-specific T cell responses in vivo. Oncotarget. 2017;8(4):6857-72.

30. Rauen J, Kreer C, Paillard A, van Duikeren S, Benckhuijsen WE, Camps MG, et al. Enhanced cross-presentation and improved CD8+ T cell responses after mannosylation of synthetic long peptides in mice. PLoS One. 2014;9(8):e103755.

31. Wassenberg JJ, Dezfulian C, Nicchitta CV. Receptor mediated and fluid phase pathways for internalization of the ER Hsp90 chaperone GRP94 in murine macrophages. J Cell Sci. 1999;112 (Pt 13):2167-75.

32. Wainszelbaum MJ, Proctor BM, Pontow SE, Stahl PD, Barbieri MA. IL4/PGE2 induction of an enlarged early endosomal compartment in mouse macrophages is Rab5-dependent. Exp Cell Res. 2006;312(12):2238-51.

33. Mahnke K, Guo M, Lee S, Sepulveda H, Swain SL, Nussenzweig M, et al. The dendritic cell receptor for endocytosis, DEC-205, can recycle and enhance antigen presentation via major histocompatibility complex class II-positive lysosomal compartments. J Cell Biol. 2000;151(3):673-84.

34. Shimada K, Takimoto H, Yano I, Kumazawa Y. Involvement of mannose receptor in glycopeptidolipid-mediated inhibition of phagosome-lysosome fusion. Microbiol Immunol. 2006;50(3):243-51.

35. Sweet L, Singh PP, Azad AK, Rajaram MV, Schlesinger LS, Schorey JS. Mannose receptor-dependent delay in phagosome maturation by Mycobacterium avium glycopeptidolipids. Infect Immun. 2010;78(1):518-26.

36. Burgdorf S, Lukacs-Kornek V, Kurts C. The mannose receptor mediates uptake of soluble but not of cell-associated antigen for cross-presentation. J Immunol. 2006;176(11):6770-6.

37. He LZ, Crocker A, Lee J, Mendoza-Ramirez J, Wang XT, Vitale LA, et al. Antigenic targeting of the human mannose receptor induces tumor immunity. J Immunol. 2007;178(10):6259-67.

38. Dasgupta S, Navarrete AM, Bayry J, Delignat S, Wootla B, Andre S, et al. A role for exposed mannosylations in presentation of human therapeutic self-proteins to CD4+ T lymphocytes. Proc Natl Acad Sci U S A. 2007;104(21):8965-70.

39. McKenzie EJ, Taylor PR, Stillion RJ, Lucas AD, Harris J, Gordon S, et al. Mannose receptor expression and function define a new population of murine dendritic cells. J Immunol. 2007;178(8):4975-83.

40. Burgdorf S, Kurts C. Endocytosis mechanisms and the cell biology of antigen presentation. Curr Opin Immunol. 2008;20(1):89-95.

41. Embgenbroich M, Burgdorf S. Current Concepts of Antigen Cross-Presentation. Front Immunol. 2018;9:1643.

42. Kreer C, Rauen J, Zehner M, Burgdorf S. Cross-presentation: how to get there - or how to get the ER. Front Immunol. 2011;2:87.

43. Sturge J, Todd SK, Kogianni G, McCarthy A, Isacke CM. Mannose receptor regulation of macrophage cell migration. J Leukoc Biol. 2007;82(3):585-93.

44. Luca ME, Kel JM, van Rijs W, Wouter Drijfhout J, Koning F, Nagelkerken L. Mannosylated PLP(139-151) induces peptide-specific tolerance to experimental autoimmune encephalomyelitis. J Neuroimmunol. 2005;160(1-2):178-87.

45. Kel J, Oldenampsen J, Luca M, Drijfhout JW, Koning F, Nagelkerken L. Soluble mannosylated myelin peptide inhibits the encephalitogenicity of autoreactive T cells during experimental autoimmune encephalomyelitis. Am J Pathol. 2007;170(1):272-80.

46. Allavena P, Chieppa M, Bianchi G, Solinas G, Fabbri M, Laskarin G, et al. Engagement of the mannose receptor by tumoral mucins activates an immune suppressive phenotype in human tumor-associated macrophages. Clin Dev Immunol. 2010;2010:547179.

47. Limmer A, Ohl J, Wingender G, Berg M, Jungerkes F, Schumak B, et al. Cross-presentation of oral antigens by liver sinusoidal endothelial cells leads to CD8 T cell tolerance. Eur J Immunol. 2005;35(10):2970-81.

48. van Vliet SJ, van Liempt E, Geijtenbeek TB, van Kooyk Y. Differential regulation of C-type lectin expression on tolerogenic dendritic cell subsets. Immunobiology. 2006;211(6-8):577-85.

49. Rothstein DM, Saito H, Streuli M, Schlossman SF, Morimoto C. The alternative splicing of the CD45 tyrosine phosphatase is controlled by negative regulatory trans-acting splicing factors. J Biol Chem. 1992;267(10):7139-47.

50. Ledbetter JA, Tonks NK, Fischer EH, Clark EA. CD45 regulates signal transduction and lymphocyte activation by specific association with receptor molecules on T or B cells. Proc Natl Acad Sci U S A. 1988;85(22):8628-32.

51. Hatzi K, Nance JP, Kroenke MA, Bothwell M, Haddad EK, Melnick A, et al. BCL6 orchestrates Tfh cell differentiation via multiple distinct mechanisms. J Exp Med. 2015;212(4):539-53.

52. Rodgaard-Hansen S, Rafique A, Christensen PA, Maniecki MB, Sandahl TD, Nexo E, et al. A soluble form of the macrophage-related mannose receptor (MR/CD206) is present in human serum and elevated in critical illness. Clin Chem Lab Med. 2014;52(3):453-61.

53. Nielsen MC, Andersen MN, Rittig N, Rodgaard-Hansen S, Gronbaek H, Moestrup SK, et al. The macrophage-related biomarkers sCD163 and sCD206 are released by different shedding mechanisms. J Leukoc Biol. 2019;106(5):1129-38.

54. Sandahl TD, Stoy SH, Laursen TL, Rodgaard-Hansen S, Moller HJ, Moller S, et al. The soluble mannose receptor (sMR) is elevated in alcoholic liver disease and associated with disease severity, portal hypertension, and mortality in cirrhosis patients. PLoS One. 2017;12(12):e0189345.

55. Bossen L, Vesterhus M, Hov JR, Farkkila M, Rosenberg WM, Moller HJ, et al. Circulating Macrophage Activation Markers Predict Transplant-Free Survival in Patients With Primary Sclerosing Cholangitis. Clin Transl Gastroenterol. 2021;12(3):e00315.

56. Andersen ES, Rodgaard-Hansen S, Moessner B, Christensen PB, Moller HJ, Weis N. Macrophage-related serum biomarkers soluble CD163 (sCD163) and soluble mannose receptor (sMR) to differentiate mild liver fibrosis from cirrhosis in patients with chronic hepatitis C: a pilot study. Eur J Clin Microbiol Infect Dis. 2014;33(1):117-22.

57. Saha B, Tornai D, Kodys K, Adejumo A, Lowe P, McClain C, et al. Biomarkers of Macrophage Activation and Immune Danger Signals Predict Clinical Outcomes in Alcoholic Hepatitis. Hepatology. 2019;70(4):1134-49.

58. Stoy S, Laursen TL, Eriksen LL, Gronbaek H, Vilstrup H, Sandahl TD. No Effect in Alcoholic Hepatitis of Gut-Selective, Broad-Spectrum Antibiotics on Bacterial Translocation or Hepatic and Systemic Inflammation. Clin Transl Gastroenterol. 2021;12(2):e00306.

59. Suzuki Y, Shirai M, Asada K, Yasui H, Karayama M, Hozumi H, et al. Macrophage mannose receptor, CD206, predict prognosis in patients with pulmonary tuberculosis. Sci Rep. 2018;8(1):13129.

60. Zou R, Gui X, Zhang J, Tian Y, Liu X, Tian M, et al. Association of serum macrophage-mannose receptor CD206 with mortality in idiopathic pulmonary fibrosis. Int Immunopharmacol. 2020;86:106732.

61. Andersen MN, Andersen NF, Lauridsen KL, Etzerodt A, Sorensen BS, Abildgaard N, et al. STAT3 is over-activated within CD163(pos) bone marrow macrophages in both Multiple Myeloma and the benign pre-condition MGUS. Cancer Immunol Immunother. 2022;71(1):177-87.

62. Andersen MN, Andersen NF, Rodgaard-Hansen S, Hokland M, Abildgaard N, Moller HJ. The novel biomarker of alternative macrophage activation, soluble mannose receptor (sMR/sCD206): Implications in multiple myeloma. Leuk Res. 2015;39(9):971-5.

63. Heftdal LD, Stengaard-Pedersen K, Ornbjerg LM, Hetland ML, Horslev-Petersen K, Junker P, et al. Soluble CD206 plasma levels in rheumatoid arthritis reflect decrease in disease activity. Scand J Clin Lab Invest. 2017;77(5):385-9.

64. Heftdal LD, Loft AG, Hendricks O, Ashouri Christiansen A, Schiottz-Christensen B, Arnbak B, et al. Divergent effects on macrophage biomarkers soluble CD163 and CD206 in axial spondyloarthritis. Scand J Clin Lab Invest. 2018;78(6):483-9.

65. Loonen AJM, Leijtens S, Serin O, Hilbink M, Wever PC, van den Brule AJC, et al. Soluble mannose receptor levels in blood correlate to disease severity in patients with community-acquired pneumonia. Immunol Lett. 2019;206:28-32.

66. Tsuchiya K, Suzuki Y, Yoshimura K, Yasui H, Karayama M, Hozumi H, et al. Macrophage Mannose Receptor CD206 Predicts Prognosis in Community-acquired Pneumonia. Sci Rep. 2019;9(1):18750.

67. Horiike Y, Suzuki Y, Fujisawa T, Yasui H, Karayama M, Hozumi H, et al. Successful classification of macrophage-mannose receptor CD206 in severity of anti-MDA5 antibody positive dermatomyositis associated ILD. Rheumatology (Oxford). 2019;58(12):2143-52.

68. Shen YW, Zhang YM, Huang ZG, Wang GC, Peng QL. Increased Levels of Soluble CD206 Associated with Rapidly Progressive Interstitial Lung Disease in Patients with Dermatomyositis. Mediators Inflamm. 2020;2020:7948095.

69. Ding D, Song Y, Yao Y, Zhang S. Preoperative serum macrophage activated biomarkers soluble mannose receptor (sMR) and soluble haemoglobin scavenger receptor (sCD163), as novel markers for the diagnosis and prognosis of gastric cancer. Oncol Lett. 2017;14(3):2982-90.

70. Andersen MN, Honge BL, Jespersen S, Medina C, da Silva Te D, Laursen A, et al. Soluble Macrophage Mannose Receptor (sCD206/sMR) as a Biomarker in Human Immunodeficiency Virus Infection. J Infect Dis. 2018;218(8):1291-5.

71. Fan W, Yang X, Huang F, Tong X, Zhu L, Wang S. Identification of CD206 as a potential biomarker of cancer stem-like cells and therapeutic agent in liver cancer. Oncol Lett. 2019;18(3):3218-26.

72. Marie Relster M, Gaini S, Moller HJ, Johansen IS, Pedersen C. The macrophage activation marker sMR as a diagnostic and prognostic marker in patients with acute infectious disease with or without sepsis. Scand J Clin Lab Invest. 2018;78(3):180-6.

73. Chavele KM, Martinez-Pomares L, Domin J, Pemberton S, Haslam SM, Dell A, et al. Mannose receptor interacts with Fc receptors and is critical for the development of crescentic glomerulonephritis in mice. J Clin Invest. 2010;120(5):1469-78.

74. Duffield JS, Tipping PG, Kipari T, Cailhier JF, Clay S, Lang R, et al. Conditional ablation of macrophages halts progression of crescentic glomerulonephritis. Am J Pathol. 2005;167(5):1207-19.

75. Ikezumi Y, Hurst LA, Masaki T, Atkins RC, Nikolic-Paterson DJ. Adoptive transfer studies demonstrate that macrophages can induce proteinuria and mesangial cell proliferation. Kidney Int. 2003;63(1):83-95.

76. Kitamura M, Suto T, Yokoo T, Shimizu F, Fine LG. Transforming growth factor-beta 1 is the predominant paracrine inhibitor of macrophage cytokine synthesis produced by glomerular mesangial cells. J Immunol. 1996;156(8):2964-71.

77. Embgenbroich M, van der Zande HJP, Hussaarts L, Schulte-Schrepping J, Pelgrom LR, Garcia-Tardon N, et al. Soluble mannose receptor induces proinflammatory macrophage activation and metaflammation. Proc Natl Acad Sci U S A. 2021;118(31).

78. Kelly B, O'Neill LA. Metabolic reprogramming in macrophages and dendritic cells in innate immunity. Cell Res. 2015;25(7):771-84.

79. Xue J, Schmidt SV, Sander J, Draffehn A, Krebs W, Quester I, et al. Transcriptome-based network analysis reveals a spectrum model of human macrophage activation. Immunity. 2014;40(2):274-88.

80. Shrivastava P, Katagiri T, Ogimoto M, Mizuno K, Yakura H. Dynamic regulation of Src-family kinases by CD45 in B cells. Blood. 2004;103(4):1425-32.

81. Chen J. The Src/PI3K/Akt signal pathway may play a key role in decreased drug efficacy in obesity-associated cancer. J Cell Biochem. 2010;110(2):279-80.

82. Abu-Amer Y, Ross FP, McHugh KP, Livolsi A, Peyron JF, Teitelbaum SL. Tumor necrosis factor-alpha activation of nuclear transcription factor-kappaB in marrow macrophages is mediated by c-Src tyrosine phosphorylation of Ikappa Balpha. J Biol Chem. 1998;273(45):29417-23.

83. Bai D, Ueno L, Vogt PK. Akt-mediated regulation of NFkappaB and the essentialness of NFkappaB for the oncogenicity of PI3K and Akt. Int J Cancer. 2009;125(12):2863-70.

84. Cheng J, Phong B, Wilson DC, Hirsch R, Kane LP. Akt fine-tunes NF-kappaB-dependent gene expression during T cell activation. J Biol Chem. 2011;286(41):36076-85.

85. Xie X, Lan T, Chang X, Huang K, Huang J, Wang S, et al. Connexin43 mediates NF-kappaB signalling activation induced by high glucose in GMCs: involvement of c-Src. Cell Commun Signal. 2013;11(1):38.

86. Weisberg SP, McCann D, Desai M, Rosenbaum M, Leibel RL, Ferrante AW, Jr. Obesity is associated with macrophage accumulation in adipose tissue. J Clin Invest. 2003;112(12):1796-808.

87. Obstfeld AE, Sugaru E, Thearle M, Francisco AM, Gayet C, Ginsberg HN, et al. C-C chemokine receptor 2 (CCR2) regulates the hepatic recruitment of myeloid cells that promote obesity-induced hepatic steatosis. Diabetes. 2010;59(4):916-25.

88. Kanda H, Tateya S, Tamori Y, Kotani K, Hiasa K, Kitazawa R, et al. MCP-1 contributes to macrophage infiltration into adipose tissue, insulin resistance, and hepatic steatosis in obesity. J Clin Invest. 2006;116(6):1494-505.

89. Lackey DE, Olefsky JM. Regulation of metabolism by the innate immune system. Nat Rev Endocrinol. 2016;12(1):15-28.

90. Lumeng CN, Bodzin JL, Saltiel AR. Obesity induces a phenotypic switch in adipose tissue macrophage polarization. J Clin Invest. 2007;117(1):175-84.

91. Hotamisligil GS, Shargill NS, Spiegelman BM. Adipose expression of tumor necrosis factor-alpha: direct role in obesity-linked insulin resistance. Science. 1993;259(5091):87-91.

92. Stienstra R, Joosten LA, Koenen T, van Tits B, van Diepen JA, van den Berg SA, et al. The inflammasome-mediated caspase-1 activation controls adipocyte differentiation and insulin sensitivity. Cell Metab. 2010;12(6):593-605.

93. Sullivan TJ, Miao Z, Zhao BN, Ertl LS, Wang Y, Krasinski A, et al. Experimental evidence for the use of CCR2 antagonists in the treatment of type 2 diabetes. Metabolism. 2013;62(11):1623-32.

94. Nawaz A, Aminuddin A, Kado T, Takikawa A, Yamamoto S, Tsuneyama K, et al. CD206(+) M2-like macrophages regulate systemic glucose metabolism by inhibiting proliferation of adipocyte progenitors. Nat Commun. 2017;8(1):286.

95. van Vliet SJ, Bay S, Vuist IM, Kalay H, Garcia-Vallejo JJ, Leclerc C, et al. MGL signaling augments TLR2-mediated responses for enhanced IL-10 and TNF-alpha secretion. J Leukoc Biol. 2013;94(2):315-23.

96. van Vliet SJ, Gringhuis SI, Geijtenbeek TB, van Kooyk Y. Regulation of effector T cells by antigen-presenting cells via interaction of the C-type lectin MGL with CD45. Nat Immunol. 2006;7(11):1200-8.

97. Westcott DJ, Delproposto JB, Geletka LM, Wang T, Singer K, Saltiel AR, et al. MGL1 promotes adipose tissue inflammation and insulin resistance by regulating 7/4hi monocytes in obesity. J Exp Med. 2009;206(13):3143-56.

98. Castoldi A, Andrade-Oliveira V, Aguiar CF, Amano MT, Lee J, Miyagi MT, et al. Dectin-1 Activation Exacerbates Obesity and Insulin Resistance in the Absence of MyD88. Cell Rep. 2017;19(11):2272-88.

99. Kingeter LM, Lin X. C-type lectin receptor-induced NF-kappaB activation in innate immune and inflammatory responses. Cell Mol Immunol. 2012;9(2):105-12.

100. Greco SH, Torres-Hernandez A, Kalabin A, Whiteman C, Rokosh R, Ravirala S, et al. Mincle Signaling Promotes Con A Hepatitis. J Immunol. 2016;197(7):2816-27.

101. Nakamura N, Shimaoka Y, Tougan T, Onda H, Okuzaki D, Zhao H, et al. Isolation and expression profiling of genes upregulated in bone marrow-derived mononuclear cells of rheumatoid arthritis patients. DNA Res. 2006;13(4):169-83.

102. Kostarnoy AV, Gancheva PG, Lepenies B, Tukhvatulin AI, Dzharullaeva AS, Polyakov NB, et al. Receptor Mincle promotes skin allergies and is capable of recognizing cholesterol sulfate. Proc Natl Acad Sci U S A. 2017;114(13):E2758-E65.

103. Ichioka M, Suganami T, Tsuda N, Shirakawa I, Hirata Y, Satoh-Asahara N, et al. Increased expression of macrophage-inducible C-type lectin in adipose tissue of obese mice and humans. Diabetes. 2011;60(3):819-26.

104. Tanaka M, Ikeda K, Suganami T, Komiya C, Ochi K, Shirakawa I, et al. Macrophage-inducible C-type lectin underlies obesity-induced adipose tissue fibrosis. Nat Commun. 2014;5:4982.

105. Tanaka M. Molecular mechanism of obesity-induced adipose tissue inflammation; the role of Mincle in adipose tissue fibrosis and ectopic lipid accumulation. Endocr J. 2020;67(2):107-11.

106. Takanabe-Mori R, Ono K, Sowa N, Wada H, Takaya T, Horie T, et al. Lectin-like oxidized low-density lipoprotein receptor-1 is required for the adipose tissue expression of proinflammatory cytokines in high-fat diet-induced obese mice. Biochem Biophys Res Commun. 2010;398(3):576-80.

107. Sawamura T, Kume N, Aoyama T, Moriwaki H, Hoshikawa H, Aiba Y, et al. An endothelial receptor for oxidized low-density lipoprotein. Nature. 1997;386(6620):73-7.

108. Yoshida H, Kondratenko N, Green S, Steinberg D, Quehenberger O. Identification of the lectin-like receptor for oxidized low-density lipoprotein in human macrophages and its potential role as a scavenger receptor. Biochem J. 1998;334 (Pt 1):9-13.

109. Kume N, Kita T. Roles of lectin-like oxidized LDL receptor-1 and its soluble forms in atherogenesis. Curr Opin Lipidol. 2001;12(4):419-23.

110. Murase T, Kume N, Kataoka H, Minami M, Sawamura T, Masaki T, et al. Identification of soluble forms of lectin-like oxidized LDL receptor-1. Arterioscler Thromb Vasc Biol. 2000;20(3):715-20.

111. Hofmann A, Brunssen C, Wolk S, Reeps C, Morawietz H. Soluble LOX-1: A Novel Biomarker in Patients With Coronary Artery Disease, Stroke, and Acute Aortic Dissection? J Am Heart Assoc. 2020;9(1):e013803.

112. Mitsuoka H, Kume N, Hayashida K, Inui-Hayashiada A, Aramaki Y, Toyohara M, et al. Interleukin 18 stimulates release of soluble lectin-like oxidized LDL receptor-1 (sLOX-1). Atherosclerosis. 2009;202(1):176-82.

113. Zhao XQ, Zhang MW, Wang F, Zhao YX, Li JJ, Wang XP, et al. CRP enhances soluble LOX-1 release from macrophages by activating TNF-alpha converting enzyme. J Lipid Res. 2011;52(5):923-33.

114. Gioia M, Vindigni G, Testa B, Raniolo S, Fasciglione GF, Coletta M, et al. Membrane Cholesterol Modulates LOX-1 Shedding in Endothelial Cells. PLoS One. 2015;10(10):e0141270.

115. Maslowska M, Vu H, Phelis S, Sniderman AD, Rhode BM, Blank D, et al. Plasma acylation stimulating protein, adipsin and lipids in non-obese and obese populations. Eur J Clin Invest. 1999;29(8):679-86.

116. Markstad H, Edsfeldt A, Yao Mattison I, Bengtsson E, Singh P, Cavalera M, et al. High Levels of Soluble Lectinlike Oxidized Low-Density Lipoprotein Receptor-1 Are Associated With Carotid Plaque Inflammation and Increased Risk of Ischemic Stroke. J Am Heart Assoc. 2019;8(4):e009874.

117. Hayashida K, Kume N, Murase T, Minami M, Nakagawa D, Inada T, et al. Serum soluble lectin-like oxidized low-density lipoprotein receptor-1 levels are elevated in acute coronary syndrome: a novel marker for early diagnosis. Circulation. 2005;112(6):812-8.

118. Pirillo A, Catapano AL. Soluble lectin-like oxidized low density lipoprotein receptor-1 as a biochemical marker for atherosclerosis-related diseases. Dis Markers. 2013;35(5):413-8.

119. Kume N, Mitsuoka H, Hayashida K, Tanaka M, Kominami G, Kita T. Soluble lectin-like oxidized LDL receptor-1 (sLOX-1) as a sensitive and specific biomarker for acute coronary syndrome--comparison with other biomarkers. J Cardiol. 2010;56(2):159-65.

120. Zhao ZW, Zhu XL, Luo YK, Lin CG, Chen LL. Circulating soluble lectin-like oxidized low-density lipoprotein receptor-1 levels are associated with angiographic coronary lesion complexity in patients with coronary artery disease. Clin Cardiol. 2011;34(3):172-7.

121. Skarpengland T, Skjelland M, Kong XY, Skagen K, Holm S, Otterdal K, et al. Increased Levels of Lectin-Like Oxidized Low-Density Lipoprotein Receptor-1 in Ischemic Stroke and Transient Ischemic Attack. J Am Heart Assoc. 2018;7(2).

122. Gazi U, Martinez-Pomares L. Influence of the mannose receptor in host immune responses. Immunobiology. 2009;214(7):554-61.

123. Paccosi S, Pala L, Cresci B, Silvano A, Cecchi M, Caporale R, et al. Insulin resistance and obesity affect monocyte-derived dendritic cell phenotype and function. Diabetes Res Clin Pract. 2020;170:108528.

124. Plazolles N, Humbert JM, Vachot L, Verrier B, Hocke C, Halary F. Pivotal advance: The promotion of soluble DC-SIGN release by inflammatory signals and its enhancement of cytomegalovirus-mediated cis-infection of myeloid dendritic cells. J Leukoc Biol. 2011;89(3):329-42.

125. Wu X, Zhang J, Ge H, Gupte J, Baribault H, Lee KJ, et al. Soluble CLEC2 Extracellular Domain Improves Glucose and Lipid Homeostasis by Regulating Liver Kupffer Cell Polarization. EBioMedicine. 2015;2(3):214-24.

126. Kazama F, Nakamura J, Osada M, Inoue O, Oosawa M, Tamura S, et al. Measurement of soluble C-type lectin-like receptor 2 in human plasma. Platelets. 2015;26(8):711-9.

127. Jaitin DA, Adlung L, Thaiss CA, Weiner A, Li B, Descamps H, et al. Lipid-Associated Macrophages Control Metabolic Homeostasis in a Trem2-Dependent Manner. Cell. 2019;178(3):686-98 e14.

128. Maquoi E, Munaut C, Colige A, Collen D, Lijnen HR. Modulation of adipose tissue expression of murine matrix metalloproteinases and their tissue inhibitors with obesity. Diabetes. 2002;51(4):1093-101.

129. Chavey C, Mari B, Monthouel MN, Bonnafous S, Anglard P, Van Obberghen E, et al. Matrix metalloproteinases are differentially expressed in adipose tissue during obesity and modulate adipocyte differentiation. J Biol Chem. 2003;278(14):11888-96.

130. de Meijer VE, Sverdlov DY, Le HD, Popov Y, Puder M. Tissue-specific differences in inflammatory infiltrate and matrix metalloproteinase expression in adipose tissue and liver of mice with diet-induced obesity. Hepatol Res. 2012;42(6):601-10.

CHAPTER 5

LKB1 signaling in dendritic cells controls whole-body metabolic homeostasis by limiting T helper 17 priming

Hendrik J.P. van der Zande, Eline C. Brombacher, Joost M. Lambooij, Leonard R. Pelgrom, Anna Zawistowska-Deniziak, Thiago A. Patente, Graham A. Heieis, Frank Otto, Arifa Ozir-Fazalalikhan, Maria Yazdanbakhsh, Bart Everts* and Bruno Guigas*

*These authors contributed equally to this study

JCI Insight (*in revision*)
bioRxiv 2021.10.14.464396
doi: 10.1101/2021.10.14.464396

Abstract

Obesity-associated metaflammation drives the development of insulin resistance and type 2 diabetes, notably through modulating innate and adaptive immune cells in metabolic organs. The nutrient sensor liver kinase B1 (LKB1) has recently been shown to control cellular metabolism and T cell priming functions of dendritic cells (DCs). Here, we report that hepatic DCs from high-fat diet (HFD)-fed obese mice display increased LKB1 phosphorylation and that LKB1 deficiency in DCs ($CD11c^{\Delta LKB1}$) worsened HFD-driven hepatic steatosis, systemic insulin resistance and glucose intolerance. Loss of LKB1 in DCs was associated with increased cellular expression of Th17-polarizing cytokines and increased hepatic $CD4^+$ $IL\text{-}17A^+$ Th17 cells in HFD-fed mice. Importantly, IL-17A neutralization rescued metabolic perturbations in HFD-fed $CD11c^{\Delta LKB1}$ mice. Mechanistically, disrupted metabolic homeostasis was independent of the canonical LKB1-AMPK axis. Instead, we provide evidence for involvement of the AMPK-related salt-inducible kinase(s) in controlling Th17-polarizing cytokine expression in LKB1-deficient DCs. Altogether, our data reveal a key role for LKB1 signaling in DCs in protection against obesity-induced metabolic dysfunctions by limiting hepatic Th17 differentiation.

Introduction

Obesity is associated with chronic low-grade inflammation, also known as metaflammation, where continuous overnutrition generates a self-sustained inflammatory loop in metabolic tissues that drives insulin resistance and type 2 diabetes (1). One of the hallmarks of metaflammation is the accumulation of myeloid cells in the main metabolic organs, *i.e.* white adipose tissue (WAT), liver and skeletal muscle (2). Macrophage-related cytokines such as tumor necrosis factor (TNF) and interleukin (IL)-1β were shown to inhibit insulin signaling (3, 4) and as such, macrophages are considered key players in the etiology of tissue-specific insulin resistance. However, dendritic cells (DCs) also accumulate in WAT and liver during obesity and are associated with metabolic dysfunctions. Indeed, depletion of the entire DC population or specific conventional DC (cDC) subsets in different genetic mouse models alleviates adipose tissue and/or hepatic inflammation, although the underlying mechanisms are incompletely understood (5-8).

DCs are specialized antigen presenting cells that govern T cell responses depending on the inflammatory and metabolic microenvironment. Moreover, modulation of T helper cell subsets in metabolic tissues has been shown to play a role in the control of immunometabolic homeostasis. For instance, T helper 2 (Th2) cells and regulatory T cells (Tregs) are enriched in lean, insulin sensitive WAT and contribute to maintenance of tissue-specific insulin sensitivity (9-11). On the contrary, Th17 cells accumulate in WAT and liver during obesity, and are associated with hepatic steatosis and insulin resistance (12-16). In addition, preventing CXCR3-dependent hepatic Th17 accrual and blocking IL-17A signaling using neutralizing antibodies both alleviated non-alcoholic fatty liver disease (NAFLD) (15, 16), suggesting an important contribution of hepatic Th17 cells to NAFLD severity. Although both DCs and T helper cell subsets in metabolic tissues have been associated with control of metabolic homeostasis, little is known about the regulation of DC-mediated T helper cell polarization in these organs during the development of obesity, and its impact on whole-body insulin sensitivity.

DC-mediated priming of Tregs and effector Th1, Th2 and Th17 cells is considered to be driven by metabolic rewiring of DCs in response to environmental cues, which controls co-stimulatory molecule and cytokine expression that shape T helper cell polarization (17). For example, *in vitro* Toll-like receptor (TLR)-activated mature DCs depend on glycolysis for fueling their anabolic demands, whereas quiescent DCs mainly rely on fatty acid oxidation and mitochondrial oxidative phosphorylation (18). As such, the obesity-induced changes in the metabolic organ microenvironment in which DCs reside may impact their T cell-polarizing capacities and contribute to metaflammation (19).

Among the bioenergetic sensors that regulate DC intrinsic metabolism and function *in vivo*, liver kinase B1 (LKB1) has recently received considerable attention (20-22). The tumor suppressor LKB1 is a serine/threonine kinase that can phosphorylate and activate AMP-

activated protein kinase (AMPK) and 12 other members of the AMPK-related family of protein kinases (23, 24), thereby controlling cell growth, survival, polarity and metabolism (25). In DCs, LKB1 was shown to be a critical regulator of effector T cell and Treg priming, thereby maintaining anti-tumor immunity (21, 22). We therefore hypothesized that LKB1 in DCs may connect the changing metabolic microenvironment during obesity to altered T cell priming, thereby impacting whole-body metabolic homeostasis.

In the present study, we investigated the role of LKB1 signaling in DC-mediated T helper cell priming in metabolic tissues and its impact on metabolic homeostasis. We demonstrate that obesity increased LKB1 phosphorylation in hepatic DCs, and that loss of LKB1 in DCs exacerbated metabolic dysfunctions by promoting AMPK-independent Th17 polarization in obese mice. Finally, we identify salt-inducible kinase(s) (SIK) as the possible LKB1 downstream mediator in repressing Th17-polarizing cytokine expression in DCs.

Results

Obesity induces DC activation in metabolic tissues and increases LKB1 phosphorylation in hepatic DCs

To investigate the role of dendritic cells (DCs) in whole-body metabolic homeostasis during obesity, male C57BL/6J mice were fed a high-fat diet (HFD) for 24 weeks, resulting in significant increases in body weight and fat mass when compared to low-fat diet (LFD)-fed control mice (Figure 1A-C). Using flow cytometry (Supplementary Figure 1), we assessed the frequency and phenotype of DCs in metabolic tissues from lean and obese mice. The number of DCs was found to be significantly increased in WAT but not in the liver from obese mice (Figure 1D-E). However, DCs from both tissues exhibited increased expression of activation markers (Figure 1F-G), a feature specific to metabolic tissues as activation status of DCs remained unchanged in the spleen (Supplementary Figure 2A). These changes in DC phenotypes were associated with alterations in the T helper cell pool in metabolic tissues. In eWAT, interferon (IFN)γ^+ Th1 cells were increased at the expense of IL-5$^+$ Th2 cells and FOXP3$^+$ regulatory T cells (Tregs), while in the liver we detected increased Th1 cells, IL-17A$^+$ Th17 cells and Tregs (Figure 1H-I). In line with unaltered expression of activation markers on splenic DCs, T cell cytokine expression in the spleen was largely unaffected in obese mice (Supplementary Figure 2B). These data suggest that the changing microenvironment in metabolic tissues during obesity alters DC activation and, consequently, DC-mediated T cell polarization.

As a bioenergetic sensor, LKB1 was recently shown to be a critical regulator of DC biology and T cell responses *in vivo* (20-22). We next investigated LKB1 signaling in spleen, eWAT and liver DCs by flow cytometry to determine its potential role in tissue-specific DC responses to

HFD. Interestingly, we found a marked increase in phosphorylation of Ser431-LKB1 specifically in hepatic DCs from obese mice, suggesting that LKB1 signaling within DC is altered during high-fat feeding, whereas Ser79-ACC phosphorylation, as a proxy for activity of the canonical LKB1 downstream target AMPK, was unchanged (Figure 1J-K; Supplementary Figure 2C). Together, these findings indicate that obesity-induced changes in the hepatic microenvironment may affect LKB1 signaling in DCs which is associated with altered hepatic T cell polarization.

LKB1 deficiency in DCs aggravates obesity-induced metabolic dysfunctions

To study the role of LKB1 in DCs in the context of obesity-induced metaflammation, we crossed *Stk11*$^{flox/flox}$ mice to *Itgax*^{cre} mice to generate mice with CD11c-specific deletion of LKB1 as previously described (22). Male conditional knockout (CD11c$^{\Delta LKB1}$) and Cre^{-} littermate control (CD11c^{WT}) mice were fed an HFD for 18 weeks (Figure 2A), which did not result in differences in body weight gain or body composition between genotypes (Figure 2B-E). Food intake, energy expenditure, and carbohydrate (CHO) and fatty acid (FA) oxidation were also not affected by loss of LKB1 in CD11c- expressing cells (Supplementary Figure 3). However, despite similar levels at baseline, CD11c$^{\Delta LKB1}$ mice developed higher fasting blood glucose levels than CD11c^{WT} littermates after 6 weeks on HFD, which was sustained throughout the experiment (Figure 2F). Furthermore, whole-body insulin resistance and glucose intolerance were worsened in CD11c$^{\Delta LKB1}$ mice, while glucose-induced insulin levels were similar (Figure 2G-I). Altogether, LKB1 in DCs is important for mitigating insulin resistance and restraining metabolic dysfunctions in mice during HFD-induced obesity.

Deletion of LKB1 in DCs promotes hepatic Tregs and Th17 cells and exacerbates hepatic steatosis

We next determined if the exacerbated metabolic dysfunctions observed in obese CD11c$^{\Delta LKB1}$ mice could be driven by tissue-specific immunometabolic changes. In eWAT, total leukocyte count and relative abundances of eosinophils, neutrophils, monocytes and CD11c/CD86-expressing macrophages were mostly unaffected (Supplementary Figure 4A-F). In line with our previous findings that LKB1-deficient DCs are more migratory (22), we found that the relative abundance of eWAT DCs was decreased in obese CD11c$^{\Delta LKB1}$ mice while frequencies of conventional DC (cDC) subsets between genotypes remained similar (Supplementary Figure 4G-H). As previous work revealed that LKB1-deficient DCs induced Tregs and effector Th17 cells mostly in lymphoid tissues of lean mice (21, 22), we next assessed whether these T helper subsets are affected in eWAT from obese CD11c$^{\Delta LKB1}$ mice. Despite similar CD4 T cell abundance, frequencies of FOXP3^{+} Tregs and IL-17A^{+} Th17 cells within the CD4 T cell pool were increased

in eWAT from obese CD11c$^{\Delta LKB1}$ mice, while IL-5^{+} Th2 cells were not (Supplementary Figure 4I-L). However, when expressed as frequencies of total leukocytes, neither Tregs nor Th17 cells were significantly increased (Supplementary Figure 4M-N). Furthermore, adipocyte mean diameter and size distribution were not affected in obese CD11c$^{\Delta LKB1}$ mice (Supplementary Figure 4O-Q).

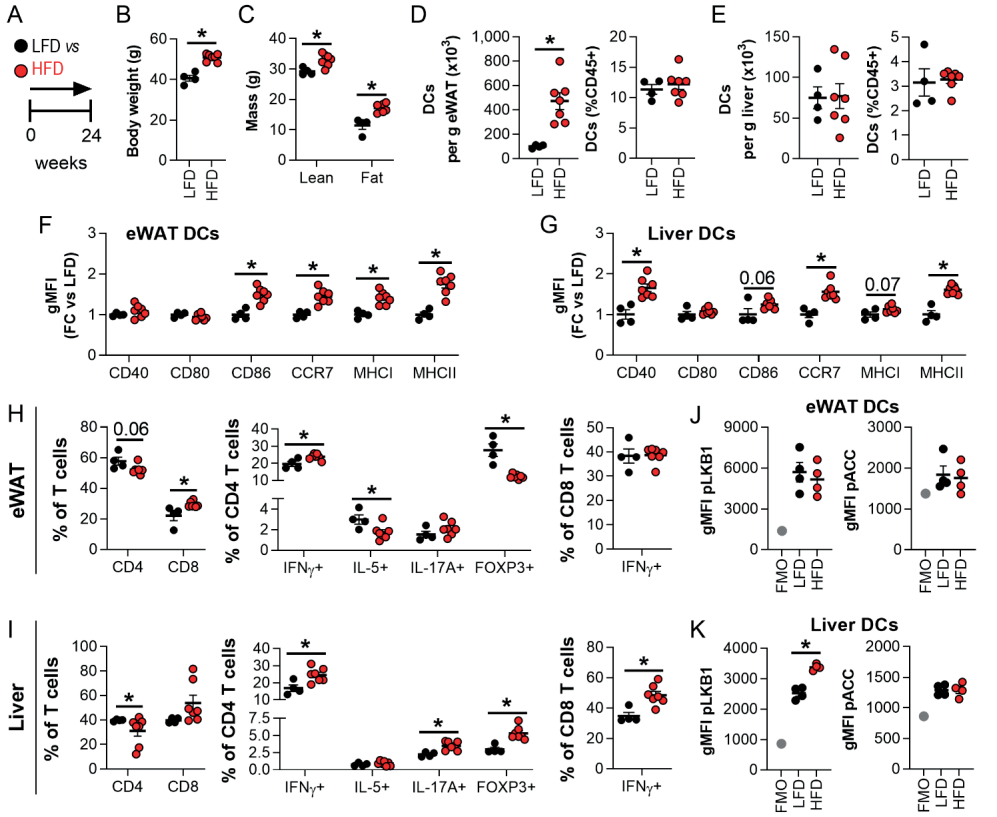

Figure 1. WAT and liver DCs are activated in obese mice. (**A**) Mice were fed a low-fat diet (LFD; black symbols) or a high fat diet (HFD; red symbols) for 24 weeks. (**B-C**) Body weight (*B*) and body composition (*C*) were measured at the end of the experiment. (**D-G**) At sacrifice, epididymal white adipose tissue (eWAT) and liver were collected and immune cells were isolated and analysed by flow cytometry. Absolute numbers of DCs per g tissue and frequencies of total leukocytes in eWAT (*D*) and liver (*E*). Relative expression of indicated DC markers by eWAT (*F*) and liver DCs (*G*). (**H-I**) Cells were restimulated with PMA/ionomycin in the presence of Brefeldin A for detection of intracellular cytokines, and were analysed by flow cytometry. CD4 and CD8 T cell, IFNγ^{+} (Th1), IL-5^{+} (Th2), IL-17A^{+} (Th17) and FOXP3^{+} (Treg) CD4 T cell and IFNγ^{+} CD8 T cell percentages in eWAT (*H*) and liver (*I*). (**J-K**) eWAT and liver were immediately formaldehyde-fixed after collection and immune cells were isolated. Phosphorylated LKB1 (Ser431) and ACC (Ser79) were measured in DCs from eWAT (*J*) and liver (*K*) by flow cytometry. Full gating strategies are shown in Supplementary Figure 1. Results are expressed as means ± SEM. * P<0.05 vs LFD (n = 4-7 mice per group).

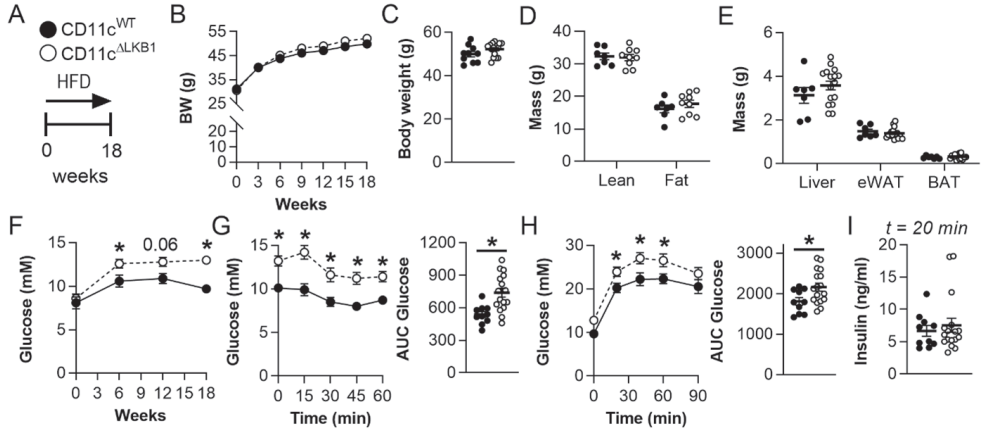

Figure 2. Deletion of LKB1 in DCs aggravates whole-body glucose intolerance and insulin resistance in obese mice. (**A**) $CD11c^{WT}$ (black symbols) and $CD11c^{\Delta LKB1}$ (open symbols) mice were fed a HFD for 18 weeks. (**B-C**) Body weight was monitored throughout the experiment. (**D-E**) Body composition (*D*) and weights of liver, eWAT and BAT (*E*) were measured at the end of the experiment. (**F**) Fasting blood glucose was measured at the indicated weeks. (**G**) An i.p. insulin tolerance test was performed 1 week before sacrifice. Blood glucose levels were measured at the indicated time points and the AUC of the glucose excursion curve was calculated. (**H**) An i.p. glucose tolerance test (GTT) was performed 1 week before sacrifice. Blood glucose levels were measured at the indicated time points and the AUC of the glucose excursion curve was calculated. (**I**) Plasma insulin was measured at 20 minutes post glucose injection during i.p. GTT. Data shown are a pool of two independent experiments. Results are expressed as means ± SEM. * P<0.05 vs $CD11c^{WT}$ (n = 7-17 mice per group).

In the liver, the abundance of total leukocytes, eosinophils, neutrophils, monocytes and macrophages, in addition to macrophage polarization, was unchanged in obese $CD11c^{\Delta LKB1}$ mice when compared to $CD11c^{WT}$ littermates (Figure 3A; Supplementary Figure 5). As was also seen in eWAT, the frequency of DCs was reduced in the livers of $CD11c^{\Delta LKB1}$ mice, although the relative abundance of DC subsets remained similar. (Figure 3B-C). Strikingly, the proportions of liver $CD4^+$ Tregs and Th17 cells were significantly increased in mice with LKB1-deficient DCs in comparison to LKB1-sufficient controls (Figure 3D-I). Moreover, the livers of $CD11c^{\Delta LKB1}$ obese mice exhibited enhanced hepatic steatosis when compared to WT littermates (Figure 3J-K). Consistent with this, hepatic triglyceride (TG) and total cholesterol (TC) levels were also increased (Figure 3L). Taken together, these results show that deletion of LKB1 in DCs induces a potent increase in Tregs and Th17 cells in the liver and exacerbates hepatic steatosis in obese mice.

IL-17A neutralization prevents exacerbated obesity-induced metabolic dysfunctions in mice lacking LKB1 in DCs

WAT and liver Th17 cells have consistently been linked to obesity-induced metabolic dysfunctions (13, 30), and hepatic steatosis in particular (12, 14-16). Accordingly, we observed elevated IL-17A-expressing CD4 T cells in the livers of obese mice lacking LKB1 in DCs, a feature that was associated with enhanced hepatic steatosis. Hence, to investigate the contribution of increased Th17 cells to worsened metabolic dysfunctions in $CD11c^{\Delta LKB1}$ obese mice, we treated them with either neutralizing antibodies for the Th17 effector cytokine IL-17A or isotype control during the first 6 weeks on HFD (Figure 4A). IL-17A neutralization did not impact body weight gain (Figure 4B-C) or hepatic Treg and Th17 cell abundances in $CD11c^{\Delta LKB1}$ mice (Supplementary Figure 6). However, IL-17A blockade led to significantly improved whole-body insulin sensitivity (Figure 4D) and reduced hepatic steatosis to comparable levels as $CD11c^{WT}$ littermates (Figure 4E-G). Thus, increased IL-17A in $CD11c^{\Delta LKB1}$ mice plays a central role in promoting liver steatosis and metabolic dysfunctions during HFD-induced obesity. Altogether our findings suggest that LKB1 in DCs mitigates hepatic inflammation during the development of obesity by restraining Th17 priming.

To explore a direct role for LKB1-deficient DCs in promoting Th17 polarization, we sorted hepatic type 2 conventional DCs (cDC2s), the main CD4 T cell-priming subset shown to induce Th17 priming (31), from lean $CD11c^{WT}$ and $CD11c^{\Delta LKB1}$ mice that were subcutaneously injected with Flt3L-secreting B16 melanomas to expand the *in vivo* DC pool (Figure 5A). Gene expression profiling validated knockout of *Stk11*, encoding LKB1, in hepatic cDC2s from $CD11c^{\Delta LKB1}$ mice (Figure 5C). While surface expression of activation markers on hepatic cDC2s was unchanged during homeostasis (Figure 5B), LPS-induced expression of the Th17-polarizing cytokines *Il6* and *Il1b* was enhanced in LKB1-deficient hepatic cDC2s when compared to controls, whereas *Il23a* was undetectable and *Tgfb1* unchanged (Figure 5C). These results show that LKB1 deficiency in DCs promotes production of cytokines, known to favor Th17 polarization, suggesting LKB1 in DCs restrains Th17 polarization by limiting IL-1β and IL-6 production.

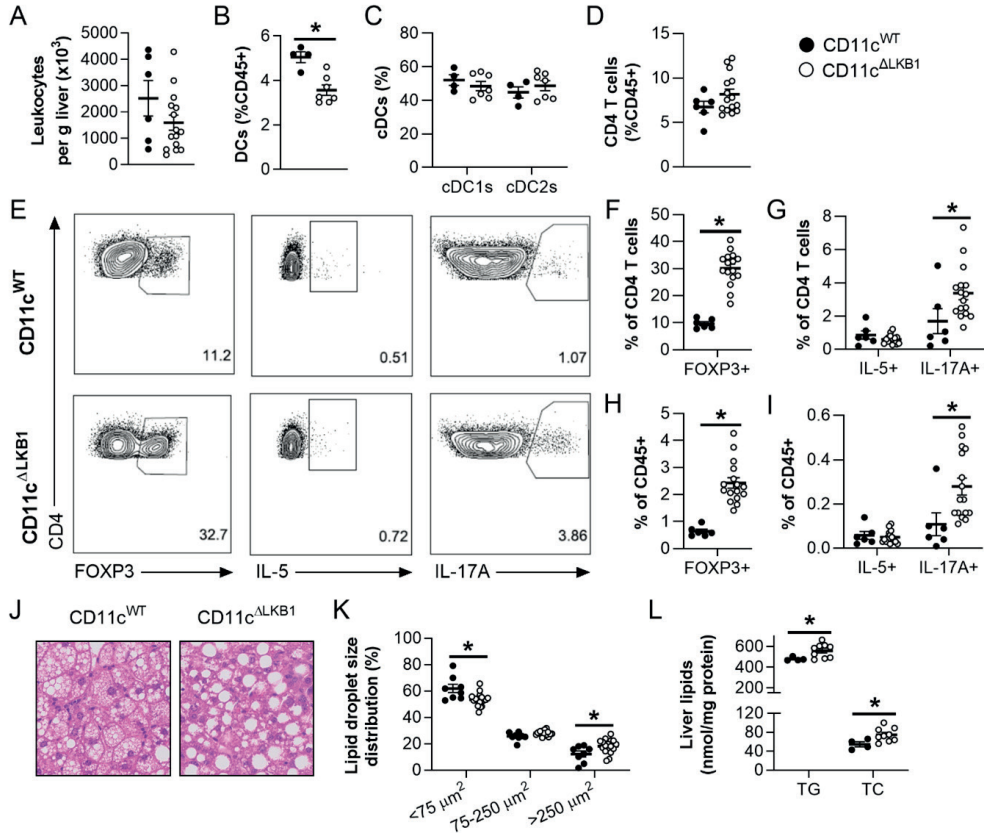

Figure 3. Obese CD11c$^{\Delta LKB1}$ mice are more susceptible to HFD-induced hepatic steatosis and have increased hepatic Treg and Th17 cells. CD11c^{WT} (black symbols) and CD11c$^{\Delta LKB1}$ (open symbols) mice were fed a HFD for 18 weeks. (**A-D**) At sacrifice, liver was collected and immune cells isolated. Total leukocytes per gram liver were quantified (*A*). Percentages of DCs (*B*), cDC subsets (*C*) and CD4 T cells (*D*) were determined by flow cytometry. (**E-I**) Liver leukocytes were restimulated with PMA and ionomycin in the presence of Brefeldin A for intracellular cytokine detection. Representative plots (*E*) and percentages of FOXP3$^+$ Tregs (*F,H*), IL-5$^+$ Th2 and IL-17A$^+$ Th17 cells (*G,I*) were determined as frequencies of CD4 T cells (*F,G*) or total leukocytes (*H,I*). (J) A part of liver was sectioned and H&E stained. (**K**) Lipid droplet sizes and size distribution were quantified from H&E-stained slides. (**L**) Hepatic triglyceride (TG) and total cholesterol (TC) contents were determined. Data shown are a pool of two independent experiments, except for B, C and L. Results are expressed as means ± SEM. * P<0.05 vs CD11c^{WT} (n = 6-17 mice per group for A, D-K; n = 4-9 mice per group for B, C and L).

The LKB1 downstream targets SIKs regulate Th17-polarizing cytokine expression in DCs independent of AMPK

Having demonstrated a role for LKB1 in DCs for preventing excessive obesity-induced metaflammation, we next investigated the signaling mediators downstream of LKB1 responsible for the altered Th17 priming function of DCs. The LKB1-AMPK axis represents a central node in the regulation of cellular energetics, where LKB1 promotes the downstream activation of AMPK though direct phosphorylation of its catalytic α-subunit (25). To assess whether AMPK is involved in the impaired metabolic homeostasis observed in CD11c$^{\Delta LKB1}$ obese mice, we generated CD11c$^{\Delta AMPK\alpha1}$ mice, in which AMPKα1, the main α-subunit expressed by DCs (32), is deleted in these cells (22). We next fed them and their CD11c^{WT} littermates an HFD for 18 weeks (Supplementary Figure 7A). Surprisingly, none of the abovementioned detrimental immunometabolic changes observed in CD11c$^{\Delta LKB1}$ obese mice, *i.e.* increased fasting glucose levels, glucose intolerance, insulin resistance, and hepatic Tregs and Th17 cells, were recapitulated in HFD-fed CD11c$^{\Delta AMPK\alpha1}$ mice (Supplementary Figure 7B-M). These data indicate that LKB1-deficiency promotes hepatic Th17 polarization in an AMPK-independent manner.

In addition to AMPK, LKB1 phosphorylates several other downstream AMPK-related kinases including MARK1-4, SIK1-3, NUAK1-2, SNRK and BRSK1-2 (23, 24). We therefore investigated which LKB1 target(s) may contribute to altering DC function by analyzing published datasets for their expression in total splenic DCs, as well as mature GM-CSF-elicited bone-marrow DCs (GMDCs; Supplementary Figure 8). The expression profiles were similar between primary splenic DCs and GMDCs, showing that all these kinases were expressed to a significant level with the notable exception of *Prkaa2* (encoding AMPKα2), confirming that only the catalytic AMPKα1 isoform is expressed by DCs (32), *Mark1* and the members of the BRSK family (Supplementary Figure 8A-B). Hence, we next determined their role in production of cytokine driving Th17 polarization by DCs. GMDCs were treated with inhibitors of MARK, SIK, NUAK and AMPK families prior to LPS stimulation, and intracellular levels of Th17-polarizing cytokines were assessed by flow cytometry. Largely consistent with liver-derived cDC2s from CD11c$^{\Delta LKB1}$ mice, LKB1-deficient GMDCs (Supplementary Figure 8C) displayed upregulated LPS-induced expression of pro-IL-1β, IL-6 and IL-23p19 when compared to wild-type GMDCs, whereas latency-associated peptide (LAP) expression, as a proxy for TGF-β production, was unchanged (Figure 5D). Strikingly, inhibition of SIKs, but not of the other LKB1 downstream kinases, recapitulated the cytokine profile of LKB1-deficient GMDCs (Figure 5D), identifying SIKs in DCs as potential regulators of Th17 polarization. Collectively, our data indicate that LKB1 signaling in DCs controls hepatic Th17 differentiation and metabolic homeostasis in obese mice, and we propose a role for SIK downstream of LKB1 in repression of Th17-polarizing cytokines.

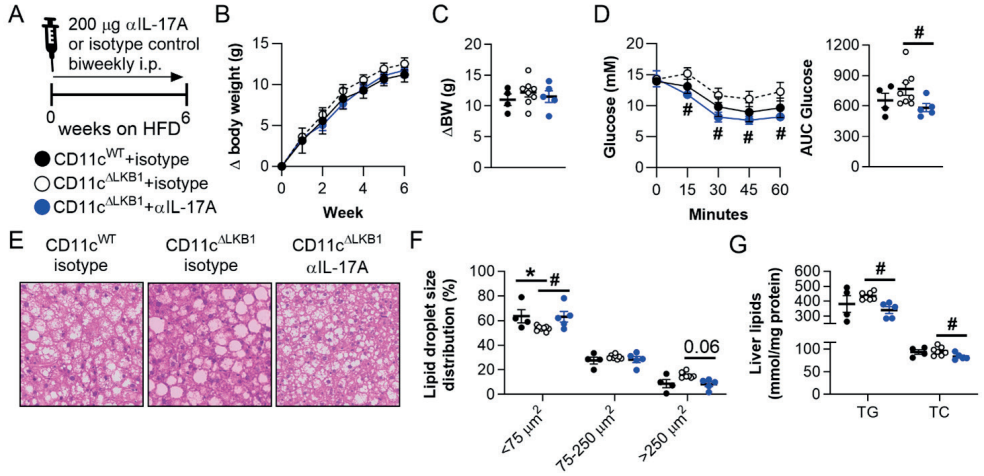

Figure 4. IL-17A neutralization rescued metabolic dysfunctions in CD11c$^{\Delta LKB1}$ mice. (**A**) CD11c^{WT} (black symbols) and CD11c$^{\Delta LKB1}$ mice were fed a HFD for 6 weeks while concomitant biweekly intraperitoneal treatment with IL-17A neutralizing antibodies (blue symbols) or isotype control (open symbols). (**B-C**) Body weight gain was monitored throughout the experiment. (**D**) An i.p. insulin tolerance test was performed during week 6. (**E**) At sacrifice, a piece of liver was sectioned and H&E stained. (**F**) Lipid droplet size distribution was quantified from H&E-stained slides. (**G**) Hepatic TG and TC content were determined. Data shown are a pool of two independent experiments. Results are expressed as means ± SEM. * P<0.05 vs CD11c^{WT}; # P<0.05 vs CD11c$^{\Delta LKB1}$ + isotype control (n = 4-8 mice per group).

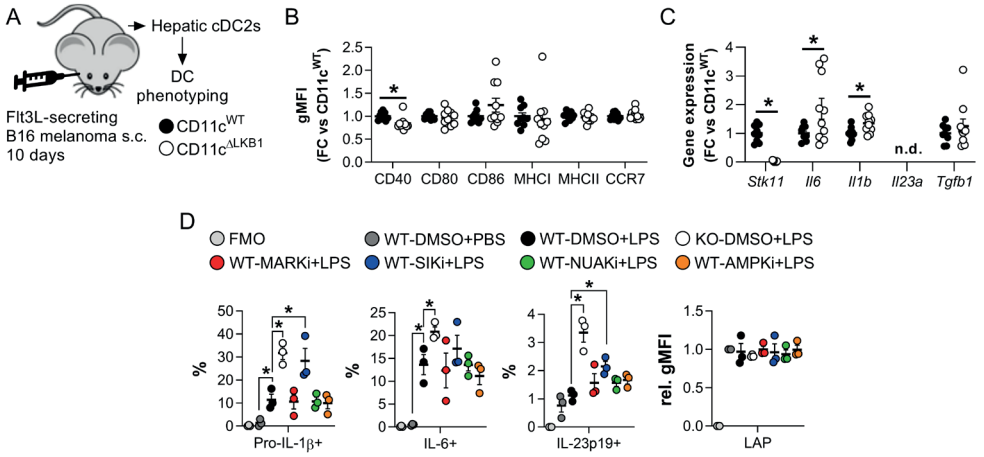

Figure 5. LKB1 deficiency increases Th17-polarizing cytokines expression in DCs, which is mediated through its downstream target SIK. (**A-C**) CD11c^{WT} (black symbols) and CD11c$^{\Delta LKB1}$ (open symbols) mice were subcutaneously injected with Flt3L-secreting B16 melanomas to expand the DC pool. After 10 days, hepatic cDC2s were FACS sorted for DC phenotyping (*A*). Expression

▲Figure 5. Legend (Continued)

of indicated DC markers was measured by flow cytometry (*B*). Expression of indicated genes was measured by RT-qPCR after *ex vivo* overnight LPS stimulation (*C*). (**D**) GM-CSF cultured bone marrow-derived DCs (GMDCs) from $CD11c^{WT}$ (WT) mice were treated with inhibitors targeting LKB1 downstream targets MARKs, SIKs, NUAKs and AMPK for 2 h, before LPS stimulation in the presence of Brefeldin A for 4 h and compared with $CD11c^{\Delta LKB1}$ GMDCs (KO). Pro-IL-1β, IL-6, IL-23p19 and LAP-expressing GMDCs were quantified by intracellular cytokine staining/flow cytometry. Data shown are a pool of three experiments. Results are expressed as means ± SEM. * $P<0.05$ vs $CD11c^{WT}$ or as indicated (n = 9-10 mice per group for A-C; n = 3 biological replicates per group for D).

Discussion

The bioenergetic sensor LKB1 was recently shown to be a critical regulator of DC metabolism, activation and T cell priming functions (20-22). Whether LKB1 signaling in DCs links the changing immunometabolic microenvironment during obesity with altered DC function and ultimately whole-body metabolic dysfunctions remained unclear. Here, we report that obesity increased LKB1 phosphorylation in hepatic DCs. Deletion of LKB1 from DCs aggravated HFD-induced insulin resistance and hepatic steatosis, and increased hepatic Tregs and Th17 cells in obese mice. These immunometabolic defects were restored by neutralizing the Th17 effector cytokine IL-17A, uncovering a role for LKB1 in restraining DC-mediated pathogenic Th17 cell differentiation, thereby controlling whole-body metabolic homeostasis.

Although DCs accumulate in WAT and liver during obesity and contribute to whole-body insulin resistance (5-8), the underlying mechanisms are incompletely understood. Indeed, obese *Flt3l*$^{-/-}$ mice lacking DCs and *Ccr7*$^{-/-}$ mice with impaired DC migration displayed reduced metaflammation and insulin resistance suggesting they have a central role in the development of metabolic dysfunctions (6, 7). Here, we report that DCs from eWAT and liver, but not spleen, of obese mice display increased expression of activation markers, indicating that the obesity-induced changes in the metabolic tissue microenvironment enhance DC activation. Interestingly, both eWAT and liver DCs from obese mice expressed higher levels of CCR7, suggestive of increased migration to draining lymph nodes where they can prime inflammatory T cells. Consistent with an increased proinflammatory activation profile of the DCs, we found that obesity altered the CD4 T helper cell pool in eWAT and liver, but not spleen, favoring Th1 cells at the expense of Th2 cells and Tregs in eWAT, and increasing Th1 cells, Th17 cells and Tregs in the liver. Some of these obesity-induced changes in T helper subsets in metabolic tissues have been reported previously (11, 16). Moreover, $XCR1^{+}$ type 1 conventional DCs (cDC1s), efficient at cross-presenting antigens to CD8 T cells, were reported to increase hepatic steatosis and contribute

to liver pathology, which was associated with inflammatory T cell reprogramming in the liver-draining lymph nodes (8). Congruent with this, we found increased HFD-induced IFNγ$^+$ CD8 T cells in the liver, most likely resulting from increased cDC1-mediated priming.

In addition to increased DC activation and altered T cell priming in metabolic tissues, we observed a significant increase of Ser431-LKB1 phosphorylation in hepatic DCs of obese mice. LKB1 is phosphorylated at Ser431 by protein kinase C ζ (PKCζ) (33), p90 ribosomal S6 kinase (p90-RSK) and cAMP-dependent protein kinase A (PKA) (34). Although the exact consequence of phosphorylation at this site remains unclear, the residue corresponding to murine Ser431 is conserved in all organisms, suggesting that its phosphorylation may play a role in modulating LKB1 signaling. Despite a lack of a phenotype and normal AMPK activation in knock-in mice carrying a homozygous Ser431 to alanine mutation in LKB1 (35), it has been suggested that Ser431 phosphorylation could promote nuclear export of LKB1 and phosphorylation of some of its cytoplasmic substrates (33, 36).

Interestingly, Ser431-LKB1 phosphorylation was unchanged in splenic and eWAT DCs, indicating that obesity-induced changes in the hepatic microenvironment may specifically alter LKB1 signaling in liver-associated DCs and change its effector functions. Obesity induces persistent changes in the gut microbiota, and endotoxemia through increased gut permeability (37). As a result, the gut and serum metabolome are altered (38, 39), promoting NAFLD pathogenesis through a gut-liver axis (40). Since LPS injection has been reported to acutely increase Ser431-LKB1 phosphorylation in whole lung and liver lysates, and in immortalized Raw264.7 macrophages (41), one may hypothesize that obesity-induced endotoxemia might contribute to increased pLKB1 levels in hepatic DCs from obese mice. Of note, in Raw264.7 macrophages, LPS-induced Ser431-LKB1 phosphorylation suppressed NF-κB signaling, suggesting that increased pLKB1 in hepatic DCs from obese mice may serve as a feedback mechanism to keep inflammation in check. In addition, butyrate, a short-chain fatty acid produced by commensal bacteria that metabolize indigestible fiber, was recently shown to increase Ser431-LKB1 phosphorylation in HepG2 hepatocytes (42), providing conceptual evidence that gut metabolites may alter LKB1 phosphorylation in liver-resident cells. Yet, the underlying mechanisms by which LKB1 signaling is selectively modulated in hepatic DCs during obesity remain to be identified.

Deletion of LKB1 from DCs increased hepatic Tregs and Th17 cells in obese mice. Though predominantly focused on adipose tissue, the role of Tregs in the regulation of metabolic homeostasis has become controversial over recent years. Seminal work revealed that adipose tissue Tregs are lost during obesity (11, 43), and replenishing the Treg pool through IL-33 treatment or adoptive transfer reduced adipose tissue inflammation and improved metabolic homeostasis (44, 45). However, aging-associated insulin resistance is

ameliorated after depletion of adipose tissue Tregs (46), and deletion of the insulin receptor, IL-10 and the transcription factor Blimp1 from Tregs all prevented insulin resistance, in part through promoting adaptive thermogenesis (47, 48). We found a trend for increased adipose tissue Tregs in CD11c$^{\Delta LKB1}$ mice, yet eWAT weight, adipocyte size distribution, BAT weight and energy expenditure were unchanged, excluding a role for adaptive thermogenesis in the metabolic phenotype of CD11c$^{\Delta LKB1}$ mice. Hepatic Tregs were rather reported to control hepatic inflammation and inhibit NASH development (49). In addition, we clearly demonstrate that neutralizing the Th17 effector cytokine IL-17A rescued the metabolic perturbations in HFD-fed CD11c$^{\Delta LKB1}$ mice, indicating an important role for Th17 cells in explaining the metabolic phenotype of obese CD11c$^{\Delta LKB1}$ mice.

Indeed, obesity-induced hepatic Th17 cells and IL-17A signaling are consistently reported to impair insulin sensitivity and promote hepatic steatosis (12-16). Th17 differentiation is dependent on the cytokines IL-6, TGFβ, IL-1β and IL-23 (50, 51), but different combinations can lead to different degrees of pathogenicity. In the context of experimental autoimmune encephalitis, IL-6 and TGFβ-induced Th17 cells were not pathogenic, whereas IL-6, IL-1β and IL-23 induced Th17 cells were pathogenic (52, 53). Furthermore, development of Th17 cells *in vivo* is dependent on SIRPα/CD172a expression on DCs (31, 54), a marker of cDC2s that efficiently prime CD4 T cells. We previously showed that LKB1-deficient splenic cDC2s produced higher levels of IL-6 (22). In addition, others showed that mRNA expression of *Il6*, *Tgfb2* and *Il23a* tended to be increased in LKB1-deficient total splenic DCs compared to WT DCs, whereas *Tgfb1* and *Tgfb3* were decreased or similar (21). Moreover, increased Th17 priming by LKB1-deficient splenic DCs was at least partly dependent on IL-6, but not TGFβ (21). Here, we find that LPS-stimulated LKB1-deficient GMDCs express significantly enhanced levels of IL-6, pro-IL-1β and IL-23p19, while TGFβ production was not affected. In addition, LKB1-deficient hepatic cDC2s express increased levels of *Il6* and *Il1b*, whereas *Tgfb1* was unchanged and *Il23a* undetectable. These data indicate that LKB1-deficient hepatic cDC2s display a cytokine profile that favors the development of pathogenic Th17 cells.

Recent single cell transcriptomics analysis of hepatic Th17 cells from HFD-fed obese mice identified two subsets, of which one was enriched during obesity. The accumulation of this inflammatory hepatic Th17 (ihTh17) subset was regulated through a CXCL9/10-CXCR3 axis, and these cells were sufficient to exacerbate NAFLD pathogenesis through glycolysis-facilitated production of proinflammatory cytokines IL-17A, TNF and IFNγ (16). Moreover, increased IL-6, TGFβ, IL-1β and IL-23 levels in steatotic livers were also reported in this study, suggesting involvement of DCs in generating these ihTh17 cells. Given their role in promoting NAFLD pathogenesis, it is tempting to speculate that LKB1-

deficient hepatic DCs promote accrual of these ihTh17 cells.

Deletion of AMPKα1 in DCs did not recapitulate the immunometabolic phenotype of CD11c$^{\Delta LKB1}$ obese mice. Indeed, we and others have recently shown that LKB1 functions independently of AMPK in governing Tregs and Th17 cell differentiation (21, 22), which corresponds with a growing line of research showing AMPK-independent effects of LKB1 in immune cells (41, 55). We rather show that SIK inhibition, but not of the other DC-expressed AMPK-related kinases, increased expression of IL-6, IL-1β and IL-23 in GMDCs, indicating that an LKB1-SIK axis is likely involved in controlling the expression of cytokines that polarize pathogenic Th17 cells. The SIK family consists of three isoforms, SIK1-3, and is involved in regulating hepatic gluconeogenesis, lipid metabolism and tumorigenesis (56), although its underlying mechanisms are only beginning to be understood. SIKs control the phosphorylation and nucleocytoplasmic transport of class IIa histone deacetylases (HDACs) and cAMP-regulated transcriptional coactivators (CRTCs), identifying a role for SIKs in transcriptional regulation (57). CRTC is a coactivator of cAMP response element-binding protein (CREB) (58), and the promotors of *Il6*, *Il1b* and *Il23a* all contain CREB binding sites (59-61). It is thus tempting to speculate that inhibition of SIKs may promote CRTC nuclear transport, thereby promoting transcription of Th17-polarizing cytokines. In support of this, SIK1 and SIK3 were shown to control IL-6 production in tumor cells (62), and IL-6 and IL-1β production in Raw264.7 macrophages (63). Conversely, pharmacological inhibition of SIKs was also reported to suppress proinflammatory cytokines production in DCs and macrophages (64, 65). As SIK family members display functional redundancy in some settings (57), future studies are required to identify which SIK family member(s) control expression of Th17-polarizing cytokines, and what the mechanistic underpinnings are.

Among the limitations of our study, we cannot formally rule out that deletion of LKB1 in other CD11c-expressing cells, such as macrophages, contributed to the immunometabolic phenotype. Indeed, LysM^{cre}-driven LKB1 deletion in macrophages increased LPS-induced proinflammatory cytokine production (41). However, these LysM$^{\Delta LKB1}$ mice have unchanged Treg numbers (20), indicating that LKB1 deletion from macrophages does not alter T cell polarization *in vivo*. In addition, only partial knockout of *Stk11* was observed in macrophages from CD11c$^{\Delta LKB1}$ mice (21, 66), which is likely attributable to lower CD11c expression by macrophages as compared to DCs. Furthermore, we found that expression of the proinflammatory/metaflammation-associated markers CD86 and CD11c on both eWAT and liver macrophages was either decreased or unchanged, as was *ex vivo* LPS-induced TNF production by macrophages from CD11c$^{\Delta LKB1}$ mice (data not shown). Together, this makes it unlikely that macrophages play a dominant role in the immunometabolic phenotype of CD11c$^{\Delta LKB1}$ mice.

Altogether, our data reveal a key role for LKB1 signaling in liver-resident DCs in limiting liver-specific and whole-body metabolic dysfunctions in the context of obesity, by

constraining hepatic Th17 accrual. We suggest the involvement of an LKB1-SIK axis to control expression of Th17-polarizing cytokines in DCs, opening interesting therapeutic options in controlling pathogenic Th17 cell development in metaflammation and other hyperinflammatory disorders.

Methods

Animals, diet and treatment

All experiments were performed in accordance with the Guide for the Care and Use of Laboratory Animals of the Institute for Laboratory Animal Research and have received approval from the Dutch Central Authority for Scientific Procedures on Animals (CCD; animal license number AVD116002015253). *Itgax*^{cre} (CD11c; PMID: 17591855), *Stk11*$^{fl/fl}$ (LKB1; PMID: 12226664), *Prkaa1*$^{fl/fl}$ (AMPKα1; PMID: 21124450) and WT mice, all on C57Bl/6J background, were purchased from The Jackson Laboratory or Envigo and crossed, housed and bred at the LUMC. Mice were housed in a temperature-controlled room with a 12-hour light-dark cycle and ad libitum access to food and tap water under specific pathogen free conditions. To reduce variation due to sex hormone cycles on whole-body metabolism, male mice were used for all in vivo experiments. An a priori power calculation was done. Analysis was performed blinded to the conditions.

8-16 weeks old age-matched WT, *Stk11*$^{fl/fl}$ (CD11c^{WT}), *Itgax*^{cre} *Stk11*$^{fl/fl}$ (CD11c$^{\Delta LKB1}$), *Prkaa1*$^{fl/fl}$ (CD11c^{WT}) and *Itgax*^{cre} *Prkaa1*$^{fl/fl}$ (CD11c$^{\Delta AMPK\alpha1}$) male mice were fed a high fat diet (HFD, 45% energy derived from fat, D12451, Research Diets) for 18-24 weeks as indicated.

For IL-17A neutralization experiments, 12-19 weeks old age-matched CD11c^{WT} and CD11c$^{\Delta LKB1}$ mice were systematically randomized over treatment groups based on body weight and fasting blood glucose levels, and fed a HFD for 6 weeks while concomitant biweekly treatment with 200 μg anti-mouse IL-17A (clone 17F3) or IgG1 κ isotype control (clone MOPC-21; both Bio X Cell). At sacrifice, spleen, visceral white adipose tissue (epididymal; eWAT), brown adipose tissue (intrascapular; BAT) and liver were weighed and collected for further processing.

Body composition and indirect calorimetry

Body composition was measured by MRI using an EchoMRI (Echo Medical Systems). Indirect calorimetry was performed in groups of 7-8 mice using a Comprehensive Laboratory Animal Monitoring System (Columbus Instruments) with free access to food and tap water.

Mice were individually housed at room temperature and a standard 12-hour light/dark cycle was maintained throughout the measurements. Mice were acclimated to the cages for a period of 48 hours before the start of 4 days of measurements at 20-minute intervals. Food intake was assessed by real-time feed weight measurements. Oxygen consumption and carbon dioxide production were measured, and based on this respirometry, energy expenditure (EE), and carbohydrate (CHO) and fatty acid (FA) oxidation were calculated as previously described (26).

Isolation of leukocytes from spleen

Spleens were collected in 500 µL RPMI 1640 + Glutamax (Life Technologies), mechanically disrupted, and digested for 20 min at 37 °C in medium supplemented with 1 mg/mL Collagenase D (Roche) and 2000 U/mL DNase I (Sigma-Aldrich). Digested samples were filtered through 100 µm filters and subjected to erythrocyte lysis buffer (0.15 M NH_4Cl, 1 mM $KHCO_3$, 0.1 mM Na_2EDTA) before counting using a hemocytometer.

Isolation of stromal vascular fraction from adipose tissue

After a 1-minute transcardial perfusion with PBS post sacrifice, eWAT samples were collected and digested as described previously (27, 28). In short, eWAT samples were minced and incubated for 1 hour at 37°C in an incubator under agitation (60 rpm) in HEPES-buffered Krebs solution, containing 0.5-1 g/L collagenase type I from *Clostridium histolyticum* (Sigma-Aldrich), 2% (w/v) dialyzed bovine serum albumin (BSA, fraction V; Sigma-Aldrich) and 6 mM D-Glucose (Sigma-Aldrich). The samples were passed through a 100 µm filter (Corning Life Sciences) which was washed with PBS supplemented with 2.5 mM EDTA and 5% FCS. After allowing the adipocytes to settle for ~10 min, the infranatant, consisting of immune cells, was collected and pelleted at 350 x g for 10 min at room temperature. The pellet was treated with erythrocyte lysis buffer, washed with PBS/EDTA/FCS, and counted using a hemocytometer.

Isolation of leukocytes from liver

Livers were collected and digested as described previously (27, 28). In short, livers were minced and incubated for 45 min at 37°C in RPMI 1640 + Glutamax containing 1 mg/mL collagenase type IV from *Clostridium histolyticum*, 200 U/mL DNase (both Sigma-Aldrich) and 1 mM $CaCl_2$. The digested tissues were passed through a 100 µm cell strainer (Corning Life Sciences) which was subsequently washed with PBS/EDTA/FCS. After

centrifugation (530 x g, 10 min at 4°C), cells were resuspended in 30 mL PBS/EDTA/FCS and spun down at 50 x g for 3 min at 4°C to pellet the hepatocytes. The supernatant was collected, treated with erythrocyte lysis buffer and $CD45^+$ leukocytes were isolated using LS columns and CD45 MicroBeads (35 µL beads per sample, Miltenyi Biotec) according to the manufacturer's protocol. Isolated liver leukocytes were counted using a hemocytometer.

Flow cytometry

For assessing LKB1/ACC phosphorylation state in spleen, eWAT and liver, tissues were collected and immediately minced in 1.85% formaldehyde solution (Sigma-Aldrich) and digested as described above. Isolated cell suspensions were permanently permeabilized using 100% methanol for 10 min at -20°C. For other purposes, spleen, eWAT and liver cell suspensions were stained using a Fixable Aqua Dead Cell Stain Kit (Invitrogen) or Zombie UV Fixable Viability Kit (Biolegend) for 20 min at room temperature. Unless sorted or measured alive, cells were fixed for 1 h at 4°C using a FOXP3/Transcription Factor Staining Buffer Set (Invitrogen, for FOXP3 detection) or 15 min at room temperature using a 1.85% formaldehyde solution in PBS (Sigma-Aldrich, for everything else). For detection of intracellular cytokines, isolated cells were cultured for 4 h in RPMI 1640 + Glutamax in the presence of 100 ng/mL phorbol myristate acetate (PMA), 1 µg/mL ionomycin, 10 µg/mL Brefeldin A (all from Sigma-Aldrich). After 4 hours, cells were washed with PBS, stained with Aqua, and fixed as described above. Cell suspensions were first pre-incubated with 2.4G2 antibody (kindly provided by Louis Boon) for blocking Fc receptors and next stained for surface markers in PBS supplemented with 0.5% BSA (Roche) and 2 mM EDTA (Sigma-Aldrich) and antibodies for 30 min at 4°C. For detection of phosphorylated proteins, FOXP3 and intracellular cytokines, cell suspensions were stained in Permeabilization Buffer (eBioscience) instead. Phosphorylated Ser79-ACC and Ser431-LKB1 were stained using unconjugated rabbit-anti-mouse antibodies prior to staining with other antibodies and goat-anti-rabbit-Alexa Fluor 647. Antibody information is provided in Supplementary Table 1 and gating strategies shown in Supplementary Figure 1. Cells were measured on a FACSCanto II or LSR II and analyzed using FlowJo (Version 10.6, TreeStar).

Plasma analysis

Blood samples were collected from the tail tip of 4 h-fasted mice using paraoxon-coated glass capillaries. Fasting blood glucose level was determined using a hand-held Glucometer (Accu-Check; Roche Diagnostics) and plasma insulin level was measured using a commercial kit as per manufacturer's instructions (Chrystal Chem).

Insulin- and glucose tolerance tests

Whole-body insulin tolerance test (ipITT) and glucose tolerance test (ipGTT) were performed 1 week before sacrifice, as previously described (27, 28). In short, a bolus of insulin (0.75U/kg body mass, NOVORAPID, Novo Nordisk) was administered intraperitoneally (i.p.) to 4 h-fasted mice, after which blood glucose levels were measured at t=0, 15, 30, 45 and 60 min post insulin administration using a Glucometer. For ipGTT, 6 h-fasted mice were injected i.p. with 2g/kg total body mass of D-Glucose (Sigma-Aldrich) and blood glucose was measured at t=0, 20, 40, 60 and 90 min post glucose injection using a Glucometer.

Histological analysis

Pieces of eWAT and liver (~30 mg) were fixed in 4% formaldehyde solution (Sigma-Aldrich), paraffin-embedded, sectioned at 4 μm and stained with Hematoxylin and Eosin (H&E). Six fields at 20x magnification (total area 1.68 mm^2) were used for the analysis of adipocyte size, crown-like structures or hepatic steatosis.

Hepatic lipid composition

Liver lipids were extracted as previously described (29). Liver triglyceride and total cholesterol concentrations were measured using commercial kits (all from Instruchemie) and expressed as nanomoles per milligram of total protein content using the Bradford protein assay kit (Sigma-Aldrich).

In vivo DC expansion, isolation and sorting

To expand the DC pool *in vivo*, 2 × 10^6 Flt3L-secreting B16 melanoma cells (kind gift from Dr. Edward Pearce) in 100 μL HBSS were injected subcutaneously into the flank of mice. After 10 days, spleen, liver and eWAT were harvested, and digested and processed as described earlier. cDC2s were further enriched from single cell suspensions by positive isolation with CD11c Microbeads (Miltenyi Biotec; per manufacturer's instructions) and FACS sorting ($MHCII^+$ $CD11c^+$ $CD64^-$ $F4/80^-$ $CD172a^+$ $XCR1^-$) on a BD FACSAria using a 100 μm nozzle at 20 PSI. Subsequently, sorted cDC2s were stimulated with 100 ng/mL LPS for 16 h for assessing cytokine expression by RT-qPCR.

BM-derived DC cultures

Bone marrow-derived DCs were cultured as described previously (22). Briefly, bone marrow cells were flushed from femurs and tibias, and 5 × 10^6 cells were plated in tissue culture-

treated petri dishes (NUNC) in 10 mL of differentiation medium, consisting of RMPI 1640 Glutamax (Gibco) supplemented with 5% FCS (Gibco), 25 nM β-mercaptoethanol (Sigma-Aldrich), 100 U/mL penicillin, 100 μg/mL streptomycin and 20 ng/mL of murine GM-CSF (PeproTech). Medium was refreshed on day 4 and day 7, after which on day 9 non-adherent GMDCs were harvested. 1 x 10^5 GMDCs were seeded in a round-bottom 96-well plate and rested overnight. The next day, GMDCs were incubated for 2 h at 37°C with 50 μM MARK inhibitor (MARK/Par-1 Activity Inhibitor, 39621; Calbiochem), 50 nM SIK inhibitor (HG-9-91-01; Cayman Chemical), 1 μM NUAK inhibitor (WZ 4003; Tocris) or 5 μM AMPK inhibitor (SBI-0206965; Sigma-Aldrich). After 2 h, LPS and Brefeldin A were added to a final concentration of 100 ng/mL and 10 μg/mL, respectively, and samples were incubated for an additional 4 h at 37°C. After 6 h, cells were stained with a viability kit, fixed using 1.85% formaldehyde and stored at 4°C until further processing for intracellular cytokine detection by flow cytometry.

RNA-isolation and RT-qPCR

RNA was extracted from LPS-stimulated sorted cDC2s or GMDCs using TriPure RNA Isolation reagent. Total RNA (200-400 ng) was reverse transcribed using the M-MLV Reverse Transcriptase kit (ThermoFisher). Real-time qPCR runs were performed on a CFX96 Real-time C1000 thermal cycler (Biorad) using the GoTaq qPCR Master Mix kit (Promega). Gene expression was normalized to the housekeeping gene *Rplp0* and expressed as fold change compared to $CD11c^{WT}$ samples. A list of primer sequences can be found in Supplementary Table 2.

Statistical analysis

All data are presented as mean ± standard error of the mean (SEM). Statistical analysis was performed using GraphPad Prism version 8 for Windows (GraphPad Software) with unpaired t-test, one-way or two-way analysis of variance (ANOVA) followed by Fisher's post-hoc test. Differences between groups were considered statistically significant at $P < 0.05$.

Acknowledgements

This study was supported by the Dutch Organization for Scientific Research (NWO) Graduate School Program (022.006.010 to HvdZ) and the LUMC fellowship (to BE). The funders had no role in study design, data collection and analysis, decision to publish,

or preparation of the manuscript. The authors thank Ko Willems van Dijk and Patrick Rensen (Leiden University Medical Center) for allowing the use of the LUMC metabolic phenotyping platform (MRI and metabolic cages). The authors also acknowledge the LUMC Flow cytometry Core Facility (FCF) for technical support and cell sorting assistance.

References

1. Gregor MF, Hotamisligil GS. Inflammatory mechanisms in obesity. Annu Rev Immunol. 2011;29:415-45.
2. van der Zande HJP, Zawistowska-Deniziak A, Guigas B. Immune Regulation of Metabolic Homeostasis by Helminths and Their Molecules. Trends Parasitol. 2019;35(10):795-808.
3. Hotamisligil GS, Shargill NS, Spiegelman BM. Adipose expression of tumor necrosis factor-alpha: direct role in obesity-linked insulin resistance. Science. 1993;259(5091):87-91.
4. Stienstra R, Joosten LA, Koenen T, van Tits B, van Diepen JA, van den Berg SA, et al. The inflammasome-mediated caspase-1 activation controls adipocyte differentiation and insulin sensitivity. Cell Metab. 2010;12(6):593-605.
5. Bertola A, Ciucci T, Rousseau D, Bourlier V, Duffaut C, Bonnafous S, et al. Identification of adipose tissue dendritic cells correlated with obesity-associated insulin-resistance and inducing Th17 responses in mice and patients. Diabetes. 2012;61(9):2238-47.
6. Stefanovic-Racic M, Yang X, Turner MS, Mantell BS, Stolz DB, Sumpter TL, et al. Dendritic cells promote macrophage infiltration and comprise a substantial proportion of obesity-associated increases in CD11c+ cells in adipose tissue and liver. Diabetes. 2012;61(9):2330-9.
7. Cho KW, Zamarron BF, Muir LA, Singer K, Porsche CE, DelProposto JB, et al. Adipose Tissue Dendritic Cells Are Independent Contributors to Obesity-Induced Inflammation and Insulin Resistance. J Immunol. 2016;197(9):3650-61.
8. Deczkowska A, David E, Ramadori P, Pfister D, Safran M, At The B, et al. XCR1(+) type 1 conventional dendritic cells drive liver pathology in non-alcoholic steatohepatitis. Nat Med. 2021;27(6):1043-54.
9. Wu D, Molofsky AB, Liang HE, Ricardo-Gonzalez RR, Jouihan HA, Bando JK, et al. Eosinophils sustain adipose alternatively activated macrophages associated with glucose homeostasis. Science. 2011;332(6026):243-7.
10. Molofsky AB, Nussbaum JC, Liang HE, Van Dyken SJ, Cheng LE, Mohapatra A, et al. Innate lymphoid type 2 cells sustain visceral adipose tissue eosinophils and alternatively activated macrophages. J Exp Med. 2013;210(3):535-49.
11. Feuerer M, Herrero L, Cipolletta D, Naaz A, Wong J, Nayer A, et al. Lean, but not obese, fat is enriched for a unique population of regulatory T cells that affect metabolic parameters. Nat Med. 2009;15(8):930-9.
12. Tang Y, Bian Z, Zhao L, Liu Y, Liang S, Wang Q, et al. Interleukin-17 exacerbates hepatic steatosis and inflammation in non-alcoholic fatty liver disease. Clin Exp Immunol. 2011;166(2):281-90.
13. Fabbrini E, Cella M, McCartney SA, Fuchs A, Abumrad NA, Pietka TA, et al. Association between specific adipose tissue CD4+ T-cell populations and insulin resistance in obese individuals. Gastroenterology. 2013;145(2):366-74 e1-3.
14. Harley IT, Stankiewicz TE, Giles DA, Softic S, Flick LM, Cappelletti M, et al. IL-17 signaling accelerates the progression of nonalcoholic fatty liver disease in mice. Hepatology. 2014;59(5):1830-9.

15. Gomes AL, Teijeiro A, Buren S, Tummala KS, Yilmaz M, Waisman A, et al. Metabolic Inflammation-Associated IL-17A Causes Non-alcoholic Steatohepatitis and Hepatocellular Carcinoma. Cancer Cell. 2016;30(1):161-75.
16. Moreno-Fernandez ME, Giles DA, Oates JR, Chan CC, Damen M, Doll JR, et al. PKM2-dependent metabolic skewing of hepatic Th17 cells regulates pathogenesis of non-alcoholic fatty liver disease. Cell Metab. 2021;33(6):1187-204 e9.
17. Patente TA, Pelgrom LR, Everts B. Dendritic cells are what they eat: how their metabolism shapes T helper cell polarization. Curr Opin Immunol. 2019;58:16-23.
18. Pearce EJ, Everts B. Dendritic cell metabolism. Nat Rev Immunol. 2015;15(1):18-29.
19. Brombacher EC, Everts B. Shaping of Dendritic Cell Function by the Metabolic Micro-Environment. Front Endocrinol (Lausanne). 2020;11:555.
20. Chen S, Fang L, Guo W, Zhou Y, Yu G, Li W, et al. Control of Treg cell homeostasis and immune equilibrium by Lkb1 in dendritic cells. Nat Commun. 2018;9(1):5298.
21. Wang Y, Du X, Wei J, Long L, Tan H, Guy C, et al. LKB1 orchestrates dendritic cell metabolic quiescence and anti-tumor immunity. Cell Res. 2019;29(5):391-405.
22. Pelgrom LR, Patente TA, Sergushichev A, Esaulova E, Otto F, Ozir-Fazalalikhan A, et al. LKB1 expressed in dendritic cells governs the development and expansion of thymus-derived regulatory T cells. Cell Res. 2019;29(5):406-19.
23. Jaleel M, McBride A, Lizcano JM, Deak M, Toth R, Morrice NA, et al. Identification of the sucrose non-fermenting related kinase SNRK, as a novel LKB1 substrate. FEBS Lett. 2005;579(6):1417-23.
24. Lizcano JM, Goransson O, Toth R, Deak M, Morrice NA, Boudeau J, et al. LKB1 is a master kinase that activates 13 kinases of the AMPK subfamily, including MARK/PAR-1. EMBO J. 2004;23(4):833-43.
25. Shackelford DB, Shaw RJ. The LKB1-AMPK pathway: metabolism and growth control in tumour suppression. Nat Rev Cancer. 2009;9(8):563-75.
26. van der Zande HJP, Lambooij JM, Chavanelle V, Zawistowska-Deniziak A, Otero Y, Otto F, et al. Effects of a novel polyphenol-rich plant extract on body composition, inflammation, insulin sensitivity, and glucose homeostasis in obese mice. Int J Obes (Lond). 2021.
27. Hussaarts L, Garcia-Tardon N, van Beek L, Heemskerk MM, Haeberlein S, van der Zon GC, et al. Chronic helminth infection and helminth-derived egg antigens promote adipose tissue M2 macrophages and improve insulin sensitivity in obese mice. FASEB J. 2015;29(7):3027-39.
28. van der Zande HJP, Gonzalez MA, de Ruiter K, Wilbers RHP, Garcia-Tardon N, van Huizen M, et al. The helminth glycoprotein omega-1 improves metabolic homeostasis in obese mice through type 2 immunity-independent inhibition of food intake. FASEB J. 2021;35(2):e21331.
29. Thomas A, Belaidi E, Moulin S, Horman S, van der Zon GC, Viollet B, et al. Chronic Intermittent Hypoxia Impairs Insulin Sensitivity but Improves Whole-Body Glucose Tolerance by Activating Skeletal Muscle AMPK. Diabetes. 2017;66(12):2942-51.
30. Teijeiro A, Garrido A, Ferre A, Perna C, Djouder N. Inhibition of the IL-17A axis in adipocytes suppresses diet-induced obesity and metabolic disorders in mice. Nat Metab. 2021;3(4):496-512.

31. Nishimura T, Saito Y, Washio K, Komori S, Respatika D, Kotani T, et al. SIRPalpha on CD11c(+) cells induces Th17 cell differentiation and subsequent inflammation in the CNS in experimental autoimmune encephalomyelitis. Eur J Immunol. 2020;50(10):1560-70.

32. Nieves W, Hung LY, Oniskey TK, Boon L, Foretz M, Viollet B, et al. Myeloid-Restricted AMPKalpha1 Promotes Host Immunity and Protects against IL-12/23p40-Dependent Lung Injury during Hookworm Infection. J Immunol. 2016;196(11):4632-40.

33. Xie Z, Dong Y, Scholz R, Neumann D, Zou MH. Phosphorylation of LKB1 at serine 428 by protein kinase C-zeta is required for metformin-enhanced activation of the AMP-activated protein kinase in endothelial cells. Circulation. 2008;117(7):952-62.

34. Sapkota GP, Kieloch A, Lizcano JM, Lain S, Arthur JS, Williams MR, et al. Phosphorylation of the protein kinase mutated in Peutz-Jeghers cancer syndrome, LKB1/STK11, at Ser431 by p90(RSK) and cAMP-dependent protein kinase, but not its farnesylation at Cys(433), is essential for LKB1 to suppress cell vrowth. J Biol Chem. 2001;276(22):19469-82.

35. Houde Vanessa P, Ritorto Maria S, Gourlay R, Varghese J, Davies P, Shpiro N, et al. Investigation of LKB1 Ser431 phosphorylation and Cys433 farnesylation using mouse knockin analysis reveals an unexpected role of prenylation in regulating AMPK activity. Biochemical Journal. 2014;458(1):41-56.

36. Song P, Xie Z, Wu Y, Xu J, Dong Y, Zou MH. Protein kinase Czeta-dependent LKB1 serine 428 phosphorylation increases LKB1 nucleus export and apoptosis in endothelial cells. J Biol Chem. 2008;283(18):12446-55.

37. Nagpal R, Newman TM, Wang S, Jain S, Lovato JF, Yadav H. Obesity-Linked Gut Microbiome Dysbiosis Associated with Derangements in Gut Permeability and Intestinal Cellular Homeostasis Independent of Diet. J Diabetes Res. 2018;2018:3462092.

38. Thaiss CA, Itav S, Rothschild D, Meijer MT, Levy M, Moresi C, et al. Persistent microbiome alterations modulate the rate of post-dieting weight regain. Nature. 2016;540(7634):544-51.

39. Liu R, Hong J, Xu X, Feng Q, Zhang D, Gu Y, et al. Gut microbiome and serum metabolome alterations in obesity and after weight-loss intervention. Nat Med. 2017;23(7):859-68.

40. Martin-Mateos R, Albillos A. The Role of the Gut-Liver Axis in Metabolic Dysfunction-Associated Fatty Liver Disease. Front Immunol. 2021;12:660179.

41. Liu Z, Zhang W, Zhang M, Zhu H, Moriasi C, Zou MH. Liver kinase B1 suppresses lipopolysaccharide-induced nuclear factor kappaB (NF-kappaB) activation in macrophages. J Biol Chem. 2015;290(4):2312-20.

42. Zhao ZH, Wang ZX, Zhou D, Han Y, Ma F, Hu Z, et al. Sodium Butyrate Supplementation Inhibits Hepatic Steatosis by Stimulating Liver Kinase B1 and Insulin-Induced Gene. Cell Mol Gastroenterol Hepatol. 2021.

43. Li C, Wang G, Sivasami P, Ramirez RN, Zhang Y, Benoist C, et al. Interferon-alpha-producing plasmacytoid dendritic cells drive the loss of adipose tissue regulatory T cells during obesity. Cell Metab. 2021.

44. Han JM, Wu D, Denroche HC, Yao Y, Verchere CB, Levings MK. IL-33 Reverses an Obesity-Induced Deficit in Visceral Adipose Tissue ST2+ T Regulatory Cells and Ameliorates Adipose Tissue Inflammation and Insulin Resistance. J Immunol. 2015;194(10):4777-83.

45. Wara AK, Wang S, Wu C, Fang F, Haemmig S, Weber BN, et al. KLF10 Deficiency in CD4(+) T Cells Triggers Obesity, Insulin Resistance, and Fatty Liver. Cell Rep. 2020;33(13):108550.

46. Bapat SP, Myoung Suh J, Fang S, Liu S, Zhang Y, Cheng A, et al. Depletion of fat-resident Treg cells prevents age-associated insulin resistance. Nature. 2015;528(7580):137-41.

47. Wu D, Wong CK, Han JM, Orban PC, Huang Q, Gillies J, et al. T reg-specific insulin receptor deletion prevents diet-induced and age-associated metabolic syndrome. J Exp Med. 2020;217(8).

48. Beppu LY, Mooli RGR, Qu X, Marrero GJ, Finley CA, Fooks AN, et al. Tregs facilitate obesity and insulin resistance via a Blimp-1/IL-10 axis. JCI Insight. 2021;6(3).

49. Ma X, Hua J, Mohamood AR, Hamad ARA, Ravi R, Li Z. A high-fat diet and regulatory T cells influence susceptibility to endotoxin-induced liver injury. Hepatology. 2007;46(5):1519-29.

50. Volpe E, Servant N, Zollinger R, Bogiatzi SI, Hupe P, Barillot E, et al. A critical function for transforming growth factor-beta, interleukin 23 and proinflammatory cytokines in driving and modulating human T(H)-17 responses. Nat Immunol. 2008;9(6):650-7.

51. Manel N, Unutmaz D, Littman DR. The differentiation of human T(H)-17 cells requires transforming growth factor-beta and induction of the nuclear receptor RORgammat. Nat Immunol. 2008;9(6):641-9.

52. Ghoreschi K, Laurence A, Yang XP, Tato CM, McGeachy MJ, Konkel JE, et al. Generation of pathogenic T(H)17 cells in the absence of TGF-beta signalling. Nature. 2010;467(7318):967-71.

53. Lee Y, Awasthi A, Yosef N, Quintana FJ, Xiao S, Peters A, et al. Induction and molecular signature of pathogenic TH17 cells. Nat Immunol. 2012;13(10):991-9.

54. Scott CL, Tfp ZM, Beckham KS, Douce G, Mowat AM. Signal regulatory protein alpha (SIRPalpha) regulates the homeostasis of CD103(+) CD11b(+) DCs in the intestinal lamina propria. Eur J Immunol. 2014;44(12):3658-68.

55. He N, Fan W, Henriquez B, Yu RT, Atkins AR, Liddle C, et al. Metabolic control of regulatory T cell (Treg) survival and function by Lkb1. Proc Natl Acad Sci U S A. 2017;114(47):12542-7.

56. Sun Z, Jiang Q, Li J, Guo J. The potent roles of salt-inducible kinases (SIKs) in metabolic homeostasis and tumorigenesis. Signal Transduct Target Ther. 2020;5(1):150.

57. Wein MN, Foretz M, Fisher DE, Xavier RJ, Kronenberg HM. Salt-Inducible Kinases: Physiology, Regulation by cAMP, and Therapeutic Potential. Trends Endocrinol Metab. 2018;29(10):723-35.

58. Altarejos JY, Montminy M. CREB and the CRTC co-activators: sensors for hormonal and metabolic signals. Nat Rev Mol Cell Biol. 2011;12(3):141-51.

59. Dendorfer U, Oettgen P, Libermann TA. Multiple regulatory elements in the interleukin-6 gene mediate induction by prostaglandins, cyclic AMP, and lipopolysaccharide. Mol Cell Biol. 1994;14(7):4443-54.

60. Chandra G, Cogswell JP, Miller LR, Godlevski MM, Stinnett SW, Noel SL, et al. Cyclic AMP signaling pathways are important in IL-1 beta transcriptional regulation. J Immunol. 1995;155(10):4535-43.

61. Kocieda VP, Adhikary S, Emig F, Yen JH, Toscano MG, Ganea D. Prostaglandin E2-induced IL-23p19 subunit is regulated by cAMP-responsive element-binding protein and C/AATT enhancer-binding protein beta in bone marrow-derived dendritic cells. J Biol Chem. 2012;287(44):36922-35.

62. Hollstein PE, Eichner LJ, Brun SN, Kamireddy A, Svensson RU, Vera LI, et al. The AMPK-Related Kinases SIK1 and SIK3 Mediate Key Tumor-Suppressive Effects of LKB1 in NSCLC. Cancer Discov. 2019;9(11):1606-27.

63. Yong Kim S, Jeong S, Chah KH, Jung E, Baek KH, Kim ST, et al. Salt-inducible kinases 1 and 3 negatively regulate Toll-like receptor 4-mediated signal. Mol Endocrinol. 2013;27(11):1958-68.

64. Lombardi MS, Gillieron C, Dietrich D, Gabay C. SIK inhibition in human myeloid cells modulates TLR and IL-1R signaling and induces an anti-inflammatory phenotype. J Leukoc Biol. 2016;99(5):711-21.

65. Sundberg TB, Choi HG, Song JH, Russell CN, Hussain MM, Graham DB, et al. Small-molecule screening identifies inhibition of salt-inducible kinases as a therapeutic strategy to enhance immunoregulatory functions of dendritic cells. Proc Natl Acad Sci U S A. 2014;111(34):12468-73.

66. Caton ML, Smith-Raska MR, Reizis B. Notch-RBP-J signaling controls the homeostasis of CD8- dendritic cells in the spleen. J Exp Med. 2007;204(7):1653-64.

Supplementary information

Supplementary Table 1. Antibodies and reagents for flow cytometry

Target	Clone	Conjugate	Source	Identifier
B220	RA3-6B2	FITC	eBioscience	11-0452
CD3	17A2	APC-eF780	eBioscience	47-0032
CD3	17A2	BV605	Biolegend	100237
CD3	17A2	FITC	eBioscience	11-0032
CD4	GK1.5	BV650	BD Biosciences	563232
CD4	GK1.5	PE-Cy7	eBioscience	25-0041
CD4	GK1.5	PerCP-eFluor 710	eBioscience	46-0041
CD8a	53-6.7	BV711	Biolegend	100759
CD8a	53-6.7	PE	eBioscience	12-0081
CD11b	M1/70	FITC	eBioscience	11-0112
CD11b	M1/70	PE-Cy7	eBioscience	25-0112
CD11c	N418	BV421	Biolegend	117330
CD11c	HL3	FITC	BD Biosciences	553801
CD11c	HL3	Horizon V450	BD Biosciences	560521
CD11c	N418	PE-Cy7	eBioscience	25-0114
CD19	MB19-1	FITC	eBioscience	11-0191
CD40	HM40-3	FITC	eBioscience	11-0402
CD44	IM7	eFluor 450	eBioscience	48-0441
CD45	30-F11	BV785	Biolegend	103149
CD45.2	104	FITC	Biolegend	109806
CD45.2	104	eFluor 450	eBioscience	48-0454
CD64	X54-5/7.1	PE	Biolegend	139304
CD64	X54-5/7.1	PE/Dazzle 594	Biolegend	139319
CD64	X54-5/7.1	PerCP-Cy5.5	Biolegend	139308
CD80	16-10A1	APC	eBioscience	17-0801
CD86	GL-1	APC/Fire 750	Biolegend	105045
CD86	GL-1	PE	BD Biosciences	553692
CD172a	P84	PE	Biolegend	144011
CD197/CCR7	4B12	PerCP-Cy5.5	Biolegend	120116
F4/80	BM8	APC	eBioscience	17-4801
F4/80	BM8	BV711	Biolegend	123147
FOXP3	FJK-16s	APC	eBioscience	17-5773
Goat-anti-Rabbit	Polyclonal	Alexa Fluor 647	Invitrogen	A21244
GR-1	RB6-8C5	FITC	BD Biosciences	553126
IFNγ	XMG1.2	FITC	eBioscience	11-7311
IL-5	TRFK5	PE	Biolegend	504303
IL-6	MP5-20F3	APC	Biolegend	504507
IL-17A	eBio17B7	PE-Cy7	eBioscience	25-7177
IL-17A	TC11-18H10.1	PerCP-Cy5.5	Biolegend	506919

Target	Clone	Conjugate	Source	Identifier
IL-23p19	fc23cpg	eFluor 660	Invitrogen	50-7023
LAP	TW7-16B4	PerCP-eF710	Invitrogen	46-9821
Ly6C	HK1.4	APC-Cy7	Biolegend	128026
MHCI/H-2Kb	AF6-88.5	Pacific Blue	Biolegend	116514
MHCII	M5/114 15.2	Alexa Fluor 700	Invitrogen	56-5321
MHCII	M5/114 15.2	APC-eFluor 780	eBioscience	47-5321
MHCII	M5/114 15.2	FITC	eBioscience	11-5321
NK1.1	PK136	FITC	eBioscience	11-5941
Phospho-ACC (Ser79)	D7D11	-	Cell Signaling	11818S
Phospho-LKB1 (Ser431)	C67A3	-	Cell Signaling	3482S
Pro-IL-1β	NJTEN3	PE	Invitrogen	12-7114
Siglec-F	E50-2440	PE	BD Biosciences	552126
XCR1	ZET	BV650	Biolegend	148220
Other reagents			**Source**	**Identifier**
LIVE/DEAD™ Fixable Aqua Dead Cell Stain Kit			Invitrogen	L34957
Zombie UV™ Fixable Viability Kit			Biolegend	423107

Supplementary Table 2. qPCR primers

Gene	Accession number	Forward primer	Reverse primer
Il1b	NM_008361	GACCCCAAAAGATGAAGGGCT	ATGTGCTGCTGCGAGATTTG
Il6	NM_031168.2	CCTCTCTGCAAGAGACTTCCAT	ACAGGTCTGTTGGGAGTGGT
Il23a	NM_031252.2	GCACCAGCGGGACATATGAA	CAAGCAGAACTGGCTGTTGTC
Rplp0	NM_007475	TCTGGAGGGTGTCCGCAACG	GCCAGGACGCGCTTGTACCC
Stk11	NM_011492.4	GTGCCAAGCTCATGGGTACT	CACCGAGGTCGGAGATCTTG
Tgfb1	NM_011577	GCTGAACCAAGGAGACGGAA	ATGTCATGGATGGTGCCCAG

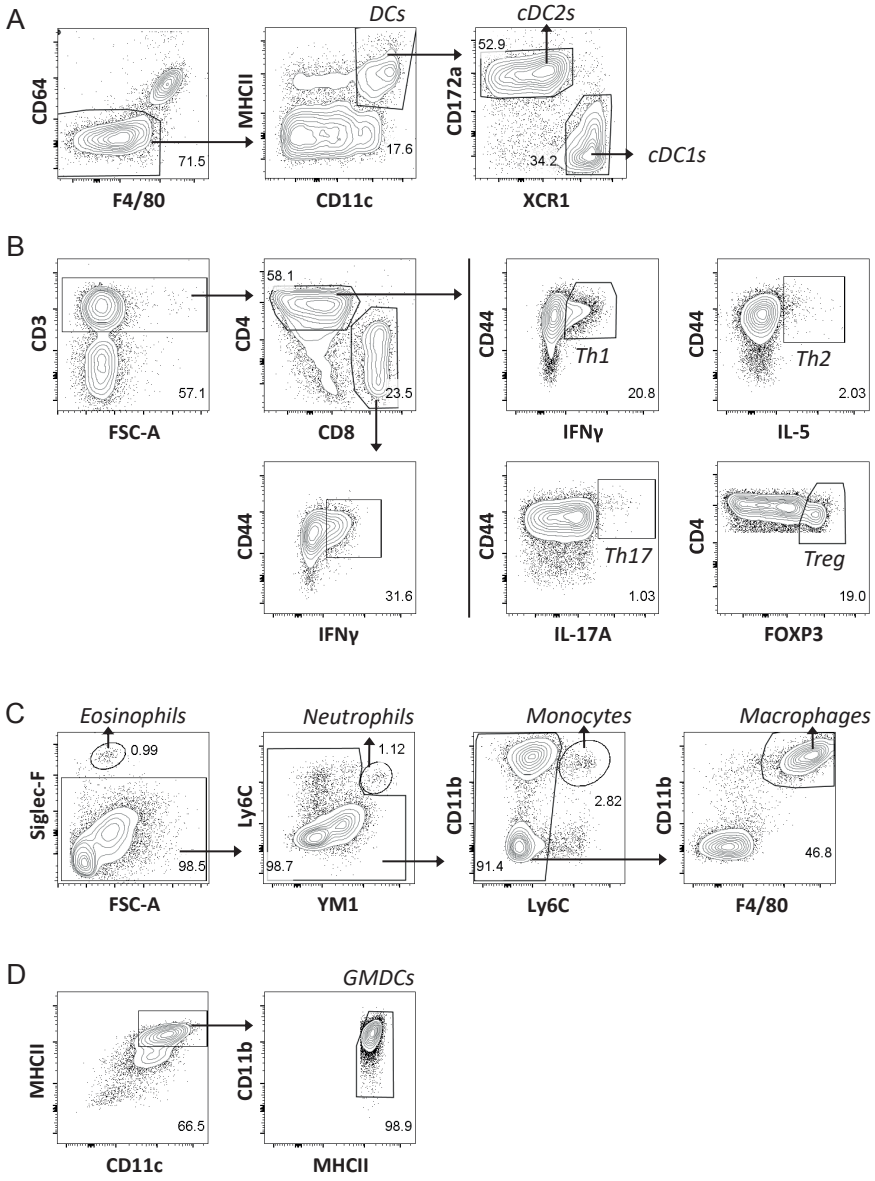

Supplementary Figure 1. Gating strategies. (**A**) Gating strategy for analysis of DCs and cDC subsets. CD11b and CD8a were used as alternatives for CD172a and XCR1, respectively. (**B**) Gating strategy for T (helper) cell subsets is shown. (**C**) Gating strategy for identification of myeloid cell subsets. (**D**) Gating strategy for identification of GMDCs. Isolated cells were pre-gated on live CD45^{+} single cells. For T (helper) cell subset analysis, cells were additionally pre-gated as lineage^{-}, which included antibodies directed against B220, CD11b, CD11c, GR-1 and NK1.1. Representative sample was chosen from eWAT samples for A-C. Gating strategies were similar for the indicated cell populations in liver and spleen.

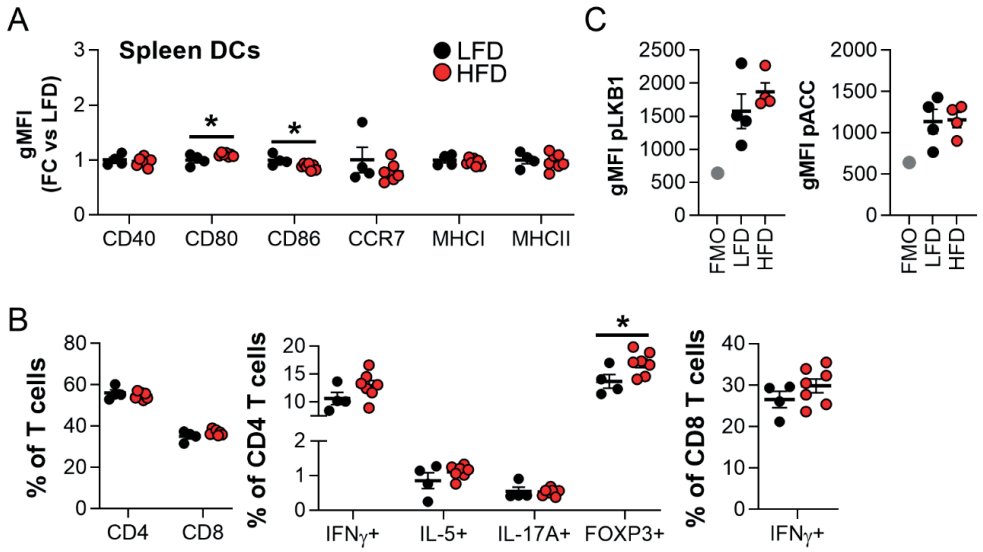

Supplementary Figure 2. Splenic DCs and T cells are mostly unaffected by obesity. Mice were fed a LFD (black symbols) or a HFD (red symbols) for 24 weeks. (**A**) At sacrifice, spleen was collected and immune cells were isolated and analyzed by flow cytometry. Relative expression of indicated DC markers by splenic DCs. (**B**) Cells were restimulated with PMA/ionomycin in the presence of Brefeldin A for detection of intracellular cytokines, and were analyzed by flow cytometry. CD4 and CD8 T cell, Th1, Th2, Th17 and Treg CD4 T cell, and IFNγ$^+$ CD8 T cell percentages in spleen. (**C**) Spleens were immediately formaldehyde-fixed after collection and immune cells were isolated. Phosphorylated LKB1 (Ser431) and ACC (Ser79) were measured in DCs from spleen by flow cytometry. Results are expressed as means ± SEM. * P<0.05 vs LFD (n = 4-7 mice per group). Related to figure 1.

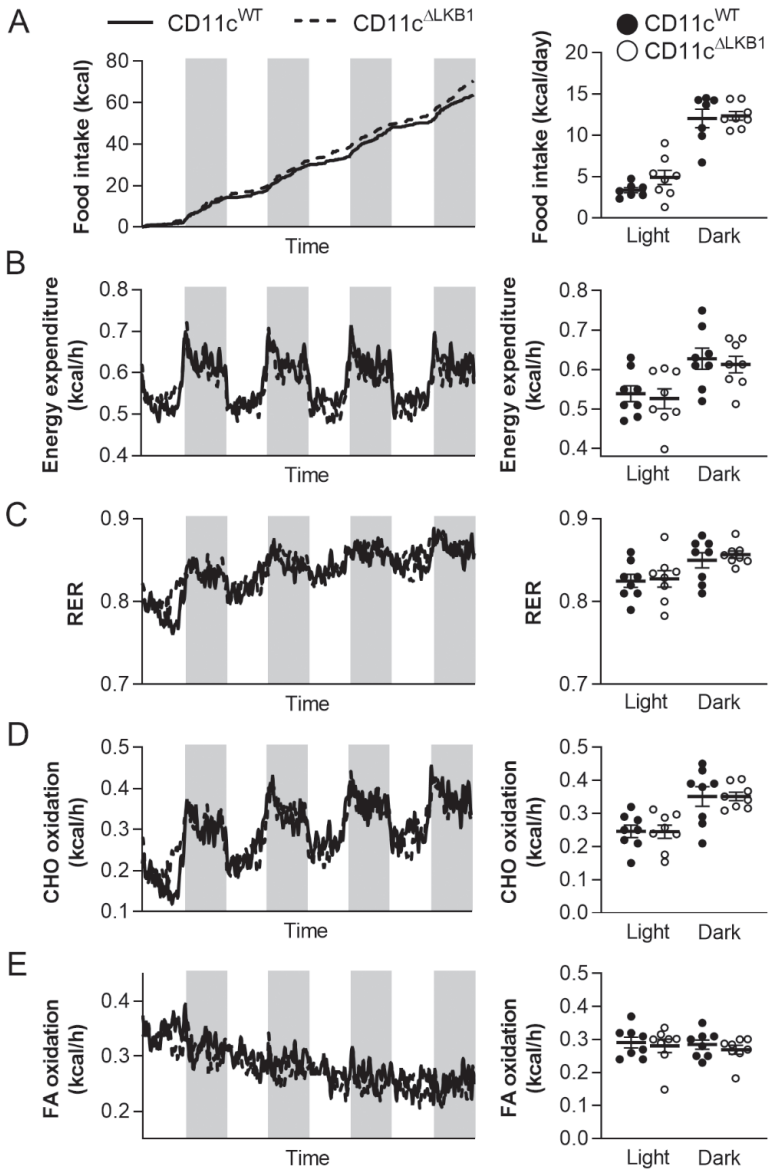

Supplementary Figure 3. LKB1 deficiency in DCs did not affect food intake and whole-body energy expenditure. CD11c^{WT} (black symbols) and CD11c$^{\Delta LKB1}$ (open symbols) mice were fed a HFD for 18 weeks. At week 15, mice were subjected to individual indirect calorimetric measurements using fully automated metabolic cages with free access to food and water. (**A-E**) Cumulative food intake (*A*), energy expenditure (EE; *B*), respiratory exchange rate (RER; *C*), carbohydrate (CHO; *D*) and fatty acid (FA; *E*) oxidation were measured for 4 consecutive days (white part = light phase; grey part = dark phase). The daily averages for each of the abovementioned parameters were calculated. Results are expressed as means ± SEM. (n = 7-8 mice per group). Related to figure 2.

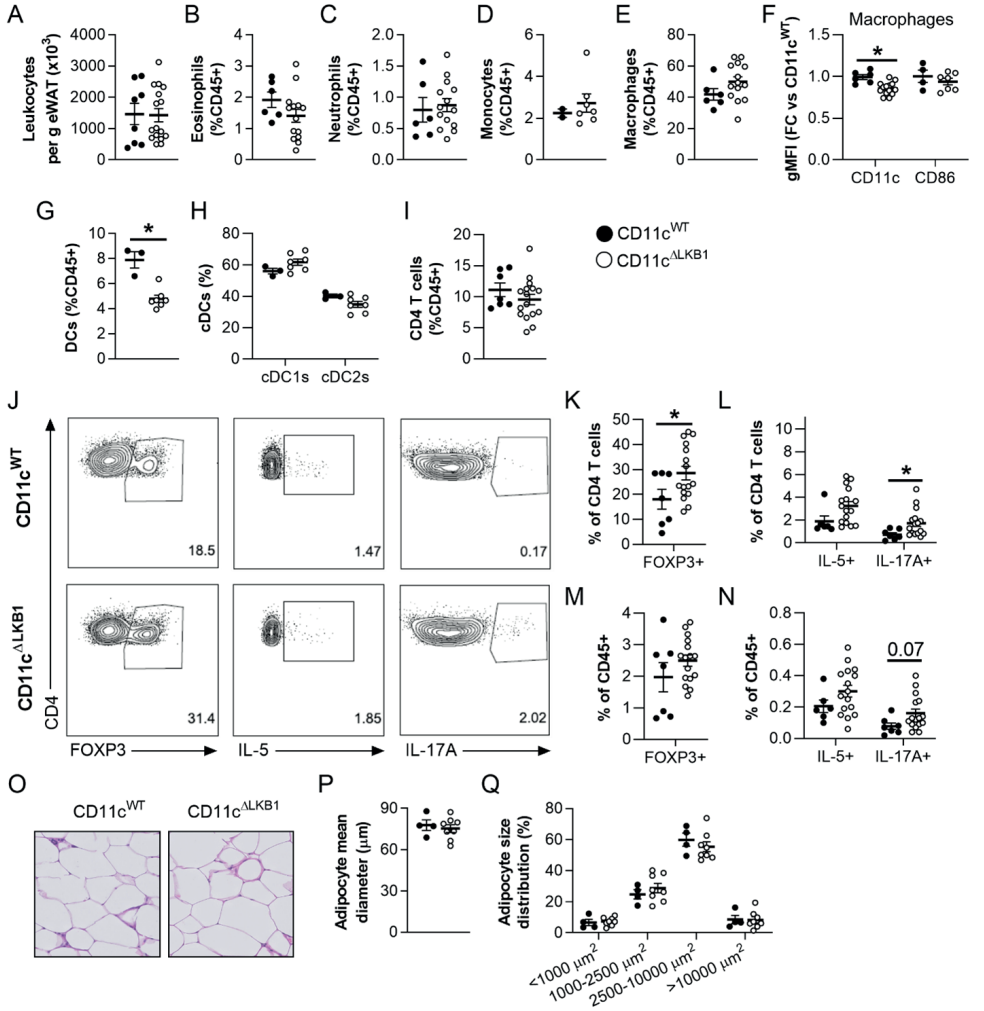

Supplementary Figure 4. LKB1 deficiency in DCs did not aggravate adipose tissue immunometabolic dysfunctions in obese mice. CD11c^{WT} (black symbols) and CD11c$^{\Delta LKB1}$ mice (open symbols) were fed a HFD for 18 weeks. (**A-I**) At sacrifice, eWAT was collected and immune cells isolated and analyzed by flow cytometry. Total leukocytes per gram eWAT were quantified (*A*). Percentages of eosinophils (*B*), neutrophils (*C*), monocytes (*D*) and macrophages (*E*) in eWAT expressed as frequencies of total leukocytes. Expression of CD11c and CD86 on eWAT macrophages relative to CD11c^{WT} mice (*F*). Abundances of DCs (*G*), cDC subsets (*H*) and CD4 T cells (*I*). (**J-N**) eWAT immune cells were restimulated with PMA and ionomycin in the presence of Brefeldin A for intracellular cytokine detection. Representative plots (*J*) and percentages of FOXP3$^+$ Treg (*K,M*), IL-5$^+$ Th2 and IL-17A$^+$ Th17 cells (*L,N*) were determined as frequencies of CD4 T cells (*K,L*) and total leukocytes (*M,N*). (**O**) A part of eWAT was sectioned and H&E-stained. (**P-Q**) Mean adipocyte diameter (*P*) and adipocyte size distribution (*Q*) were quantified from H&E stained slides. Data shown are a pool of two independent experiments, except for D, F-H and O-Q. Results are expressed as means ± SEM. * P<0.05 vs CD11c^{WT} (n = 7-16 mice per group for A-C, E and I-N; n = 3-8 mice per group for D, F-H and O-Q).

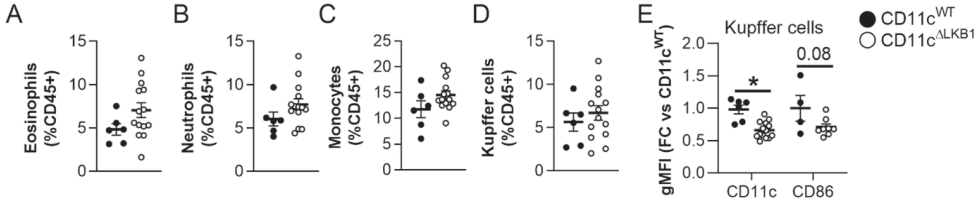

Supplementary Figure 5. Effects of LKB1 deletion from DCs on myeloid cell subsets in the liver. $CD11c^{WT}$ (black symbols) and $CD11c^{\Delta LKB1}$ (open symbols) mice were fed a HFD for 18 weeks. At sacrifice, liver was collected and immune cells were isolated and analyzed by flow cytometry. (**A-E**) Percentages of hepatic eosinophils (*A*), neutrophils (*B*), monocytes (*C*) and Kupffer cells (*D*) expressed as frequencies of total leukocytes. Expression of CD11c and CD86 on Kupffer cells, expressed as fold change *vs* $CD11c^{WT}$ (*E*). Data shown are a pool of two independent experiments, except for CD86 expression in E. Results are expressed as means ± SEM. * P<0.05 vs $CD11c^{WT}$ (n = 4-14 mice per group). Related to figure 3.

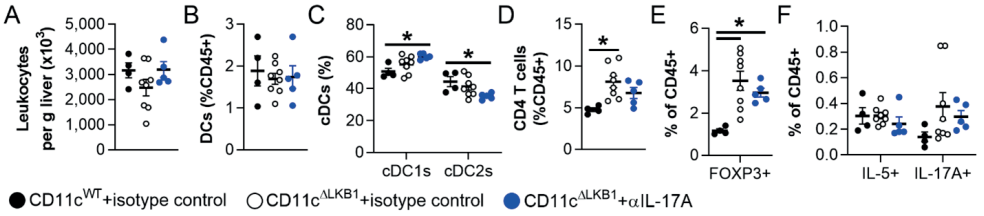

Supplementary Figure 6. Effects of IL-17A neutralization on hepatic immune cells. Mice were treated as described in the legend of figure 5. (**A-D**) At sacrifice, liver was collected and immune cells were isolated and phenotyped by flow cytometry. Total number of leukocytes per gram liver (*A*), and frequencies of DCs (*B*), cDC subsets (*C*) and CD4 T cells (*D*) were determined. (**E-F**) Hepatic leukocytes were restimulated with PMA/ionomycin in the presence of Brefeldin A for detection of intracellular cytokines. Abundance of $FOXP3^+$ Tregs (*E*), $IL\text{-}5^+$ Th2 cells and $IL\text{-}17A^+$ Th17 cells (*F*) were determined as frequencies of total leukocytes. Data shown are a pool of two independent experiments. Results are expressed as means ± SEM. * P<0.05 vs $CD11c^{WT}$ (n = 4-8 mice per group). Related to figure 4.

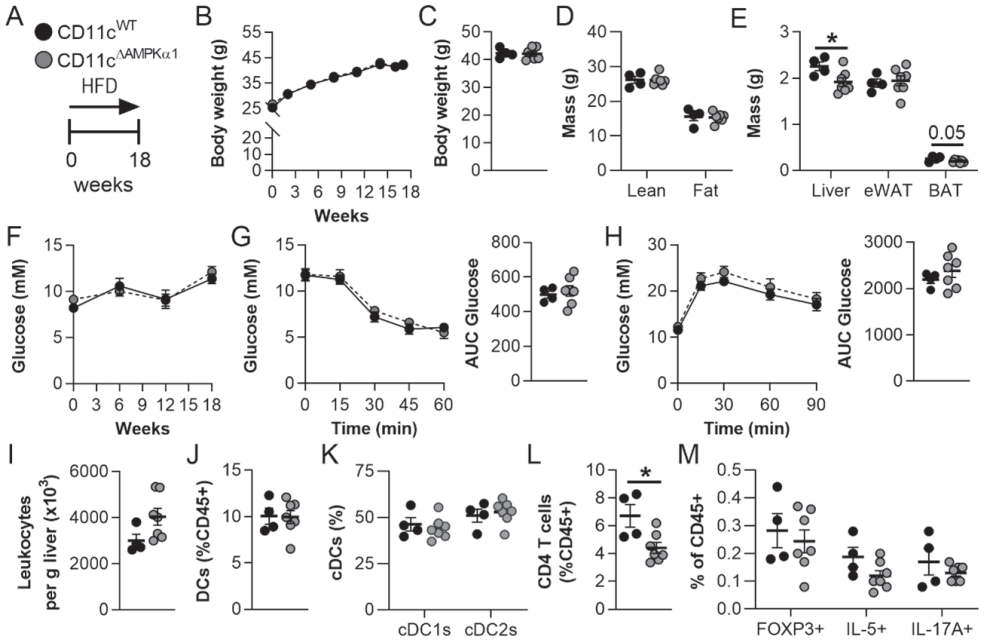

Supplementary Figure 7. Deletion of AMPKα1 from DCs did not recapitulate the immunometabolic phenotype of CD11c$^{\Delta LKB1}$ mice. (**A**) CD11c^{WT} (black symbols) and CD11c$^{\Delta AMPK\alpha1}$ mice (grey symbols) were fed a HFD for 18 weeks. (**B-C**) Body weight was monitored throughout the experiment. (**D-E**) Body composition (*D*) and weights of liver, eWAT and BAT (*E*) were measured at the end of the experiment. (**F**) Fasting blood glucose was measured at the indicated weeks. (**G**) An i.p. insulin tolerance test was performed 1 week before sacrifice and AUC calculated. (**H**) An i.p. glucose tolerance test was performed 1 week before sacrifice and AUC calculated. (**I-L**) At sacrifice, liver was collected and immune cells isolated. Total leukocytes per gram liver were quantified (*I*). Percentages of DCs (*J*), cDC subsets (*K*) and CD4 T cells (*L*) were determined by flow cytometry. (**M**) Liver leukocytes were restimulated with PMA and ionomycin in the presence of Brefeldin A for intracellular cytokine detection. Percentages of FOXP3$^+$ Treg, IL-5$^+$ Th2 and IL-17A$^+$ Th17 cells were determined as frequencies of total leukocytes. Results are expressed as means ± SEM. * P<0.05 vs CD11c^{WT} (n = 4-7 mice per group).

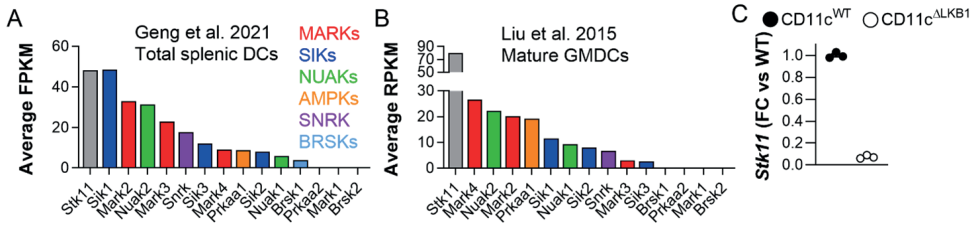

Supplementary Figure 8. Transcriptional analysis of LKB1 and its substrates in DCs. (**A-B**) Expression of *Stk11* (encoding LKB1) and its downstream targets *Mark1-4*, *Sik1-3*, *Nuak1-2*, *Prkaa1-2* (encoding AMPKα1-2), *Snrk* and *Brsk1-2* in total splenic DCs (Geng et al., *Immunology*. 2021; *A*) and mature GM-CSF-elicited bone marrow DCs (GMDCs; Liu et al., *J. Immunol.* 2015; *B*). (**C**) *Stk11* expression in GMDCs from CD11c^{WT} (black symbols) and CD11c$^{\Delta LKB1}$ mice (open symbols) at day 10 of culture. Related to figure 5.

PART II

IMMUNOMODULATORY (HELMINTH) MOLECULES AND OBESITY-INDUCED METABOLIC DYFSUNCTIONS

CHAPTER 6

Immune regulation of metabolic homeostasis by helminths and their molecules

Hendrik J.P. van der Zande[#], Anna Zawistowska-Deniziak[#], Bruno Guigas

[*]These authors contributed equally to this review

Trends in Parasitology. 35(10):795-808. (2019)
PMID: 31492623
doi: 10.1016/j.pt.2019.07.014

Abstract

Since time immemorial, humans have coevolved with a wide variety of parasitic helminths that have contributed to shape their immune system. The recent eradication of helminth infections in modern societies has coincided with a spectacular rise in inflammatory metabolic diseases, such as obesity, nonalcoholic steatohepatitis, and type 2 diabetes. Landmark studies in the emerging field of immunometabolism have highlighted the central role of the immune system in regulating metabolic functions, notably in adipose tissue, liver, and the gut. In this review we discuss how helminths, which are among the strongest natural inducers of type 2 immunity, and some of their unique immunomodulatory molecules, may contribute to the maintenance of tissue-specific and whole-body metabolic homeostasis and protection against obesity-associated meta-inflammation.

Glossary

Alternatively activated macrophage (AAM): an innate immune cell involved in protection against parasites, resolution of inflammation, and tissue repair.

Beiging: occurs when white adipose tissue develops features of thermogenic brown adipose tissue.

Brown adipose tissue (BAT): involved in thermogenesis during cold exposure owing to high expression of mitochondrial uncoupling protein UCP1.

Eosinophil: a short-lived granulocyte induced by helminths and involved in type 2 immune responses.

Extracellular vesicles (EVs): lipid bilayer-delimited particles that are released by most eukaryotic cells and involved in intercellular communication.

Group 2 innate lymphoid cells (ILC2s): one of the cell types involved in the initiation of type 2 immune responses via specific damage signals (alarmins) and cytokines.

Helminths: multicellular parasitic worms, including roundworms, tapeworms, and flukes.

Hepatic steatosis: ectopic accumulation of lipids in hepatocytes, resulting in a fatty liver.

Homeostatic Model Assessment for Insulin Resistance (HOMA-IR): calculated from fasting plasma insulin and glucose levels and used as a proxy for whole-body insulin resistance.

Hygiene hypothesis: proposes that the increases in hyperinflammatory disease prevalence in modern societies result from higher hygiene care and reduced exposure to pathogens and microorganisms, such as early-life parasitic infections.

Insulin resistance: impaired insulin action on its target metabolic organs/cells.

Interleukin-33 (IL-33): an alarmin cytokine released by stromal/epithelial cells that promotes type 2 immune responses

Meta-inflammation: chronic low-grade inflammation occurring in metabolic organs

Microbiota: is composed of a wide array of bacteria, archaea, viruses, fungi, and parasites that reside at mucosal surfaces, notably in the gastrointestinal tract.

Nonalcoholic fatty liver disease (NAFLD): a metabolic disorder characterized by excessive fat accumulation in the liver (see hepatic steatosis).

Nonalcoholic steatohepatitis (NASH): NALFD combined with hepatic inflammation and liver damage.

Regulatory T cell (Treg): a specialized T cell restricting excessive immune responses.

Soluble Egg Antigens (SEA): a mixture of soluble molecules extracted from *Schistosoma mansoni* eggs.

Type 2 diabetes: a metabolic disease characterized by insulin resistance and chronically elevated blood glucose levels.

Type 2 immunity: immune response characterized by increased ILC2s, eosinophils, T_H2 cells, mast cells, basophils, and alternatively-activated macrophages.

Type 2 T helper cell (T_H2): a specialized T helper cell involved in asthma, allergies and immune responses against helminth parasites.

White adipose tissue (WAT): an endocrine organ with a high storage capacity for triglycerides.

Helminths and inflammatory metabolic diseases

Helminth (see Glossary) parasites have a long coevolutionary history with humans, and about one quarter of the world's inhabitants are still infected with a wide variety of these worms (1). In tropical and subtropical areas, where hygiene and sanitation are poor, soil-transmitted helminth infections are highly prevalent, including infections with *Ascaris lumbricoides*, *Trichuris trichiura*, and hookworms, together with filarial nematodes and schistosomes such as *Schistosoma mansoni* and *Schistosoma haematobium* (1, 2). By contrast, most Western countries have successfully eradicated helminths and other pathogens during the second half of the last century, contributing to an almost complete disappearance of chronic helminth infections and significant changes in the whole **microbiota** composition, notably in the gastrointestinal tract. However, a concomitant increase in autoimmune and allergic diseases, such as multiple sclerosis, type 1 diabetes, and asthma, has been observed. This suggests that exposure to pathogens and microorganisms, such as parasites, contributes to shaping our immune system and is protective against inflammatory diseases, a general concept known as the '**hygiene hypothesis**' (3, 4).

Importantly, the prevalence of inflammatory metabolic diseases, such as obesity, **nonalcoholic fatty liver disease** (**NAFLD**) and **type 2 diabetes**, is also dramatically increasing in Western societies and some developing countries that have recently experienced a rapid urbanization (5). Among various pathophysiological underlying mechanisms, the obesity-associated chronic low-grade inflammation, also called **meta-inflammation**, contributes to the development of **insulin resistance** and dysregulated glucose/lipid metabolism, ultimately leading to type 2 diabetes, **nonalcoholic steatohepatitis** (**NASH**) and associated cardiovascular diseases (6, 7). During the last decade, landmark studies have highlighted the central role played by the immune system in the regulation of metabolic homeostasis in both rodents and humans. These studies have identified a repertoire of innate and adaptive immune cell subsets that populate metabolic organs and contribute to tissue-specific maintenance of biological functions through complex and yet incompletely understood crosstalk with metabolic cells (8, 9).

Remarkably, chronic infections with various helminths, which result in potent **type 2 immunity** and T cell hyporesponsiveness through induction of a regulatory network (10, 11), were associated with reduced insulin resistance and a lower prevalence of metabolic syndrome and type 2 diabetes in populations living in endemic areas (12-16). This suggests that the modulation of the host immune system by worms may protect against metabolic diseases (17, 18). Similar beneficial effects were reported in preclinical rodent models of type 2 diabetes, where both infection with various helminth species and treatment with helminth-derived molecules promote type 2 immune responses, dampen meta-inflammation, and improve metabolic homeostasis during obesity (19-28).

In this review we discuss our current understanding of the immune-mediated mechanisms by which helminths and some of their unique molecules may contribute to maintenance of tissue-specific and whole-body metabolic homeostasis in their host and prevent obesity-associated meta-inflammation.

(Dys)regulation of metabolic homeostasis by immune cells

The concept of immune cells contributing to metabolic homeostasis is now well recognized and supported by a large body of recent literature. One of the cornerstones that has fueled the development of the immunometabolism field was the discovery that the increase in macrophage-derived proinflammatory cytokine Tumor Necrosis Factor (TNF) in adipose tissue contributes to insulin resistance during obesity (29). In the following section we describe how immune cells control tissue-specific metabolic homeostasis, focusing specifically on macrophages that are considered to play a central role in the etiology of obesity-associated meta-inflammation and regulation of insulin sensitivity in most of the metabolic tissues (9).

White adipose tissue

White adipose tissue (WAT) is by far the metabolic tissue that has been studied most in terms of immune cell phenotyping. During the past decade, a growing body of innate and adaptive immune cells have been shown to be involved in regulating adipose tissue biology (9). In 2011, a landmark study revealed the role of interleukin (IL)-4-producing WAT **eosinophils** in the maintenance of insulin sensitivity (27), establishing the conceptual basis that type 2 immunity could be involved in adipose tissue metabolic homeostasis in mice. In lean WAT, eosinophils are relatively abundant and are maintained through IL-5 and IL-13 produced by tissue-resident **group 2 innate lymphoid cells** (**ILC2s**) and **type 2 T helper** (**T_H2**) cells (30). Moreover, stromal cells expressing **IL-33** and thymic stromal lymphopoietin (TSLP) were recently shown to sustain ILC2s in WAT (31, 32). IL-4 and IL-13, produced locally by eosinophils, T_H2 cells, and/or ILC2s, are thought to promote alternative activation of adipose tissue macrophages (ATMs) (30), which are considered to be the effector cells of an immune cascade that regulates insulin sensitivity. Although the underlying molecular mechanisms remain mostly unknown, these **alternatively-activated macrophages** (**AAMs**) have been suggested to control WAT inflammation through enhanced production of the immunosuppressive cytokine IL-10 (33) and/or induction of **regulatory T cells** (**Tregs**) (34). It has recently been shown that the vast majority of these M2-like AAMs are tissue-resident, tightly associated with WAT vasculature, and displaying high endocytic capacity that might act as a buffer for adipocyte-derived lipids during homeostasis (35).

During obesity, this type 2 immune environment is perturbed. Prolonged caloric excess causes hypertrophic adipocytes to produce chemokines and proinflammatory cytokines. These, in turn, recruit circulating monocytes, which subsequently differentiate into $CD11c^+$ proinflammatory macrophages upon encountering the inflammatory milieu (33). These newly recruited macrophages also produce proinflammatory cytokines and chemokines that directly interfere with canonical insulin signaling and recruit more monocytes, leading to a vicious circle that exacerbates WAT inflammation (9). Due to their expression of some canonical markers, such as inducible nitric oxide synthase (iNOS), and enhanced production of TNF, IL-6, and IL-1β, these macrophages were initially considered to be classically activated, M1-like macrophages (33). However, several reports have recently challenged this concept by providing a more subtle classification and phenotyping of ATMs, along with paradoxical functions (Box 1) (35-39). Taken together, ATMs appear to exist in multiple flavors and are versatile cells with a high degree of plasticity, yielding a spectrum of activation states likely dependent on their changing microenvironment during the development of obesity.

Box 1. The recent evolution of obesity-associated adipose tissue macrophage classification

During the course of obesity, adipose tissue macrophages (ATMs) have long been thought to acquire a proinflammatory phenotype that resembles the M1 polarization state induced by LPS in bone marrow-derived macrophages (BMDMs). However, recent studies have led to an evolution in ATM classification by reporting unexpected new phenotypes and functions. Among the newly identified subsets, ATMs expressing lipid metabolism genes under the control of peroxisome proliferator-activated receptor gamma (PPARγ), and producing TNF and IL-1β, were found to be increased in obese mice and termed 'metabolically-activated macrophages' (MMes). Their transcriptomic signature is similar to in vitro bone marrow-derived macrophages stimulated with high concentrations of glucose, insulin, and palmitate, mimicking the nutrient abundance encountered in the obese WAT microenvironment (36). These MMes potentiate WAT inflammation, but, owing to their lipid metabolism machinery, could also exert protective beneficial action by buffering excess adipocyte lipid release and preventing ectopic lipid deposition, as well as clearing dead adipocytes through lysosomal exocytosis (37). Unbiased single-cell analyses in obese WAT have recently allowed different research groups to characterize ATM subsets more in-depth: (i) a lipid-laden and proinflammatory macrophage population expressing CD9 and exclusively found in crown-like structures surrounding dead adipocytes (38), (ii) a monocyte-derived $CD11c^+CD64^+$ macrophage population expressing CD9 but also an array of anti-inflammatory/detoxifying genes and displaying a low endocytic capacity (35), and (iii) a lipid-associated $CD9^+$ macrophage subset expressing a high level of the lipid receptor Trem2 involved in counteracting inflammation and adipocyte hypertrophy (39). Thus, multiple subtle flavors of obesity-associated ATMs exist, being either protective or detrimental for the regulation of metabolic homeostasis, depending on the adipose tissue micro-environment and diseasåe progression.

Liver

During obesity, an overflow of lipolysis-derived nonesterified free fatty acids (NEFAs) released from insulin-resistant WAT is taken up and stored in ectopic tissues, notably in the liver, where triglyceride accumulation in the form of lipid droplets causes **hepatic steatosis** and NAFLD (40). NAFLD-associated lipotoxicity triggers both oxidative and endoplasmic reticulum stress and hepatic inflammation through various mechanisms that are still incompletely understood, ultimately resulting in NASH and progressive liver damage (40). This inflammatory process is thought to be mediated, at least in part, by liver macrophages that can be divided into two main categories: the liver-resident Kupffer cells (KCs), which are embryonically derived and self-sustained through local proliferation, and newly recruited macrophages which originate from circulating monocytes (41).

Although accumulation of hepatic $CD8^+$ T cells and $CD4^+$ T helper 17 (T_H17) cells during obesity might also contribute (42, 43), many studies have shown that KCs are central players in the initiation of liver inflammation. Once activated, notably by lipid metabolites and/or gut-derived endotoxins, KCs promote the recruitment of circulating monocytes that differentiate into proinflammatory macrophages, driving NAFLD progression and insulin resistance (44-47). In line with this, depletion of KCs protects against hepatic steatosis and insulin resistance (48), as does genetic or therapeutic interference with hepatic recruitment of monocytes through the monocyte chemoattractant protein (MCP)1-CCR2 axis (49, 50). The effects of KCs on hepatic insulin resistance have often been associated with the production of TNF and IL-1β (41), yet, a recent report suggests that hepatic macrophages rather stimulate gluconeogenesis and lipogenesis through the release of insulin-like growth factor-binding protein 7 (IGFBP7), a noninflammatory protein that directly binds to the insulin receptor and triggers activation of extracellular-signal-regulated kinase (ERK) signaling (51). Of note, although AAMs are associated with improved insulin sensitivity in WAT, their function remains unclear in the liver. Furthermore, type 2 immunity was rather shown to promote hepatic fibrosis and progression of NAFLD through IL-4 and IL-13, notably in response to liver injury or *Schistosoma mansoni* infection (52-54).

Other metabolic tissues

The obesity-induced inflammation driven by tissue-specific changes in immune cell composition and/or activation states is also observed in skeletal muscle, pancreas and some hypothalamic areas in the brain and may have profound effects on whole-body metabolic homeostasis (see recent reviews (55-57)).

In skeletal muscle, only a few immune cells can be detected during homeostasis. By contrast, obesity leads to recruitment of monocytes/macrophages and T cells into the

expanding adipose depots surrounding the muscle fibers and their subsequent polarization towards a proinflammatory phenotype (56). The release of cytokines and chemokines from inflamed myocytes further accelerates immune cell recruitment, forming a feed-forward inflammatory loop that negatively regulates skeletal muscle insulin sensitivity and metabolic functions, and contributes to whole-body metabolic dysfunctions (56).

In the pancreas, obesity-associated islet inflammation is involved in the failure of insulin secretion by β-cells during type 2 diabetes progression (57). This is partly mediated by glucose-induced metabolic stress that triggers IL-1β secretion by β-cells, resulting in recruitment of circulating monocytes and polarization towards proinflammatory macrophages, β-cell death, and impaired insulin production (58). In addition, islet-resident macrophages were recently shown to proliferate during obesity and engulf β-cell insulin secretory granules, which may contribute to restricting insulin secretion (59). Recently, it has also been shown that **IL-33-** and ILC2-dependent maintenance of islet-resident retinoic-acid-producing myeloid cells promotes glucose-induced insulin secretion by β-cells in homeostatic conditions, a finely-tuned system that is impaired during obesity (60).

In the brain, microglia are embryonically derived tissue-resident macrophage-like cells that control organ homeostasis, notably through clearance of dead neurons, but they also contribute to the regulation of feeding behavior and whole-body energy expenditure (55, 61). Excess calorie intake activates microglia in the mediobasal hypothalamus (MBH), notably through dietary components like saturated NEFAs and peripheral hormones, leading to secretion of proinflammatory cytokines such as TNF, IL-1β, and IL-6, and chemokines. These microglia-derived signals contribute to recruitment and/or proliferation of monocyte-derived macrophages in both the MBH and arcuate nucleus, thereby amplifying hypothalamic inflammation and leading to central leptin resistance, increased food intake and decreased energy expenditure (62, 63).

Altogether, proinflammatory activation of macrophages in metabolic tissues is associated with impaired insulin sensitivity and metabolic homeostasis, which drives progression towards type 2 diabetes. Repolarizing macrophages to an anti-inflammatory state may therefore contribute to restore tissue homeostasis and limit obesity-induced metabolic dysfunctions.

Helminth immunomodulation and metabolic health

Helminth infection and metabolic homeostasis in humans

A number of epidemiological cross-sectional studies conducted in helminth-endemic areas spread over the entire world have reported inverse correlations between infection with various nematode and trematode species and insulin resistance assessed by **homeostatic**

model assessment for insulin resistance (**HOMA-IR**) or prevalence of metabolic syndrome and type 2 diabetes, in both lean and obese individuals (12-16) (Figure 1). Although the beneficial effects of helminth infection on metabolic homeostasis were usually associated with increased markers of type 2 immunity, such as eosinophilia, IgE, and/or circulating type 2 cytokines, other factors might also be involved, and the observational nature of these studies makes it difficult to draw definitive conclusions about a causal relationship between the two. However, it has recently been reported that deworming individuals infected with soil-transmitted helminths using anthelmintic drugs significantly reduced worm burden and serum markers of type 2 immunity, and resulted in increased HOMA-IR or circulating glucose and insulin levels. These results indicate the worsening of whole-body insulin sensitivity and glucose homeostasis upon deworming (16, 64) and further support the notion that helminth infection protects against metabolic dysfunctions in humans.

Helminths and type 2 immune responses in metabolic organs

Since the seminal preclinical study showing that infection of obese mice with the rodent nematode *Nippostrongylus brasiliensis* resulted in WAT eosinophilia and improved high-fat diet (HFD)-induced metabolic dysfunctions (27), many publications have reported similar effects of helminth infection and/or helminth-derived molecules on metabolic homeostasis, associated or not with induction of a type 2 immune response in metabolic organs (Table 1). *N. brasiliensis* infection also increased WAT YM1-expressing AAMs and had beneficial effects on hepatic steatosis in a signal transducer and activator of transcription 6 (STAT6)-dependent manner (28), establishing a link between helminth-induced type 2 immunity and improved metabolic homeostasis. Infection of genetically or diet-induced obese mice with other nematode and trematode species, including *Heligmosomoides polygyrus*, *Litosomoides sigmodontis, Strongyloides venezuelensis* and *S. mansoni*, also increased eosinophils and various AAM markers in WAT and improved whole-body glucose tolerance and insulin sensitivity (19, 23-25, 28). A key role for these ATMs was established by adoptive transfer of *H. polygyrus*-induced WAT AAMs, which improved whole-body glucose tolerance (26). However, with the exception of the overexpression of a few canonical markers, the identity and functional properties of these AAMs, and the underlying molecular mechanism(s) by which they exert their beneficial metabolic effects, remain unknown.

Importantly, these effects were not merely a result of host parasitism, as treatment of obese mice with *S. mansoni* **soluble egg antigens** (SEA) also increased WAT eosinophils, T_H2 cells and AAMs, and ameliorated hepatic steatosis and whole-body metabolic dysfunctions (20, 23, 65). Similarly, *L. sigmodontis* worm antigens were also able to induce WAT type 2 immunity and improve whole-body glucose tolerance (19). Remarkably, these immunometabolic beneficial effects were also reported with some single molecules.

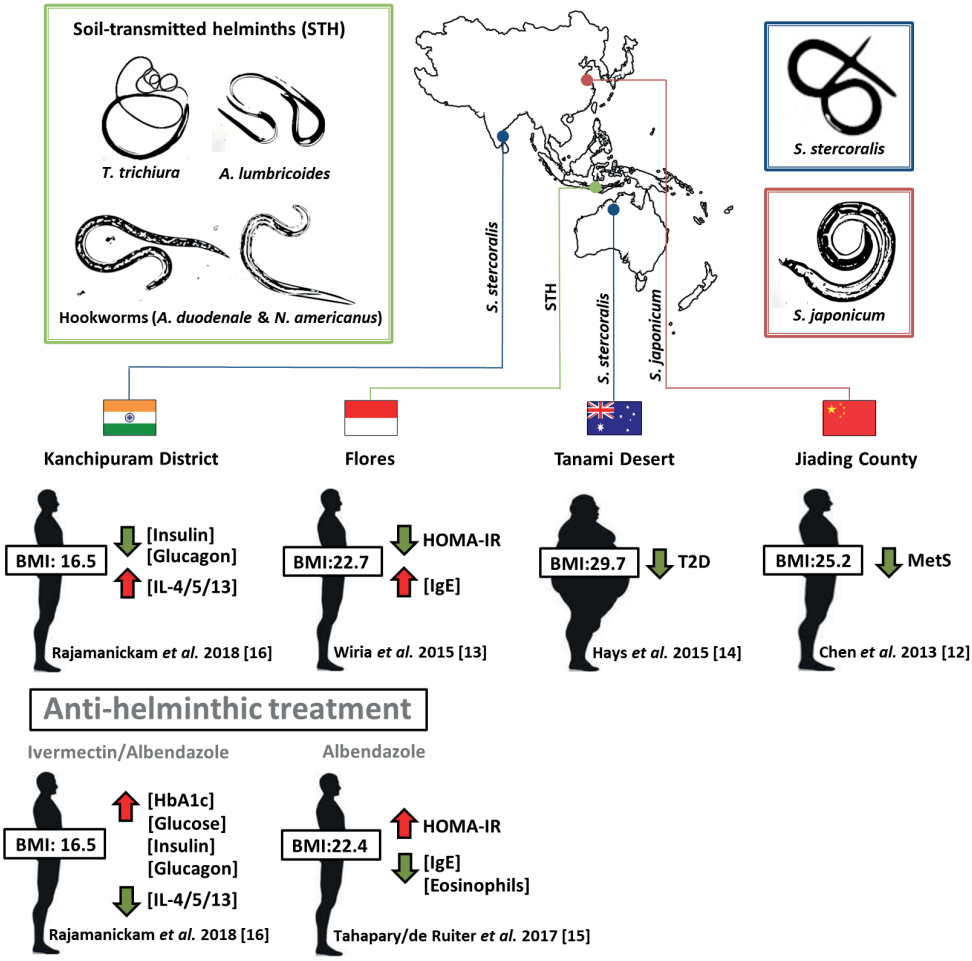

Figure 1. Associations between helminth infection and protection against metabolic diseases. Epidemiological studies conducted in endemic countries have reported an inverse association between infection with the trematode *Schistosoma japonicum* and the nematode *Strongyloides stercoralis* and the prevalence of metabolic syndrome and type 2 diabetes in lean and obese subjects, respectively. Improvements of the homeostatic model assessment for insulin resistance (HOMA-IR), hyperinsulinemia and hyperglucagonemia, hallmarks of whole-body insulin resistance and metabolic dysfunctions, were also observed in rural populations infected with various species of soil-transmitted helminths. These effects were associated with eosinophilia and increased serum levels of total IgE and prototypical type 2 cytokines interleukin (IL)-4, IL-5, and IL-13, suggesting that the helminth-induced type 2 immune response might play a role. Antihelminthic treatment was shown to reduce circulating markers of type 2 immunity and to impair metabolic homeostasis, as characterized by elevated HOMA-IR and hemoglobin A1c (glycated hemoglobin) (HbA1c). Abbreviations: BMI, body mass index; MetS, metabolic syndrome; T2D, type 2 diabetes. Species names: *A. duodenale, Ancylostoma duodenale*; *A. lumbricoides, Ascaris lumbricoides*; *N. americanus, Necator americanus*; *T. trichiura, Trichuris trichiura*. References: (12-16).

For instance, recombinant omega-1, a T_H2-inducing T2-RNAse glycoprotein present in *S. mansoni* egg excretory/secretory products (66), increased WAT type 2 immunity, promoted **WAT beiging**, reduced body weight and improved whole-body glucose tolerance in obese mice by a mannose receptor-, IL-33- and ILC2-dependent mechanism (22).

Furthermore, *Acanthocheilonema viteae*-purified native ES-62 was also recently shown to induce mild WAT eosinophilia and ameliorate HFD-induced liver fibrosis, although the impact on whole-body metabolic homeostasis was rather minimal (21).

Taken together, helminth infection, mixtures of helminth antigens and some helminth-derived single molecules induce type 2 immunity in metabolic tissues, which were either associated with or causal in the improvement of obesity-associated metabolic dysfunctions.

Table 1. Immunometabolic effects of parasite infection or treatment with native and/or recombinant parasite molecules in obese micea

	Mouse models	Immunomodulatory effects	Metabolic effects	Refs
Parasite infection				
Nippostrongylus brasiliensis	DIO male C57BL/6	↑ WAT eosinophils	↓ Fasting blood glucose ↑ Whole-body insulin sensitivity ↑ Whole-body glucose tolerance	(27)
	DIO male C57BL/6 WT, Stat6$^{-/-}$, Il13$^{-/-}$ RIP2-Opa1$^{\downarrow}$KO	↑ WAT YM1 and Arg1 gene expression ↑ YM1^{+} ATMs	↓ Body weight ↓ Hepatic steatosis (STAT6-dependent) ↑ Whole-body glucose tolerance	(28)
Heligmosomoides polygyrus	Chow-fed male KK-Ay/TaJcl	↑ small intestine AAM markers and IL-4, IL-13 and IL-10 genes expression	↓ Hepatic steatosis ↓ HOMA-IR ↑ Whole-body glucose tolerance	(24)
	DIO female C57BL/6	↑ WAT AAM genes expression ↑ AAM markers on ATMs	↓ Body weight gain ↑ Whole-body glucose tolerance ↑ WAT beiging (M2 macrophage dependent)	(26)
	DIO male C57BL/6	N/A	↓ Body weight gain ↑ WAT beiging Altered microbiota composition	(74)
Litosomoides sigmodontis	DIO male BALB/c WT, ΔdblGATA	↑ WAT eosinophils and RELMα+ AAMs ↑ CD4^{+} T cells in WAT	↑ Whole-body glucose tolerance (eosinophil-dependent)	(19)

	Mouse models	Immunomodulatory effects	Metabolic effects	Refs
Strongyloides venezuelensis	DIO male Swiss	↑ MGL1$^+$ ATMs	↑ Whole-body glucose tolerance ↑ Insulin-stimulated glucose uptake Altered microbiota composition	(25)
Schistosoma mansoni	DIO male C57BL/6	↑ WAT eosinophils and YM1$^+$ AAMs	↓ Body weight gain ↓ HOMA-IR ↑ Whole-body insulin sensitivity ↑ Whole-body glucose tolerance	(23)
Parasite antigen mixtures				
L. sigmodontis worm antigens	DIO male C57BL/6 WT and DEREG	↑ WAT RELMα$^+$ AAMs, eosinophils, ILC2s, CD4$^+$ T cells and Foxp3$^+$ Tregs ↓ CD11c$^+$ ATMs	↑ Whole-body glucose tolerance (Treg-independent)	(19)
S. mansoni egg antigens	DIO male C57BL/6	↑ WAT AAM genes expression ↓ WAT CAM genes expression ↑ serum IL-4 and IL-10 levels	↓ HOMA-IR ↑ Whole-body insulin sensitivity (IL-10-dependent) ↑ Whole-body glucose tolerance ↓ Hepatic steatosis	(20)
	DIO male C57BL/6	↑ WAT eosinophils, YM1$^+$ ATMs ↑ IL-4, -5, and -13-expressing T_H2 cells	↓ HOMA-IR ↑ Whole-body insulin sensitivity ↑ Whole-body glucose tolerance	(23)
	DIO male C57BL/6	↑ WAT eosinophils	↔ BAT activation and WAT beiging	(65)
Trichuris suis soluble products	DIO male C57BL/6	↑ WAT eosinophils	↔ BAT activation and WAT beiging	(65)
Parasite single molecules				
HEK-produced recombinant *S. mansoni* omega-1	DIO male C57BL/6 WT, Cd206$^{-/-}$, Rora$^{fl/sg}$ Il7r^{cre}, Il1rl1$^{-/-}$	↑ IL-33 release by adipocytes ↑ WAT T_H2 cells, Tregs, CD206^{hi} AAMs, eosinophils and ILC2s ↓ WAT T_H1 cells and CD206^{low} classically-activated ATMs	↓ Body weight ↓ Fasting blood glucose ↑ Whole-body insulin sensitivity ↑ Whole-body glucose tolerance (CD206-, IL-33- and ILC2-dependent) ↑ WAT beiging	(22)

	Mouse models	Immunomodulatory effects	Metabolic effects	Refs
Acanthocheilonema viteae ES-62	DIO male C57BL/6 DIO female C57BL/6	↑ WAT eosinophils ↑ WAT IL-4 and IL-5 mRNA levels	↓ Liver fibrosis	(21)

[a] AAMs, alternatively-activated macrophages; ATMs, adipose tissue macrophages; BAT, brown adipose tissue; CAMs, classically activated macrophages; DIO, diet-induced obesity; HOMA-IR, Homeostatic Model Assessment for Insulin Resistance; IHC, Immunohistochemistry; WAT, white adipose tissue; WT, wild type; DEREG, Tg(Foxp3-DTR/EGFP)

Novel helminth-induced pathways: role in immunometabolic effects?

Modulation of gut microbiota by helminths

The gut microbiota is composed of a large number of microorganisms that are key determinants of both immune and metabolic homeostasis, including type 2 immunity (67). Alterations in their abundance and diversity, the so-called dysbiosis, can affect local and systemic immune responses and contribute to the development of immune and metabolic disorders (68, 69). In recent years, an increasing number of studies have reported the impact of helminth infections, especially those associated with the gastrointestinal tract, on the composition of intestinal microbiota in various mammalian hosts, including in humans (see recent reviews (70-72)). Although the bacterial species found to be affected by helminths vary widely depending on the helminth species, host type, and duration of the infection, those belonging to the family *Lactobacillaceae* are most commonly reported to be affected. Interestingly, these bacteria also contribute to the induction of a regulatory immune response (71, 73).

Dietary imbalance and calorie overload lead to microbiota dysbiosis and increased intestinal permeability, resulting in higher levels of circulating endotoxins such as lipopolysaccharides (LPS) that contribute to meta-inflammation and insulin resistance in peripheral tissues (69). Infection with *S. venezuelensis* has recently been shown to affect microbiota composition in the small intestine of HFD-fed obese mice (Table 1). Specifically, there was a decrease in the phylum *Bacteroidetes* and a concomitant increase in the phylum *Firmicutes*, the latter mostly attributed to a potent increase in *Lactobacillus* species (25). These helminth-induced changes in gut microbiota were associated with improved insulin sensitivity and glucose tolerance that could result, at least in part, from the decrease in gut permeability and plasma LPS levels, the increase in circulating IL-10, and/or the shift of macrophage polarization towards an M2-like phenotype (25). Another recent study has reported that infection with *H. polygyrus* also altered the composition of intestinal microbiota

in HFD-fed obese mice, with increased gut colonization by *Bacillus* and *Escherichia* species (74), which was associated with body weight loss, increased serum levels of norepinephrine (NE) and visceral WAT beiging. The effects were abolished by both antibiotic treatment and pharmacological antagonism of the b3-adrenergic receptor. This suggests that *H. polygyrus* promotes microbiota-derived NE, presumably generated by enriched *Bacillus* and *Escherichia* species, triggering a b3-adrenergic receptor-mediated thermogenic program in adipocyte progenitors and WAT beiging (74). However, the roles of WAT type 2 immune cells and other bacterial metabolites, such as short-chain fatty acids (SCFAs), both previously shown to regulate WAT beiging (75, 76), were not investigated and deserve further investigation. Altogether, it remains an open question whether the changes in gut microbiota, the helminth-induced type 2 immunity in metabolic tissues, or both, are the main driver of the metabolic health improvements. Interestingly, some gut microbiota-derived metabolites have recently been shown to directly regulate WAT inflammation by controlling the expression of a family of miRNAs, leading to the development of obesity and insulin resistance in mice (77). Whether helminth-induced changes in gut microbiota composition observed in obese mice could also affect this gut-WAT axis and significantly contribute to improvements in host metabolic homeostasis remains to be addressed.

Tuft cells

The induction of type 2 immunity by helminths is partly dependent on the epithelial cytokines IL-25, IL-33, and TSLP. Tuft cells, which are rare intestinal taste-chemosensory epithelial cells, have recently been shown to be involved in the initiation of type 2 mucosal immunity to the gastrointestinal helminth *N. brasiliensis* (78-80). Indeed, upon infection, tuft-cell-derived IL-25 activates ILC2s to secrete IL-13, which promotes goblet cell hyperplasia and tuft cell expansion that contribute to epithelial remodeling in the small intestine (79, 80). This circuit was later shown to be dependent on the calcium channel TRPM5 signaling and the succinate receptor SUCNR1 (GPR91) (79, 81, 82). However, both SUCNR1 and helminth-derived SUCNR1-ligand succinate were dispensable for type 2 immunity induction by *N. brasiliensis* (82).

Interestingly, tuft cells and some other chemosensory epithelial cells also link nutritional signals from dietary food in the gastrointestinal tract to afferent neuronal circuits controlling feeding behavior, peripheral nutrient disposal, and energy expenditure (83). While this will require further study, one may speculate that gastrointestinal helminths could affect this gut-brain axis through modulation of tuft cell-mediated chemosensory signaling. This can be either type 2 immunity-dependent or -independent and impact the regulation of food intake and/or peripheral glucose/lipid metabolism during nutritional overload.

Neuromedin U

The gut mucosa is densely innervated, and several immune cells, such as macrophages, mast cells, and ILC2s, have been reported to colocalize and interact with neurons from the enteric nervous system (84). Two landmark studies have recently reported that enteric, cholinergic neurons expressing the neuropeptide neuromedin U (NmU) colocalize with ILC2s that selectively express the NmU receptor 1 (NMUR1) (85, 86). Remarkably, *N. brasiliensis* infection increases NmU expression in enteric neurons of the intestinal lamina propria and triggers NMUR1-dependent ILC2 activation. This leads to the production of prototypical type 2 cytokines, such as IL-5 and IL-13, ultimately resulting in type 2 immunity and accelerated intestinal worm expulsion (85, 86).

Interestingly, NmU was also found to regulate whole-body metabolism, as transgenic mice overexpressing NmU exhibited reduced food intake as well as body weight gain during HFD feeding, and improved whole-body insulin sensitivity and glucose tolerance when compared with wild-type mice (87). Mechanistically, NmU was found to delay gastric emptying by directly triggering contractions of the pylorus and by indirectly activating vagal afferent neurons (88). Whether this NmU-mediated regulation of intestinal motility contributes to the beneficial effect of gastrointestinal nematode infection on glucose tolerance and insulin sensitivity in obese mice remains to be investigated.

Extracellular vesicles

Extracellular vesicles (**EVs**), including microvesicles, exosomes, and apoptotic bodies, are secreted by virtually all eukaryotic cells and have recently emerged as a new mode of intercellular communication by conveying complex mixtures of regulatory factors, such as proteins, lipids, miRNAs, and other structural components (89). Helminths have also been reported to produce EVs and use this mode of communication to manipulate the host immune responses (90, 91). For example, *H. polygyrus*-derived EVs have been shown to be taken up by activated macrophages and to potently suppress IL-33 receptor expression and both effector molecules of type 1 and type 2 immunity *in vitro* (92). But they can also generate strong antibody responses and protective immunity against infection (92) and suppress type 2 inflammation after allergen challenge *in vivo* (93). Of note, the helminth-derived EV composition is generally species- and life-stage-specific and mainly consists of excretory/secretory proteins and small noncoding RNAs, but can also be decorated by membrane-associated glycans (94) that might contribute to their immunomodulatory functions (90).

Interestingly, it has recently been shown that the production rate, size, and cargo composition of WAT-derived EVs, released from both macrophages and adipocytes, are altered

during obesity, contributing to meta-inflammation and insulin resistance through modulation of adipocyte-macrophage crosstalk and/or alteration of communication between WAT and other metabolic organs (95-97). It is therefore tempting to speculate that either worm-derived EVs or EVs released from host immune cells and/or metabolic cells primed by helminth molecules could, directly or indirectly, contribute to the crosstalk between organs that regulate tissue-specific and whole-body metabolic homeostasis. Exploring this hypothesis would be interesting and might result in the identification of specific helminth-derived EVs that could ultimately be used as potential new vectors for modulating meta-inflammation.

Immune-independent effects of helminth molecules on metabolic cells

Due to the plethora of molecules released by helminths inside their host, including some unique glycoproteins, it is finally conceivable that some helminth-derived molecules could also directly manipulate metabolic processes, potentially via glycan-mediated interactions with specific cell-surface receptors on metabolic cells. As such, *S. mansoni* SEA was shown to reduce hepatic steatosis, at least in part by direct inhibition of *de novo* lipogenesis in hepatocytes (20), and *Schistosoma japonicum* SEA was shown to inhibit TNF-induced activation of nuclear factor kappa B (NF-κB) pathway in hepatic stellate cells *in vitro* (98), an effect that might eventually contribute to reduce NASH. Recombinant omega-1 was also shown to promote IL-33 expression and release by adipocytes, presumably through interaction with mannose receptor (22).

Concluding Remarks and Future Directions

During recent years, and in line with results from cross-sectional studies conducted in populations from several endemic regions, it has been shown that infection with various helminth species - but also treatment with helminth-derived SEA mixtures or single molecules from SEA - can improve whole-body metabolic homeostasis in rodent models of obesity and type 2 diabetes. Various mechanisms have been proposed, including induction of type 2 immunity in metabolic organs, promotion of WAT beiging, decrease in hepatic steatosis, and/or changes in gut microbiota composition (Figure 2). However, the exact underlying molecular mechanism(s) by which helminths and their molecules exert their beneficial effects on insulin sensitivity and glucose/lipid homeostasis in obese mice, through either immune-dependent and/or -independent pathways, remain to be fully elucidated (see Outstanding Questions Box). As such, identifying new molecules, but also the exact molecular patterns, targeted receptors, and downstream cellular signaling pathways involved in their immunometabolic effects constitute important future directions.

Finally, whether helminthic therapies and/or development of helminth-derived therapeutics might hold promise for treating metabolic dysfunctions in obese subjects and type 2 diabetic patients is yet to be established. Importantly, controlled human infection (CHI) with *Necator americanus* shows promising results in terms of safety and tolerability (99) while efforts to establish a CHI model with single-sex *S. mansoni* are also ongoing (Trial NCT02755324; (100)). Although currently aimed at developing vaccines, clinical trials using CHI with helminths could be envisaged in the near future for inflammatory metabolic diseases such as obesity, NASH, and type 2 diabetes.

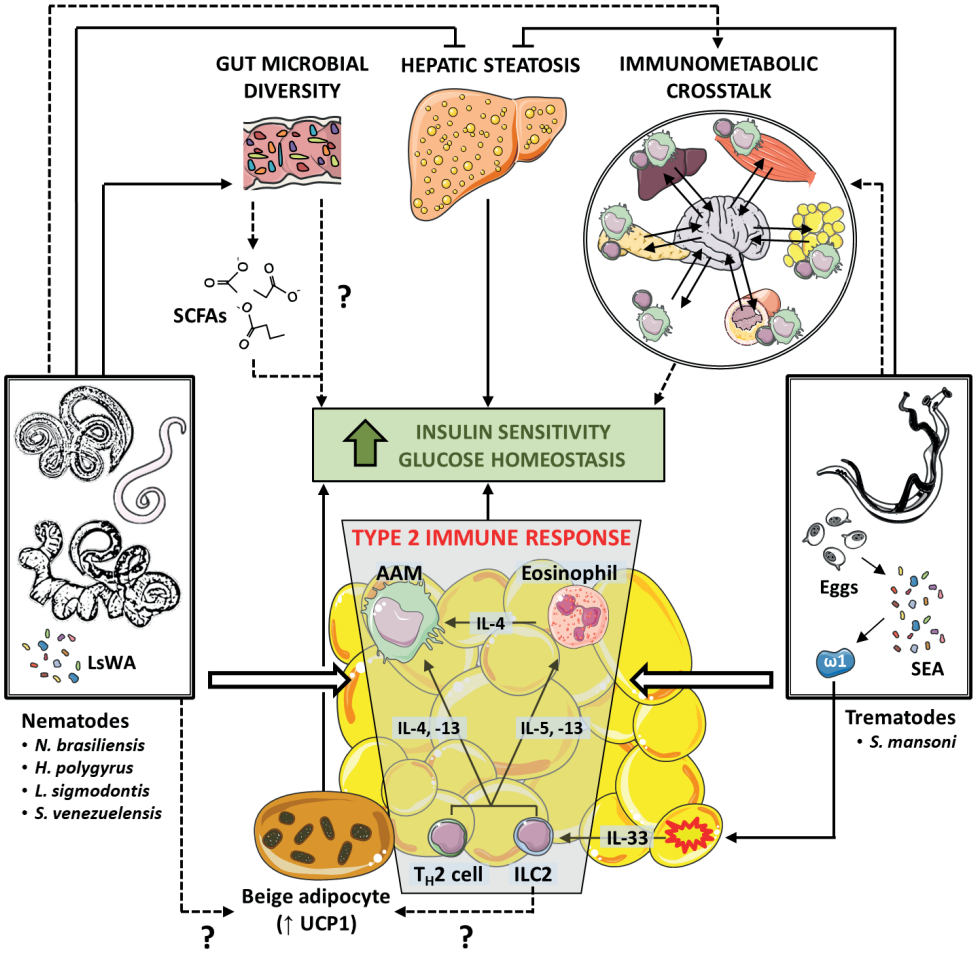

Figure 2. Regulation of metabolic homeostasis by helminths and their molecules. Both nematode and trematode infections were shown to improve whole-body metabolic homeostasis in obese mice through various mechanisms involving induction of type 2 immune responses and alternatively

◀Figure 2. Legend (Continued)

activated macrophages in white adipose tissue (WAT), WAT beiging, and/or reduction in hepatic steatosis. Some gastrointestinal nematodes were reported to change gut microbial composition and diversity, which may contribute to increased WAT beiging, notably through enhanced bacterial production of specific short-chain fatty acids (SCFAs). These SCFAs could improve whole-body metabolic homeostasis directly or indirectly via peripheral and/or brain-mediated mechanisms that are still incompletely understood. Lastly, the type 2 immune response induced by helminths in peripheral tissues may also affect the crosstalk between the brain and metabolic organs (liver, skeletal muscle, WAT, gut, and pancreas) through efferent and afferent pathways and contribute to improved whole-body insulin sensitivity and glucose homeostasis. Treatment with various mixtures of egg antigens and with either native or recombinant single-helminth-derived molecules was also shown to recapitulate some of the beneficial immunometabolic effects observed in helminth-infected obese mice, although the underlying molecular mechanisms proposed might sometimes differ. Abbreviations: AAM, alternatively activated macrophages; IL, interleukin; ILC2, group 2 innate lymphoid cell; LsWA, *L. sigmodontis* worm antigens; SEA, soluble egg antigens; T_H2, type 2 T helper cell; UCP1, uncoupling protein 1. Species names: *H. polygyrus*, *Heligmosomoides polygyrus*; *L. sigmodontis*, *Litosomoides sigmodontis*; *N. brasiliensis*, *Nippostrongylus brasiliensis*; *S. mansoni*, *Schistosoma mansoni*; *S. venezuelensis*, *Strongyloides venezuelensis.*

Outstanding Questions Box

What is the contribution of helminth-induced type 2 immunity in other metabolic organs than adipose tissue, i.e. liver, skeletal muscle, gut and pancreas, on whole-body metabolic homeostasis? What are the immune cells or cell subsets involved?

Does induction of adipose tissue alternatively-activated macrophages in obese mice play a central role in the improvement of insulin sensitivity by helminth molecules? If yes, what are their phenotypical characteristics and by which mechanism(s) do these polarized macrophages modulate adipocyte functions?

Do helminth infections and/or helminth molecules affect WAT beiging and/or BAT activation through type 2 immune response-dependent mechanism(s)?

To what extent do changes in gut microbiota diversity induced by gastrointestinal worms contribute to regulating whole-body metabolic homeostasis?

Do helminth-derived extracellular vesicles play a role in the immune-mediated regulation of tissue-specific insulin sensitivity and glucose/lipid metabolism?

Could direct interactions of helminth molecules with metabolic cells, e.g. adipocytes, hepatocytes, myocytes and/or beta-cells, contribute to the improvement of obesity-associated metabolic dysfunctions?

Is helminth-induced type 2 immunity in metabolic tissues, as observed in rodents, also present in humans, and is it involved in regulating whole-body metabolic homeostasis? If yes, what would have been the evolutionary advantage of this metabolic trade for the worms and their host?

Does helminthic therapy using controlled human infection and/or helminth-derived drugs hold promise as innovative therapeutic approaches for obesity and inflammatory metabolic diseases?

Acknowledgments

The authors want to thank Professor Maria Yazdanbakhsh for her critical reading of the manuscript. This work was supported by funding from the European Federation for the Study of Diabetes (EFSD/Lilly Research Grant Fellowship to B.G.), the Dutch Organization for Scientific Research (ZonMW TOP Grant 91214131 to B.G.), the NWO Graduate School Program 022.006.010 (to H.v.d.Z.), and the Polish Ministry of Science and Higher Education project Mobilność V (DN/MOB/278/V/2017 to A.Z.).

References

1. Hotez PJ, Alvarado M, Basanez MG, Bolliger I, Bourne R, Boussinesq M, et al. The global burden of disease study 2010: interpretation and implications for the neglected tropical diseases. PLoS Negl Trop Dis. 2014;8(7):e2865.
2. Karagiannis-Voules DA, Biedermann P, Ekpo UF, Garba A, Langer E, Mathieu E, et al. Spatial and temporal distribution of soil-transmitted helminth infection in sub-Saharan Africa: a systematic review and geostatistical meta-analysis. Lancet Infect Dis. 2015;15(1):74-84.
3. Bach JF. The hygiene hypothesis in autoimmunity: the role of pathogens and commensals. Nat Rev Immunol. 2018;18(2):105-20.
4. Yazdanbakhsh M, Kremsner PG, van Ree R. Allergy, parasites, and the hygiene hypothesis. Science. 2002;296(5567):490-4.
5. IDF. IDF Diabetes Atlas. 2017;8th edn:http://www.diabetesatlas.org/.
6. Hotamisligil GS. Inflammation, metaflammation and immunometabolic disorders. Nature. 2017;542(7640):177-85.
7. Saltiel AR, Olefsky JM. Inflammatory mechanisms linking obesity and metabolic disease. J Clin Invest. 2017;127(1):1-4.
8. Brestoff JR, Artis D. Immune regulation of metabolic homeostasis in health and disease. Cell. 2015;161(1):146-60.
9. Lackey DE, Olefsky JM. Regulation of metabolism by the innate immune system. Nat Rev Endocrinol. 2016;12(1):15-28.
10. Maizels RM, McSorley HJ. Regulation of the host immune system by helminth parasites. J Allergy Clin Immunol. 2016;138(3):666-75.
11. Harris NL, Loke P. Recent Advances in Type-2-Cell-Mediated Immunity: Insights from Helminth Infection. Immunity. 2017;47(6):1024-36.
12. Chen Y, Lu J, Huang Y, Wang T, Xu Y, Xu M, et al. Association of previous schistosome infection with diabetes and metabolic syndrome: a cross-sectional study in rural China. J Clin Endocrinol Metab. 2013;98(2):E283-7.
13. Wiria AE, Hamid F, Wammes LJ, Prasetyani MA, Dekkers OM, May L, et al. Infection with Soil-Transmitted Helminths Is Associated with Increased Insulin Sensitivity. PLoS One. 2015;10(6):e0127746.
14. Hays R, Esterman A, Giacomin P, Loukas A, McDermott R. Does Strongyloides stercoralis infection protect against type 2 diabetes in humans? Evidence from Australian Aboriginal adults. Diabetes Res Clin Pract. 2015;107(3):355-61.
15. Tahapary DL, de Ruiter K, Martin I, Brienen EAT, van Lieshout L, Djuardi Y, et al. Effect of anthelmintic treatment on leptin, adiponectin and leptin to adiponectin ratio: a randomized-controlled trial. Nutr Diabetes. 2017;7(10):e289.
16. Rajamanickam A, Munisankar S, Bhootra Y, Dolla C, Thiruvengadam K, Nutman TB, et al. Metabolic consequences of concomitant Strongyloides stercoralis infection in Type 2 diabetes mellitus. Clin Infect Dis. 2018.
17. Guigas B, Molofsky AB. A worm of one's own: how helminths modulate host adipose tissue function and metabolism. Trends Parasitol. 2015;31(9):435-41.

18. Guigas B. Editorial - Parasites and metabolic diseases. Parasite Immunol. 2017;39(5).

19. Berbudi A, Surendar J, Ajendra J, Gondorf F, Schmidt D, Neumann AL, et al. Filarial Infection or Antigen Administration Improves Glucose Tolerance in Diet-Induced Obese Mice. J Innate Immun. 2016;8(6):601-16.

20. Bhargava P, Li C, Stanya KJ, Jacobi D, Dai L, Liu S, et al. Immunomodulatory glycan LNFPIII alleviates hepatosteatosis and insulin resistance through direct and indirect control of metabolic pathways. Nat Med. 2012;18(11):1665-72.

21. Crowe J, Lumb FE, Doonan J, Broussard M, Tarafdar A, Pineda MA, et al. Parasitic worm product ES-62 promotes healthspan and lifespan in a model of obesity induced ageing. BioRxiv. 2019;. Posted June 22 2019. https://doi.org/10.1101/622753.

22. Hams E, Bermingham R, Wurlod FA, Hogan AE, O'Shea D, Preston RJ, et al. The helminth T2 RNase omega1 promotes metabolic homeostasis in an IL-33- and group 2 innate lymphoid cell-dependent mechanism. FASEB J. 2016;30(2):824-35.

23. Hussaarts L, Garcia-Tardon N, van Beek L, Heemskerk MM, Haeberlein S, van der Zon GC, et al. Chronic helminth infection and helminth-derived egg antigens promote adipose tissue M2 macrophages and improve insulin sensitivity in obese mice. FASEB J. 2015;29(7):3027-39.

24. Morimoto M, Azuma N, Kadowaki H, Abe T, Suto Y. Regulation of type 2 diabetes by helminth-induced Th2 immune response. J Vet Med Sci. 2017;78(12):1855-64.

25. Pace F, Carvalho BM, Zanotto TM, Santos A, Guadagnini D, Silva KLC, et al. Helminth infection in mice improves insulin sensitivity via modulation of gut microbiota and fatty acid metabolism. Pharmacol Res. 2018;132:33-46.

26. Su CW, Chen CY, Li Y, Long SR, Massey W, Kumar DV, et al. Helminth infection protects against high fat diet-induced obesity via induction of alternatively activated macrophages. Sci Rep. 2018;8(1):4607.

27. Wu D, Molofsky AB, Liang HE, Ricardo-Gonzalez RR, Jouihan HA, Bando JK, et al. Eosinophils sustain adipose alternatively activated macrophages associated with glucose homeostasis. Science. 2011;332(6026):243-7.

28. Yang Z, Grinchuk V, Smith A, Qin B, Bohl JA, Sun R, et al. Parasitic nematode-induced modulation of body weight and associated metabolic dysfunction in mouse models of obesity. Infect Immun. 2013;81(6):1905-14.

29. Hotamisligil GS, Shargill NS, Spiegelman BM. Adipose expression of tumor necrosis factor-alpha: direct role in obesity-linked insulin resistance. Science. 1993;259(5091):87-91.

30. Molofsky AB, Nussbaum JC, Liang HE, Van Dyken SJ, Cheng LE, Mohapatra A, et al. Innate lymphoid type 2 cells sustain visceral adipose tissue eosinophils and alternatively activated macrophages. J Exp Med. 2013;210(3):535-49.

31. Dahlgren MW, Jones SW, Cautivo KM, Dubinin A, Ortiz-Carpena JF, Farhat S, et al. Adventitial Stromal Cells Define Group 2 Innate Lymphoid Cell Tissue Niches. Immunity. 2019;50(3):707-22 e6.

32. Rana BMJ, Jou E, Barlow JL, Rodriguez-Rodriguez N, Walker JA, Knox C, et al. A stromal cell niche sustains ILC2-mediated type-2 conditioning in adipose tissue. J Exp Med. 2019;. Published Online First: June 27 2019. http://dx.doi.org/10.1084/jem.20190689.

33. Lumeng CN, DelProposto JB, Westcott DJ, Saltiel AR. Phenotypic switching of adipose tissue macrophages with obesity is generated by spatiotemporal differences in macrophage subtypes. Diabetes. 2008;57(12):3239-46.

34. Gundra UM, Girgis NM, Ruckerl D, Jenkins S, Ward LN, Kurtz ZD, et al. Alternatively activated macrophages derived from monocytes and tissue macrophages are phenotypically and functionally distinct. Blood. 2014;123(20):e110-22.

35. Silva HM, Bafica A, Rodrigues-Luiz GF, Chi J, Santos PDA, Reis BS, et al. Vasculature-associated fat macrophages readily adapt to inflammatory and metabolic challenges. J Exp Med. 2019;216(4):786-806.

36. Kratz M, Coats BR, Hisert KB, Hagman D, Mutskov V, Peris E, et al. Metabolic dysfunction drives a mechanistically distinct proinflammatory phenotype in adipose tissue macrophages. Cell Metab. 2014;20(4):614-25.

37. Coats BR, Schoenfelt KQ, Barbosa-Lorenzi VC, Peris E, Cui C, Hoffman A, et al. Metabolically Activated Adipose Tissue Macrophages Perform Detrimental and Beneficial Functions during Diet-Induced Obesity. Cell Rep. 2017;20(13):3149-61.

38. Hill DA, Lim HW, Kim YH, Ho WY, Foong YH, Nelson VL, et al. Distinct macrophage populations direct inflammatory versus physiological changes in adipose tissue. Proc Natl Acad Sci U S A. 2018;115(22):E5096-E105.

39. Jaitin DA, Adlung L, Thaiss CA, Weiner A, Li B, Descamps H, et al. Lipid-Associated Macrophages Control Metabolic Homeostasis in a Trem2-Dependent Manner. Cell. 2019;178(3):686-98.

40. Friedman SL, Neuschwander-Tetri BA, Rinella M, Sanyal AJ. Mechanisms of NAFLD development and therapeutic strategies. Nat Med. 2018;24(7):908-22.

41. Kazankov K, Jorgensen SMD, Thomsen KL, Moller HJ, Vilstrup H, George J, et al. The role of macrophages in nonalcoholic fatty liver disease and nonalcoholic steatohepatitis. Nat Rev Gastroenterol Hepatol. 2019;16(3):145-59.

42. Gomes AL, Teijeiro A, Buren S, Tummala KS, Yilmaz M, Waisman A, et al. Metabolic Inflammation-Associated IL-17A Causes Non-alcoholic Steatohepatitis and Hepatocellular Carcinoma. Cancer Cell. 2016;30(1):161-75.

43. Ghazarian M, Revelo XS, Nohr MK, Luck H, Zeng K, Lei H, et al. Type I Interferon Responses Drive Intrahepatic T cells to Promote Metabolic Syndrome. Sci Immunol. 2017;2(10).

44. Lanthier N, Molendi-Coste O, Horsmans Y, van Rooijen N, Cani PD, Leclercq IA. Kupffer cell activation is a causal factor for hepatic insulin resistance. Am J Physiol Gastrointest Liver Physiol. 2010;298(1):G107-16.

45. Morinaga H, Mayoral R, Heinrichsdorff J, Osborn O, Franck N, Hah N, et al. Characterization of distinct subpopulations of hepatic macrophages in HFD/obese mice. Diabetes. 2015;64(4):1120-30.

46. Tencerova M, Aouadi M, Vangala P, Nicoloro SM, Yawe JC, Cohen JL, et al. Activated Kupffer cells inhibit insulin sensitivity in obese mice. FASEB J. 2015;29(7):2959-69.

47. Krenkel O, Hundertmark J, Abdallah AT, Kohlhepp M, Puengel T, Roth T, et al. Myeloid cells in liver and bone marrow acquire a functionally distinct inflammatory phenotype during obesity-related steatohepatitis. Gut. 2019;. Published Online First: 10 May 2019. http://dx.doi.org/10.1136/gutjnl-2019-318382.

48. Huang W, Metlakunta A, Dedousis N, Zhang P, Sipula I, Dube JJ, et al. Depletion of liver Kupffer cells prevents the development of diet-induced hepatic steatosis and insulin resistance. Diabetes. 2010;59(2):347-57.

49. Obstfeld AE, Sugaru E, Thearle M, Francisco AM, Gayet C, Ginsberg HN, et al. C-C chemokine receptor 2 (CCR2) regulates the hepatic recruitment of myeloid cells that promote obesity-induced hepatic steatosis. Diabetes. 2010;59(4):916-25.

50. Krenkel O, Puengel T, Govaere O, Abdallah AT, Mossanen JC, Kohlhepp M, et al. Therapeutic inhibition of inflammatory monocyte recruitment reduces steatohepatitis and liver fibrosis. Hepatology. 2018;67(4):1270-83.

51. Morgantini C, Jager J, Li X, Levi L, Azzimato V, Sulen A, et al. Liver macrophages regulate systemic metabolism through non-inflammatory factors. Nature Metabolism. 2019;1:445-59.

52. Gieseck RL, 3rd, Ramalingam TR, Hart KM, Vannella KM, Cantu DA, Lu WY, et al. Interleukin-13 Activates Distinct Cellular Pathways Leading to Ductular Reaction, Steatosis, and Fibrosis. Immunity. 2016;45(1):145-58.

53. Weng SY, Wang X, Vijayan S, Tang Y, Kim YO, Padberg K, et al. IL-4 Receptor Alpha Signaling through Macrophages Differentially Regulates Liver Fibrosis Progression and Reversal. EBioMedicine. 2018;29:92-103.

54. Hart KM, Fabre T, Sciurba JC, Gieseck RL, 3rd, Borthwick LA, Vannella KM, et al. Type 2 immunity is protective in metabolic disease but exacerbates NAFLD collaboratively with TGF-beta. Sci Transl Med. 2017;9(396).

55. Jais A, Bruning JC. Hypothalamic inflammation in obesity and metabolic disease. J Clin Invest. 2017;127(1):24-32.

56. Wu H, Ballantyne CM. Skeletal muscle inflammation and insulin resistance in obesity. J Clin Invest. 2017;127(1):43-54.

57. Eguchi K, Nagai R. Islet inflammation in type 2 diabetes and physiology. J Clin Invest. 2017;127(1):14-23.

58. Ehses JA, Boni-Schnetzler M, Faulenbach M, Donath MY. Macrophages, cytokines and beta-cell death in Type 2 diabetes. Biochem Soc Trans. 2008;36(Pt 3):340-2.

59. Ying W, Lee YS, Dong Y, Seidman JS, Yang M, Isaac R, et al. Expansion of Islet-Resident Macrophages Leads to Inflammation Affecting beta Cell Proliferation and Function in Obesity. Cell Metab. 2019;29(2):457-74 e5.

60. Dalmas E, Lehmann FM, Dror E, Wueest S, Thienel C, Borsigova M, et al. Interleukin-33-Activated Islet-Resident Innate Lymphoid Cells Promote Insulin Secretion through Myeloid Cell Retinoic Acid Production. Immunity. 2017;47(5):928-42 e7.

61. Valdearcos M, Myers Jr MG, Koliwad SK. Hypothalamic microglia as potential regulators of metabolic physiology. Nature Metabolism. 2019;1:314-20.

62. Valdearcos M, Douglass JD, Robblee MM, Dorfman MD, Stifler DR, Bennett ML, et al. Microglial Inflammatory Signaling Orchestrates the Hypothalamic Immune Response to Dietary Excess and Mediates Obesity Susceptibility. Cell Metab. 2017;26(1):185-97 e3.

63. Lee CH, Kim HJ, Lee YS, Kang GM, Lim HS, Lee SH, et al. Hypothalamic Macrophage Inducible Nitric Oxide Synthase Mediates Obesity-Associated Hypothalamic Inflammation. Cell Rep. 2018;25(4):934-46 e5.

64. Tahapary DL, de Ruiter K, Martin I, Brienen EAT, van Lieshout L, Cobbaert CM, et al. Effect of Anthelmintic Treatment on Insulin Resistance: A Cluster-Randomized, Placebo-Controlled Trial in Indonesia. Clin Infect Dis. 2017;65(5):764-71.

65. van den Berg SM, van Dam AD, Kusters PJH, Beckers L, den Toom M, van der Velden S, et al. Helminth antigens counteract a rapid high-fat diet-induced decrease in adipose tissue eosinophils. J Mol Endocrinol. 2017;59(3):245-55.

66. Everts B, Perona-Wright G, Smits HH, Hokke CH, van der Ham AJ, Fitzsimmons CM, et al. Omega-1, a glycoprotein secreted by Schistosoma mansoni eggs, drives Th2 responses. J Exp Med. 2009;206(8):1673-80.

67. McCoy KD, Ignacio A, Geuking MB. Microbiota and Type 2 immune responses. Curr Opin Immunol. 2018;54:20-7.

68. Honda K, Littman DR. The microbiota in adaptive immune homeostasis and disease. Nature. 2016;535(7610):75-84.

69. Cani PD. Microbiota and metabolites in metabolic diseases. Nature Reviews Endocrinology. 2019;15(2):69-70.

70. Reynolds LA, Finlay BB, Maizels RM. Cohabitation in the Intestine: Interactions among Helminth Parasites, Bacterial Microbiota, and Host Immunity. J Immunol. 2015;195(9):4059-66.

71. Peachey LE, Jenkins TP, Cantacessi C. This Gut Ain't Big Enough for Both of Us. Or Is It? Helminth-Microbiota Interactions in Veterinary Species. Trends Parasitol. 2017;33(8):619-32.

72. Rapin A, Harris NL. Helminth-Bacterial Interactions: Cause and Consequence. Trends Immunol. 2018;39(9):724-33.

73. Zaiss MM, Harris NL. Interactions between the intestinal microbiome and helminth parasites. Parasite Immunol. 2016;38(1):5-11.

74. Shimokawa C, Obi S, Shibata M, Olia A, Imai T, Suzue K, et al. Suppression of Obesity by an Intestinal Helminth through Interactions with Intestinal Microbiota. Infect Immun. 2019;87(6).

75. Villarroya F, Cereijo R, Villarroya J, Gavalda-Navarro A, Giralt M. Toward an Understanding of How Immune Cells Control Brown and Beige Adipobiology. Cell Metab. 2018;27(5):954-61.

76. Li B, Li L, Li M, Lam SM, Wang G, Wu Y, et al. Microbiota Depletion Impairs Thermogenesis of Brown Adipose Tissue and Browning of White Adipose Tissue. Cell Rep. 2019;26(10):2720-37 e5.

77. Virtue AT, McCright SJ, Wright JM, Jimenez MT, Mowel WK, Kotzin JJ, et al. The gut microbiota regulates white adipose tissue inflammation and obesity via a family of microRNAs. Sci Transl Med. 2019;11(496).

78. Gerbe F, Sidot E, Smyth DJ, Ohmoto M, Matsumoto I, Dardalhon V, et al. Intestinal epithelial tuft cells initiate type 2 mucosal immunity to helminth parasites. Nature. 2016;529(7585):226-30.

79. Howitt MR, Lavoie S, Michaud M, Blum AM, Tran SV, Weinstock JV, et al. Tuft cells, taste-chemosensory cells, orchestrate parasite type 2 immunity in the gut. Science. 2016;351(6279):1329-33.

80. von Moltke J, Ji M, Liang HE, Locksley RM. Tuft-cell-derived IL-25 regulates an intestinal ILC2-epithelial response circuit. Nature. 2016;529(7585):221-5.

81. Schneider C, O'Leary CE, von Moltke J, Liang HE, Ang QY, Turnbaugh PJ, et al. A Metabolite-Triggered Tuft Cell-ILC2 Circuit Drives Small Intestinal Remodeling. Cell. 2018;174(2):271-84 e14.

82. Nadjsombati MS, McGinty JW, Lyons-Cohen MR, Jaffe JB, DiPeso L, Schneider C, et al. Detection of Succinate by Intestinal Tuft Cells Triggers a Type 2 Innate Immune Circuit. Immunity. 2018;49(1):33-41 e7.

83. Reimann F, Tolhurst G, Gribble FM. G-protein-coupled receptors in intestinal chemosensation. Cell Metab. 2012;15(4):421-31.

84. Veiga-Fernandes H, Mucida D. Neuro-Immune Interactions at Barrier Surfaces. Cell. 2016;165(4):801-11.

85. Cardoso V, Chesne J, Ribeiro H, Garcia-Cassani B, Carvalho T, Bouchery T, et al. Neuronal regulation of type 2 innate lymphoid cells via neuromedin U. Nature. 2017;549(7671):277-81.

86. Klose CSN, Mahlakoiv T, Moeller JB, Rankin LC, Flamar AL, Kabata H, et al. The neuropeptide neuromedin U stimulates innate lymphoid cells and type 2 inflammation. Nature. 2017;549(7671):282-6.

87. Kowalski TJ, Spar BD, Markowitz L, Maguire M, Golovko A, Yang S, et al. Transgenic overexpression of neuromedin U promotes leanness and hypophagia in mice. J Endocrinol. 2005;185(1):151-64.

88. Jarry AC, Merah N, Cisse F, Cayetanot F, Fiamma MN, Willemetz A, et al. Neuromedin U is a gut peptide that alters oral glucose tolerance by delaying gastric emptying via direct contraction of the pylorus and vagal-dependent mechanisms. FASEB J. 2019;33(4):5377-88.

89. Mathieu M, Martin-Jaular L, Lavieu G, Thery C. Specificities of secretion and uptake of exosomes and other extracellular vesicles for cell-to-cell communication. Nat Cell Biol. 2019;21(1):9-17.

90. Kuipers ME, Hokke CH, Smits HH, Nolte-'t Hoen ENM. Pathogen-Derived Extracellular Vesicle-Associated Molecules That Affect the Host Immune System: An Overview. Front Microbiol. 2018;9:2182.

91. Tritten L, Geary TG. Helminth extracellular vesicles in host-parasite interactions. Curr Opin Microbiol. 2018;46:73-9.

92. Coakley G, McCaskill JL, Borger JG, Simbari F, Robertson E, Millar M, et al. Extracellular Vesicles from a Helminth Parasite Suppress Macrophage Activation and Constitute an Effective Vaccine for Protective Immunity. Cell Rep. 2017;19(8):1545-57.

93. Buck AH, Coakley G, Simbari F, McSorley HJ, Quintana JF, Le Bihan T, et al. Exosomes secreted by nematode parasites transfer small RNAs to mammalian cells and modulate innate immunity. Nat Commun. 2014;5:5488.

94. de la Torre-Escudero E, Gerlach JQ, Bennett APS, Cwiklinski K, Jewhurst HL, Huson KM, et al. Surface molecules of extracellular vesicles secreted by the helminth pathogen Fasciola hepatica direct their internalisation by host cells. PLoS Negl Trop Dis. 2019;13(1):e0007087.

95. Pan Y, Hui X, Hoo RLC, Ye D, Chan CYC, Feng T, et al. Adipocyte-secreted exosomal microRNA-34a inhibits M2 macrophage polarization to promote obesity-induced adipose inflammation. J Clin Invest. 2019;129(2):834-49.

96. Ying W, Riopel M, Bandyopadhyay G, Dong Y, Birmingham A, Seo JB, et al. Adipose Tissue Macrophage-Derived Exosomal miRNAs Can Modulate In Vivo and In Vitro Insulin Sensitivity. Cell. 2017;171(2):372-84 e12.

97. Huang-Doran I, Zhang CY, Vidal-Puig A. Extracellular Vesicles: Novel Mediators of Cell Communication In Metabolic Disease. Trends Endocrinol Metab. 2017;28(1):3-18.

98. Chen L, Yu Y, Liu E, Duan L, Zhu D, Chen J, et al. Schistosoma japonicum soluble egg antigen inhibits TNF-alpha-induced IL-34 expression in hepatic stellate cells. Parasitol Res. 2019;118(2):551-7.

99. Loukas A, Hotez PJ, Diemert D, Yazdanbakhsh M, McCarthy JS, Correa-Oliveira R, et al. Hookworm infection. Nat Rev Dis Primers. 2016;2:16088.

100. Roestenberg M, Hoogerwerf MA, Ferreira DM, Mordmuller B, Yazdanbakhsh M. Experimental infection of human volunteers. Lancet Infect Dis. 2018;18(10):e312-e22.

CHAPTER 7

The helminth glycoprotein omega-1 improves metabolic homeostasis in obese mice through type-2 immunity-independent inhibition of food intake

Hendrik J.P. van der Zande, Michael A. Gonzalez, Karin de Ruiter, Ruud H.P. Wilbers, Noemí García-Tardón, Mariska van Huizen, Kim van Noort, Leonard R. Pelgrom, Joost M. Lambooij, Anna Zawistowska-Deniziak, Frank Otto, Arifa Ozir-Fazalalikhan, Danny van Willigen, Mick Welling, Jordan Poles, Fijs van Leeuwen, Cornelis H. Hokke, Arjen Schots, Maria Yazdanbakhsh, P'ng Loke, Bruno Guigas

The FASEB Journal. 35:e21331. (2021)
PMID: 33476078
doi: 10.1096/fj.202001973R

Abstract

Type 2 immunity plays an essential role in the maintenance of metabolic homeostasis and its disruption during obesity promotes meta-inflammation and insulin resistance. Infection with the helminth parasite *Schistosoma mansoni* and treatment with its soluble egg antigens (SEA) induces a type 2 immune response in metabolic organs and improve insulin sensitivity and glucose tolerance in obese mice, yet a causal relationship remains unproven. Here, we investigated the effects and underlying mechanisms of the T2 ribonuclease omega-1 (ω1), one of the major *S. mansoni* immunomodulatory glycoproteins, on metabolic homeostasis. We show that treatment of obese mice with plant-produced recombinant ω1, harboring similar glycan motifs as present on the native molecule, decreased body fat mass and improved systemic insulin sensitivity and glucose tolerance in a time- and dose-dependent manner. This effect was associated with an increase in white adipose tissue (WAT) type 2 T helper cells, eosinophils and alternatively-activated macrophages, without affecting type 2 innate lymphoid cells. In contrast to SEA, the metabolic effects of ω1 were still observed in obese STAT6-deficient mice with impaired type 2 immunity, indicating that its metabolic effects are independent of the type 2 immune response. Instead, we found that ω1 inhibited food intake, without affecting locomotor activity, WAT thermogenic capacity or whole-body energy expenditure, an effect also occurring in leptin receptor-deficient obese and hyperphagic *db/db* mice. Altogether, we demonstrate that while the helminth glycoprotein ω1 can induce type 2 immunity, it improves whole-body metabolic homeostasis in obese mice by inhibiting food intake via a STAT6-independent mechanism.

Introduction

Obesity is associated with chronic low-grade inflammation in metabolic organs (1). This so-called meta-inflammation plays a prominent role in the etiology of insulin resistance and type 2 diabetes (1-3), and is associated with increased numbers of proinflammatory macrophages, notably in white adipose tissue (WAT) (4) and liver (5). In WAT, these macrophages mainly originate from newly-recruited blood monocytes that differentiate into proinflammatory macrophages upon entering the inflammatory milieu (4) and/or being activated by elevated local concentration of free fatty acids (6). These proinflammatory macrophages produce cytokines, such as tumor necrosis factor (TNF) and interleukin 1-beta (IL-1β), which directly inhibit canonical insulin signaling [as reviewed in (2)] and contribute to tissue-specific insulin resistance and whole-body metabolic dysfunctions. In the liver, activation of Kupffer cells, the tissue-resident macrophages, promote the recruitment of proinflammatory monocytes and neutrophils which trigger hepatic inflammation and insulin resistance through the production of proinflammatory cytokines and elastase, respectively (5, 7, 8). In contrast, a type 2 cytokine environment predominates in lean metabolic tissues under homeostatic conditions, notably in WAT where IL-4, IL-5 and IL-13 produced by type 2 innate lymphoid cells (ILC2s), T helper 2 (Th2) cells and/or eosinophils promote alternatively activated macrophages (AAM) (9, 10). According to the current paradigm, AAMs are the final effector cells of this type 2 immune response, contributing to the maintenance of WAT insulin sensitivity by underlying molecular mechanism(s) that are still largely unknown (2, 11).

Parasitic helminths are the strongest natural inducers of type 2 immunity (12). Interestingly, several studies have reported an association between helminth-induced type 2 immunity and improved whole-body metabolic homeostasis in both humans and rodents [(13), and as reviewed in (11)]. We also showed that chronic treatment with *S. mansoni* soluble egg antigens (SEA) promoted eosinophilia, Th2 cells, type 2 cytokines expression and AAMs in WAT, and improved both tissue-specific and systemic insulin sensitivity in obese mice (14). SEA drives dendritic cell (DC)-mediated Th2 skewing at least partly through glycosylated molecules [(15), and reviewed in (16)], particularly the T2 RNase glycoprotein omega-1 [ω1; (17, 18)]. Interestingly, acute treatment with human embryonic kidney 293 (HEK-293)-produced recombinant ω1 was recently shown to decrease body weight and improve whole-body glucose tolerance in obese mice, through ILC2-mediated type 2 immunity and induction of WAT beiging (19). In this study, the metabolic effect of ω1 was reported to be glycan-dependent, yet we have previously shown that the glycosylation pattern of HEK-293-produced ω1 differs significantly from the *S. mansoni* native molecule, which notably harbors immunogenic Lewis-X (Le^X) glycan motifs (18, 20). By exploiting the flexible N-glycosylation machinery of *Nicotiana benthamiana* plants, we successfully

produced large amounts of recombinant ω1 glycosylation variants, either carrying Le^X motifs on one of its glycan branches or not (21).

In the present study, we investigate the effects and underlying immune-dependent mechanisms of both SEA and two plant-produced ω1 glycovariants on whole-body metabolic homeostasis in obese mice. Remarkably, we demonstrate that while SEA improved metabolic homeostasis in obese mice through a STAT6-dependent type 2 immune response, recombinant pLe^X-ω1 did so independent of its type 2 immunity-inducing capacity, by reducing food intake in a leptin receptor-independent manner.

Results

S. mansoni soluble egg antigens (SEA) improve metabolic homeostasis in obese mice by a STAT6-dependent mechanism

In order to investigate the role of type 2 immunity in the beneficial metabolic effects of SEA, we used mice deficient for STAT6 (*Stat6*$^{-/-}$), a key transcription factor involved in signature type 2 cytokines interleukin (IL)-4/IL-13 signaling and maintenance of Th2 effector functions (22, 23). In line with previous studies (14, 24), we treated HFD-fed obese WT and *Stat6*$^{-/-}$ with SEA for 4 weeks (Figure 1A). We confirmed that chronic treatment with SEA increased IL-5 and IL-13-expressing Th2 cells (Figure 1B), eosinophils (Figure 1C) and $YM1^+$ AAMs (Figure 1D) in WAT from HFD-fed obese WT mice while, as expected, this type 2 immune response was abrogated in *Stat6*$^{-/-}$ mice. SEA slightly reduced body weight (Figure 1E) and similarly affected body composition (Supplementary Figure 2A) in both WT and *Stat6*$^{-/-}$ obese mice, without affecting food intake (Figure 1F). In line with our previous study, we showed that SEA reduced fasting plasma insulin levels (Supplementary Figure 2C) and HOMA-IR (Figure 1G), and improved whole-body glucose tolerance in WT obese mice (Figure 1H,J). Strikingly, this beneficial metabolic effect was completely abolished in *Stat6*$^{-/-}$ mice (Figure 1I,J), indicating that SEA improves whole-body metabolic homeostasis in obese mice through STAT6-mediated type 2 immunity.

Plant-produced recombinant ω1 glycovariants increase adipose tissue Th2 cells, eosinophils and alternatively-activated macrophages, without affecting innate lymphoid cells

One of the major type 2 immunity-inducing molecules in SEA is the T2 ribonuclease glycoprotein ω1 (18). To study the effect of ω1 on metabolic homeostasis and the role of its immunomodulatory glycans, we generated two recombinant glycosylation variants using glycol-engineered *N. benthamiana* plants: one carrying wild-type plant glycans (pWT-ω1) and one harboring terminal Le^X motifs (pLe^X-ω1;

(21)). For both ω1 glycovariants, 4 weeks treatment markedly increased WAT CD4 T cells in HFD-fed obese mice, with pWT-ω1 being slightly more potent than pLe^{X}-ω1, while total ILCs were unaffected (Figure 2A-B). Interestingly, a specific increase in WAT IL-5 and IL-13-expressing Th2 cells was seen for both ω1 glycovariants, while the other CD4 T cell subsets, *i.e.* regulatory T cells (Treg) and Th1 cells, were not affected (Figure 2C). In addition, we confirmed that HFD reduced WAT IL-5^{+}/IL-13^{+} ILC2s, as previously reported (9), an effect that was even further pronounced with ω1 glycovariants (Figure 2D). The type 2 cytokines IL-5 and IL-13 produced by either ILC2s and/or Th2 cells have been reported to maintain WAT eosinophils (9). Congruent with our data on Th2 cells, we found a potent increase in WAT eosinophils upon ω1 treatment that was of similar extent for both glycovariants (Figure 2E). Finally, both pWT-ω1 and pLe^{X}-ω1 increased WAT YM1^{+} AAMs while obesity-associated CD11c^{+} macrophages were not affected (Figure 2F-G). This ω1-induced WAT type 2 immunity was dose-dependent (Supplementary Figure 3) and already observed after one week of treatment, when ILC2s were also not affected (Supplementary Figure 4).

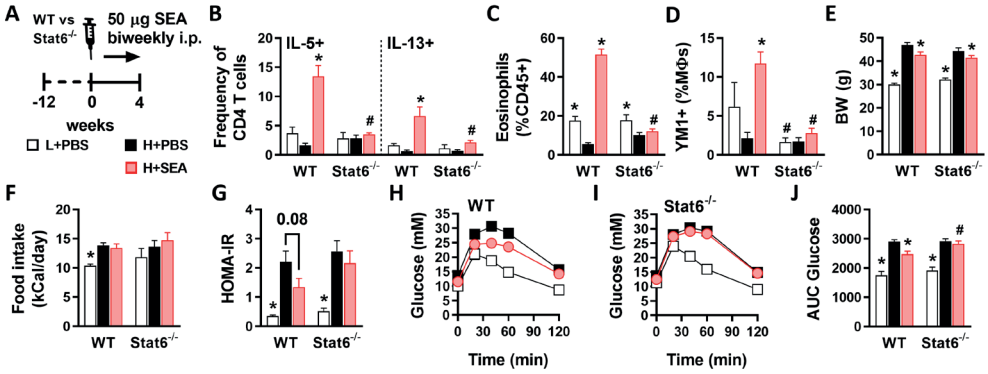

Figure 1. *S. mansoni* soluble egg antigens improve metabolic homeostasis in obese mice by a STAT6-dependent mechanism. (**A**) WT and *Stat6*$^{-/-}$ mice were fed a LFD (white bars) or a HFD for 12 weeks and next received intraperitoneal injections of PBS (black bars) or 50 µg *S. mansoni* soluble egg antigens (SEA; red bars) every 3 days for 4 weeks. At sacrifice, epididymal WAT was collected and SVF was isolated and analyzed by flow cytometry. The complete gating strategy is shown in Supplementary Figure 1. (**B**) Frequencies of IL-5 and IL-13 expressing Th2 cells in WAT were determined after PMA/ionomycin/Brefeldin A restimulation. (**C-D**) Abundances of eosinophils (*C*) and YM1^{+} macrophages (AAMs; *D*) were determined. (**E**) Body weight was measured after 4 weeks of treatment. (**F**) Food intake was monitored throughout the experimental period. (**G**) HOMA-IR was calculated using fasting blood glucose and plasma insulin levels at week 4. (**H-J**) An i.p. glucose tolerance test was performed at week 3. Blood glucose levels were measured at the indicated time points (*H-I*) and the AUC of the glucose excursion curve was calculated (*J*). Data shown are a pool of two independent experiments. Results are expressed as means ± SEM. **P*<0.05 *vs* HFD, #*P*<0.05 *vs* WT (n = 9-12 mice per group).

AAMs are considered the effector cells of WAT type 2 immunity in the maintenance of tissue insulin sensitivity (2), although the mechanisms are not fully understood. Monocyte-derived macrophages can irreversibly be labelled upon tamoxifen administration in *Cx3cr1*$^{\text{CreERT2-IRES-EYFP}}$ *Rosa26*$^{\text{LoxP-stop-LoxP-tdTomato}}$ (*Cx3cr1*$^{\text{CreER}}$ *Rosa26*$^{\text{tdTomato}}$) mice, as described elsewhere (25). In order to characterize newly recruited, ω1-induced adipose tissue macrophages (ATMs) during obesity, we performed RNA sequencing on FACS-sorted tdTomato^{+} macrophages from eWAT SVF of obese *Cx3cr1*$^{\text{CreER}}$ *Rosa26*$^{\text{tdTomato}}$ mice that were treated with PBS or pLe^{X}-ω1, the glycovariant that resembles native ω1 most (Supplementary Figure 5A). Genes associated with alternative activation, *e.g. Tmem26*, *Slc7a2, Chil3* and *Arg1*, were upregulated ($\log_2$FC > 2) in ATMs from pLe^{X}-ω1-treated mice as compared to controls, while genes associated with proinflammatory or obesity-associated macrophages, *e.g. Igfbp7, Cxcl12, Bgn, Dcn* and *Cd86*, were downregulated ($\log_2$FC < -2; Supplementary Figure 5B-C). Macrophage function is increasingly recognized to be supported by their metabolism to meet energy demands, and as such, AAMs display increased oxidative phosphorylation (26). In PD-L2^{+} WAT macrophages (Supplementary Figure 5D), pLe^{X}-ω1 indeed increased mitochondrial mass, while displaying decreased mitochondrial membrane potential and similar total reactive oxygen species production (Supplementary Figure 5E-G), a metabolic phenotype in line with alternative macrophage activation.

Similar to WAT, maintenance of insulin sensitivity in the liver is also associated with type 2 immunity (27), whereas obesity-driven activation of Kupffer cells increases the recruitment of proinflammatory monocytes and triggers hepatic insulin resistance (2, 7). In our conditions, while ω1 glycovariants increased Th2 cells in the liver, we did not find alternative activation of Kupffer cells (Supplementary Figure 6A-D). Instead, ω1 glycovariants increased the number of CD11c^{+} proinflammatory Kupffer cells (Supplementary Figure 6D), hepatic expression of proinflammatory cytokines *Ccl2, Tnf* and *Il1b* (Supplementary Figure 6E), and newly recruited monocytes (Supplementary Figure 6F), with a more potent effect in pLe^{X}-ω1-treated mice. Taken together, these data indicate that both ω1 glycovariants potently induce type 2 immunity in obese mice, triggering an alternative activation profile in WAT, but not liver macrophages.

ω1 glycovariants reduce body weight, fat mass and food intake, and improve whole-body metabolic homeostasis in obese mice

We next investigated the metabolic effects of ω1 glycovariants and showed that they both induced a rapid and gradual body weight loss in HFD-fed mice (Figure 3A-B), which was exclusively due to a decrease in fat mass (Figure 3C). The ω1 glycovariants significantly reduced visceral eWAT mass, but had no or only marginal effects on subcutaneous iWAT,

brown adipose tissue (BAT) and liver mass (Supplementary Figure 2D). This reduction in fat mass was associated with smaller adipocytes (Supplementary Figure 7A-B), reduced leptin expression (Supplementary Figure 7C-D), and opposite changes in expression of proinflammatory (decrease in *Itgax*) and alternatively-activated (increase in *Arg1*) canonical macrophage markers in both eWAT and iWAT (Supplementary Figure 7C-D). However, the lower fat mass gain was clearly not due to increased WAT beiging, as ω1 glycovariants neither increased expression of thermogenic gene markers (*Ucp1*, *Cox8b* and *Cidea*) in both eWAT and iWAT from obese mice (Supplementary Figure 7C-D), nor whole-body energy expenditure (Supplementary Figure 7E). In addition, ω1 glycovariants did not affect hepatic steatosis (Supplementary Figure 6G-I) but increased the expression of fibrotic gene markers (Supplementary Figure 8A), without detectable collagen accumulation (Supplementary Figure 8B-C). An increase in circulating alanine transaminase levels was also observed (Supplementary Figure 8D), indicating that ω1 may also have some cytotoxic effects in the liver, as previously reported (28, 29).

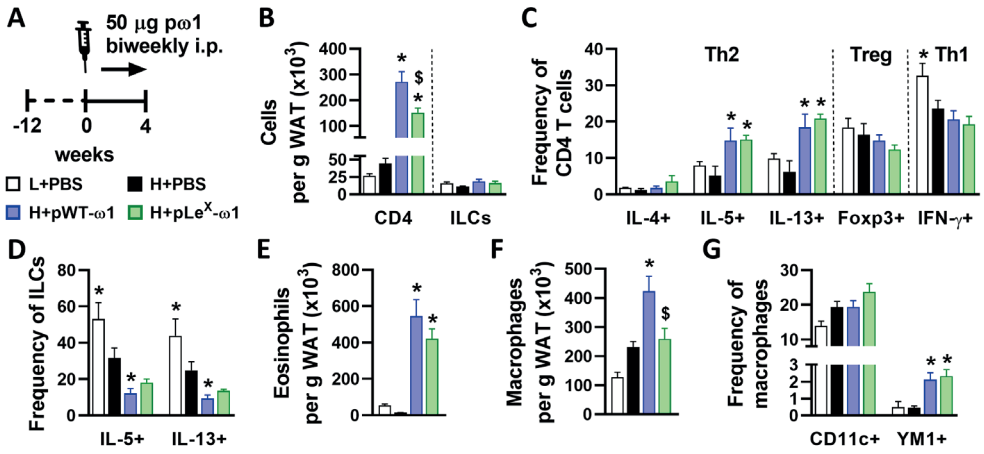

Figure 2. Plant-produced recombinant ω1 glycovariants increase adipose tissue Th2 cells, eosinophils and alternatively-activated macrophages, without affecting innate lymphoid cells. (**A**) Mice were fed a LFD (white bars) or a HFD for 12 weeks, and next received intraperitoneal injections of PBS (black bars) or either 50 µg pWT-ω1 (blue bars) or 50 µg pLe^{X}-ω1 (green bars) every 3 days for 4 weeks. At the end of the experiment, eWAT was collected, processed and analyzed as described in the legend of Figure 1. (**B-G**) Numbers of CD4 T cells, ILCs (*B*), eosinophils (*E*) and macrophages (*F*) per gram tissue were determined. Frequencies of CD4 T helper subsets (*C*) and cytokine-expressing ILCs (*D*) were determined. Percentages of CD11c^{+}YM1^{-} and CD11c^{-}YM1^{+} macrophages (*G*) were measured. Data shown are a pool of at least two independent experiments. Results are expressed as means ± SEM. **P*<0.05 *vs* HFD, $*P*<0.05 *vs* pWT-ω1 (n = 6-19 mice per group in B, E-G, and 3-9 mice per group in C and D).

Interestingly, we found that both ω1 glycovariants induced a significant decrease in food intake (Figure 3D-E), while locomotor activity was not affected (Figure 3F-G). Treatment with both ω1 glycovariants significantly reduced fasting blood glucose, plasma insulin levels (Supplementary Figure 2E-F) and HOMA-IR (Figure 3H) in obese mice, with a trend towards a stronger effect with pLe^{X}-ω1, indicating improved insulin sensitivity. Congruent with these data, we observed a significant improvement in whole-body glucose tolerance (Figure 3I-J) and insulin sensitivity (Figure 3K-L) in both pWT-ω1 and pLe^{X}-ω1-treated obese mice. Furthermore, except in eWAT, the ω1 glycovariants restored the expression the insulin receptor (IRβ) and the insulin-induced phosphorylation of PKB in the main metabolic organs, confirming enhanced insulin sensitivity (Figure 3M-P). In line with enhanced hepatic insulin sensitivity, we also found that pWT-ω1 and pLe^{X}-ω1 lowered the glucose levels during an intraperitoneal pyruvate tolerance test (Supplementary Figure 6J-K) and decreased the expression of gluconeogenic genes in the livers of obese mice (Supplementary Figure 6L), suggesting an improved insulin-induced inhibition of hepatic gluconeogenesis.

Of note, the effects of ω1 glycovariants on food intake, plasma metabolic parameters and whole-body insulin sensitivity were all dose-dependent (Supplementary Figure 3) and already observed after one week of treatment, when body weight and fat mass were only mildly affected (Supplementary Figure 4). Altogether, these data show that both recombinant ω1 glycovariants improve whole-body metabolic homeostasis in insulin-resistant obese mice.

pLe^{X}-ω1 improves metabolic homeostasis in obese mice by a STAT6-independent mechanism

We next investigated the role of type 2 immunity in the metabolic effects of ω1, using pLe^{X}-ω1 as the most potent and native-like glycovariant. As expected, while 4 weeks pLe^{X}-ω1 treatment (Figure 4A) increased WAT Th2 cells, eosinophils and YM1^{+} AAMs in obese WT mice, this type 2 immune response was abrogated in obese *Stat6*$^{-/-}$ mice (Figure 4B-D). However, treatment with pLe^{X}-ω1 still reduced body weight (Figure 4E-G) and food intake (Figure 4H), and affected body composition (Supplementary Figure 2G) in *Stat6*$^{-/-}$ obese mice to the same extent as in WT mice. In addition, both plasma insulin levels and HOMA-IR were markedly decreased in both genotypes (Supplementary Figure 2H-I and Figure 4I). The improvements in whole-body glucose tolerance (Figure 4J-L) and insulin sensitivity (Figure 4M-O) were also still observed in *Stat6*$^{-/-}$ mice, indicating that pLe^{X}-ω1's type 2 immunity-inducing capacity does not play a major role in restoration of metabolic homeostasis in obese mice. Of note, in contrast to its implication in maintenance of WAT metabolic homeostasis, IL-13 signaling has recently also been shown to play a role in the development of liver fibrosis (30, 31). Interestingly, the increase in liver IL-5^{+} and IL-13^{+}

Th2 cells in response to pLe^{X}-ω1 was also abrogated in *Stat6*$^{-/-}$ mice (Supplementary Figure 8E), and the expression of fibrotic gene markers were markedly reduced in *Stat6*$^{-/-}$ mice as compared to WT mice (Supplementary Figure 8F). Taken together, these results show that pLe^{X}-ω1 improves whole-body metabolic homeostasis independent of STAT6-mediated type 2 immunity, while promoting early markers of hepatic fibrosis at least partly through an IL-13-STAT6-mediated mechanism.

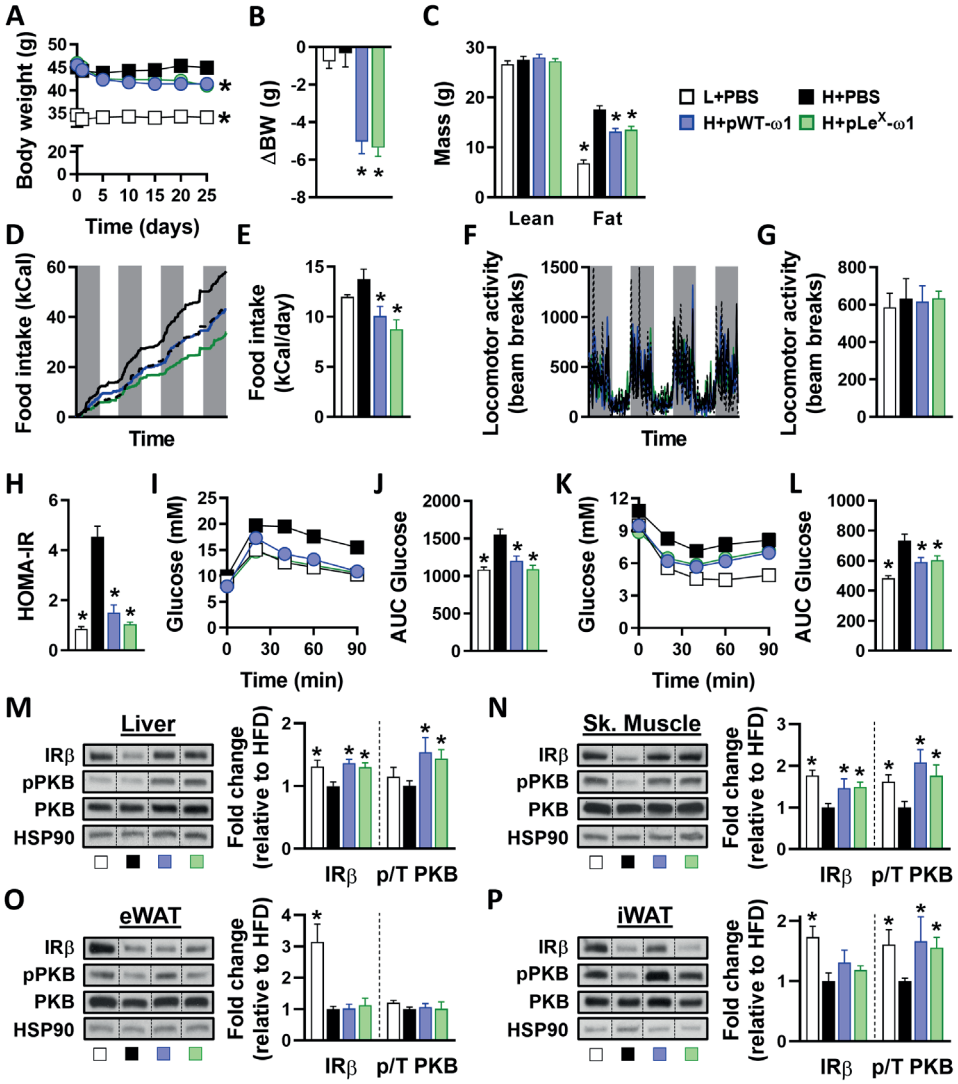

Figure 3. ω1 glycovariants reduce body weight, fat mass and food intake, and improve whole-body metabolic homeostasis in obese mice. Mice were fed a LFD (white bars) or a HFD for 12 weeks, and

▲Figure 3. Legend (Continued)

next received biweekly intraperitoneal injections of PBS (black bars) or 50 µg pWT-ω1 (blue bars) or pLe^X-ω1 (green bars) for 4 weeks. (**A-B**) Body weight was monitored throughout the experimental period. (**C**) Body composition was measured after 4 weeks of treatment. (**D-G**) Food intake (*D-E*) and locomotor activity (*F-G*) were assessed using fully automated single-housed metabolic cages during the first week of treatment. (**H**) HOMA-IR at week 4 was calculated. (**I-L**) Intraperitoneal glucose (*I-J*) and insulin (*K-L*) tolerance tests were performed during week 3. Blood glucose levels were measured at the indicated time points (*I, K*) and the AUC of the glucose excursion curve were calculated (*J, L*). (**M-P**) After 4 weeks of treatment, mice received an i.p. injection of insulin (1 U/kg lean body mass) and after 15 minutes, pieces of liver (*M*), skeletal muscle (*N*), eWAT (*O*) and iWAT (*P*) were collected and snap frozen immediately. The protein expression of IRβ and the phosphorylation state of PKB-Ser473 (pPKB) were assessed by Western blot and quantified by densitometry analysis. HSP90 expression was used as internal housekeeping protein, and phosphorylation of PKB is expressed as a ratio of phosphorylated over total PKB. Representative Western blots are shown. Data shown are a pool of at least two independent experiments. Results are expressed as means ± SEM. **P*<0.05 *vs* HFD (n = 11-20 mice per group in A-C, H-L, and 4-9 mice per group in D-G, M-P).

pLeX-ω1 improves metabolic homeostasis through leptin receptor-independent inhibition of food intake in obese mice

As ω1 significantly reduced food intake in obese mice, we next investigated its impact on feeding behavior. We found that a single intraperitoneal injection of pLe^X-ω1 in overnight fasted obese mice markedly reduced food intake during refeeding for at least 24 hours, resulting in decreased body weight gain as compared to PBS-injected mice (Figure 5A-C). To determine whether reduced food intake drives the beneficial metabolic effects of ω1, we treated HFD-fed mice with pLe^X-ω1 or PBS, and included a pair-fed group that received daily adjusted HFD meals based on the food intake of the pLe^X-ω1-treated animals (Figure 5D). While pLe^X-ω1 induced IL-13$^+$ Th2 cells, eosinophils and YM1$^+$ AAMs in WAT, reducing caloric intake in pair-fed mice did not affect WAT type 2 immunity, as expected (Figure 5E-G). Yet, food restriction in the pair-fed group decreased body weight (Figure 5H), fasting blood glucose and plasma insulin levels (Supplementary Figure 2K-L), and HOMA-IR (Figure 5I) as well as whole-body glucose tolerance to the same extent as in pLe^X-ω1-treated animals (Figure 5J-K).

The central regulation of feeding behavior and whole-body energy homeostasis involves complex neuronal networks, notably in the hypothalamus and brain stem (32, 33). To investigate whether pLe^X-ω1 accumulates in the brain to directly regulate hypothalamic neurons controlling food intake, we performed in vivo imaging experiments with pLe^X-ω1 conjugated to a hybrid tracer (^{111}In-DTPA-Cy5-pLe^X-ω1). Both Single Photo Emission Computed Tomography (SPECT) imaging and radioactivity biodistribution revealed that ^{111}In-DTPA-Cy5-pLe^X-ω1 mainly accumulated in abdominal organs, *e.g.* adipose tissues,

liver and intestines, and peritoneal draining lymph nodes, whereas no substantial amounts of radioactivity could be detected in the hypothalamus and other brain regions 24h after tracer administration (Supplementary Figure 9A-B). Of note, both glycovariants did not affect HFD-induced expression of various inflammatory genes in the whole hypothalamus (Supplementary Figure 9C), suggesting that dampening of hypothalamic inflammation is probably not involved in the anorexigenic effects of ω1. Hence, ω1 does not distribute to the brain and likely regulates food intake through peripheral effects.

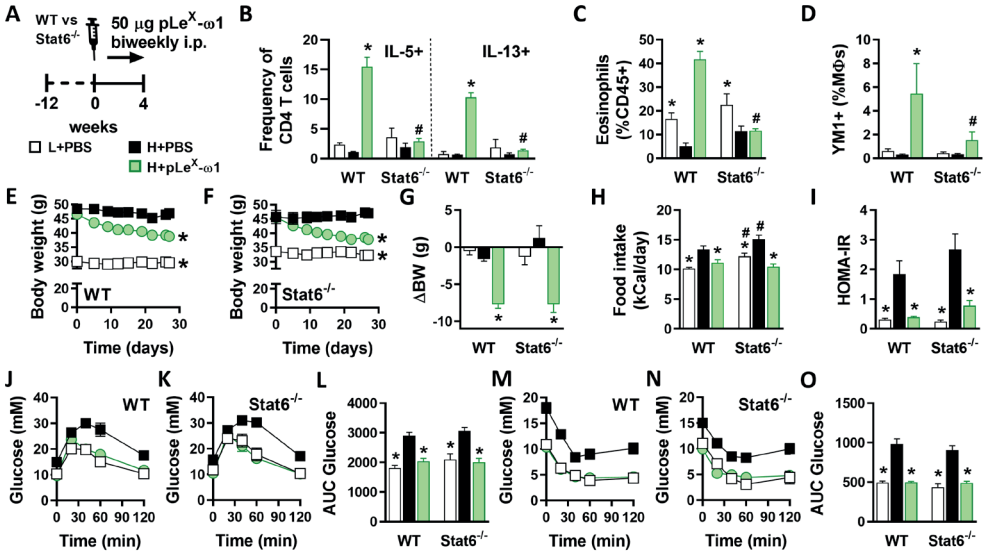

Figure 4. pLeX-ω1 improves metabolic homeostasis in obese mice by a STAT6-independent mechanism. (**A**) WT and *Stat6*$^{-/-}$ mice were fed a LFD (white bars) or a HFD for 12 weeks and next received biweekly intraperitoneal injections of PBS (black bars) or 50 µg pLe^{X}-ω1 (green bars) for 4 weeks. At the end of the experiment, eWAT was collected, processed and analyzed as described in the legend of Figure 1. (**B**) The frequencies of cytokine-expressing CD4 T cells were determined. (**C-D**) Abundances of eosinophils (*C*) and YM1^{+} macrophages (*D*) were determined. (**E-H**) Body weight (*E-G*) and food intake (*H*) were monitored throughout the experimental period. (**I**) HOMA-IR at week 4 was calculated. (**J-O**) Intraperitoneal glucose (*J-L*) and insulin (*M-O*) tolerance tests were performed as described in the legend of Figures 1 and 3. Results are expressed as means ± SEM. **P*<0.05 *vs* HFD, #*P*<0.05 *vs* WT (n = 3-5 mice per group).

The hypothalamus and brain stem also integrate signals from both the enteric nervous system and circulating hormones derived from adipose tissue and other peripheral tissues. Leptin is by far the best studied peripheral hormone that regulates food intake, increasing satiety by triggering STAT3-mediated pathways in the hypothalamic arcuate nucleus (32).

In order to study the role of leptin signaling in the metabolic effects of pLe^X-ω1, we used leptin receptor-deficient *db/db* mice that are hyperphagic and naturally develop obesity and severe metabolic dysfunctions (34). In this model, pLe^X-ω1 also increased WAT IL-13$^+$ Th2 cells, eosinophils and YM1$^+$ AAMs (Figure 6A-D). Furthermore, pLe^X-ω1 still reduced body weight (Figure 6E-F), fat mass gain (Supplementary Figure 2M-N) and food intake (Figure 6G), indicating that leptin signaling is not involved in the anorexigenic effect of ω1. Lastly, plasma insulin levels (Supplementary Figure 2P), HOMA-IR (Figure 6H) and whole-body glucose tolerance and insulin sensitivity (Figure 6I-L) were still significantly improved.

Collectively, our results show that ω1 improves whole-body metabolic homeostasis independent of its type 2 immunity-inducing capacity, but by inhibiting food intake through a leptin receptor-independent mechanism.

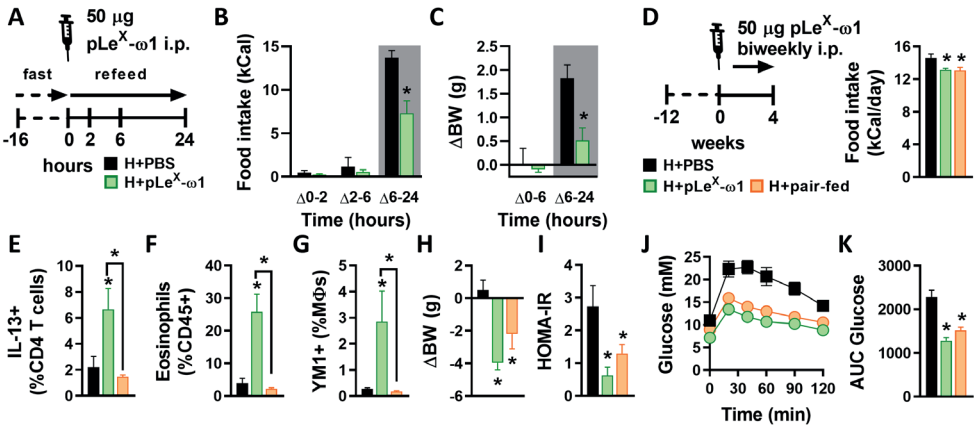

Figure 5. pLeX-ω1 inhibits fasting-induced refeeding and improves metabolic homeostasis through inhibition of food intake in obese mice. (**A**) Mice were fed a HFD for 12 weeks and fasted overnight prior to intraperitoneal injections of either PBS (black bars) or 50 µg pLe^X-ω1 (green bars). (**B-C**) Food intake (*B*) and body weight changes (*C*) were next monitored during 24 hours after refeeding. (**D**) Mice were fed a HFD for 12 weeks, single-housed, and next received biweekly intraperitoneal injections of PBS or 50 µg pLe^X-ω1 for 4 weeks. In one group (H+pair-fed; orange bars), the amount of food available for PBS-treated mice was adjusted daily in order to match the food intake of the pLe^X-ω1-treated group. At the end of the experiment, eWAT was collected, processed and analyzed as described in the legend of Figure 1. (**E-G**) The frequencies of IL-13-expressing CD4 T cells (*E*), eosinophils (*F*) and YM1$^+$ macrophages (*G*) were determined. (**H**) Body weight change was determined after 4 weeks. (**I**) HOMA-IR was calculated at week 4. (**J-K**) An i.p. glucose tolerance test was performed at week 3, as described in the legend of Figure 1. Results are expressed as means ± SEM. **P*<0.05 *vs* HFD or as indicated (n = 3-5 mice per group).

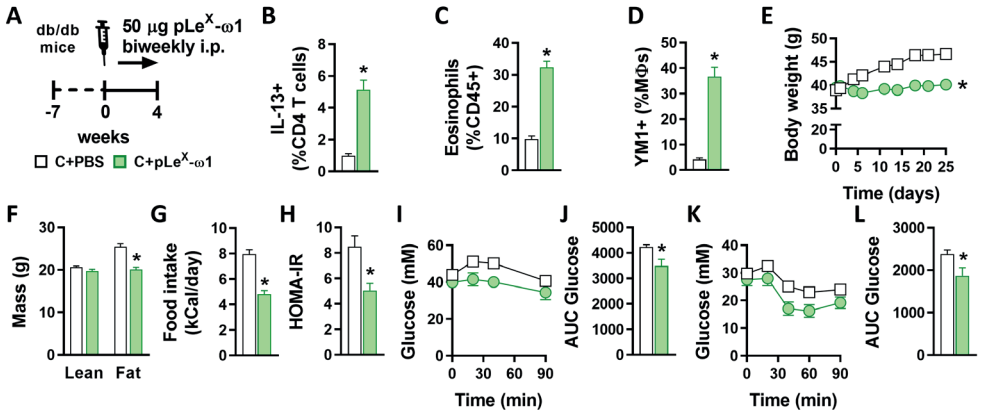

Figure 6. The metabolic effects of pLeX-ω1 are independent of leptin signaling in hyperphagic obese mice. (**A**) 7 weeks-old obese *db/db* mice received biweekly intraperitoneal injections of PBS (white bars) or 50 µg pLe^X-ω1 (green bars) for 4 weeks. At the end of the experiment, eWAT was collected, processed and analyzed as described in the legend of Figure 1. (**B-D**) The frequencies of IL-13-expressing CD4 T cells (*B*), eosinophils (*C*) and YM1$^+$ macrophages (*D*) were determined. (**E-G**) Body weight (*E*) and food intake (*G*) were monitored throughout the experimental period, and body composition (*F*) was measured after 4 weeks. (**H**) HOMA-IR was calculated at week 4. (**I-L**) Intraperitoneal glucose (*I-J*) and insulin (*K-L*) tolerance tests were performed as described in the legend of Figures 1 and 3. Results are expressed as means ± SEM. **P*<0.05 *vs* PBS (n = 5-6 mice per group).

Discussion

Obesity-associated metaflammation promotes insulin resistance, while metabolic homeostasis is maintained by type 2 immunity (1). Since helminths are well known for inducing a potent type 2 immune response, their putative beneficial effects on insulin sensitivity and glucose homeostasis, together with the identification of specific helminth-derived molecules capable of driving such type 2 immune responses, have gained increasing attention (11, 16, 35). The assumption has been that induction of type 2 immunity is the main mechanism by which helminths and helminth-derived molecules can improve metabolic homeostasis. The glycoprotein ω1, a T2 ribonuclease which is secreted from *S. mansoni* eggs, is one of the major immunomodulatory components in SEA and has previously been shown to condition DCs to prime Th2 responses, at least partly through its glycan-mediated uptake and intracellular RNase activity (17, 18). Here, we report that two plant-produced recombinant ω1 glycovariants induced a rapid and sustained reduction in body weight and improved whole-body insulin sensitivity and glucose tolerance in obese mice. This improvement was associated with a strong type 2 immune response in WAT,

characterized by a significant increase in Th2 cells, eosinophils and AAMs. Contrary to SEA, ω1 still improved metabolic homeostasis in *Stat6*-deficient obese mice, indicating that its type 2 immunity-inducing capacity does not play a major role. Indeed, we find that ω1 regulates energy consumption independent of leptin receptor signaling, which drives most of its metabolic effects. Altogether, these findings indicate that helminth-derived molecules may act through multiple distinct pathways for improving obesity-associated metabolic dysfunctions and further characterization of these molecules may lead to new therapeutic strategies for combating obesity.

A recent study from Hams et al. also reported that acute treatment of HFD-fed obese mice with HEK-293-produced recombinant ω1 induced long-lasting weight loss, and improved glucose tolerance by a mechanism involving IL-33 and ILC2-mediated WAT type 2 immunity and adipose tissue beiging (19). In contrast to this report, while we also observed increased IL-33 mRNA expression in eWAT using the same ω1 concentrations (*data not shown*), we found no increase in WAT ILC2s after either one, or four weeks of treatment with both plant-produced ω1 glycovariants. Moreover, we did not find evidence of WAT beiging in both eWAT and iWAT from obese mice. Lastly, we also found that STAT6-mediated type 2 immunity was dispensable for the metabolic effects of ω1. It should be noted that despite similar RNase activity when compared to native ω1 (21), the recombinant ω1 produced by HEK-293 cells and the glyco-engineered molecules from *N. benthamiana* plants harbor significantly different N-glycosylation patterns (18), which may partly explain the different outcomes between studies. Interestingly, as compared to pWT-ω1, we observed a trend for a stronger effect on insulin sensitivity and food intake with pLe^X-ω1, of which the glycans resemble the ones of native helminth ω1 the most.

In our study, both ω1 glycovariants were found to induce a type 2 immune response in WAT, characterized by a significant increase in Th2 cells, eosinophils and AAMs. WAT eosinophilia is dependent on IL-5 and IL-13, which are predominantly expressed by ILC2s, and, to a lower extent, by Th2 cells in lean mice (9). As previously described for SEA (14), we showed that the ω1-induced increase in type 2 cytokines is clearly derived from CD4$^+$ T cells, suggesting that DC-mediated Th2 skewing is required, rather than ILC2 activation, to induce WAT eosinophilia and AAM polarization. Of note, it was previously shown that pLe^X-ω1, compared to pWT-ω1, induced a stronger Th2 polarization *in vivo* using a footpad immunization model in mice (21). In our conditions, both glycovariants induced a similar increase in the percentage of Th2 cells in metabolic tissues from obese mice, whereas pLe^X–ω1 increased total CD4$^+$ T cells to a greater extent in the liver and to a lesser extent in WAT when compared to pWT-ω1. Altogether, this suggests that the different glycans on ω1 glycovariants might lead to tissue-specific targeting of ω1 and resulting differences in total Th2 cells.

While the type 2 immune response seems not to be significantly involved in the beneficial metabolic effects of ω1, we found that treatment with both ω1 glycovariants reduced food intake, with a trend for pLe^X-ω1 being more potent than pWT-ω1. This anorexigenic effect, which was not observed previously when mice were chronically infected with *S. mansoni* or treated with SEA [Figure 1F and (14)], was dose-dependent and also observed in *Stat6*-deficient mice. Importantly, since both locomotor activity and lean body mass were not affected by ω1, this inhibition of food intake is unlikely to be caused by illnesses associated with catatonia. Using fast-refeeding and paired feeding experiments, we clearly showed that ω1 rapidly inhibited food intake, an effect that mainly contributed to the improvements in metabolic homeostasis. This inhibition of food intake persisted throughout the four weeks of treatment, indicating a long-lasting effect, and was already achieved by injecting 10 µg pLe^X-ω1 (*data not shown*). Of note, in the study from Hams *et al.* using HEK-produced recombinant ω1 in the same concentration range as us, the effect of ω1 on feeding behavior and its putative contribution to the observed decrease in body weight and improvement of glucose tolerance in obese mice have not been specifically investigated (19).

Anorexia is one of the clinical manifestations of infection with different helminth species in both animals and humans. As such, deworming children infected with the hookworms *Ascaris lumbricoides* and/or *Trichuris trichuria* has been reported to increase appetite (36), suggesting a relationship between helminth infection and food intake. In rodents, infection with *Taenia taeniaformis* and *N. brasiliensis* both induced anorexia by modulating neuropeptide expression in the hypothalamus (37, 38), indicating that helminths and/or helminth products may regulate feeding behavior. The mechanism by which ω1 inhibits food intake is however still unknown and will require further neuroscience-driven approaches to be elucidated. Regulation of food intake by the central nervous system is a complex process involving both local and peripheral neuro-immuno-endocrine inputs that are mainly integrated in the hypothalamic arcuate nucleus and the brain stem *nucleus tractus solitarius* (32, 33). In our study, we did not detect accumulation of radioactively-labelled ω1 in the brain 24 hours after intraperitoneal injection, suggesting that the glycoprotein may exerts its anorexigenic effects via peripheral rather than central action(s). Upon meal ingestion, several anorexigenic peptides and hormones are produced by metabolic organs, including adipose tissues and the intestine, and can either directly act on specific neurons after crossing the blood-brain barrier or signal from the periphery via vagal nerve-mediated pathways that contribute to satiety regulation (39, 40). Leptin is a key adipose tissue-derived anorexigenic hormone which signals through the leptin receptor expressed in specific neurons located in the arcuate nucleus of the hypothalamus to reduce food intake (32). During obesity,

hypothalamic inflammation has been reported to impair whole-body energy homeostasis, at least partly by inducing central leptin resistance and subsequent increased food intake (41-43). However, despite some evidence of improved systemic leptin sensitivity by ω1 (data not shown), we showed that the hypothalamic expression of key inflammatory genes was not affected by ω1 in obese mice, suggesting that modulation of hypothalamic inflammation is likely not involved in its anorexigenic effect. Furthermore, we found that its anorexigenic and metabolic effects were still present in leptin receptor-deficient mice, allowing us to exclude a significant contribution of peripheral/central leptin signaling. Among the peripheral signals that regulate feeding behavior, it would be interesting to explore the involvement of a gut-brain axis, potentially secondary to changes in gut microbiota, through vagal nerve ablation (40). Recently, *N. brasiliensis* infection and its products were also shown to increase production of the neuropeptide Neuromedin U by mucosal neurons, allowing the host to mount an effective type 2 immune response (44-46). Neuromedin U also has anorexigenic effects (47), thus it is tempting to speculate that some helminth molecules may indirectly trigger anorexia through neuro-immune interactions in the gut.

It is worth mentioning that ω1 also increased IL-13 producing Th2 cells in the liver, but, unlike SEA (14), promoted CD11c expression in Kupffer cells while not affecting the expression of YM1, suggesting that macrophages are rather polarized towards a proinflammatory state in this tissue. An increase in hepatic expression of fibrotic gene markers and circulating ALAT levels was also observed, both indicating increased liver damage induced by ω1. Interestingly, the ω1-induced increase in IL-13$^+$ Th2 cells and IL-13 gene expression in the liver were markedly reduced in *Stat6*-deficient mice, which was accompanied by a decreased expression of fibrotic gene markers. Collectively, these findings confirmed previous studies describing that IL-13 plays a role in the development of liver fibrosis (30, 31), and that ω1 has cytotoxic effects in the liver (28, 29).

In conclusion, we report here that the helminth glycoprotein ω1 improved metabolic homeostasis in insulin-resistant obese mice independent of its type 2 immunity-inducing capacity. Rather, the ω1-induced metabolic improvements in obese mice were mostly attributable to leptin receptor-independent inhibition of food intake. Further studies are required to unravel such underlying mechanisms, notably exploring the role of gut hormones on peripheral and/or central regulation of feeding behavior. Of note, with regards to its putative therapeutic potential for metabolic disorders, it is important to underline that despite beneficial effects on whole-body metabolic homeostasis, ω1 also induced early markers of mild hepatic fibrosis, partly through a type 2 immunity-mediated mechanism. Finally, by contrast to ω1, the complex mixture of SEA does not have detrimental effects on the liver and improves metabolic homeostasis through a STAT6-mediated type 2 immune

response, suggesting that it may contain some other unidentified molecules, such as Dectin 2 ligands (48), with potentially beneficial immunometabolic properties.

Methods

Animals, diet and treatment

All mouse experiments were performed in accordance with the Guide for the Care and Use of Laboratory Animals of the Institute for Laboratory Animal Research and have received approval from the university Ethical Review Board (Leiden University Medical Center, Leiden, The Netherlands; DEC12199) or the Institutional Animal Care and Use Committee (IACUC, New York University School of Medicine, New York, USA; protocol ID IA16-00864). All mice were housed in a temperature-controlled room with a 12-hour light-dark cycle with *ad libitum* access to food and tap water. Group randomization was systematically performed before the start of each experiment, based on body weight, fat mass, and fasting plasma glucose levels. At the end of the experiment, mice were sacrificed through an overdose of ketamine/xylazine.

8-10 weeks old male wild-type (WT) and 7 weeks old male *db/db* mice, both on C57BL6/J background, were purchased from Envigo (Horst, The Netherlands) and housed at Leiden University Medical Center. WT mice were fed a low-fat diet (LFD, 10% energy derived from fat, D12450B, Research Diets, Wijk bij Duurstede, The Netherlands) or a high-fat diet (HFD, 45% energy derived from fat, D12451) for 12 weeks, and *db/db* mice were fed a chow diet (RM3 (P), Special Diet Services, Witham, UK) throughout the experimental period.

8-10 weeks-old male wild-type (WT), *Stat6*$^{-/-}$ mice and *Rosa26*$^{\text{LoxP-STOP-LoxP-tdTomato/+}}$ (*Rosa26*$^{\text{tdTomato}}$), were purchased from The Jackson Laboratory (Bar Harbor, ME, USA), and *Cx3cr1*$^{\text{CreERT2-IRES-YFP/+}}$ (*Cx3cr1*$^{\text{CreER}}$) mice, all on C57BL/6J background, were generously provided by Dr. Dan Littman (Skirball Institute, New York University Medical Center). Mice were housed at New York University School of Medicine, and either put on a HFD (60% energy derived from fat; D12492; Research Diets, New Brunswick, NJ, USA) or LFD (10% energy derived from fat; D12450J; Research Diets) for 10 weeks. To exclude effects of genotype-dependent microbiota differences on metabolic and immunological outcomes, the beddings of WT and *Stat6*$^{-/-}$ mice were frequently mixed within similar diet groups throughout the run-in period. At 14 days and 7 days before sacrifice, *Cx3cr1*$^{\text{CreER}}$ *Rosa26*$^{\text{tdTomato}}$ reporter mice received an oral gavage with tamoxifen to label monocytes.

SEA was prepared as described previously (49). Recombinant ω1 was produced in *N. benthamiana* plants through transient expression of ω1 alone (pWT-ω1) or ω1 in combination with exogenous glycosyltransferases to yield Le^X glycan motifs (pLe^X-ω1), as

described previously (21). SEA, pWT/pLe^X-ω1 (10-50 μg) or vehicle control (sterile-filtered PBS) were injected i.p. every 3 days for 1 or 4 weeks, as indicated in the legends of the figures. For fast-refeeding experiments, WT HFD-fed mice received an i.p. injection of 50 μg pLe^X-ω1 or vehicle control after an overnight fast (5pm-9am), followed by refeeding and frequent measurements of food intake and body weight for 24 hours. For assessing the contribution of reduced food intake on the immunometabolic effects of pLe^X-ω1, WT HFD-fed mice were single-housed and, in a pair-fed group of PBS-injected mice, daily food availability was adjusted to the calorie intake of the pLe^X-ω1-treated group.

Body composition and indirect calorimetry

Body composition was measured by MRI using an EchoMRI (Echo Medical Systems, Houston, TX, USA). Groups of 4-8 mice with free access to food and water were subjected to individual indirect calorimetric measurements during the initiation of the treatment with recombinant ω1 for a period of 7 consecutive days using a Comprehensive Laboratory Animal Monitoring System (Columbus Instruments, Columbus, OH, USA). Before the start of the measurements, single-housed animals were acclimated to the cages for a period of 48 hours. Feeding behavior was assessed by real-time food intake. Oxygen consumption and carbon dioxide production were measured at 15-minute intervals. Energy expenditure (EE) was calculated and normalized for lean body mass (LBM), as previously described (14). Spontaneous locomotor activity was determined by the measurement of beam breaks.

At sacrifice, visceral white adipose tissue (epididymal; eWAT), subcutaneous white adipose tissue (inguinal; iWAT), supraclavicular brown adipose tissue (BAT) and liver were weighed and collected for further processing and analyses.

Isolation of stromal vascular fraction from adipose tissue

eWAT was collected at sacrifice after a 1-minute perfusion with PBS through the heart left ventricle and digested as described previously (14). In short, collected tissues were minced and incubated for 1 hour at 37°C in an agitated incubator (60 rpm) in HEPES buffer (pH 7.4) containing 0.5 g/L collagenase type I from *Clostridium histolyticum* (Sigma-Aldrich, Zwijndrecht, The Netherlands) and 2% (w/v) dialyzed bovine serum albumin (BSA, fraction V; Sigma-Aldrich). The disaggregated adipose tissue was passed through a 100 μm cell strainer that was washed with PBS supplemented with 2.5 mM EDTA and 5% FCS. After centrifugation (350 x g, 10 minutes at room temperature), the supernatant was discarded and the pellet was treated with erythrocyte lysis buffer (0.15 M NH_4Cl; 1 mM $KHCO_3$; 0.1 mM Na_2EDTA). Cells were next washed with PBS/EDTA/FCS, and counted manually.

Isolation of leukocytes from liver tissue

Livers were collected and digested as described previously (14). In short, livers were minced and incubated for 45 minutes at 37°C in RPMI 1640 + Glutamax (Life Technologies, Bleiswijk, The Netherlands) containing 1 mg/mL collagenase type IV from *C. histolyticum*, 2000 U/mL DNase (both Sigma-Aldrich) and 1 mM $CaCl_2$. The digested liver tissues were passed through a 100 µm cell strainer that was washed with PBS/EDTA/FCS. Following centrifugation (530 x g, 10 minutes at 4°C), the supernatant was discarded, after which the pellet was resuspended in PBS/EDTA/FCS and centrifuged at 50 x g to pellet hepatocytes (3 minutes at 4°C). Next, supernatants were collected and pelleted (530 x g, 10 minutes at 4°C). The cell pellet was first treated with erythrocyte lysis buffer and next washed with PBS/EDTA/FCS. $CD45^+$ leukocytes were isolated using LS columns and CD45 MicroBeads (35 µL beads per liver, Miltenyi Biotec) according to manufacturer's protocol and counted manually.

Processing of isolated immune cells for flow cytometry

For analysis of macrophage and lymphocyte subsets, both WAT stromal vascular cells and liver leukocytes were stained with the live/dead marker Aqua (Invitrogen, Bleiswijk, The Netherlands) or Zombie-UV (Biolegend, San Diego, CA, USA), fixed with either 1.9% formaldehyde (Sigma-Aldrich) or the eBioscience™ FOXP3/Transcription Factor Staining Buffer Set (Invitrogen), and stored in FACS buffer (PBS, 0.02% sodium azide, 0.5% FCS) at 4°C in the dark until subsequent analysis. For analysis of cytokine production, isolated cells were cultured for 4 hours in culture medium in the presence of 100 ng/mL phorbol myristate acetate (PMA), 1 µg/mL ionomycin and 10 µg/mL Brefeldin A (all from Sigma-Aldrich). After 4 hours, cells were washed with PBS, stained with Aqua, and fixed as described above.

Flow cytometry

For analysis of CD4 T cells and innate lymphoid cell (ILC) subsets, SVF cells were stained with antibodies against B220 (RA3-6B2), CD11b (M1/70), CD3 (17A2), CD4 (GK1.5), NK1.1 (PK136) and Thy1.2 (53-2.1; eBioscience), CD11c (HL3) and GR-1 (RB6-8C5; both BD Biosciences, San Jose, CA, USA), and CD45.2 (104; eBioscience, Biolegend or Tonbo Biosciences, San Diego, CA, USA). CD4 T cells were identified as $CD45^+$ $Thy1.2^+$ $Lineage^+$ $CD4^+$, and ILCs as $CD45^+$ $Thy1.2^+$ $Lineage^-$ $CD4^-$ cells, in which the lineage cocktail included antibodies against CD11b, CD11c, B220, GR-1, NK1.1 and CD3.

CD4 T cell subsets and cytokine production by ILCs were analyzed following permeabilization with either 0.5% saponin (Sigma-Aldrich) or eBioscience™ FOXP3/ Transcription Factor Staining Buffer Set. Subsets were identified using antibodies against CD11b, CD11c, GR-1, B220, NK1.1, CD3, CD45.2, CD4, Thy1.2, IL-4 (11B11), IL-13 (eBio13A), Foxp3 (FJK-16s; all eBioscience), IL-5 (TRFK5) and IFN-γ (XMG1.2; both Biolegend).

For analysis of macrophages, eosinophils, monocytes and neutrophils, cells were permeabilized as described above. Cells were then incubated with an antibody against YM1 conjugated to biotin (polyclonal; R&D Systems, Minneapolis, MN, USA), washed, and stained with streptavidin-PerCP (BD Biosciences) or streptavidin-PerCP-Cy5.5 (Biolegend), and antibodies directed against CD45 (30-F11, Biolegend), CD45.2, CD11b, CD11c [HL3 (BD Biosciences) or N418 (Biolegend)], F4/80 (BM8; Invitrogen or Biolegend), Siglec-F (E50-2440; BD Biosciences), and Ly6C (HK1.4; Biolegend).

Mitochondrial mass, membrane potential and total ROS were quantified by staining with MitoTracker Green (20 nM), Tetramethylrhodamine, Methyl Ester, Perchlorate (TMRM; 20 nM) and CM-H2DCFDA (5 μM; all Invitrogen), respectively, for 30 minutes at 37°C before staining with other antibodies. For sorting adipose tissue macrophages, cells were stained with the live/dead marker Blue, followed by staining for surface markers. Macrophages were fluorescence-assisted cell sorted from adipose tissue on an Aria II cell sorter (BD Biosciences), by gating on singlet, live, $CD45.2^+$ $Ly6C^-$ $CD3^-$ $CD19^-$ $NK1.1^-$ $Siglec\text{-}F^-$ $CD11b^+$ $F4/80^+$ $tdTomato^+$.

All cells were stained and measured within 4 days post fixation. Flow cytometry was performed using a FACSCanto or LSR-II (both BD Biosciences), and gates were set according to Fluorescence Minus One (FMO) controls. Representative gating schemes are shown in Supplementary Figure 1 and all antibodies used are listed in Supplementary Table 1.

Plasma analysis

Blood samples were collected from the tail tip of 4h-fasted mice (food removed at 9 am) using chilled paraoxon-coated capillaries. Fasting blood glucose level was determined using a Glucometer (Accu-Check; Roche Diagnostics, Almere, The Netherlands) and plasma insulin level was measured using a commercial kit according to the instructions of the manufacturer (Chrystal Chem, Zaandam, The Netherlands). The homeostatic model assessment of insulin resistance (HOMA-IR) adapted to mice (50) was calculated as ([glucose (mg/dl)*0.055] × [insulin (ng/ml) × 172.1])/3857, and used as a surrogate measure of whole-body insulin resistance. Plasma concentrations of alanine aminotransferase (ALAT) were measured using

a Reflotron® kit (Roche diagnostics) using a pool of plasma samples from each group (n = 4-6 mice per group) in 2 separate experiments.

Glucose, insulin and pyruvate tolerance tests

Whole-body glucose tolerance test (ipGTT) was performed at week 3 of treatment in 6h-fasted mice, as previously reported (14). In short, after an initial blood collection by tail bleeding (t = 0), a glucose load (2 g/kg total body weight of D-Glucose [Sigma-Aldrich]) was administered i.p., and blood glucose was measured at 20, 40, 60, and 90 min after glucose administration using a Glucometer. For *db/db* mice, blood samples were collected at 0, 20, 40 and 90 min after glucose administration, and plasma glucose levels were measured using the hexokinase method (HUMAN, Wiesbaden, Germany).

Whole-body insulin tolerance test (ipITT) was performed at week 1 or week 3 of treatment in 4h-fasted mice, as described previously (14). In short, after an initial blood collection by tail bleeding (t = 0), a bolus of insulin (1 U/kg (lean) body mass [NOVORAPID, Novo Nordisk, Alphen aan den Rijn, Netherlands]) was administered i.p., and blood glucose was measured at 20, 40, 60, and 90 min after insulin administration using a Glucometer.

Whole-body pyruvate tolerance test (ipPTT) was performed at week 4 of treatment in overnight-fasted mice. In short, after an initial blood collection by tail bleeding (t = 0), a pyruvate load (2 g/kg total body weight of sodium pyruvate [Sigma-Aldrich]) was administered i.p. Blood glucose was measured at 20, 60, 90 and 120 min after pyruvate administration using a Glucometer.

Western blot analysis

A piece of liver, skeletal muscle, eWAT and iWAT from mice that were sacrificed 15 min after an acute i.p. injection of insulin (1 U/kg lean body mass, NOVORAPID, Novo Nordisk, Alphen aan den Rijn, Netherlands) was collected and immediately freeze-clamped. Snap-frozen samples (~50 mg) were lysed in ice-cold buffer containing: 50 mM HEPES (pH 7.6), 50 mM NaF, 50 mM KCl, 5 mM NaPPi, 1 mM EDTA, 1 mM EGTA, 1 mM DTT, 5 mM β-glycerophosphate, 1 mM sodium vanadate, 1% NP40 and protease inhibitors cocktail (Complete, Roche, Mijdrecht, The Netherlands). Western blots were performed as previously described (51). The primary antibodies used were pSer473-PKB (#9271, Cell Signaling Technology), PKB (#4691, Cell Signaling Technology), IRb (sc-711, Santa Cruz Biotechnology) and HSP90 (sc-7947, Santa Cruz Biotechnology). Bands were visualized by enhanced chemiluminescence and quantified using Image J (NIH, US).

RNA isolation and qRT-PCR

RNA was extracted from snap-frozen adipose tissue and liver samples using Tripure RNA Isolation reagent (Roche Diagnostics). Total RNA (1 μg) was reverse transcribed and quantitative real-time PCR was performed with SYBR Green Core Kit on a MyIQ thermal cycler (Bio-Rad) using specific primers sets (available on request). mRNA expression was normalized to ribosomal protein, large, P0 (*RplP0*) mRNA content and expressed as fold change compared to LFD-fed or HFD-fed mice as indicated, using the ΔΔCT method.

Transcriptomic analysis by RNA-sequencing

RNA isolation from FACS-purified adipose tissue macrophages was done as described previously with the QIAGEN RNeasy micro kit (QIAGEN, Venlo, the Netherlands) (25). Libraries were generated for each sample using the CelSeq2 protocol (52) and were sequenced on Illumina HiSeq. Reads were mapped by Bowtie2.3.1 (53) to the *mus musculus* reference genome, and uniquely mapped indices were determined by HTSeq-counts (54). Gene read counts were normalized to *B2m* and *Rplp0*. Transcriptome data was visualized with an MA-plot. Upregulated (log_2 fold change > 2 *vs* HFD) and downregulated (log_2 fold change < -2 *vs* HFD) genes were visualized in a heat map using the online software tool Morpheus (https://software.broadinstitute.org/morpheus).

Hepatic triglyceride content

Liver lipids were extracted as previously described (55). Briefly, ~50 mg liver samples were homogenized in 10:1 (vol/wt) ice-cold methanol using a FastPrep-24 5GTM High Speed Homogenizer (MP Biomedicals, Santa Ana, CA, USA). Subsequently, lipids were extracted from the homogenate using methanol-chloroform (1:3 v/v) extraction. Protein concentration of the homogenate was determined by Pierce™ BCA protein assay (Thermo Fisher Scientific). Triglyceride (TG) of the lipid extract were determined using a commercially available kit (Roche Diagnostics).

Histological analysis

A piece of liver was fixed in 4% formaldehyde (Sigma-Aldrich), paraffin-embedded, sectioned at 4 μm and stained with Hematoxylin and Eosin (H&E), or Sirius Red to visualize collagen. Six fields at 20x magnification (total area 1.68 mm^2) were used for the analysis of hepatic steatosis in H&E-stained sections. On Sirius Red-stained sections, fibrosis was scored on 10 fields at 40x magnification (total area 1.23 mm^2) as absent (score 0), present in the

perisinusoidal or periportal area (score 1), present in the perisinusoidal and periportal (score 2), bridging fibrosis (score 3) or cirrhosis (score 4) as described elsewhere (56).

Biodistribution of pLe^X-ω1

Synthesis of N3-Cy5-pLeX-ω1

DTPA-DBCO click chelate and Cy5-N_3 dye were synthesized as described previously (57), with one deviation for Cy5-N_3 synthesis being the use of 1-(5-carboxypentyl)-2,3,3-trimethyl-3H-indol-1-ium-5-sulfonate instead of 1-(5-carboxypentyl)-2,3,3-trimethyl-3H-indol-1-ium. Cy5-N_3 molecular mass was calculated to be 823.8 and found to be 824.0 using MALDI-TOF (Bruker, Leiderdorp, Netherlands). To allow for N_3-Cy5-pLe^X-ω1 formation, 200 µL of phosphate buffer (100 mM, pH 8.5) was added to 200 µg (6.5 nmol) pLe^X-ω1 (1.9 mg/mL in PBS), followed by 9.5 µL (58.1 nmol) of Cy5-N_3 (5 mg/mL stock solution in DMSO). After mixing for 60 minutes at room temperature, 90 µL of PBS was added and the unreacted Cy5 was removed using a PD MiniTrap G-25 column (Merck KGaA, Darmstadt, Germany). The labelling ratio was estimated to be 0.9 dye/protein using UV/Vis spectroscopy (Nanodrop) and the eluate (1 mL) was stored at 7°C prior to use.

Radiolabeling of pLeX-ω1

DTPA-DBCO (2.6 nmol) was dissolved in 17.3 µL of ammonium acetate buffer (250 mM, pH 5.5), and 9.6 MBq or 48.0 MBq of $^{111}InCl_3$ (370 MBq/mL, Mallinckrodt Medical, Petten, The Netherlands) was added for biodistribution or SPECT imaging, respectively. The mixture was shaken for 60 minutes at room temperature followed by addition of PBS (200 mM, pH 7.5). Of this mixture, 4.1 MBq or 20.7 MBq was added to 1.3 nmol or 0.7 nmol of N_3-Cy5-pLe^X-ω1 and stirred overnight at room temperature to form ^{111}In-DTPA -Cy5-pLe^X-ω1. The reaction mixture was directly used for injection.

SPECT imaging

10-week HFD-fed mice were injected intraperitoneally with 10 µg ^{111}In-DTPA-Cy5-pLe^X-ω1 (10 MBq/mouse). 24 hours post injection, *in vivo* biodistribution was assessed after the animals were placed and fixed on a dedicated positioned bed of a three-headed U-SPECT-2 (MILabs, Utrecht, The Netherlands) under continuous 1-2% isoflurane anesthesia. Radioactivity counts from total body scans and a second one of a head and neck area were acquired for 20 min and images were reconstructed as described before (58). After imaging, mice were euthanized by an intraperitoneal injection of 0.25 mL Euthasol (ASTfarma, Oudewater, The Netherlands).

Biodistribution

For biodistribution experiments, organs were harvested, weighed and radioactivity was counted (Wizard2 2470 automatic gamma scintillation counter, PerkinElmer, Groningen, the Netherlands). Total injected dose was determined by counting full and empty syringes in a gamma counter (2470 automatic gamma counter, Perkin-Elmer), and data are represented as % injected dose per gram tissue (%ID/g), which was calculated as follows: ((([MBq] tissue/[MBq]injected)*100)/g tissue).

Statistical analysis

All data are presented as mean ± standard error of the mean (SEM). Statistical analysis was performed using GraphPad Prism version 8 for Windows (GraphPad Software, La Jolla, CA, USA) with unpaired t-test, or either one-way or two-way analysis of variance (ANOVA) followed by Fisher's post-hoc test. Differences between groups were considered statistically significant at $P < 0.05$.

Acknowledgements

The authors thank Gerard van der Zon and Tessa Buckle (Leiden University Medical Center, Leiden, the Netherlands), and Uma Mahesh Gundra, Ada Weinstock, Jian-Da Lin and Mei San Tang (New York University School of Medicine, New York, USA) for their invaluable technical assistance. The authors also thank Ko Willems van Dijk and Patrick Rensen (Leiden University Medical Center) for allowing the use of the LUMC metabolic phenotyping platform (MRI and metabolic cages). This study was supported by Dutch Organization for Scientific Research (NWO; ZonMW TOP Grant 91214131 to CH, AS, MY and BG) and the NWO Graduate School Program (022.006.010 to HvdZ). This work was also supported in part by the Division of Intramural Research, National Institutes of Health (NIH)/National Institute of Allergy and Infectious Diseases (NIAID) and Awards AI130945 and AI133977, NIH/National Heart, Lung, and Blood Institute Award HL084312, and U.S. Department of Defense Award W81XWH-16-1-0256 (to PL). The funders had no role in study design, data collection and analysis, decision to publish, or preparation of the manuscript.

Conflict of interest

The authors have stated there are no conflicts of interest in connection with this article.

References

1. Donath MY, Shoelson SE. Type 2 diabetes as an inflammatory disease. Nat Rev Immunol. 2011;11(2):98-107.
2. Lackey DE, Olefsky JM. Regulation of metabolism by the innate immune system. Nat Rev Endocrinol. 2016;12(1):15-28.
3. Kolb H, Mandrup-Poulsen T. The global diabetes epidemic as a consequence of lifestyle-induced low-grade inflammation. Diabetologia. 2010;53(1):10-20.
4. Lumeng CN, DelProposto JB, Westcott DJ, Saltiel AR. Phenotypic switching of adipose tissue macrophages with obesity is generated by spatiotemporal differences in macrophage subtypes. Diabetes. 2008;57(12):3239-46.
5. Obstfeld AE, Sugaru E, Thearle M, Francisco AM, Gayet C, Ginsberg HN, et al. C-C chemokine receptor 2 (CCR2) regulates the hepatic recruitment of myeloid cells that promote obesity-induced hepatic steatosis. Diabetes. 2010;59(4):916-25.
6. Kratz M, Coats BR, Hisert KB, Hagman D, Mutskov V, Peris E, et al. Metabolic dysfunction drives a mechanistically distinct proinflammatory phenotype in adipose tissue macrophages. Cell Metab. 2014;20(4):614-25.
7. Lanthier N, Molendi-Coste O, Horsmans Y, van Rooijen N, Cani PD, Leclercq IA. Kupffer cell activation is a causal factor for hepatic insulin resistance. Am J Physiol Gastrointest Liver Physiol. 2010;298(1):G107-16.
8. Talukdar S, Oh DY, Bandyopadhyay G, Li D, Xu J, McNelis J, et al. Neutrophils mediate insulin resistance in mice fed a high-fat diet through secreted elastase. Nat Med. 2012;18(9):1407-12.
9. Molofsky AB, Nussbaum JC, Liang HE, Van Dyken SJ, Cheng LE, Mohapatra A, et al. Innate lymphoid type 2 cells sustain visceral adipose tissue eosinophils and alternatively activated macrophages. J Exp Med. 2013;210(3):535-49.
10. Wu D, Molofsky AB, Liang HE, Ricardo-Gonzalez RR, Jouihan HA, Bando JK, et al. Eosinophils sustain adipose alternatively activated macrophages associated with glucose homeostasis. Science. 2011;332(6026):243-7.
11. van der Zande HJP, Zawistowska-Deniziak A, Guigas B. Immune Regulation of Metabolic Homeostasis by Helminths and Their Molecules. Trends Parasitol. 2019;35(10):795-808.
12. Maizels RM, Yazdanbakhsh M. Immune regulation by helminth parasites: cellular and molecular mechanisms. Nat Rev Immunol. 2003;3(9):733-44.
13. Zinsou JF, Janse JJ, Honpkehedji YY, Dejon-Agobe JC, Garcia-Tardon N, Hoekstra PT, et al. Schistosoma haematobium infection is associated with lower serum cholesterol levels and improved lipid profile in overweight/obese individuals. PLoS Negl Trop Dis. 2020;14(7):e0008464.
14. Hussaarts L, Garcia-Tardon N, van Beek L, Heemskerk MM, Haeberlein S, van der Zon GC, et al. Chronic helminth infection and helminth-derived egg antigens promote adipose tissue M2 macrophages and improve insulin sensitivity in obese mice. FASEB J. 2015;29(7):3027-39.
15. Okano M, Satoskar AR, Nishizaki K, Abe M, Harn DA, Jr. Induction of Th2 responses and IgE is largely due to carbohydrates functioning as adjuvants on Schistosoma mansoni egg antigens. J Immunol. 1999;163(12):6712-7.

16. Hussaarts L, Yazdanbakhsh M, Guigas B. Priming dendritic cells for th2 polarization: lessons learned from helminths and implications for metabolic disorders. Front Immunol. 2014;5:499.

17. Everts B, Perona-Wright G, Smits HH, Hokke CH, van der Ham AJ, Fitzsimmons CM, et al. Omega-1, a glycoprotein secreted by Schistosoma mansoni eggs, drives Th2 responses. J Exp Med. 2009;206(8):1673-80.

18. Everts B, Hussaarts L, Driessen NN, Meevissen MH, Schramm G, van der Ham AJ, et al. Schistosome-derived omega-1 drives Th2 polarization by suppressing protein synthesis following internalization by the mannose receptor. J Exp Med. 2012;209(10):1753-67, S1.

19. Hams E, Bermingham R, Wurlod FA, Hogan AE, O'Shea D, Preston RJ, et al. The helminth T2 RNase omega1 promotes metabolic homeostasis in an IL-33- and group 2 innate lymphoid cell-dependent mechanism. FASEB J. 2016;30(2):824-35.

20. Meevissen MH, Wuhrer M, Doenhoff MJ, Schramm G, Haas H, Deelder AM, et al. Structural characterization of glycans on omega-1, a major Schistosoma mansoni egg glycoprotein that drives Th2 responses. J Proteome Res. 2010;9(5):2630-42.

21. Wilbers RH, Westerhof LB, van Noort K, Obieglo K, Driessen NN, Everts B, et al. Production and glyco-engineering of immunomodulatory helminth glycoproteins in plants. Sci Rep. 2017;7:45910.

22. Takeda K, Tanaka T, Shi W, Matsumoto M, Minami M, Kashiwamura S, et al. Essential role of Stat6 in IL-4 signalling. Nature. 1996;380(6575):627-30.

23. Takeda K, Kamanaka M, Tanaka T, Kishimoto T, Akira S. Impaired IL-13-mediated functions of macrophages in STAT6-deficient mice. J Immunol. 1996;157(8):3220-2.

24. Bhargava P, Li C, Stanya KJ, Jacobi D, Dai L, Liu S, et al. Immunomodulatory glycan LNFPIII alleviates hepatosteatosis and insulin resistance through direct and indirect control of metabolic pathways. Nat Med. 2012;18(11):1665-72.

25. Gundra UM, Girgis NM, Gonzalez MA, San Tang M, Van Der Zande HJP, Lin JD, et al. Vitamin A mediates conversion of monocyte-derived macrophages into tissue-resident macrophages during alternative activation. Nat Immunol. 2017;18(6):642-53.

26. Van den Bossche J, O'Neill LA, Menon D. Macrophage Immunometabolism: Where Are We (Going)? Trends Immunol. 2017;38(6):395-406.

27. Ricardo-Gonzalez RR, Red Eagle A, Odegaard JI, Jouihan H, Morel CR, Heredia JE, et al. IL-4/STAT6 immune axis regulates peripheral nutrient metabolism and insulin sensitivity. Proc Natl Acad Sci U S A. 2010;107(52):22617-22.

28. Dunne DW, Lucas S, Bickle Q, Pearson S, Madgwick L, Bain J, et al. Identification and partial purification of an antigen (omega 1) from Schistosoma mansoni eggs which is putatively hepatotoxic in T-cell deprived mice. Trans R Soc Trop Med Hyg. 1981;75(1):54-71.

29. Abdulla MH, Lim KC, McKerrow JH, Caffrey CR. Proteomic identification of IPSE/alpha-1 as a major hepatotoxin secreted by Schistosoma mansoni eggs. PLoS Negl Trop Dis. 2011;5(10):e1368.

30. Gieseck RL, 3rd, Ramalingam TR, Hart KM, Vannella KM, Cantu DA, Lu WY, et al. Interleukin-13 Activates Distinct Cellular Pathways Leading to Ductular Reaction, Steatosis, and Fibrosis. Immunity. 2016;45(1):145-58.

31. Hart KM, Fabre T, Sciurba JC, Gieseck RL, 3rd, Borthwick LA, Vannella KM, et al. Type 2 immunity is protective in metabolic disease but exacerbates NAFLD collaboratively with TGF-beta. Sci Transl Med. 2017;9(396).

32. Schwartz MW, Woods SC, Porte D, Jr., Seeley RJ, Baskin DG. Central nervous system control of food intake. Nature. 2000;404(6778):661-71.

33. Schneeberger M, Gomis R, Claret M. Hypothalamic and brainstem neuronal circuits controlling homeostatic energy balance. J Endocrinol. 2014;220(2):T25-46.

34. Hummel KP, Dickie MM, Coleman DL. Diabetes, a new mutation in the mouse. Science. 1966;153(3740):1127-8.

35. de Ruiter K, Tahapary DL, Sartono E, Soewondo P, Supali T, Smit JWA, et al. Helminths, hygiene hypothesis and type 2 diabetes. Parasite Immunol. 2017;39(5).

36. Hadju V, Stephenson LS, Abadi K, Mohammed HO, Bowman DD, Parker RS. Improvements in appetite and growth in helminth-infected schoolboys three and seven weeks after a single dose of pyrantel pamoate. Parasitology. 1996;113 (Pt 5):497-504.

37. Lohmus M, Moalem S, Bjorklund M. Leptin, a tool of parasites? Biol Lett. 2012;8(5):849-52.

38. Horbury SR, Mercer JG, Chappell LH. Anorexia induced by the parasitic nematode, Nippostrongylus brasiliensis: effects on NPY and CRF gene expression in the rat hypothalamus. J Neuroendocrinol. 1995;7(11):867-73.

39. Murphy KG, Bloom SR. Gut hormones and the regulation of energy homeostasis. Nature. 2006;444(7121):854-9.

40. Li Z, Yi CX, Katiraei S, Kooijman S, Zhou E, Chung CK, et al. Butyrate reduces appetite and activates brown adipose tissue via the gut-brain neural circuit. Gut. 2018;67(7):1269-79.

41. Cai D, Liu T. Hypothalamic inflammation: a double-edged sword to nutritional diseases. Ann N Y Acad Sci. 2011;1243:E1-39.

42. Valdearcos M, Douglass JD, Robblee MM, Dorfman MD, Stifler DR, Bennett ML, et al. Microglial Inflammatory Signaling Orchestrates the Hypothalamic Immune Response to Dietary Excess and Mediates Obesity Susceptibility. Cell Metab. 2017;26(1):185-97 e3.

43. Lee CH, Kim HJ, Lee YS, Kang GM, Lim HS, Lee SH, et al. Hypothalamic Macrophage Inducible Nitric Oxide Synthase Mediates Obesity-Associated Hypothalamic Inflammation. Cell Rep. 2018;25(4):934-46 e5.

44. Cardoso V, Chesne J, Ribeiro H, Garcia-Cassani B, Carvalho T, Bouchery T, et al. Neuronal regulation of type 2 innate lymphoid cells via neuromedin U. Nature. 2017;549(7671):277-81.

45. Klose CSN, Mahlakoiv T, Moeller JB, Rankin LC, Flamar AL, Kabata H, et al. The neuropeptide neuromedin U stimulates innate lymphoid cells and type 2 inflammation. Nature. 2017;549(7671):282-6.

46. Wallrapp A, Riesenfeld SJ, Burkett PR, Abdulnour RE, Nyman J, Dionne D, et al. The neuropeptide NMU amplifies ILC2-driven allergic lung inflammation. Nature. 2017;549(7672):351-6.

47. Hanada R, Teranishi H, Pearson JT, Kurokawa M, Hosoda H, Fukushima N, et al. Neuromedin U has a novel anorexigenic effect independent of the leptin signaling pathway. Nat Med. 2004;10(10):1067-73.

48. Kaisar MMM, Ritter M, Del Fresno C, Jonasdottir HS, van der Ham AJ, Pelgrom LR, et al. Dectin-1/2-induced autocrine PGE2 signaling licenses dendritic cells to prime Th2 responses. PLoS Biol. 2018;16(4):e2005504.

49. Grogan JL, Kremsner PG, Deelder AM, Yazdanbakhsh M. Elevated proliferation and interleukin-4 release from CD4+ cells after chemotherapy in human Schistosoma haematobium infection. Eur J Immunol. 1996;26(6):1365-70.

50. Lee S, Muniyappa R, Yan X, Chen H, Yue LQ, Hong EG, et al. Comparison between surrogate indexes of insulin sensitivity and resistance and hyperinsulinemic euglycemic clamp estimates in mice. Am J Physiol Endocrinol Metab. 2008;294(2):E261-70.

51. Stephenne X, Foretz M, Taleux N, van der Zon GC, Sokal E, Hue L, et al. Metformin activates AMP-activated protein kinase in primary human hepatocytes by decreasing cellular energy status. Diabetologia. 2011;54(12):3101-10.

52. Hashimshony T, Senderovich N, Avital G, Klochendler A, de Leeuw Y, Anavy L, et al. CEL-Seq2: sensitive highly-multiplexed single-cell RNA-Seq. Genome Biol. 2016;17:77.

53. Langmead B, Salzberg SL. Fast gapped-read alignment with Bowtie 2. Nat Methods. 2012;9(4):357-9.

54. Anders S, Pyl PT, Huber W. HTSeq--a Python framework to work with high-throughput sequencing data. Bioinformatics. 2015;31(2):166-9.

55. Thomas A, Belaidi E, Aron-Wisnewsky J, van der Zon GC, Levy P, Clement K, et al. Hypoxia-inducible factor prolyl hydroxylase 1 (PHD1) deficiency promotes hepatic steatosis and liver-specific insulin resistance in mice. Sci Rep. 2016;6:24618.

56. Kleiner DE, Brunt EM, Van Natta M, Behling C, Contos MJ, Cummings OW, et al. Design and validation of a histological scoring system for nonalcoholic fatty liver disease. Hepatology. 2005;41(6):1313-21.

57. Hensbergen AW, van Willigen DM, Welling MM, van der Wijk FA, de Korne CM, van Oosterom MN, et al. Click Chemistry in the Design and Production of Hybrid Tracers. ACS Omega. 2019;4(7):12438-48.

58. Spa SJ, Welling MM, van Oosterom MN, Rietbergen DDD, Burgmans MC, Verboom W, et al. A Supramolecular Approach for Liver Radioembolization. Theranostics. 2018;8(9):2377-86.

Supplementary information

Supplementary Table 1. Antibodies and reagents for flow cytometry.

Target	Clone	Conjugate	Source	Identifier
B220	RA3-6B2	FITC	eBioscience	11-0452
CD3	17A2	Alexa Fluor 700	Biolegend	100216
CD3	17A2	APC-eF780	eBioscience	47-0032
CD3	17A2	eF450	eBioscience	48-0032
CD3	17A2	FITC	eBioscience	11-0032
CD4	GK1.5	PE-Cy7	eBioscience	25-0041
CD4	GK1.5	PerCP-eF710	eBioscience	46-0041
CD11b	M1/70	APC-Cy7	Biolegend	101226
CD11b	M1/70	FITC	eBioscience	11-0112
CD11b	M1/70	PE-Cy7	eBioscience	25-0112
CD11c	N418	BV421	Biolegend	117330
CD11c	HL3	HV450	BD Biosciences	560521
CD19	6D5	Alexa Fluor 700	Biolegend	115528
CD45	30-F11	BV785	Biolegend	103149
CD45.2	104	FITC	Biolegend	109806
CD45.2	104	eF450	eBioscience	48-0454
CD45.2	104	PerCP-Cy5.5	Tonbo Biosciences	65-0454
F4/80	BM8	APC	eBioscience	17-4801
F4/80	BM8	PE-Cy7	Biolegend	123114
F4/80	BM8	BV711	Biolegend	123147
Foxp3	FJK-16s	PE	eBioscience	12-5773
GR-1	RB6-8C5	FITC	BD Biosciences	553126
IFN-γ	XMG1.2	APC	eBioscience	17-7311
IL-4	11B11	APC	eBioscience	17-7041
IL-5	TRFK5	PE	Biolegend	504303
IL-13	eBio13A	eF450	eBioscience	48-7133
Ly6C	HK1.4	Alexa Fluor 700	Biolegend	128024
Ly6C	HK1.4	APC-Cy7	Biolegend	128026
NK1.1	PK136	Alexa Fluor 700	Biolegend	108730
NK1.1	PK136	FITC	eBioscience	11-5941
Siglec-F	E50-2440	BV421	BD Biosciences	562681
Siglec-F	E50-2440	BV605	BD Biosciences	740388
Siglec-F	E50-2440	PE	BD Biosciences	552126
Thy1.2	53-2.1	APC-eF780	eBioscience	47-0902
YM1	Polyclonal	Biotin	R&D Systems	BAF2446
Other reagents			**Source**	**Identifier**
CM-H2DCFDA			Invitrogen	C6827
LIVE/DEAD™ Fixable Aqua Dead Cell Stain Kit			Invitrogen	L34957
LIVE/DEAD™ Fixable Blue Dead Cell Stain Kit			Invitrogen	L23105
MitoTracker™ Green FM			Invitrogen	M7514
Streptavidin-PerCP			BD Biosciences	554064
Streptavidin-PerCP-Cy5.5			Biolegend	405214
TMRM			Invitrogen	T668
Zombie UV™ Fixable Viability Kit			Biolegend	423107

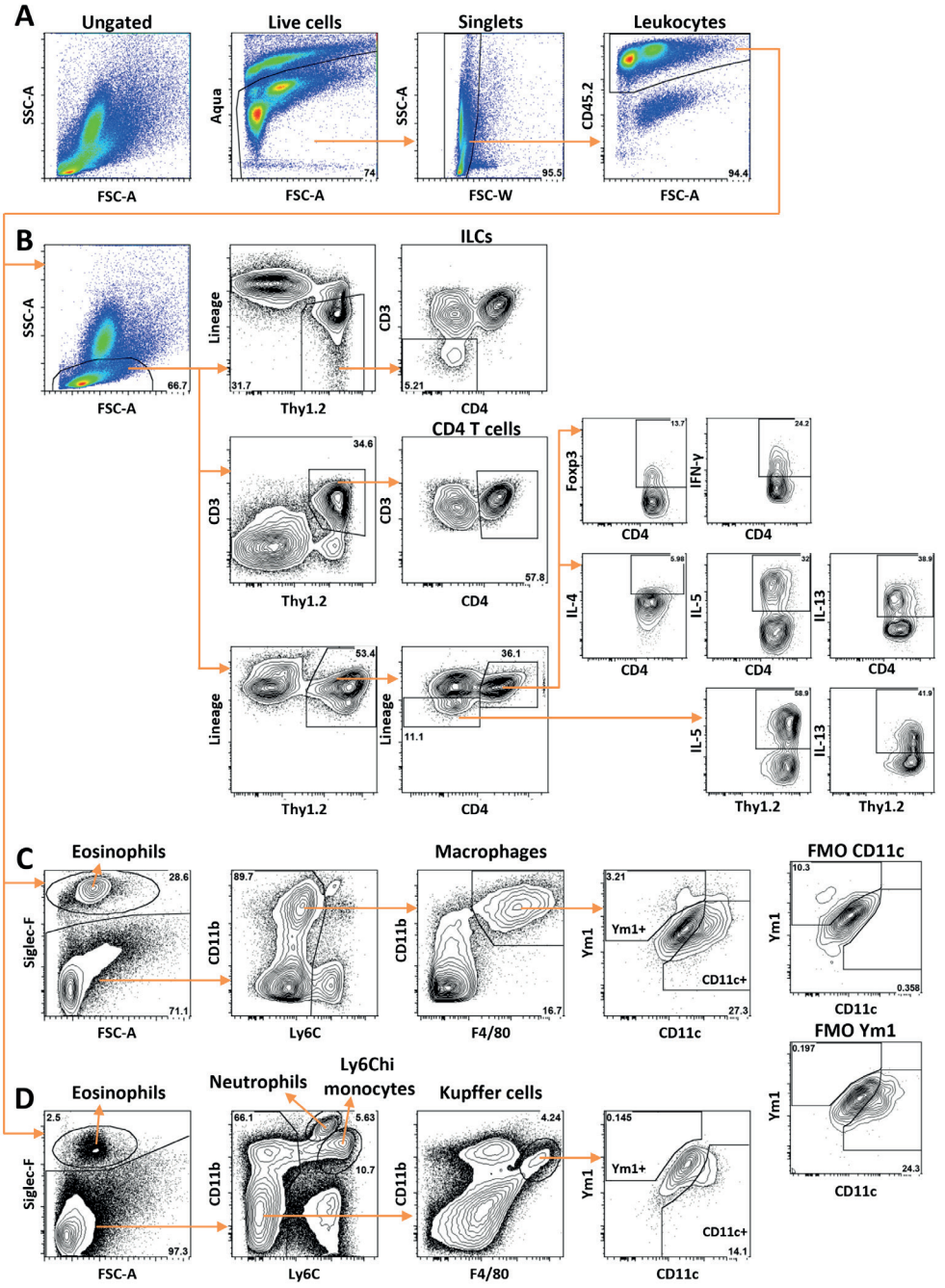

Supplementary Figure 1. Gating strategies. (**A**) Isolated cells were pre-gated on Aqua^{-}CD45^{+} single cells. (**B**) The gating strategy for eWAT and liver analyses of ILCs, CD4 T cells and intracellular cytokine production is shown. The lineage channel includes antibodies against CD11b, CD11c, B220,

◀Supplementary Figure 1. Legend (Continued)

GR-1, NK1.1 and CD3. (**C**) The gating strategies for eWAT eosinophils, $CD11c^{+}YM1^{-}$ macrophages and $CD11c^{-}YM1^{+}$ macrophages are shown, including Fluorescence Minus One (FMO) controls for CD11c and Ym1. (**D**) The gating strategy for liver eosinophils, monocytes, $CD11c^{+}YM1^{-}$ Kupffer cells and $CD11c^{-}YM1^{+}$ Kupffer cells is shown.

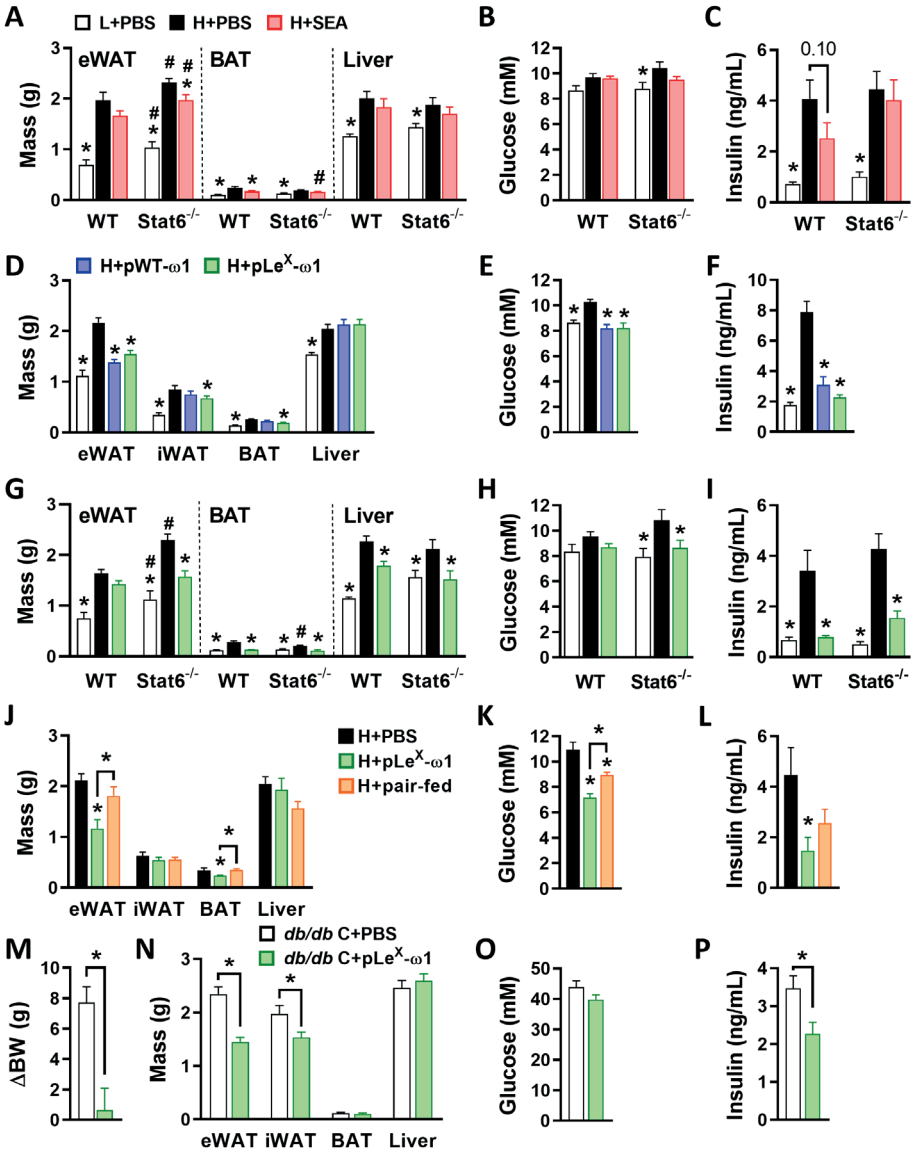

Supplementary Figure 2. Body composition and fasting blood glucose and plasma insulin levels after SEA and pLeX-ω1 treatment in obese mice. (**A-P**) Supplementary data for Figure 1 (*A-C*), 3 (*D-F*), 4 (*G-I*), 5 (*J-L*) and 6 (*M-P*). Mice were fed a LFD or a HFD and treated as described in the corresponding figure legends. The weights of epididymal WAT (eWAT), inguinal WAT (iWAT), intrascapular brown adipose tissue (BAT) and the liver were measured after 4 weeks (*A, D, G, J* and *N*). Blood glucose (*B, E, H, K* and *O*) and plasma insulin (*C, F, I, L* and *P*) were measured at week 4 in 4h-fasted mice. Body weight change after 4 weeks was determined in *db/db* mice treated with PBS or 50 µg pLe^{X}-ω1 (*M*). Results are expressed as means ± SEM. **P*<0.05 *vs* HFD or as indicated, #*P*<0.05 *vs* WT (n = 3-6 mice per group in A-C, G-P and 11-18 mice per group in D-F).

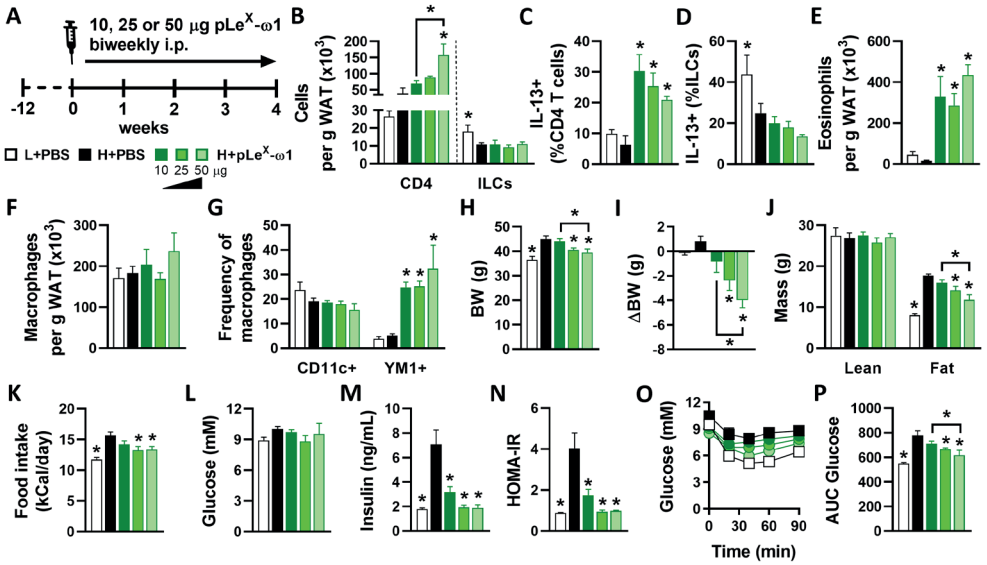

Supplementary Figure 3. pLeX-ω1 increases adipose tissue type 2 immune cells and improves whole-body insulin sensitivity in a dose-dependent manner. (**A**) Mice were fed a LFD (white bars) or a HFD for 12 weeks, and next received biweekly intraperitoneal injections of PBS (black bars) or 10 µg, 25 µg or 50 µg pLe^{X}-ω1 (green bars) for 4 weeks. At the end of the experiment, eWAT was collected, processed and analyzed as described in the legend of Figure 1. (**B-G**) The numbers of CD4 T cells and ILCs per gram tissue (*B*), and the frequencies of IL-13^{+} CD4 T cells (*C*) and ILCs (*D*) were determined. Numbers of eosinophils (*E*) and macrophages (*F*) per gram tissue, and percentages of CD11c^{+}YM1^{-} and CD11c^{-}YM1^{+} macrophages (*G*) were determined. (**H-J**) Body weight (*H-I*) and body composition (*J*) were determined after 4 weeks. (**K**) Food intake was monitored throughout the treatment period. (**L-N**) Fasting blood glucose (*L*) and plasma insulin levels (*M*) were determined at week 4, and HOMA-IR (*N*) was calculated. (**O-P**) An i.p. insulin tolerance test (*O-P*) was performed at week 3. Results are expressed as means ± SEM. * *P*<0.05 *vs* HFD or as indicated (n = 3-4 mice per group).

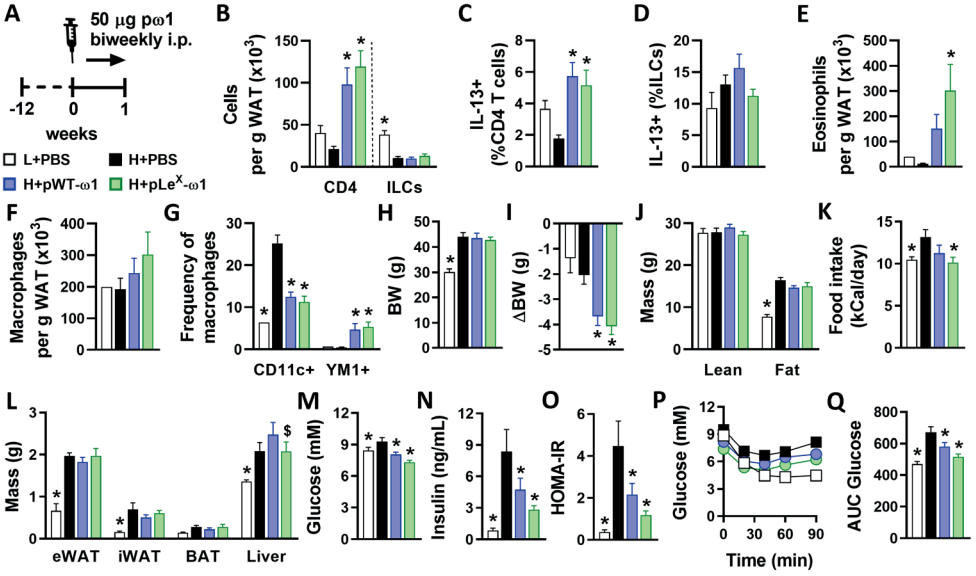

Supplementary Figure 4. ω1 glycovariants increase adipose tissue type 2 immune cells and improve whole-body insulin sensitivity after 1 week of treatment. (**A**) Mice were fed a LFD (white bars) or a HFD for 12 weeks, and next received biweekly intraperitoneal injections of PBS (black bars) or 50 µg pWT-ω1 (blue bars) or pLe^{X}-ω1 (green bars) for 1 week. At the end of the experiment, eWAT was collected, processed and analyzed as described in the legend of Figure 1. (**B-G**) The numbers of CD4 T cells and ILCs per gram tissue (*B*), and the frequencies of IL-13^{+} CD4 T cells (*C*) and ILCs (*D*) were determined. Numbers of eosinophils (*E*) and macrophages (*F*) per gram tissue, and frequencies of CD11c^{+}YM1^{-} and CD11c^{-}YM1^{+} macrophages (*G*) were determined. (**H-L**) Body weight (*H*), body weight change (*I*), body composition (*J, L*) and food intake (*K*) were measured after 1 week of treatment. (**M-O**) Fasting blood glucose (*M*) and plasma insulin levels (*N*) were determined in 4h-fasted mice at the end of week 1, and HOMA-IR (*O*) was calculated. (**P-Q**) An i.p. insulin tolerance test was performed. Results are expressed as means ± SEM. **P*<0.05 *vs* HFD, $*P*<0.05 *vs* pWT-ω1 (n = 1-9 mice per group).

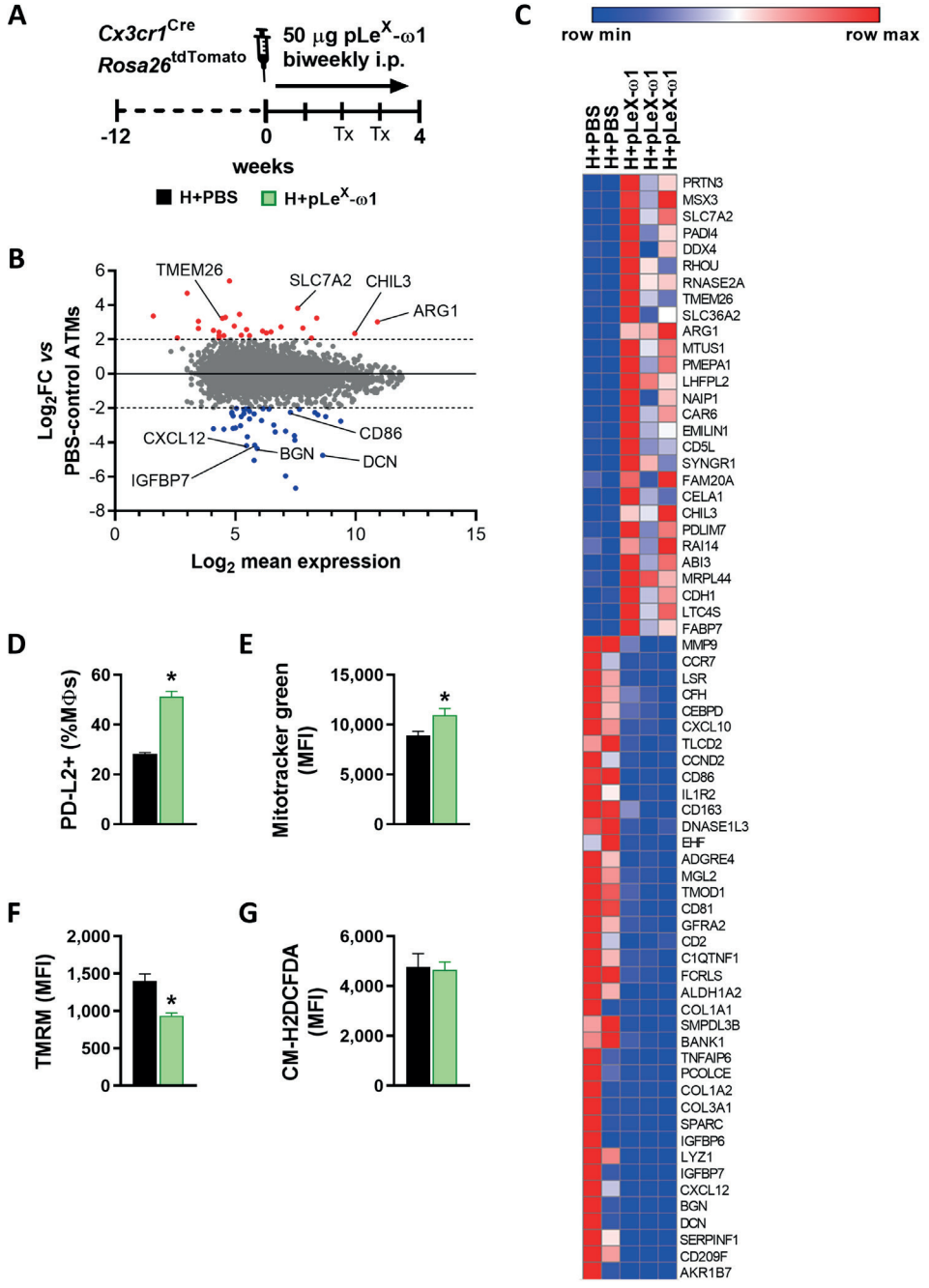

Supplementary Figure 5. Adipose tissue macrophages from mice treated with pLeX-ω1 display some alternatively-activated phenotypic features. (**A**) *Cx3cr1*^{CreER} *R26*^{tdTomato} mice were fed a HFD

▲Supplementary Figure 5. Legend (Continued)

for 12 weeks, and next received biweekly intraperitoneal injections of PBS or 50 μg pLe^{X}-ω1 for 4 weeks. At week 2 and 3, mice received an oral gavage with tamoxifen (Tx) to label CX3CR1^{+} cells. At the end of the experiment, adipose tissue macrophages (ATMs) from eWAT SVF were FACS-sorted and RNA was isolated and sequenced. (**B**) MA plot shows the mean gene expression in pLe^{X}-ω1 ATMs, as expressed in $\log_2$ fold change *versus* PBS-control ATMs. Upregulated genes ($\log_2$ fold change > 2) are indicated in red and downregulated genes ($\log_2$ fold change < -2) are indicated in blue. (**C**) Normalized read counts of upregulated and downregulated genes are visualized in a heatmap. (**D-G**) WT mice were fed a HFD for 12 weeks, and next received biweekly intraperitoneal injections of PBS (black bars) or 50 μg pLe^{X}-ω1 (green bars) for 4 weeks. Percentage of PD-L2^{+} macrophages (*D*) was determined. MitoTracker Green (mitochondrial mass; *E*), TMRM (mitochondrial membrane potential; *F*) and CM-H2CFDA (total ROS; *G*) fluorescence intensities were determined in PD-L2^{+} macrophages. Results are expressed as means ± SEM. *P<0.05 *vs* HFD (n = 2-3 mice per group in B-C, and 3-4 mice per group in D-G).

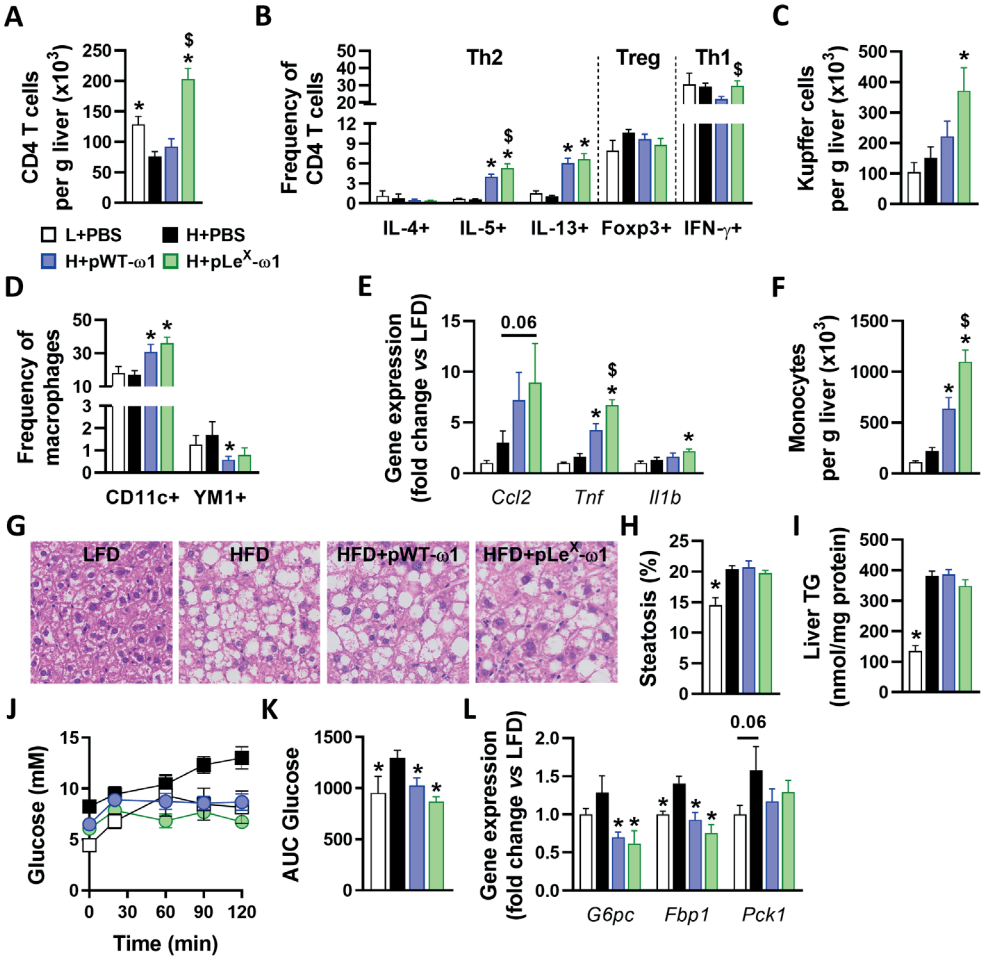

Supplementary Figure 6. ω1 glycovariants do not affect hepatic steatosis, but reduce gluconeogenesis in obese mice. Mice were fed a LFD (white bars) or a HFD for 12 weeks, and next received biweekly intraperitoneal injections of PBS (black bars) or 50 µg pWT-ω1 (blue bars) or pLe^{X}-ω1 (green bars) for 4 weeks, as described in the legend of Figure 2. At sacrifice, CD45^{+} liver cells were isolated and analyzed by flow cytometry. (**A-F**) The numbers of CD4 T cells (*A*), Kupffer cells (KC, *C*) and Ly6C^{hi} monocytes (*F*) per gram tissue, and the frequencies of T helper (*B*) and KC subsets (*D*) were determined. The mRNA expression of proinflammatory genes (*E*) was determined. (**G-I**) Hepatic steatosis was assessed using hematoxylin/eosin staining in fixed tissues (*G-H*) and hepatic triglycerides content was determined (*I*). (**J-K**) An intraperitoneal pyruvate tolerance test was performed during week 4. Blood glucose levels were measured at the indicated time points (*J*) and the AUC of the glucose excursion curve was calculated (*K*). (**L**) The mRNA expression of the main gluconeogenic genes was determined. Data shown are a pool of at least two independent experiments, except for J-K. Results are expressed as means ± SEM. *P<0.05 *vs* HFD, \$$P$<0.05 *vs* pWT-ω1 (n = 5-18 mice per group in A-I, L, and 3-6 mice per group in J-K).

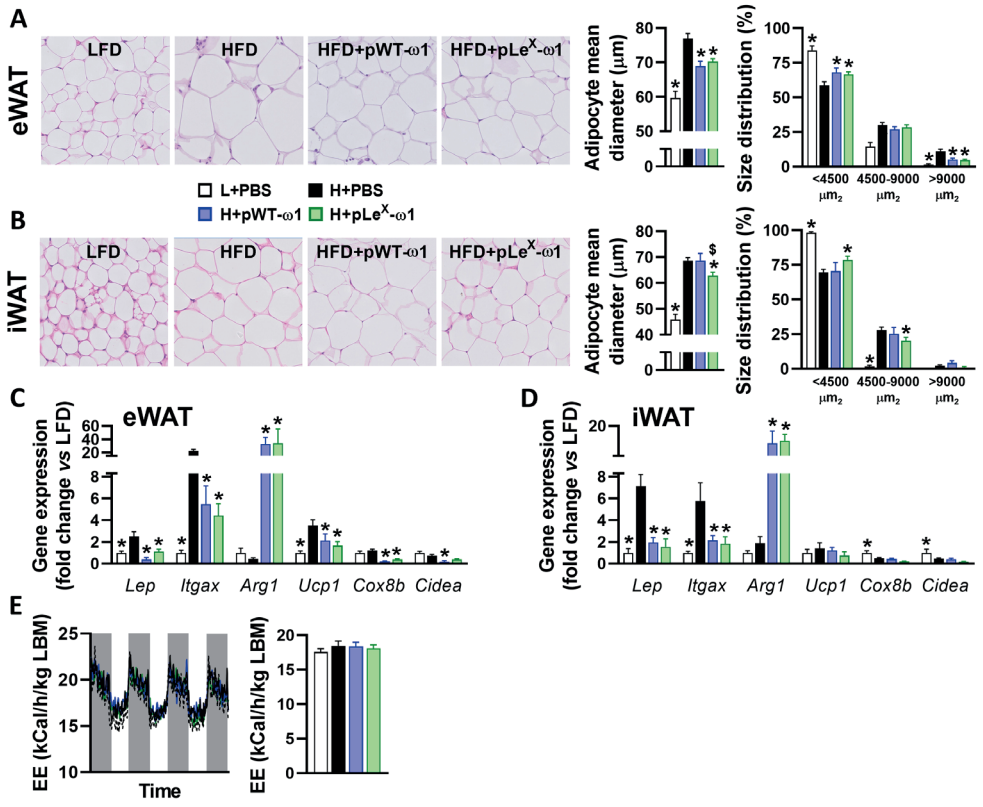

Supplementary Figure 7. ω1 glycovariants reduce adipocyte size, but neither increase adipose tissue beiging nor whole-body energy expenditure in obese mice. (**A-D**) Mice were fed a LFD (white bars) or a HFD for 12 weeks, and next received biweekly intraperitoneal injections of PBS (black bars) or 50 µg pWT-ω1 (blue bars) or pLe^X-ω1 (green bars) as described in the legend of Figure 2. At sacrifice, the eWAT (*A,C*) or iWAT (*B,D*) were collected. Adipocyte diameter and size distribution were determined after H&E staining (*A,B*). mRNA expressions of the indicated genes were determined by RT-PCR and expressed relative to the *RplP0* gene as fold change versus LFD-fed mice (*C,D*). (**E**) Energy expenditure, corrected for lean body mass, was measured for three consecutive days using fully automated single-housed metabolic cages during the first week of treatment. Data shown are a pool of two independent experiments. Results are expressed as means ± SEM. *P<0.05 *vs* HFD (n = 4-10 mice per group).

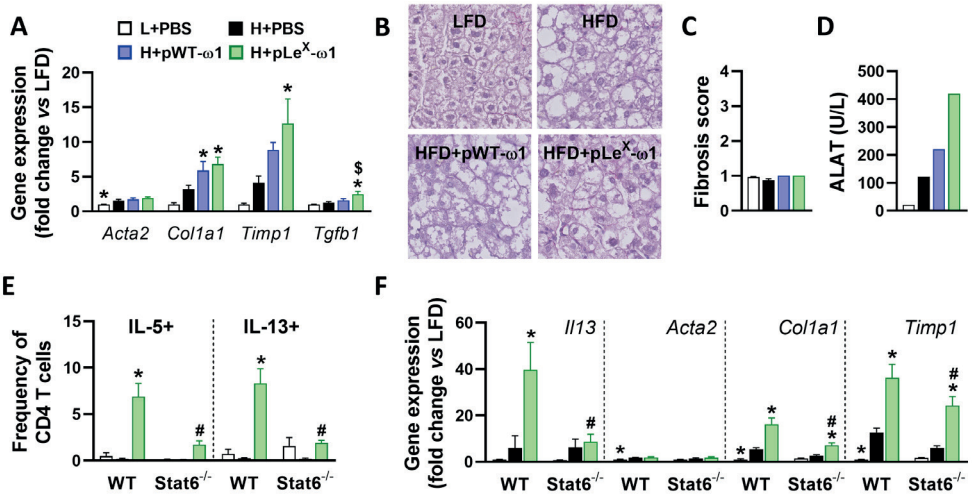

Supplementary Figure 8. ω1 glycovariants increase fibrosis gene markers and liver damage in obese mice. Mice were fed a LFD (white bars) or a HFD for 12 weeks, and next received biweekly intraperitoneal injections of PBS (black bars) or 50 µg pWT-ω1 (blue bars) or pLe^{X}-ω1 (green bars) for 4 weeks, as described in the legend of Figure 2. (**A**) The mRNA expression of fibrosis gene markers was determined. (**B-C**) Sirius Red-stained sections of fixed tissues (*B*) were scored for fibrosis (*C*). (**D**) Plasma alanine aminotransferase levels were determined at week 4. (**E-F**) WT and *Stat6*$^{-/-}$ mice were fed a LFD or a HFD and next received biweekly intraperitoneal injections of PBS or 50 µg pWT/pLeX-ω1 for 4 weeks, as described in the legend of Figure 4. Hepatic frequencies of IL-5 and IL-13-expressing CD4 T cells (*E*), and mRNA expression of *Il13* and fibrosis gene markers (*F*) were determined. Data shown are a pool of at least two independent experiments, except for E-F. Results are expressed as means ± SEM. **P*<0.05 *vs* HFD, $*P*<0.05 *vs* pWT-ω1, #*P*<0.05 *vs* WT (n = 5-18 mice per group in A-D, and 3-5 mice per group in E-F).

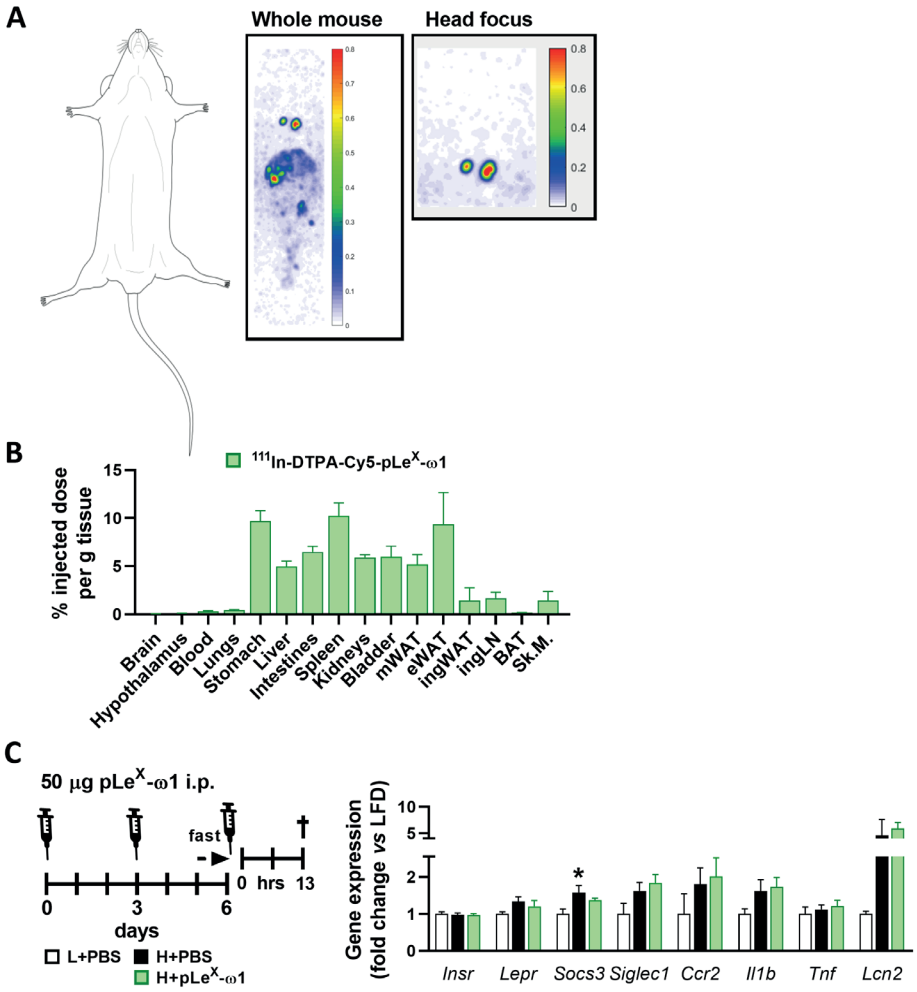

Supplementary Figure 9. Fluorescent and radioactive hybrid-labelled pLeX-ω1 distributes to abdominal organs, but not to the brain; pLeX-ω1 does not affect HFD-induced hypothalamic inflammation. (**A-B**) Mice were fed a HFD for 12 weeks, and next received a single intraperitoneal injection of 10 µg of either 1 (*A*) or 10 (*B*) MBq ^{111}In-DTPA-Cy5-pLe^{X}-ω1. After 24h, the biodistribution was visualized by SPECT scan of the whole mouse (*A*), with a head focus (*insert*), and organs were collected and weighed after sacrifice. The organ-specific ^{111}In radioactivity was counted and data expressed as mean % injected dose per g tissue ± SEM (*B*; n = 6 mice per group). (**C**) Mice were fed a LFD (white bars) or HFD (black/green bars) for 12 weeks and fasted prior to intraperitoneal injections of either PBS (white/black bars) or 50 µg pLeX-ω1 (green bars; *C*). The hypothalami were collected and freeze-clamped 13h post-injection, at the peak of the inhibitory effect observed on food intake during the dark phase (see Figure 5). mRNA expression of the indicated genes (*C*) was determined by RT-PCR and expressed relative to the *RplP0* gene as fold change versus LFD-fed mice. Results are expressed as means ± SEM. *P<0.05 vs HFD (n = 4-6 mice per group).

CHAPTER 8

Effects of a novel polyphenol-rich plant extract on body composition, inflammation, insulin sensitivity and glucose homeostasis in obese mice

Hendrik J.P. van der Zande, Joost M. Lambooij, Vivien Chavanelle, Anna Zawistowska-Deniziak, Yolanda Otero, Frank Otto, Louise Lantier, Owen P. McGuinness, Florian Le Joubioux, Martin Giera, Thierry Maugard, Sébastien L. Peltier, Pascal Sirvent and Bruno Guigas

International Journal of Obesity. 45:2016–2027 (2021)
PMID: 34079069
doi: 10.1038/s41366-021-00870-x

Abstract

Background/Objectives: The worldwide prevalence of obesity, metabolic syndrome and type 2 diabetes (T2D) is reaching epidemic proportions that urge the development of new management strategies. Totum-63 is a novel, plant-based polyphenol-rich active principle that has been shown to reduce body weight, fasting glycemia, glucose intolerance and fatty liver index in obese subjects with prediabetes. Here, we investigated the effects and underlying mechanism(s) of Totum-63 on metabolic homeostasis in insulin-resistant obese mice.

Methods: Male C57BL6/J mice were fed a high-fat diet for 12 weeks followed by supplementation with Totum-63 for 4 weeks. The effects on whole-body energy and metabolic homeostasis, as well as on tissue-specific inflammation and insulin sensitivity were assessed using a variety of immunometabolic phenotyping tools.

Results: Totum-63 decreased body weight and fat mass in obese mice, without affecting lean mass, food intake and locomotor activity, and increased fecal energy excretion and whole-body fatty acid oxidation. Totum-63 reduced fasting plasma glucose, insulin and leptin levels, and improved whole-body insulin sensitivity and peripheral glucose uptake. The expression of insulin receptor β and the insulin-induced phosphorylation of Akt/PKB were increased in liver, skeletal muscle, white adipose tissue (WAT) and brown adipose tissue (BAT). Hepatic steatosis was also decreased by Totum-63 and associated with a lower expression of genes involved in fatty acid uptake, *de novo* lipogenesis, inflammation and fibrosis. Furthermore, a significant reduction in proinflammatory macrophages was also observed in epididymal WAT. Finally, a potent decrease in BAT mass associated with enhanced tissue expression of thermogenic genes was found, suggesting BAT activation by Totum-63.

Conclusions: Our results show that Totum-63 reduces inflammation and improves insulin sensitivity and glucose homeostasis in obese mice through pleiotropic effects on various metabolic organs. Altogether, plant-derived Totum-63 might constitute a promising novel nutritional supplement for alleviating metabolic dysfunctions in obese people with or without T2D.

Introduction

The dramatic worldwide rise in obesity, insulin resistance (IR), metabolic associated fatty liver disease (MAFLD), and type 2 diabetes (T2D) poses a serious global threat to public health. The most recent data from the World Health Organization indicate that more than a third of the world's adult population is overweight (1) and 465 million suffer from T2D (2), with an associated yearly health care cost estimated to exceed 760 billion dollars (3). T2D is a complex and multifactorial disease that develops as a result of synergistic dysfunctions of metabolic pathways in interconnected organs, such as the intestine, pancreas, liver, skeletal muscle, adipose tissues and the brain (4, 5). During the last decade it also became clear that the immune system plays a central role in disease progression, with the obesity-associated chronic low-grade inflammation, or metaflammation (6), being one of the major contributors to tissue-specific IR and impaired glucose/lipid homeostasis (7-10). While some treatments with various drug classes are available, the multiplicity of the pathophysiological mechanisms involved in T2D development makes pharmacological interventions targeting a single pathway generally insufficient. In this context, therapeutic strategies simultaneously targeting several dysfunctional mechanisms in different organs may constitute the most efficient option for tackling these complex and multifactorial metabolic disorders.

The concepts of functional foods and nutraceuticals have recently emerged and refer to a wide range of bioactive compounds contained in food and natural products with potentially relevant benefits on human health (11, 12). As such, several plants used in traditional medicines or as dietary supplements contain antioxidants, fibers and phytochemicals, like polyphenols and alkaloids, that have been shown to exert anti-obesogenic and antidiabetic properties through concomitant modulation of diverse cellular pathways and metabolic processes (13-17). Although still mechanistically unclear, these bioactive compounds can exert pleiotropic actions on multiple tissues, leading to beneficial metabolic effects such as appetite reduction, modulation of intestinal nutrient absorption and metabolism, enhanced thermogenesis, improvement of tissue-specific insulin sensitivity and/or changes in both gut microbiota and local/systemic inflammation (13).

Totum-63 is a novel, polyphenol-rich plant-based active principle composed of a mixture of five plant extracts that has been designed to act in combination to target the risk factors associated with developing T2D. Totum-63 has recently been shown to reduce body weight, fasting glycemia, glucose intolerance and fatty liver index in a clinical study conducted in obese subjects with prediabetes (18). In the present study, we aimed to investigate the effects and underlying mechanism(s) of Totum-63 on metabolic homeostasis in high-fat diet (HFD)-induced obese mice, a model of established T2D.

Results

Totum-63 decreases body weight and fat mass, and reduces food efficiency in obese mice

To study the effects of Totum-63 on metabolic homeostasis in insulin resistant obese mice, C57BL/6 male mice were first fed a high-fat diet (HFD) for 12 weeks, followed by supplementation with or without Totum-63 (2.7% w/w) for 4 additional weeks (Figure 1A). Totum-63 induced a rapid decrease in body weight in HFD-fed obese mice, which was already significant after 6 days of supplementation (Figure 1B). At the end of the experimental period, the body weight remained significantly lower in the Totum-63-supplemented mice (Figure 1C), an effect exclusively due to a reduction in body fat mass (Figure 1D) and associated with lower liver (Figure 1E) and BAT (Figure 1F) masses while both WAT and heart weights were not affected (Figure 1G-H). Food intake, assessed by regular weighing of food pellets, was found to be transiently reduced during the first days of Totum-63 supplementation, without affecting the average food intake throughout the entire study (Figure 1I-J). Next, using individual metabolic cages, we confirmed that Totum-63 neither altered food intake after the first day of supplementation (Supplementary Figure 1A) nor spontaneous locomotor activity (Supplementary Figure 1B) and total energy expenditure (Supplementary Figure 1C) in HFD-fed obese mice. However, indirect calorimetry revealed that Totum-63 significantly decreased the respiratory exchange ratio (RER; Supplementary Figure 1D), indicating that whole-body fatty acid oxidation was increased while carbohydrate oxidation was concomitantly decreased (Supplementary Figure 1E-F). Of note, although the fecal energy content was not affected by Totum-63 supplementation in HFD-fed mice (Figure 1L), the feces production rate was increased (Figure 1K) and, as such, the daily amount of excreted energy (Figure 1M). Since the daily ingested energy was not different (Figure 1N), the calculated apparent energy assimilation efficiency (AEAE) was therefore reduced by Totum-63 in obese mice (Figure 1O), suggesting that an alteration of nutrient absorption in the digestive tract may partly contribute to the reduction in body weight. Of note, no significant changes in the expression of the main fatty acid (FA) and carbohydrate (CHO) intestinal transporters were observed, at least in the ileum, while the expression of the biliary cholesterol transporters *Abcg5* and *Abcg8* were significantly upregulated by Totum-63 (Figure 1P). Congruent with this, ileal expression of the bile acid (BA)-regulated gene *Fgf15* (19) was also upregulated by Totum-63, whereas the expression of other gut-derived hormones was unchanged (Supplementary Figure 2A). Moreover, Totum-63 supplementation restored the gene expression of tight junction proteins involved in HFD-induced intestinal permeability (Figure 1Q), but did not affect the expression of inflammatory markers in the ileum (Supplementary Figure 2B).

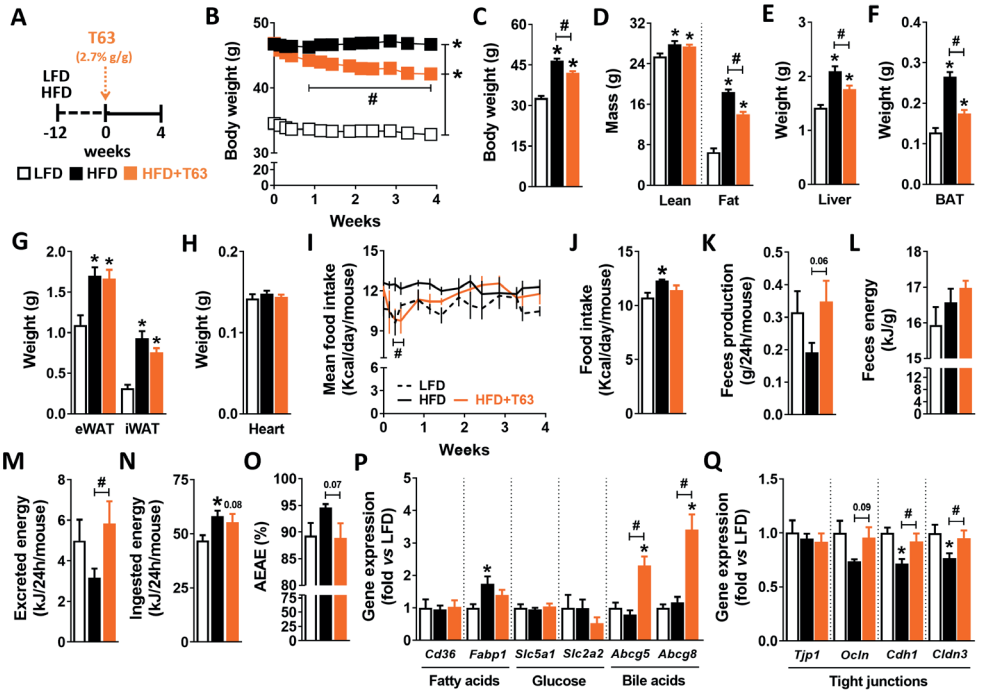

Figure 1. Totum-63 decreases body weight, fat mass and energy assimilation efficiency in HFD-fed mice. (**A**) C57BL6/J mice were fed either a low-fat diet (LFD, open squares/bars) or high-fat diet (HFD) for a period of 12 weeks after which the HFD was supplemented with Totum-63 (T63, 2.7% g/g; orange squares/bars) or not (control; black squares/bars) for an additional 4 weeks. (**B**) Body weight was monitored throughout the supplementation period. (**C-D**) At week 4, body weight and body composition were determined. (**E-H**) After sacrifice, the weights of the liver (*E*), BAT (*F*), eWAT, iWAT (*G*) and heart (*H*) were measured. (**I-J**) Mean food intake per mouse was monitored throughout the supplementation period. (**K**) The feces production was assessed during 24 hours. (**L**) The fecal energy content was determined by bomb calorimetry. (**M-O**) The excreted (*M*) and ingested (*N*) energy, and the apparent energy assimilation efficiency (AEAE, *O*) were calculated. (**P-Q**) The expression of key genes involved in nutrient and bile transport (*P*) and epithelial tight junctions (*Q*), was measured in the ileum section of the intestine by RT-qPCR. Results are expressed as mean ± SEM. * P ≤ 0.05 *vs* LFD, # P ≤ 0.05 *vs* HFD (n=10-12 mice per group from 2 independent experiments; feces: n=3-5 cages per group; qPCR: n=5-6 mice per group).

Totum-63 improves glucose homeostasis and insulin sensitivity in obese mice

We next investigated the effects of Totum-63 on whole-body metabolic homeostasis in HFD-fed obese mice. As expected, HFD feeding increased fasting plasma glucose, insulin and leptin levels (Figure 2A-C), HOMA-IR (HOmeostatis Model Assessment of Insulin Resistance; Figure 2D), as well as blood HbA1c levels (Figure 2E) when compared to LFD-fed mice. Furthermore, HFD impaired whole-body insulin sensitivity (Figure 2F) and glucose

homeostasis (Figure 2G-H), as assessed by intraperitoneal insulin and glucose tolerance tests, respectively. Totum-63 supplementation in HFD-fed mice restored glucose, insulin and HOMA-IR, as well as blood HbA1c to the LFD-fed mice levels (Figure 2A-B, D-E) while circulating leptin concentrations were significantly reduced (Figure 2C). Congruent with HOMA-IR data, Totum-63 improved whole-body insulin sensitivity and glucose homeostasis in obese mice, as respectively assessed by insulin and glucose tolerance tests (Figure 2F-G), without affecting glucose-induced insulin levels (Figure 2H). Importantly, all these beneficial effects were still observed in a subset of body weight-paired control and supplemented obese mice (Supplementary Fig 3), indicating that the improvement of metabolic homeostasis by Totum-63 is not only secondary to reduced body weight. Of note, the effect on glucose, insulin and HOMA-IR was already observed after 2 weeks of Totum-63 supplementation whereas fasting total cholesterol (TC) and triglycerides (TG) were not affected (Supplementary Figure 4). Moreover, the HFD-induced increase in total blood leukocyte counts and circulating levels of monocytes and B cells was still present after Totum-63 supplementation, while other myeloid (neutrophils, eosinophils) and lymphoid (NK, T) cells were not affected whatever the conditions (Supplementary Figure 5).

In order to decipher the respective contribution of the main metabolic organs to the improvement of systemic insulin sensitivity by Totum-63 in obese mice, we performed a hyperinsulinemic-euglycemic clamp. Blood glucose levels were maintained at euglycemia in all mice during the clamp whereas insulinemia was found to be significantly lower at steady state in HFD-fed mice treated with Totum-63 (Figure 3A-B). As expected, the glucose infusion rate (GIR) was markedly reduced in HFD-fed obese mice when compared to lean mice, but the extent of this detrimental effect was significantly lower in Totum-63-treated mice (Figure 3C). Although the endogenous glucose production rate (EndoRa) was unchanged (Figure 3D), the glucose disappearance rate (Rd) was found to be significantly improved by Totum-63 in HFD-fed obese mice (Figure 3E-F). Administration of 2-^{14}C-DG during the clamp was used to determine insulin-stimulated glucose uptake (Rg) in various tissues. As shown in Figure 3G-H, Totum-63 increased insulin-induced skeletal muscle Rg in HFD-fed mice, regardless of muscle type, while a borderline significant trend for an increase was also observed in heart, eWAT and BAT. In line with this, the insulin receptor β expression (IRβ) and insulin-induced phosphorylation of protein kinase B (PKB) were found to be increased by Totum-63 in all tissues (Figure 3I-L), indicating improvement in both hepatic and peripheral insulin sensitivity in HFD-fed mice.

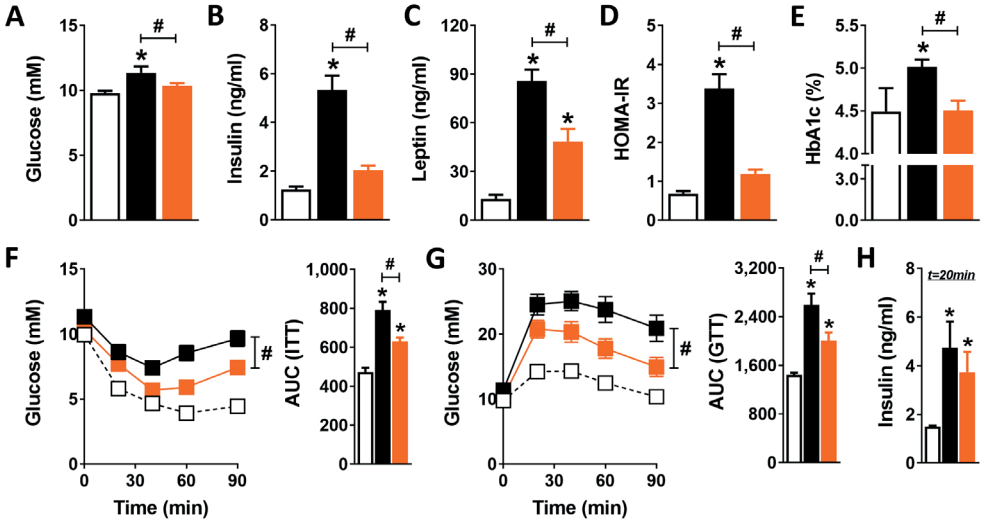

Figure 2. Totum-63 improves whole body metabolic homeostasis in obese mice. LFD- and HFD-fed C57BL6/J mice were treated as described in the legend of Figure 1. (**A-E**) Fasting blood glucose (*A*) and plasma insulin (*B*) levels were measured at week 4 of supplementation and used to calculate the HOMA-IR (*D*). Fasting plasma leptin (*C*) and blood HbA1c (*E*) levels were also determined at the same time point. (**F**) At week 3, whole-body insulin sensitivity was determined by an intraperitoneal (i.p.) insulin tolerance test (ITT) in 4-h fasted mice. Blood glucose levels were measured at the indicated timepoints after i.p. insulin injection and the AUC was calculated. (**G-H**) An i.p. glucose tolerance test (GTT) was performed at week 4 of supplementation in 6-h fasted mice. Blood glucose levels were measured at the indicated timepoints and the AUC was calculated (*G*). Plasma insulin levels during GTT were determined 20 min after glucose injection (*H*). Results are expressed as mean ± SEM. * P ≤ 0.05 *vs* LFD, # P ≤ 0.05 *vs* HFD (n=10-12 mice per group from 2 independent experiments).

Totum-63 reduces hepatic steatosis, inflammation and fibrosis in obese mice

Totum-63 supplementation almost completely reverted HFD-induced hepatic steatosis in obese mice, as assessed by H&E staining (Figure 4A-B) and liver total TG content (Figure 4C). Using quantitative lipidomics, we confirmed that Totum-63 significantly reduced the liver content of all TG species (Supplementary Figure 6). Furthermore, except for phosphatidylcholine levels that were found to be increased, the hepatic lipid composition of obese mice supplemented with Totum-63 resembled LFD-fed lean mice more than HFD-fed mice (Supplementary Figure 6A-C). This effect was associated with decreased gene expression of the major hepatic lipid transporters *Cd36* and *Fabp1*, and the lipogenic enzymes *Acaca*, *Fas* and *Scd1* when compared to HFD-fed control mice, whereas genes involved in FA oxidation were not affected (Figure 4D). Of note, Totum-63 also lowered the expression of *Fbp1*, one of the key gluconeogenic enzyme involved in hepatic glucose production (Figure 4E).

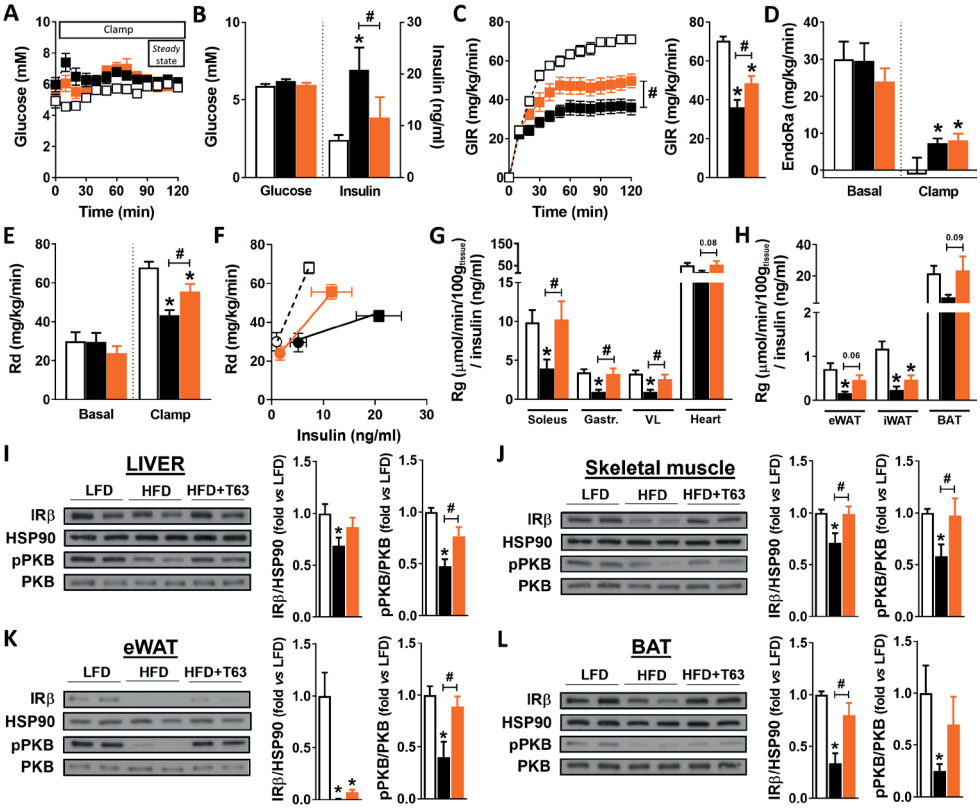

Figure 3. Totum-63 improves systemic and tissue-specific insulin sensitivity in obese mice. LFD- and HFD-fed C57BL6/J mice were treated as described in the legend of Figure 1. (**A**) A hyperinsulinemic-euglycemic clamp was performed in 5 h–fasted conscious mice. Blood glucose was monitored throughout the clamp at 10 min intervals by sampling from the arterial catheter. (**B**) Blood glucose and serum insulin levels were determined at steady-state (90-120 min). (**C**) The glucose infused rate (GIR) required to maintain euglycemia is shown. (**D-E**) The endogenous glucose production (EndoRa, *D*) and glucose disappearance rate (Rd, *E*) were determined using continuous infusion of ^{3}H-glucose. (**F**) The changes in Rd from basal to clamp state were plotted against the corresponding serum insulin levels. (**G-H**) The tissue-specific glucose uptake (Rg) was determined in soleus, gastrocnemius, vastus lateralis (VL), heart, eWAT, iWAT and BAT by administration of nonmetabolizable 2-[^{14}C]-deoxy-glucose and the data corrected for differences in serum insulin levels at steady state. (**I-L**) Tissue-specific insulin signaling was assessed in liver (*I*), quadriceps skeletal muscle (*J*), eWAT (*K*), and BAT (*L*) 15 min after an acute i.p. insulin injection. The protein expression of IRn PKB, and HSP90, and the phosphorylation (p) state of Ser473-PKB were determined by Western blot and quantified by densitometric analysis. The IRβ/HSP90 and pPKB/PKB ratios were calculated and expressed as fold change relative to LFD-fed mice. Results are expressed as mean ± SEM. * P ≤ 0.05 *vs* LFD, # P ≤ 0.05 *vs* HFD (clamp: n=6-8 mice per group; WB: n=5-10 mice per group from 2 independent experiments).

Activation of Kupffer cells (KCs), the tissue-resident macrophages, together with increased recruitment of monocyte-derived macrophages play a key role in obesity-induced hepatic inflammation and progression towards NASH and liver fibrosis (8). Using flow cytometry (see Supplementary Figure 7A for gating strategy), we showed that despite a trend for an increase, Totum-63 supplementation neither significantly affected total hepatic KCs content (Figure 4F) nor the HFD-induced increase in both $CD11c^+$ KCs (Figure 4G-H) and newly recruited monocytes (Figure 4I) in obese mice. This was also confirmed by the absence of differences in the hepatic gene expression of the pan monocyte/macrophage marker *Cd68* and KC marker *Clec4f* (Figure 4J). However, the expression of the proinflammatory chemokine/cytokine *Ccl2*, *Il1b* and *Tnf* were found to be significantly reduced by Totum-63 (Figure 4J), suggesting a reduction in HFD-induced KC activation. Furthermore, although the expression of the hepatic stellate cell marker *Hhipf* was not altered, those of early fibrotic markers *Acta2* and *Col1a1* were significantly reduced by Totum-63 in HFD-fed obese mice (Figure 4K).

Totum-63 reduces inflammation in white adipose tissues and promotes thermogenesis in brown adipose tissue from obese mice

Morphometric analysis of eWAT and iWAT using H&E staining revealed that Totum-63 supplementation in obese mice did not change mean adipocyte diameter and adipocyte size distribution (Figure 5A-B, F-G), a result in line with the absence of differences observed in tissue weights at sacrifice (Figure 1G). Using flow cytometry (see Supplementary Figure 7B for gating strategy), we showed that Totum-63 did not affect adipose tissue monocyte and total macrophage (ATM) contents (Figure 5C-D) but significantly lowered the percentage of obesity-associated $CD11c^+$ ATMs in eWAT (Figure 5E). In iWAT, a beneficial effect of Totum-63 on tissue inflammation was still observed, with a decrease in the number of immune cells per adipocyte observed by H&E staining (Figure 5H) and a reduction in the expression of proinflammatory gene markers (Figure 5I). Of note, the gene expression of thermogenic markers was not changed in iWAT from HFD-fed obese mice, indicating that Totum-63 did not promote WAT beiging (Figure 5I). By contrast to WAT, a significant reduction in both large adipocytes and adipocyte mean diameter was observed in BAT from obese mice supplemented with Totum-63 (Figure 6A-B). This result was in line with the potent decrease in organ weight observed at sacrifice and associated with an upregulation of most of the thermogenic genes (Figure 6C) and an increase in UCP1 protein expression (Figure 6D), suggesting BAT activation in obese mice supplemented with Totum-63. A decrease in the expression of HFD-induced proinflammatory genes was also evidenced in BAT (Figure 6E), highlighting again the beneficial impact of Totum-63 on metabolic tissue inflammation in obese mice.

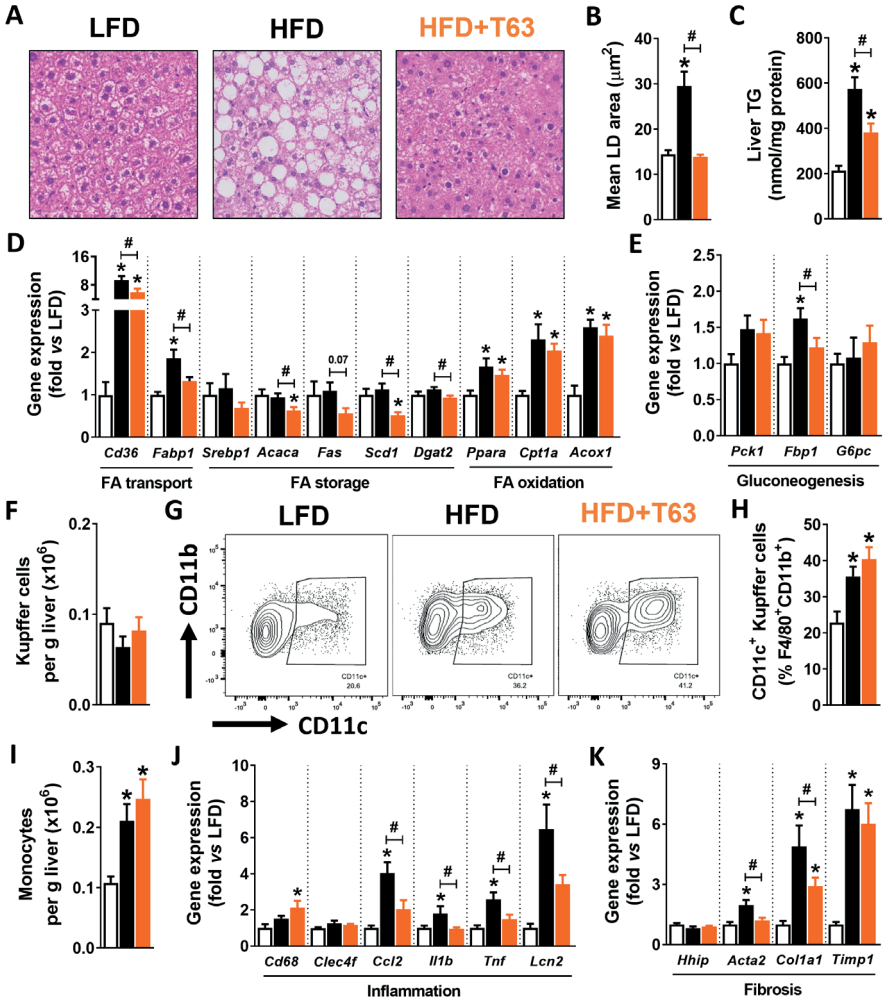

Figure 4. Totum-63 reduces hepatic steatosis, inflammation and fibrosis in obese mice. LFD- and HFD-fed C57BL6/J mice were treated as described in the legend of Figure 1. (**A-C**) Hepatic lipid droplet (LD) area by H&E staining (*A-B*) and liver triglyceride (TG) content (*C*) were determined to assess hepatic steatosis. (**D-E**) The hepatic expression of key genes involved in lipid metabolism (*D*) and gluconeogenesis (*E*) were measured by RT-qPCR. (**F-I**) The liver content of Kupffer cells (*F*) and monocytes (*I*) and the percentage of proinflammatory CD11c⁺ Kupffer cells (*G-H*) were determined by flow cytometry. (**J-K**) The hepatic expression of key genes involved in inflammation (*J*) and fibrosis (*K*) was measured by RT-qPCR. Results are expressed as mean ± SEM. * $P \leq 0.05$ *vs* LFD, # $P \leq 0.05$ *vs* HFD (hepatic steatosis: n=5-6 mice per group; flow cytometry: n=4-6 mice per group; qPCR: n=7-11 mice per group from 2 independent experiments).

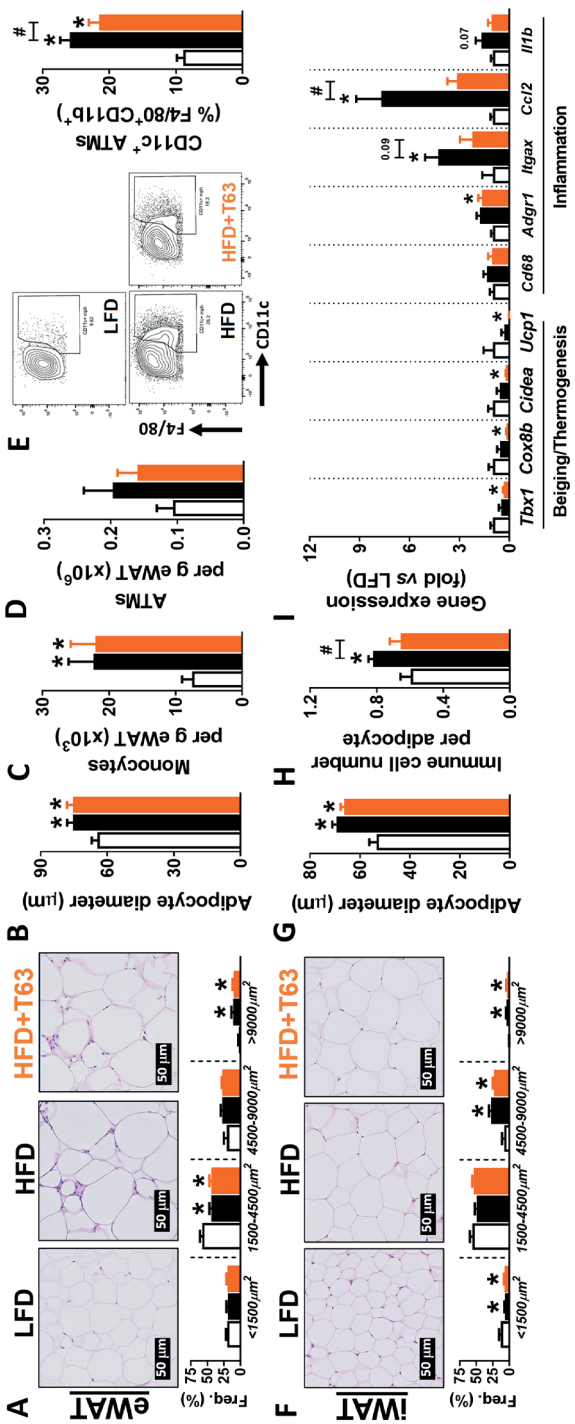

Figure 5. Totum-63 reduces inflammation in white adipose tissues from obese mice. LFD- and HFD-fed C57BL6/J mice were treated as described in the legend of Figure 1. (**A-G**) Adipocyte mean diameter and size distribution were determined by H&E staining in epididymal (eWAT, *A-B*) and inguinal (iWAT, *F-G*) adipose tissues. The number of eWAT monocytes (*C*) and adipose tissue macrophages (ATMs, *D*), and the percentage of obesity-associated CD11c$^+$ ATMs (*E*) were determined by flow cytometry. (**H-I**) The number of immune cell per adipocyte (*H*) and the expression of key genes involved in WAT beiging/thermogenesis and inflammation (*I*) were determined in iWAT by H&E staining and RT-qPCR, respectively. Results are expressed as mean ± SEM. * $P \leq 0.05$ *vs* LFD, # $P \leq 0.05$ *vs* HFD (adipocyte size/distribution: n=4-6 mice per group; flow cytometry: n=5-9 mice per group from 2 independent experiments; qPCR: n=5-6 mice per group).

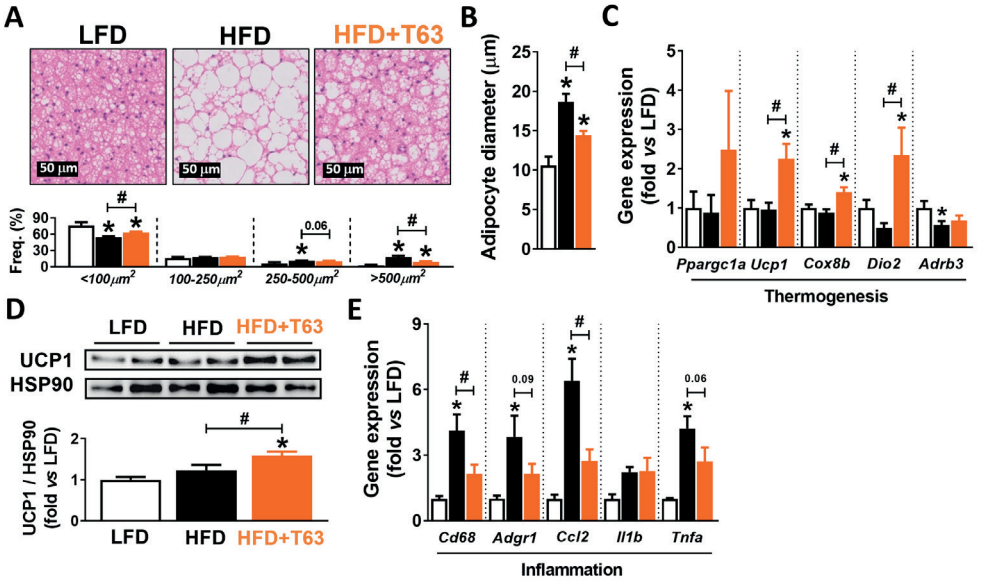

Figure 6. Totum-63 promotes thermogenic program and reduces inflammation in brown adipose tissue from obese mice. LFD- and HFD-fed C57BL6/J mice were treated as described in the legend of Figure 1. (**A-B**) Adipocyte mean diameter and size distribution were determined by H&E staining of subclavicular brown adipose tissue (BAT). (**C-E**) The expression of key genes involved in thermogenesis (*C*) and inflammation (*E*) was measured by RT-qPCR. The expression of UCP1 was assessed by Western Blot, and expressed relative to HSP90 (*D*). Results are expressed as mean ± SEM. * P ≤ 0.05 *vs* LFD, # P ≤ 0.05 *vs* HFD (adipocyte size/distribution: n=4-6 mice per group; qPCR: n=9-11 mice per group; WB: n=4 mice per group).

Discussion

The obesity and T2D epidemics urge new effective management strategies. The main objectives of the present study were to investigate the effects of Totum-63, a new polyphenol-rich plant-based nutritional supplement, on metabolic homeostasis in a mouse model of diet-induced obesity and T2D, and to decipher its underlying mechanism(s) of action. Here, we show that Totum-63 supplementation lowered body fat mass, reduced metaflammation, and improved both whole-body insulin sensitivity and glucose homeostasis in obese, insulin-resistant mice. These beneficial effects on obesity-associated low-grade inflammation and metabolic homeostasis were associated with either partial or almost complete restoration of various metabolic dysfunctions induced by HFD in different organs, suggesting a pleiotropic mode-of-action of Totum-63 owing to its chemical composition rich in various bioactive compounds.

We report that chronic consumption of Totum-63 through dietary supplementation significantly reduced body weight and fat mass in obese mice, a feature that was sustained

for at least 4 weeks while only associated with a transient reduction of food intake during the first days of supplementation, probably due to the bitterness of some flavonoids and saponins components of Totum-63. Whole-body EE was also not affected by Totum-63 throughout the study, a feature confirmed by ANCOVA analysis (data not shown), indicating that increased energy dissipation did not likely contribute in a significant and measurable extent to the reduction of body weight. By contrast, the daily feces production was increased and the AEAE was therefore significantly reduced, suggesting altered nutrient absorption and/or metabolism in the gastrointestinal tract. Interestingly, some bioactive compounds present in Totum-63, notably several polyphenols, have been previously reported to inhibit various digestive enzymes that may ultimately lead to a reduction in both carbohydrate and lipid absorption during the gastrointestinal transit (20-22). Among them, anthocyanins, chlorogenic acid, oleuropein and some luteolin derivatives have been shown to reduce both pancreatic α-amylase and lipase activities and inhibit intestinal α-glucosidase (20-22). Altogether, one can speculate that inhibition of digestive enzymes by various specific component(s) of Totum-63 may have contributed to the higher energy excretion in the feces observed in supplemented obese mice.

Since absorption of CHO and FA mostly takes place in the small intestine (23), we also measured ileal expression of some of the players involved in nutrient uptake and trafficking into enterocytes, but did not find any significant changes in response to Totum-63 supplementation. However, we cannot exclude that different intestinal segments could be affected and/or that alterations of other intestinal lumen-related processes might contribute to lower nutrient absorption, for instance through a decrease in passive diffusion of dietary TG-derived free FA (FFA) secondary to changes in gut permeability. In this context, it is worth mentioning that preliminary lipidomic analyses performed on pooled feces samples may support this hypothesis, as mean levels of various FFA species measured in Totum-63-supplemented mice were increased when compared to HFD-fed control mice (Supplementary Figure 8). In line with this, we also showed that Totum-63 can restore the HFD-induced downregulation of genes encoding tight junction proteins involved in obesity-associated intestinal permeability, dysbiosis and metaflammation (24). Once again, some Totum-63 components, including fibers and polyphenols, could directly and indirectly affect this interface, notably through modulation of local production of microbiota-derived metabolites that can act as signaling molecules and/or exert direct effects on the epithelial barrier (24). Altogether, further experiments are definitely required to explore the impact of Totum-63 on the gastrointestinal tract more in depth, not only focusing on nutrient absorption in various intestinal sections but also on microbiome composition and diversity, local immune responses and enterocyte-specific metabolic functions, which all can contribute to its beneficial effects.

The other important outcome of this study was the demonstration that Totum-63 can improve insulin sensitivity and glucose tolerance, an effect that is not entirely due to the observed reduction in body weight. Indeed, body weight-matching of control and supplemented obese mice showed that Totum-63 still exerted some intrinsic beneficial effects on metabolic homeostasis. Remarkably, we showed that Totum-63 supplementation in HFD-fed obese mice could restore insulin sensitivity and glucose uptake in various peripheral organs, notably in skeletal muscle, the tissue that contributes the most to the insulin-mediated glucose clearance from the circulation. Mechanistically, the obesity-associated metaflammation, which results from changes in the composition and activation states of various innate and adaptive immune cells in metabolic organs, has been suggested to underlie part of tissue-specific alterations of insulin signaling, notably in WAT and the liver (8-10). Interestingly, we found a mild but significant reduction in the $CD11c^+$ ATMs, a proinflammatory macrophage subset that is believed to mediate part of the detrimental effect on tissue insulin sensitivity (9, 25). In the liver, although $CD11c^+$ KC content was not affected, the decrease in gene expression of KC-derived cytokines such as *Ccl2* (MCP-1) and *Tnfa* suggests a reduction in HFD-induced KC proinflammatory activation by Totum-63. In line with this, Totum-63 also improved tissue-specific insulin sensitivity and induced a potent reduction in hepatic TG accumulation. This beneficial effect on liver steatosis was associated with a significant downregulation of genes involved in FA transport and *de novo* lipogenesis, while those involved in FA oxidation were unchanged. Taken together, this suggests that the reduction in ectopic lipid deposition in the liver may result from a decrease in both hepatic FA transport and TG biosynthesis, although we cannot exclude that it could also partly be the consequence of reduced lipid availability secondary to improved insulin-mediated inhibition of lipolysis in WAT and/or increased FA oxidation in BAT. Interestingly, we also found a decrease in BAT mass associated with an increased tissue expression of thermogenic genes, including *Ucp1*, in Totum-63-supplemented obese mice, suggesting BAT activation. However, we do not find a significant increase in EE, suggesting that the quantitative contribution of this effect to whole-body energy homeostasis is rather mild. Here again, some compounds present in Totum-63, notably chlorogenic acid and oleuropein, have been reported to promote BAT activation (26), at least partly through activation of the sympathetic nervous system (27). Alternatively, we show that Totum-63 increased ileal expression of BA-regulated genes, a feature that may suggest a higher BA bioavailability. In addition to their role in lipid absorption, BAs are increasingly recognized as signaling molecules that, among others, promote BAT activation and energy expenditure (28). Whether Totum-63 can affect liver and intestinal BA metabolism and whether this can contribute to some of its metabolic effects, notably through BA receptor-mediated BAT

activation, would require further studies. Of note, despite decreased hepatic expression of some early fibrotic gene markers by Totum-63, the HFD used in the framework of this study does not induce detectable levels of liver fibrosis, as assessed by Sirius red staining (data not shown). As such, further studies with appropriate NASH mouse models and/or pro-fibrotic diet regimens are also required to assess the impact of Totum-63 on fibrosis regression.

In conclusion, our current study shows that Totum-63, a new polyphenol-rich plant-based nutritional supplement, reduces body fat mass, hepatic steatosis, inflammation and insulin resistance in obese mice, likely through pleiotropic effects on various metabolic organs, including skeletal muscle, intestine, liver, and WAT/BATs. It is important to mention that in addition to the absence of an effect on locomotor activity, we have also not observed any abnormal behavioral/physiological parameters throughout the study that would have suggested some harmful effects. Furthermore, the impact of a 6-month supplementation with Totum-63 has also recently been evaluated in the framework of a phase 2a clinical trial in subjects with prediabetes (NCT02868177) and no detrimental side effects have been reported [18]. Altogether, although additional mechanistic and long-term studies are required, plant-derived Totum-63 appears to be a promising novel nutritional supplement for alleviating metabolic dysfunctions in obese people with or without T2D.

Materials and Methods

Totum-63

Totum-63 is a patented blend of 5 plant extracts designed to act in combination to target the risk factors of developing T2D. The mixture contains extracts from olive leaf (*Olea europaea*), bilberry (*Vaccinium myrtillus*), artichoke (*Cynara scolymus*), chrysanthellum (*Chrysanthellum indicum* subsp*. afroamericanum B.L. Turner*) and black pepper (*Piper nigrum*). Its chemical characterization is shown in Supplementary Table 1.

Animals and diet

All experiments were performed in accordance with the Guide for the Care and Use of Laboratory Animals of the Institute for Laboratory Animal Research and have received approval from the local Ethical Review Boards (Leiden University Medical Center, Leiden, The Netherlands; C2E2A, Clermont-Ferrand, France; Vanderbilt Animal Care and Use Committee, Nashville, USA). 10-week-old C57BL/6JOlaHsd male mice were purchased from Envigo (Horst, The Netherlands) and housed in a temperature-controlled room with a 12-hour light-dark cycle and *ad libitum* access to food and tap water. Mice were fed a low-fat diet (LFD, 10% energy derived from fat, D12450H, Research Diets, USA) or high fat diet (HFD, 45% energy derived

from fat, D12451, Research Diets, USA) for 12 weeks after which HFD was supplemented with or without Totum-63 (2.7% w/w, Valbiotis SA, Perigny, France) for an additional 4 weeks. A pilot study was performed *a priori* to select the most appropriate dosage of Totum-63 for reducing T2D risk factors in obese mice (data not shown). The experimental groups were randomized after removal of HFD low responders (~5%; body weight gain <6 g), according to total body weight, lean and fat mass, and fasting plasma glucose. An *a priori* power calculation was done. The experimenters were not blinded to the diet supplementation on the test days, however, most of the subsequent analyses were performed in blinded conditions.

Body composition and indirect calorimetry

Body weight was frequently measured during the 4 weeks of supplementation using a conventional weighing scale. Food intake was also frequently assessed by weighing food pellets in every cage. Body composition was measured at week 4 by MRI in conscious unrestrained mice using an EchoMRI (Echo Medical Systems). At sacrifice, visceral white adipose tissue (epididymal; eWAT), subcutaneous white adipose tissue (inguinal; iWAT), supraclavicular brown adipose tissue (BAT), heart and liver were weighed and collected for further processing. For indirect calorimetric measurements, 12-week HFD-fed mice were transferred to individual metabolic cages (8-channel multiplex system, Promethion, Sable Systems, USA) with free access to food and water, and followed for 4 weeks after the start of supplementation as previously reported (29) and described in the Appendix.

Insulin- and glucose tolerance tests

Whole-body insulin tolerance (ipITT) and glucose tolerance (ipGTT) tests were performed at week 3 and 4 of Totum-63 supplementation, respectively, as previously reported (29, 30) and described in the Appendix.

Hyperinsulinemic-euglycemic clamp

Hyperinsulinemic-euglycemic (HI-EU) clamp was performed at week 4 of supplementation. One week before HI-EU clamps, carotid artery and jugular vein catheters were surgically placed for sampling and infusions. Mice were fasted for 5h and then clamped unrestrained and in conscious state, as previously reported (31) and described in the Appendix.

Plasma analysis

Blood samples were collected from the tail vein of 4h-fasted mice using paraoxon-coated glass capillaries. Plasma total cholesterol (TC, Instruchemie #10015), triglycerides (TG,

Instruchemie #2913), insulin (Chrystal Chem #90080) and leptin (Chrystal Chem #90030), and whole blood HbA1c (Chrystal Chem #80310) were determined using commercially available kits per manufacturer's instructions. The homeostatic model assessment of insulin resistance (HOMA-IR) adjusted for mice (32) was calculated as followed ([glucose (mg/dl)*0.055]*[insulin (ng/ml)*172.1])/3875.

Feces analyses

Feces were carefully collected from 24h cage bedding during week 4 and weighed. Fecal energy density was determined by bomb calorimetry (IKA C200, Germany). The apparent energy assimilation efficiency (AEAE) was calculated as (fecal energy density x averaged daily feces production / averaged daily energy intake over the collection period).

Hepatic lipid composition

Liver lipids were measured as previously reported (33, 34) and described in the Appendix.

Histological analysis

Pieces of eWAT, iWAT, BAT and liver (~30 mg) were fixed in 4% formaldehyde (Sigma-Aldrich), paraffin-embedded, sectioned at 4 μm and stained with Hematoxylin and Eosin (H&E) (30). Six fields at 20x magnification were used for the analysis of adipocyte diameter and hepatic steatosis.

Isolation of leukocytes from blood, adipose tissue and liver for flow cytometry

At sacrifice, blood was collected retro-orbitally in heparin-coated tubes for leukocytes isolation as described in the Appendix and previously reported (29, 30). After a 1-minute post sacrifice transcardial perfusion with PBS, eWAT and liver samples were collected and digested for isolation of either stromal vascular fraction or leukocytes, respectively, as previously reported (29, 30) and described in the Appendix.

Flow cytometry

Analysis of blood, WAT and liver myeloid/lymphocyte subsets were done as previously reported (29, 30) and described in the Appendix.

RNA-isolation and RT-qPCR

RNA was extracted from snap-frozen liver, eWAT, iWAT, BAT or intestine samples using TriPure RNA Isolation reagent (Roche Diagnostics). Total RNA (1-2 μg) was reverse

transcribed using the M-MLV Reverse Transcriptase kit (ThermoFisher). Real-time qPCR runs were performed on a CFX96 Real-time C1000 thermal cycler (Biorad) using the GoTaq qPCR Master Mix kit (Promega). Gene expression was normalized using housekeeping gene *RplP0* and expressed as fold change compared to LFD-fed mice. Primer sequences can be found in Supplementary Table 2.

Western blot analysis

Snap-frozen liver, skeletal muscle (quadriceps), eWAT and BAT samples (~50 mg) collected 15 min after an acute i.p. insulin injection (1U/kg lean body mass) were lysed in ice-cold buffer containing: 50 mM Hepes (pH 7.6), 50 mM NaF, 50 mM KCl, 5 mM NaPPi, 1 mM EDTA, 1 mM EGTA, 1 mM DTT, 5 mM β-glycerophosphate, 1 mM sodium vanadate, 1% NP40 and protease inhibitors cocktail (Complete, Roche). Western blots were performed as previously described (35). Bands were visualized by enhanced chemiluminescence and quantified using Image J. Primary antibodies used are listed in Supplementary Table 3.

Statistical analysis

All data are presented as mean ± standard error of the mean (SEM). Statistical analysis was performed using GraphPad Prism 8.0 (GraphPad Software, La Jolla, CA, USA) with unpaired t-test, one-way or two-way analysis of variance (ANOVA) followed by Fisher's post-hoc test. Differences between groups were considered statistically significant at $P < 0.05$. Outliers were identified according to the two-standard deviation method.

Competing Interests statement

V. Chavanelle, Y. Otero, F. Le Joubioux, S.L. Peltier and P. Sirvent are all employees of Valbiotis. S.L. Peltier and P. Sirvent are listed as co-inventors on Totum-63 patent and possess company stock. None of the other authors have any potential conflict of interest. This work was supported in part by National Institute of Diabetes and Digestive and Kidney Diseases grants DK059637 and S10RR028101 (L.L., O. McG.), the NWO project 184.034.019 (M.G.), and Valbiotis (B.G.). Study design, collection of the data, analysis and interpretation of the results, writing and decision to submit the article for publication was performed by Guigas' group at the Leiden University Medical Center, in agreement with Valbiotis.

References

1. WHO. Obesity and overweight. Key facts.;https://www.who.int/news-room/fact-sheets/detail/obesity-and-overweight.
2. IDF. IDF Diabetes Atlas. 2019;9th edn:http://www.diabetesatlas.org/.
3. Williams R, Karuranga S, Malanda B, Saeedi P, Basit A, Besancon S, et al. Global and regional estimates and projections of diabetes-related health expenditure: Results from the International Diabetes Federation Diabetes Atlas, 9th edition. Diabetes Res Clin Pract. 2020;162:108072.
4. DeFronzo RA, Ferrannini E, Groop L, Henry RR, Herman WH, Holst JJ, et al. Type 2 diabetes mellitus. Nat Rev Dis Primers. 2015;1:15019.
5. Roden M, Shulman GI. The integrative biology of type 2 diabetes. Nature. 2019;576(7785):51-60.
6. Hotamisligil GS. Inflammation, metaflammation and immunometabolic disorders. Nature. 2017;542(7640):177-85.
7. Jais A, Bruning JC. Hypothalamic inflammation in obesity and metabolic disease. J Clin Invest. 2017;127(1):24-32.
8. Kazankov K, Jorgensen SMD, Thomsen KL, Moller HJ, Vilstrup H, George J, et al. The role of macrophages in nonalcoholic fatty liver disease and nonalcoholic steatohepatitis. Nat Rev Gastroenterol Hepatol. 2019;16(3):145-59.
9. Lackey DE, Olefsky JM. Regulation of metabolism by the innate immune system. Nat Rev Endocrinol. 2016;12(1):15-28.
10. Lee YS, Wollam J, Olefsky JM. An Integrated View of Immunometabolism. Cell. 2018;172(1-2):22-40.
11. Castejon-Vega B, Giampieri F, Alvarez-Suarez JM. Nutraceutical Compounds Targeting Inflammasomes in Human Diseases. Int J Mol Sci. 2020;21(14).
12. Granato D, Barba FJ, Bursac Kovacevic D, Lorenzo JM, Cruz AG, Putnik P. Functional Foods: Product Development, Technological Trends, Efficacy Testing, and Safety. Annu Rev Food Sci Technol. 2020;11:93-118.
13. Martel J, Ojcius DM, Chang CJ, Lin CS, Lu CC, Ko YF, et al. Anti-obesogenic and antidiabetic effects of plants and mushrooms. Nat Rev Endocrinol. 2017;13(3):149-60.
14. Alkhatib A, Tsang C, Tiss A, Bahorun T, Arefanian H, Barake R, et al. Functional Foods and Lifestyle Approaches for Diabetes Prevention and Management. Nutrients. 2017;9(12).
15. Kumar S, Pandey AK. Chemistry and biological activities of flavonoids: an overview. ScientificWorldJournal. 2013;2013:162750.
16. Hussain T, Tan B, Murtaza G, Liu G, Rahu N, Saleem Kalhoro M, et al. Flavonoids and type 2 diabetes: Evidence of efficacy in clinical and animal studies and delivery strategies to enhance their therapeutic efficacy. Pharmacol Res. 2020;152:104629.
17. Cory H, Passarelli S, Szeto J, Tamez M, Mattei J. The Role of Polyphenols in Human Health and Food Systems: A Mini-Review. Front Nutr. 2018;5:87.

18. Peltier S, Chavanelle V, Otero YF, Bargetto M, Cazaubiel M, Sirvent P, et al. Totum-63 Lowers Fasting Glycemia in Subjects with Prediabetes: A Phase 2A Clinical Trial. Diabetes. 2020;69(Supplement 1):848-P.
19. Inagaki T, Choi M, Moschetta A, Peng L, Cummins CL, McDonald JG, et al. Fibroblast growth factor 15 functions as an enterohepatic signal to regulate bile acid homeostasis. Cell Metab. 2005;2(4):217-25.
20. Tadera K, Minami Y, Takamatsu K, Matsuoka T. Inhibition of alpha-glucosidase and alpha-amylase by flavonoids. J Nutr Sci Vitaminol (Tokyo). 2006;52(2):149-53.
21. McDougall GJ, Kulkarni NN, Stewart D. Current developments on the inhibitory effects of berry polyphenols on digestive enzymes. Biofactors. 2008;34(1):73-80.
22. Tan Y, Chang SKC. Digestive enzyme inhibition activity of the phenolic substances in selected fruits, vegetables and tea as compared to black legumes. J Funct Foods. 2017;38:644-55.
23. Ko CW, Qu J, Black DD, Tso P. Regulation of intestinal lipid metabolism: current concepts and relevance to disease. Nat Rev Gastroenterol Hepatol. 2020;17(3):169-83.
24. Khoshbin K, Camilleri M. Effects of dietary components on intestinal permeability in health and disease. Am J Physiol Gastrointest Liver Physiol. 2020;319(5):G589-G608.
25. Patsouris D, Li PP, Thapar D, Chapman J, Olefsky JM, Neels JG. Ablation of CD11c-positive cells normalizes insulin sensitivity in obese insulin resistant animals. Cell Metab. 2008;8(4):301-9.
26. Han X, Zhang Y, Guo J, You Y, Zhan J, Huang W. Chlorogenic Acid Stimulates the Thermogenesis of Brown Adipocytes by Promoting the Uptake of Glucose and the Function of Mitochondria. J Food Sci. 2019;84(12):3815-24.
27. Oi-Kano Y, Kawada T, Watanabe T, Koyama F, Watanabe K, Senbongi R, et al. Oleuropein, a phenolic compound in extra virgin olive oil, increases uncoupling protein 1 content in brown adipose tissue and enhances noradrenaline and adrenaline secretions in rats. J Nutr Sci Vitaminol (Tokyo). 2008;54(5):363-70.
28. Ahmad TR, Haeusler RA. Bile acids in glucose metabolism and insulin signalling - mechanisms and research needs. Nat Rev Endocrinol. 2019;15(12):701-12.
29. Hussaarts L, Garcia-Tardon N, van Beek L, Heemskerk MM, Haeberlein S, van der Zon GC, et al. Chronic helminth infection and helminth-derived egg antigens promote adipose tissue M2 macrophages and improve insulin sensitivity in obese mice. FASEB J. 2015;29(7):3027-39.
30. van der Zande HJP, Gonzalez MA, de Ruiter K, Wilbers RHP, Garcia-Tardon N, van Huizen M, et al. The helminth glycoprotein omega-1 improves metabolic homeostasis in obese mice through type 2 immunity-independent inhibition of food intake. FASEB J. 2021;35(2):e21331.
31. Lantier L, Williams AS, Williams IM, Guerin A, Bracy DP, Goelzer M, et al. Reciprocity Between Skeletal Muscle AMPK Deletion and Insulin Action in Diet-Induced Obese Mice. Diabetes. 2020;69(8):1636-49.
32. Lee S, Muniyappa R, Yan X, Chen H, Yue LQ, Hong EG, et al. Comparison between surrogate indexes of insulin sensitivity and resistance and hyperinsulinemic euglycemic clamp estimates in mice. Am J Physiol Endocrinol Metab. 2008;294(2):E261-70.

33. Thomas A, Belaidi E, Aron-Wisnewsky J, van der Zon GC, Levy P, Clement K, et al. Hypoxia-inducible factor prolyl hydroxylase 1 (PHD1) deficiency promotes hepatic steatosis and liver-specific insulin resistance in mice. Sci Rep. 2016;6:24618.

34. Zinsou JF, Janse JJ, Honpkehedji YY, Dejon-Agobe JC, Garcia-Tardon N, Hoekstra PT, et al. Schistosoma haematobium infection is associated with lower serum cholesterol levels and improved lipid profile in overweight/obese individuals. PLoS Negl Trop Dis. 2020;14(7):e0008464.

35. Thomas A, Belaidi E, Moulin S, Horman S, van der Zon GC, Viollet B, et al. Chronic Intermittent Hypoxia Impairs Insulin Sensitivity but Improves Whole-Body Glucose Tolerance by Activating Skeletal Muscle AMPK. Diabetes. 2017;66(12):2942-51.

Supplementary Materials and Methods

Body composition and indirect calorimetry

Before the start of the measurements, the animals were acclimated to the cages and single housing for 48h. A standard 12h light/dark cycle was maintained throughout the calorimetry study. Spontaneous locomotor activity was determined by the measurement of beam breaks. Oxygen consumption and carbon dioxide production were measured at 30 sec intervals. Energy expenditure (EE) and carbohydrate (CHO) and fatty acid (FA) oxidation were calculated based on respirometry, as previously described (29). The ANCOVA analysis of EE was done using the NIDDK Mouse Metabolic Phenotyping Centers (www.mmpc.org).

Insulin- and glucose tolerance tests

For ipITT, a bolus of insulin (1U/kg lean body mass, Novorapid, Novo Nordisk) was administered i.p. in 4h-fasted mice after which blood glucose levels were measured at t=0, 20, 40, 60 and 90 min post insulin administration using a Glucometer (Accu-Check, Roche Diagnostics). For ipGTT, a bolus of glucose (2g D-Glucose/kg total body weight, Sigma-Aldrich) was administered i.p. in 6h-fasted mice and blood glucose was measured at t=0, 20, 40, 60 and 90 min post glucose injection.

Hyperinsulinemic-euglycemic clamp

Briefly, [3-^{3}H]-D-glucose was first primed and continuously infused (t=-90 to 0 min, 0.04 mCi/min). The insulin clamp was next initiated at t=0 min with a continuous insulin infusion (4 mU/kg/min) followed by variable glucose infusion rate (GIR) until t=155 min in order to maintain euglycemia. Arterial glucose levels were monitored every 10 min to provide feedback for adjustment of the GIR (50% dextrose + [3-^{3}H]-D-glucose). [3-^{3}H]-D-glucose kinetics were determined at t=-10 min and at steady state (from 80 to 120 min) to assess endogenous glucose production (EndoRa) and whole-body glucose disappearance (Rd) rates. An intravenous bolus of 2-[^{14}C]-deoxy-D-glucose (13 μCi) was administered at t=120 min. The mice were sacrificed at t=155 min and their tissues immediately harvested and freeze-clamped to determine glucose metabolic index (Rg), an index of tissue-specific glucose uptake. Plasma and tissue processing were performed as previously described (31). Full step-by-step descriptions of the HI-EU clamp and calculations are available from the Vanderbilt Mouse Metabolic Phenotyping Center website (www.vmmpc.org).

Hepatic lipid composition

Liver TG and TC concentrations were measured using the commercial kits described above and expressed as mg per mg of total protein content using the Bradford protein assay kit (Sigma-Aldrich). For lipidomics, lipids were extracted from 10 mg of liver by the methyl-tert-butylether method and analyzed using the Lipidyzer™, a direct infusion-tandem mass spectrometry (DI-MS/MS)-based platform (Sciex, Redwood City, USA), as previously described (34). Lipid concentrations were expressed as pmol/mg of liver.

Feces lipid composition

Lipids were extracted from 50 mg of collected 24h after cage refreshment by the same method described above for the liver and analyzed using the Lipidyzer™ platform. Lipid concentrations were expressed as pmol/mg of fresh feces.

Isolation of stromal vascular fraction from adipose tissue

eWAT samples were minced and incubated for 1 hour at 37°C in an incubator under agitation (60 rpm) containing 0.5 g/L collagenase type I from *Clostridium histolyticum* (Sigma-Aldrich), 100 mM HEPES (ThermoFisher), 2% (w/v) dialyzed bovine serum albumin (BSA, fraction V; Sigma-Aldrich) and 6 mM D-Glucose. The samples were passed through a 236 µm filter which was washed with PBS supplemented with 2.5 mM EDTA and 1% FCS. Adipocytes and stromal vascular fraction (SVF) were separated by collecting the infranatant. SVF was next pelleted at 350 x g for 10 min at room temperature and treated with erythrocyte lysis buffer (0.15 M NH_4Cl; 1 mM $KHCO_3$; 0.1 mM Na_2EDTA). Cells were washed with PBS/EDTA/FCS, and counted using a hematocytometer, as previously described (29, 30).

Isolation of liver leukocytes

Livers were minced and incubated for 45 min at 37°C in RPMI 1640 + Glutamax (Life Technologies) containing 1 mg/ml collagenase type IV from *Clostridium histolyticum*, 200 U/ml DNase (both Sigma-Aldrich) and 1 mM $CaCl_2$. The digested tissues were passed through a 100 µm cell strainer which was subsequently washed with PBS/EDTA/FCS. After washing the pellet once with PBS/EDTA/FCS, the samples were centrifuged at 50 x g for 3 minutes at 4°C to pellet the hepatocytes. The supernatant was collected and spun down at 530 x g for 10 min at 4°C. The pellet was subsequently treated with erythrocyte lysis buffer and next washed with PBS/EDTA/FCS. $CD45^+$ leukocytes were isolated using LS columns and CD45 MicroBeads (35 µL beads per sample, Miltenyi Biotec) according to the manufacturer's protocol and the isolated cells were counted using a hematocytometer, as described previously (29, 30).

Isolation of blood leukocytes

Blood was treated with erythrocyte lysis buffer. After washing, cells were centrifuged (530 x g, 10 min at 4°C), resuspended in FACS buffer, counted, and processed as described above for the SVF from eWAT.

Flow cytometry

For analysis of WAT and liver myeloid subsets, cells were first permeabilized with 0.5% saponin (Sigma-Aldrich) and stained with an antibody against YM1 conjugated to biotin. After washing, cells were next stained with streptavidin-PerCP (BD Biosciences) and antibodies directed against CD45.2, Siglec-F, CD11b, Ly6C, F4/80 and CD11c in 0.5% saponin/FACS buffer. For analysis of blood monocyte and lymphocyte subsets, cells were first permeabilized or not with 0.5% saponin (Sigma-Aldrich), respectively. After washing, cells were stained with antibodies directed against CD45.2, Siglec-F, CD11b, Ly6C, B220 and CCR2 (monocyte subset) or CD45.2, CD19, NK1.1, CD3, CD4 and CD8 (lymphocyte subset). Cells were measured on a FACSCanto or LSR-II flow cytometer (BD Biosciences), and gates were set according to Fluorescence Minus One (FMO) controls. Antibody information is provided in Supplementary Table 4.

Supplementary references

1. L. Hussaarts, N. Garcia-Tardon, L. van Beek, M.M. Heemskerk, S. Haeberlein, G.C. van der Zon, A. Ozir-Fazalalikhan, J.F. Berbee, K. Willems van Dijk, V. van Harmelen, M. Yazdanbakhsh, and B. Guigas, Chronic helminth infection and helminth-derived egg antigens promote adipose tissue M2 macrophages and improve insulin sensitivity in obese mice. FASEB J 29 (2015) 3027-39.
2. L. Lantier, A.S. Williams, I.M. Williams, A. Guerin, D.P. Bracy, M. Goelzer, M. Foretz, B. Viollet, C.C. Hughey, and D.H. Wasserman, Reciprocity Between Skeletal Muscle AMPK Deletion and Insulin Action in Diet-Induced Obese Mice. Diabetes 69 (2020) 1636-1649.
3. J.F. Zinsou, J.J. Janse, Y.Y. Honpkehedji, J.C. Dejon-Agobe, N. Garcia-Tardon, P.T. Hoekstra, M. Massinga-Loembe, P. Corstjens, G.J. van Dam, M. Giera, P.G. Kremsner, M. Yazdanbakhsh, A.A. Adegnika, and B. Guigas, Schistosoma haematobium infection is associated with lower serum cholesterol levels and improved lipid profile in overweight/obese individuals. PLoS Negl Trop Dis 14 (2020) e0008464.
4. H.J.P. van der Zande, M.A. Gonzalez, K. de Ruiter, R.H.P. Wilbers, N. Garcia-Tardon, M. van Huizen, K. van Noort, L.R. Pelgrom, J.M. Lambooij, A. Zawistowska-Deniziak, F. Otto, A. Ozir-Fazalalikhan, D. van Willigen, M. Welling, J. Poles, F. van Leeuwen, C.H. Hokke, A. Schots, M. Yazdanbakhsh, P. Loke, and B. Guigas, The helminth glycoprotein omega-1 improves metabolic homeostasis in obese mice through type 2 immunity-independent inhibition of food intake. FASEB J 35 (2021) e21331.

Supplementary information

Supplementary Table 1. Chemical characterization of Totum-63.

Compound type	Extract content (g/100 g dry weight)
Total polyphenols	14.36
Total anthocyanins	0.81
Monocaffeoylquinic acids	1.18
Chlorogenic acid	0.85
Other monocaffeoylquinic acids	0.33
Dicaffeoylquinic acids	0.98
Cynarin	0.24
Other dicaffeoylquinic acids	0.74
Caffeic acid	0.01
Oleuropein	3.72
Oleuropein isomers	0.20
Hydroxytyrosol	0.04
Luteolin	0.01
Luteolin-7-O-glucoside	0.38
Luteolin-7-O-glucuronide	0.38
Apigenin	0.01
Apigenin-7-O-glucoside	0.01
Apigenin-7-O-glucuronide	0.25
Apigenin 6-C-glucoside-8-C-arabinoside (Shaftoside)	0.06
Apigenin 6,8-C-diglucoside (Vicenin 2)	0.06
Eriodictyol	<0.01
Eriodictyol-7-O-glucoside	0.11
Okanin-4-O-glucoside (Marein)	0.05
Isookanin-7-O-glucoside (Flavanomarein)	0.05
Maritimetin-6-O-glucoside (Maritimein)	0.08
Saponins	
Chrysanthellin A	0.01
Chrysanthellin B	0.27
Alkaloid	
Piperin	0.004
Fiber	
Soluble Fiber	13.7
Insoluble Fiber	3.3

Supplementary Table 2. qPCR primers.

Gene	Accession number	Forward primer	Reverse primer
Abcg5	NM_031884	TGTCCTACAGCGTCAGCAACC	GGCCACTCTCGATGTACAAGG
Abcg8	NM_026180	TCCTGTGAGCTGGGCATCCGA	CCCGCAGCCTGAGCTCCCTAT
Acaca	NM_133360.2	CAGCTGGTGCAGAGGTACCG	TCTACTCCGCAGGTACTGCCG
Acox1	NM_015729	GGGACCCACAAGCCTCTGCCA	GTGCCGTCAGGCTTCACCTGG
Acta2	NM_007392.3	AGCCATCTTTCATTGGGATGG	CCCCTGACAGGACGTTGTTA
Adgr1	NM_010130.4	CTTTGGCTATGGGCTTCCAGTC	GCAAGGAGGACAGAGTTTATCGTG
Adrb3	NM_013462.3	CACCGCTCAACAGGTTTGATG	TCTTGGGGCAACCAGTCAAG
Cck	NM_031161.4	CTGCCCTCAACTTAGCTGGA	TTCATGGCTTTGGATGGGGAA
Ccl2	NM_011333.3	TCAGCCAGATGCAGTTAACGCCC	GCTTCTTTGGGACACCTGCTGCT
Cd3e	NM_007648.4	CAGGACGATGCCGAGAACATT	CGTCACTGTCTAGAGGGCAC
Cd36	NM_001159558	GCAAAGAACAGCAGCAAAATC	CAGTGAAGGCTCAAAGATGG
Cd68	NM_009853.1	CCTCCACCCTCGCCTAGTC	TTGGGTATAGGATTCGGATTTGA
Cdh1	NM_009864.3	CCAAGCACGTATCAGGGTCA	ACTGCTGGTCAGGATCGTTG
Cidea	NM_007702	CTCGGCTGTCTCAATGTCAA	CCGCATAGACCAGGAACTGT
Cidec	NM_178373	CCATCAGAACAGCGCAAGAAG	AGAGGGTTGCCTTCACGTTC
Cldn3	NM_009902.4	CCTAGGAACTGTCCAAGCCG	CCCGTTTCATGGTTTGCCTG
Clec4f	NM_016751.3	ACTGAAGTACCAAATGGACAATGTTAGT	GTCAGCATTCACATCCTCCAGA
Col1a1	NM_007742.3	GAGAGGTGAACAAGGTCCCG	AAACCTCTCTCGCCTCTTGC
Cox8b	NM_007751.3	GACCCCGAGAATCATGCCAA	CCTGCTCCACGGCGGAA
Cpt1a	NM_013495	AGGAGACAAGAACCCCAACA	AAGGAATGCAGGTCCACATC
Dgat2	NM_026384.3	GTCTCCTGGCTAGGGACACG	GGATATGCGCCAGAGCAACG
Dio2	NM_010050	CGCTCCAAGTCCACTCGCGG	CGGCCCCATCAGCGGTCTTC
Fabp1	NM_017399.4	GCCACCATGAACTTCTCCGGCA	GGTCCTCGGGCAGACCTATTGC
Fas	NM_007988	CACAGGCATCAATGTCAACC	TTTGGGAAGTCCTCAGCAAC
Fbp1	NM_019395.2	GCATCGCACAGCTCTATGGT	ACAGGTAGCGTAGGACGACT
Fgf15	NM_008003.2	CGGTCGCTCTGAAGACGATT	CCTCCGAGTAGCGAATCAGC
G6pc	NM_008061	CCATGGGCGCAGCAGGTGTA	AGCCACGACCTGGTGGGGAA
Gcg	NM_008100.4	TTGAGAGGCATGCTGAAGGG	TCTTCTGGGAAGTCTCGCCT

Gene	Accession number	Forward primer	Reverse primer
Gdf15	NM_011819.3	GTCCAGAGGTGAGATTGGGG	CTTCAGGGGCCTAGTGATGTC
Ghrl	NM_021488.5	CCAGAAAGCCCAGCAGAGAAAG	ATGCCAACATCGAAGGGAGC
Hhip	NM_020259.4	ATACCACCAACCAGGAACGG	GGGGGTTTTTCCTGGATACTGT
Infg	NM_008337	CGGCACAGTCATTGAAAGCC	TGTCACCATCCTTTTGCCAGT
Il1b	NM_008361	GACCCCAAAAGATGAAGGGCT	ATGTGCTGCTGCGAGATTTG
Il10	NM_010548	GACAACATACTGCTAACCGACTC	ATCACTCTTCACCTGCTCCACT
Itgax	NM_021334.2	GCCACCAACCCTTCCTGGCTG	TTGGACACTCCTGCTGTGCAGTTG
Lcn2	NM_008491	GCCACTCCATCTTTCCTGTTG	AAGAGGCTCCAGATGCTCCTT
Lep	NM_008493	CCCTGTGTCGGTTCCTGTGGC	GCGGATACCGACTGCGTGTGT
Ncub2	NM_001360375.1	GTATCATCAGGCCGTCCAGC	CAAACTTCAGCTCTCCCGCT
Ocln	NM_001360536.1	GTCCTCCTGGCTCAGTTGAA	AGATAAGCGAACCTTGGCGG
Pck1	NM_011044.2	GGGCCGCTGGATGTCGGAAG	GGTGCGGCCTTTCATGCACC
Ppara	NM_011144	CAACCCGCCTTTTGTCATAC	CCTCTGCCTCTTTGTCTTCG
Ppargc1a	NM_008904.2	CCCAGAGTCACCAAATGACCCCA	CCTCTTGGTTGGCGGTGGCA
Pyy	NM_145435.1	GGCAGCGGTATGGAAAAAGA	CCACTGGTCCAAACCTTCTG
Rplp0	NM_007475	TCTGGAGGGTGTCCGCAACG	GCCAGGACGCGCTTGTACCC
Scd1	NM_009127.4	GCTCTACACCTGCCTCTTCGGGAT	TCCAGAGGCGATGAGCCCCG
Slc2a2	NM_031197.2	TCATGTCGGTGGGACTTGTG	CCCAAGGAAGTCCGCAATGT
Slc5a1	NM_019810.4	AGTGGGCTGTACCAACATCG	CAGGCCTCGCAGTCCATTAG
Srebp1	NM_011480	CTGGCTGAGGCGGGATGA	TACGGGCCACAAGAAGTAGA
Tbx1	NM_011532.2	CAAGGCAGGCAGACGAATGT	TACCGGTAGCGCTTGTCATC
Timp1	NM_011593	AGTGCCTGCAGCTTCTTGGT	CAGCCAGCACTATAGGTCTTTGAG
Tjp1	NM_009386.2	GGAGATGTTTATGCGGACGG	CCATTGCTGTGCTCTTAGCG
Tnfa	NM_013693	GTCCCCAAAGGGATGAGAAG	CACTTGGTGGTTTGCTACGA
Ucp1	NM_009463	TCAGGATTGGCCTCTACGAC	TGCATTCTGACCTTCACGAC

Supplementary Table 3. Western Blot antibodies.

Primary antibody	Residue	Supplier	Reference	Dilution
HSP90	-	Santa Cruz	sc-7947	1:1000
IRβ	-	Santa Cruz	sc-711	1:1000
PKBα	-	Upstate	07-416	1:1000
PKBβ	-	Upstate	07-372	1:1000
Phospho-PKB	Ser473	Cell Signaling	#9271	1:1000
UCP1	-	Abcam	ab10983	1:1000

Supplementary Table 4. FACS antibodies.

Target	Clone	Conjugate	Source	Identifier
B220	RA3-6B2	FITC	eBioscience	11-0452
B220	RA3-6B2	eF450	eBioscience	48-0452
CCR2	475301	APC	R&D Systems	FAB5538A
CD3e	17A2	APC	eBioscience	17-0032
CD4	GK1.5	PE-Cy7	eBioscience	25-0041
CD8a	53-6.7	APC-Cy7	Biolegend	100714
CD11b	M1/70	PE-Cy7	eBioscience	25-0112
CD11c	N418	BV421	Biolegend	117330
CD19	eBio1D3	eF450	eBioscience	48-0193
CD45	30-F11	BV785	Biolegend	103149
CD45.2	104	FITC	Biolegend	109806
F4/80	BM8	APC	eBioscience	17-4801
Ly6C	HK1.4	APC-Cy7	Biolegend	128025
NK1.1	PK136	PE	BD Biosciences	557391
Siglec-F	E50-2440	BV605	BD Biosciences	740388
Siglec-F	E50-2440	PE	BD Biosciences	552126
Other reagents			**Source**	**Identifier**
LIVE/DEAD™ Fixable Aqua Dead Cell Stain Kit			Invitrogen	L34957
Zombie UV™ Fixable Viability Kit			Biolegend	423107

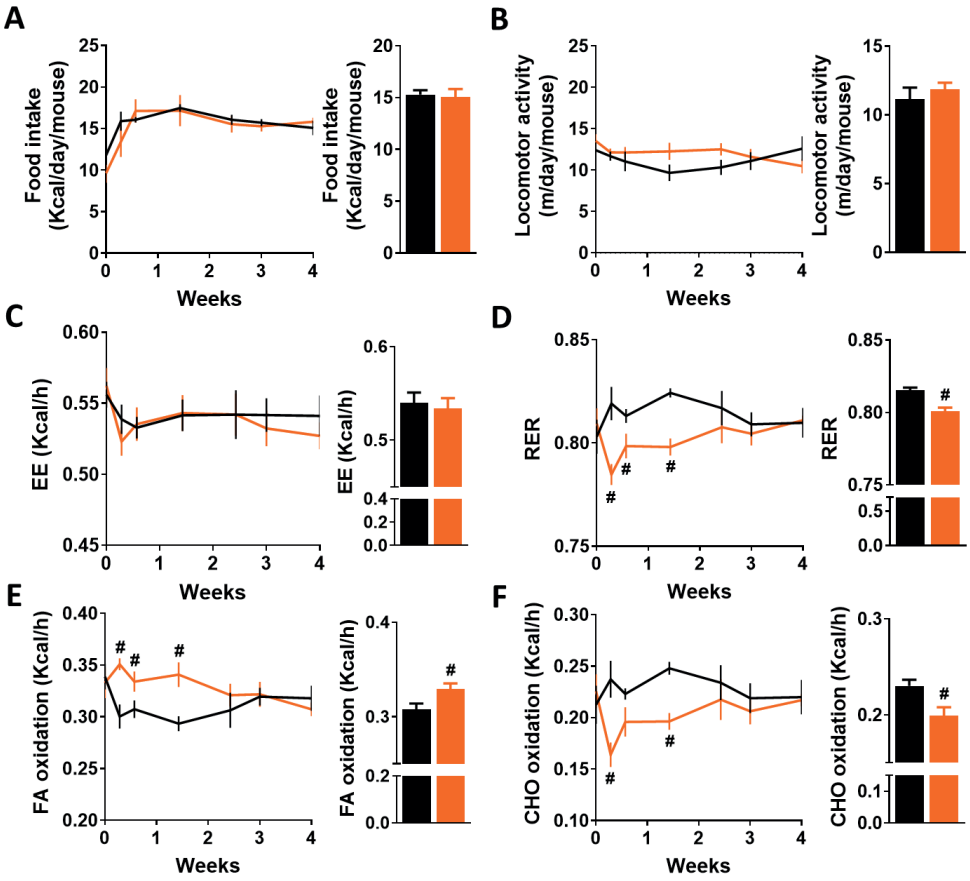

Supplementary Figure 1. Totum-63 does not affect food intake, locomotor activity and total energy expenditure, but promotes a shift towards fatty acid oxidation in obese mice. C57BL6/J mice were fed a HFD for 12 weeks and next transferred to individual metabolic cages. After 48 hours of acclimatization, mice received HFD supplemented or not with Totum-63 (2.7% w/w) for 4 weeks. (**A-B**) Food intake (*A*) and locomotor activity (*B*) were monitored throughout the study. (**C-F**) Oxygen consumption and carbon dioxide production were measured at 30 sec intervals and total energy expenditure (EE, *C*), respiratory exchange ratio (RER, *D*), and fatty acid (FA, *E*) and carbohydrate (CHO, *F*) oxidation rates were calculated, and the averaged data during 4 weeks were shown. Results are expressed as mean ± SEM. # P ≤ 0.05 *vs* HFD (n=8 mice per group from 2 independent experiments).

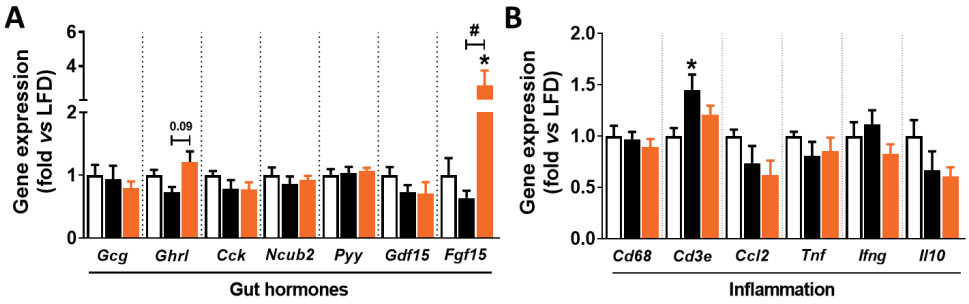

Supplementary Figure 2. Totum-63 does not affect the gene expression of main gut hormones and inflammatory markers in ileum from obese mice. LFD- and HFD-fed C57BL6/J mice were treated as described in the legend of Figure 1. (**A-B**) The expression of key genes involved in gut hormone synthesis (*A*) and inflammation (*B*) was measured in the ileum section of the intestine by RT-qPCR. Results are expressed as mean ± SEM. * P ≤ 0.05 *vs* LFD, # P ≤ 0.05 *vs* HFD (n=5-6 mice per group).

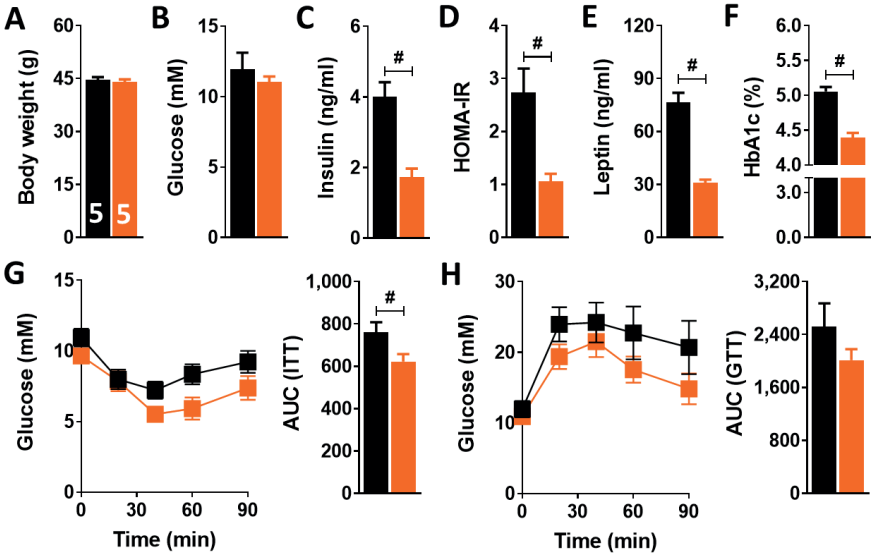

Supplementary Figure 3. Totum-63 improves metabolic homeostasis in obese mice independently of its effect on body weight. (**A**) C57BL6/J obese mice on HFD supplemented with Totum-63 (T63, 2.7% w/w; orange squares/bars) or not (control; black squares/bars) were weight-paired after 4 weeks of supplementation. (**B-F**) Fasting blood glucose (*B*) and HbA1c (*F*) levels together with plasma insulin (*C*) and leptin (*E*) levels, and HOMA-IR (*D*) were determined. (**G-H**) Intraperitoneal ITT (*G*) and GTT (*H*) were performed and the respective AUC calculated, as described in the legend of Figure 3. Results are expressed as mean ± SEM. * P ≤ 0.05 *vs* LFD, # P ≤ 0.05 *vs* HFD (n=5 mice selected per group from 2 independent experiments).

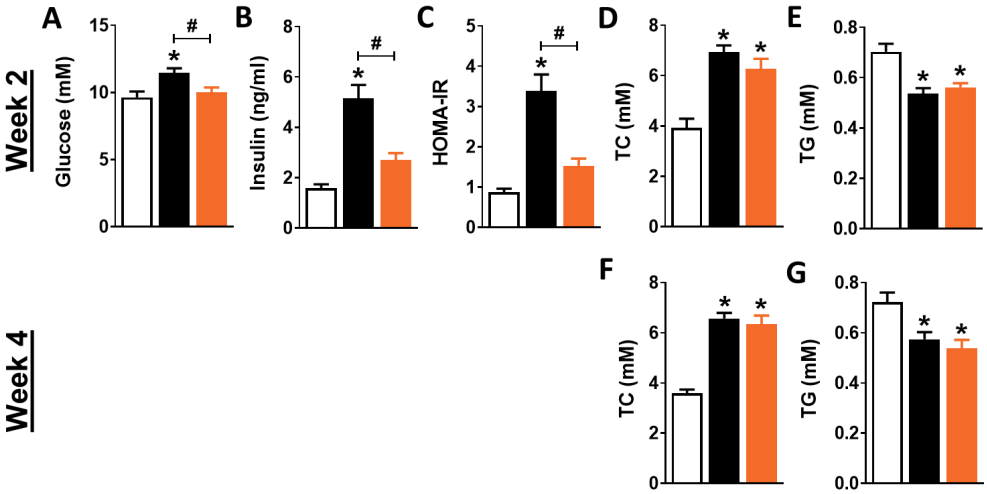

Supplementary Figure 4. Totum-63 reduces hyperglycemia and hyperinsulinemia already after 2 weeks but does not affect plasma TC and TG levels in obese mice. LFD- and HFD-fed C57BL6/J mice were treated as described in the legend of Figure 1. (**A-C**) Fasting blood glucose (*A*) and plasma insulin (*B*) levels were measured at week 2 of supplementation and used to calculate the HOMA-IR (*C*). (**D-G**) Fasting plasma total cholesterol (TC, *D,F*) and triglycerides (TG, *E,G*) were also determined at week 2 (*D-E*) and 4 (*F-G*). Results are expressed as mean ± SEM. * P ≤ 0.05 *vs* LFD, # P ≤ 0.05 *vs* HFD (n=10-12 mice per group from 2 independent experiments).

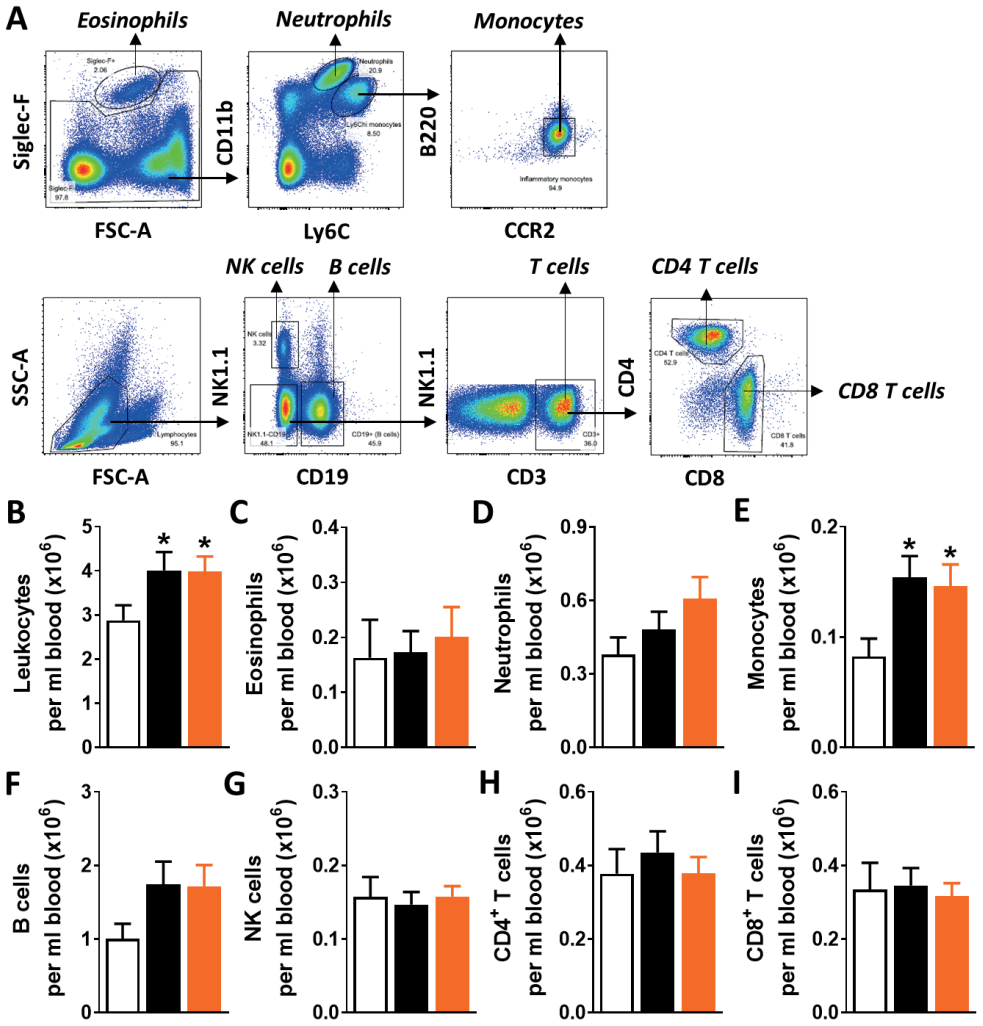

Supplementary Figure 5. Totum-63 does not affect blood immune cell subsets in obese mice. LFD- and HFD-fed C57BL6/J mice were treated as described in the legend of Figure 1. (**A**) The gating strategy for analysis of blood eosinophils, neutrophils, monocytes, NK cells, B cells, and CD4/CD8 T cells is shown for a representative sample. Isolated cells were pre-gated on $CD45^+$ single cells. (**B-I**) The blood levels of $CD45^+$ leukocytes (*B*), monocytes (*C*), neutrophils (*D*), eosinophils (*E*), B cells (*F*), NK cells (*G*), CD4 T cells (*H*) and CD8 T cells (*I*) were determined by flow cytometry. Results are expressed as mean ± SEM. * $P \leq 0.05$ *vs* LFD, # $P \leq 0.05$ *vs* HFD (n=4-6 mice per group).

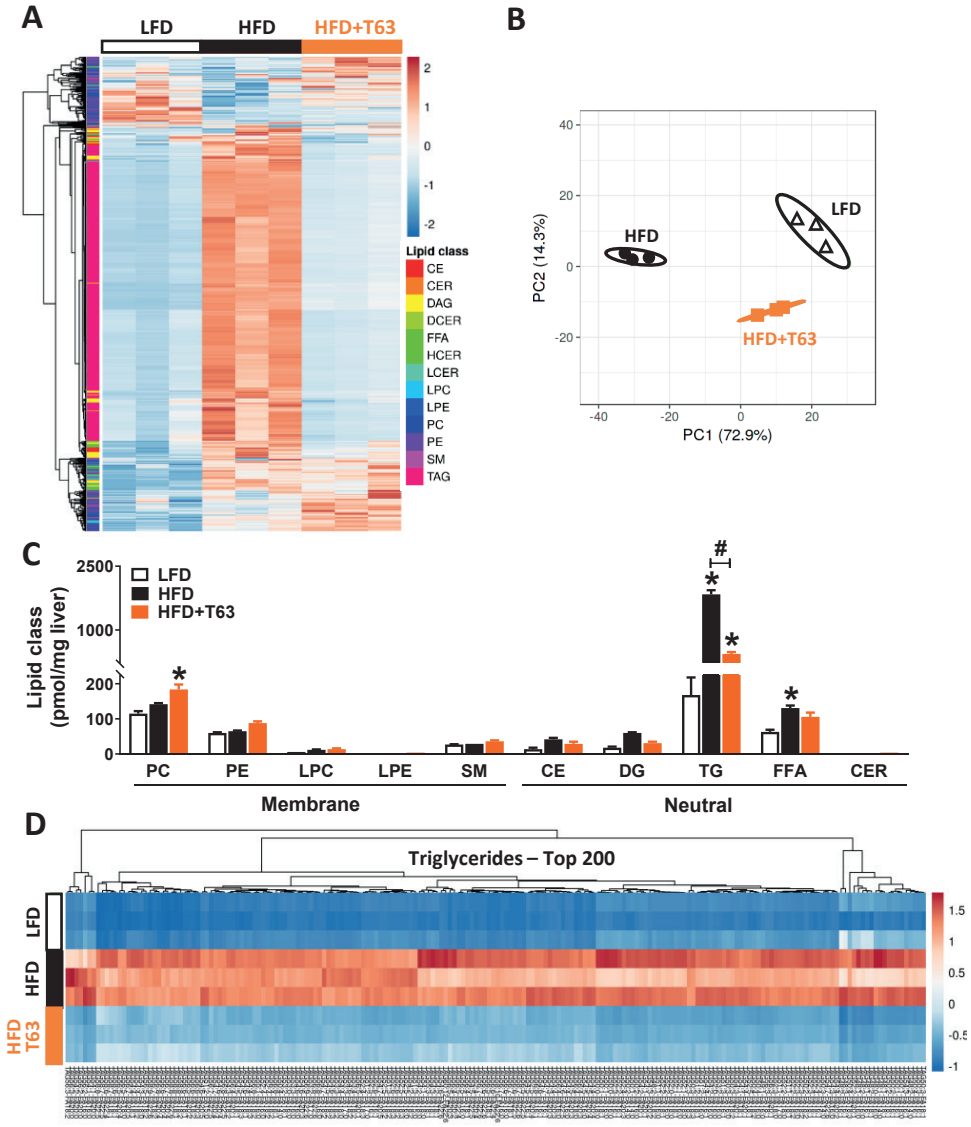

Supplementary Figure 6. Totum-63 reduces accumulation of hepatic triglyceride species in obese mice. LFD- and HFD-fed C57BL6/J mice were treated as described in the legend of Figure 1. (**A-D**) At sacrifice, a piece of liver was collected and freeze-clamped. After lipid extraction, the hepatic lipid species concentrations were quantified by targeted lipidomics using the Lipidyzer platform. The heatmap (*A*) and PCA plot (*B*) depicting the effect of T63 on >800 individual lipid species are shown. The levels of the individual lipid species were summed up for each lipid class (*C*) and the heatmap for the top 200 triglyceride species expressed is shown (*D*). PC, Phosphatidylcholine; PE, Phosphatidylethanolamine; LPC, Lysophosphatidylcholine; LPE, Lysophosphatidylethanolamine; SM, Sphingomyelin; CE, Cholesterylester; DG, Diglycerides; TG, Triglycerides; FFA, Free-fatty acids; CER, Ceramides. Results are expressed as mean ± SEM. * P ≤ 0.05 *vs* LFD, # P ≤ 0.05 *vs* HFD (n=3 mice per group).

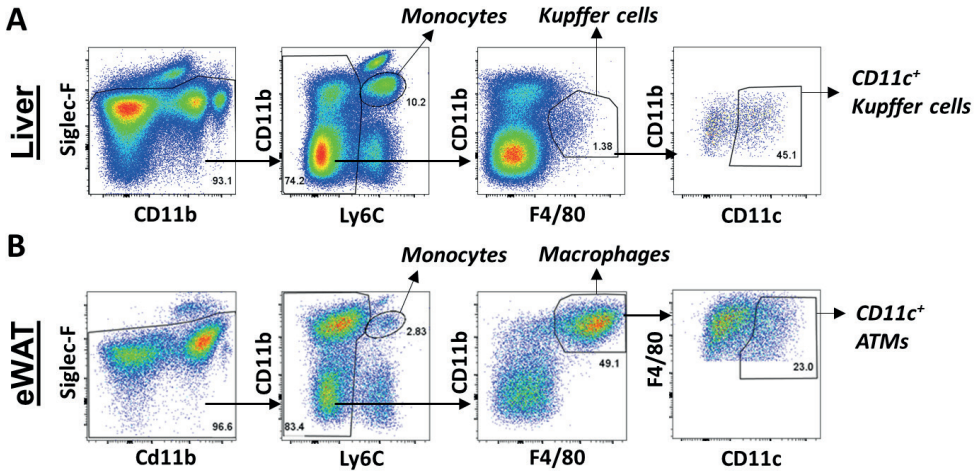

Supplementary Figure 7. Gating strategies for liver and adipose tissue immune cell phenotyping. (**A-B**) Isolated cells from liver (*A*) or eWAT (*B*) were pre-gated on Aqua^{-}CD45^{+} single cells. The gating strategy for analysis of monocytes, Kupffer cells (KC)/adipose tissue macrophages (ATMs) and CD11c^{+} KC/ATMs is shown for a representative sample.

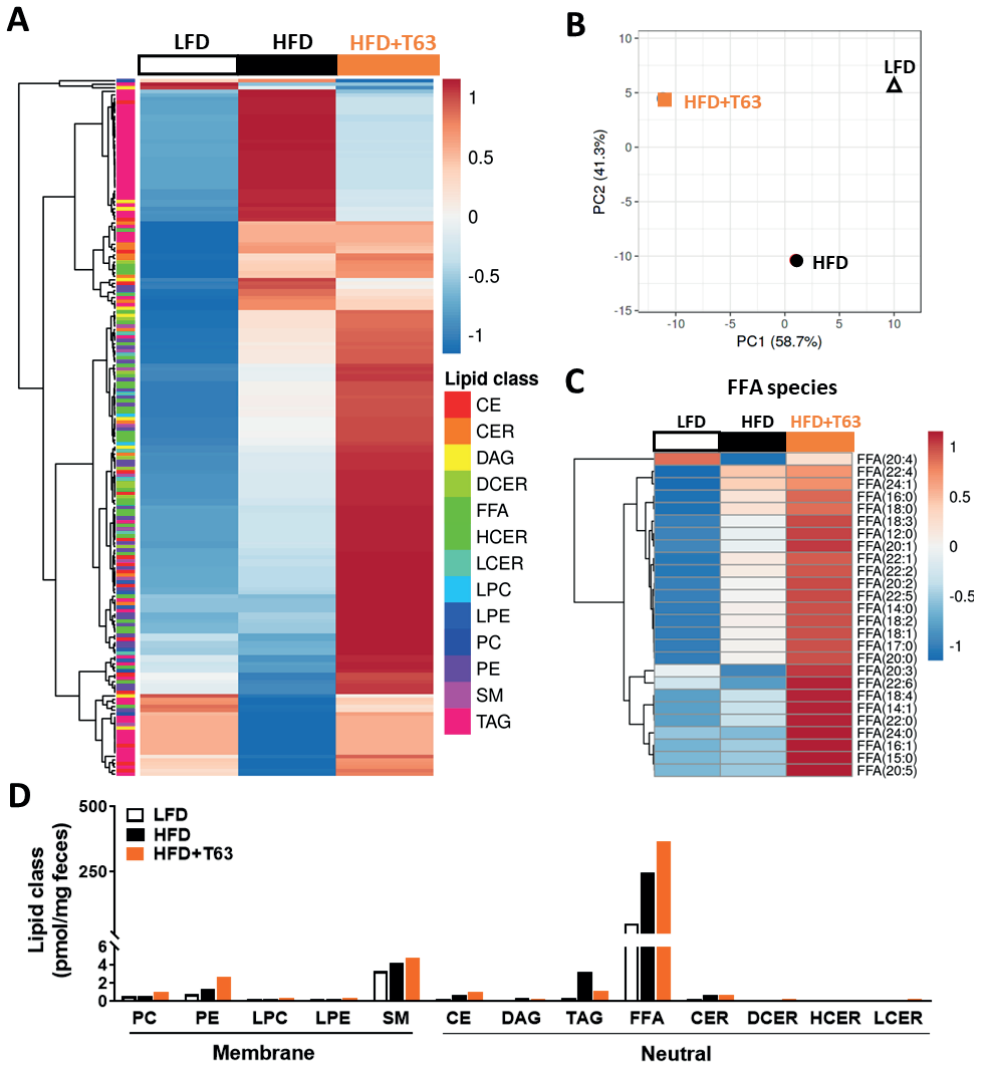

Supplementary Figure 8. Feces lipid composition from obese mice is affected by Totum-63. LFD- and HFD-fed C57BL6/J mice were treated as described in the legend of Figure 1. (**A-D**) Overnight-produced feces were collected and freeze-clamped. After lipid extraction, the feces lipid species concentrations were quantified by targeted lipidomics using the Lipidyzer platform. The heatmap (*A*) and PCA plot (*B*) depicting the effect of T63 on >800 individual lipid species are shown. The heatmap for the free fatty acid species expressed is shown (*C*) and the individual lipid species were summed up for each lipid class (*D*). PC, Phosphatidylcholine; PE, Phosphatidylethanolamine; LPC, Lysophosphatidylcholine; LPE, Lysophosphatidylethanolamine; SM, Sphingomyelin; CE, Cholesterylester; DG, Diglycerides; TG, Triglycerides; FFA, Free-fatty acids; CER, Ceramides. Results are data from pooled feces per group (n=3-4 cages per group).

CHAPTER 9

Summarizing discussion and future perspectives

Summarizing discussion

The work presented in this thesis aimed to contribute to a better understanding of the mechanisms responsible for the immunological control of metabolic homeostasis. In addition, the potency and underlying mechanisms of (helminth-derived) immunomodulatory molecules for alleviating obesity-induced metaflammation, insulin resistance and metabolic dysfunctions were investigated. This chapter summarizes the main findings and discusses these results in a broader perspective.

What was known about immunological control of metabolic homeostasis?

A plethora of evidence currently supports that chronic low-grade inflammation in insulin target tissues, *i.e.* adipose tissues, cardiac and skeletal muscle, liver and pancreas, contributes to the development of insulin resistance and type 2 diabetes (1, 2). Such control of tissue and whole-body metabolism by the immune system is one of the central themes in the emerging field of immunometabolism.

Increased expression of the inflammatory cytokine tumor necrosis factor (TNF) in obese white adipose tissue (WAT), which was found to induce insulin resistance by inhibiting canonical insulin signaling, was one of the landmark discoveries that fueled the interest in immunometabolism (3, 4). Additionally, macrophages were found to accumulate in obese WAT and account for the majority of TNF production, along with other proinflammatory mediators such as inducible nitric oxide synthase (iNOS) and interleukin (IL)-6 (5, 6). These adipose tissue macrophages (ATMs) were shown to express increased levels of the integrin CD11c and to predominantly localize around necrotic adipocytes in so-called crown-like structures (7-10), likely protecting their environment from lipotoxicity through lysosomal exocytosis and digestion of apoptotic/necrotic adipocytes (11). Conceivably, the flip side of this protective mechanism is inflammatory activation of ATMs (12), contributing to increased cytokine and chemokine production, immune cell recruitment, and the generation of a vicious circle that exacerbates inflammation and insulin resistance. Indeed, genetic manipulation to inhibit the monocyte chemoattractant protein 1 (MCP-1)-CCR2-axis, which coordinates circulating monocyte recruitment into tissues, alleviates inflammation and insulin resistance (13, 14). In the liver, activation of the liver-resident macrophages (Kupffer cells; KCs) and recruitment of monocytes that develop into proinflammatory monocyte-derived KCs (MoKCs) have also been demonstrated to drive the pathogenesis of non-alcoholic fatty liver disease (NAFLD) and progression towards non-alcoholic steatohepatitis (NASH) (15-17). Although the contribution of macrophages to the etiology

and pathogenesis of insulin resistance, NAFLD/NASH and type 2 diabetes has been well-established, other immune cells were also shown to accumulate in adipose tissue and liver during obesity (2). The underlying mechanisms responsible for deterioration of metabolic homeostasis by both macrophages and other immune cells are still incompletely resolved, and dissecting such mechanisms may provide novel therapeutic leads.

How did our studies advance the field?

Elucidating some of the processes involved in the regulation of proinflammatory macrophage activation may provide therapeutic leads to combat obesity-induced metabolic disorders. Immune cell function is increasingly recognized to be dictated by cellular metabolism (18). The cytosolic enzyme ATP citrate lyase (Acly) was recently shown to link cellular metabolism to inflammatory responses in LPS-activated macrophages (19). By converting mitochondrial-exported citrate resulting from increased glycolytic flux into oxaloacetate and acetyl-CoA, Acly provides metabolic intermediates allowing biosynthesis of fatty acids and cholesterol, as well as histone acetylation to regulate gene expression (19-21). Acly-deficient BMDMs were previously shown to exhibit enhanced LPS-induced cytokine production and surface marker expression, indicative of proinflammatory activation (22). Hence, in **chapter 2**, we studied the consequence of myeloid Acly-deficiency in the context of inflammatory disorders, including metaflammation. We confirmed that LPS treatment of Acly-deficient BMDMs indeed promoted a proinflammatory transcriptomic signature when compared to control BMDMs. Surprisingly, neither acute LPS-induced peritonitis, experimental autoimmune encephalomyelitis nor obesity-induced metabolic dysfunctions and metaflammation were significantly affected by myeloid Acly deficiency, indicating that the proinflammatory transcriptomic signature observed *in vitro* did not translate into worsening of inflammatory disorders *in vivo* (**Figure 1A**).

Acly was previously shown to link metabolism to inflammatory responses in LPS-stimulated macrophages by supporting histone acetylation and proinflammatory gene transcription (19, 21). These studies utilized small interfering RNAs for Acly knockdown *in vitro* or small molecule Acly inhibitors to study the role of Acly in macrophage biology, which may generate different outcomes when compared to constitutive genetic deletion of Acly. For example, Acly-deficient BMDMs may rewire cellular metabolism to rescue defects in cholesterol biosynthesis and lipogenesis (22). These processes are fueled by acetyl-CoA generated by Acly, and Acly-deficient BMDMs indeed displayed deregulated cholesterol metabolism. However, total cholesterol content was unchanged, indicating Acly-deficient macrophages employ strategies to compensate for the loss of Acly-derived acetyl-CoA. In

support of this, differentially regulated genes in Acly-deficient BMDMs compared with control BMDMs indicated an upregulation of genes involved in cholesterol biosynthesis and import, while cholesterol efflux genes were downregulated. In addition, acyl-coenzyme A synthetase short-chain family member 2 (*Acss2*), converting acetate into acetyl-CoA, was upregulated in Acly-deficient BMDMs, suggesting that this pathway may contribute to maintenance of acetyl-CoA levels in the absence of Acly (22). Hence, constitutive deletion of Acly may rewire cells to rescue the metabolic perturbation, which may explain the discrepancies between using small molecule Acly inhibitors and genetic deletion of Acly on macrophage inflammation *in vivo*. Of note, we found that *Acly* expression was upregulated in adipose tissue macrophages from obese mice, leading to speculate that Acly may play a role in obesity-induced proinflammatory activation of adipose tissue macrophages. Future studies could benefit from the use of inducible, macrophage-specific knockout models, such as the tamoxifen-inducible *Lyz2*$^{\text{Cre-ERT2}}$, or the *Cx3cr1*$^{\text{Cre-ERT2-IRES-YFP}}$ mouse model used in **chapter 7**.

Macrophages express a plethora of cell surface receptors that sense perturbations in the microenvironment, enabling their maintenance of homeostasis (23, 24). One of these receptors, the mannose receptor (MR/CD206), is a C-type lectin receptor that recognizes molecular patterns for internalization, processing and cross-presentation of antigens (25, 26). Interestingly, the MR can be proteolytically cleaved from the membrane and released as a soluble form (27, 28), which was recently shown to correlate with the pathogenesis of diverse inflammatory diseases (29-33). The effects of the MR and its soluble form (sMR) on proinflammatory macrophage activation in the context of metaflammation was studied in **chapter 3**. Here, we demonstrated that sMR reprogrammed mouse BMDMs and human monocyte-derived macrophages towards a proinflammatory phenotype *in vitro*. By binding to and inhibiting the phosphatase and pan-leukocyte marker CD45, sMR initiated a novel Src-Akt-NF-κB-mediated signaling pathway that resulted in proinflammatory cytokine production. sMR serum levels were increased in obese mice and humans, and correlated with adiposity. Strikingly, whole-body MR-deficient mice were completely protected against high fat diet (HFD)-induced hepatic steatosis, insulin resistance and glucose intolerance, which was associated with decreased CD11c-expressing obesity-associated macrophages that correlated with insulin resistance. Lastly, we found that treatment of lean, MR-sufficient mice with sMR increased insulin resistance and promoted proinflammatory activation of adipose tissue macrophages, unequivocally demonstrating a role for sMR in proinflammatory macrophage activation in the context of metaflammation (**Figure 1B**). These results and additional roles of the MR and other C-type lectins in regulating inflammation were reviewed in-depth in a broader context in **chapter 4**.

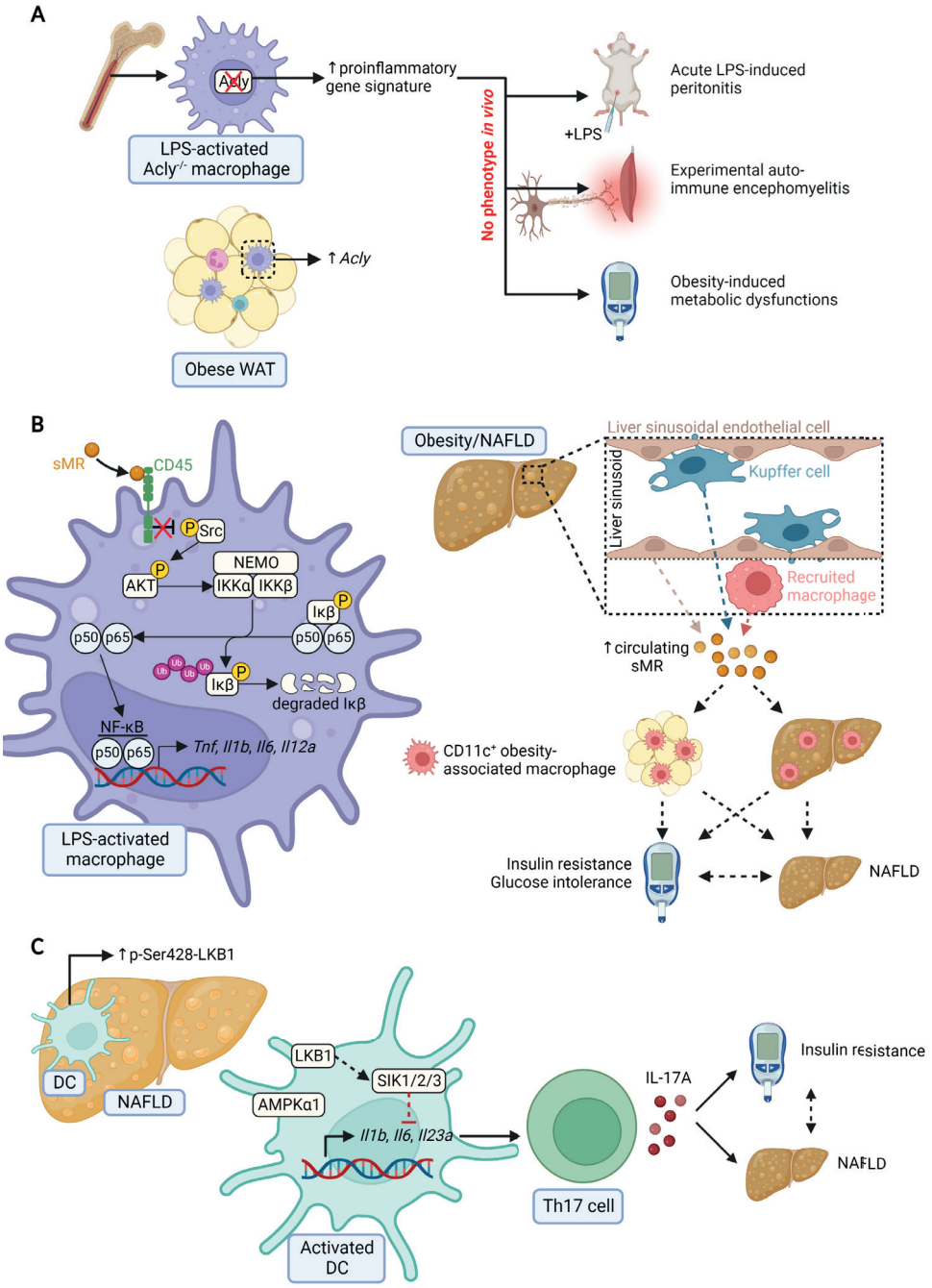

Figure 1. Mechanisms of immunological control of metabolic homeostasis. (**A**) Graphical summary of chapter 2. LPS-activated Acly-deficient bone marrow-derived macrophages (BMDMs)

Figure 1. Continued

display a proinflammatory gene signature compared to WT control BMDMs. However, myeloid Acly deletion did not impact acute LPS-induced peritonitis, experimental autoimmune encephalomyelitis and obesity-associated metabolic dysfunctions, although Acly was upregulated in adipose tissue macrophages of obese WT mice. (**B**) Graphical summary of chapter 3. Soluble mannose receptor (sMR) interacts with CD45 on the surface of macrophages, inhibiting its phosphatase activity. This enables Src-AKT-NF-κB-mediated signaling to promote proinflammatory macrophage activation and production of TNF, IL-1β, IL-6 and IL-12. Obesity increases circulating sMR levels, associated with increased CD11c-expressing obesity-associated macrophages in WAT and liver, which correlated with insulin resistance and glucose intolerance. Liver sinusoidal endothelial cells represent the majority of MR-expressing cells, while obesity increased MR-expressing macrophages in the liver. (**C**) Graphical summary of chapter 5. Obesity increased LKB1 phosphorylation at Serine428 in hepatic dendritic cells (DCs). LKB1 limits Th17 polarizing cytokine expression in DCs, potentially through SIK. In addition, LKB1 limits IL-17A+ Th17 cells in vivo, thereby controlling insulin resistance and NAFLD. Created with BioRender.com.

The MR is expressed by macrophages, DCs and endothelial cells (34). We show that liver sinusoidal endothelial cells constitute the majority of cells expressing the MR in metabolic tissues, yet MR-expressing macrophage numbers were increased particularly in livers of obese mice. Hence, one of the hypotheses is that obesity-induced liver macrophages are the main source of increased serum sMR in obesity, yet this remains to be verified. Unfortunately, no conditional knockout model for MR is available to date. Future studies could, however, rely on adoptive transfer of MR-deficient bone marrow to irradiated, MR-sufficient acceptor mice to address whether hematopoietic cells are the source of increased sMR in obesity.

Local increased expression and shedding of sMR might act in an autocrine fashion to promote proinflammatory macrophage activation and deteriorate insulin resistance. MR shedding is regulated by currently unidentified metalloproteases, and appears to occur constitutively as sMR levels in supernatant positively correlate with MR expression of cells in culture (27, 28). In this regard, it is worth noting that MR expression is regulated by PPAR-γ (35), a transcription factor that regulates expression of genes involved in glucose and lipid metabolism, and has been shown to be upregulated in both lipid-associated hepatic and WAT macrophages (36, 37). Strikingly, a recent study demonstrated that a novel subset of MR-expressing KCs is increased in steatotic livers of HFD-fed mice (38). These KCs display transcriptomic features of lipid metabolism and contribute to NASH pathogenesis at least partly through the fatty acid transporter CD36. As such, one may speculate that obesity could result in PPAR-γ-mediated upregulation of MR expression and shedding by lipid-associated macrophages in metabolic tissues, contributing to insulin resistance. Yet, given the beneficial effects of PPAR-γ agonists on whole-body insulin sensitivity (39), and the contribution of PPAR-γ to alternative activation of macrophages (40), this is a paradoxical

and challenging hypothesis that requires follow-up research. Alternatively, obesity was demonstrated to impact the expression of metalloproteinases in metabolic tissues (41), which may also contribute to increased MR shedding and warrants further studies.

Although we provide evidence for a role of sMR in proinflammatory macrophage activation and metaflammation through both loss-of-function experiments and exogenous administration of sMR, its *in vivo* cellular and molecular mechanisms are yet to be established. We demonstrated that sMR-mediated inflammatory reprogramming of macrophages is dependent on the interaction of sMR with CD45, which is expressed by macrophages but also other immune cells. Interfering with this interaction may provide clues to underlying mechanisms. For this, antibody-mediated neutralization or targeted mutagenesis of the region of CD45 interacting with sMR could be envisaged, although this first requires in-depth characterization of the sMR-CD45 molecular synapse. In addition, development of a CD45 conditional knockout model to delete CD45 from macrophages or other immune cells is of interest. Of note, after publication of our manuscript, an independent study demonstrated that MR-expressing adipose tissue macrophages in humans positively correlated with markers of metabolic dysfunctions, *i.e.* HbA1c, fasting blood glucose and criteria for metabolic syndrome (42). Moreover, these MR-expressing macrophages were enriched in visceral adipose tissue of obese, type 2 diabetics compared to both lean and obese non-diabetic humans, supporting a role for MR-expressing macrophages in contributing to metaflammation also in humans. Altogether, we propose that inhibiting sMR release, neutralizing sMR or interfering with the sMR-CD45 molecular synapse may hold promise to alleviate metaflammation and other inflammatory diseases.

Besides a well-established role for macrophages in the etiology of metaflammation, DCs also accumulate in metabolic tissues and contribute to insulin resistance (43-45). DCs are specialized antigen presenting cells that govern T cell responses depending on the inflammatory and metabolic microenvironment (46, 47). Indeed, T cell subset abundances were reported to change in metabolic tissues during obesity (48), indicative of altered DC function. The nutrient sensor liver kinase B1 (LKB1) was recently shown to control DC-mediated immune homeostasis and T cell priming in the context of allergic asthma and tumor development (49-51). In **chapter 5**, we report that Ser428-LKB1 phosphorylation is increased in hepatic DCs from obese mice, and that deletion of LKB1 from DCs increased HFD-induced hepatic steatosis, insulin resistance and glucose intolerance in obese mice. These metabolic perturbations were associated with increased regulatory T cells (Tregs) and T helper 17 (Th17) cells particularly in the liver, and were rescued through antibody-mediated neutralization of the canonical Th17 cytokine IL-17A. Indeed, LKB1-deficient DCs displayed increased expression of the Th17-polarizing cytokines IL-6, IL-1β and IL-23,

suggesting increased Th17 priming by LKB1-deficient DCs in line with previous work (51). Taken together, we identified LKB1 as a repressor of pathogenic Th17 cell priming in the liver, thereby controlling whole-body metabolic homeostasis (**Figure 1C**).

The tumor suppressor LKB1 is a serine/threonine kinase that controls cell polarity, growth and metabolism (52) by phosphorylating and activating AMP-activated protein kinase (AMPK) and 12 other AMPK-related kinases (53, 54). LKB1 activates AMPK in low-nutrient conditions, and its effects on cellular metabolism has been studied extensively in multiple *in vitro* and *in vivo* models (55). However, although reduced phosphorylation of the AMPK target acetyl-CoA carboxylase (ACC) was previously shown in LKB1-deficient splenic DCs (50), we show that increased Treg and Th17 priming as well as aggravated metabolic dysfunctions in LKB1-deficient obese mice was independent of AMPK. Instead, using pharmacological inhibitors in bone marrow DCs, we provide evidence for involvement of the LKB1 downstream salt-inducible kinase (SIK) family in repressing expression of the Th17-polarizing cytokines IL-6, IL-1β and IL-23. The SIK family consists of three isoforms (SIK1-3) and is involved in regulating gluconeogenesis, lipid metabolism and tumorigenesis (56). Interestingly, activation of SIKs retains class IIa histone deacetylases (HDACs) and cAMP-regulated transcriptional coactivators (CRTCs) in the cytoplasm, thereby either promoting or inhibiting transcription, respectively (57). CRTCs are coactivators of the transcription factor cAMP response element-binding protein (CREB) (58). The promotors of *Il6*, *Il1b* and *Il23a* genes all contain CREB binding sites (59-61), which leads to speculate that the absence of SIK activation in LKB1-deficient DCs may promote nuclear translocation of CRTCs and enhanced CREB-dependent *Il6*, *Il1b* and *Il23a* expression. Supporting this, SIK1 and SIK3 deficiencies were both reported to increase IL-6 production in tumor cells (62), and IL-6 and IL-1β production in immortalized Raw264.7 macrophages (63). However, SIK inhibition was also reported to inhibit TLR-induced proinflammatory cytokine production in macrophages and DCs (64, 65). As such, investigating whether SIK inhibition indeed increases nuclear translocation of CRTCs, thereby promoting Th17 polarization, would definitely be of interest. In addition, future transgenic studies are also required to identify the SIK isoforms involved in regulating Th17-polarizing cytokine expression in DCs. However, deleting individual SIK isoforms revealed that SIK family members display functional redundancy in some settings (57). Identification of the isoform involved may thus require the development of a DC-specific, inducible triple knockout (SIK1/2/3) model, which is currently not available and would be difficult to achieve. Finally, it is necessary to confirm that increased Th17-polarizing cytokine expression after SIK inhibition or deletion indeed results in polarization of Th17 cells *in vivo*, for instance via adoptive transfer of DCs that were *ex vivo* pulsed with a SIK inhibitor.

The composition of the cytokine milieu in which Th17 differentiation takes place was shown to determine pathogenicity of the effector Th17 cells, where the presence of IL-6, IL-1β and IL-23

promoted the development proinflammatory Th17 cells (66, 67). As we found increased expression of these cytokines in LKB1-deficient DCs, the increased Th17 cells in the livers of these mice are likely pathogenic in the context of obesity. However, the phenotype of these Th17 cells and underlying mechanisms for promoting hepatic steatosis and insulin resistance are still unclear. Since antibody-mediated neutralization of IL-17A in $CD11c^{\Delta LKB1}$ mice rescued metabolic perturbations, the Th17 effector cytokine IL-17A likely plays a role. Indeed, Th17 cells and IL-17A signaling have previously been shown to impair whole-body insulin sensitivity and drive hepatic steatosis (68-71). Mechanistically, IL-17A was suggested to either exert its effects on hepatocytes directly (68, 69), or signal through the IL-17RA on myeloid cells (71) to increase insulin resistance and hepatic steatosis. Recent single-cell transcriptomic analysis of Th17 cells in the liver identified an obesity-induced inflammatory hepatic Th17 (ihTh17) cell subset with increased expression the surface receptor CXCR3 and co-expression of the inflammatory cytokines IL-17A, interferon (IFN)γ and TNF (72). Here, the ihTh17 cells exacerbated NAFLD pathogenesis, which was at least partly dependent on their IFNγ-expression and increased glycolysis. Although in our settings the Th17 cells induced by LKB1-deficient DCs did not co-express IFNγ (data not shown), it would be interesting to investigate similarities with the ihTh17 phenotype by mapping the transcriptomic signature of ihTh17 cells onto transcriptomic data of hepatic Th17 cells of $CD11c^{\Delta LKB1}$ mice (73). This could be done by either performing single cell RNA sequencing of total liver leukocytes or bulk RNA sequencing on sorted Th17 cells from livers of $CD11c^{\Delta LKB1}$ mice.

Obesity increased Ser428-LKB1 phosphorylation in hepatic DCs. Although many posttranslational modifications of LKB1 have been identified, how these modifications affect LKB1 activity is only beginning to be resolved (74). LKB1 phosphorylation at Ser428 (in mice) or Ser431 (in humans) is dependent on the upstream kinases p90 Ribosomal S6 Kinase (p90RSK), protein kinase A and protein kinase C (PKC)ζ, and has been reported to increase LKB1 nucleocytoplasmic translocation and phosphorylation of downstream AMPK-related kinases (75-78). However, the role of this phosphorylation site remains controversial, as AMPK-related kinase phosphorylation by LKB1 has been reported to be normal in multiple tissues from homozygous knockin mice in which Ser431 is mutated to alanine (79). We currently cannot explain why and how Ser428-LKB1 phosphorylation is increased in hepatic DCs from obese mice, and what the exact functional consequence is, *i.e.* whether kinase activity and/or subcellular localization is altered. Still, we may hypothesize that this posttranslational modification constitutes a compensatory mechanism to limit pathogenic Th17 cell priming. While Ser428-LKB1 phosphorylation was increased in hepatic DCs from obese mice, it was unaltered in splenic and adipose tissue DCs, suggesting obesity-induced changes in the hepatic microenvironment that may alter LKB1 activation and DC effector functions. Obesity compromises the intestinal barrier function, resulting in increased gut permeability and altered serum metabolome (80). As

a result, increased transport of gut-derived bacterial products through the mesenteric and portal veins first targets the liver through a gut-liver axis. Indeed, LPS injection was previously reported to increase Ser428-LKB1 phosphorylation in whole lung and liver lysates, and in Raw264.7 macrophages (81). In addition, sodium butyrate, an indigestible fiber that is metabolized by the gut microbiome, was also demonstrated to increase Ser428-LKB1 phosphorylation in an *in vitro* model of hepatocytes (82), supporting that gut-derived metabolites may increase pLKB1 in hepatic resident cells. Obesity-induced gut permeability and/or metabolic endotoxemia might thus explain increased pLKB1 selectively in hepatic DCs. Future studies are required to elucidate the upstream molecular mechanisms that increase Ser428-LKB1 phosphorylation in hepatic DCs from obese mice. Interestingly, although obesity increased pLKB1 in hepatic DCs, phosphorylation of the AMPK downstream target ACC was unchanged, supporting AMPK-independent effects of LKB1 in DCs. Whether this increase in pLKB1 indeed results in downstream SIK-mediated repression of Th17-polarizing cytokines is currently unknown. In sum, we identified LKB1 as a regulator of DC function that empowers DC-mediated control of metabolic homeostasis. Targeting the LKB1-SIK axis in DCs may thus constitute a novel therapeutic approach for alleviating obesity-induced metabolic dysfunctions.

Altogether, our work identified novel mechanisms of myeloid cell-mediated control of whole-body metabolic homeostasis, that may present new therapeutic targets for treating metaflammation.

Box: Summary of main findings

- Myeloid Acly expression controls proinflammatory macrophage activation *in vitro*, without affecting acute peritonitis, chronic encephalomyelitis and metaflammation models *in vivo* (**chapter 2**)
- A soluble form of the mannose receptor (sMR) reprograms macrophages towards a proinflammatory phenotype by interacting with CD45 and a novel Src/Akt/NK-κB-mediated signaling pathway (**chapter 3**)
- MR-deficient mice are protected against HFD-induced hepatic steatosis, insulin resistance and glucose intolerance, associated with reduced proinflammatory macrophages in metabolic tissues (**chapter 3**)
- Serum sMR levels correlate with adiposity in both mice and humans, and sMR promotes metaflammation as well as obesity-induced metabolic dysfunctions (**chapter 3**)
- Mice with LKB1-deficient DCs develop worse insulin resistance, glucose intolerance and hepatic steatosis upon HFD feeding, which is dependent on the canonical Th17 cytokine IL-17A (**chapter 5**)
- LKB1 limits LPS-induced expression of Th17-polarizing cytokines IL-6, IL-1β and IL-23 in bone marrow DCs, potentially through its downstream target SIK (**chapter 5**)

What was known about immunomodulatory molecules and obesity-induced metabolic dysfunctions?

Obesity-induced metaflammation could be seen as a protective mechanism of physiologic inflammation that aims to prevent tissue damage and/or restore homeostasis (83), but ultimately fails and promotes chronic low-grade inflammation. Indeed, apart from its role in defense against pathogens, the immune system is increasingly recognized to support tissue function and control homeostasis (83, 84). Lean, insulin-sensitive adipose tissue is populated by type 2 innate lymphoid cells (ILC2s), T helper 2 (Th2) cells, eosinophils and alternatively activated macrophages (AAMs) (2). These cells, belonging to type 2 immunity, display a self-maintaining network through production of the type 2 cytokines IL-4, IL-5 and IL-13 that culminates in the alternative activation of macrophages (85-87). These AAMs are thus considered the effector type 2 immune cells in lean adipose tissue that control insulin sensitivity (2), although the underlying molecular mechanisms are not fully understood. In the liver, IL-4 and IL-13-mediated signaling, engaging their downstream transcription factors STAT6 and/or STAT3, have also been shown to increase glucose oxidation, decrease gluconeogenesis and reduce hepatic steatosis (88-90). Although the homeostatic type 2 immune network in liver of lean individuals is ill-defined, these findings suggest that type 2 immunity plays a significant role in the control of metabolic homeostasis both in adipose tissue and the liver. During obesity, these type 2 immune cells are lost, thus it is tempting to speculate that restoring type 2 immunity in obese metabolic tissues may reinstall tissue homeostasis and improve insulin sensitivity. Parasitic helminths are the strongest natural inducers of type 2 immunity, characterized by tissue eosinophilia, production of type 2 cytokines, Th2 cells and alternative activation of macrophages (91). As such, helminths and their immunomodulatory molecules have gained considerable interest as a potential resource to manipulate the immune system and combat insulin resistance (92). Indeed, cross-sectional studies conducted in helminth-endemic areas demonstrate an inverse correlation between helminth infection and metabolic dysfunctions (93-95). Experimental infection of obese mice has allowed for investigating isolated effects of helminth infection on metabolic homeostasis, showing that different helminth species induced type 2 immunity in metabolic tissues and alleviated metabolic dysfunctions in obese mice (85, 96-99). Importantly, our group and others have also shown that treatment of obese mice with helminth-expressed immunomodulatory molecules in a pathogen-free setting recapitulated these immunometabolic effects (97, 98, 100). However, hitherto there was little evidence for a causal role of helminth-induced type 2 immunity to increased insulin action. Altogether, harnessing immunomodulation to improve whole-body metabolic homeostasis is a promising and exciting area of research that may build on lessons learned from helminths (101).

How did our studies advance the field?

Helminth immunomodulatory molecules

As sentinels of homeostasis (23, 24), AAMs are believed to control insulin sensitivity in metabolic tissues (2). These AAMs are maintained through a type 2 immune axis involving ILC2s, Th2 cells and eosinophils (85-87). Obesity induces chronic low-grade inflammation in metabolic tissues, where these type 2 immune cells are lost and proinflammatory macrophages accumulate that contribute to insulin resistance (2). Exploiting the type 2 immunity-inducing properties of parasitic helminths and their immunomodulatory molecules (91) to improve obesity-associated metabolic complications has sparked an interesting line of research. **Chapter 6** provided an overview of the literature concerning the regulation of metabolic homeostasis by helminths and their molecules. Here, we discussed cross-sectional studies conducted in helminth-endemic areas showing an inverse correlation between helminth infection and metabolic dysfunctions (93-95, 102). In support of this correlation, deworming helminth-infected individuals using antihelminthic drugs increased proxies of systemic insulin resistance (102-104). Furthermore, we discussed that experimental infection of obese mice with different types of helminths improved whole-body metabolic homeostasis (85, 96-99, 105-107). In fact, our group has previously shown that both infection of obese mice with the helminth *Schistosoma mansoni*, but also treatment with the Th2-inducing soluble egg antigens (SEA) of *S. mansoni*, induced type 2 immunity in adipose tissue and liver, and improved whole-body glucose tolerance and insulin sensitivity (97). However, only few studies have described a dependency of metabolic effects to helminth-induced immunomodulation (105, 108). In **chapter 7**, we investigated the contribution of type 2 immunity to the metabolic effects of SEA using mice deficient for STAT6, a key transcription factor transducing canonical type 2 cytokines IL-4 and IL-13 signaling (109, 110). As expected, in obese *Stat6*$^{-/-}$ mice, SEA failed to induce the Th2-eosinophil-AAM axis in WAT that was observed in wildtype mice. Strikingly, the beneficial effect of SEA on whole-body glucose tolerance was lost in *Stat6*$^{-/-}$ mice, indicating that induction of type 2 immunity is required for the metabolic effects of SEA (**Figure 2A**). While this reinforces the paradigm that AAMs are the effector cells of a type 2 immune cascade that maintains insulin sensitivity, these data were obtained using a whole-body *Stat6*$^{-/-}$ mouse model and do not demonstrate a causal role for AAMs in the metabolic effects of SEA.

Infection of obese mice with the gastrointestinal helminth *Heligmosomoides polygyrus* was also shown to increase markers of type 2 immunity and improve whole-body glucose tolerance (99, 105). Interestingly, adoptive transfer of *H. polygyrus*-induced AAMs to uninfected mice via tail vein injection blunted HFD-induced adiposity and glucose intolerance

(105), highlighting a role for AAMs in promoting insulin sensitivity. Adoptive transfer of these macrophages was associated with increased expression of uncoupling protein 1 (UCP-1) in adipose tissues, indicative of brown adipose tissue (BAT) activation or WAT beiging. These are physiological responses to cold exposure to induce non-shivering thermogenesis, producing heat at the expense of ATP production by uncoupling mitochondrial oxidative phosphorylation, thereby combusting large amounts of glucose and lipids and significantly increasing energy expenditure (111-113). As such, BAT activation and beiging have gained considerable attention as therapeutic goals for combating metabolic disorders (114). Although AAMs were previously suggested to promote beiging through the release of catecholamines (115, 116), this concept was later refuted by an elegant study showing that AAMs are incapable of producing catecholamines and do not contribute to beiging (117). In our studies, we have not observed effects of helminth infection or SEA/ω1 treatment on white adipose tissue beiging or BAT activation (**chapter 7** and unpublished results), while AAMs were increased in adipose tissue in all settings. The transferred macrophages from *H. polygyrus*-infected mice are thus unlikely to improve metabolic homeostasis through beiging. In addition, these macrophages were not selected for AAM markers and derived from spleen and peritoneal cavity, rather than AAMs from metabolic tissues. Moreover, the fate of these macrophages after transfer and mechanisms for improving whole-body glucose tolerance were not investigated. Together, this hinders the interpretation of the data showing that *H. polygyrus*-induced AAMs promote metabolic homeostasis, and more work is undoubtedly required to elucidate mechanisms by which helminth-induced AAMs may govern insulin sensitivity.

In addition to *S. mansoni* SEA, we also investigated the effects and underlying mechanisms of recombinantly produced ω1, one of the major immunomodulatory molecules present in SEA (118), on whole-body metabolic homeostasis in **chapter 7**. SEA and other helminth worm or egg antigen mixtures are crude, heterogeneous preparations that display batch variability. This impedes detailed, batch-transcending molecular and functional characterization, which leaves room for potential off-target effects. Hence, dissecting underlying mechanisms of type 2 immunity induction and improvement of metabolic homeostasis by single molecules expressed by helminths may aid in identifying therapeutic targets. SEA-induced type 2 immunity, through dendritic cell (DC)-mediated T helper 2 (Th2) polarization, is at least partly dependent on glycosylated antigens present in SEA (101, 119). Among these antigens is the T2 RNase glycoprotein ω1 that licenses DCs to polarize Th2 cells dependent on glycan-mediated uptake and its enzymatic activity (118, 120). Interestingly, treatment of obese mice with ω1, that was recombinantly produced using human embryonic kidney 293 (HEK293) cells, acutely reduced body weight and improved whole-body glucose tolerance (108).

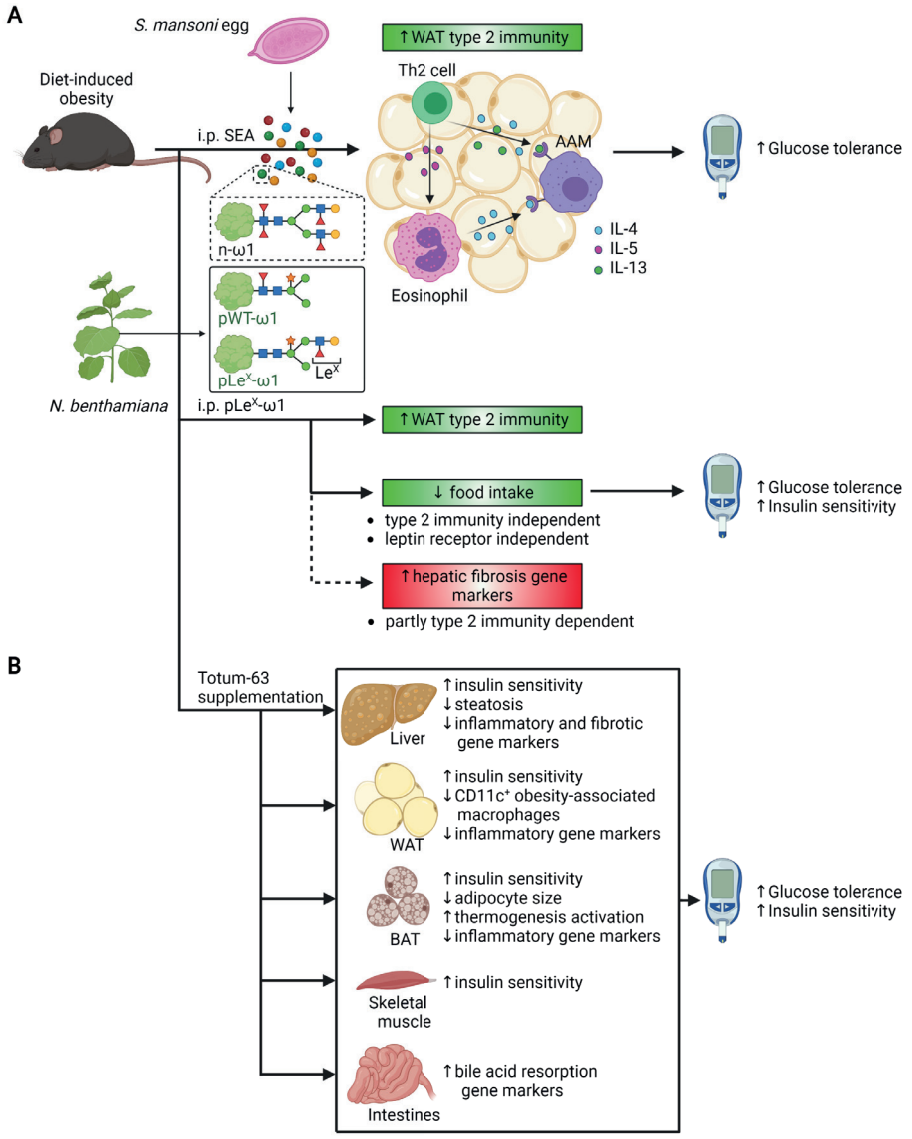

Figure 2: Mechanisms employed by immunomodulatory (helminth) molecules to alleviate obesity-induced metabolic dysfunctions. (**A**) Graphical summary of chapter 7. *Schistosoma mansoni* soluble egg antigens (SEA) improved whole-body glucose tolerance in obese mice through STAT6-mediated type 2 immunity. *Nicotiana benthamiana*-produced glycosylation variants of ω1 also induced WAT type 2 immunity, but improved whole-body glucose tolerance and insulin sensitivity by reducing food intake, which was independent of type 2 immunity and leptin receptor signaling. Furthermore, pLe^X-ω1 upregulated hepatic fibrosis gene markers, which was partly dependent on type 2 immunity. (**B**) Graphical summary of chapter 8. Totum-63 supplementation improved whole-body metabolic homeostasis through pleiotropic effects on various metabolic organs. Created with BioRender.com.

However, glycan structures of HEK293-produced ω1 differ from the *S. mansoni* native molecule, specifically lacking immunogenic Lewis-X (Le^X) motifs on glycan termini (120, 121). Glycans on protein may profoundly affect protein function, *e.g.* by affecting protein folding, receptor binding and biodistribution (122), and play important roles in controlling immune responses (123). By exploiting the flexible N-glycosylation machinery of *Nicotiana benthamiana* plants (124), we investigated the immunometabolic effects of two ω1 glycosylation variants, either carrying the Le^X motif on one of its glycan branches or not, in obese mice (**Figure 2A**).

Both of these plant-produced, glyco-engineered ω1 molecules induced type 2 immunity in metabolic tissues, which was associated with reduced fat mass and improvements in both tissue-specific and whole-body insulin sensitivity. In stark contrast to SEA, ω1 glycovariants significantly improved whole-body metabolic homeostasis in obese *Stat6*$^{-/-}$ mice in the absence of type 2 immunity. The ω1 glycovariants rather inhibited food intake, without affecting locomotor activity, lean mass, or behavior of the mice, indicating that discomfort is unlikely to explain decreased appetite. Nonetheless, reduced food intake explained most of the beneficial metabolic effects of at least the Le^X-glycoengineered ω1 (pLe^X-ω1), which occurred independent of leptin receptor signaling, a central hormone involved in regulation of energy intake (**Figure 2A**; 125).

The regulation of food intake by plant-produced ω1 glycovariants was surprising, as HEK293-produced ω1 was previously not suggested to affect feeding behavior (108), although this was not assessed in detail. Interestingly, deworming helminth-infected school children was found to be associated with increased appetite and growth (126), leading to speculate that helminth-expressed molecules may regulate satiety. We showed that plant-produced ω1 does not accumulate in the brain, indicating its effect is likely mediated by peripheral rather than central mechanisms. Bidirectional communication between the gastrointestinal tract and the central nervous system, the so-called gut-brain axis, has gained interest in the context of metabolic disorders, where it has been shown to be involved in regulation of energy intake and energy expenditure (127). Interestingly, several mechanisms for sensing gastrointestinal helminths to induce mucosal type 2 immunity and expel the worms have also recently been identified. For instance, the gastrointestinal helminth *Nippostrongylus brasiliensis* activates an intestinal tuft cell-ILC2 program that results in epithelial remodeling and increased mucus production (128-130). Tuft cells are rare, secretory epithelial cells that closely interact with enteroendocrine cells and enteric neurons (131). Although underlying mechanisms are still largely elusive, tuft cells and other chemosensory cells are hypothesized to relay nutritional signals to brain regions that control food intake, and are thereby potentially involved in the regulation of appetite (132, 133). In

addition, *N. brasiliensis* is sensed by intestinal neurons, initiating type 2 immunity through production of neuromedin U (NmU) and activating NmU receptor-expressing ILC2s (134, 135). Both intracerebroventricular (136) as well as peripheral administration of NmU (137) or a NmU receptor-selective agonist (138) have been demonstrated to suppress food intake. Mechanistically, peripherally administered NmU was suggested to inhibit food intake by signaling to brain regions that regulate satiety through the vagal nerve (137). Although speculative, whether plant-produced ω1 glycovariants alter energy intake, through potential changes in tuft cell activation or intestinal neuroimmune interactions that affect the gut-brain axis, would be an interesting new angle to explore in future studies.

In addition to its beneficial effects on whole-body glucose tolerance and insulin sensitivity, ω1 also increased fibrotic gene marker expression in the liver and alanine aminotransferase (ALAT) levels in serum, indicative of liver injury. During *S. mansoni* infection, adult worms reside in hepatic veins where they release eggs that lodge in the liver (139). This triggers granuloma formation through IL-4 and IL-13, and consequently hepatic fibrosis surrounding egg granulomas via IL-13 (140). Indeed, also in the absence of *S. mansoni* infection, IL-13 was shown to be pro-fibrotic in the liver (141). Given that we found increased hepatic IL-13-expressing Th2 cells in ω1-treated mice, it is likely that this effect may underlie increased fibrotic gene marker expression in the liver. In line with this, we found that fibrotic gene expression in the liver was at least partly dependent on STAT6 (**Figure 2A**). Interestingly, *S. mansoni* eggs in which ω1 has been knocked down also generated smaller granulomas *in vivo* (142), further supporting a role for ω1 in driving hepatic fibrosis. Using radioactively-labelled pLe^X-ω1, we found that pLe^X-ω1 distributes throughout abdominal organs after intraperitoneal injection, while single-photon emission computerized tomography (SPECT) identified apparent accumulation of pLe^X-ω1 in the liver 24 hours post injection. Although both glycovariants increased leukocyte numbers in WAT and liver, these effects were more pronounced in WAT for pWT-ω1 and liver for pLe^X-ω1, respectively, suggesting that the glycans present on the molecule may affect its biodistribution. Congruent with this, *in vivo* administration of different glycoconjugates have been shown to display glycan-dependent, specific distribution kinetics [as reviewed in (122, 143)]. Specific tissue and/or cell targeting approaches using glycans are currently conducted. For example, triantennary N-acetyl galactosamine improved targeting of antisense oligonucleotides to the liver through interacting with the hepatocyte-specific asialoglycoprotein receptor (ASGPR) (144), and glucan-encapsulated particles containing siRNAs specifically target phagocytic cells expressing Dectin-1 or other β-glucan recognizing receptors (145). This would suggest that manipulating ω1 glycosylation may have potential to bypass the liver and specifically target adipose tissue DCs to elicit type 2 immunity and

improve whole-body metabolic homeostasis, although the glycan structures and valency to achieve this are yet to be identified.

To conclude, our work has provided evidence for involvement of SEA-induced type 2 immunity in improvement of metabolic homeostasis in obese mice. In addition, we found that the *S. mansoni*-expressed Th2-inducing molecule ω1 unexpectedly regulates food intake through a peripheral mechanism independent of its Th2-inducing capacity. One of our hypotheses is that ω1 may regulate the gut-brain axis involved in the control of food intake. As bidirectional gut-brain communication is mediated by the vagal nerve (146), future studies may benefit from vagotomy as recently used in other studies assessing the gut-brain axis in the context of obesity (147, 148). In addition, follow-up studies should address whether helminth-induced AAMs contribute to improvements in insulin sensitivity and elucidate underlying mechanisms, which may be facilitated through the development of inducible mouse models with defective alternative activation of macrophages.

The polyphenol-rich plant extract Totum-63 and metabolic homeostasis

The types of food we eat may impact inflammatory conditions (149) and nutritional supplements have thus gained attention for modulating immune responses (150). Using dietary supplements for weight management and improving metabolic health is not novel, yet provides an interesting, non-invasive method for prevention or amelioration of obesity-induced metabolic disorders (151-153). Given the immunomodulatory properties of some of these nutraceuticals, they may function as a double-edged sword: both ameliorating systemic metaflammation as well as improving insulin sensitivity and/or glucose homeostasis directly in metabolic organs. In **chapter 8**, the effects and underlying mechanisms of Totum-63, a recently developed dietary supplement consisting of a blend of polyphenol-rich plant extracts with potential immunomodulatory effects, on metabolic homeostasis in obese, insulin resistant mice was investigated. In-depth metabolic phenotyping revealed that Totum-63 reduced body weight, completely attributable to a decrease in fat mass, and improved whole-body insulin sensitivity and glucose tolerance independent of body weight changes. Totum-63 improved metabolic and immunological parameters in various metabolic tissues, including intestines, liver, skeletal muscle, visceral and subcutaneous WAT, and BAT, indicating the principle promotes metabolic homeostasis through pleiotropic effects, likely owing to its chemical composition containing a variety of bioactive molecules (**Figure 2B**).

We demonstrated that Totum-63 reduced CD11c-expressing obesity-associated macrophages in visceral WAT and reduced inflammatory gene markers in subcutaneous WAT, BAT and liver. As hepatic steatosis was almost completely reversed in Totum-63-

supplemented mice, reduced inflammation in BAT and liver probably results from reduced ectopic lipid deposition and lipotoxicity, potentially through insulin-mediated inhibition of WAT lipolysis. However, Totum-63 is rich in polyphenols, and several of these micronutrients possess intrinsic immunomodulatory properties, *e.g.* by inhibiting NF-κB-mediated proinflammatory cytokine production (154, 155). Hence, we cannot completely exclude potential immunomodulatory effects of polyphenols or other components (*i.e.* saponins, alkaloids and fibers) of Totum-63 that may impact metaflammation and thereby promote tissue-specific and whole-body insulin sensitivity.

Although whole-body energy expenditure was unchanged, Totum-63 increased BAT activation, as illustrated by decreased BAT mass and increased expression of UCP-1 and other thermogenic gene markers. Some polyphenols were reported to increase BAT activation (153, 156), yet we also found increased ileal expression of bile acid transporters, indicative of increased bile acid resorption. Bile acids are increasingly recognized as signaling molecules that impact whole-body metabolism, immunity and also BAT activation (157, 158). Interestingly, polyphenols have been demonstrated to regulate bile acid bioavailability (159). Whether Totum-63 increased systemic bile acid levels and whether bile acids may contribute to the pleiotropic effects of Totum-63, for instance through immunomodulation and/or direct effects on metabolic organs, remains to be determined. Future studies supplementing mice that are deficient for bile acid receptors, such as FXR or TGR5, could be considered for answering such questions.

Totum-63 was developed for the treatment of pre-diabetes and to reduce the risk of developing type 2 diabetes. As such, the bioactive principle was shown to protect against obesity-induced metabolic dysfunction in a progression model, when lean mice received HFD supplemented with Totum-63 (160). Our work indicates that Totum-63 may also hold potential in treating established type 2 diabetes by exerting pleiotropic effects on multiple metabolic organs. Importantly, safety and tolerability of Totum-63 were also recently demonstrated in pre-diabetic men, where 6 months supplementation induced body weight loss, reduced fasting blood glucose and improved glucose tolerance (160, 161). Together, our work has illuminated the potential mechanistic underpinnings of Totum-63-mediated improvements in metabolic homeostasis. Increased bile acid bioavailability and immunomodulation by Totum-63 may contribute to the immunometabolic effects of Totum-63, yet this remains to be investigated.

Box: Summary of main findings

- The beneficial metabolic effects of *S. mansoni* SEA on whole-body glucose tolerance in obese mice are dependent on SEA-induced type 2 immunity (**chapter 7**)
- Glyco-engineered, plant-produced ω1 improves whole-body metabolic homeostasis in obese mice through leptin receptor-independent inhibition of food intake; not through its type 2 immunity-inducing properties (**chapter 7**)
- The polyphenol-rich plant extract Totum-63 improves whole-body metabolic homeostasis in obese mice through pleiotropic effects on multiple metabolic organs, including a reduction in proinflammatory macrophages in adipose tissue (**chapter 8**)

Future perspectives and concluding remarks

This thesis deepens our understanding of how immune cells control whole-body metabolic homeostasis. Developments in immunology and immunometabolism research have provided new tools and perspectives to propel the field forward, of which several will be highlighted below.

Single-cell and spatial transcriptomics

Analyses of immune cells in metabolic tissues have long relied on conventional flow cytometry, with a limitation in the number of parameters to be measured based on the number of detectors that are assigned to a single fluorophore. Historically, based on the expression of a selected set of markers, macrophages in lean WAT were considered to resemble *in vitro* IL-4-polarized M2 macrophages, whereas proinflammatory macrophages in obese WAT were thought to be similar to *in vitro* LPS + IFNγ-polarized M1 macrophages. While this dichotomy was at the time already reported to be an oversimplification (162), recent technological advances have confirmed that metabolic tissue macrophage phenotypes *in vivo* are indeed much more complex. The development of single-cell transcriptomics during the last decade now allows an unbiased approach to obtain unprecedented insights into the cellular heterogeneity of complex samples (163). Single-cell RNA sequencing (scRNAseq) has recently been extensively employed to investigate the immune cell composition of adipose tissue (36, 164) and liver (37, 38, 165) isolated from lean and obese mice and humans. This has provided novel insights into phenotypes and mechanisms underlying immune-mediated control of metaflammation. Among the key findings is the identification of an evolutionary conserved lipid-associated macrophage phenotype expressing CD9, Trem2 and/or CD36 in both obese WAT and fatty liver, which contributes to obesity and NASH pathogenesis (36-38).

Of note, whereas hepatocytes and other parenchymal cells in the liver can readily be identified using scRNAseq, mature adipocytes are too fragile to survive the procedure.

Isolating nuclei from snap-frozen adipose tissue samples and performing single-nuclei RNAseq was shown to be a valuable strategy to overcome this problem and revealed a previously unrecognized heterogeneity in adipocyte subsets during obesity (164). Although nuclei carry fewer RNA which may hinder resolution, single-nuclei RNAseq uncouples sample acquisition from processing and may represent a goldmine allowing the analysis of previously biobanked tissue samples.

scRNAseq enables detailed characterization of the cellular composition of metabolic organs, yet it does not resolve cellular microenvironmental niches and cell-cell interactions. As a spectacular recent example, a spatial proteogenomic atlas was generated for healthy and obese mouse and human livers by integrating single-cell proteomic and transcriptomic information with spatial transcriptomics (166). This provided clues regarding the development and function of cell subsets based on their microanatomical niche, and strategies for identifying and further studying specific hepatic cell subsets. Similar endeavors to provide spatial resolution of cell subsets identified in snRNAseq of adipose tissue may deepen our understanding of immunological control of obesity-induced metabolic dysfunctions.

In the timespan during which our studies took place, the development of these tools and their applications in immunometabolism research have contributed a wealth of new knowledge to the field. Unfortunately, at the time, we could not implement these cutting-edge new tools in our work and have thus mostly relied on a selected set of markers by conventional flow cytometry for identifying macrophages in adipose tissue and liver (i.e. CD11b, CD64 and F4/80), as well as to predict their function (e.g. YM1 for AAMs and CD11c for proinflammatory obesity-associated macrophages). As such, one of the limitations of our work is that this approach did not allow to fully capture the heterogeneity of the macrophage pool in metabolic tissues. Consequently, during the course of our own studies we were not able to assess in depth some of the new macrophage subsets identified by others using single cell transcriptomic and proteomic technologies (36-38, 164-166). For example, obese adipose tissue accommodates a broad spectrum of macrophages, such as lipid-associated macrophages (LAMs) (36), vascular-associated macrophages (167) and sympathetic neuron-associated macrophages (168) that display phenotypical and functional diversity at least partly based on their localization within adipose tissue. Likewise, in the liver, $CD64^{+}CD11c^{+}CLEC4F^{-}$ monocyte-derived KCs were shown to be more inflammatory as compared to $CLEC4F^{+}TIM4^{+}$ resident KCs, which are lost during obesity (37, 169). Furthermore, osteopontin-expressing monocyte-derived macrophages in the liver were also shown to resemble WAT LAMs and to be enriched in fibrotic liver (37). Our studies could have benefited from mapping the transcriptional signatures defining these diverse macrophage subsets onto the myeloid cells-of-interest in our studies. This may have provided

more detailed and broad insights into the effects of given genetic or pharmacological interventions on the leukocyte pool in metabolic tissues, and likely left fewer questions unanswered. Finally, how (helminth-induced) AAMs contribute to insulin sensitivity is still poorly understood. Further studies will likely benefit from in-depth characterization of these cells by scRNAseq and establishing their microenvironmental niche.

Neuroimmunometabolism and the gut-brain axis

Besides bidirectional communication with metabolic cells, immune cells can also interact with neurons. Such interactions are particularly apparent at mucosal areas, *e.g.* the intestines and the lungs, where immune cells interact with dense neuronal networks to preserve tissue homeostasis and assist in establishing immune responses (170). For example, several recent studies demonstrated that the neuropeptide NmU promotes ILC2 responses in the intestines and the lung (134, 135, 171). Strikingly, the excretory/secretory products of the gastrointestinal helminth *N. brasiliensis* were found to be sensed by neuronal organoids, resulting in increased NmU expression, thereby likely contributing to increased worm expulsion through ILC2-mediated type 2 immunity (134). Such neuro-immune circuits have not only been reported for enteric ILC2s, but also for muscularis macrophages in the gut wall. These macrophages were shown to protect enteric neurons from infection-induced cell death (172), and by this way, to preserve the self-sustaining crosstalk between muscularis macrophages and enteric neurons that regulates gastrointestinal motility (173). Altogether, this may lead one to speculate that at least some of the metabolic effects of helminth molecules and the nutritional supplement Totum-63 may be secondary to altered neuro-immune circuits in the intestines, as a result of sensing of these molecules either by enteric neurons or muscularis macrophages. As vagal afferent nerves are known to relay intestinal sensory information to regulate food intake (147, 174), such interactions could potentially also contribute to the regulation of satiety by ω1.

The findings that subsets of macrophages co-localize and interact with sympathetic neurons in BAT and WAT has sparked the research topic of neuroimmunometabolism (175). Sympathetic innervation promotes lipolysis in BAT and WAT, and regulates adaptive thermogenesis (112, 176). BAT macrophages were found to control tissue innervation, which increased HFD-induced adiposity upon disruption (177). In WAT, obesity promotes the accrual of sympathetic neuron-associated macrophages that scavenges norepinephrine to reduce its extracellular bioavailability and WAT lipolysis (168). Removing the norepinephrine importer Slc6a2 from myeloid cells increased lipolysis and limited weight gain upon HFD feeding. WAT sympathetic neurons also indirectly interact with ILC2s through mesenchymal cells (178). Neuronal-derived norepinephrine stimulates glial-derived neurotrophic factor

(GDFN) release by mesenchymal cells, which binds to its receptor tyrosine kinase RET on ILC2s to increase cytokine production. Loss of RET on ILC2s promoted HFD-induced metabolic dysfunctions, whereas gain of function had an opposite effect, presumably by controlling WAT beiging (178). Whether (helminth-induced) AAMs also interact with sympathetic neurons in their microenvironmental niche, and whether such neuro-immune interactions could contribute to regulation of tissue insulin sensitivity, is a novel perspective that warrants further study.

Immunomodulatory helminth molecules and controlled human infections

Experimental infection of obese, insulin-resistant mice has unequivocally demonstrated that different helminth species alleviate whole-body metabolic dysfunctions in mice. In **chapter 6** we provided an overview of immune regulation of metabolic homeostasis by helminths and their molecules. We described in **chapter 7** that both *S. mansoni* SEA as well as the Th2-inducing molecule ω1, one of the molecules present in SEA, improve whole-body glucose tolerance. SEA is a crude mixture containing many (glyco)proteins with potential Th2-inducing properties, such as currently unidentified Dectin-1/2 ligands (179). Identification of such molecules, either expressed by *S. mansoni* or other helminths, and assessment of their potency to improve whole-body metabolic homeostasis remains a promising undertaking.

Cross-sectional studies in helminth-endemic areas indicate that an inverse correlation between helminth infection and insulin sensitivity also exists in humans (**chapter 6**). However, whether therapeutic helminth infection holds promise for patients with type 2 diabetes remains to be studied. Given the risks associated with experimental infection, such studies require thorough ethical consideration. Still, controlled human infection trials have provided a wealth of scientific insights and contributed to the development of vaccines and drugs for infectious diseases, such as infection with rhinovirus, influenza and the malaria parasite *Plasmodium falciparum* (180). Interestingly, controlled infection of humans with the soil-transmitted helminth *Necator americanus* has been reported to be well tolerated (181, 182). Moreover, a recent landmark study described experimental infection of volunteers with *S. mansoni*, albeit with only male cercariae - the infectious larval form of *S. mansoni* - to prevent egg deposition and associated pathogenesis (183). Even though these trials are currently focused on drug and vaccine development, they may potentially pave the way for applying controlled experimental helminth infection in the context of obesity-associated metabolic dysfunctions or other inflammatory disorders.

To conclude, our works describes novel mechanisms by which immune cells control whole-body metabolic homeostasis, and that (helminth) immunomodulatory molecules are potent candidates for alleviating metaflammation. We provide new insights, but our

studies also raised new questions that remain to be addressed (see Outstanding questions box). While one should not overlook the efficacy of lifestyle modifications, harnessing immunomodulation through helminths, their expressed molecules or other sources presents a potent means for improving obesity-associated metabolic dysfunctions that warrants follow-up.

Box: Outstanding questions

- What is the source of increased sMR serum levels in obesity, and how is increased sMR shedding regulated?
- What are the effector cells and molecular mechanism(s) of sMR-induced metaflammation?
- What is the role of SIKs in controlling Th17 polarization by DCs?
- What is the contribution of helminth-induced AAMs to the control of whole-body metabolic homeostasis, and what are their phenotypes and underlying mechanisms?
- Does the gut-brain axis mediate the inhibitory effects of ω1 on food intake?
- What is the contribution of neuroimmunometabolism and the gut-brain axis to the metabolic effects of helminth molecules and the polyphenol-rich nutritional supplement Totum-63?
- Does controlled human helminth infection hold promise as a translational model to explore the impact of helminth-induced immunomodulation on metabolic homeostasis ?

References

1. Brestoff JR, Artis D. Immune regulation of metabolic homeostasis in health and disease. Cell. 2015;161(1):146-60.
2. Lackey DE, Olefsky JM. Regulation of metabolism by the innate immune system. Nature Reviews Endocrinology. 2016;12(1):15-28.
3. Hotamisligil GS, Shargill NS, Spiegelman BM. Adipose expression of tumor necrosis factor-alpha: direct role in obesity-linked insulin resistance. Science. 1993;259(5091):87.
4. Yuan M, Konstantopoulos N, Lee J, Hansen L, Li ZW, Karin M, et al. Reversal of obesity- and diet-induced insulin resistance with salicylates or targeted disruption of Ikkbeta. Science. 2001;293(5535):1673-7.
5. Weisberg SP, McCann D, Desai M, Rosenbaum M, Leibel RL, Ferrante AW, Jr. Obesity is associated with macrophage accumulation in adipose tissue. J Clin Invest. 2003;112(12):1796-808.
6. Xu H, Barnes GT, Yang Q, Tan G, Yang D, Chou CJ, et al. Chronic inflammation in fat plays a crucial role in the development of obesity-related insulin resistance. J Clin Invest. 2003;112(12):1821-30.
7. Lumeng CN, Bodzin JL, Saltiel AR. Obesity induces a phenotypic switch in adipose tissue macrophage polarization. The Journal of Clinical Investigation. 2007;117(1):175-84.
8. Nguyen MT, Favelyukis S, Nguyen AK, Reichart D, Scott PA, Jenn A, et al. A subpopulation of macrophages infiltrates hypertrophic adipose tissue and is activated by free fatty acids via Toll-like receptors 2 and 4 and JNK-dependent pathways. J Biol Chem. 2007;282(48):35279-92.
9. Cinti S, Mitchell G, Barbatelli G, Murano I, Ceresi E, Faloia E, et al. Adipocyte death defines macrophage localization and function in adipose tissue of obese mice and humans. J Lipid Res. 2005;46(11):2347-55.
10. Murano I, Barbatelli G, Parisani V, Latini C, Muzzonigro G, Castellucci M, et al. Dead adipocytes, detected as crown-like structures, are prevalent in visceral fat depots of genetically obese mice. J Lipid Res. 2008;49(7):1562-8.
11. Haka AS, Barbosa-Lorenzi VC, Lee HJ, Falcone DJ, Hudis CA, Dannenberg AJ, et al. Exocytosis of macrophage lysosomes leads to digestion of apoptotic adipocytes and foam cell formation. J Lipid Res. 2016;57(6):980-92.
12. Kratz M, Coats Brittney R, Hisert Katherine B, Hagman D, Mutskov V, Peris E, et al. Metabolic Dysfunction Drives a Mechanistically Distinct Proinflammatory Phenotype in Adipose Tissue Macrophages. Cell Metabolism. 2014;20(4):614-25.
13. Kanda H, Tateya S, Tamori Y, Kotani K, Hiasa K, Kitazawa R, et al. MCP-1 contributes to macrophage infiltration into adipose tissue, insulin resistance, and hepatic steatosis in obesity. J Clin Invest. 2006;116(6):1494-505.
14. Weisberg SP, Hunter D, Huber R, Lemieux J, Slaymaker S, Vaddi K, et al. CCR2 modulates inflammatory and metabolic effects of high-fat feeding. J Clin Invest. 2006;116(1):115-24.
15. Lanthier N, Molendi-Coste O, Horsmans Y, van Rooijen N, Cani PD, Leclercq IA. Kupffer cell activation is a causal factor for hepatic insulin resistance. Am J Physiol Gastrointest Liver Physiol. 2010;298(1):G107-16.

16. Krenkel O, Puengel T, Govaere O, Abdallah AT, Mossanen JC, Kohlhepp M, et al. Therapeutic inhibition of inflammatory monocyte recruitment reduces steatohepatitis and liver fibrosis. Hepatology. 2018;67(4):1270-83.
17. Morinaga H, Mayoral R, Heinrichsdorff J, Osborn O, Franck N, Hah N, et al. Characterization of distinct subpopulations of hepatic macrophages in HFD/obese mice. Diabetes. 2015;64(4):1120-30.
18. O'Neill LAJ, Kishton RJ, Rathmell J. A guide to immunometabolism for immunologists. Nature Reviews Immunology. 2016;16(9):553-65.
19. Lauterbach MA, Hanke JE, Serefidou M, Mangan MSJ, Kolbe C-C, Hess T, et al. Toll-like Receptor Signaling Rewires Macrophage Metabolism and Promotes Histone Acetylation via ATP-Citrate Lyase. Immunity. 2019;51(6):997-1011.e7.
20. Wellen KE, Hatzivassiliou G, Sachdeva UM, Bui TV, Cross JR, Thompson CB. ATP-Citrate Lyase Links Cellular Metabolism to Histone Acetylation. Science. 2009;324(5930):1076.
21. Langston PK, Nambu A, Jung J, Shibata M, Aksoylar HI, Lei J, et al. Glycerol phosphate shuttle enzyme GPD2 regulates macrophage inflammatory responses. Nature Immunology. 2019;20(9):1186-95.
22. Baardman J, Verberk SGS, van der Velden S, Gijbels MJJ, van Roomen CPPA, Sluimer JC, et al. Macrophage ATP citrate lyase deficiency stabilizes atherosclerotic plaques. Nature Communications. 2020;11(1):6296.
23. Wynn TA, Chawla A, Pollard JW. Macrophage biology in development, homeostasis and disease. Nature. 2013;496(7446):445-55.
24. Okabe Y, Medzhitov R. Tissue biology perspective on macrophages. Nature Immunology. 2016;17(1):9-17.
25. Burgdorf S, Lukacs-Kornek V, Kurts C. The mannose receptor mediates uptake of soluble but not of cell-associated antigen for cross-presentation. J Immunol. 2006;176(11):6770-6.
26. Burgdorf S, Kautz A, Bohnert V, Knolle PA, Kurts C. Distinct pathways of antigen uptake and intracellular routing in CD4 and CD8 T cell activation. Science. 2007;316(5824):612-6.
27. Martinez-Pomares L, Mahoney JA, Kaposzta R, Linehan SA, Stahl PD, Gordon S. A functional soluble form of the murine mannose receptor is produced by macrophages in vitro and is present in mouse serum. J Biol Chem. 1998;273(36):23376-80.
28. Jordens R, Thompson A, Amons R, Koning F. Human dendritic cells shed a functional, soluble form of the mannose receptor. Int Immunol. 1999;11(11):1775-80.
29. Andersen ES, Rodgaard-Hansen S, Moessner B, Christensen PB, Moller HJ, Weis N. Macrophage-related serum biomarkers soluble CD163 (sCD163) and soluble mannose receptor (sMR) to differentiate mild liver fibrosis from cirrhosis in patients with chronic hepatitis C: a pilot study. Eur J Clin Microbiol Infect Dis. 2014;33(1):117-22.
30. Rodgaard-Hansen S, Rafique A, Weis N, Wejse C, Nielsen H, Pedersen SS, et al. Increased concentrations of the soluble mannose receptor in serum from patients with pneumococcal bacteraemia, and prediction of survival. Infect Dis (Lond). 2015;47(4):203-8.
31. Ding D, Song Y, Yao Y, Zhang S. Preoperative serum macrophage activated biomarkers soluble mannose receptor (sMR) and soluble haemoglobin scavenger receptor (sCD163), as novel markers for the diagnosis and prognosis of gastric cancer. Oncol Lett. 2017;14(3):2982-90.

32. Suzuki Y, Shirai M, Asada K, Yasui H, Karayama M, Hozumi H, et al. Macrophage mannose receptor, CD206, predict prognosis in patients with pulmonary tuberculosis. Scientific Reports. 2018;8(1):13129.

33. Loonen AJM, Leijtens S, Serin O, Hilbink M, Wever PC, van den Brule AJC, et al. Soluble mannose receptor levels in blood correlate to disease severity in patients with community-acquired pneumonia. Immunol Lett. 2019;206:28-32.

34. Taylor PR, Gordon S, Martinez-Pomares L. The mannose receptor: linking homeostasis and immunity through sugar recognition. Trends Immunol. 2005;26(2):104-10.

35. Klotz L, Hucke S, Thimm D, Classen S, Gaarz A, Schultze J, et al. Increased Antigen Cross-Presentation but Impaired Cross-Priming after Activation of Peroxisome Proliferator-Activated Receptor γ Is Mediated by Up-Regulation of B7H1. The Journal of Immunology. 2009;183(1):129.

36. Jaitin DA, Adlung L, Thaiss CA, Weiner A, Li B, Descamps H, et al. Lipid-Associated Macrophages Control Metabolic Homeostasis in a Trem2-Dependent Manner. Cell. 2019;178(3):686-98.e14.

37. Remmerie A, Martens L, Thoné T, Castoldi A, Seurinck R, Pavie B, et al. Osteopontin Expression Identifies a Subset of Recruited Macrophages Distinct from Kupffer Cells in the Fatty Liver. Immunity. 2020;53(3):641-57.e14.

38. Bleriot C, Barreby E, Dunsmore G, Ballaire R, Chakarov S, Ficht X, et al. A subset of Kupffer cells regulates metabolism through the expression of CD36. Immunity. 2021;54(9):2101-16 e6.

39. Gross B, Pawlak M, Lefebvre P, Staels B. PPARs in obesity-induced T2DM, dyslipidaemia and NAFLD. Nat Rev Endocrinol. 2017;13(1):36-49.

40. Odegaard JI, Ricardo-Gonzalez RR, Goforth MH, Morel CR, Subramanian V, Mukundan L, et al. Macrophage-specific PPARgamma controls alternative activation and improves insulin resistance. Nature. 2007;447(7148):1116-20.

41. de Meijer VE, Sverdlov DY, Le HD, Popov Y, Puder M. Tissue-specific differences in inflammatory infiltrate and matrix metalloproteinase expression in adipose tissue and liver of mice with diet-induced obesity. Hepatol Res. 2012;42(6):601-10.

42. Muir LA, Cho KW, Geletka LM, Baker NA, Flesher CG, Ehlers AP, et al. Human CD206+ macrophages associate with diabetes and adipose tissue lymphoid clusters. JCI Insight. 2022;7(3).

43. Cho KW, Zamarron BF, Muir LA, Singer K, Porsche CE, DelProposto JB, et al. Adipose Tissue Dendritic Cells Are Independent Contributors to Obesity-Induced Inflammation and Insulin Resistance. The Journal of Immunology. 2016:1600820.

44. Deczkowska A, David E, Ramadori P, Pfister D, Safran M, At the B, et al. XCR1+ type 1 conventional dendritic cells drive liver pathology in non-alcoholic steatohepatitis. Nature Medicine. 2021;27(6):1043-54.

45. Stefanovic-Racic M, Yang X, Turner MS, Mantell BS, Stolz DB, Sumpter TL, et al. Dendritic Cells Promote Macrophage Infiltration and Comprise a Substantial Proportion of Obesity-Associated Increases in CD11c⁺ Cells in Adipose Tissue and Liver. Diabetes. 2012;61(9):2330.

46. Brombacher EC, Everts B. Shaping of Dendritic Cell Function by the Metabolic Micro-Environment. Front Endocrinol (Lausanne). 2020;11:555.

47. Patente TA, Pelgrom LR, Everts B. Dendritic cells are what they eat: how their metabolism shapes T helper cell polarization. Curr Opin Immunol. 2019;58:16-23.

48. Van Herck MA, Weyler J, Kwanten WJ, Dirinck EL, De Winter BY, Francque SM, et al. The Differential Roles of T Cells in Non-alcoholic Fatty Liver Disease and Obesity. Front Immunol. 2019;10(82).

49. Chen S, Fang L, Guo W, Zhou Y, Yu G, Li W, et al. Control of Treg cell homeostasis and immune equilibrium by Lkb1 in dendritic cells. Nat Commun. 2018;9(1):5298.

50. Pelgrom LR, Patente TA, Sergushichev A, Esaulova E, Otto F, Ozir-Fazalalikhan A, et al. LKB1 expressed in dendritic cells governs the development and expansion of thymus-derived regulatory T cells. Cell Res. 2019;29(5):406-19.

51. Wang Y, Du X, Wei J, Long L, Tan H, Guy C, et al. LKB1 orchestrates dendritic cell metabolic quiescence and anti-tumor immunity. Cell Res. 2019;29(5):391-405.

52. Shackelford DB, Shaw RJ. The LKB1-AMPK pathway: metabolism and growth control in tumour suppression. Nat Rev Cancer. 2009;9(8):563-75.

53. Lizcano JM, Goransson O, Toth R, Deak M, Morrice NA, Boudeau J, et al. LKB1 is a master kinase that activates 13 kinases of the AMPK subfamily, including MARK/PAR-1. EMBO J. 2004;23(4):833-43.

54. Jaleel M, McBride A, Lizcano JM, Deak M, Toth R, Morrice NA, et al. Identification of the sucrose non-fermenting related kinase SNRK, as a novel LKB1 substrate. FEBS Lett. 2005;579(6):1417-23.

55. Lin SC, Hardie DG. AMPK: Sensing Glucose as well as Cellular Energy Status. Cell Metab. 2018;27(2):299-313.

56. Sun Z, Jiang Q, Li J, Guo J. The potent roles of salt-inducible kinases (SIKs) in metabolic homeostasis and tumorigenesis. Signal Transduct Target Ther. 2020;5(1):150.

57. Wein MN, Foretz M, Fisher DE, Xavier RJ, Kronenberg HM. Salt-Inducible Kinases: Physiology, Regulation by cAMP, and Therapeutic Potential. Trends Endocrinol Metab. 2018;29(10):723-35.

58. Altarejos JY, Montminy M. CREB and the CRTC co-activators: sensors for hormonal and metabolic signals. Nat Rev Mol Cell Biol. 2011;12(3):141-51.

59. Dendorfer U, Oettgen P, Libermann TA. Multiple regulatory elements in the interleukin-6 gene mediate induction by prostaglandins, cyclic AMP, and lipopolysaccharide. Mol Cell Biol. 1994;14(7):4443-54.

60. Chandra G, Cogswell JP, Miller LR, Godlevski MM, Stinnett SW, Noel SL, et al. Cyclic AMP signaling pathways are important in IL-1 beta transcriptional regulation. J Immunol. 1995;155(10):4535-43.

61. Kocieda VP, Adhikary S, Emig F, Yen JH, Toscano MG, Ganea D. Prostaglandin E2-induced IL-23p19 subunit is regulated by cAMP-responsive element-binding protein and C/AATT enhancer-binding protein beta in bone marrow-derived dendritic cells. J Biol Chem. 2012;287(44):36922-35.

62. Hollstein PE, Eichner LJ, Brun SN, Kamireddy A, Svensson RU, Vera LI, et al. The AMPK-Related Kinases SIK1 and SIK3 Mediate Key Tumor-Suppressive Effects of LKB1 in NSCLC. Cancer Discov. 2019;9(11):1606-27.

63. Yong Kim S, Jeong S, Chah KH, Jung E, Baek KH, Kim ST, et al. Salt-inducible kinases 1 and 3 negatively regulate Toll-like receptor 4-mediated signal. Mol Endocrinol. 2013;27(11):1958-68.

64. Lombardi MS, Gillieron C, Dietrich D, Gabay C. SIK inhibition in human myeloid cells modulates TLR and IL-1R signaling and induces an anti-inflammatory phenotype. J Leukoc Biol. 2016;99(5):711-21.

65. Sundberg TB, Choi HG, Song JH, Russell CN, Hussain MM, Graham DB, et al. Small-molecule screening identifies inhibition of salt-inducible kinases as a therapeutic strategy to enhance immunoregulatory functions of dendritic cells. Proc Natl Acad Sci U S A. 2014;111(34):12468-73.

66. Ghoreschi K, Laurence A, Yang XP, Tato CM, McGeachy MJ, Konkel JE, et al. Generation of pathogenic T(H)17 cells in the absence of TGF-beta signalling. Nature. 2010;467(7318):967-71.

67. Lee Y, Awasthi A, Yosef N, Quintana FJ, Xiao S, Peters A, et al. Induction and molecular signature of pathogenic TH17 cells. Nat Immunol. 2012;13(10):991-9.

68. Tang Y, Bian Z, Zhao L, Liu Y, Liang S, Wang Q, et al. Interleukin-17 exacerbates hepatic steatosis and inflammation in non-alcoholic fatty liver disease. Clin Exp Immunol. 2011;166(2):281-90.

69. Fabbrini E, Cella M, McCartney SA, Fuchs A, Abumrad NA, Pietka TA, et al. Association between specific adipose tissue CD4+ T-cell populations and insulin resistance in obese individuals. Gastroenterology. 2013;145(2):366-74 e1-3.

70. Harley IT, Stankiewicz TE, Giles DA, Softic S, Flick LM, Cappelletti M, et al. IL-17 signaling accelerates the progression of nonalcoholic fatty liver disease in mice. Hepatology. 2014;59(5):1830-9.

71. Gomes AL, Teijeiro A, Buren S, Tummala KS, Yilmaz M, Waisman A, et al. Metabolic Inflammation-Associated IL-17A Causes Non-alcoholic Steatohepatitis and Hepatocellular Carcinoma. Cancer Cell. 2016;30(1):161-75.

72. Moreno-Fernandez ME, Giles DA, Oates JR, Chan CC, Damen M, Doll JR, et al. PKM2-dependent metabolic skewing of hepatic Th17 cells regulates pathogenesis of non-alcoholic fatty liver disease. Cell Metab. 2021;33(6):1187-204 e9.

73. Pont F, Tosolini M, Fournie JJ. Single-Cell Signature Explorer for comprehensive visualization of single cell signatures across scRNA-seq datasets. Nucleic Acids Res. 2019;47(21):e133.

74. Kullmann L, Krahn MP. Controlling the master-upstream regulation of the tumor suppressor LKB1. Oncogene. 2018;37(23):3045-57.

75. Xie Z, Dong Y, Scholz R, Neumann D, Zou MH. Phosphorylation of LKB1 at serine 428 by protein kinase C-zeta is required for metformin-enhanced activation of the AMP-activated protein kinase in endothelial cells. Circulation. 2008;117(7):952-62.

76. Xie Z, Dong Y, Zhang M, Cui MZ, Cohen RA, Riek U, et al. Activation of protein kinase C zeta by peroxynitrite regulates LKB1-dependent AMP-activated protein kinase in cultured endothelial cells. J Biol Chem. 2006;281(10):6366-75.

77. Martinez-Lopez N, Varela-Rey M, Fernandez-Ramos D, Woodhoo A, Vazquez-Chantada M, Embade N, et al. Activation of LKB1-Akt pathway independent of phosphoinositide 3-kinase plays a critical role in the proliferation of hepatocellular carcinoma from nonalcoholic steatohepatitis. Hepatology. 2010;52(5):1621-31.

78. Sapkota GP, Kieloch A, Lizcano JM, Lain S, Arthur JS, Williams MR, et al. Phosphorylation of the protein kinase mutated in Peutz-Jeghers cancer syndrome, LKB1/STK11, at Ser431 by p90(RSK) and cAMP-dependent protein kinase, but not its farnesylation at Cys(433), is essential for LKB1 to suppress cell vrowth. J Biol Chem. 2001;276(22):19469-82.

79. Houde VP, Ritorto MS, Gourlay R, Varghese J, Davies P, Shpiro N, et al. Investigation of LKB1 Ser431 phosphorylation and Cys433 farnesylation using mouse knockin analysis reveals an unexpected role of prenylation in regulating AMPK activity. Biochem J. 2014;458(1):41-56.

80. Liu R, Hong J, Xu X, Feng Q, Zhang D, Gu Y, et al. Gut microbiome and serum metabolome alterations in obesity and after weight-loss intervention. Nat Med. 2017;23(7):859-68.

81. Liu Z, Zhang W, Zhang M, Zhu H, Moriasi C, Zou MH. Liver kinase B1 suppresses lipopolysaccharide-induced nuclear factor kappaB (NF-kappaB) activation in macrophages. J Biol Chem. 2015;290(4):2312-20.

82. Zhao ZH, Wang ZX, Zhou D, Han Y, Ma F, Hu Z, et al. Sodium Butyrate Supplementation Inhibits Hepatic Steatosis by Stimulating Liver Kinase B1 and Insulin-Induced Gene. Cell Mol Gastroenterol Hepatol. 2021.

83. Medzhitov R. The spectrum of inflammatory responses. Science. 2021;374(6571):1070-5.

84. Meizlish ML, Franklin RA, Zhou X, Medzhitov R. Tissue Homeostasis and Inflammation. Annu Rev Immunol. 2021;39:557-81.

85. Wu D, Molofsky AB, Liang HE, Ricardo-Gonzalez RR, Jouihan HA, Bando JK, et al. Eosinophils sustain adipose alternatively activated macrophages associated with glucose homeostasis. Science. 2011;332(6026):243-7.

86. Molofsky AB, Nussbaum JC, Liang H-E, Van Dyken SJ, Cheng LE, Mohapatra A, et al. Innate lymphoid type 2 cells sustain visceral adipose tissue eosinophils and alternatively activated macrophages. Journal of Experimental Medicine. 2013;210(3):535-49.

87. Nussbaum JC, Van Dyken SJ, von Moltke J, Cheng LE, Mohapatra A, Molofsky AB, et al. Type 2 innate lymphoid cells control eosinophil homeostasis. Nature. 2013;502(7470):245-8.

88. Ricardo-Gonzalez RR, Red Eagle A, Odegaard JI, Jouihan H, Morel CR, Heredia JE, et al. IL-4/STAT6 immune axis regulates peripheral nutrient metabolism and insulin sensitivity. Proc Natl Acad Sci U S A. 2010;107(52):22617-22.

89. Wang AJ, Yang Z, Grinchuk V, Smith A, Qin B, Lu N, et al. IL-25 or IL-17E Protects against High-Fat Diet-Induced Hepatic Steatosis in Mice Dependent upon IL-13 Activation of STAT6. J Immunol. 2015;195(10):4771-80.

90. Stanya KJ, Jacobi D, Liu S, Bhargava P, Dai L, Gangl MR, et al. Direct control of hepatic glucose production by interleukin-13 in mice. J Clin Invest. 2013;123(1):261-71.

91. Maizels RM, Yazdanbakhsh M. Immune Regulation by helminth parasites: cellular and molecular mechanisms. Nature Reviews Immunology. 2003;3(9):733-44.

92. Guigas B, Molofsky AB. A worm of one's own: how helminths modulate host adipose tissue function and metabolism. Trends Parasitol. 2015;31(9):435-41.

93. Chen Y, Lu J, Huang Y, Wang T, Xu Y, Xu M, et al. Association of Previous Schistosome Infection With Diabetes and Metabolic Syndrome: A Cross-Sectional Study in Rural China. The Journal of Clinical Endocrinology & Metabolism. 2013;98(2):E283-E7.

94. Hays R, Esterman A, Giacomin P, Loukas A, McDermott R. Does Strongyloides stercoralis infection protect against type 2 diabetes in humans? Evidence from Australian Aboriginal adults. Diabetes Research and Clinical Practice. 2015;107(3):355-61.

95. Wiria AE, Hamid F, Wammes LJ, Prasetyani MA, Dekkers OM, May L, et al. Infection with Soil-Transmitted Helminths Is Associated with Increased Insulin Sensitivity. PLOS ONE. 2015;10(6):e0127746.

96. Yang Z, Grinchuk V, Smith A, Qin B, Bohl Jennifer A, Sun R, et al. Parasitic Nematode-Induced Modulation of Body Weight and Associated Metabolic Dysfunction in Mouse Models of Obesity. Infection and Immunity. 2013;81(6):1905-14.

97. Hussaarts L, García-Tardón N, van Beek L, Heemskerk MM, Haeberlein S, van der Zon GC, et al. Chronic helminth infection and helminth-derived egg antigens promote adipose tissue M2 macrophages and improve insulin sensitivity in obese mice. The FASEB Journal. 2015;29(7):3027-39.

98. Berbudi A, Surendar J, Ajendra J, Gondorf F, Schmidt D, Neumann AL, et al. Filarial Infection or Antigen Administration Improves Glucose Tolerance in Diet-Induced Obese Mice. Journal of Innate Immunity. 2016;8(6):601-16.

99. Morimoto M, Azuma N, Kadowaki H, Abe T, Suto Y. Regulation of type 2 diabetes by helminth-induced Th2 immune response. Journal of Veterinary Medical Science. 2016;78(12):1855-64.

100. Bhargava P, Li C, Stanya KJ, Jacobi D, Dai L, Liu S, et al. Immunomodulatory glycan LNFPIII alleviates hepatosteatosis and insulin resistance through direct and indirect control of metabolic pathways. Nature Medicine. 2012;18(11):1665-72.

101. Hussaarts L, Yazdanbakhsh M, Guigas B. Priming dendritic cells for th2 polarization: lessons learned from helminths and implications for metabolic disorders. Front Immunol. 2014;5:499-.

102. Rajamanickam A, Munisankar S, Bhootra Y, Dolla C, Thiruvengadam K, Nutman TB, et al. Metabolic Consequences of Concomitant Strongyloides stercoralis Infection in Patients With Type 2 Diabetes Mellitus. Clinical Infectious Diseases. 2019;69(4):697-704.

103. Tahapary DL, de Ruiter K, Martin I, Brienen EAT, van Lieshout L, Cobbaert CM, et al. Effect of Anthelmintic Treatment on Insulin Resistance: A Cluster-Randomized, Placebo-Controlled Trial in Indonesia. Clinical Infectious Diseases. 2017;65(5):764-71.

104. Tahapary DL, de Ruiter K, Martin I, Brienen EAT, van Lieshout L, Djuardi Y, et al. Effect of anthelmintic treatment on leptin, adiponectin and leptin to adiponectin ratio: a randomized-controlled trial. Nutrition & Diabetes. 2017;7(10):e289-e.

105. Su Cw, Chen C-Y, Li Y, Long SR, Massey W, Kumar DV, et al. Helminth infection protects against high fat diet-induced obesity via induction of alternatively activated macrophages. Scientific Reports. 2018;8(1):4607.

106. Pace F, Carvalho BM, Zanotto TM, Santos A, Guadagnini D, Silva KLC, et al. Helminth infection in mice improves insulin sensitivity via modulation of gut microbiota and fatty acid metabolism. Pharmacological Research. 2018;132:33-46.

107. Khudhair Z, Alhallaf R, Eichenberger RM, Whan J, Kupz A, Field M, et al. Gastrointestinal Helminth Infection Improves Insulin Sensitivity, Decreases Systemic Inflammation, and Alters the Composition of Gut Microbiota in Distinct Mouse Models of Type 2 Diabetes. Frontiers in Endocrinology. 2021;11(1132).

108. Hams E, Bermingham R, Wurlod FA, Hogan AE, O'Shea D, Preston RJ, et al. The helminth T2 RNase ω1 promotes metabolic homeostasis in an IL-33- and group 2 innate lymphoid cell-dependent mechanism. The FASEB Journal. 2016;30(2):824-35.

109. Takeda K, Kamanaka M, Tanaka T, Kishimoto T, Akira S. Impaired IL-13-mediated functions of macrophages in STAT6-deficient mice. The Journal of Immunology. 1996;157(8):3220.

110. Takeda K, Tanaka T, Shi W, Matsumoto M, Minami M, Kashiwamura S-i, et al. Essential role of Stat6 in IL-4 signalling. Nature. 1996;380(6575):627-30.

111. Nicholls DG, Locke RM. Thermogenic mechanisms in brown fat. Physiological Reviews. 1984;64(1):1-64.

112. Cannon B, Nedergaard JAN. Brown Adipose Tissue: Function and Physiological Significance. Physiological Reviews. 2004;84(1):277-359.

113. Wu J, Boström P, Sparks Lauren M, Ye L, Choi Jang H, Giang A-H, et al. Beige Adipocytes Are a Distinct Type of Thermogenic Fat Cell in Mouse and Human. Cell. 2012;150(2):366-76.

114. Betz MJ, Enerbäck S. Targeting thermogenesis in brown fat and muscle to treat obesity and metabolic disease. Nature Reviews Endocrinology. 2018;14(2):77-87.

115. Nguyen KD, Qiu Y, Cui X, Goh YPS, Mwangi J, David T, et al. Alternatively activated macrophages produce catecholamines to sustain adaptive thermogenesis. Nature. 2011;480(7375):104-8.

116. Qiu Y, Nguyen KD, Odegaard JI, Cui X, Tian X, Locksley RM, et al. Eosinophils and type 2 cytokine signaling in macrophages orchestrate development of functional beige fat. Cell. 2014;157(6):1292-308.

117. Fischer K, Ruiz HH, Jhun K, Finan B, Oberlin DJ, van der Heide V, et al. Alternatively activated macrophages do not synthesize catecholamines or contribute to adipose tissue adaptive thermogenesis. Nature Medicine. 2017;23(5):623-30.

118. Everts B, Perona-Wright G, Smits HH, Hokke CH, van der Ham AJ, Fitzsimmons CM, et al. Omega-1, a glycoprotein secreted by Schistosoma mansoni eggs, drives Th2 responses. Journal of Experimental Medicine. 2009;206(8):1673-80.

119. Okano M, Satoskar AR, Nishizaki K, Abe M, Harn DA. Induction of Th2 Responses and IgE Is Largely Due to Carbohydrates Functioning as Adjuvants on Schistosoma mansoni Egg Antigens. The Journal of Immunology. 1999;163(12):6712.

120. Everts B, Hussaarts L, Driessen NN, Meevissen MHJ, Schramm G, van der Ham AJ, et al. Schistosome-derived omega-1 drives Th2 polarization by suppressing protein synthesis following internalization by the mannose receptor. Journal of Experimental Medicine. 2012;209(10):1753-67.

121. Meevissen MHJ, Wuhrer M, Doenhoff MJ, Schramm G, Haas H, Deelder AM, et al. Structural Characterization of Glycans on Omega-1, a Major Schistosoma mansoni Egg Glycoprotein That Drives Th2 Responses. Journal of Proteome Research. 2010;9(5):2630-42.

122. Varki A. Biological roles of glycans. Glycobiology. 2017;27(1):3-49.

123. van Kooyk Y, Rabinovich GA. Protein-glycan interactions in the control of innate and adaptive immune responses. Nature Immunology. 2008;9(6):593-601.

124. Wilbers RHP, Westerhof LB, van Noort K, Obieglo K, Driessen NN, Everts B, et al. Production and glyco-engineering of immunomodulatory helminth glycoproteins in plants. Scientific Reports. 2017;7(1):45910.

125. Schwartz MW, Woods SC, Porte D, Seeley RJ, Baskin DG. Central nervous system control of food intake. Nature. 2000;404(6778):661-71.

126. Hadju V, Stephenson LS, Abadi K, Mohammed HO, Bowman DD, Parker RS. Improvements in appetite and growth in helminth-infected schoolboys three and seven weeks after a single dose of pyrantel pamoate. Parasitology. 1996;113 (Pt 5):497-504.

127. Richards P, Thornberry NA, Pinto S. The gut–brain axis: Identifying new therapeutic approaches for type 2 diabetes, obesity, and related disorders. Molecular Metabolism. 2021;46:101175.

128. Gerbe F, Sidot E, Smyth DJ, Ohmoto M, Matsumoto I, Dardalhon V, et al. Intestinal epithelial tuft cells initiate type 2 mucosal immunity to helminth parasites. Nature. 2016;529(7585):226-30.

129. Howitt MR, Lavoie S, Michaud M, Blum AM, Tran SV, Weinstock JV, et al. Tuft cells, taste-chemosensory cells, orchestrate parasite type 2 immunity in the gut. Science. 2016;351(6279):1329.

130. von Moltke J, Ji M, Liang H-E, Locksley RM. Tuft-cell-derived IL-25 regulates an intestinal ILC2–epithelial response circuit. Nature. 2016;529(7585):221-5.

131. Cheng X, Voss U, Ekblad E. Tuft cells: Distribution and connections with nerves and endocrine cells in mouse intestine. Exp Cell Res. 2018;369(1):105-11.

132. Reimann F, Tolhurst G, Gribble Fiona M. G-Protein-Coupled Receptors in Intestinal Chemosensation. Cell Metabolism. 2012;15(4):421-31.

133. Arora P, Andersen D, Moll JM, Danneskiold-Samsoe NB, Xu L, Zhou B, et al. Small Intestinal Tuft Cell Activity Associates With Energy Metabolism in Diet-Induced Obesity. Front Immunol. 2021;12:629391.

134. Cardoso V, Chesné J, Ribeiro H, García-Cassani B, Carvalho T, Bouchery T, et al. Neuronal regulation of type 2 innate lymphoid cells via neuromedin U. Nature. 2017;549(7671):277-81.

135. Klose CSN, Mahlakõiv T, Moeller JB, Rankin LC, Flamar A-L, Kabata H, et al. The neuropeptide neuromedin U stimulates innate lymphoid cells and type 2 inflammation. Nature. 2017;549(7671):282-6.

136. Howard AD, Wang R, Pong SS, Mellin TN, Strack A, Guan XM, et al. Identification of receptors for neuromedin U and its role in feeding. Nature. 2000;406(6791):70-4.

137. Jarry A-C, Merah N, Cisse F, Cayetanot F, Fiamma M-N, Willemetz A, et al. Neuromedin U is a gut peptide that alters oral glucose tolerance by delaying gastric emptying via direct contraction of the pylorus and vagal-dependent mechanisms. The FASEB Journal. 2019;33(4):5377-88.

138. Kaisho T, Nagai H, Asakawa T, Suzuki N, Fujita H, Matsumiya K, et al. Effects of peripheral administration of a Neuromedin U receptor 2-selective agonist on food intake and body weight in obese mice. Int J Obes (Lond). 2017;41(12):1790-7.

139. Llanwarne F, Helmby H. Granuloma formation and tissue pathology in Schistosoma japonicum versus Schistosoma mansoni infections. Parasite Immunol. 2021;43(2):e12778.

140. Fallon PG, Richardson EJ, McKenzie GJ, McKenzie AN. Schistosome infection of transgenic mice defines distinct and contrasting pathogenic roles for IL-4 and IL-13: IL-13 is a profibrotic agent. J Immunol. 2000;164(5):2585-91.

141. Gieseck RL, 3rd, Ramalingam TR, Hart KM, Vannella KM, Cantu DA, Lu WY, et al. Interleukin-13 Activates Distinct Cellular Pathways Leading to Ductular Reaction, Steatosis, and Fibrosis. Immunity. 2016;45(1):145-58.

142. Hagen J, Young ND, Every AL, Pagel CN, Schnoeller C, Scheerlinck JP, et al. Omega-1 knockdown in Schistosoma mansoni eggs by lentivirus transduction reduces granuloma size in vivo. Nat Commun. 2014;5:5375.

143. Ogura A, Kurbangalieva A, Tanaka K. Exploring the glycan interaction in vivo: Future prospects of neo-glycoproteins for diagnostics. Glycobiology. 2016;26(8):804-12.

144. Prakash TP, Graham MJ, Yu J, Carty R, Low A, Chappell A, et al. Targeted delivery of antisense oligonucleotides to hepatocytes using triantennary N-acetyl galactosamine improves potency 10-fold in mice. Nucleic Acids Res. 2014;42(13):8796-807.

145. Barreby E, Sulen A, Aouadi M. Glucan-Encapsulated siRNA Particles (GeRPs) for Specific Gene Silencing in Adipose Tissue Macrophages. Methods Mol Biol. 2019;1951:49-57.

146. Berthoud HR, Albaugh VL, Neuhuber WL. Gut-brain communication and obesity: understanding functions of the vagus nerve. J Clin Invest. 2021;131(10).

147. Li Z, Yi CX, Katiraei S, Kooijman S, Zhou E, Chung CK, et al. Butyrate reduces appetite and activates brown adipose tissue via the gut-brain neural circuit. Gut. 2018;67(7):1269-79.

148. Holland J, Sorrell J, Yates E, Smith K, Arbabi S, Arnold M, et al. A Brain-Melanocortin-Vagus Axis Mediates Adipose Tissue Expansion Independently of Energy Intake. Cell Rep. 2019;27(8):2399-410 e6.

149. Thorburn AN, Macia L, Mackay CR. Diet, metabolites, and "western-lifestyle" inflammatory diseases. Immunity. 2014;40(6):833-42.

150. Kim JH, Kim DH, Jo S, Cho MJ, Cho YR, Lee YJ, et al. Immunomodulatory functional foods and their molecular mechanisms. Exp Mol Med. 2022;54(1):1-11.

151. Riccardi G, Capaldo B, Vaccaro O. Functional foods in the management of obesity and type 2 diabetes. Curr Opin Clin Nutr Metab Care. 2005;8(6):630-5.

152. Rios-Hoyo A, Gutierrez-Salmean G. New Dietary Supplements for Obesity: What We Currently Know. Curr Obes Rep. 2016;5(2):262-70.

153. Martel J, Ojcius DM, Chang CJ, Lin CS, Lu CC, Ko YF, et al. Anti-obesogenic and antidiabetic effects of plants and mushrooms. Nat Rev Endocrinol. 2017;13(3):149-60.

154. Ding S, Jiang H, Fang J. Regulation of Immune Function by Polyphenols. Journal of Immunology Research. 2018;2018:1264074.

155. Yahfoufi N, Alsadi N, Jambi M, Matar C. The Immunomodulatory and Anti-Inflammatory Role of Polyphenols. Nutrients. 2018;10(11).

156. Han X, Zhang Y, Guo J, You Y, Zhan J, Huang W. Chlorogenic Acid Stimulates the Thermogenesis of Brown Adipocytes by Promoting the Uptake of Glucose and the Function of Mitochondria. J Food Sci. 2019;84(12):3815-24.

157. Fiorucci S, Biagioli M, Zampella A, Distrutti E. Bile Acids Activated Receptors Regulate Innate Immunity. Front Immunol. 2018;9:1853.

158. Ahmad TR, Haeusler RA. Bile acids in glucose metabolism and insulin signalling — mechanisms and research needs. Nature Reviews Endocrinology. 2019;15(12):701-12.

159. Chambers KF, Day PE, Aboufarrag HT, Kroon PA. Polyphenol Effects on Cholesterol Metabolism via Bile Acid Biosynthesis, CYP7A1: A Review. Nutrients. 2019;11(11):2588.

160. Chavanelle V, Otero YF, Le Joubioux F, Ripoche D, Bargetto M, Vluggens A, et al. Effects of Totum-63 on glucose homeostasis and postprandial glycemia: a translational study. Am J Physiol Endocrinol Metab. 2021;320(6):E1119-E37.

161. Peltier S, Chavanelle V, Otero YF, Bargetto M, Cazaubiel M, Pereira B, et al. 848-P: Totum-63 Lowers Fasting Glycemia in Subjects with Prediabetes: A Phase 2A Clinical Trial. Diabetes. 2020;69(Supplement 1):848-P.

162. Murray PJ, Allen JE, Biswas SK, Fisher EA, Gilroy DW, Goerdt S, et al. Macrophage activation and polarization: nomenclature and experimental guidelines. Immunity. 2014;41(1):14-20.

163. Ginhoux F, Yalin A, Dutertre CA, Amit I. Single-cell immunology: Past, present, and future. Immunity. 2022;55(3):393-404.

164. Emont MP, Jacobs C, Essene AL, Pant D, Tenen D, Colleluori G, et al. A single-cell atlas of human and mouse white adipose tissue. Nature. 2022;603(7903):926-33.

165. Seidman JS, Troutman TD, Sakai M, Gola A, Spann NJ, Bennett H, et al. Niche-Specific Reprogramming of Epigenetic Landscapes Drives Myeloid Cell Diversity in Nonalcoholic Steatohepatitis. Immunity. 2020;52(6):1057-74 e7.

166. Guilliams M, Bonnardel J, Haest B, Vanderborght B, Wagner C, Remmerie A, et al. Spatial proteogenomics reveals distinct and evolutionarily conserved hepatic macrophage niches. Cell. 2022;185(2):379-96 e38.

167. Silva HM, Bafica A, Rodrigues-Luiz GF, Chi J, Santos PDA, Reis BS, et al. Vasculature-associated fat macrophages readily adapt to inflammatory and metabolic challenges. J Exp Med. 2019;216(4):786-806.

168. Pirzgalska RM, Seixas E, Seidman JS, Link VM, Sanchez NM, Mahu I, et al. Sympathetic neuron-associated macrophages contribute to obesity by importing and metabolizing norepinephrine. Nat Med. 2017;23(11):1309-18.

169. Tran S, Baba I, Poupel L, Dussaud S, Moreau M, Gelineau A, et al. Impaired Kupffer Cell Self-Renewal Alters the Liver Response to Lipid Overload during Non-alcoholic Steatohepatitis. Immunity. 2020;53(3):627-40 e5.

170. Huh JR, Veiga-Fernandes H. Neuroimmune circuits in inter-organ communication. Nat Rev Immunol. 2020;20(4):217-28.

171. Wallrapp A, Riesenfeld SJ, Burkett PR, Abdulnour RE, Nyman J, Dionne D, et al. The neuropeptide NMU amplifies ILC2-driven allergic lung inflammation. Nature. 2017;549(7672):351-6.

172. Matheis F, Muller PA, Graves CL, Gabanyi I, Kerner ZJ, Costa-Borges D, et al. Adrenergic Signaling in Muscularis Macrophages Limits Infection-Induced Neuronal Loss. Cell. 2020;180(1):64-78 e16.

173. Muller PA, Koscso B, Rajani GM, Stevanovic K, Berres ML, Hashimoto D, et al. Crosstalk between Muscularis Macrophages and Enteric Neurons Regulates Gastrointestinal Motility. Cell. 2014;158(5):1210.

174. Cork SC. The role of the vagus nerve in appetite control: Implications for the pathogenesis of obesity. J Neuroendocrinol. 2018;30(11):e12643.

175. Larabee CM, Neely OC, Domingos AI. Obesity: a neuroimmunometabolic perspective. Nat Rev Endocrinol. 2020;16(1):30-43.

176. Zeng W, Pirzgalska RM, Pereira MM, Kubasova N, Barateiro A, Seixas E, et al. Sympathetic neuro-adipose connections mediate leptin-driven lipolysis. Cell. 2015;163(1):84-94.

177. Wolf Y, Boura-Halfon S, Cortese N, Haimon Z, Sar Shalom H, Kuperman Y, et al. Brown-adipose-tissue macrophages control tissue innervation and homeostatic energy expenditure. Nat Immunol. 2017;18(6):665-74.

178. Cardoso F, Klein Wolterink RGJ, Godinho-Silva C, Domingues RG, Ribeiro H, da Silva JA, et al. Neuro-mesenchymal units control ILC2 and obesity via a brain-adipose circuit. Nature. 2021;597(7876):410-4.

179. Kaisar MMM, Ritter M, Del Fresno C, Jonasdottir HS, van der Ham AJ, Pelgrom LR, et al. Dectin-1/2-induced autocrine PGE2 signaling licenses dendritic cells to prime Th2 responses. PLoS Biol. 2018;16(4):e2005504.

180. Roestenberg M, Hoogerwerf MA, Ferreira DM, Mordmuller B, Yazdanbakhsh M. Experimental infection of human volunteers. Lancet Infect Dis. 2018;18(10):e312-e22.

181. Hoogerwerf MA, Koopman JPR, Janse JJ, Langenberg MCC, van Schuijlenburg R, Kruize YCM, et al. A Randomized Controlled Trial to Investigate Safety and Variability of Egg Excretion After Repeated Controlled Human Hookworm Infection. J Infect Dis. 2021;223(5):905-13.

182. Chapman PR, Webster R, Giacomin P, Llewellyn S, Becker L, Pearson MS, et al. Vaccination of human participants with attenuated Necator americanus hookworm larvae and human challenge in Australia: a dose-finding study and randomised, placebo-controlled, phase 1 trial. Lancet Infect Dis. 2021;21(12):1725-36.

183. Langenberg MCC, Hoogerwerf MA, Koopman JPR, Janse JJ, Kos-van Oosterhoud J, Feijt C, et al. A controlled human Schistosoma mansoni infection model to advance novel drugs, vaccines and diagnostics. Nat Med. 2020;26(3):326-32.

APPENDICES

Begrippenlijst

Adipocyten: Vetcellen
Antigenen: Stukjes van cellen of ziekteverwekkers waar het immuunsysteem op kan reageren

ATP citraat lyase (Acly): Enzym betrokken bij het metabolisme, belangrijk voor het maken van vetten en cholesterol, en het reguleren van de expressie van genen

Acly-deficiënte macrofagen: Macrofagen die geen Acly kunnen maken

Cytokines/chemokines: Signaalstofjes die gemaakt worden door cellen om met elkaar te communiceren

$DC^{\Delta LKB1}$ muizen: Muizen waarvan de dendritische cellen geen LKB1 kunnen maken

Dendritische cellen: Cellen van het aspecifieke immuunsysteem die gespecialiseerd zijn in het controleren van hun omgeving op ziekteverwekkers en het instrueren van T cellen

Genen: Stukje DNA dat de code beschrijft voor het maken van eiwitten

Genexpressie: De mate van uitlezen van een gen, wat de hoeveelheid te maken eiwit bepaald

Glycanen: Koolhydraatstructuren verbonden aan eiwitten en vetten

Glycoproteïnen: Eiwitten waaraan koolhydraatstructuren verbonden zijn

Helminten: Groep parasitaire wormen die bekend staan als sterkste natuurlijke opwekkers van type 2 immuunreacties

Homeostase: Gezonde balans

Immunomodulatoire moleculen: Moleculen die het immuunsysteem kunnen beïnvloeden

Inflammatie: Ontstekingsreactie

Insulineresistentie: Ongevoeligheid voor het hormoon insuline, wat de bloedsuikerspiegel reguleert

In vitro: Type onderzoek wat zich afspeelt buiten een levend wezen, bijvoorbeeld in een reageerbuis in het laboratorium

In vivo: Type onderzoek wat zich afspeelt in een levend wezen, bijvoorbeeld een muis

Lever kinase B1 (LKB1): Eiwit betrokken bij het metabolisme dat in dendritische cellen een rol speelt bij T cel priming

Macrofagen: Veelzijdige cellen van het aspecifieke immuunsysteem die hun omgeving beschermen door (delen van) cellen en ziekteverwekkers op te eten en onschadelijk te maken. Spelen ook een rol bij het behouden van homeostase

Metabole homeostase: Gezonde balans van het metabolisme, waarin metabole weefsels gevoelig zijn voor insuline

Metabole weefsels: Weefsels betrokken bij het metabolisme, zoals vetweefsel, de lever en spieren

Metaflammatie: Ontsteking in metabole weefsels die leidt tot insulineresistentie

pLe^{X}-ω1: Belangrijk immunomodulatoir glycoproteïne dat voorkomt in SEA en type 2 immuunreacties induceert. Geproduceerd in gemodificeerde planten waardoor de glycanen meer lijken op het ω1 uit SEA

Pro-inflammatoir: Ontstekingsbevorderend

Schistosoma mansoni: Soort binnen de helminten

SEA: 'Soluble egg antigens', een mix van (immunomodulatoire) moleculen uit *Schistosoma mansoni* eitjes

sMR: Oplosbaar extracellulair gedeelte van de mannose receptor dat afgeknipt kan worden en in verband gebracht is met ontstekingsziekten

$Stat6^{-/-}$ muizen: Muizen die geen STAT6 maken en zodoende geen type 2 immuunreactie kunnen starten

T cel priming: Het instrueren van T cellen door dendritische cellen, waardoor ze vermenigvuldigen en een specifieke immuunreactie opwekken tegen hetgeen de dendritische cel ze presenteert

T cellen: Cellen van het specifieke immuunsysteem die een specifieke immuunreactie kunnen opwekken op basis van instructies van dendritische cellen

Totum-63: Voedingssupplement op basis van plantextracten ontwikkeld voor het voorkomen van diabetes type 2 in mensen met een hoog risico op het ontwikkelen van diabetes type 2

Type 2 immuunreactie: Soort immuunreactie waarbij type 2 T helper cellen, eosinofielen en alternatief geactiveerde macrofagen een rol spelen. Wordt onder andere opgewekt door helminten en lijkt gunstig voor het behouden van insulinegevoeligheid in metabole weefsel

Nederlandse samenvatting

Obesitas, diabetes type 2 en metaflammatie

Een chronisch hogere energie-inname dan -verbruik leidt tot overgewicht en obesitas, en verhoogt het risico op het ontwikkelen van verschillende ziekten zoals diabetes type 2, hart- en vaatziekten, en sommige vormen van kanker. Obesitas is momenteel een epidemie ondanks dat het voorkomen kan worden. Volgens de laatste cijfers van de World Health Organisation leden in 2016 wereldwijd 650 miljoen volwassenen aan obesitas, en 450 miljoen volwassenen in 2019 aan diabetes type 2. Leefstijlinterventies – zoals aanpassingen in het dieet, meer bewegen, psychologische begeleiding of een combinatie daarvan – hebben bewezen effect op het verlagen van de risico's van obesitas en het verbeteren van de kwaliteit van leven. Het behouden van gewichtsverlies is voor velen echter een grote uitdaging. Mensen die zijn afgevallen hebben zelfs een verhoogd risico op versnelde gewichtstoename, wat de voordelen van eerder gewichtsverlies teniet doet. Er wordt veel onderzoek naar obesitas en diabetes type 2 gedaan, en diabetes type 2 is dan ook behandelbaar met medicijnen. Helaas pakken deze behandelingen vooral symptomen aan en niet de oorzaak, en zijn we nog niet in staat het tij te keren. Daarom zijn nieuwe, innovatieve behandelmethoden nodig die (betere) alternatieven bieden voor de huidige medicijnen, en/of die leefstijlinterventies ondersteunen om de druk van de ziekte op de maatschappij te verlichten.

Een beter begrip van de mechanismen achter obesitas en bijbehorende complicaties draagt mogelijk bij aan het ontwikkelen van zulke behandelmethoden. Langdurig te veel voeding consumeren zorgt ervoor dat vetcellen (de ***adipocyten***) groeien en dat nieuwe adipocyten worden gemaakt. In het vetweefsel wordt hierbij een ontstekingsreactie aangewakkerd, ook wel ***inflammatie*** genoemd. Hierdoor worden cellen van het immuunsysteem geactiveerd en produceren zij signaalstofjes (zogenaamde ***cytokines en chemokines***) die ervoor zorgen dat meer immuuncellen zich verplaatsen naar het ontstoken vetweefsel. Hoe meer immuuncellen, hoe meer cytokines en chemokines. Zo ontstaat een vicieuze cirkel waarbij er steeds meer immuuncellen ophopen in het vetweefsel. Daarnaast verminderen bepaalde cytokines de gevoeligheid van adipocyten voor insuline, het hormoon dat de bloedsuikerspiegel reguleert. Hierdoor neemt het vetweefsel minder glucose op uit het bloed en laat het meer vetten vrij in het bloed. Deze vetten kunnen zich ophopen in spieren en de lever, wat de gezonde balans (***homeostase***) en functie van deze organen belemmerd. Een dergelijke verstoring van de homeostase zorgt voor inflammatie zoals in het vetweefsel, ongevoeligheid van de spieren en de lever voor insuline (***insulineresistentie***), en verhoogde glucoseproductie door de lever. Tezamen leidt dit tot een verhoogde bloedsuikerspiegel en het is deze chronisch verhoogde bloedsuikerspiegel in diabetes type 2 die schade met zich meebrengt, zoals aan bloedvaten

en zenuwen, met alle gevolgen van dien. Diabetes type 2 als gevolg van obesitas wordt dus veroorzaakt door chronische inflammatie in weefsels betrokken bij het metabolisme (***metabole weefsels***), zoals het vetweefsel, spieren en de lever. Dit fenomeen noemen we ***metaflammatie***.

Om metaflammatie te begrijpen is een basaal begrip van het immuunsysteem nodig. Dit systeem is essentieel voor de bescherming van het lichaam voor gevaren van buitenaf, maar ook van binnenuit. Zo beschermt het immuunsysteem tegen infecties met bacteriën, virussen, schimmels en parasieten, maar ruimt het ook dode cellen en zelfs tumorcellen op. Het immuunsysteem kan grofweg worden onderverdeeld in twee takken: het aspecifieke immuunsysteem en het specifieke immuunsysteem. Zoals de naam aangeeft, beschermt het aspecifieke immuunsysteem op een niet specifieke manier tegen ziekteverwekkers. Dat wil zeggen dat verschillende ziekteverwekkers op een soortgelijke manier aangepakt worden. Neutrofielen, eosinofielen, monocyten en macrofagen zijn enkele cellen van deze tak van het immuunsysteem die ziekteverwekkers kunnen opeten en/of onschadelijk maken. ***Dendritische cellen*** (DCs) zijn bijzondere cellen van het aspecifieke immuunsysteem omdat ze de schakel vormen tussen het aspecifieke en specifieke immuunsysteem. Zij doen dit door hun omgeving te scannen op ziekteverwekkers en kleine stukje hiervan, zogenoemde ***antigenen,*** te presenteren aan ***T cellen***. Dit noemen we ***T cel priming***. T cellen zijn cellen van het specifieke immuunsysteem, die na priming door DCs alleen een ontstekingsreactie in gang zetten tegen deze specifieke antigenen. Mits zij de juiste signalen ontvangen van DCs, kunnen T cellen zich snel vermenigvuldigen en het immuunsysteem helpen om ziekteverwekkers efficiënt op te ruimen. Daartoe zijn er verschillende typen T cellen die specifiek zijn voor verschillende soorten ziekteverwekkers, en allen hun eigen cytokines produceren. Naast de rol van immuuncellen in bescherming tegen ziekteverwekkers, zijn ze ook in veel gezonde weefsels aanwezig om weefselfunctie te ondersteunen, bijvoorbeeld door dode of beschadigde cellen op te ruimen.

Bij metaflammatie is de homeostase van het immuunsysteem in metabole weefsels dus verstoord. Bij het meeste onderzoek naar metaflammatie is gekeken naar het vetweefsel, aangezien dit wordt beschouwd als de oorsprong van een ontstekingsreactie die leidt tot insulineresistentie. Zowel cellen van ons aspecifieke als specifieke immuunsysteem hopen zich op in het vetweefsel tijdens obesitas, en spelen een rol bij het ontwikkelen van insulineresistentie. Eén van de belangrijke concepten hierbij is de verplaatsing van monocyten uit het bloed naar het obese vetweefsel die zich aldaar ontwikkelen tot ***macrofagen*** in de inflammatoire omgeving. De cytokines die geproduceerd worden door deze inflammatoire macrofagen, zoals tumor necrose factor (TNF) en interleukine 1β (IL-1β), remmen de werking van insuline in adipocyten (zie **Figuur 1**). Net als in het vetweefsel, zorgt obesitas in de lever voor activatie van de macrofagen aldaar. Langdurige obesitas zorgt voor celdood van deze macrofagen, waardoor opnieuw monocyten worden aangetrokken die zich ontwikkelen in macrofagen om de ontstane niche op te vullen.

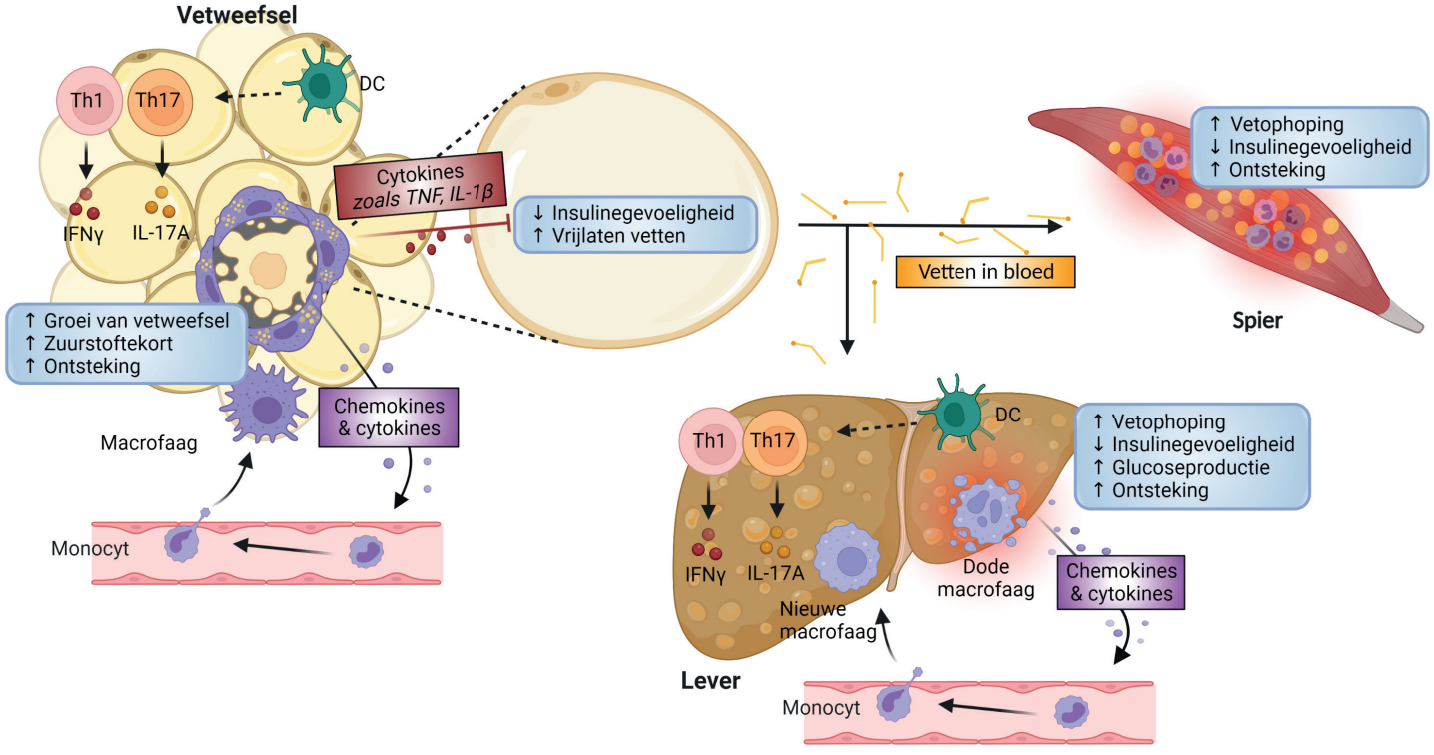

Figuur 1. Processen van metaflammatie bij obesitas die leiden tot complicaties. Zie tekst voor details. Th: T helper cel, DC: dendritische cel, IFNγ: interferon gamma, IL: interleukine, TNF: tumor necrose factor. Figuur gemaakt met BioRender.com.

Deze nieuwe macrofagen, afkomstig van monocyten, zijn echter ontstekingsbevorderend (***pro-inflammatoir***), wat bijdraagt aan ophoping van vet in de lever, insulineresistentie en uiteindelijk het ziektebeloop van diabetes type 2 (zie **Figuur 1**). De precieze omgevingsfactoren in het vetweefsel en de lever, en veranderingen in de macrofaag die zorgen voor activatie van macrofagen tijdens obesitas en het bevorderen van metaflammatie, zijn tot op heden nog niet volledig bekend. Het bepalen van deze omgevingsfactoren en/of veranderingen kan leiden tot aanknopingspunten voor nieuwe of verbeterde behandelmethoden.

Naast macrofagen dragen ook DCs bij aan het ziektebeloop van obesitas en bijbehorende complicaties. De hoeveelheid DCs in metabole weefsels stijgt tijdens obesitas, en muizen die geen DCs hebben of waarvan DC migratie is verstoord, zijn beschermd tegen metaflammatie en insulineresistentie. De DCs in metabole weefsels zorgen voor priming van T cellen, die ook in grote mate aanwezig zijn in metabole weefsels. Obesitas vergroot het aandeel T cellen in deze weefsels die de pro-inflammatoire cytokines interferon gamma (IFNγ) en IL-17A produceren. Deze cellen worden type 1 T helper cellen (Th1 voor IFNγ-producerende T helper cellen) en Th17 cellen (voor IL-17A-producerende T helper cellen) genoemd. Deze Th1 en Th17 cellen worden beschouwd als cellen die bijdragen aan insulineresistentie (zie **Figuur 1**). Welk type T cel ontstaat na activatie door DCs wordt onder andere bepaald door het metabolisme van de DCs. Voor het maken van cytokines en andere moleculen die een rol spelen bij T cel priming heeft de DC bouwstenen/nutriënten nodig. Deze komen uit de omgeving, van moleculen die al aanwezig zijn in de cel, of een combinatie daarvan. Als gevolg hiervan weten we dat de omgeving waarin de DC zich bevindt en de aanwezigheid van nutriënten invloed heeft op T cel priming. Tijdens obesitas is de beschikbaarheid van nutriënten in metabole weefsels anders dan tijdens homeostase, wat dus invloed kan hebben op DCs en T cel priming. De exacte mechanismen die ten grondslag liggen aan T cel priming in metabole weefsels tijdens obesitas zijn echter nog niet volledig bekend.

Type 2 immuunreacties, metabole homeostase en parasitaire wormen

Het behoud van insulinegevoeligheid van metabole weefsels wordt gecontroleerd door het immuunsysteem. In gezond vetweefsel bevinden zich met name T cellen die de cytokines IL-4, IL-5 en IL-13 produceren. Dit zijn de type 2 T helper cellen (Th2 cellen). Van deze cytokines zorgt IL-5 ervoor dat eosinofielen behouden blijven in het vetweefsel. Deze eosinofielen zijn cellen van ons aspecifieke immuunsysteem die onder andere bijdragen aan de bescherming tegen parasieten, maar in het vetweefsel zijn zij de belangrijkste producent van IL-4 en daarmee het behoud van weefsel homeostase. IL-4 zorgt namelijk samen met IL-13 voor het alternatief activeren van macrofagen. Deze alternatief geactiveerde macrofagen worden beschouwd als ontstekingsremmende cellen en één van de hoofdrolspelers in het behoud van

insulinegevoeligheid van het vetweefsel, ook wel ***metabole homeostase*** genoemd (zie **Figuur 2**). Terwijl dit in de lever niet zo uitvoerig is bestudeerd, is er bewijs voor vergelijkbare processen die aldaar metabole homeostase behouden. Deze ***type 2 immuunreactie*** in metabole weefsels verdwijnt tijdens obesitas. Het herstellen van deze (type 2) immuunreactie in personen met obesitas zou mogelijk de insulinegevoeligheid kunnen verbeteren, en de complicaties van obesitas kunnen verminderen.

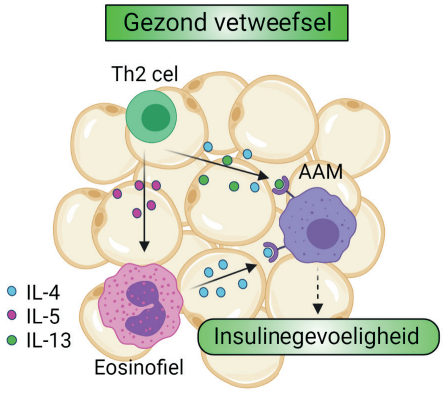

Figuur 2. Type 2 immuunreactie in gezond vetweefsel. Zie tekst voor details. Th: T helper cel, IL: interleukine, AAM: alternatief geactiveerde macrofaag. Figuur gemaakt met BioRender.com.

Helminten, een groep parasitaire wormen, zijn de belangrijkste natuurlijke opwekkers van type 2 immuunreacties. Onderzoek wijst uit dat obesitas minder vaak voorkomt bij mensen die in gebieden wonen waar infecties met helminten veel voorkomen. Het is zelfs zo dat het ontwormen van mensen die geïnfecteerd zijn met helminten de insulinegevoeligheid van deze mensen vermindert. Dit geeft aan dat er mogelijk een omgekeerd verband is tussen infectie met helminten en de complicaties van obesitas. Infectie van muizen met helminten zorgt dus voor een type 2 immuunreactie, ook in het vetweefsel van obese muizen. Deze immuunreactie is gericht tegen antigenen van deze helminten, maar zorgt ook voor het verbeteren van de insulinegevoeligheid. Het injecteren van de antigenen van de eitjes of de wormen zelf, in afwezigheid van levende parasieten, wakkert ook een type 2 immuunreactie in het vetweefsel aan en verbetert de insulinegevoeligheid van muizen met obesitas. Tezamen suggereert dit dat het opwekken van een type 2 immuunreactie, door helminten of hun antigenen, een veelbelovende strategie kan zijn voor het bestrijden van obesitas en diabetes type 2. Of de type 2 immuunreactie daadwerkelijk belangrijk is voor het verbeteren van de insulinegevoeligheid en hoe dit precies werkt is nog niet bekend.

Onderzoek beschreven in dit proefschrift

Dit proefschrift beschrijft hoe immuuncellen metabole homeostase controleren. Om dit goed te kunnen bestuderen is onderzoek in muizen nodig. Voor dit onderzoek is dan ook met name gebruik gemaakt van een muismodel voor obesitas, insulineresistentie en diabetes type 2. Hierbij worden muizen een dieet gevoerd met veel vetten, waardoor ze overgewicht en insulineresistentie ontwikkelen.

Dit proefschrift bestaat uit twee delen. In deel 1 wordt beschreven hoe cellen van het aspecifieke immuunsysteem, met name macrofagen en dendritische cellen, metabole homeostase bewaken. Als we beter begrijpen hoe dit mis gaat tijdens obesitas, kan dit leiden tot nieuwe behandelmethoden voor obesitas en bijbehorende complicaties. De functie van immuuncellen wordt gefaciliteerd door hun metabolisme. Het enzym ***ATP citraat lyase (Acly)*** vormt een link tussen het metabolisme van macrofagen en hun activatie. Acly zorgt er namelijk voor dat geactiveerde macrofagen voldoende Acetyl-Coenzym A (Acetyl-CoA) hebben, wat een bouwsteen is om nieuwe vetten en cholesterol te maken, en om expressie van ***genen*** te beïnvloeden. Genen zijn stukken DNA die de blauwdruk vormen van eiwitten, zoals cytokines of enzymen. De informatie in deze genen moet worden gelezen en vertaald, en de mate waarin genen worden afgelezen noemen we ***expressie***, wat uiteindelijk bepaald hoeveel eiwit wordt gemaakt. Recent onderzoek wijst uit dat macrofagen die het enzym Acly niet kunnen maken (aangeduid als ***Acly-deficiënte macrofagen***), meer genen tot expressie brengen die coderen voor cytokines en bepaalde eiwitten betrokken bij ontstekingsreacties. De verhoogde productie van deze cytokines en eiwitten duidt op inflammatoire activatie. In **hoofdstuk 2** hebben we de consequenties van het verwijderen van Acly uit macrofagen bestudeerd in verschillende inflammatoire ziekten, waaronder metaflammatie. We bevestigen dat activatie van Acly-deficiënte macrofagen in het laboratorium (***in vitro***) leidt tot sterkere inflammatoire activatie vergeleken met controle macrofagen. Dit zou er toe kunnen leiden dat ***in vivo***, oftewel in een compleet levend lichaam, ontstekingen verergeren. Echter, buikvliesontsteking, multiple sclerose en metaflammatie waren allen onveranderd in muizen met Acly-deficiënte macrofagen. Dit geeft aan dat het pro-inflammatoire profiel van Acly-deficiënte macrofagen *in vitro* zich niet vertaalde tot verergering van verschillende inflammatoire ziekten in de muis. Mogelijk compenseren Acly-deficiënte macrofagen voor het verlies van Acly, om zo toch aan voldoende Acetyl-CoA te komen voor belangrijke processen in de cel. Dit zou de discrepantie van onze resultaten met eerdere studies kunnen verklaren. Om dit vast te kunnen stellen is meer onderzoek nodig.

Macrofagen hebben een grote verscheidenheid aan eiwitten op hun oppervlakte waarmee veranderingen in de omgeving kunnen worden gedetecteerd; informatie die door de macrofaag wordt gebruikt om homeostase te kunnen bewaken. Een van deze eiwitten is

de mannose receptor (MR), een eiwit dat moleculen kan binden en opnemen. Het gedeelte van de MR dat zich aan de buitenkant van de cel bevindt, heeft de eigenaardige eigenschap om afgeknipt te kunnen worden en op te lossen in vloeistoffen in de omgeving van de cel. Deze vorm van de MR (***sMR***) is recent in verband gebracht met verschillende inflammatoire ziekten en blijkt het beloop en de ernst van deze ziekten te kunnen voorspellen. De rol die de MR en sMR spelen bij macrofaag activatie is bestudeerd in **hoofdstuk 3.** We laten hier *in vitro* zien dat het behandelen van macrofagen met sMR de activatie van macrofagen versterkt, en we laten in detail zien welke eiwitten en processen in de cel hiervoor verantwoordelijk zijn. Zowel in muizen als in mensen met obesitas vonden we meer sMR in het bloed, en dit voorspelde de hoeveelheid vet in het lichaam. Muizen die geen mannose receptor kunnen maken, kregen wel obesitas na het voeren van een dieet hoog in vetten, maar bleken volledig beschermt tegen vervetting van de lever en insulineresistentie. Tegelijkertijd waren er minder pro-inflammatoire macrofagen in zowel het vetweefsel als de lever, en dit was voorspellend voor de mate van insulineresistentie. Tot slot resulteerde het injecteren van sMR in gezonde, slanke muizen in insulineresistentie en inflammatoire activatie van macrofagen in het vetweefsel. Tezamen toont dit aan dat de sMR macrofagen pro-inflammatoir maakt en dat dit een rol speelt bij metaflammatie. Welke cellen tijdens obesitas meer sMR produceren, en hoe dit precies werkt, moet nog onderzocht worden. Mogelijk is het remmen van de productie van sMR of het wegvangen van sMR een interessante nieuwe strategie om obesitas en bijbehorende complicaties tegen te gaan. De resultaten van hoofdstuk 3 en andere manieren die de MR en gelijksoortige receptoren gebruiken om ontstekingsreacties te beïnvloeden zijn geëvalueerd in **hoofdstuk 4**.

Voor macrofagen is dus een belangrijke rol weggelegd in metaflammatie, maar zoals eerder genoemd neemt ook het aandeel DCs toe in metabole weefsels tijdens obesitas. Daarnaast is er een verandering in het aantal en type T helper cellen in metabole weefsels tijdens obesitas, wat aangeeft dat de functie van DCs is veranderd. Recent onderzoek toont aan dat het eiwit ***lever kinase B1 (LKB1)*** de T cel priming door DCs beïnvloedt bij verschillende inflammatoire ziekten. **Hoofdstuk 5** beschrijft dat muizen waarvan de DCs geen LKB1 kunnen maken (***DC$^{\Delta LKB1}$ muizen***) verergerde vervetting van de lever en insulineresistentie hadden na het ontwikkelen van obesitas. Daarnaast vonden we in vergelijking met controlemuizen met obesitas meer regulatoire T cellen (Tregs), die over het algemeen ontstekingsremmend zijn, en IL-17A-producerende Th17 cellen, met name in de lever van DC$^{\Delta LKB1}$ muizen. DCs die geen LKB1 kunnen maken, produceerden meer cytokines die zorgen voor Th17 cel priming. Het wegvangen van IL-17A remde leververvetting en insulineresistentie af in DC$^{\Delta LKB1}$ muizen. Dit toont aan dat Th17 cellen belangrijk zijn bij het ontwikkelen van metabole complicaties bij obese DC$^{\Delta LKB1}$ muizen. Meer onderzoek is nodig

om aan te tonen welke processen in deze DCs zorgen voor verhoogde Th17 cel priming, en of deze processen gemanipuleerd kunnen worden om obesitas en bijbehorende complicaties tegen te gaan.

In deel 2 van dit proefschrift hebben we onderzocht of moleculen die het immuunsysteem beïnvloeden (***immunomodulatoire moleculen***), geproduceerd door helminten of met een andere oorsprong, ingezet kunnen worden in de strijd tegen obesitas en bijbehorende complicaties. Tevens hebben we geprobeerd de processen die hieraan ten grondslag liggen te ontrafelen. Helminten wekken een type 2 immuunreactie op in de gastheer. Deze type 2 immuunreactie vinden we tijdens homeostase in gezond vetweefsel, maar gaat verloren tijdens obesitas. De capaciteit van helminten en hun immunomodulatoire moleculen om een type 2 immuunreactie aan te wakkeren, heeft geleid tot de ontwikkeling van een interessante nieuwe onderzoekslijn waarbij onderzocht wordt of dit obesitas en bijbehorende complicaties kan verbeteren. In **hoofdstuk 6** geven we een overzicht van wat hierover bekend is in de literatuur. Hierin beschrijven we onder andere eerder werk van onze groep waarin gebruik werd gemaakt van een helmint genaamd ***Schistosoma mansoni***. Infectie van obese muizen met deze helmint, maar ook behandeling met de immunomodulatoire moleculen uit de eitjes (***SEA***), zorgden voor een type 2 immuunreactie in vetweefsel en de lever, en verbeterde de insulinegevoeligheid van de muizen. Er zijn bijna geen studies die bewijzen dat de gunstige effecten van helminten op metabole homeostase daadwerkelijk afhankelijk zijn van de effecten van helminten op het immuunsysteem. In **hoofdstuk 7** hebben we onderzocht of dit soort gunstige effecten van SEA inderdaad afhankelijk zijn van de type 2 immuunreactie, door gebruik te maken van muizen die geen type 2 immuunreactie kunnen opstarten (***Stat6$^{-/-}$ muizen***). Zoals verwacht was SEA in *Stat6$^{-/-}$* muizen met obesitas niet in staat om een type 2 immuunreactie op te wekken in vetweefsel, in tegenstelling tot controlemuizen met obesitas. Echter, in *Stat6$^{-/-}$* muizen had SEA ook geen gunstig effect op de metabole homeostase, wat aangeeft dat het opwekken van de type 2 immuunreactie door SEA inderdaad belangrijk is voor het verbeteren van de gezondheid van muizen. Hoewel dit past bij een model waarin alternatief geactiveerde macrofagen insulinegevoeligheid bewaken, moet nog bevestigd worden of deze cellen hier daadwerkelijk een rol bij spelen.

SEA wordt gemaakt door de eitjes van *S. mansoni* te breken en de eischalen te verwijderen. Hierdoor blijft een ongezuiverde mix van veel verschillende moleculen over die mogelijk uiteenlopende effecten hebben. Het isoleren en onderzoeken of afzonderlijke moleculen een type 2 immuunreactie kunnen opwekken en metabole homeostase kunnen verbeteren, zou tot nieuwe behandelstrategieën kunnen leiden. Het veroorzaken van een type 2 immuunreactie door SEA is voor een belangrijk deel afhankelijk van eiwitten waaraan koolhydraatstructuren verbonden zijn, die we ook wel ***glycoproteïnen*** noemen. Deze

glycoproteïnen worden opgenomen door DCs, die op hun beurt zorgen voor de priming van Th2 cellen. Eén van deze glycoproteïnen in SEA met sterke immunomodulatoire eigenschappen is omega-1 (ω1). Er zit te weinig ω1 in SEA om voldoende materiaal te isoleren voor onderzoek, waardoor we afhankelijk zijn van productie in levende cellen. Eerder onderzoek heeft laten zien dat behandeling van obese muizen met ω1 geproduceerd in humane embryonale niercellen leidde tot gewichtsverlies en verbeterde metabole homeostase. Echter, de immunomodulatoire eigenschappen van ω1 zijn voor een deel afhankelijk van de koolhydraatstructuren (***glycanen***) op het eiwit, en de soort glycanen op ω1 geproduceerd in humane cellen verschilt significant van de glycanen op ω1 uit SEA. Specifiek mist een koolhydraatstructuur op het eind van de glycanen dat we Lewis X (Le^X) noemen, waarvan bekend is dat het een immuunreactie veroorzaakt. Aangezien glycanen belangrijk zijn voor het opwekken van een type 2 immuunreactie door SEA en ω1, is in **hoofdstuk 7** een andere strategie gebruikt voor het produceren van ω1. In samenwerking met onderzoekers van de Wageningen Universiteit hebben we ω1 gemaakt in planten van de familie *Nicotiana benthamiana*. In deze planten is het bouwproces van deze glycanen gemanipuleerd, waardoor de glycanen op ω1 uit *N. benthamiana* (***pLe^X-ω1***) meer lijken op de glycanen van ω1 uit SEA.

Behandeling van obese muizen met pLe^X-ω1 veroorzaakte een type 2 immuunreactie in metabole weefsels, verlaagde de vetmassa en verbeterde de insulinegevoeligheid. Echter, in tegenstelling tot SEA verbeterde pLe^X-ω1 ook metabole homeostase in *Stat6*$^{-/-}$ muizen met obesitas die geen type 2 immuunreactie kunnen opwekken. pLe^X-ω1 verminderde de voedselinname, maar niet de beweeglijkheid van de muizen, wat aangeeft dat het onwaarschijnlijk is dat ongerief de eetlust heeft beïnvloed. Deze lagere energie-inname verklaarde voor een belangrijk deel de verbeterde metabole homeostase. Het ontrafelen van de processen die hieraan ten grondslag liggen, kunnen mogelijk leiden tot nieuwe behandelmethoden voor obesitas-gerelateerde complicaties.

In **hoofdstuk 8** hebben we de effecten van een recent ontwikkeld voedingssupplement op metabole homeostase in muizen met obesitas onderzocht. Ons dieet heeft invloed op ontstekingsziekten, onderzoek naar voedingssupplementen om immuunreacties te beïnvloeden is daarom in trek. Het gebruik van voedingssupplementen voor het verbeteren van metabole gezondheid is niet nieuw, maar is wel een interessante, niet-invasieve manier om obesitas-gerelateerde complicaties te voorkomen of verbeteren. Aangezien sommige voedingssupplementen immunomodulatoire eigenschappen hebben, zouden ze twee vliegen in één klap kunnen slaan: zowel het verminderen van metaflammatie, als het verbeteren van de insulinegevoeligheid van adipocyten, spiercellen en/of levercellen. ***Totum-63*** is een mix van plantextracten met mogelijk immunomodulatoire eigenschappen dat recent is

ontwikkeld voor het voorkomen van diabetes type 2 in mensen met een verhoogd risico op het ontwikkelen van diabetes type 2. In **hoofdstuk 8** is onderzocht of het voedingssupplement ook metabole homeostase kan verbeteren wanneer diabetes type 2 reeds is ontwikkeld, en op welke manier(en) Totum-63 dit doet. Totum-63 suppletie in muizen met obesitas leidde tot gewichtsverlies, verlies van vetmassa en verbetering van insulinegevoeligheid. Het voedingssupplement had effect op meerdere metabole weefsels, zoals de darmen, de lever, de spieren, vetweefsel rond de organen en onderhuids vetweefsel. In deze organen verminderde Totum-63 ontsteking en verbeterde het de insulinegevoeligheid. Daarnaast activeerde Totum-63 bruin vetweefsel. Bruin vetweefsel is een type vetweefsel dat niet primair dient als opslag voor vetten, maar als orgaan dat warmte produceert door glucose en vetten te verbranden. Het lijkt er daarom op dat Totum-63 op veel verschillende manieren werkt, wat mogelijk verklaard wordt door de samenstelling, bestaande uit verscheidene plantextracten. Desalniettemin is Totum-63 een veelbelovend voedingssupplement dat mogelijk kan bijdragen aan het bestrijden van obesitas en bijbehorende complicaties.

Conclusie

Dit proefschrift beschrijft nieuw ontdekte manieren die immuuncellen gebruiken om insulinegevoeligheid te behouden. Daarnaast laten we zien dat immunomodulatoire moleculen, bijvoorbeeld van helminten, het immuunsysteem beïnvloeden en complicaties van obesitas verbeteren. Hoewel we de effectiviteit van leefstijlinterventies niet over het hoofd moeten zien, is het manipuleren van het immuunsysteem met helminten, de moleculen van helminten, of andere immunomodulatoire moleculen een veelbelovend aanknopingspunt in de strijd tegen obesitas en bijbehorende complicaties, waarvoor meer onderzoek nodig is.

Curriculum vitae

Hendrik Johannes Petrus (Patrick) van der Zande was born on 20 November 1991 in Dordrecht, the Netherlands. He completed grammar school (gymnasium) at the Norbertuscollege in Roosendaal, the Netherlands, in 2009. That same year, he moved to Leiden, the Netherlands, to start the bachelor program Biomedical Sciences at the Leiden University Medical Center (LUMC).

During this bachelor program, he passionately engaged in student participation at the LUMC and Leiden University through different platforms: as a full-time board member with portfolio student participation at his study association (Medische Faculteit der Leidse Studenten, Leiden, 2012-2013), as chair of the student council of the LUMC (2013-2014), as member of the Leiden University Student Platform (2013-2014) and as student member of the Medicine and Biomedical Sciences program board of the LUMC (2013-2014).

At the end of his bachelor program, he was a student research intern at the department of Nephrology (LUMC) under the supervision of prof.dr. A.J. van Zonneveld, dr. E.P. van der Veer and dr. R.G. de Bruin in 2014. He studied the role of the RNA-binding protein Quaking on regulating alternative splicing events in monocyte to macrophage differentiation. He presented this work at the bi-annual Leiden International Medical Student Conference (LIMSC, LUMC) in 2015, for which he received the prize for best oral presentation. His contributions to this work culminated in his first co-authorship on a 2016 Nature Communications article.

In 2014 he received his bachelor's degree and started the master program Biomedical Sciences at LUMC. He conducted research as an intern at the department of Parasitology (LUMC) in 2015, under the supervision of dr. B.G.A Guigas and prof.dr. C.H. Hokke. Here, he investigated the effects of helminth-derived glycoproteins on adipogenesis of human mesenchymal stem cells, introducing him to and fascinating him about the work presented in this thesis. In 2016, he moved to Brooklyn, NY, USA, to work in the lab of dr. P. Loke at New York University School of Medicine for which he received several scholarships. He combined in vivo metabolic tests and flow cytometry-based immunological assessments to investigate the contribution of type 2 immunity to the beneficial metabolic effects of helminth glycoproteins. This led to the work described in chapter 7 of this thesis. During this time, he was awarded an Immunity, Infection and Tolerance graduate program grant at LUMC to continue this work, funding his subsequent PhD position at the department of Parasitology under the supervision of prof.dr. M. Yazdanbakhsh and dr. B.G.A. Guigas. He started this work in late 2016 and graduated a Master of Science in 2017.

He gave several oral presentations on his PhD work, at the Annual Dutch Diabetes Research Meetings (ADDRM, Oosterbeek and Wageningen, the Netherlands, from 2016-

2019), the annual meeting of the Dutch Association for Parasitology (NVP, Utrecht, the Netherlands, in 2017), the Conference on Molecular and Cellular Biology of Helminth Parasites (Hydra, Greece, in 2018), the European Workshop on AMPK (Louvain-La-Neuve, Belgium, in 2019), the virtual meeting of the Immunometabolism Network Netherlands (ImmunoMetNet, 2020) and the International Meeting on AMPK (Evian-les-Bains, France, in 2021). He was awarded the best oral presentation prize at the European Workshop on AMPK (2019).

In 2021, he started his post-doctoral training at Wageningen University & Research, Wageningen, the Netherlands, supervised by dr. R. Stienstra. Here, he studies the impact of timing of lifestyle interventions in pre-diabetics on metabolic health and immune responses through the consortium "The right timing to prevent type 2 diabetes (TIMED)".

List of publications

Publications related to this thesis

1. **van der Zande HJP**, Brombacher EC, Lambooij JM, Pelgrom LR, Zawistowska-Deniziak A, Patente TA, Heieis GA, Otto F, Ozir-Fazalalikhan A, Yazdanbakhsh M, Everts B* and Guigas B*. LKB1 signaling in dendritic cells controls whole-body metabolic homeostasis by limiting T helper 17 priming. *bioRxiv*, 2021.10.14.464396.
   (* shared senior authorship)
2. **van der Zande HJP**#, Nitsche D#, Schlautmann L#, Guigas B*, Burgdorf S*. The mannose receptor: from endocytic receptor and biomarker to regulator of (meta)inflammation. *Front Immunol.* 2021 Oct 14;12:765034.
   (# shared first authorship, * shared senior authorship)
3. **van der Zande HJP**, Lambooij JM, Chavanelle V, Zawistowska-Deniziak A, Otero Y, Otto F, Lantier L, McGuinness OP, Le Joubioux F, Giera M, Maugard T, Peltier SL, Sirvent P and Guigas B. Effects of a novel polyphenol-rich plant extract on body composition, inflammation, insulin sensitivity, and glucose homeostasis in obese mice. *Int J Obes (Lond).* 2021 Sep;45(9):2016-2027.
4. Embgenbroich M#, **van der Zande HJP**#, Hussaarts L#, Schulte-Schrepping J, Pelgrom LR, García-Tardón N, Schlautmann L, Stoetzel I, Händler K, Lambooij JM, Zawistowska-Deniziak A, Hoving L, de Ruiter K, Wijngaarden M, Pijl H, Willems van Dijk K, Everts B, van Harmelen V, Yazdanbakhsh M, Schultze JL, Guigas B*, Burgdorf S*. Soluble mannose receptor induces proinflammatory macrophage activation and metaflammation. *Proc Natl Acad Sci U S A*. 2021 Aug 3;118(31):e2103304118.
   (# shared first authorship, * shared senior authorship)
5. Verberk SGS#, **van der Zande HJP**#, Baardman J, de Goede KE, Harber KJ, Keuning ED, Lambooij JM, Otto F, Zawistowska-Deniziak A, de Vries HE, de Winther MPJ, Guigas B, Van den Bossche J. Myeloid ATP Citrate Lyase Regulates Macrophage Inflammatory Responses In Vitro Without Altering Inflammatory Disease Outcomes. *Front Immunol.* 2021 Apr 26;12:669920.
   (# shared first authorship)
6. **van der Zande HJP**, Gonzalez MA, de Ruiter K, Wilbers RHP, García-Tardón N, van Huizen M, van Noort K, Pelgrom LR, Lambooij JM, Zawistowska-Deniziak A, Otto F, Ozir-Fazalalikhan A, van Willigen D, Welling M, Poles J, van Leeuwen F, Hokke CH, Schots A, Yazdanbakhsh M, Loke P, Guigas B. The helminth glycoprotein omega-1 improves metabolic homeostasis in obese mice through type-2 immunity-independent inhibition of food intake. *FASEB J.* 2021 Feb;35(2):e21331.
7. **van der Zande HJP**#, Zawistowska-Deniziak A#, Guigas B. Immune regulation of metabolic homeostasis by helminths and their molecules. *Trends Parasitol.* 2019 Oct;35(10):795-808.
   (# shared first authorship)

Publications outside this thesis

8. Pelgrom LR#, Patente TA#, Otto F, Nouwen LV, Ozir-Fazalalikhan A, van der Ham AJ, **van der Zande HJP**, Heieis GA, Arens R, Everts B. mTORC1 signaling in antigen-presenting cells of the skin restrains CD8$^+$ T cell priming. *Cell Reports*. 2022 Jul;40:111032.
(# shared first authorship)
9. Zawistowska-Deniziak A, Lambooij JM, Kalinowska A, Patente TA, Łapiński M, **van der Zande HJP**, Basałaj K, de Korne CM, Chayé MAM, Gasan TA, Norbury LJ, Giera M, Zaldumbide A, Smits HH, Guigas B. Fasciola hepatica Fatty Acid Binding Protein 1 modulates T cell polarization by promoting dendritic cell Thrombospondin-1 secretion without affecting metabolic homeostasis in obese mice. *Front Immunol*. 2022 May 26;13:884663.
10. de Bruin RG, Vogel G, Prins J, Duijs JMJG, Bijkerk R, **van der Zande HJP**, van Gils JM, de Boer HC, Rabelink TJ, van Zonneveld AJ, van der Veer EP, Richard S. Targeting the RNA-binding protein QKI in myeloid cells ameliorates macrophage-induced renal interstitial fibrosis. *Epigenomes*. 2020 Feb 13;4(1):2.
11. Pelgrom LR, Patente TA, Sergushichev A, Esaulova E, Otto F, Ozir-Fazalalikhan A, **van der Zande HJP**, van der Ham AJ, van der Stel S, Artyomov MN, Everts B. LKB1 expressed in dendritic cells governs the development and expansion of thymus-derived regulatory T cells. *Cell Res*. 2019 May;29(5):406-419.
12. Hoving LR, **van der Zande HJP**, Pronk A, Guigas B, Willems van Dijk K, van Harmelen V. Dietary yeast-derived mannan oligosaccharides have immune-modulatory properties but do not improve high fat diet-induced obesity and glucose intolerance. *PLoS One*. 2018 May 3;13(5):e0196165.
13. Gundra UM#, Girgis NM#, Gonzalez MA#, San Tang M, **Van Der Zande HJP**, Lin JD, Ouimet M, Ma LJ, Poles J, Vozhilla N, Fisher EA, Moore KJ, Loke P. Vitamin A mediates conversion of monocyte-derived macrophages into tissue-resident macrophages during alternative activation. *Nat Immunol*. 2017 Jun;18(6):642-653.
(# shared first authorship)
14. de Bruin RG, Shiue L, Prins J, de Boer HC, Singh A, Fagg WS, van Gils JM, Duijs JM, Katzman S, Kraaijeveld AO, Böhringer S, Leung WY, Kielbasa SM, Donahue JP, **van der Zande PH**, Sijbom R, van Alem CM, Bot I, van Kooten C, Jukema JW, Van Esch H, Rabelink TJ, Kazan H, Biessen EA, Ares M Jr, van Zonneveld AJ, van der Veer EP. Quaking promotes monocyte differentiation into pro-atherogenic macrophages by controlling pre-mRNA splicing and gene expression. *Nat Commun*. 2016 Mar 31;7:10846.

Dankwoord / acknowledgements

Velen hebben bijgedragen aan de realisatie van dit proefschrift, waar ik iedereen voor wil bedanken. In het bijzonder wil ik een aantal mensen benoemen.

First and foremost: thank you, Bruno. I am grateful for you nurturing me in science, your trust in me, and helping me develop both as a scientist and person. I hope our scientific paths cross again in the future. Professor Yazdanbakhsh, dear Maria, thank you for supporting me from being a Master's student until working at your wonderful department of parasitology. I will be forever grateful for you connecting me with P'ng, allowing me to embark on the biggest adventure of my life.

Paranimfen, ik ben blij jullie naast me te hebben tijdens de verdediging van mijn proefschrift. Eline, bedankt voor het lachen en je steun als buurvrouw in P4-28. Ik koester onze fijne gesprekken, zowel de wetenschappelijke als de persoonlijke. Sven, ik bewonder hoe je altijd weet wat je moet zeggen. Ik ben trots op onze vriendschap, die zich alsmaar verder blijft ontwikkelen.

Professor Hokke, beste Ron, bedankt dat je mijn interesse hebt aangewakkerd voor glycobiologie, en je enthousiaste begeleiding tijdens mijn masterstage en daarna. Bart, bedankt voor je creativiteit, het sparren over data en de mooie fietsritten. Joost, ik waardeer je toewijding en kijk met plezier terug op onze samenwerking als PhD studenten bij Bruno; dat liep als een trein. Graham, thanks for reigniting my passion for science and for sharing our enthusiasm for cycling. Leonard, je ontfermde je over me tijdens mijn masterstage en promotietraject. Ik heb veel van je geleerd, waar ik je erg dankbaar voor ben. Alice, Alwin, Angela, Anna, Arifa, Astrid, Frank, Hermelijn, Leonie, Linh, Noémi, Thiago, Tom and Yvonne: thank you for your guidance and instrumental help during experiments. All other roommates and colleagues at PARA: thanks for your help, advice and support.

Bedankt professor Fijs van Leeuwen, Danny en Mick, voor jullie hulp en fijne samenwerking bij het onderzoeken van de biodistributie van omega-1. Professor Anton-Jan van Zonneveld, Ruben en in het bijzonder Eric, jullie hebben mij mijn eerste stapjes in de wetenschap laten zetten tijdens mijn bachelorstage aan Quaking. Eric, ik kan me geen betere eerste mentor bedenken. Bedankt voor je aanstekelijke enthousiasme, je vertrouwen, en de ruimte die je me hebt gegeven om dit promotietraject te starten. Maarten van Tol, bedankt voor je ondersteuning van de beursaanvraag die tot dit proefschrift heeft geleid, onze fijne gesprekken, en je hart voor onderwijs en studenten. Je bent een inspiratie voor me.

Jan en Sanne, bedankt voor de gezellige en prettige samenwerking die heeft geresulteerd in het Acly paper. Professor Burgdorf and Maria Embgenbroich, thank you for our fruitful

collaboration resulting in two chapters of this thesis. Bedankt professor Arjen Schots, Kim en Ruud, voor de interessante consortiummeetings in Wageningen en Leiden, en de samenwerking die heeft geleid tot het omega-1 paper. Many thanks to Michael and P'ng. Working with you at New York University has been a life-changing event for me. Thank you for your guidance and mentoring during this time. I hope our paths will cross again. Collega's in Wageningen, in het bijzonder Brecht, Frank, Lisa en Rinke: bedankt voor het warme welkom.

Victoria, ik waardeer onze gesprekken. Bedankt voor al je hulp.

Mensen die me goed kennen, weten dat ik niet snel ergens trots op ben. Ik ben echter wel ontzettend trots op mijn vrienden en familie, die mij op allerlei manieren hebben ondersteund tijdens het maken van dit proefschrift. Coach Niels, bedankt voor je begeleiding in het combineren van mijn sportambities met het leven van een wetenschapper. Coverband An Apple A Day: Armand, Esmée, Hans, Koen en Tom, bedankt voor al het plezier, lachen en de prachtige avonturen. Bedankt Jelle, Roy, Martijn, Yvo, Lennart, Féline, Ramzi, Lisa, Niels, Suzanne en Wessel: onze vriendschap betekent veel voor me. Dear Doug, you are a wonderful person. Thank you for your care during my New York visits. Doug and Miho, thank you for your help designing the cover of this thesis. BrooklynTriClub friends, thank you for the early morning suffering. Kees, Mariëlle, Sanne, Ward, Eva, Jordi, Joost en Christine, bedankt voor jullie interesse en zorgen. Zelfs Almere voelt nu een beetje als thuis.

Lieve papa en mama, bedankt voor jullie onvoorwaardelijke steun. Jullie hebben me veel ruimte gegeven om mezelf in een nieuwe, onbekende omgeving te ontwikkelen. Dat waardeer ik enorm. Lieve zus Hannalie, Roland, Axel en Demi; jullie maken thuis compleet.

Liefste Maartje, jij bént thuis. Bedankt voor het aanhoren van zowel mijn enthousiaste verhalen over succesvolle proeven, als frustraties wanneer het niet goed ging. Je bent tijdens dit traject mijn reddingsboei, anker en golfbreker geweest. Bedankt voor je rust en empathie. Ik ben trots op je en kijk reikhalzend uit naar onze toekomst.